INDEX

ACTA
TECHNICA

ACADEMIAE SCIENTIARUM HUNGARICAE

REDIGIT: M. MAJOR

ACTA
TECHNICA

ACADEMIAE SCIENTIARUM HUNGARICAE

REDIGIT: M. MAJOR

IN MEMORY OF NIKOLA TESLA*

Nikola TESLA was born in the Yugoslav Smiljan 120 years ago. He acquired world fame in the field of technical sciences with the discoveries in the fields of both industrial electricity and telecommunication. One of his greatest inventions is the discovery of the rotating magnetic field principle, which permitted the utilization of electrical energy for power transmission, in addition to lighting uses.

In telecommunication his wireless telegraphs excited by electrical discharges and coupled into a high-frequency oscillating circuit permitted to construct, already at the end of the last century, a 200 kW transmitter and to transmit over a distance of 1000 km. At the same period he succeeded in realizing a 25 km wireless transmission for lighting and, according to some sources, also for driving electric motors.

At this time he realized his iron-free high-frequency, high-woltage, oil transformer which already at the end of the last century was able to produce a 12 million V voltage.

For the oil insulation he was the first to introduce the vacuum treatment of the winding. A long list of inventions prove his magnificent creative power; he is the first to use the antenna dimensioned for a quarter of a wavelength, amongst his inventions there are numerous high-frequency patents, his remotely-controlled electrically driven ship and various other control systems.

Already in the secondary school he strove at mastering foreign languages as perfectly as possible and this permitted him, in later periods of his life, to become acquaintanced with the results of natural and technical sciences, and to get into the international front line of the great technical upswing which started at the end of the last century. In Graz he finished the Technical University; there he concentrated mainly on mathematics, physics and their experimental carried out in the laboratory of his professor of experimental physics, while making experiments with a d.c. machine which had arrived

---

* Lecture delivered at the 1976, October 5 session of the Department of Technical Sciences of the Hungarian Academy of Sciences.

from Paris, he first had the idea that instead of the d.c. commutator machine some other solution could to be found, e.g. with the aid of the rotating magnetic field. His professor considered this solution as completely impossible, as if somebody would wish to change the gravitational force of the earth or to invent the perpetuum mobile. He finished his studies at the humanistic branch of Prague University. He was able to develop a generalized picture of the different phenomena of life, which still better permits the realization of creations useful for humanity.

After finishing the university he starts his professional work in Budapest, where he becomes a draughtsman at the Hungarian Government Central Telegraph Office. His superiors immediately notice his special abilities and allow him take part in the work of the Telephone Exchange then under construction. His first inventions are from this time. By mechanical sound amplification of the Telephonograph (loudspeaker and microphone in series) he increases the transmission distance arousing the great interest of the PUSKÁS brothers. But the idea of the rotating field which was born during his stay in Graz, did not let him rest. The search for the solution nearly led to a complete nervous breakdown, the liberation from which, as he writes in his memories, was brought about by Goethe's poem "Faust". One afternoon in February of 1882 he was walking with a friend of his in the Budapest City Park. At sunset the following lines of the poem came to his mind:

"The glow retreats, done is the day of toil,
It yonder hastes, new fields of life exploring;
Ah, that no wing can lift me from the soil,
Upon its track to follow, follow soaring!"

After reciting this thought urging progress he suddenly found the solution, and with a stick in his hand he traced it in the sand, explaining it to his friend, so that he understood it at once. After one year with the aid of the PUSKÁS brothers he gets to France and in 1883 in Strasbourg constructs the first rotating-current motor.

According to some sources he also worked with Károly ZYPERNOWSKY and it is possible that the realization of the multi-phase power transmission principle — which later, beginning from 1893, Kálmán KANDÓ represented in the Ganz Factory — in our country, was furthered by this encounter.

Posterity will always gratefully remember Nikola TESLA, thanks to his great and outstanding theoretical and technical creations.

B. ZORKÓCZY

1898—1975

Béla ZORKÓCZY, Doctor of Technical Sciences between 1950 and 1969 was an active Professor of the Chair of Mechanical Technology of the Miskolc Technical University of Heavy Industry and during the years 1950—1968 he was its head. His death is a great loss to the University and in a larger sense to the whole of Hungarian Mechanical Engineering. The reputation of his scientific work have extended beyond the borders of Hungary.

Béla ZORKÓCZY was born on 27th March 1898 in the town of Moson-magyaróvár. He finished his schooling at the same place in 1916 and was immediately drafted into the Army. He was obliged to participate in World War I, at the end of which he became a prisoner of war in Italy. In 1919 he returned and enrolled at the present Budapest Technical University. In 1924 he obtained the Engineer's diploma in Mechanical Engineering. From 1924 to 1934 he was an assistant of the Chair of Mechanical Technology of the same University and later became chief assistant.

In the years 1934—1944 he was the plant manager, technical director and finally the general manager of the Hubert and Sigmund Steel and Metal Works in Budapest. After the liberation of Budapest, in the early spring of 1945 he organized the production of light metal pistons for supplying the Red Army and parallel to this commission he operated as deputy professor at the Chair of Mechanical Technology of the Budapest Technical University.

From the summer 1945 until 1950 he accepted the post of the technical manager of the Hungarian Matchworks Co.Ltd.

In January, 1950 he was invited to organize the Chair of Mechanical Technology of the new Miskolc Technical University for Heavy Industries and to lecture on the subjects of the chair (Metallography, Technology of structural materials, Heat treatment, Welding). In September, 1950 he was promoted to Ordinary professor, a post which he filled until his retirement in 1969.

Meanwhile, on April 1, 1950 he was appointed as director of the Welding Department of the Iron Industries' Research Institute in Budapest. Until 1962 he carried on both posts, later he devoted his time to his professorial duties only.

The Miskolc Heavy Industries Technical University organized from 1960 on the Academic Working Group for Heavy Machinery, which carried out the complex tasks of several Chairs — under the direction of B. ZORKÓCZY and with the support of the Hungarian Academy of Sciences — until 1970.

At the Miskolc Heavy Industries Technical University, in 1961 he organized the branch of specialized welding engineers, where graduated mechanical engineers could continue their studies during 4 half-years and could obtain a second diploma.

In addition to these tasks he also undertook numerous scientific assignments. For many years he was the chairman of the Welding Branch of the Scientific Association for Mechanical Engineering, for about five years he was chairman of the Mechanical-Siderurgical Commission of the National Postgraduate Degree Granting Board and from 1951 was a member of the Commission on Mechanical Engineering of the Hungarian Academy of Sciences.

From 1963 he was the Chairman of the National Commission of the International Institute of Welding, and a member of the Board of this international organization.

Amongst his many scientific lectures held at home and abroad, let us mention the lecture on "The Stress Corrosion of Welded Steelplate Stacks of Open Hearth Furnaces" which he achieved in 1965 in Paris.

As an academic tutor and research worker he dealt in the first place with welding and in this field he achieved success which was recognized also internationally. Within a short time he created a Hungarian School in this field. Outstanding specialists of heat treatment and welding grew up under his hand, to whom he implanted the love of creative scientific work.

His literary work started in 1930 and lasted almost to the time of his death. Already his first paper concerned the technology of welding and its modern application. This was followed by nearly 80 papers, books or contribution to books, university or postgraduate scripts.

His scientific results were recognized in 1952 by the degree of Candidate of Technical Sciences. The Miskolc Technical University in 1960 granted him the title of Technical Doctor and later, at the Silver Jubilee (25 years) of the University, he was presented with the Honorary Doctorate.

The outstanding results of his teaching, educational and research work were recognized by several govermental, ministerial and scientific honours, the highest of which he obtained in 1956 for his scientific results: the KOSSUTH-prize.

At the end of October, 1975 he became ill and on November 18, 1975 he died unexpectedly.

In the spring of 1976 the National Postgraduate Degree Granting Board declared him posthumously, on the base of his theses submitted the year before "Doctor of Technical Sciences".

Z. Terplán

L. SZÉLL

1903—1976

Das Ableben des Professors László Széll bedeutet sowohl für die Berufs-
ausbildung der ungarischen Architekten, als auch für die Pflege der ungari-
schen Architekturwissenschaften einen überaus großen Verlust. Seine nahezu
ein halbes Jahrhundert währende, hingebungsvolle, schöpferische, pädagogi-
sche und wissenschaftliche Tätigkeit im Dienste der Vertiefung der Baukunst,
der Fortentwicklung der Bautechnik, die eingehende Pflege der Fachliteratur,
die stete Forschung und Suche nach Neuem und Modernem kennzeichnen
sein arbeitsreiches Leben. Er war bei seinen Kollegen beliebt und erwarb
die Wertschätzung seiner Mitarbeiter und die Achtung seiner Schüler.

L. Széll wurde am 9. Mai 1903 in Makó geboren. Seine Mittelschulstudien
absolvierte er an den staatlichen Obergymnasien in Torda und Makó und
erwarb 1928 das Architektendiplom an der Fakultät für Architektur der
Technischen Universität zu Budapest.

Im Jahre 1945 erlangte er "summa cum laude" den Titel eines Doktor-
ingenieurs und wurde 1947 auf dem Fachgebiet "Bautechnologie" zum Privat-
dozenten an der Technischen Universität zu Budapest promoviert.

Auf Grund seines Werkes "Hochbaukunde I.—II." hat ihm 1962 das
Wissenschaftliche Qualifizierungskomitee der Ungarischen Akademie der
Wissenschaften den wissenschaftlichen Grad C. Sci. zuerkannt und für seine
Abhandlung "Grundsätze der Flächengestaltung Zeitgemäßer Gebäude" am
31. Oktober 1973 zum Doktor der technischen Wissenschaften qualifiziert.

Von 1929 betätigte sich L. Széll am Lehrstuhl für Baukonstruktionen
der Budapester Technischen Universität erst als Assistent, dann von 1940
bis 1948 als Dozent und seit 1951 als Universitätsprofessor.

In den Jahren 1951—1959 war er erst Leiter des Lehrstuhls für Hochbau-
kunde, später des Lehrstuhles für Bautechnologie. Im Schuljahr 1957—58
bekleidete er das Amt das stellvertretenden Dekans, in 1959—60 des Dekans
der Fakultät für Architektur. Seit 1960 betätigte er sich am Lehrstuhl für
Bauausführung.

In den Jahren 1930—1957 befaßte er sich mit praktischen Planungs-
arbeiten, beteiligte sich an zahlreichen Wettbewerben und gewann zahlreiche

I. Preise. Auf Grund seiner Pläne wurden mehrere Wohnhäuser und öffentliche Gebäude gebaut. Seine architektonisch-künstlerische Auffassung bezeugt sein in der Zeit von 1930 bis 1950 angefertigtes, in 10 Bänden mehrere tausend Seiten umfassendes Skizzenbuch. In diesem entwickelte er seine Ideen und veröffentlichte Studien über die Eindrücke, die er während seiner Studienreisen im In- und Ausland gewann und entnahm Veröffentlichungen der Fachliteratur, soweit diese mit seinen Ideen, seinen Wettbewerbsplänen und den für seine Auftraggeber angefertigten Entwürfen zusammenhingen.

Seine wissenschaftliche Tätigkeit übte er — außer in Form seiner zahlreichen Publikationen — auch im Auftrag verschiedener Behörden aus. So bekleidete Prof. SZÉLL im Jahre 1973 den Posten eines Vizepräsidenten der — damals neu geschaffenen — juridisch-technischen Fachkommission und wurde zugleich zum Leiter des Unterausschußes für Architektur dieser Institution ernannt.

Das Ministerium für Bauwesen hat 1973 Professor SZÉLL "in Anerkennung seiner auf dem Gebiet der architektonischen Planung, der technischen Literatur und des Unterrichtswesens während mehrerer Jahrzehnte geleiteten hervorragenden Tätigkeit" den Miklós Ybl-Preis I. Klasse verliehen.

Die wissenschaftliche Arbeit des Professors SZÉLL kennzeichnen in erster Reihe seine Fach- und Lehrbücher. Diese Werke — besonders jene, die sich mit der Bauausführung befassen — genügen vollauf ihrer zweifachen Zielsetzung, indem sie einerseits die Grundlagen dieser in Ungarn spät entfalteten und noch später zur Selbstständigkeit gelangten Wissenschaft klären und ihre wichtigsten Bereiche eingehend bearbeiten, andererseits sowohl dem Hochschulunterricht, als auch der Baupraxis vorzügliche Dienste leisten.

Die in seinen Büchern zum Ausdruck gebrachte Betrachtungsweise ist richtig, da die Wahl der Bautechnik und -technologie stets der Vorstellung und Intention des Architekten entsprechend getroffen wurde und das Problem vom Gesichtspunkt des Architekten betrachtet wird, der bestrebt ist die mannigfaltigen Faktoren zu einer harmonischen Einheit zusammenzufassen. Inhaltlich sind die Werke sorgfältig und nützlich gestaltet, da sie in gut verständlicher Weise, anhand von zahlreichen und schönen Bildern einen guten Überblick der wichtigsten Konstruktionen, Einrichtungen und Technologien bieten.

L. Gábor

L. Széll's fachliterarische Tätigkeit

Épületek költségvetése és egyéb anyagi vonatkozásai (Kostenvoranschlag und sonstige materielle Belange von Gebäuden; 87 Seiten, 18 Bildtafeln; Lehrstuhl für Baukonstruktionen, 1944).

Szerkezet és forma viszonya az építészetben (Beziehung zwischen Konstruktion und Form in der Architektur; Doktorarbeit, Manuskript; 109 Seiten, 13 Bildtafeln, 1946).

Korszerű nyílászáró szerkezetek (Zeitgemäße Fenster und Türen; 56 Seiten, 54 Bilder; Fortbildungsinstitut für Ingenieure, 1949).

Kőművesszerkezet (Mauerkonstruktionen; 240 Seiten, 686 Bilder; Tankönyvkiadó, 1951).

Lakóházak építésének nagyipari módszerei a Szovjetunióban (Großindustrielle Methoden des Wohnhausbaues in der Sowjetunion; 76 Seiten, 22 Bildseiten; Institut für Bauwissenschaften, 1960).

Hőszigetelő üvegek (Wärmedämmende Glassorten; 45 Seiten, 26 Bilder, Institut für Bauwissenschaften, 1962).

Nyílászáró szerkezetek vasalatainak és szerelvényeinek fejlesztése (Entwicklung der Beschläge und Armaturen von Fenstern und Türen; 40 Seiten, 65 Bilder; Institut für Bauwissenschaften, 1962).

Üvegtermékek gyártásának és alkalmazásának fejlesztése az építőiparban (Entwicklung der Herstellung und Anwendung von Glasprodukten in der Bauindustrie; 10 Seiten, 22 Bilder; *Magyar Építőipar*, Jg. 1962. Seiten 545—554).

Magasépítéstan I. (Hochbaukunde I. (umgearbeitete zweite Auflage), 58 Bogen bzw. 464 Seiten, 920 Bilderfolgen, 53 Tafeln; Tankönyvkiadó, Budapest, 1963).

SZÉLL—BRUZSA: Épületszerkezetek (Baukonstruktionen; Mérnöki Kézikönyv Band IV., Seiten 17—254, 237 Seiten, 384 Bilder; Műszaki Könyvkiadó, Budapest, 1965).

Beziehungen zwischen Baukonstruktionen, Form und Technologie. Bedeutung der Bautechnologie und des technologischen Unterrichts (4 Seiten, 1 Bild; Teubner Verlag, Leipzig, 1966).

Új szakipari szerkezetek és technológiák (Neue fachgewerbliche Konstruktionen und Technologien; 196 Seiten, 178 Bilder; Tankönyvkiadó, Budapest, 1966).

Magasépítéstan II. (Hochbaukunde II. (umgearbeitete zweite Auflage), 50,5 Bogen, bzw. 402 Seiten, 746 Bilder, 36 Tafeln; Tankönyvkiadó, Budapest, 1967).;

Nyersbeton felületképzés (Rochbetonflächengestaltung, 10 Seiten, 29 Bilder; *Magyar Építőipar*, Jg. 1967. Seiten 740—749).

Technologija Gradenja I.—II. (Bautechnologie, 506 Seiten, 480 Bilder; Izdanje, Beograd, 1968).

A hőszigetelő üveg alkalmazásával kapcsolatosan felmerülő kérdések, különös tekintettel az üveg meghibásodására (Probleme der Anwendung wärmedämmenden Glases unter besonderer Berücksichtigung von Glasschäden; 58 Seiten, 34 Bilder, 3 Tafeln; Budapester Technische Universität, Lehrstuhl für Bauausführung, 1969).

A hőszigetelő üveg alkalmazása, az üveg meghibásodása (Anwendung des wärmedämmenden Glases, Glasschäden; 24 Seiten, 33 Bilder, 3 Tafeln; *Szakipari Technika*, Jg. 1970. Heft. 1.—2.).

Építéstechnológia (Bautechnologie; 44 Bogen bzw. 350 Seiten, 496 Bilder, 18 Tafeln; Tankönyvkiadó, Budapest. 1970).

Felület, ill. homlokzatképzések vizsgálata (Untersuchung von Flächen- bzw. Fassadengestaltungen; 324 Seiten, 277 Bilder, 16 Tafeln; Budapester Technische Universität, Lehrstuhl für Bauausführung, 1971).

A BME Építészmérnöki Kar munkássága az 1963—70 években (Tätigkeit der Fakultät für Bauingenieure der Budapester Technischen Universität in den Jahren 1963—70; Fakultät für Bauingenieure der Technischen Universität zu Budapest, 1971).

Épülethomlokzatok burkolatának tisztítása (Reinigung der Fassadenverkleidungen; 23 Seiten, 40 Bilder, 1 Tafel; *Szakipari Technika*, Jg. 1972. Seiten 40—71).

Homlokzatképzések (Fassadengestaltungen; 27 Bogen bzw. 207 Seiten, 281 Bilder, 8 Tabellen, 12 Tafeln; Műszaki Könyvkiadó, Budapest 1973).

László Gábor

THE SPEED EFFECT IN PAVEMENT DEFLECTION

I. ALPAN* and R. BAKER**

[Manuscript received August 4, 1976]

The influence of vehicle speed on pavement deflection is a problem of obvious importance related to the evaluation of pavement performance. The fact that the deflections diminish with increasing speed implies a dissipative component in the system. A simple visco-elastic model is analysed which furnishes results in good agreement with empirical evidence and may be used in assessing the distortion pattern of pavements under idealized service conditions. Furthermore, relatively simple experimental procedures may be used to determine the required material parameters.

1. Introduction

The bituminous surface layer of a flexible pavement as well as the underlying base and subgrade materials are known to exhibit dissipative properties, that is to say energy is lost when cyclic loading is being applied to these materials. Under sinusoidal stress application the strain is found to lag behind the stress, the time delay depending, in most cases, on the frequency which may be regarded as a measure of the time-rate of loading.

Consequently, the deflection of road structures of the type referred to above may be expected to be time-dependent, an assumption which has been amply verified by observation as discussed, e.g., by BAUM [1958], by HEUKELOM [1961] or by PERLOFF and MOAVENZADEH [1968].

The implications are of obvious importance: since traffic loads are essentially dynamic, the evaluation of performance and life expectancy of flexible pavements must include the consideration of the influence of vehicle speed.

A successful analysis of the problem requires an appropriate model of the road structure and here the theory of visco-elastic materials appears to have offered the most promising approach. Indeed, HARR [1962], PISTER and WESTMANN [1963], WESTMANN [1967], PERLOFF and MOAVENZADEH [1968] and FERRARI [1972], to mention but a few, use viscoelastic models in their analysis of our problem.

* I. ALPAN, Professor of Civil Engineering, Israel Institute of Technology; Haifa.
** R. BAKER, Lecturer, Faculty of Civil Engineering, Israel Institute of Technology.

The present paper is no exception in this respect. Its contribution lies mainly in the choice of a model which, while amenable to a simple analysis, appears to provide satisfactory agreement of prediction with performance.

2. The model

We consider a point load (the wheel), moving with constant speed over the surface of an infinite elastic plate, supported by springs (a so-called Winkler foundation). The resulting deflection is assumed, as a first approximation, to be in accordance with the classic Hertz theory of floating elastic plates. The radial distance, corresponding to zero deflection, is designated as the radius of influence, R_0.
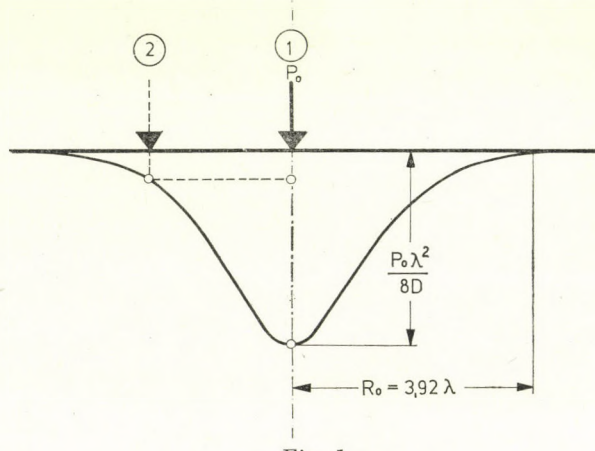
Fig. 1

The deflection curve, constructed from a tabulation given by Hetényi [1946], is shown in Fig. 1. Consider the point load, P_0, in the two positions indicated in the figure: according to Betti's Reciprocal Theorem the deflection at the centre (point "1") for P_0 at position "2" equals the deflection at "2" for P_0 at position "1". Thus the deflection curve should represent the shape of the time function of the deflection at the centre for a point load, moving with constant speed along a straight line passing through the centre.

This time-space correspondence would be strictly valid for an elastic (i.e. non-dissipative) system. However, due to the time-dependence mentioned before, the shape of the time function may be taken to deviate from symmetry as, indeed, indicated by the work of Ferrari [1972]. Thus the rigorous use of the functional relations of the Hertz theory (zero order Hankel functions) does not appear warranted and, instead, a much simpler time function was chosen.

Finally, the road structure (pavement and support) was idealized as a lumped parameter Kelvin model, subjected to a time-dependent force. In contradistinction from the model used by HARR [1962], no inertial component was introduced, a decision supported by the work of FERRARI [1972] and, indirectly, by the investigations of BAUM and HÜRTGEN [1969].

3. The analysis of a single moving load

The system is shown schematically in Fig. 2. The point load, P_0, moves with the constant speed v.
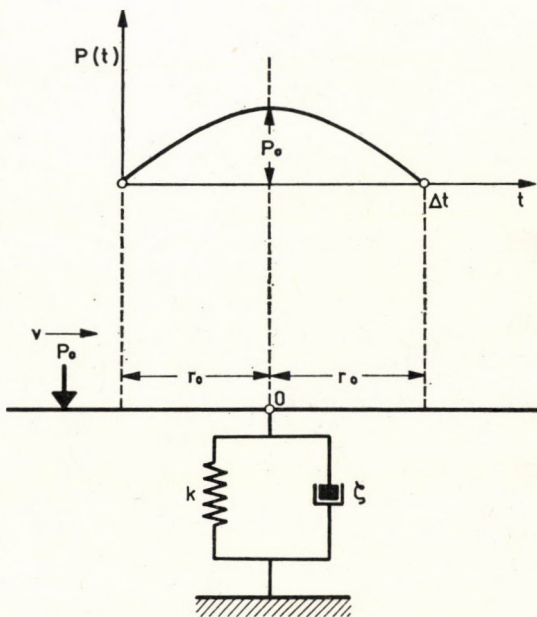
Fig. 2

We shall consider the deflection at point 0 on the surface, rigidly connected to a Kelvin model. During the time interval

$$\Delta t = 2r_0/v \tag{1}$$

the load is supposed to produce a deflection at 0 corresponding to that produced by an equivalent time-dependent load, $P(t)$, applied at that point and given by

$$P(t) = P_0 \sin \pi \frac{t}{\Delta t} \tag{2}$$

as shown in Fig. 2. The influence radius, r_0, will be discussed further on.

The rheological equations, governing the deflection Δ at point 0, read

$$k\Delta + \zeta\dot{\Delta} = P_0 \sin \pi \frac{t}{\Delta t}, \quad (0 \leq t \leq \Delta t) \tag{3}$$

$$k\Delta + \zeta\dot{\Delta} = 0 \quad (\Delta t < t) \tag{4}$$

where k is the spring constant and ζ the viscous resistance of the model.
With the definitions

$$\Delta_S = \frac{P_0}{k}, \quad \text{(static deflection)} \tag{5}$$

$$\tau_0 = \frac{\zeta}{k}, \quad \text{(retardation time)} \tag{6}$$

$$\tan \varphi = \pi \frac{\tau_0}{\Delta t} \quad \text{(loss tangent)} \tag{7}$$

the solution of Eqs 3 and 4 may be written as follows:

for $0 \leq t \leq \Delta t$:

$$\frac{\Delta}{\Delta_S} = \cos \varphi \left[\sin \left(\pi \frac{t}{\Delta t} - \varphi \right) + \sin \varphi \cdot e^{-t/\tau_0} \right], \tag{8}$$

and for $\Delta t \leq t$:

$$\frac{\Delta}{\Delta_S} = \sin \varphi \cdot \cos \varphi [1 + e^{-\Delta t/\tau_0}] \cdot e^{-(t-\Delta t)/\tau_0} . \tag{9}$$

The time function of the deflection ratio, as expressed by Eqs 8 and 9, is shown in Fig. 3 for a particular value of the loss tangent. We note the gradual recovery of the deflection with time, also remarked on by HARR [1962] as being typical for flexible pavements (and leading to the use of critical damping in his analysis).

The maximum deflection, Δ_m, occurs approximately at the time

$$t_m = \left(\frac{1}{2} - \frac{\varphi}{\pi} \right) \Delta t \tag{10}$$

and may be expressed as follows:

$$\frac{\Delta_m}{\Delta_S} \frac{1}{\sqrt{1 + \tan^2\varphi}} \left[1 + \sin \varphi \cdot \exp\left(-\frac{\pi/2 + \varphi}{\tan \varphi} \right) \right]. \tag{11}$$
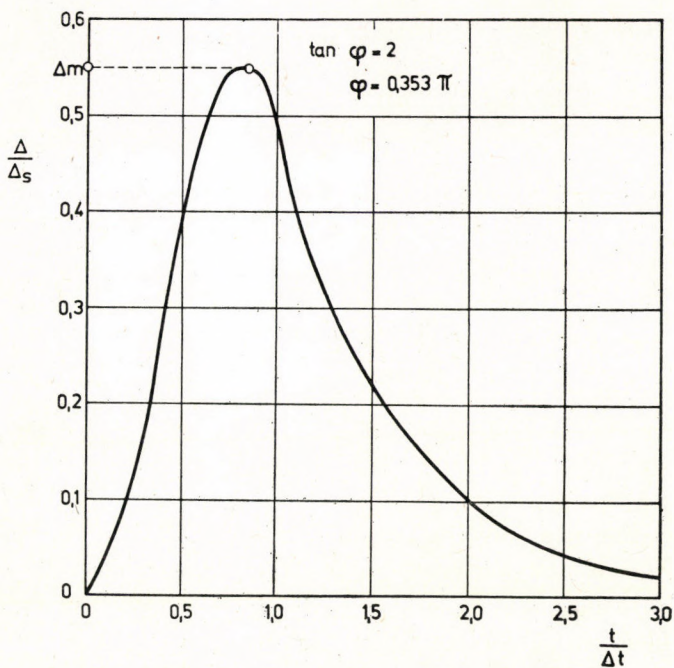
Fig. 3
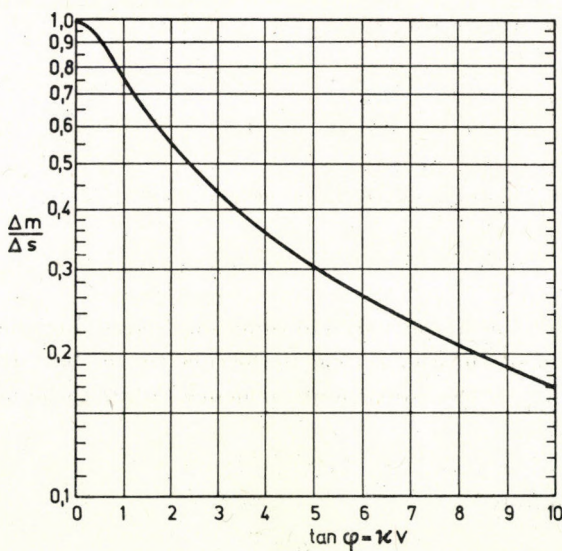
Fig. 4

Combining Eqs 1, 6 and 7, we may write

$$\tan \varphi = \pi \frac{\zeta}{k} \cdot \frac{v}{2r_0} = \varkappa v . \tag{12}$$

Thus the maximum deflection (Eq. 11) is seen to depend on the pavement parameter $\varkappa$ and the velocity of the moving load, as shown in Fig. 4.

4. The parameter $\varkappa$

By definition

$$\varkappa = \frac{\pi \zeta}{2kr_0} = \frac{\pi \tau_0}{2r_0} . \tag{13}$$

Hence, in order to evaluate the parameter, we require, on the one hand, the constants of our model and, on the other, the geometrical quantity r_0.

The influence radius, R_0, according to Hertz as shown in Fig. 1, depends on the pavement stiffness D and the "spring" reaction per unit surface k_s. Let E and ν denote Young's modulus and Poisson's ratio of the pavement and h its thickness; the pavement stiffness is, then,

$$D = \frac{Eh^3}{12(1 - \nu^2)} . \tag{14}$$

Defining a "characteristic length" by

$$\lambda = \sqrt[4]{\frac{D}{k_s}} \tag{15}$$

the radius of influence referred to above is given by

$$R_0 = 3{,}92\lambda . \tag{16}$$

However, in view of the simplified load function used in our analysis, an appropriate modification of the theoretical deflection curve (based on a sine curve of equal area) furnishes the equivalent influence radius to be used in Eq. 13 as

$$r_0 = 2{,}28\lambda \tag{17}$$

whence, approximately,

$$\varkappa = 0{,}7 \frac{\tau_0}{\lambda} . \tag{18}$$

Although having the same dimensions, the spring reaction k_s should not be confused with the so-called "subgrade modulus" used in foundation engineering since the latter presupposes a semi-infinite continuum as support.

Using the theory of an infinite plate on an elastic half-space, as presented by TIMOSHENKO and WOINOWSKY-KRIEGER [1959], it is possible to establish an approximate relation between k_s and the elastic modulus of the supporting half-space.

Denoting by E_0 and ν_0 the elastic constants of the continuum and defining a "subgrade coefficient" as

$$k_0 = \frac{E_0}{2(1 - \nu_0^2)} \tag{19}$$

and a characteristic length for this model as

$$\lambda_E = \sqrt[3]{\frac{D}{k_0}}, \tag{20}$$

it appears that, for equal maximum deflections under a point load,

$$\lambda = 1{,}241\,\lambda_E. \tag{21}$$

Thus, taking a typical average value for ν_0,

$$k_s \cong \frac{E_0}{3\lambda}. \tag{22}$$

5. An illustration

Fig. 5 shows AASHO Road Test data, as presented by HARR [1962], which may conveniently be used to check Eq. 11. Two experimental points were chosen for each axle load and used with Fig. 4 to obtain the loss tangent, and thus $\varkappa$, as summarised in Table 1.

With the parameter $\varkappa$ given, the maximum deflections for intermediate vehicle speeds could be determined as shown by the dotted curves in Fig. 5: the agreement of the interpolation with the experimental points is quite satisfactory.

From Hertz' theory the following relation can be easily derived:

$$k = 8\sqrt{Dk_s} \tag{23}$$
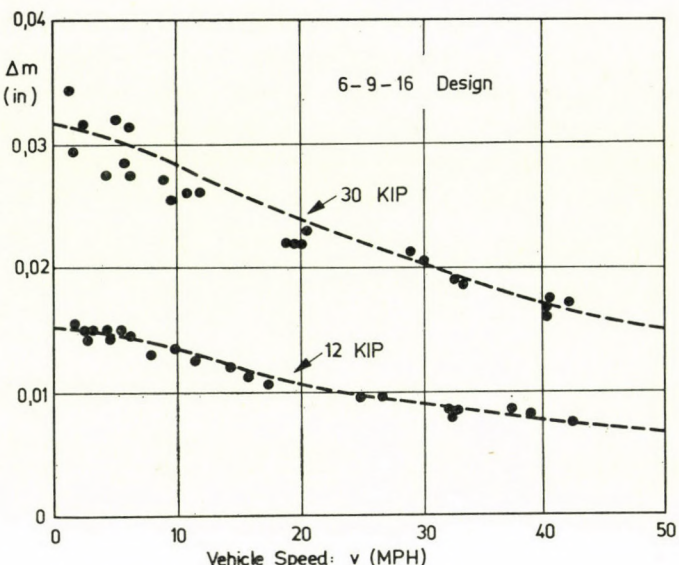
Fig. 5

Table 1

Axle load (KIP)	v (MPH)	$\Delta_m \cdot 10^2$ (in)	tan φ	$\varkappa$ (hrs/mile)
12	1,85	1,55	2,5	0,06
	42,3	0,74		
30	1,69	3,19	2,1	0,05
	42,0	1,71		

(The deflections at low speeds were taken to approximate to a sufficient degree the static values, Δ_s).

which, by Eq. 22 and the relevant definitions, enables the pavement parameter to be expressed as

$$\varkappa = 0,124 \frac{\zeta}{\sqrt[3]{D^2 E_0}} \ . \tag{24}$$

The deformation characteristics of granular soils, loaded by large plates, are known to be pressure-dependent due, in particular, to confinement effects. Thus Eq. 24 may explain the difference in $\varkappa$ for the two axle loads (cf. Table 1).

In order to form some idea concerning the magnitude of the retardation time, we note that WISEMAN [1973] reports, for several typical pavements,

values of λ ranging between 30 and 90 cm. Thus, using Eq. 18, we find τ_0 to vary approximately between 50 and 160 ms. The evaluation of data, presented by BERGER [1973], furnishes a retardation time range of 100 to 300 ms at a pavement temperature of 30 °C. Retardation times of a similar order of magnitude may be recovered from the work of FERRARI [1972]. However, it should be mentioned that much smaller values have been quoted by HEUKE-LOM [1961] as typical.

6. Field testing

In order to be able to construct deflection-speed functions such as shown in Fig. 5 we require the following quantities of a given pavement structure: a. the static spring constant k; b. the characteristic length λ; and c. the retardation time τ_0.

Having evaluated the pavement parameter $\varkappa$ (eq. 18), we are in a position to determine, using Fig. 4, the function

$$\Delta_m = \frac{P_0}{k} f(v) \ . \tag{25}$$

A most convenient field testing device appears to be the Road Rater, discussed i.a. by WISEMAN [1973] and BERGER [1973], capable of applying to a pavement a periodic force, superimposed on a constant static reference load.

The static load application evidently furnishes the required quantities k and λ, whereas the periodic loading enables the retardation time to be evaluated. Concerning the static loading, it may be mentioned that the deflection Δ practically reaches the ultimate value Δ_s after $t = 5\,\tau_0$, that is within a matter of seconds.

Now, let the periodic forcing function applied by the road rater be of the form

$$P(t) = P_0 \sin \omega t \tag{26}$$

with ω the circular frequency.

The steady-state solution of the rheological equation of our model (Eq. 3), with the above forcing function, reads

$$\frac{\Delta(t)}{\Delta_s} = \frac{\sin(\omega t - \varphi)}{\sqrt{1 + \tan^2 \varphi}} \ , \tag{27}$$

the loss tangent, for this case, given as

$$\tan \varphi = \omega \tau_0 \ . \tag{28}$$

Defining the pavement stiffness under dynamic load application as

$$S = \frac{P_0}{\varDelta} \qquad (29)$$

where

$$\varDelta = \varDelta_s(1 + \tan^2 \varphi)^{-1/2} \text{ (cf. eq. 27),}$$

we evidently have

$$\frac{\varDelta_s}{\varDelta} = \frac{S}{k} = \sqrt{1 + \omega^2 \tau_0^2} \ , \qquad (30)$$

and are thus able to recover the retardation time from an experimental plot such as shown in Fig. 6.
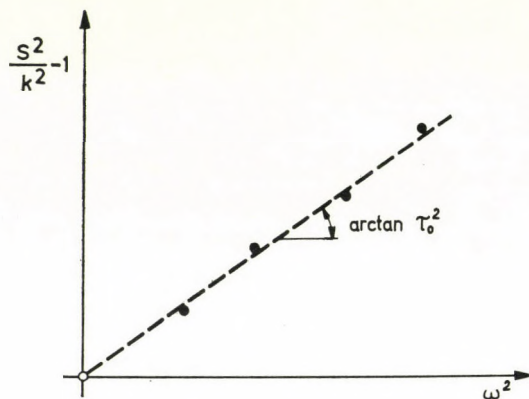
Fig. 6

WISEMAN [1973] presents data showing the stiffness ratio, S/k, to vary between 1 and 5 approximately, corresponding, for an assumed frequency of 10 Hz, to a retardation time range of 0 to 80 ms.

It is important to note that the characteristic length λ must be determined from static loading tests, for it has been observed to change with the frequency of the dynamic load applications. As the data, presented by BAUM and HÜRTGEN [1969], show, the problem is rather complicated but it appears that, at relatively low frequencies λ increases with the frequency. It seems probable that the deviations recorded for higher frequencies are due to the increased influence of inertial effects.

Let us denote by E_p and E_s the elastic moduli of the pavement and the supporting soil. Combining Eqs 14, 15 and 22 we can write (with $E_s = E_0$):

$$\lambda^3 = \alpha \frac{E_p}{E_s} \ . \qquad (31)$$

Assuming both the pavement material and the soil to be adequately represented by Kelvin models with retardation times τ_p and τ_s, we may express the respective dynamic moduli as follows (the subscript 0 indicating the static values):

$$E_p = E_{p0}(1 + \omega^2\tau_p^2)^{1/2}, \tag{32}$$

and

$$E_s = E_{s0}(1 + \omega^2\tau_s)^{1/2}. \tag{33}$$
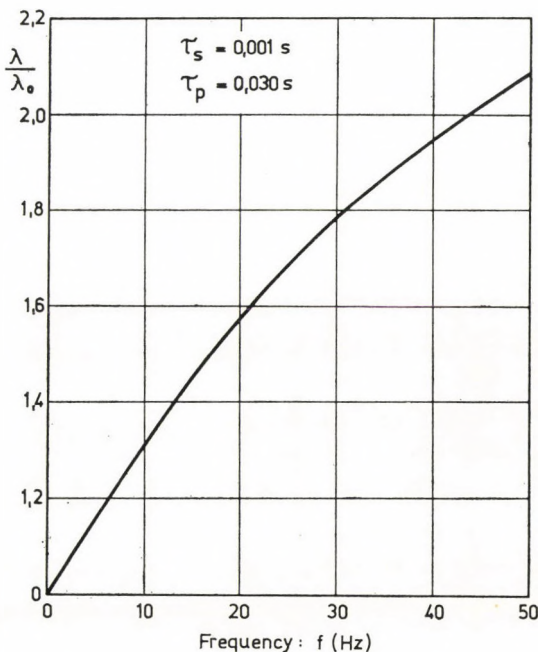
Fig. 7

Substituting Eqs 32 and 33 in Eq. 31, we obtain the characteristic length ratio as

$$\frac{\lambda}{\lambda_0} = \left[\frac{1 + \omega^2\tau_p^2}{1 + \omega^2\tau_s^2} \right]^{1/6} \tag{34}$$

with $\lambda_0 = \lambda\,(\omega = 0)$.

If, as indeed indicated by tests, typical pavement materials (asphalt concrete for example) have larger retardation times than the supporting soil, Eq. 34 shows λ to increase with frequency as shown in Fig. 7. It will be noted that the retardation times, chosen for our illustration, are considerably lower than those discussed previously. However, it should be remembered that our original model was intended to represent the composite road structure as a whole, whereas, with Fig. 7, we chose retardation times typical for specific materials.

7. Sequence of moving point loads

In this section, we shall be concerned to establish the time history of the deflection at a point of our idealized pavement structure due to the passage of an infinite row of equally spaced point loads. Furthermore, the distortion pattern of the pavement will be investigated.

As an obvious extension of our introductory discussion, we shall assume the time function of the equivalent applied load at the point in question as a series of half-waves, as shown in Fig. 2, separated by the time interval $T - \Delta t$. We present the time function in Fig. 8: since the chain of point loads is taken to proceed indefinitely, the position of the origin is immaterial and. hence, an even function was chosen for convenience.
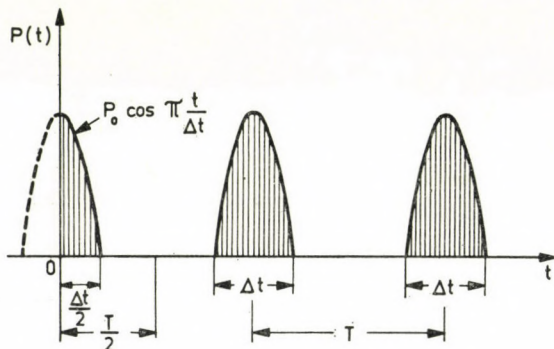
Fig. 8

The governing differential equation may be expressed as follows (cf. Eq. 3):

$$\dot{\Delta} + \frac{1}{\tau_0} \Delta = \frac{P_0}{\zeta} f(t) \,. \tag{35}$$

The function $f(t)$ is an even, periodic function, containing Δt and T as parameters and requires its expansion in an appropriate Fourier series in order to enable the solution of Eq. 35.

With $p = \Delta t/T$, we can write with sufficient approximation

$$f(t) = \frac{2p}{\pi} \left[1 + \sum_{n=1}^{N} \bar{a}_n \cdot \cos 2\pi \, \frac{npt}{\Delta t} \right] \tag{36}$$

subject to

$$N \geq 7/p \tag{37}$$

and where

$$\bar{a}_n = \begin{cases} \dfrac{2 \cos \pi np}{1 - (2np)^2} & \text{for} \quad n \neq \dfrac{1}{2p}, \\[4mm] \dfrac{\pi}{2} & \text{for} \quad n = \dfrac{1}{2p}. \end{cases} \qquad (38)$$
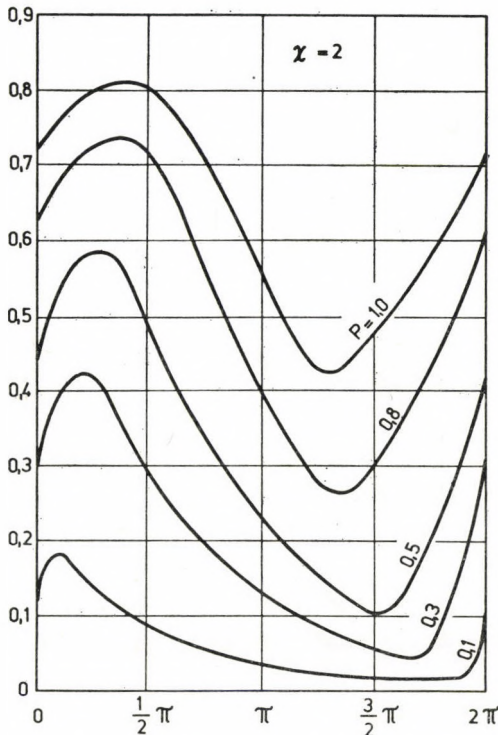
Fig. 9

The steady-state solution of Eq. 35 will be given in terms of the following dimensionless variables and parameters:

$$\eta = 2\pi \frac{t}{T}, \quad \chi = 2\pi \frac{\tau_0}{T} \quad \text{and} \quad p = \frac{\Delta t}{T} \qquad (39)$$

and reads

$$\xi(t) = \frac{\Delta}{\Delta_s} = \frac{2p}{\pi} \left[1 + \sum_{n=1}^{N} \frac{\bar{a}_n}{1 + (n\chi)^2} (\cos n\eta + n\chi \sin n\eta) \right] \qquad (40)$$

(Δ_s as given by Eq. 5).

The variation with time of the amplitude ratio ξ is shown in Fig. 9 for a particular value of the dissipation parameter χ. The deflection extremes are

seen to be influenced by the parameter p which, in turn, depends on vehicle speed and traffic density (cf. Eqs 1 and 39).

The fluctuating part of the deflection, i.e.

$$\Delta \xi = \xi_{\max} - \xi_{\min} \qquad (41)$$

is shown in Fig. 10 as a function of p with χ as parameter and with maximum values in the range $0{,}6 < p < 0{,}8$.
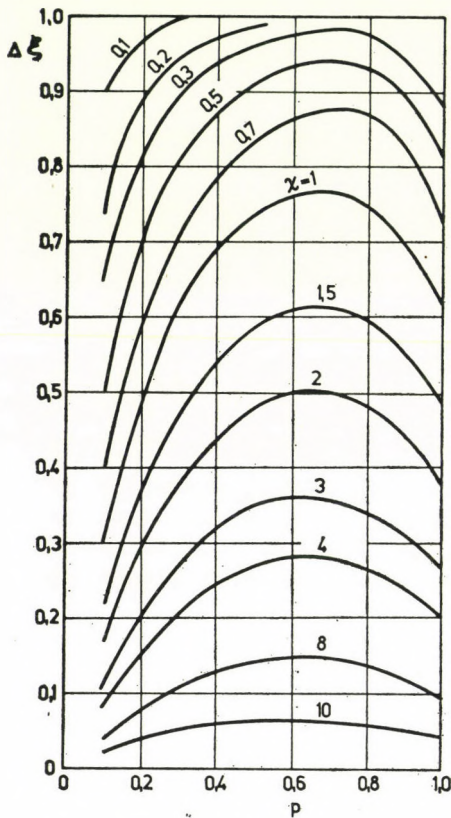
Fig. 10

There can be little doubt that the durability of a pavement is related to the phenomenon of fatigue due to its continuing flexing under traffic loads as discussed, i.e., by TAYLOR and PELL [1969]. Thus it appears reasonable to examine the changes in curvature likely to occur in a pavement under moving loads.

We consider the disturbance pattern Δ in analogy with a one-dimensional wave, travelling in the x-direction with the propagation velocity v. Thus, we may exchange in our non-dimensional time variable η (Eq. 39) the time t

with x/v and define a non-dimensional space variable as

$$\eta_0 = 2\pi \frac{x}{vT} \qquad (42)$$

which replaces η in Eq. 40 to transform it into the space representation $\xi(\chi)$ of the sequence of pavement distortions, similarly represented by Fig. 9, of course in terms of the new space variable.
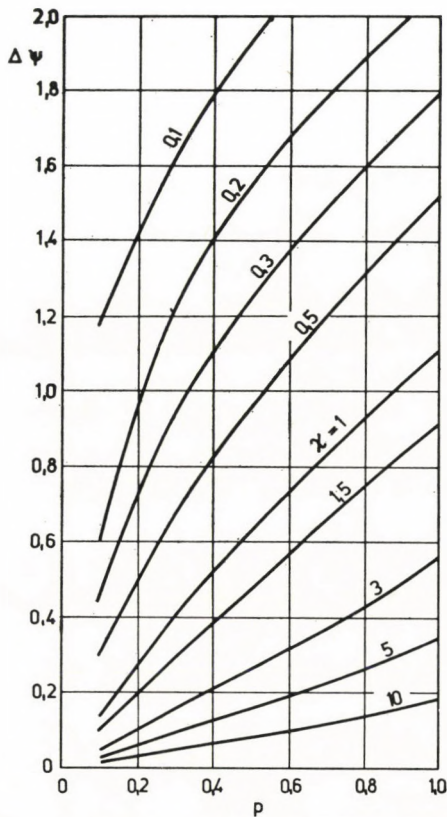
Fig. 11

Denoting by ϱ the relevant radius of curvature, we approximate the curvature by

$$\frac{1}{\varrho} \cong \frac{d^2\varDelta}{dx^2} = \varDelta_s \left(\frac{2\pi}{vT}\right)^2 \cdot \frac{d^2\xi}{dx^2} \qquad (43)$$

in view of Eq. 42, or, in view of Eqs 1 and 39, by

$$\frac{1}{\varrho} = \varDelta_s \left(\frac{\pi p}{r_0}\right)^2 \cdot \frac{d^2\xi}{dx^2} \ . \qquad (44)$$

Differentiating twice the transformed Eq. 40 and introducing the result in Eq. 44, we conveniently define a function ψ as

$$\psi = \frac{r^2}{2\pi\varrho\Delta_s} = -p^3 \sum_{n=1}^{N} \frac{n^2\bar{a}_n}{1 + (n\chi)^2} \left(\cos n\eta_0 + n\chi \sin n\eta_0\right) \tag{45}$$

whence the curvature (see Eq. 17)

$$\frac{1}{\varrho} = \frac{2\pi\Delta_s}{r_0^2} \psi \simeq 1{,}21 \frac{\Delta_s}{\lambda^2} \psi . \tag{46}$$

Since, here again, we are interested in the maximum variation of the curvature, the difference

$$\Delta\psi = \psi_{\max} - \psi_{\min} \tag{47}$$

was computed as a function of p with χ as parameter, as shown in Fig. 11.

8. Conclusions

The main objective of the analysis of the speed effect of a single moving load was to establish the suitability of our simple visco-elastic model. The satisfactory agreement with experimental data, as illustrated by Fig. 5, tends to justify the use of the model in the analysis of pavement performance under conditions more representative of traffic loads, such as the sequence of moving, equally spaced, point loads.

More specifically, if we consider the phenomenon of fatigue, the results of our analysis, summarized in Fig. 11, should furnish a more rational basis for evaluating the life expectancy of pavements in terms of significant and measurable parameters.

Consider, for example, the empirical relation given by JOSEPH and HALL [1972] which expresses the number of load applications to failure N_f as a function of the elastic deflection Δ_s early in the life of road and airfield pavements:

$$N_f \simeq 1{,}8(10^6) \cdot \Delta_s^{-4,3} \tag{48}$$

(Δ_s in mm).

The data on which the above equation was based show very considerable scatter, only to be expected in view of the inclusive character of the formula.

The results of our analysis, presented in Fig. 11, suggest that a more explicit grouping of experimental data is likely to lead to improved correlations.

Consider Eq. 46: if more severe distortion, as measured by curvature, shortens the life of a pavement, then the dependence of the curvature on Δ_S appears to validate empirical relationships of the type of Eq. 48. However, as mentioned above, we should expect better correlations from an evaluation of data which would include the influence of the parameters λ and $\Delta \Psi$.

It is, perhaps, not out of place to speculate on the form a more rational fatigue criterion might take. According to Hertz' theory (see Fig. 1):

$$\frac{\Delta_s}{\lambda^2} = \frac{P_0}{8D} \; .$$
(49)

Thus, based on Eqs 46 and 48, we may write tentatively

$$N_f = m \left(\frac{P_0}{D} \right)^{-\alpha} \cdot (\Delta \psi)^{-\beta}$$
(50)

where α, β and m are positive constants. The number of load applications to failure is thus seen to be reduced by

    a. higher loads (not surprising);

    b. higher traffic density (again not surprising);

    c. lower vehicle speeds (confirmed by experience);

    d. lower road structure stiffness and

    e. shorter retardation time of the road structure.

REFERENCES

BAUM, G.: Das dynamische Verhalten von Strassenkonstruktionen. *Straßen und Tiefbau* **12** (1958), 674—680.

BAUM, G.—HÜRTGEN, H.: Die dynamischen Prüfverfahren an Strassen. Pt. 4 of "Die Reaktion von Strassen bei zeitabhängiger Belastung", *Wiss. Ber. Bundesanst. f. Strassenwesen*, Heft 8, Verlag W. Ernst & Sohn, (1969), 20 pp.

BERGER, L.: Pavement Evaluation and Design by Nondestructive Methods. *Conf. Road Engg. Asia and Australasia*, Kuala Lumpur (1973), 11 pp.

FERRARI, P.: Calculations of the Deformations caused by Vehicles to Flexible Pavements. *Proc. 3rd U. of Michigan Int. Conf. on the Structural Design of Asphalt Pavements*, vol. **1**, Ann Arbor (1972), 382—391.

HARR, M. E.: Influence of Vehicle Speed on Pavement Deflections. *Proc. Highway Res. Bd.*, **41** (1962), 77—82.

HETÉNYI, M.: Beams on Elastic Foundations. The U. of Michigan Press, Ann Arbor (1946), 255 pp.

HEUKELOM, W.: Analysis of Dynamic Deflexions of Soils and Pavements. *Géotechnique* **11**, (1961), 224—243.

JOSEPH, A. H.—HALL, J. W., JR.: Nondestructive Vibratory Pavement Evaluation Techniques. *Proc. 3rd U. of Michigan Int. Conf. on the Structural Design of Asphalt Pavements,* **1,** Ann Arbor (1972), 844—848.

PERLOFF, W. H.—MOAVENZADEH, F.: Deflection of Viscoelastic Medium due to a Moving Load. *Proc. 2nd U. of Michigan Int. Conf. on the Structural Design of Asphalt Pavements,* Ann Arbor (1968), 269—276.

PISTER, K. S.—WESTMANN, R. A.: Analysis of Viscoelastic Pavements subjected to Moving Loads. *Proc. 1st U. of Michigan Int. Conf. on the Structural Design of Asphalt Pavements,* Ann Arbor (1963), 522—529.

TAYLOR, I. F.— PELL, P. S.: Could Fatigue be a Problem in Flexible Pavements? *Roads and Road Construction* **47,** (1969), 236—243.

TIMOSHENKO, S.—WOINOWSKY-KRIEGER, S.: Theory of Plates and Shells. McGraw-Hill Book Co. (1959), 580 pp.

WESTMANN, R. A.: Viscoelastic Layered System subjected to Moving Loads. *Proc. ASCE, J. EMD,* **93,** No. EM3 (1967), 201—218.

WISEMAN, G.: Flexible Pavement Evaluation using Hertz Theory. *Proc. ASCE, TEJ.,* **99,** No. TE3 (1973) 449—466.

Auswirkung der Fahrgeschwindigkeit auf die Verformung der Straßendecke — Die Auswirkung der Fahrgeschwindigkeit auf die Verformung des Straßendecke ist von offenbarer Wichtigkeit in der Auswertung des Verhaltens der Straßendecke unter den Verkehrsbelastungen. Die Tatsache, daß die Durchbiegungen sich mit der zunehmenden Geschwindigkeit vermindern, verweist auf das Vorhandensein einer Streuungskomponente im System. Es wird ein einfaches viscoelastisches Modell analysiert, das Ergebnisse in guter Übereinstimmung mit den Erfahrungsangaben liefert und in der Abschätzung des Verformungszustands von unter idealisierten Betriebsverhältnissen befindlichen Straßendecken angewandt werden kann. Außerdem können auch verhältnismäßig einfache Versuchsverfahren zur Ermittlung der erforderlichen Materialeigenschaften verwendet werden.

Воздействие скорости транспортного средства на прогиб дорожного покрытия. Воздействие скорости транспортного средства на деформацию дорожного покрытия является таким вопросом, который, естественно, играет важную роль при определении поведения дорожного покрытия. Тот факт, что масштабы пробиба падают с ростом скорости, показывает присутствие в системе некоторой слагающей разброса. Результаты, полученные на основе детального исследования простой вязко-упругой модели, хорошо совпадают с практическими данными. Кроме того, могут быть использованы при определении деформации дорожных покрытий при идеальных условиях нагрузки. Наряду с тем необходимые материальные параметры можно определить с помощью простых экспериментальных методов.

MATHEMATICAL STATISTICAL ANALYSIS
OF THE EXPLOITABILITY FUNCTIONS

SZ. PETHŐ*

DOCTOR OF TECHN. SCI.

and

J. PATVAROS**

The exploitability functions can be derived from the distribution function of one of the components of the mineral occurrence (e.g. its metal content). With the aid of the distribution function the mean component of the two truncated functions and its variance can be determined for any mass proportion. One truncated function refers to the exploited part, the other one to the part left back. Exploitability functions are called the distribution function and the continuous variations, as functions of the constituent of the mean component of the two truncated functions and their variances as well as the losses of the valuable constituent.

1. Introduction

The estimation of exploitability or minability of a block of mineral resources within a mineral occurrence is a problem which often appears in mining practice. Decision-making is affected by both the engineering and economical factors from which the content and distribution of the useful component to be exploited are of the greatest significance wherefrom the economy of minability of the mineral occurrence or blocks greatly depends [3, 4, 8, 9, 10].

In this paper, from the distribution functions concerning the quality characteristics of the mineral resources (metal content, ash content, etc.) the method for the determination of the average quality characteristics and variances of the mass proportions to be exploited and that left back is presented in case where the limiting value of exploitability changes uninterruptedly. Such functions might be called exploitability functions since by knowing the proportion of mineral resources to be exploited and their average quality characteristics, the expenses of mining and productive development as well as the profits from the marketing may continuously be compared with each other, and the quality limit of the exploitability may definitely be determined [5, 6, 8, 9, 10].

* Prof. Dr. Sz. PETHŐ, H-3529 Miskolc, Csabai kapu 36, Hungary.
** Dr. J. PATVAROS, H-3529 Miskolc, Csabai kapu 36, Hungary.

It is convenient to continuously determine the distribution of the useful components and the most significant parameters of the proportions to be exploited and that left back not only referring to the whole mineral resources but to each strip whereby the establishment of the operational production plan may be facilitated. Recognizing the distribution and parameters of the various components of each strip a detailed production program may be established; and the location of the work sites may be forecast with the view of assuring the most efficient performance of the plans of the mining plant, prescribed with respect to the quality and quantity of the production [3, 5, 6, 7].

2. Analysis of the distribution functions

2.1. *General investigation*

The general solution of the given problem is represented in Figs 1 and 2.

In Fig. 1 the random variable $x_{min} \leq x \leq x_{max}$. (Content of component, for example, metal content, t/m^2 specific component), the frequency of $f(x)$ and the distribution function $F(x)$ is depicted [1], [2]: the mean value is $M(\bar{x})$ the variance $D^2(x)$.

If the limiting value $x_{min} \leq x_a \leq x_{max}$ continuously changes, so the mean values of the two subsets $M(\bar{x}_I)$ and $M(\bar{x}_{II})$ are the abscissae of the centres of gravity S_I and S_{II}, respectively, of the surface parts

$$\int_{x_{min}}^{x_a} f(x) \cdot dx = F(x_a) \quad \text{and} \quad \int_{x_a}^{x_{max}} f(x) \cdot dx = 1 - F(x_a) . \tag{1}$$

$$M(\bar{x}_I) = \frac{1}{F(x_a)} \cdot \int_{x_{min}}^{x_a} f(x) \cdot x \cdot dx \tag{2}$$

$$M(x_{II}) = \frac{1}{1 - F(x_a)} \cdot \int_{x_a}^{x_{max}} f(x) \cdot x \cdot dx . \tag{3}$$

The ordinates of the centres of gravity are

$$y_I = \frac{1}{2 \cdot F(x_a)} \cdot \int_{x_{min}}^{x_a} f^2(x) \cdot dx \tag{4}$$

and

$$y_{II} = \frac{1}{2 \cdot [1 - F(x)]} \cdot \int_{x_a}^{x_{max}} f^2(x) \cdot dx . \tag{5}$$

In Fig. 2 which serves to determine the corresponding variances, the density functions of the subsets are transformed in a such way that the parts
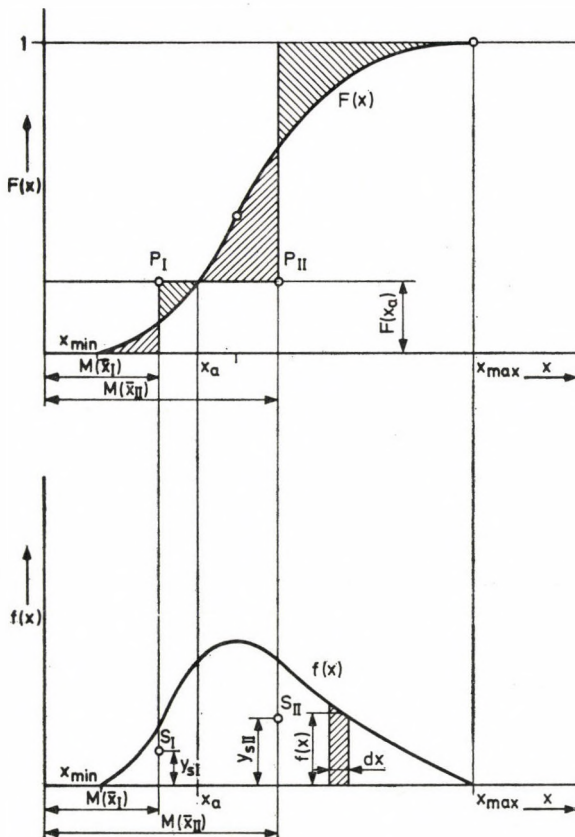
Fig. 1. Characteristic parameters of the distribution and density functions of a subset

of surface areas should be equal to 1:

$$\int_{x_{min}}^{x_a} \frac{f(x)}{F(x_a)} \cdot dx = 1$$

and

$$\int_{x_a}^{x_{max}} \frac{f(x)}{1 - F(x_a)} \cdot dx = 1. \tag{5a}$$

Thus, the variances of the subsets $D^2(\bar{x}_I)$ and $D^2(\bar{x}_{II})$ are

$$D^2(x_I) = \int_{x_{min}}^{x_a} \frac{f(x)}{F(x_a)} \cdot [x - M(\bar{x}_I)]^2 \cdot dx = \frac{1}{F(x_a)} \cdot \int_{x_{min}}^{x_a} \cdot$$
$$\cdot f(x) \cdot x^2 \cdot dx - M^2(\bar{x}_I) \tag{6}$$

and

$$D^2(x_{II}) = \int_{x_a}^{x_{max}} \frac{f(x)}{1 - F(x_a)} \cdot [x - M(\bar{x}_{II})]^2 \cdot dx =$$

$$= \frac{1}{1 - F(x_a)} \cdot \int_{x_a}^{x_{max}} f(x) \cdot x^2 \cdot dx - M^2(\bar{x}_{II}) \ . \qquad (7)$$
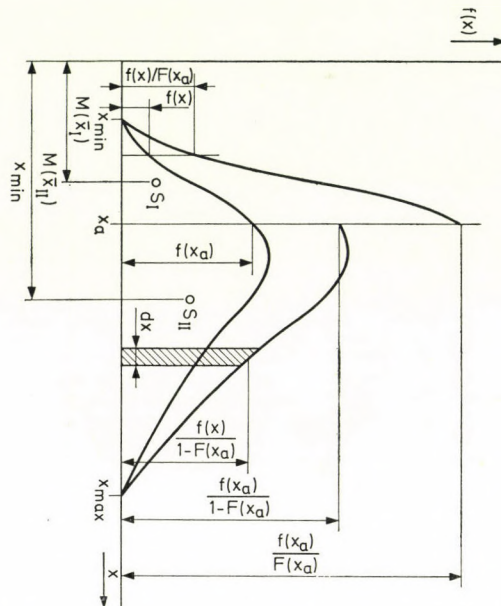
Fig. 2. Transformed density functions of subsets

2.2. *Case of the functions of normal distribution*

In the case of a normal distribution of zero mean value and σ scatter, the mean values and variances of the subsets [4] (if $\varphi(x)$ and $\Phi(x)$ are the density and distribution functions, respectively, of the normal distribution of zero mean value and unit scatter) will be [2, 4]:

$$f(x) = \frac{1}{\sqrt{2\pi} \cdot \sigma} \cdot e^{-x^2/2\sigma^2} \qquad (8)$$

and by making use of (2) of (3)

$$M(\bar{x}_I) = - \frac{\dfrac{\sigma}{\sqrt{2\pi}} \cdot e^{-x^2/2\sigma^2}}{\Phi\left(\dfrac{x_a}{\sigma}\right)} = - \frac{\sigma \cdot \varphi(x_a)}{\Phi\left(\dfrac{x_a}{\sigma}\right)} \qquad (9)$$

$$M(\bar{x}_{II}) = \frac{\dfrac{\sigma}{\sqrt{2\pi}} \cdot e^{-x^2/2\sigma^2}}{1 - \varPhi\left(\dfrac{x_a}{\sigma}\right)} = \frac{\sigma \cdot \varphi(x_a)}{1 - \varPhi\left(\dfrac{x_a}{\sigma}\right)} \; . \tag{10}$$

The ordinates of the two centres of gravity are

$$y_I = \frac{\dfrac{1}{4\sigma\sqrt{\pi}} \cdot \varPhi\left(\dfrac{x_a \cdot \sqrt{2}}{\sigma}\right)}{\varPhi\left(\dfrac{x_a}{\sigma}\right)} \tag{11}$$

$$y_{II} = \frac{\dfrac{1}{4\sigma\sqrt{\pi}} \cdot \left[1 - \varPhi\left(\dfrac{x_a \cdot \sqrt{2}}{\sigma}\right)\right]}{1 - \varPhi\left(\dfrac{x_a}{\sigma}\right)} \; . \tag{12}$$

The associated variances, by using (6) and (7), are

$$D^2(x_I) = \sigma^2 - \frac{1}{\sqrt{2\pi}} \cdot \frac{\sigma \cdot x_a}{\varPhi\left(\dfrac{x_a}{\sigma}\right)} \cdot e^{-x^2/2\sigma^2} - M^2(\bar{x}_I) \; , \tag{13}$$

$$D^2(x_{II}) = \sigma^2 + \frac{1}{\sqrt{2\pi}} \cdot \frac{\sigma \cdot x_a}{1 - \varPhi\left(\dfrac{x_a}{\sigma}\right)} \cdot e^{-x_a/2\sigma^2} - M^2(\bar{x}_{II}) \; . \tag{14}$$

By the replacement $\sigma = 1$ the associated parameters of the normal distribution of zero mean value and unit scatter may be defined. From (9) and (10) the variances are:

$$M(\bar{x}_I) = -\frac{\varphi(x_a)}{\varPhi(x_a)} \; , \tag{15}$$

$$M(x_{II}) = \frac{\varphi(x_a)}{1 - \varPhi(x_a)} \; . \tag{16}$$

And the variances from Eqs (13) and (14):

$$D^2(x_I) = 1 - x_a \cdot \frac{\varphi(x_a)}{\varPhi(x_a)} - \frac{\varphi^2(x_a)}{\varPhi^2(x_a)} \; , \tag{17}$$

$$D^2(x_{II}) = 1 + x_a \frac{\varphi(x_a)}{\varPhi(x_a)} - \frac{\varphi^2(x_a)}{[1 - \varPhi(x_a)]^2} \; . \tag{18}$$

In Fig. 3, besides the diagrams of the density and distribution functions of zero mean value and scatter 1 also show the changes of the mean values $M(\bar{x}_I)$ and $M(\bar{x}_{II})$, i.e., those of the relationships (15) and (16) have been plotted.
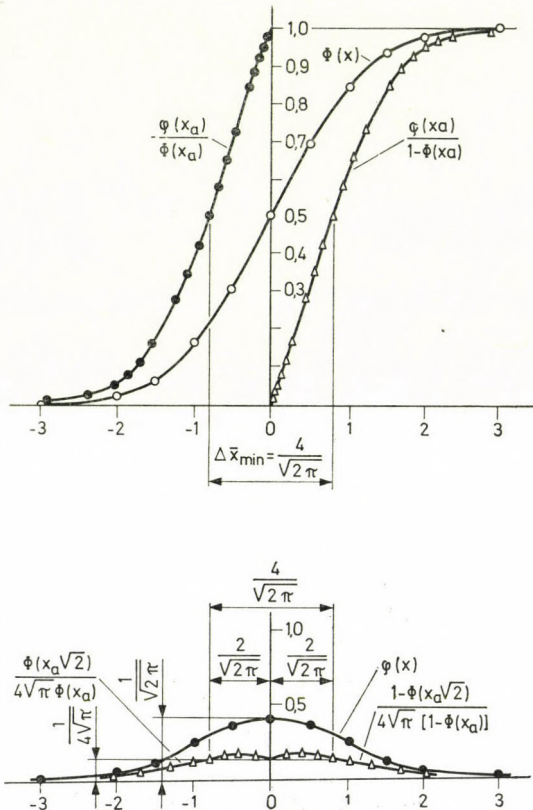
Fig. 3. Distribution and density function of the standard normal probability; change of the values $M(\bar{x}_I)$ and $M(\bar{x}_{II})$

By drawing a horizontal line through the point of intersection of the vertical line drawn at the limit value x_a and the distribution function, the associated values of $M(\bar{x}_I)$ and $M(\bar{x}_{II})$ may be defined; in the diagram of the density function the loci of the centres of gravity of the corresponding surface area parts are marked.

The function

$$y_I = \frac{\Phi(x_a \cdot \sqrt{2})}{4 \cdot \sqrt{\pi} \cdot \Phi(x_a)} \tag{19}$$

obtained by replacing $\sigma = 1$ into Eq. (11) [4], and defining the loci of the centres of gravity on the diagram of the density function, has an extreme value where

its first derivative is equal to zero. The value of x_a which may be calculated from the conditions $y_I' = 0$, is

$$x_a = \sqrt{\ln 2 + 2 \cdot \ln \frac{\Phi(x_a)}{\Phi(x_a) \cdot \sqrt{2}}}.$$ (20)

The value of x_a ($x_a = 0{,}7003$) furnishing the maximum value of y_I should satisfy the transcendent equation (20);

$$y_I = 0{,}156161 .$$

Also the difference $\Delta \bar{x}$ of $M(\bar{x}_{II})$ and $M(\bar{x}_I)$ is the function of x_a:

$$\Delta \bar{x} = \frac{\varphi(x_a)}{\Phi(x_a) \cdot [1 - \Phi(x_a)]} .$$ (21)

In Eq. (21) both the numerator and denominator have maximum values at $x_a = \Phi$, however, since the change of $\varphi(x_a)$ is not so rapid as that of

$$\Phi(x_a) \cdot [1 - \Phi(x_a)] ,$$

therefore, Eq. (21) has a minimum value at $x_a = 0$.

$$\Delta \bar{x}_{\min} = \frac{4}{\sqrt{\pi}}$$ (22)

and a maximum value at x_a,

$$(\Delta \bar{x}_{\max} \to \infty) .$$

The variances are
at $x_a = 0$

$$D^2(x_I) = D^2(x_{II}) = 1 - \frac{2}{\pi},$$ (23a)

and at $x_a \to \infty$

$$D^2(x_I) \to 1 \quad \text{and} \quad D^2(x_{II}) \to 0 .$$ (23b)

In Fig. 4, for the normal distribution of zero mean value and scatter 1, the mean values of $M(x_I)$ and $M(x_{II})$ as well as the variances $D^2(x_I)$ and $D^2(x_{II})$ are plotted depending on the limiting value of x_a, while in Table 1 the numerical values of the parameters mentioned above are listed for the various values of x_a.

3*

Table 1

Parameters of the standard normal distribution

x_a	$M(\bar{x}_I)$	$M(\bar{x}_{II})$	$M(\bar{y}_I)$	$M(\bar{y}_{II})$	$D^2(x_I)$	$D^2(x_{II})$
0,00	0,797885	0,797885	0,141047	0,141047	0,363380	0,363380
0,01	0,791530	0,804261	0,141510	0,140578	0,365565	0,361207
0,02	0,785196	0,810660	0,141965	0,140100	0,367763	0,359044
0,03	0,778885	0,817080	0,142412	0,139616	0,369971	0,356893
0,04	0,772596	0,823522	0,142852	0,139124	0,372191	0,353753
0,05	0,766328	0,829986	0,143285	0,138624	0,374425	0,352623
0,06	0,760084	0,836470	0,143709	0,138118	0,376667	0,350507
0,07	0,753862	0,842975	0,144127	0,137604	0,378922	0,348401
0,08	0,747663	0,849501	0,144537	0,137083	0,381187	0,346308
0,09	0,741486	0,856049	0,144939	0,136555	0,383464	0,344225
0,10	0,735332	0,862618	0,145333	0,136020	0,385754	0,342152
0,11	0,729012	0,869206	0,145720	0,135477	0,388053	0,340094
0,12	0,723093	0,875815	0,146100	0,134928	0,390365	0,338046
0,13	0,717008	0,882446	0,146471	0,134372	0,392689	0,336007
0,14	0,710947	0,889095	0,146836	0,133809	0,395022	0,333983
0,15	0,704908	0,895766	0,147192	0,133239	0,397368	0,331968
0,16	0,698895	0,902455	0,147541	0,132662	0,399723	0,329968
0,17	0,692903	0,909166	0,147883	0,132079	0,402092	0,327975
0,18	0,686936	0,915897	0,148216	0,131489	0,404471	0,325994
0,19	0,680993	0,922645	0,148543	0,130892	0,406860	0,324028
0,20	0,675073	0,929416	0,148861	0,130290	0,409262	0,322068
0,21	0,669178	0,936205	0,149172	0,129680	0,411673	0,320124
0,22	0,663307	0,943012	0,149477	0,129064	0,414096	0,318190
0,23	0,657460	0,949841	0,149772	0,128442	0,416531	0,316266
0,24	0,651637	0,956688	0,150062	0,127814	0,418976	0,314353
0,25	0,645840	0,963553	0,150343	0,127179	0,421431	0,312454
0,26	0,640066	0,970439	0,150617	0,126539	0,423898	0,310563
0,27	0,634317	0,977343	0,150883	0,125893	0,426376	0,308683
0,28	0,628594	0,984265	0,151142	0,125240	0,428864	0,306817
0,29	0,622895	0,991207	0,151395	0,124582	0,431363	0,304959
0,30	0,617221	0,998165	0,151639	0,123919	0,433872	0,303116
0,31	0,611572	1,005145	0,151876	0,123250	0,436393	0,301278
0,32	0,605949	0,012141	0,152107	0,122575	0,438923	0,299456
0,33	0,600351	0,109155	0,153330	0,121895	0,441463	0,297645

Table 1 (cont.)

x_a	$\overline{Mx}_{(I)}$	$M(\overline{x}_{II})$	$M(\overline{y}_I)$	$M(\overline{y}_{II})$	$D^2(x_I)$	$D^2(x_{II})$
0,34	0,594778	1,026188	0,152546	0,121209	0,444015	0,295842
0,35	0,589231	0,033239	0,152754	0,120519	0,446577	0,294051
0,36	0,583710	1,040305	0,152957	0,119822	0,449147	0,292275
0,37	0,578214	1,047393	0,153151	0,119122	0,451730	0,290503
0,38	0,572744	1,054495	0,153340	0,118416	0,454321	0,288748
0,39	0,567300	0,061618	0,153521	0,117705	0,456923	0,286998
0,40	0,561882	1,068757	0,153695	0,116990	0,459535	0,285261
0,41	0,556491	1,075912	0,153863	0,116269	0,462156	0,283537
0,42	0,551126	1,083085	0,154024	0,115546	0,464787	0,281823
0,43	0,545787	1,090275	0,154178	0,114817	0,467428	0,280118
0,44	0,540475	1,097482	0,154326	0,114084	0,470078	0,278426
0,45	0,535188	1,104708	0,154467	0,113347	0,472739	0,276739
0,46	0,529929	1,111949	0,154603	0,112605	0,475408	0,275067
0,47	0,524697	1,119204	0,154731	0,111860	0,478085	0,273408
0,48	0,519491	1,126479	0,154853	0,111111	0,480773	0,271755
0,49	0,514312	1,133771	0,154969	0,110359	0,483470	0,270112
0,50	0,509161	1,141076	0,155079	0,109602	0,486175	0,268483
0,51	0,505036	1,148400	0,155183	0,108842	0,488889	0,266861
0,52	0,498938	1,155740	0,155280	0,108080	0,491612	0,265250
0,53	0,493868	0,163096	0,155372	0,107312	0,494344	0,263649
0,54	0,488826	1,170466	0,155457	0,106544	0,497084	0,262062
0,55	0,483810	1,177854	0,155537	0,105771	0,499832	0,260480
0,56	0,478822	1,185257	0,155612	0,104996	0,502589	0,258910
0,57	0,473862	1,192676	0,155680	0,104218	0,505354	0,257349
0,58	0,468929	1,200112	0,155743	0,103437	0,508127	0,255796
0,59	0,464024	1,207562	0,155800	0,102655	0,510908	0,254255
0,60	0,459147	1,215026	0,155853	0,101869	0,513696	0,252725
0,61	0,454298	1,222506	0,155899	0,101081	0,516491	0,251208
0,62	0,449477	1,230001	0,155941	0,100291	0,519295	0,249698
0,63	0,444684	1,237513	0,155977	0,099499	0,522106	0,248194
0,64	0,439919	1,245039	0,156008	0,098706	0,524923	0,246703
0,65	0,435182	0,252579	0,156035	0,097909	0,527748	0,245223
0,66	0,430474	1,260133	0,156056	0,097113	0,530579	0,243753
0,67	0,425794	1,267702	0,156072	0,096314	0,533417	0,242291
0,68	0,421142	1,275288	0,156084	0,095514	0,536262	0,240836
0,69	0,416519	1,282887	0,156091	0,094713	0,539113	0,239394

PETHŐ, SZ.—PATVAROS, J.

Table 1 (cont.)

x_a	$M(\bar{x}_I)$	$M(\bar{x}_{II})$	$M(\bar{y}_I)$	$M(\bar{y}_{II})$	$D^2(x_I)$	$D^2(x_{II})$
0,70	0,411925	1,290497	0,146094	0,093909	0,541970	0,238964
0,71	0,407359	1,298127	0,156091	0,093108	0,544834	0,236536
0,72	0,402821	1,305771	0,156085	0,092303	0,547704	0,235117
0,73	0,398313	1,313425	0,156074	0,091498	0,550579	0,233715
0,74	0,393833	1,321094	0,156059	0,090693	0,553459	0,232320
0,75	0,389382	1,328780	0,156040	0,089885	0,556345	0,230929
0,76	0,384960	1,336477	0,156016	0,089080	0,559236	0,229551
0,77	0,380567	1,344187	0,155989	0,088273	0,562132	0,228186
0,78	0,376202	1,351915	0,155958	0,087467	0,565034	0,226820
0,79	0,371868	1,359650	0,155923	0,086659	0,567939	0,225476
0,80	0,367561	1,367405	0,155884	0,085852	0,570850	0,224128
0,81	0,363284	1,375168	0,155841	0,085046	0,573764	0,222799
0,82	0,359037	1,382947	0,155796	0,084238	0,576683	0,221475
0,83	0,354818	1,390741	0,155746	0,083434	0,579605	0,220155
0,84	0,350629	1,398544	0,155694	0,082629	0,582531	0,218851
0,85	0,346469	1,406358	0,155638	0,081825	0,585461	0,217562
0,86	0,342338	1,414188	0,155578	0,081021	0,588394	0,216273
0,87	0,338237	1,422037	0,155516	0,080217	0,591330	0,214983
0,88	0,334165	1,429890	0,155540	0,079417	0,594269	0,213719
0,89	0,330122	1,437751	0,155382	0,078616	0,597211	0,212451
0,90	0,326109	1,445644	0,155311	0,077818	0,600155	0,211193
0,91	0,322125	1,543539	0,155237	0,077020	0,603102	0,209944
0,92	0,318171	1,461447	0,155160	0,076223	0,606050	0,208703
0,93	0,314246	1,469359	0,155081	0,075430	0,609000	0,207487
0,94	0,310351	1,477293	0,154999	0,074635	0,611952	0,206262
0,95	0,306485	1,485239	0,154915	0,073846	0,614906	0,205042
0,96	0,302649	1,493190	0,154828	0,073056	0,617860	0,203846
0,97	0,298842	1,501163	0,154739	0,072269	0,620816	0,202635
0,98	0,295065	1,509141	0,154495	0,072227	0,623772	0,201451
0,99	0,291318	1,517133	0,154555	0,070701	0,626729	0,200270
1,00	0,287600	1,525138	0,154450	0,069923	0,629686	0,199093
1,01	0,283912	1,533147	0,154362	0,069145	0,632643	0,197939
1,02	0,280253	1,541179	0,154263	0,068370	0,635601	0,196770
1,03	0,276624	1,549215	0,154162	0,067598	0,638557	0,195625
1,04	0,273024	1,557264	0,154060	0,066827	0,641513	0,194484

Table 1 (cont.)

x_a	$M(\bar{x}_{\mathrm{I}})$	$M(\bar{x}_{\mathrm{II}})$	$M(\bar{y}_{\mathrm{I}})$	$M(\bar{y}_{\mathrm{II}})$	$D^2(x_{\mathrm{I}})$	$D^2(x_{\mathrm{II}})$
1,05	0,269454	1,565326	0,153955	0,066063	0,644468	0,193348
1,06	0,265913	1,573400	0,153850	0,065297	0,647422	0,192216
1,07	0,262402	1,581477	0,153742	0,064538	0,60374	0,191112
1,08	0,258921	1,589576	0,153633	0,063780	0,653326	0,189990
1,09	0,255469	1,597676	0,153523	0,063025	0,656274	0,188899
1,10	0,252046	1,605798	0,153411	0,062276	0,659222	0,187791
1,11	0,248653	1,613919	0,152299	0,061529	0,662166	0,186716
1,12	0,245290	1,622062	0,153185	0,060784	0,665109	0,185625
1,13	0,241955	1,630214	0,153070	0,060043	0,668048	0,184545
1,14	0,238651	1,638374	0,152915	0,059572	0,670984	0,183477
1,15	0,235375	1,646542	0,152837	0,058574	0,673917	0,182423
1,16	0,232129	1,654729	0,152719	0,057844	0,676847	0,181357
1,17	0,228912	1,662922	0,152601	0,057120	0,679772	0,180310
1,18	0,225724	1,671119	0,152481	0,056398	0,682694	0,179282
1,19	0,222566	1,679332	0,152361	0,055682	0,685611	0,178249
1,20	0,219437	1,687547	0,152241	0,054968	0,688524	0,177241
1,21	0,216336	1,695792	0,152119	0,054259	0,691432	0,176199
1,22	0,213265	1,704034	0,151997	0,053556	0,694335	0,175199
1,23	0,210223	1,712274	0,151875	0,052854	0,697232	0,174255
1,24	0,207210	1,720539	0,151752	0,052159	0,700124	0,173244
1,25	0,204226	1,728813	0,151629	0,051468	0,703010	0,772222
1,26	0,201270	1,737094	0,151506	0,050781	0,705890	0,171243
1,27	0,198343	1,745397	0,151383	0,050099	0,708764	0,170243
1,28	0,195445	1,753687	0,151259	0,049419	0,711631	0,169302
1,29	0,192576	1,762012	0,151135	0,048749	0,714492	0,168309
1,30	0,189735	1,770337	0,151011	0,048080	0,717345	0,167346
1,31	0,186923	1,778657	0,150887	0,047417	0,720191	0,166419
1,32	0,184139	1,786990	0,150763	0,046759	0,723029	0,165493
1,33	0,181383	1,795352	0,150639	0,046104	0,725860	0,164529
1,34	0,178656	1,803702	0,150516	0,045457	0,728683	0,163619
1,35	0,175957	1,812077	0,150392	0,044812	0,731497	0,162680
1,36	0,173286	1,820454	0,150269	0,044174	0,734303	0,161764
1,37	0,170643	1,828852	0,150145	0,043541	0,737100	0,160728
1,38	0,168028	1,837245	0,150023	0,042912	0,739888	0,159928
1,39	0,165441	1,845653	0,149900	0,042289	0,742667	0,159023

Table 1 (cont.)

x_a	$M(\bar{x}_\mathrm{I})$	$M(\bar{x}_\mathrm{II})$	$M(\bar{y}_\mathrm{I})$	$M(\bar{y}_\mathrm{II})$	$D^2(x_\mathrm{I})$	$D^2(x_\mathrm{II})$
1,40	0,162881	1,854049	0,149778	0,041669	0,745436	0,158170
1,41	0,160349	1,862476	0,149656	0,041058	0,748195	0,157273
1,42	0,157845	1,870908	0,149535	0,040450	0,750945	0,156392
1,43	0,155368	1,879340	0,149414	0,039848	0,753684	0,155537
1,44	0,152919	1,887794	0,149293	0,039251	0,756413	0,154657
1,45	0,150496	0,896266	0,149174	0,038658	0,749131	0,153760
1,46	0,148101	1,904727	0,149054	0,038073	0,761838	0,152916
1,47	0,145733	1,913198	0,148936	0,037492	0,764534	0,152075
1,48	0,143392	1,921674	0,148817	0,036917	0,767219	0,151246
1,49	0,141078	1,930180	0,148700	0,036346	0,769892	0,150373
1,50	0,138790	1,938683	0,148583	0,035782	0,772553	0,149533
1,51	0,136529	1,947177	0,148467	0,035223	0,775202	0,148738
1,52	0,134294	1,955718	0,148352	0,034669	0,777839	0,147859
1,53	0,132085	1,964239	0,148238	0,034121	0,780463	0,147050
1,54	0,129903	0,972767	0,148124	0,033579	0,783075	0,146252
1,55	0,127747	1,981295	0,148011	0,033041	0,785673	0,145478
1,56	0,125616	1,989850	0,147899	0,032511	0,788259	0,144663
1,57	0,123512	1,998394	0,147788	0,031982	0,790831	0,143900
1,58	0,121433	2,006990	0,147678	0,793390	0,793390	0,143035
1,59	0,119380	2,015562	0,147568	0,030948	0,795935	0,142252
1,60	0,117352	2,024140	0,147460	0,030441	0,798466	0,141482
1,61	0,115349	2,032715	0,147352	0,029937	0,800983	0,140741
1,62	0,113371	2,041320	0,147246	0,029438	0,803486	0,139952
1,63	0,111419	2,049908	0,147140	0,028946	0,805974	0,139226
1,64	0,109491	2,058513	0,147036	0,028356	0,808447	0,138485
1,65	0,107587	2,067169	0,146932	0,027978	0,801906	0,137641
1,66	0,105709	2,075786	0,146830	0,027502	0,813349	0,136917
1,67	0,103854	2,084397	0,146728	0,027029	0,815777	0,136233
1,68	0,102024	2,093037	0,146628	0,026566	0,818190	0,135498
1,69	0,100218	2,101700	0,146528	0,026104	0,820588	0,134729
1,70	0,098436	2,110380	0,146430	0,025654	0,822969	0,133943
1,71	0,096677	2,119018	0,146333	0,025203	0,825335	0,133282
1,72	0,094943	2,127703	0,146236	0,024761	0,827685	0,132528
1,73	0,093231	2,136377	0,146141	0,024325	0,830018	0,131824
1,74	0,091543	2,145030	0,146047	0,023892	0,832335	0,131199
1,75	0,089878	2,153756	0,145954	0,023467	0,834636	0,130408

Table 1 (cont.)

x_a	$M(\bar{x}_I)$	$M(\bar{x}_{II})$	$M(\bar{y}_I)$	$M(\bar{y}_{II})$	$D^2(x_I)$	$D^2(x_{II})$
1,76	0,088236	2,162442	0,145862	0,023043	0,836920	0,129743
1,77	0,086616	2,171129	0,145745	0,023277	0,839187	0,129098
1,78	0,085019	2,179765	0,145682	0,022220	0,841438	0,128348
1,79	0,083445	2,188584	0,145593	0,021813	0,843671	0,127667
1,80	0,081893	2,197333	0,145506	0,021416	0,845887	0,126928
1,81	0,080362	2,206040	0,145420	0,021020	0,848086	0,126320
1,82	0,078854	2,214755	0,145335	0,020632	0,850267	0,125715
1,83	0,077368	2,223532	0,145251	0,020248	0,852431	0,124969
1,84	0,075903	2,232296	0,145168	0,019868	0,854578	0,124280
1,85	0,074459	2,241032	0,145086	0,019495	0,856706	0,123684
1,86	0,073037	2,249798	0,145005	0,019126	0,858817	0,123034
1,87	0,071636	2,258581	0,144926	0,018766	0,860910	0,122357
1,88	0,070255	2,267371	0,144847	0,018407	0,862985	0,121686
1,89	0,068896	2,276153	0,144770	0,018056	0,865042	0,121057
1,90	0,067556	2,284912	0,144964	0,017708	0,867080	0,120510
1,91	0,066237	2,293714	0,144619	0,017364	0,869101	0,119870
1,92	0,064938	2,302547	0,144545	0,017027	0,871103	0,119168
1,93	0,063659	2,311399	0,144472	0,016695	0,870386	0,118435
1,94	0,062399	2,320167	0,144401	0,016367	0,875051	0,117950
1,95	0,061160	2,329010	0,144330	0,016044	0,876998	0,117282
1,96	0,059939	2,337825	0,144260	0,015726	0,878926	0,116712
1,97	0,058738	2,346689	0,144193	0,015412	0,880836	0,116029
1,98	0,057556	2,355490	0,144125	0,015102	0,882726	0,115538
1,99	0,056393	2,364409	0,144058	0,014801	0,884599	0,114745
2,00	0,055248	2,373229	0,143993	0,014499	0,886452	0,114241
2,02	0,053014	2,390908	0,143866	0,013917	0,890102	0,113193
2,04	0,050851	2,408710	0,143743	0,013351	0,893677	0,111883
2,06	0,048760	2,426498	0,143624	0,012804	0,897177	0,110695
2,08	0,046738	2,444229	0,143510	0,012275	0,900600	0,109740
2,10	0,044784	2,462136	0,143399	0,011762	0,903949	0,108372
2,12	0,042895	2,479922	0,143292	0,011269	0,907222	0,107423
2,14	0,041072	2,497840	0,143189	0,010791	0,910419	0,106174
2,16	0,039312	2,515719	0,143090	0,010328	0,913541	0,105110
2,18	0,037613	2,533523	0,142995	0,009881	0,916589	0,104341

Table 1 (cont.)

x_a	$M(\bar{x}_I)$	$M(\bar{x}_{II})$	$M(\bar{y}_I)$	$M(\bar{y}_{II})$	$D^2(x_I)$	$D^2(x_{II})$
2,20	0,035975	2,551578	0,142903	0,009446	0,919561	0,102920
2,22	0,034395	2,569518	0,142814	0,009037	0,922460	0,101907
2,24	0,032873	2,587506	0,142730	0,008633	0,925285	0,100825
2,26	0,031406	2,605317	0,142648	0,008245	0,928036	0,100339
2,28	0,029994	2,623371	0,142570	0,007877	0,930715	0,099211
2,30	0,028634	2,641462	0,142495	0,007518	0,922322	0,098041
2,32	0,027326	2,659597	0,142423	0,007174	0,935857	0,096809
2,34	0,026068	2,677512	0,142354	0,006835	0,938322	0,096306
2,36	0,024858	2,695772	0,142288	0,06525	0,940716	0,094835
2,38	0,023696	2,713838	0,142225	0,006222	0,943042	0,094016
2,40	0,022580	2,731707	0,142164	0,005920	0,945299	0,093875
2,42	0,021508	2,750092	0,142106	0,005641	0,947489	0,092216
2,44	0,020479	2,768022	0,142051	0,005365	0,949612	0,092027
2,46	0,019492	2,786278	0,141998	0,005115	0,951671	0,090896
2,48	0,018545	2,804584	0,141948	0,004863	0,953664	0,089678
2,50	0,017638	2,822593	0,141900	0,004624	0,955594	0,089452
2,52	0,016768	2,840849	0,141854	0,004383	0,957462	0,088157
2,54	0,015936	0,259026	0,141810	0,004166	0,959269	0,087898
2,56	0,015139	2,878267	0,141769	0,003956	0,961015	0,087138
2,58	0,014376	2,895771	0,141729	0,003759	0,962703	0,085599
2,60	0,013647	2,914175	0,141691	0,003577	0,964333	0,084439
2,62	0,012949	2,932695	0,141655	0,003398	0,965906	0,082962
2,64	0,012282	2,950911	0,141621	0,003219	0,967424	0,082529
2,66	0,011646	2,969065	0,141589	0,003049	0,968887	0,082367
2,68	0,011038	2,987486	0,141558	0,002873	0,970297	0,081389
2,70	0,010457	3,005750	0,141529	0,002739	0,971665	0,090992
2,72	0,009903	3,024251	0,141501	0,002593	0,972964	0,079870
2,74	0,009375	3,042526	0,141475	0,002434	0,974334	0,079558
2,76	0,008872	3,061057	0,141450	0,002311	0,975434	0,078448
2,78	0,008392	3,079356	0,141426	0,002172	0,976598	0,078177
2,80	0,007936	3,098024	0,141403	0,002045	0,977717	0,076714
2,82	0,007501	2,116565	0,141382	0,001950	0,978791	0,075736
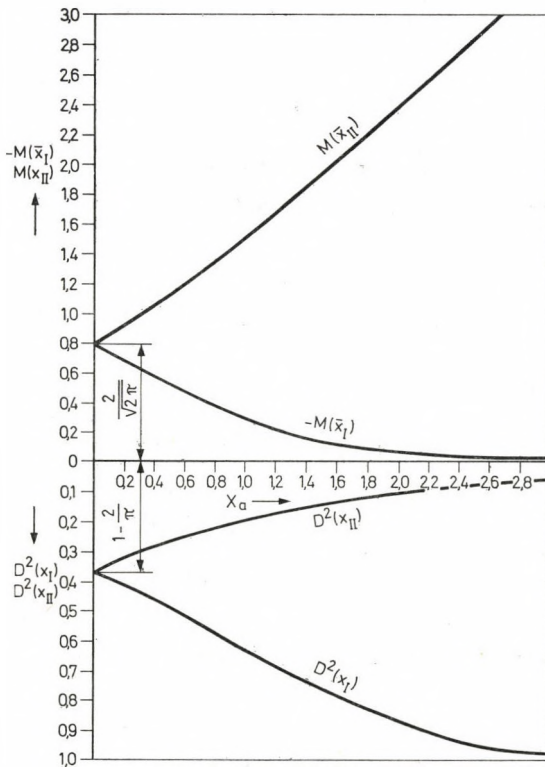
Fig. 4. Change of the mean values $M(\bar{x}_{\mathrm{I}})$ and $M(\bar{x}_{\mathrm{II}})$ as well as that of the variances $D^2(\bar{x}_{\mathrm{I}})$ and $D^2(\bar{x}_{\mathrm{II}})$ in dependence on $\bar{x}_a$

2.3. *Case of functions of lognormal distribution*

With the aid of the density function of lognormal distribution

$$f(x) = \frac{1}{\sqrt{2\pi} \cdot x \cdot \sigma} \cdot \exp - \frac{(\ln x - m)^2}{2\sigma^2} \tag{24}$$

the abscissae and ordinates of the centres of gravity of the subsets may be calculated as follows [1], [2]:

$$M(\bar{x}_{\mathrm{I}}) = \frac{e^{m+\sigma^2/2} \cdot \displaystyle\int_{-\infty}^{T_{x_a}} e^{-T^2} \cdot dT}{\displaystyle\int_{-\infty}^{t_{x_a}} e^{-t^2} \cdot dt} \tag{25}$$

wherein

$$T_{x_a} = \frac{\ln x_a - m - \sigma^2}{\sigma \cdot \sqrt{2}}, \tag{26}$$

and

$$t_{x_a} = \frac{\ln x_a - m}{\sigma \cdot \sqrt{2}} \; . \tag{27}$$

Performing the operations one obtains for the mean value of the subset, containing lower values than x_a, the following relationship [1, 2, 4]:

$$M(\overline{x}_{\mathrm{I}}) = e^{m + \sigma^2/2} \cdot \frac{\Phi\left(\dfrac{\ln x_a - m - \sigma^2}{\sigma}\right)}{\Phi\left(\dfrac{\ln x_a - m}{\sigma}\right)} \; . \tag{28}$$

The mean value of the subset comprising values higher than x_a:

$$M(\overline{x}_{\mathrm{II}}) = \frac{e^{m + \sigma^2/2} \cdot \displaystyle\int_{T_{x_a}}^{+\infty} e^{-T^2} \cdot dT}{\displaystyle\int_{t_{x_a}}^{+\infty} e^{-t^2} \cdot dt} \; . \tag{29}$$

Performing the designated operations the following relationship is given:

$$M(\overline{x}_{\mathrm{II}}) = e^{m + \sigma^2/2} \cdot \frac{1 - \Phi\left(\dfrac{\ln x_a - m - \sigma^2}{\sigma}\right)}{1 - \Phi\left(\dfrac{\ln x_a - m}{\sigma}\right)} \; . \tag{30}$$

Wherefrom, the difference of the abscissae of the centres of gravity of the subsets is

$$\Delta\overline{x}_s = e^{m + \sigma^2/2} \cdot \frac{\Phi\left(\dfrac{\ln x_a - m}{\sigma}\right) - \Phi\left(\dfrac{\ln x_a - m - \sigma^2}{\sigma}\right)}{\Phi\left(\dfrac{\ln x_a - m}{\sigma}\right) - \left[1 - \Phi\left(\dfrac{\ln x_a - m}{\sigma}\right)\right]} =$$

$$= e^{m + \sigma^2/2} \cdot \frac{\Phi_0(z) - \Phi_0(z - \sigma)}{0{,}25 - [\Phi_0(z)]^2} \tag{31}$$

wherein:

$$z = \frac{\ln x_a - m}{\sigma} \tag{32}$$

and

$$\Phi_0(z) = \Phi(z) - \frac{1}{2} \, , \tag{33}$$

further

$$\Phi_0(z) = \frac{1}{\sqrt{2\pi}} \cdot \int_0^t e^{-t^2/2} \cdot dt \qquad (34)$$

and

$$z = t_{x_a} \cdot \sqrt{2} . \qquad (35)$$

Replacements of certain terms yield the difference of the abscissae of the centres of gravity [4]:

$$\Delta \bar{x}_s = M(\xi) \cdot \frac{\Phi_0(z) - \Phi_0(z - \sigma)}{0{,}25 - [\Phi_0(z)]^2} = M(\xi) \cdot h(z) . \qquad (36)$$

By finding the extreme value of the function $h(z)$ entering in Eq. (36) the value $z = z_0$ minimalizing Δx_s may be determined by the solution to the transcendent equation

$$z_0 = \frac{1}{2} + \ln \frac{0{,}25 + \Phi_0(z_0) \cdot [\Phi_0(z_0) - 2\Phi_0(z_0 - 1)]}{0{,}25 - [\Phi_0(z_0)]^2} . \qquad (37)$$

Recognizing z_0, the minimum value of the function $h(z)$ will be, by making use of of Eqs (36) and (37):

$$h(z)_{\min} = \frac{\Phi_0(z_0) - \Phi_0(z_0 - \sigma)}{0{,}25 - [\Phi_0(z_0)]^2} . \qquad (38)$$

Denoting by x_0 the value of x_a associated with the minimum, results in

$$x_0 = e^{m + z_0 \cdot \sigma} = e^m \cdot e^{z_0 \cdot \sigma} . \qquad (39)$$

The quotients p_1 and p_2 of this x_0 and the mean value, i.e., the mode x_m $\left(x_m = e^{m - \sigma^2}\right)$ are

$$p_1 = \frac{x_0}{M(\xi)} = e^{\left(z_0 - \frac{\sigma}{2}\right) \cdot \sigma} \qquad (40)$$

and

$$p_2 = \frac{x_0}{x_m} = e^{(z_0 + \sigma) \cdot \sigma} \qquad (41)$$

respectively.

In Table 2 those numerical values are given which have been calculated for the values $\sigma = 1; 0{,}9; \dots; 0{,}2$, namely, the values of z_0 according to Eq. (37), $h(z_{\min})$ according to Eq. (38), the value of $e^{z_0 \sigma}$ involved in Eq. (39) and lastly those of the quotients p_1 and p_2 with the aid of the relationships (40) and (41). From the values of Table 2 it may be seen that $z_0 \leq 0$, consequently $e^{z_0 \sigma} \leq 1$, $p_1 \leq 1$ and $p_2 \leq 1$; with the decreasing value of σ, p_1 and p_2 are approaching 1,

more and more, i.e., x_0 associated with $h(z)_{\min}$ with the decreasing value of σ approximates more and more the mode locus of the lognormal distribution, where the density function of the distribution has a maximum and also $h(z)_{\min}$ decreases.

Similar conclusions may be drawn from the data of Tables 3 and 4, wherein, to the given σ and m parameters of the lognormal distribution ($\sigma = 1$; $0,9$; ...; $0,2$; $m = 2$; $1,6$; ...; $0,2$) the loci of minima x_0 (Table 3) and the values $\Delta \bar{x}_{s\min}$ (Table 4) are given [4].

The ordinate of the centre of gravity of the subset before x_a, may be calculated with the aid of the formula

$$
y_{\mathrm{I}} = \frac{\dfrac{1}{4\pi \cdot \sigma} \cdot \exp \dfrac{\sigma^2}{4} - m \cdot \displaystyle\int_{-\infty}^{vx_a} e^{-v^2} \cdot dv}{\dfrac{1}{\sqrt{\pi}} \cdot \displaystyle\int_{-\infty}^{tx_a} e^{-t^2} \cdot dt} , \tag{42}
$$

wherein

$$
v_{xa} = \frac{\sigma^2 - 2m + \ln x_a^2}{2 \cdot \sigma} . \tag{43}
$$

Performing the designated operations and certain convenient replacements one obtains the value of the ordinate of the centre of gravity

$$
y_{\mathrm{I}} = \frac{1}{4\sigma \cdot \sqrt{\pi}} \exp \left(\frac{\sigma^2}{4} - m \right) \cdot \frac{\Phi \left(\dfrac{\sigma^2 - 2m + \ln x_a^2}{\sigma \cdot \sqrt{2}} \right)}{\Phi \left(\dfrac{\ln x_a - m}{\sigma} \right)} . \tag{44}
$$

The ordinate of the centre of gravity of the area behind x_a may be determined with the aid of the formula

$$
y_{\mathrm{II}} = \frac{\dfrac{1}{4\sqrt{\pi} \cdot \sigma} \cdot \exp \left(\dfrac{\sigma^2}{4} - m \right) \cdot \displaystyle\int_{vx_a}^{+\infty} e^{-v^2} \cdot dv}{\dfrac{1}{\sqrt{\pi}} \displaystyle\int_{vx_a}^{+\infty} e^{-t^2} \cdot dt} . \tag{45}
$$

Carrying out the operations marked in the formula, the ordinate y_{II} may be obtained

$$
y_{\mathrm{II}} = \frac{1}{4\sigma \cdot \sqrt{\pi}} \cdot \exp \left(\frac{\sigma^2}{4} - m \right) \cdot \frac{1 - \Phi \left(\dfrac{\sigma^2 - 2m + \ln x_a^2}{\sigma \cdot \sqrt{2}} \right)}{1 - \Phi \left(\dfrac{\ln x_a - m}{\sigma} \right)} . \tag{46}
$$

Table 2

Change of $z_0\sigma$ $h(z)_{min}$, $e^{z_0\sigma}$, p_1 and p_2 in dependence on p_1 and p_2

	1	0,9	0,8	0,7	0,6	0,5	0,4	0,3	0,2
$z_0\sigma$	$-1,966$	$-1,748$	$-1,534$	$-1,330$	$-1,130$	$-0,934$	$-0,741$	$-0,553$	$-0,366$
$h(z)_{min}$	0,962527	0,937071	0,898503	0,846908	0,776847	0,687778	0,579426	0,453031	0,311344
$e^{z_0\sigma}$	0,140016	0,207381	0,293112	0,394159	0,507327	0,626880	0,743490	0,847131	0,929415
p_1	0,0849	0,1383	0,2128	0,3985	0,4238	0,5532	0,6863	0,8099	0,9110
p_2	0,3806	0,4662	0,5559	0,6434	0,7272	0,8049	0,8725	0,9269	0,9673

Table 3

Minimum loci x_0 of the differences $\bar{x}_{s\,min}$ at given σ and m

m \ σ	1	0,9	0,8	0,7	0,6	0,5	0,4	0,3	0,2
2	1,0345846	1,532346155	2,16582206	2,91246554	3,748665838	4,63205251	5,4936899028	6,259498061	6,867899043
1,6	0,633502	1,0271618	1,4517932	1,952283	2,512805	3,104956	3,682528	4,195865	4,603420
1,2	0,464869	0,688528	0,9731675	1,308656	1,6843857	2,081317	3,468476	2,812576	3,085769
1	0,380602	0,563719	0,796761	1,071436	1,379057	1,704037	2,021015	2,302741	2,526412
0,9	0,344383	0,510074	0,720940	0,969476	1,247822	1,541876	1,828690	2,083606	2,285992
0,8	0,311611	0,461534	0,652333	0,877218	1,129076	1,395147	1,654667	1,885325	2,068451
0,7	0,281957	0,417613	0,590255	0,793739	1,021631	1,262381	1,497205	1,705912	1,871612
0,6	0,255125	0,377872	0,534085	0,718205	0,924410	1,142250	1,354727	1,543573	1,693504
0,5	2,230847	0,341913	0,483260	0,649859	0,836440	1,033551	1,225808	1,396683	1,532346
0,4	0,208879	0,309375	0,437272	0,588017	0,756843	0,935195	1,109157	1,263771	1,386524
0,3	0,189002	0,279934	0,395660	0,532059	0,684819	0,846200	1,003606	1,143507	1,254579
0,2	0,171016	0,253295	0,358008	0,481427	0,619650	0,765673	0,908101	1,034688	1,135190

Table 4

Values of $\bar{x}_{s\,min}$ in case of given σ and m values

m \ σ	1	0,9	0,8	0,7	0,6	0,5	0,4	0,3	0,2
2	11,72598	10,381280	9,153049	7,995166	6,872226	5,758692	4,637998	3,501468	2,347013
1,6	7,860156	6,958777	6,135469	5,359317	4,606589	3,860165	3,108952	2,347103	1,573249
1,2	5,268828	4,664614	4,112734	3,592463	3,087893	2,587550	2,083989	1,573313	1,054582
1	4,313747	3,819060	3,367219	2,941257	2,528151	2,118505	1,706224	1,288118	0,863418
0,9	3,903240	3,455628	3,046785	2,661360	2,287565	1,916902	1,543855	1,165538	0,781253
0,8	3,531197	3,126782	2,765845	2,408098	2,069875	1,734485	1,396938	1,054622	0,706907
0,7	3,195702	2,829229	2,494497	2,178937	1,872900	1,569427	1,264002	0,954261	0,639636
0,6	2,819591	2,559992	2,257114	1,971584	1,694670	1,420076	1,154716	0,863451	0,578766
0,5	2,616420	2,316377	2,042321	1,783963	1,533401	1,284938	1,034877	0,781283	0,523689
0,4	2,367435	2,095944	1,847969	1,614196	1,387479	1,162660	0,936396	0,706934	0,473854
0,3	2,142143	1,896489	1,672111	1,640585	1,255443	1,052018	0,874286	0,639661	0,428761
0,2	1,938292	1,716014	1,512989	1,321592	1,135971	0,951905	0,877756	0,578789	0,387959

Table 5

Metal-content distribution data for an ore sample of Gyöngyösoroszi

Interval	g_i	a_i (Zn content) %	$a_i \cdot g_i$	$\Sigma a_i \cdot g_i \downarrow$	$\Sigma g_i \downarrow$	$b_i = \dfrac{\Sigma a_i g_i \Sigma g_i}{\Sigma a_i g_i} \downarrow$	$\Sigma a_i \cdot g_i \uparrow$	$\Sigma g_i \uparrow$	c_i	y_{I}	y_{II}	v
1	2	3	4	5	6	7	8	9	10	11	12	13
0 — 2	0,0517	1	0,0517	0,0517	0,0517	1,0000	6,5018	1,0000	6,5018	0,0129	0,0499	0,0079
2 — 4	0,2244	3	0,6732	0,7249	0,2761	2,6255	6,4501	0,9483	6,8018	0,0480	0,0461	0,1115
4 — 6	0,2482	5	1,2410	1,9659	0,5243	3,7496	5,7789	0,7239	7,9802	0,0547	0,0431	0,3024
6 — 8	0,2000	7	1,4000	3,3659	0,7234	4,6471	4,5359	0,4759	9,5352	0,0534	0,0332	0,5177
8 — 10	0,1344	9	1,2096	4,5755	0,8587	5,3284	3,1359	0,2757	11,3743	0,0503	0,0220	0,7037
10 — 12	0,0552	11	0,6072	5,1827	0,9139	5,6710	1,9263	0,1413	13,6327	0,0481	0,0090	0,7971
12 — 14	0,0310	13	0,4030	5,5857	0,9449	5,9114	1,3191	0,0861	15,3206	0,0467	0,0058	0,8591
14 — 16	0,0241	15	0,3615	5,9472	0,9690	6,1375	0,9161	0,0551	16,6261	0,0475	0,0048	0,9147
16 — 18	0,0172	17	0,2924	6,2396	0,9862	6,3269	0,5446	0,0310	17,8903	0,0459	0,0039	0,9597
18 — 20	0,0138	19	0,2622	6,5018	1,0000	6,5018	0,2622	0,0138	19,0000	0,0443	0,0034	1,0000

By making use of Formulae (28), (30), (44), (46) the abscissae and ordinates of the centres of gravity of the subsets may be determined for arbitrary values of x_a, σ and m with the aid of the values of the standard normal distribution function listed in the table.

3. Practical application

Table 5 shows the distribution of the zinc content in one of the ore bodies of the ore mine in Gyöngyösoroszi. By using the actual data the values of the basic diagram (a) have been defined, i.e., the distribution of the average
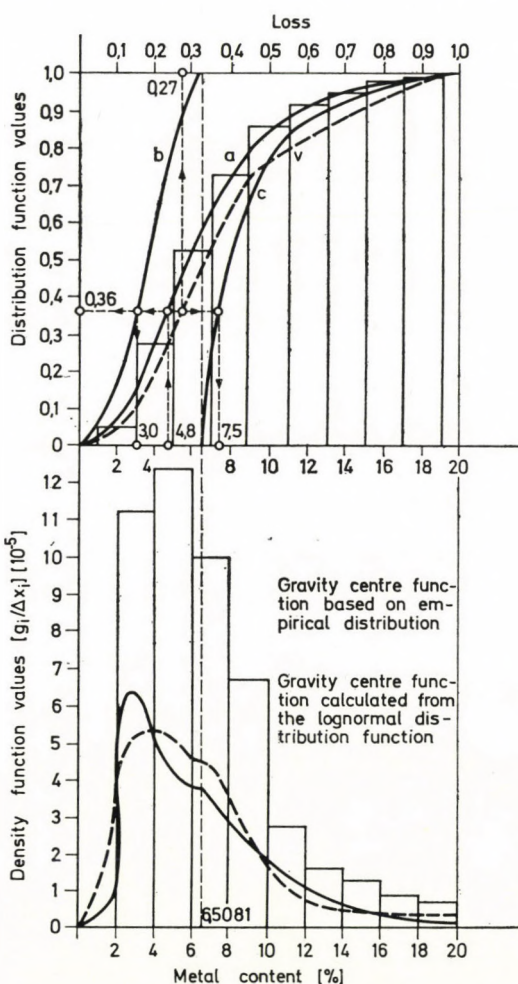
Fig. 5. Gravity centre distribution of a subset based on empirical data

metal content to be found in the whole ore assembly, as well as the mineral resources to be exploited (c) and left back (b) [3].

With the aid of the empirical density function to the values x_a given in column 3 of Table 5, the mean values $M(\bar{x}_I)$ presented in column 7 and those $M(\bar{x}_{II})$ listed in column 10, as well as the ordinates of the centres of gravity y_I to be found in column 11 and those of y_{II} in column 12 have been calculated.

With the relevant data of the table the exploitability functions presented in Fig. 5 are plotted, namely [3], [6]:

— the distribution of the metal content of the whole ore body (a);
— the distribution of the average metal content of the parts to be exploited and left back (c and b);
— the distribution of the metal loss (v)

Table 6

Values of the abscissae and ordinates of the centres of gravity in case of theoretical lognormal distribution

x_a	$M(\bar{x}_I)$	$M(\bar{x}_{II})$	y_I	y_{II}	$\varPhi\left(\dfrac{\ln x_a - m}{\sigma}\right)$
1	2	3	4	5	6
2	1,664446	6,6225835	0,058953	0,376395	0,0250
4	2,616389	7,275157	0,646357	0,313146	0,1660
6	4,031643	9,446277	0,475582	0,240766	0,5438
8	4,798822	11,404632	0,448386	0,138351	0,7422
10	5,347288	13,460507	0,416960	0,076126	0,8577
12	5,734022	15,602649	0,396067	0,041203	0,9222
14	5,989217	17,745740	0,384216	0,022817	0,9564
16	6,159038	19,869500	0,377529	0,014738	0,9750
18	6,271526	22,043774	0,373768	0,009448	0,9854
20	6,335523	30,787934	0,370945	0,005418	0,9932

The calculations were made with the following parameters:

$$M(\xi) = 6,5018$$

$$D^2(\xi) = [0,0517(1-6,5018)^2 + 0,3244(3-6,5018)^2 + \ldots + 0,0138(19-6,5018)^2 - \varDelta^2/12] =$$
$$= 13,700862,$$

wherein $\varDelta^2/12$ is the Sheppard's correction. According to column 1 of Table 5 the value of $\varDelta$ is equal to 2, which is the proportion of the metal content.

The variance is

$$\sigma^2 = \ln[(D(\xi)^2/M(\xi)) + 1] = 0,280773,$$

and the scatter

$$\sigma = 0,529842$$

and the parameter m

$$m = \ln M(\xi) - \sigma^2/2 = 1,874151\,.$$

in the function of the mass proportion of the part of the occurrence left back. In the upper part of the figure the distribution functions and in the lower the density functions are to be seen; on the horizontal axis the metal contents, i.e., the metal losses are plotted, on the vertical axis the associated distribution and density values are marked. The utilization of the table is shown by straight lines marked with arrows. According to the example demonstrated the limiting value of the metal content x_a (4,8 per cent) is fixed.

In Table 6 the abscissae and ordinates of the gravity centres of the subsets are given for the case where the empirical function is approximated by the lognormal distribution. The approximation is justified by the calculations [1], [4].

The parameters σ and m being known the values $M(x_I)$, $M(\bar{x}_{II})$, y_I and y_{II} to the limit metal content x_a may be found by making use of the listed values of the standard normal distribution function in the Table 6 already mentioned.

In Fig. 5 the curve connecting the gravity centres of the subsets is presented, calculated by the empirical and lognormal density functions. In case of both gravity centre distribution functions two local maxima may be pointed out in the proximity of the mean value, however, contrary to the normal distribution functions, they do not appear symmetrically.

REFERENCES

[1] Vincze I.: Mathematical Statistics and its Industrial Applications. Műszaki Könyvkiadó, Budapest 1968
[2] Prékopa A.: Theory of Probability and its Practical Engineering Applications. Műszaki Könyvkiadó, Budapest 1972
[3] Tarján G.: Ore Dressing I. Manuscript. Tankönyvkiadó, Budapest 1969
[4] Raisz I.: Report for the Working Party of Mining of the Hungarian Academy of Sciences (made on a commission proposed by the authors of this paper). Manuscript, Miskolc 1979
[5] Zambó J.: Theory of Settlement in Mining. Műszaki Könyvkiadó, Budapest 1966
[6] Tarján G.: Calculation Method for the Determination of Critical Values of the Economy of Ore Mines. BKL Mining (BKL Bányászat) (1973), 649—651
[7] Hoványi L.—Kolozsvári G.: Geometry of Mining. Tankönyvkiadó, Budapest 1973
[8] Tóth M.: Interpretation of the Relationship Between the Losses Occurring in the Exploitation of the Mineral Raw Materials and Exploitability. BKL Bányászat. (1975), 7—11
[9] Faller G.: Some Problems in Connection with the Estimation of Exploitability. Földtani Kutatás 10 (1967), 9—16
[10] Faller G.—Tóth M.: Results of the Research Work Formulated in Theorems Performed in the Fields of Mining Economy and Mining Resources Management. Manuscript. Budapest 1972

Über die mathematisch-statistische Untersuchung der Abbauwürdigkeitsfunktionen. — Die Abbauwürdigkeitsfunktionen können aus der Wahrscheinlichkeitsverteilungsfunktionen einer Komponente (z. B. des Metallgehalts) des Mineralvorkommens abgeleitet werden. Mit Hilfe der Verteilungsfunktion kann bei jedem Massenverhältnis die durchschnittliche Komponente der beiden Teilfunktionen und deren Varianz bestimmt werden. Eine Teilfunktion bezieht sich auf den gewonnenen, die andere auf den restlichen Teil. Unter Abbauwürdigkeitsfunktio-

nen, ferner die in Abhängigkeit von der restlichen Komponente kontinuierliche Änderung der durchschnittlichen Komponente der beiden Teilfunktionen und ihrer Streuung, sowie der Verluste der wertvollen Komponente.

Об исследования с помощью методов математической статистики функций вероятности разработки. Функции вероятности разработки можно вывести на основе функции распределения компонента (напр. металлического содержания) нефтяного месторождения. С помощью функции распределения при любом значении частной массы можнно определит среднюю составляющую двух частных функций, а также ее квадрат рассева Один изв частных функций относится к добытой части, а другой к оставшейся части. Под функциями вероятности разработки следует понимать функцию распределения, далее непрерывное изменение средней составляющей и квадрата рассева двух частных функций, а также потерь ценных компонентов в функции компонента.

COMBINED STRENGTH PATTERN OF THIN-WALLED BOX GIRDERS IN TORSION

B. GOSCHY*

CAND. OF TECHN. SCI

In this paper the theory of torsion of thin-walled box girders is extended to the general case of combined torsion by taking also into account the effects of the shear deformations. The purpose of the paper is to formulate mathematically the mechanical phenomenon of combined torsion for the engineering practice as well as to demonstrate the application of the formulae presented in the framework of a numerical example. In addition, besides the more familiar procedures WANNSLEBEN, URBAN, etc. also the significance of the secondary shear deformation is emphasized in the paper.

1. Introduction

In this paper the combined torsional strength pattern of thin walled closed sections are presented as following
— box section in combined warping and torsion,
— box section in combined warping and distorsion,
— box section in combined torsion and distorsion.

For all three cases the effect of shear will be also investigated. The purpose is to give the mathematical formulation of the phenomena of combined torsion for the engineering practice.

The calculation is carried out by using the well known force method.

2. Symbols

The following symbols are used in this paper:

m_T	distributed torsional moment (torque)
p_x, p_y	uniformly distributed load
$t(z)$	shear flow
q_x, q_y	shear forces
m_t, m_b	moments at corner points (t = top; b = bottom)
$\xi(z)$, $\eta(z)$, $\zeta(z)$	displacements in the directions x, y, z, respectively
$\varphi(z)$	angle of torsion
$\gamma(z)$	angle of distortion
x, y, z	system of coordinates

* Dr. B. GOSCHY, H-1056 — Budapest, Bástya u. 10, Hungary.

J_{T_0} moment of inertia in pure torsion of a box shaped cross section
J_{Ti} moment of inertia in torsion of a wall unit i of the box section
J_w warping (sectorial) moment of inertia
F_w warping (sectorial) moment of inertia from shear
J_x, J_y principal moments of inertia in bending of walls of the box section
J_v, J_t, J_b moments of inertia in bending of webs, top and bottom flanges, respectively
F_x, F_y equivalent shear cross-sectional area of wall units of the closed profile
h, a height and width of middle surface of the cross section
v wall thickness
E Young's modulus of elasticity
G shear modulus
μ Poisson's ratio.

3. Assumptions

3.1 The material of the thin-walled box girder under investigation is elastic, homogeneous, isotropic, to which the principles of the theory of elasticity hold true.

3.2 The cross section is constant along the full length of the girder.

3.3 The supports cannot be twisted and the cross section above the supports is absolutely rigid.

3.4 The box girder is subjected to uniformly distributed antisymmetrical loads, which generate a uniformly distributed torque.

$$m_T = p_y a + p_x h \qquad (1)$$

and a uniformly distributed distortional moment

$$m_G = p_y a - p_x h . \qquad (2)$$

3.5 The model investigated is considered to be continuous, thus, the solution may be given in a closed form.

3.6 The profile investigated is simply a symmetric, box shaped rectangular cross section with rigid corners the thickness of the two webs is equal v_g, those of the flanges are different (v_t, v_b).

4. Combined torsion and warping of an undeformable box girder

It is assumed that with a sufficient number of stiff diaphragms the cross section keeps its shape i.e., its undeformability during twisting process.

The statically determined basic profile is produced by the fictive cut at corner points (Fig. 1). Redundant quantities are: shear flow t acting on the middle surfaces of the wall cross section as well as the shear forces q_x and q_y.

Continuity conditions at the cut provide the above redundant forces.

The continuity conditions at cuttings W_1 and W_2 (Fig. 1) may be expressed in the concise forms

$$\varepsilon_{w_1}(z) = \varepsilon_{f_1}(z) \quad \text{and} \quad \varepsilon_{w_2}(z) = \varepsilon_{f_2}(z) \tag{3}, (4)$$
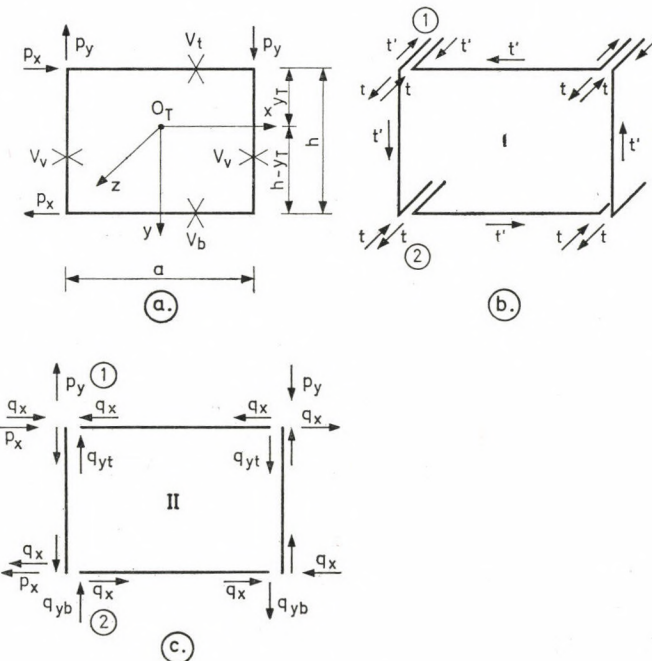
Fig. 1

of, in a more detailed form

$$- \eta_l''(-y_T) = - \xi_t''\left(-\frac{a}{2}\right), \tag{5}$$

$$- \eta_l''(h - y_T) = - \xi_b''\left(-\frac{a}{2}\right), \tag{6}$$

wherein y_T is the ordinate of the centre of torsion.

Subtraction of the two equations yields the relation

$$\eta_l'' h = (\xi_t'' - \xi_b'')\frac{a}{2} \tag{7}$$

wherein, besides bending deformation, (M) also the deformation caused by the shear force (Q) and the shear flow (T) are taken into account in the vertical

and horizontal displacements of the web and flanges respectively such as

$$\eta_l'' = \eta_{lM}'' + \eta_{lQ}'' + \eta_{lT}'' = -\frac{M_{xl}}{EJ_{xl}} + \frac{M_{xl}''}{GF_{xl}} - \frac{t'}{Gv_v}, \tag{8}$$

$$\xi_t'' = \xi_{tM}'' + \xi_{tQ}'' + \xi_{tT}'' = +\frac{M_{yt}}{EJ_{yt}} - \frac{M_{yt}''}{GF_{yt}} + \frac{t'}{Gv_t} \tag{9}$$

$$\xi_b'' = \xi_{bM}'' + \xi_{bQ}'' + \xi_{bT}'' = +\frac{M_{yb}}{EJ_{yb}} - \frac{M_{yb}''}{GF_{yb}} + \frac{t'}{Gv_b} \tag{10}$$

(where the subscripts l means "left-hand side" t and b, "top" and "bottom").

In the expressions of the displacements, flexural stiffness will be expressed as follows:

$$EJ = \frac{EJ_0}{1 - \mu^2}; \quad J_{0x} = \frac{vh^3}{12}; \quad J_{0y} = \frac{va^3}{12},$$

while the shear stiffness is given by the formulae

$$GF = GkF_0; \quad F_{0x} = vh; \quad F_{0y} = va,$$

wherein, in case of a rectangular cross section $k = 5/6$.

It is to be noted that the calculation of the centre of torsion may be carried out by adding Eqs (5) and (6):

$$\xi_l''(2y_T - h) = (\xi_t'' + \xi_b'')\frac{a}{2}. \tag{11}$$

The geometric condition is expressed by the equalities

$$\eta_{bM}'' + \eta_{bQ}'' = \varphi_f''\left(-\frac{a}{2}\right); \quad \xi_{tM}'' + \xi_{tQ}'' = -\varphi_v''(-y_T); \quad \xi_{bM}'' + \xi_{bQ}'' = -\varphi_i''(h - y_T). \tag{12}$$

Since, due to the undeformability

$$\varphi_v = \varphi_f = \varphi(z) \tag{13}$$

Eq. (7) may be brought to the form

$$-\varphi''\frac{ah}{2} - \frac{t'h}{Gv_v} = +\varphi''\frac{ha}{2} + \frac{t'a}{2Gv_t} + \frac{t'a}{2Gv_b} - \tag{7a}$$

by making use of the equalities (12).

By reducing the above equation

$$\varphi'' ah = \frac{t'}{G} \left(\frac{h}{v_v} + \frac{a}{2v_t} + \frac{a}{2v_b} \right)$$ (14)

is obtained which by further multiplication with 2 gives

$$-2FG\varphi'' = t' \oint \frac{ds}{v} .$$ (15)

This is the well known equation of deformation due to torsion (St. Venant's torsion), wherein

$$F = ah .$$

The pure torsional part of the torque may be evaluated from equation

$$m_{T1} = 2aht' = 2Ft' .$$ (16)

Consequently, Eq. (16) may be written in the form

$$-GJ_{T0}\varphi'' = m_{T1}$$ (17)

where

$$GJ_{T0} = G \frac{4F^2}{\oint \dfrac{ds}{v}}$$

is the torsional stiffness due to the pure torsion of the closed cross section.

Knowing the relationship between the geometrical conditions and deformations, one can write

$$
\begin{aligned}
\eta_{bM}^{IV} &= - \frac{p_y - (q_{yt} + q_{yb}) - t'h}{EJ_{xl}} = + \varphi_M^{IV} \left(-\frac{a}{2} \right) , \\[2mm]
\eta_{bQ}^{IV} &= + \frac{p_y'' - (q_{yt}'' + q_{yb}'')}{GF_{xl}} = + \varphi_Q^{IV} \left(-\frac{a}{2} \right) , \\[2mm]
\xi_{tM}^{IV} &= + \frac{p_x - 2q_x - t'a}{EJ_{yt}} = - \varphi_M^{IV}(-y_{T1}) , \\[2mm]
\xi_{tQ}^{IV} &= - \frac{p_x'' - 2q_x''}{GF_{yt}} = - \varphi_Q^{IV}(-y_{T2}) , \\[2mm]
\xi_{bM}^{IV} &= - \frac{p_x - 2q_x - t'a}{EJ_{yb}} = - \varphi_M^{IV}(h - y_{T1}) , \\[2mm]
\xi_{bQ}^{IV} &= + \frac{p_x'' - 2q_x''}{GF_{yb}} = - \varphi_Q^{IV}(h - y_{T2}) .
\end{aligned}
$$ (18)

From Eqs (18) by multiplication with a and h, one can obtain the expressions

$$p_y a - (q_{yt} + q_{yb})\, a - ah\, t' = \varphi_M^{IV} E \frac{a^2}{2} J_{xl} \,.$$

$$-p_y'' a + (q_{yt}'' + q_{yb}'')\, a \qquad\qquad = \varphi_Q^{IV} G \frac{a^2}{2} F_{xl} \,.$$

$$p_x h - 2q_x h - ah\, t' \qquad\qquad = \varphi_M^{IV} E h^2 \frac{J_{yt} J_{yb}}{J_{yt} + J_{yb}} \,. \qquad (19)$$

$$-p_x'' h + 2q_x'' h \qquad\qquad = \varphi_Q^{IV} G h^2 \frac{F_{yt} F_{yb}}{F_{yt} + F_{yb}} \,.$$

The warping stiffness may be written briefly as follows:

$$EJ_{wx} = E \frac{a^2}{2} J_{xl} \,, \qquad EJ_{wy} = E h^2 \frac{J_{yt} J_{yb}}{J_{yt} + J_{yb}} \,,$$

$$GF_{wx} = G \frac{a^2}{2} F_{xl} \,, \qquad GF_{wy} = G a^2 \frac{F_{yt} F_{yb}}{F_{yt} + F_{yb}} \,. \qquad (19a)$$

Summarizing flexural deformation equations (19) yields

$$p_y a + p_x h - (q_{yt} + q_{yb})a - 2q_x h - 2ah\, t' = \varphi_M^{IV} EJ_w \qquad (20)$$

$$-p_y'' a - p_x'' h + (q_{yt}'' + q_{yb}'')\, a + 2q_x'' h = \varphi_Q^{IV} GF_w \qquad (21)$$

wherein

$$J_w = J_{wx} + J_{wy}, \quad F_w = F_{wx} + F_{wy} \,.$$

The full torsion of the box section may be determined from the common effect of bending and shear [1], on the basis of equation

$$\varphi = \varphi_M + \varphi_Q \,. \qquad (22)$$

The values of φ_M and φ_Q may be expressed from Eqs (20) and (21). Forming the sum of the above Eqs we may obtain

$$p_y a + p_x h - (q_{yt} + q_{yb})a - 2q_x h - 2ah\, t' -$$
$$- (p_y'' a + p_x'' h)\frac{EJ_w}{GF_w} + \left[(q_{yt}'' + q_{yb}'')\, a + 2q_x'' h\right]\frac{EJ_w}{GF_w} = EJ_w \varphi^{IV} \,. \qquad (23)$$

Eq. (23) also satisfies the condition of equilibrium, i.e.,

$$m_T = m_{T1} + m_{T2} + m_{Ti}$$

wherein

$$m_{Ti} = (q_{yt} + q_{yb})\, a + 2q_x h = -G(J_{Tt} + J_{Tb} + 2J_{Tv})\, \varphi'' = -\, G\Sigma J_{Ti}\varphi''$$

$$m_{T1} = -\, GJ_{T0}\varphi'' = 2ah\, t'\ , \tag{23a}$$

$$m_{T2} = -\, B_w'' = +\, EJ_w \varphi^{\mathrm{IV}}\ .$$

The equation of the combined torsion is expressed by a fourth order inhomogeneous differential equation with constant coefficients:

$$EJ_w \left(1 + \frac{\sum\limits_i J_{Ti}}{F_w}\right) \varphi^{\mathrm{IV}} - G\left(J_{T0} + \sum\limits_i J_{Ti}\right)\varphi'' = m_T - \frac{EJ_w}{GF_w}\, m_T''\ . \tag{24}$$

Neglecting the shear deformation due to warping ($F_w \to \infty$), the equation of torsion becomes

$$EJ_w \varphi^{\mathrm{IV}} - G(J_{T0} + \Sigma J_{Ti})\, \varphi'' = m_T\ . \tag{25}$$

In case of thin-walled profiles one might assume that $\sum\limits_i J_{Ti} = 0$ when

$$EJ_w \varphi^{\mathrm{IV}} - GJ_{T0}\varphi'' = m_T\ . \tag{26}$$

The solution to the differential equation (24) may be carried out in the following steps:

$$k^2 \varphi^{\mathrm{IV}} - \varphi'' = +\frac{m_T}{G\bar{J}_T}\ , \tag{26a}$$

where

$$k^2 = \frac{E\bar{J}_w}{G\bar{J}_T} = \frac{EJ_w \left(1 + \dfrac{\Sigma J_{Ti}}{F_w}\right)}{G(J_{T0} + \Sigma J_{Ti})} \tag{26b}$$

wherefrom

$$\varphi'' = C_1 \cosh \frac{z}{k} + C_2 \sinh \frac{z}{k} - \frac{m_T}{G\bar{J}_T}\ , \tag{27}$$

and finally the full solution will be

$$\varphi(z) = C_1 \cosh \frac{z}{k} + C_2 \sinh \frac{z}{k} - \frac{m_T}{G\bar{J}_T}\frac{z^2}{2} + C_3 z + C_4\ . \tag{28}$$

The constants of integration may be determined from the following boundary conditions (L denotes the length of the bar):

— in case of a cantilever beam

  with shear   *without shear* $(F_w = \infty)$

  $$\varphi(o) = 0 \,,$$ $$\varphi(o) = 0 \,,$$

  $$\varphi'(o) = \frac{M_T(o)}{G(F_w + \bar{J}_T)} = \frac{m_T L}{G(F_w + \bar{J}_T)} \,,$$ $$\varphi'(o) = 0 \,,$$

  $$\varphi''(L) = -\frac{m_T}{G(F_w + \bar{J}_T)} \,,$$ $$\varphi''(L) = 0 \,,$$

  $$k^2\varphi'''(L) - \varphi'(L) = \frac{-M_T(L)}{G\bar{J}_T} = 0 \,;$$ $$k^2\varphi'''(L) = \varphi'(L) \,; \quad (28a)$$

— in case of a simply supported beam

  with shear   *without shear* $(F_w = \infty)$

  $$\varphi(o) = \varphi(L) = 0 \,,$$ $$\varphi(o) = \varphi(L) = 0 \,,$$

  $$\varphi''(o) = \varphi''(L) = -\frac{m_T}{G(F_w + \bar{J}_T)} \,,$$ $$\varphi''(o) = \varphi''(L) = 0 \,. \quad (28b)$$

5. Distorsional deformation of a thin-walled closed profile in warping torsion

In this chapter the effect of torsion will be disregarded and the strength due to cross sectional distorsion will be investigated (Fig. 2).

Lack of the stiffening diaphragms causes the distortion of the cross section which may be described with the angle of distorsion $\gamma(z)$.

The equations of displacement, may be written in the form of

$$\eta_l^{IV} = \eta_{lM}^{IV} + \eta_{lQ}^{IV} = -\frac{p_y - q_{ym}}{EJ_{xl}} + \frac{p_y'' - q_{ym}''}{GF_{xl}} \,,$$

$$\xi_t^{IV} = \xi_{tM}^{IV} + \xi_{tQ}^{IV} = +\frac{p_x - q_{xm}}{EJ_{yt}} - \frac{p_x'' - q_{xm}''}{GF_{yt}} \,, \qquad (29)$$

$$\xi_b^{IV} = \xi_{bM}^{IV} + \xi_{bQ}^{IV} = -\frac{p_x - q_{xm}}{EJ_{yb}} + \frac{p_x'' - q_{xm}''}{GF_{yb}}$$

where the shear forces might be determined in possession of the restraining moments at corners m_t and m_b according to the formulae

$$q_{ym} = \frac{2(m_t + m_b)}{a} \,; \qquad q_{xm} = \frac{2(m_t + m_b)}{h} \,. \qquad (30)$$
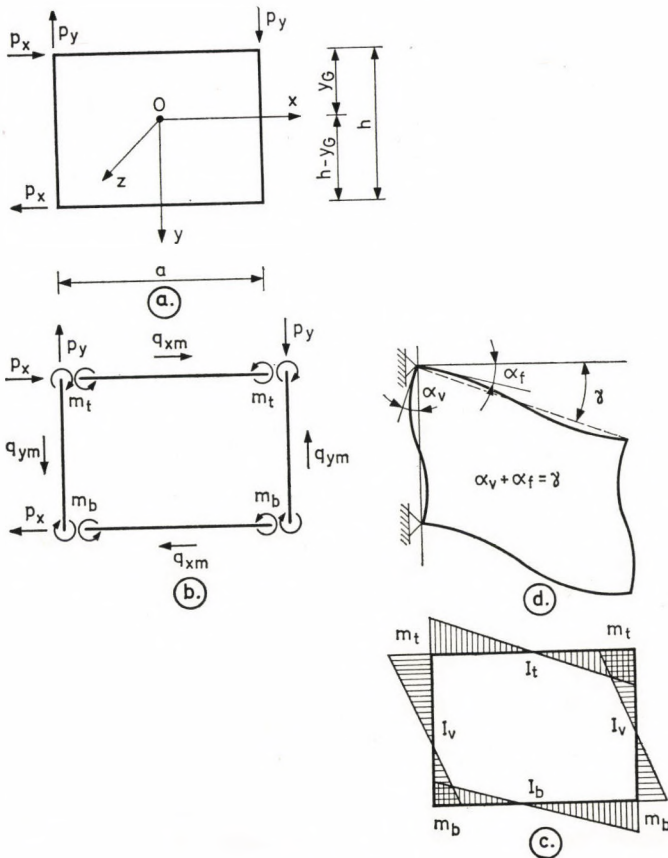
Fig. 2

Hence

$$q_{ym} = \frac{h}{a}\, q_{xm} \;.$$

The relationship between the restraining moments is expressed with the aid of the theory of frameworks by the equality

$$\left(1 + \frac{a}{3h}\,\frac{J_v}{J_t}\right) m_t = \left(1 + \frac{a}{3h}\,\frac{J_v}{J_b}\right) m_b \;. \tag{31}$$

The value of the angle of deformation may be determined by making use of the elementary framework model (Figs 2/c and 2/d) from the formula

$$\gamma = -\left(\frac{a}{6EJ_t} + \frac{h}{3EJ_v}\right) m_t + \frac{h}{6EJ_g}\, m_b \;. \tag{32}$$

From Eqs (31) and (32)

$$\gamma = - \left[\frac{a}{6EJ_t} + \frac{h}{6EJ_v} \left(2 - \frac{1 + \dfrac{a}{3h} \dfrac{J}{J_t}}{1 + \dfrac{a}{3h} \dfrac{J}{J_b}} \right) \right] m_t \, , \tag{33}$$

wherefrom the moments at corners are

$$m_t = - EK_t\gamma \, , \quad m_b = - EK_b\gamma$$

wherein K_t and K_b are stiffness coefficients.

By establishing the geometric conditions

$$\eta_{lM}^{IV} = - \frac{p_y - q_{ym}}{EJ_{xl}} = - \frac{\gamma_M^{IV}}{2} \left(- \frac{a}{2} \right) \, ,$$

$$\eta_{lQ}^{IV} = + \frac{p_y'' - q_{ym}''}{GF_{xl}} = - \frac{\gamma_Q^{IV}}{2} \left(- \frac{a}{2} \right) \, ,$$

$$\xi_{tm}^{IV} = + \frac{p_x - q_{xm}}{EJ_{yt}} = + \frac{\gamma_M^{IV}}{2} \left(- y_M \right) \, ,$$

$$\xi_{tQ}^{IV} = - \frac{p_x'' - q_{xm}''}{GF_{yt}} = + \frac{\gamma_Q^{IV}}{2} \left(- y_Q \right) \, ,$$

$$\xi_{bM}^{IV} = - \frac{p_x - q_{xm}}{EJ_{yb}} = + \frac{\gamma_M^{IV}}{2} \left(h - y_M \right) \, ,$$

$$\xi_{bQ}^{IV} = + \frac{p_x'' - q_{xm}''}{GF_{yb}} = + \frac{\gamma_Q^{IV}}{2} \left(h - y_Q \right) \tag{34}$$

after reduction the following relations are obtained

$$p_y a - q_y a = - \frac{\gamma_M^{IV}}{2} E \frac{a^2}{2} J_{xl} = - EJ_{wx} \frac{\gamma_M^{IV}}{2} \, ,$$

$$-(p_y'' a - q_y'' a) = - \frac{\gamma_Q^{IV}}{2} G \frac{a^2}{2} F_{xl} = - GF_{wx} \frac{\gamma_Q^{IV}}{2} \, ,$$

$$-(p_x h - q_x h) = - \frac{\gamma_M^{IV}}{2} E h^2 \frac{J_{yt} J_{yb}}{J_{yt} + J_{yb}} = - EJ_{wy} \frac{\gamma_M^{IV}}{2} \, ,$$

$$p_x'' h - q_x'' h = - \frac{\gamma_Q^{IV}}{2} G h^2 \frac{F_{yt} F_{yb}}{F_{yt} + F_{yb}} = - GF_{wy} \frac{\gamma_Q^{IV}}{2} \, . \tag{35}$$

Separately summarizing the effects of bending and shear, results in the following equations

$$p_y a - p_x h - (q_y a + q_x h) = \frac{-\gamma_M^{IV}}{2} EJ_w , \tag{36}$$

$$-(p_y'' a - p_p'' h) + q_y'' a + q_x'' h = -\frac{\gamma_Q^{IV}}{2} GF_w . \tag{37}$$

By superposition of angles of deformation due to bending and shear [2]

$$\gamma = \gamma_M + \gamma_Q \tag{38}$$

one arrives to the relation

$$(p_y a - p_x h) - (p_y'' a - p_x'' h) \frac{EJ_w}{GF_w} - (q_y a + q_x h) + (q_y'' a + q_x'' h) \frac{EJ_w}{GF_w} =$$

$$= -EJ_w \frac{\gamma^{IV}}{2} . \tag{39}$$

Replacing the equalities

$$q_y a = 2(m_t + m_b) = -2E(K_t + K_b) \gamma = -4E(K_t + K_b)\frac{\gamma}{2}, \tag{40}$$

$$q_x h = 2(m_t + m_b) = -2E(K_t + K_b) \gamma = -4E(K_t + K_b)\frac{\gamma}{2} \tag{41}$$

into Eq. (39) results in the fourth order differential equation of constant coefficients of the following form [2]:

$$EJ_w \frac{\gamma^{IV}}{2} - 8E(K_t + K_b) \frac{EJ_w}{GF_w} \frac{\gamma''}{2} + 8E(K_t + K_b)\frac{\gamma}{2} =$$

$$= -(p_y a - p_x h) + (p_y'' a - p_x'' h) \frac{EJ_w}{GF_w} . \tag{42}$$

Neglecting the effect of shear $(GF_w = \infty)$, equation (42) may be written more simply

$$EJ_w \frac{\gamma^{IV}}{2} + 8E(K_t + K_b)\frac{\gamma}{2} = -(p_y a - p_x h) . \tag{42a}$$

The shape of the differential equation (42a) is the same as that of a beam on elastic support. This recognition may be used in solving Eqs (42) and (42a).

From Eq. (42a) it might be seen that the moment of distortion, just like torsional moment, may be divided into two parts, as follows

$$m_{G1} + m_{G2} = m_G \tag{43}$$

wherein

$m_{G1} = -8E(K_t + K_b)\ \gamma/2$ is the distributed moment of the pure distortion;

$m_{G2} = -EJ_w\ \gamma^{IV}/2$ is the distributed moment of warping distortion.

In case of distortion, the strength associated with a bimoment similar to the theory of plates, is expressed by the relationship

$$R_G = +\ EJ_w \frac{\gamma''}{2}, \tag{44}$$

further on called distortional bimoment [4].

The complete solution to the differential equation of the warping deformation (42) may expressed in the form

$$\frac{\gamma(z)}{2} = C_1 \cosh \alpha z \sin \beta z + C_2 \cosh \alpha z \cos \beta z + C_3 \sinh \alpha z \sin \beta z +$$

$$+ C_4 \sinh \alpha z \cos \beta z + \frac{\gamma_p(z)}{2}$$

where
$C_1,\ C_2,\ C_3,\ C_4$ are constants of integration,

$$\alpha^2 = \frac{R_2^2}{2} + \frac{R_1^2}{4},$$

$$\beta^2 = \frac{R_2^2}{2} - \frac{R_1^2}{4},$$

$$R_1^2 = \frac{8E(K_t + K_b)}{GF_w},$$

$$R_2^4 = \frac{8E(K_t + K_b)}{EJ_w},$$

$$\frac{\gamma_p}{2} = -\ \frac{m_G}{8E(K_t + K_b)} \tag{42c}$$

$\gamma_p(z)$ is the particular solution.

When the shear effect is neglected, one can make use of the simplification $\alpha = \beta$ in Eq. (42).

The constants of integration are determined from the boundary conditions. Due to the application of stiffening diaphragms at the ends of the box girder the following conditions might be written:

$$\gamma(o) = \gamma(L) = 0 \, . \tag{42d}$$

$$\gamma''(o) = \gamma''(L) = \frac{2m_G}{GF_w} \, .$$

6. Warping and distorsional twist of the thin-walled box girder

The equation of the closed profiles being in the state of combined torsion and distortion (Fig. 3) can be deduced with the help of the results described in Chapters 4 and 5.

The investigation will be carried out disregarding the own torsional stiffnesses of the bordering walls $(\Sigma I_{Ti} = 0)$.

By writing the condition of continuity similar to Eq. (7a), the relation

$$2\varphi_f'' \left(-\frac{a}{2} \right) - \frac{2t'}{Gv_v} = -\varphi_v''(-h) + \frac{t'}{Gv_t} + \frac{t'}{Gv_b} \tag{43a}$$

is obtained, hence the equation of the pure torsion

$$-GJ_{T0} \frac{\varphi_f'' + \varphi_v''}{2} = 2ah \, t' = m_{T1} \, . \tag{44a}$$
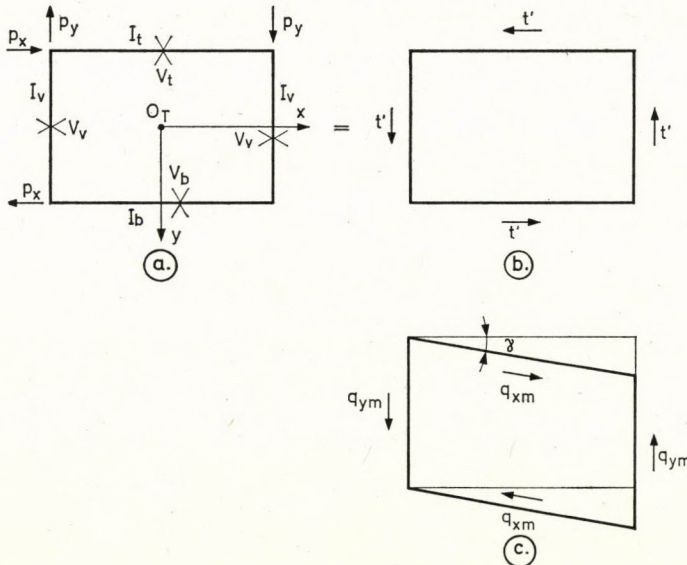
Fig. 3

In the following, we are setting up the relations between the vertical displacements and torsional rotations from bending and shear such as

$$\eta_{lM}^{IV} = -\frac{p_y - t'h - q_{ym}}{EJ_{xl}} = +\varphi_{Mf}^{IV}\left(-\frac{a}{2}\right),$$ (45a)

and

$$\eta_{lQ}^{IV} = +\frac{p_y'' - q_{ym}''}{GF_{pl}} = +\varphi_{Qf}^{IV}\left(-\frac{a}{2}\right)$$

respectively.

To the horizontal displacements the following equations may be established

$$\xi_{tM}^{IV} = \frac{p_x - t'a + q_{xm}}{EJ_{yt}} = -\varphi_{Mv}^{IV}(-y_{T1}),$$

$$\xi_{tQ}^{IV} = -\frac{p_x'' + q_{xm}''}{GF_{yt}} = -\varphi_{Qv}^{IV}(-y_{T2}),$$

$$\xi_{bM}^{IV} = -\frac{p_x - t'a + q_{xm}}{EJ_{yb}} = -\varphi_{Mv}^{IV}(h - y_{T1}),$$

$$\xi_{bQ}^{IV} = +\frac{p_x'' + q_{xm}''}{GF_{yb}} = -\varphi_{Qv}^{IV}(h - y_{T2}).$$ (45b)

Developing the equalities (45) and replacing the values of the warping stiffnesses, the following expressions are obtained:

$$p_y a - t'ah - 2(m_t + m_b) = EJ_{wx}\varphi_{Mf}^{IV},$$
$$p_x h - t'ah + 2(m_t + m_b) = EJ_{wy}\varphi_{Mv}^{IV},$$ (46)
$$-[p_y''a - 2(m_t'' + m_b'')] = GF_{wx}\varphi_{Qf}^{IV},$$
$$-[p_x''h + 2(m_t'' + m_b'')] = GF_{wy}\varphi_{Qv}^{IV}.$$

Adding the above four equations two-by-two, then subtracting two-by-two, we may find:

$$p_y a + p_x h - 2ah\,t' = EJ_{wx}\varphi_{Mf}^{IV} + EJ_{wy}\varphi_{Mv}^{IV},$$
$$-(p_y''a + p_x''h) = GF_{wx}\varphi_{Qf}^{IV} + GF_{wy}\varphi_{Qv}^{IV},$$ (47)
$$p_y a - p_x h - 4(m_t + m_b) = EJ_{wx}\varphi_{Mf}^{IV} - EJ_{wy}\varphi_{Mv}^{IV},$$
$$-(p_y''a - p_x''h) + 4(m_t'' + m_b'') = GF_{wx}\varphi_{Qf}^{IV} - GF_{wy}\varphi_{Qv}^{IV}.$$

According to the equilibrium condition the left-hand sides of the first and third equation of the system of equations (47) may be written as follows:

$$m_T - m_{T1} = m_{T2}; \quad m_G - m_{G1} = m_{G2}.$$ (48)

Accordingly, the right-hand side of the equations represents the distributed warping moment in case of torsion and distortion, i.e.,

$$m_{T2} = EJ_{wx}\varphi_{Mf}^{IV} + EJ_{wy}\varphi_{Mv}^{IV} , \tag{49}$$

$$m_{G2} = EJ_{wx}\varphi_{Mf}^{IV} - EJ_{wy}\varphi_{Mv}^{IV} .$$

By introducing the matrix notation equations (49) may be brought to the form

$$E(\bar{\bar{J}}_w)\,\bar{\varphi}_M^{IV} = \bar{m}_2 . \tag{50}$$

Hence

$$\bar{\varphi}^{IV} = \frac{1}{E}\,(\bar{\bar{J}}_w)^{-1}\bar{m}_2 , \tag{50a}$$

where

$$(\bar{\bar{J}}_w) = \begin{bmatrix} J_{wx} & J_{wy} \\ J_{wx} & -J_{wy} \end{bmatrix}, \quad \bar{\varphi}_M^{IV} = \begin{bmatrix} \varphi_{Mf}^{IV} \\ \varphi_{Mv}^{IV} \end{bmatrix}, \quad \bar{m}_2 = \begin{bmatrix} m_{T2} \\ m_{G2} \end{bmatrix}. \tag{50b}$$

It may be written in a similar way

$$-m_{T2}'' = GF_{wx}\varphi_{Qf}^{IV} + GF_{wy}\varphi_{Qv}^{IV} , \tag{51}$$

$$-m_{G2}'' = GF_{wx}\varphi_{Qf}^{IV} - GF_{wy}\varphi_{Qv}^{IV} ,$$

or

$$\bar{\varphi}_Q^{IV} = -\frac{1}{G}\,(\bar{\bar{F}}_w)^{-1}\bar{m}_2'' . \tag{51a}$$

By summing up the torsions due to bending and shear the complete torsion may be obtained, i.e.,

$$\bar{\varphi}^{IV} = \bar{\varphi}_M^{IV} + \bar{\varphi}_Q^{IV} = \frac{1}{E}\,(\bar{\bar{J}}_w)^{-1}\bar{m}_2 - \frac{1}{G}\,(\bar{\bar{F}}_w)^{-1}\bar{m}_2'' , \tag{52}$$

and the equation of warping torsion of the deformable closed profile is given by the matrix differential equation

$$E(\bar{\bar{J}}_w)\,\bar{\varphi}^{IV} = \bar{m}_2 - \frac{E}{G}\,(\bar{\bar{F}}_w)^{-1}\,(\bar{\bar{J}}_w)\,\bar{m}_2'' \tag{53}$$

wherein

$$\bar{m}_2 = \begin{bmatrix} m_{T2} \\ m_{G2} \end{bmatrix} = \begin{bmatrix} m_T \\ m_G \end{bmatrix} - \begin{bmatrix} m_{T1} \\ m_{G1} \end{bmatrix} = \bar{m} - \bar{m}_1 ,$$

$$\bar{m}_2'' = \begin{bmatrix} m_{T2}'' \\ m_{G2}'' \end{bmatrix} = \begin{bmatrix} m_T'' \\ m_G'' \end{bmatrix} - \begin{bmatrix} o \\ m_G'' \end{bmatrix} = \bar{m} - \bar{m}_1'' , \tag{53a}$$

and

$$m_{T1} = -GJ_{T0}\frac{\varphi''_f + \varphi''_v}{2} = 2ah\,t'\,,\tag{44}$$

$$m_{G1} = 4E(K_t + K_b)(\varphi_f - \varphi_v) = 4(m_t + m_b)\,.\tag{44a}$$

Eq. (53) may be rewritten in the following form

$$E(\bar{\bar{J}}_w)\,\bar{\varphi}^{IV} - \left[\frac{GJ_{T0}}{2}(\bar{\bar{I}}) + 4E(K_t + K_b)\frac{E}{G}(\bar{\bar{F}}_w)^{-1}(\bar{\bar{J}}_w)(\bar{\bar{Y}})\right]\bar{\varphi}'' +$$

$$+ 4E(K_t + K_b)(\bar{\bar{Y}})\,\bar{\varphi} = \bar{m} - \frac{E}{G}(\bar{\bar{F}}_w)^{-1}(\bar{\bar{J}}_w)\,\bar{m}''\,,\tag{54}$$

where the matrices $(\bar{\bar{I}})$ and $(\bar{\bar{Y}})$ are as follows:

$$(\bar{\bar{I}}) = \begin{bmatrix} 1 & 1 \\ 0 & 0 \end{bmatrix},$$

$$(\bar{\bar{Y}}) = \begin{bmatrix} 0 & 0 \\ 1 & -1 \end{bmatrix}.\tag{54a}$$

The general solution to the inhomogeneous differential equation (54) is [3]:

$$\bar{\varphi}_h(z) = \sum_{i=1}^{2}\bar{y}_i(A_i \cosh \alpha_i z \sin \beta_i z + B_i \cosh \alpha_i z \cos \beta_i z +$$

$$+ C_i \sinh \alpha_i z \sin \beta_i z + D_i \sinh \alpha_i z \cos \beta_i z)\,.\tag{55}$$

The full solution, knowing the particular one, $-\ \bar{\varphi}_p(z),\ -$ is

$$\bar{\varphi}(z) = \bar{\varphi}_h(z) + \bar{\varphi}_p(z)\,.\tag{56}$$

The constants of integration may be determined by making use of the boundary conditions as is presented in Chapters 4 and 5.

In the case of a simply supported beam lying on forklike supports, the boundary conditions may be expressed by the equalities

$$\bar{\varphi}(o) = \bar{\varphi}(L) = 0;\quad \bar{\varphi}''(o) = \bar{\varphi}''(L) = 0\,.\tag{56a}$$

The magnitude of the distorsional angle may be determined with the equality

$$\varphi_f(z) - \varphi_v(z) = \gamma(z)\,.\tag{57}$$

For practical cases the accuracy of the calculation will be satisfactory if one applies the following approximations:

$$\varphi_f = \varphi - \frac{\gamma}{2} \; ; \quad \varphi_v = \varphi + \frac{\gamma}{2} \; . \tag{58}$$

In this case, the torsion and angular rotation will be described by the relations

$$\frac{\varphi_f + \varphi_v}{2} = \varphi \quad \text{and} \quad \varphi_f - \varphi_v = -\gamma \; , \tag{58a}$$

further, considering Eqs (44) and (44a) the following equality may be written:

$$m_{T1} = - GJ_{T0}\varphi'' \; ,$$

$$m_{G1} = -8E(K_t + K_b)\frac{\gamma}{2} \; . \tag{58b}$$

The matrix differential equation may be written in its developed form

$$E(\bar{\bar{J}}_w)\,(\bar{\bar{J}})\,\bar{u}^{IV} - \left[(\bar{\bar{T}}) + \frac{E}{G}\,(\bar{\bar{F}}_w)^{-1}\,(\bar{\bar{J}}_w)\,(\bar{\bar{K}})\right]\bar{u}'' + K\bar{u} = \bar{m} - \frac{E}{G}\,(\bar{\bar{F}}_w)^{-1}(\bar{\bar{J}}_w)\bar{m}'' \tag{59}$$

wherein

$$(\bar{\bar{J}}) = (\bar{\bar{I}}) + (\bar{\bar{Y}}) = \begin{bmatrix} 1 & +1 \\ 1 & -1 \end{bmatrix}, \quad (\bar{\bar{T}}) = \begin{bmatrix} GJ_{T_0} & 0 \\ 0 & 0 \end{bmatrix}, \quad \bar{\bar{K}} = \begin{bmatrix} 0 & 0 \\ 0 & 8E(K_t + K_b) \end{bmatrix},$$

$$\bar{u} = \begin{bmatrix} \varphi \\ -\dfrac{\gamma}{2} \end{bmatrix} . \tag{59a}$$

Neglecting the effect of shear, the simplified equation yields

$$(\bar{\bar{F}}_w)^{-1} \to \infty \; ,$$

$$E(\bar{\bar{J}}_w)\,(\bar{\bar{J}})\,\bar{u}^{IV} - (\bar{\bar{T}})\,\bar{u}'' + (\bar{\bar{K}})\,\bar{u} = \bar{m} \; , \tag{60}$$

or, in detailed form

$$EJ_w\varphi^{IV} - GJ_{T0}\varphi'' - E(J_{wx} - J_{wy})\frac{\gamma^{IV}}{2} = m_T \; ,$$

$$EJ_w\frac{\gamma^{IV}}{2} + 8E(K_f + K_a)\frac{\gamma}{2} - E(J_{wx} - J_{wy})\,\varphi^{IV} = -m_G \; . \tag{61}$$

The first equation describes the torsion without distorsion if $\gamma = 0$; the second one expresses the distorsion in transversal bending without torsion if $\varphi = 0$.

REFERENCES

1. COURBON, J.: Résistance des matériaux. Dunod, Paris 1968
2. KRISTEK, V.: Tapered Box Girders of Deformable Cross Section. *Journal of the Structural Division. Proceedings of the A.S.C.E.* Aug. 1970
3. KOLLBRUNNER, C.—HAJDIN, N.—KRAJCINOVIC, D.: Matrix Analyses of Thin-walled Structures. Institute for Eng. Research Zürich, Dec. 1969
4. WLASOV, V. Z.: Thin-walled Elastic Beams, Ed. 2., Moscow 1959

Beanspruchungszustand von Trägern mit dünnwandigem geschlossenem Querschnitt in Torsion. — Die Torsionstheorie von Trägern mit dünnwandigem geschlossenem Querschnitt wird auf allgemeine Fälle der Wölbkrafttorsion der deformierbaren Querschnitten, sowie auf den Einfluß der Schubverformungen erstreckt. Das Anliegen der Abhandlung ist die mathematische Erfassung der mechanischen Erscheinung der zusammengesetzten Torsion für die Ingenieurpraxis, weiters die Anwendung der mitgeteilten Formeln im Rahmen eines numerischen Beispiels. Ausser den bekannten Verfahren (WANNSLEBEN, URBAN, usw.) weist der Verfasser auch auf die Bedeutung der sekundären Schubverformungen hin.

Состояние нагрузки тонкостенных балок закрытого профиля. В данной работе теория тонкостенных балок закрытого профиля распространяется для специальных случаев чистого, коробляющегося — и искажающего кручения при учете воздействия деформаций среза. Работой ставится цель математической формулировки механических явлений комбинированного кручения для инженерной практики, далее демонстрация сообщенных формул в рамках числовых примеров. В работе сверх наиболее известных методик (Ванслебен, Урбан и т. д.) указывается также на значение вторичных деформаций среза.

EXAMINATION OF THE BUILD UP CHARACTERISTICS OF HIGH-PRESSURE WALL-STABILIZED DISCHARGES

I. BOLLA*—I. CSÁNYI**

The physical and chemical phenomena during the build-up period of high-pressure gas discharge systems with $Hg : TlI : DyI_3$ additives were investigated by simultaneously measuring the terminal voltage and the spectral characteristics of the discharge. The influence of each additive on the electrical characteristics during the evaporation processes, which are parallel to the build-up of the dicharge tube wall temperature, was determined. The results were evaluated from the point of view of the energy dissipation phenomena — ionization/recombination, photoemission/absorption, dissociation — in the discharge.

1. Introduction

It is well known that in the high-pressure wall-stabilized discharge light sources the working medium is formed by mercury and by various metals (Na, Tl, In, Dy, Sc, Th etc.) introduced in the form of metal haloids (generally iodide). The partial pressures and concentrations are basically determined by the temperature distribution of the discharge tube. Under normal operating conditions — depending on the geometry of the discharge tube and the electrical input power — the temperature of the tube wall varies between 400 and 750 °C and thus the total pressure of the metal vapours introduced into the system may change from 1 to 5 atm, depending on quantity of the additions.

It is known furthermore that in the mentioned pressure range and at the temperature of $2 \ldots 5 \times 10^3$ K the main characteristics of the plasma: the electron temperature T_e, the electron concentration n_e, the ion concentration n_i etc. can be determined on the base of the model assuming Local Thermodynamical Equilibrium (LTE). This theme has at present a vast literature, and embraces the widely varied fields of application of the collision-dominated plasmas [1, 2, 3].

But a completely new approach is required by the description and interpretation of the phenomena occuring in the build up period which follows the breakdown in the wall-stabilized discharges. In this transient range the

* I. Bolla, Korvin O. u. 47, H-1036 Budapest, Hungary.
** I. Csányi Felszabadulás u. 60, H-2120 Dunakeszi, Hungary.

concentration of the metal iodides and Hg evaporated in the argon ignition gas of about $10 \div 30$ Torr pressure increases continuously, due to the increasing wall temperature, which is a direct reason for the power dissipation by the argon discharge.

In this transient state of the discharge system, not the knowledge of the concentration and temperature distribution functions are important, which determine the spectral characteristics — in the absence of equilibrium state such functions cannot be defined — but the energy dissipation phenomena, which in the first line influence the electric characteristics of the discharge.

That is, if during the stabilization period of the discharge the ionization, excitation, dissociation, and heat conduction losses exceed a critical value, the terminal voltage of the discharge suddenly jumps up and the discharge drops out.

Therefore in the build up characteristics of the terminal voltage of the wall-stabilized discharges an important role can be assigned to the definitions of the various intervals — the elucidation of basic interaction during the characteristic periods.

2. Basic phenomena during the build up period of the wall-stabilized metal vapour discharges

As it is known, in the high-pressure wall-stabilized metal vapour discharges, besides the quantity of additions introduced into the quartz tube, the wall temperature determines the density of the plasma. After the breakdown phenomena (ca. 10^{-1} sec), by the action of the heat dissipated by the arc discharge in the ignition gas, this temperature rises from ambient to $400-750$ °C. Because of the increase of the metal vapour concentration in the ca. 10 Torr argon and the metal vapour, mixture gradually diminishes the mean free path of the energizing electrons λ_e and thus the mean energy $\bar{\varepsilon}$ assumed cy the electrons for a given field strength $\bar{E}$, needed for maintaining an adequate degree of ionization in the positive column, must be increased.

Inasmuch as the field strengths in the cathode and anode spaces are determined by other methods [4], the evaporation and energy dissipation phenomena during the build up period can directly be followed through the terminal voltage of the discharge.

The most simple form of the build up characteristics $\bar{U}(t)$ of the wall-stabilized discharges is provided by the so-called single component systems, such as mercury vapour discharges, where the increase of the field intensity of the positive column and therefore of the terminal voltage of the system is determined by the concentration of the evaporating mercury vapour [2, 4]. The typical form of the characteristic $\bar{U}(t)$ is shown in Fig. 1.

Taking into account that the terminal voltage and thus the field strength of the positive column is a function of the concentration of the Hg atoms in the first line, the characteristic presented in Fig. 1. is relatively simple to interpret:

— in the interval AB due to the Townsend avalanche phenomena, first a glow and then an arc discharge develops; the conductivity of the positive column (~ 10 Torr Ar $+ \sim 10^{-3}$ Torr Hg) is very high, the terminal voltage is approximately the sum of anode and cathode drops;
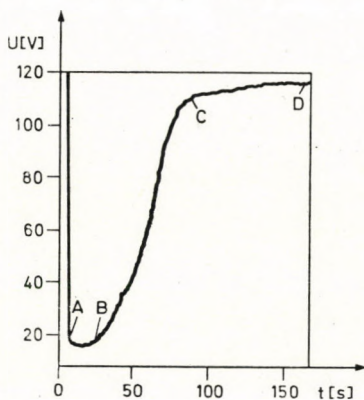
Fig. 1. Typical build up characteristic of Hg vapour discharge

— in the interval BC raises the wall temperature continuously due to the dissipated heat quantity Q, by the Ar-discharge increases the concentration of Hg, decreases the mean free paths λ_e and increases the field strength $\bar{E}$;
— in point C the total quantity of Hg evaporates, the system gets in the state of an unsaturated vapour and a further increase of wall temperature and plasma temperature results only in a pressure rise of

$$p_{H_g} \sim kT$$

— in point D the system reaches its normal state — it reaches local thermodynamical equilibrium (LTE) [2], and the mean value of the field strength by time and radius $\bar{\bar{E}}$ can be calculated by the following relation deduced on the base of the LTE-assumptions [5]:

$$\bar{E}_z = C \frac{P^{1/2}}{P(P - P_v/V_i) \cdot 4\bar{V}} \cdot \frac{m^{(V_i/4V)+1/4}}{d^{3/2}} \qquad (1)$$

where

$P = \bar{E}_z I$ is the input electrical power — the product of the axial component of field strength and discharge current,

$P_v = $ thermal conduction loss,

$V_i = $ the ionization potential of the Hg atoms,

$V = $ the mean excitation potential of the Hg atoms,

$d = $ the length of the positive column,

$C = $ a constant depending on the conditions of discharge.

Far more complicated is the interpretation of the bild up characteristics with the so-called multicomponents systems, where in addition to the evaporation phenomena of individual components (which in themselves cause very complicated changes of conductivity because of arc contraction and broadening phenomena) an important role is played by the various dissociation phenomena and by the elctron capture phenomena of the electronegative gases (e.g. iodine).

Subsequently the build up characteristics $U(t)$ of such multicomponent systems and the characteristic points occurring with the various additions are dealt with, thus permitting a better understanding of transient phenomena which cannot be described within the frame of the LTE model and so far not treated in literature.

3. Examination of the voltage build up characteristics of the multicomponent discharge systems

3.1. Measuring method

The characteristics $\bar{U}(t)$ of the above mentioned multicomponent wall-stabilized discharges have been examined in the first line with including systems TlI-, DyI$_3$- and Hg-additions which are important in the field of light generation.

For the investigation 23 mm dia. quartz discharge tubes with Th-activated tungsten electrodes, 50 mm electrode distance, 20 Torr argon starting gas and suitable additions were used. For reducing heat losses they were enveloped in vacuum bulbs. These outer bulbs were each provided with a quartz window for absorption-free measuring of the UV radiation of the discharge.

For the current limitation of the discharge an $L = 100$ mH coil served and in the circuit a 0,5 Ω resistor was inserted in series for measuring the current in the dischaige tube. The variation within one half period of the voltage-current characteristic $\tilde{U}_s(t)$ was measured with an oscilloscope (Fig. 2b), the changes of the $\bar{U}(t)$ characteristic in the section BD were recorded by an instrument equally suitable for measuring of the peak and effective voltages. The circuit diagram of the discharge tube operated with an alternating voltage is shown in Fig. 2a.

In order to elucidate the mutual influences in the discharge, as a first step, simultaneously with the voltage characteristic $\bar{U}(t)$ the relative intensities of the spectrum lines emitted by the atoms of the additive metals were recorded with an UM-2 type monochromator. According to earlier meas-

$R_1 = 0.5 \ \Omega$
$P_1 = 100 \ k\Omega$
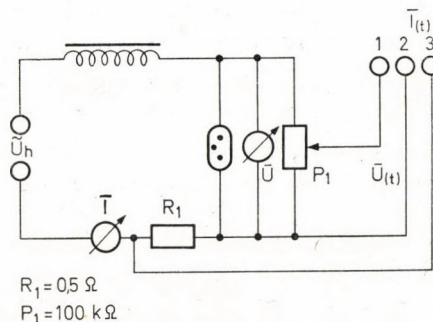
Fig. 2a. Electrical scheme of the discharge tube
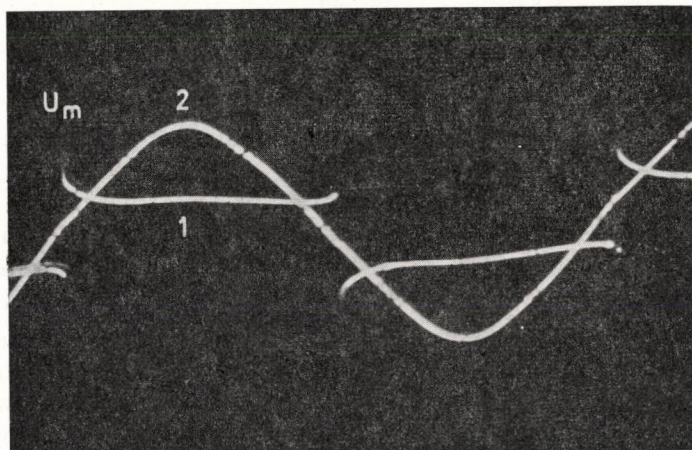
Fig. 2b. The voltage-current characteristic $\bar{U}(t) - \bar{I}(t)$ of the a.c. wall-stabilized discharge

urements in the initial period of the pressure build-up of the additives the plasma behaved optically, from the point of view of the emitted spectrum lines, as a plasma thin layer. Hence, as a first approximation it can be assumed that the increase of intensity is proportionate to the increase of concentration.

It is to be remarked that the fully exact discussion would require the function $T_f(t, z, \varphi)$ when analyzing the build up characteristics, i.e. the knowledge of the wall temperature distribution, but under operational conditions there is no possibility for determining it.

The measurements have shown that the build up characteristic $\overline{U}(t)$ shows typical breaking points at those times t_i when the increase of intensity of the spectrum lines emitted by the various metals has started or has passed into saturation.

Since the monochromator measurements have not explained some typical intervals of the characteristic, in the second part of the examinations on the typical points of the characteristis $\overline{U}(t)$ the complete spectrum of the discharge was recorded with a PGS-2 spectrographs in the range 2300 ... ... 6500 Å, in order to clarify the effects which are presumably due to molecular phenomena. The voltage-current characteristic $\widetilde{U}_s(t) - \widetilde{I}_s(t)$ was recorded with a two-beam oscilloscope (Fig. 2b). The arrangement of the spectral measurement is shown in Fig. 3.
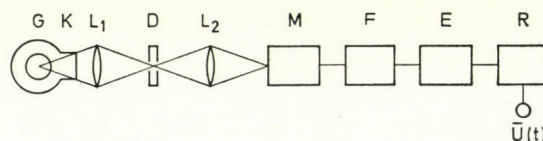
Fig. 3. Arrangement of the spectrographic measurements: G Gas discharge tube with outer bulb; M Monochromator; K Quartz window; F Photoelectronmultiplier; L_1 Lens $f_1 = 150$ mm; E Amplifier; D Diaphragm; R Recorder; L_2 Lens $f_2 = 75$ mm

3.2. *Measurements in multi-component discharge systems*

During the first step the investigations were carried out in a discharge system consisting of Hg, DyI_3, TlI, Ar, and the $\overline{U}(t)$ voltage characteristic was measured, as well as the intensities of the discrete spectral lines emitted by the atoms of various metal additives evaporating into the discharge (Hg, Dy, Tl). The relative intensities $I_i(t)$ of the spectral lines belonging to the transitions Hg $7^3S_1 - 6^3P_1$, $7^3S_1 - 6^3P_2$, $7^3S_1 - 6^3P_0$, Tl $7^2S_{1/2} - 6^2P_{3/2}$, $9^2P_{1/2} - 7^2S_{1/2}$ were determined as a function of time. For Dy only the absolute values of the energy levels belonging to the given line are indicated, because the electron configuration of the rare earth metals is only partly known. So in the given case the data for energies above 15 000 cm^{-1} are lacking [6]; the intensities of the spectral lines belonging to the energy transitions 23 736 cm^{-1}—0, 27 837—4134 cm^{-1} and 30 778—7050 cm^{-1} were measured. As an example the intensity changes, as functions of time, of the 436 nm mercury line (Fig. 4), the 535 nm line belonging to the transition Tl $7^2S_{2/2} - 6^2P_{3/2}$ (Fig. 5), and of the double line of Dy 421,12—421,32 nm (Fig. 6) (lower enveloping curves) are shown. The upper envelopes of the three figures show the build up characteristic $\overline{U}(t)$. It is to be remarked here that in the Dy spectrum the lines are so close to each other that the monochromator used was unable to separate the above mentioned line pairs.

The characteristics presented show that on the $\bar{U}(t)$ voltage graph until the equilibrium (LTE) five typical ranges can be distinguished (Fig. 4).

I. As the partial pressure of the iodides of the additions is negligible at room temperature, the discharge takes place in a Penning mixture of ca. 20 Torr argon and 10^{-3} Torr mercury, and the 20 V terminal voltage measured after the build-up of the arc is the sum of the anode and the cathode drops. This can also be seen on Fig. 7, where the $\bar{U}(t_1)$ terminal voltage is shown for 20 °C wall temperature and for various electrode distances.
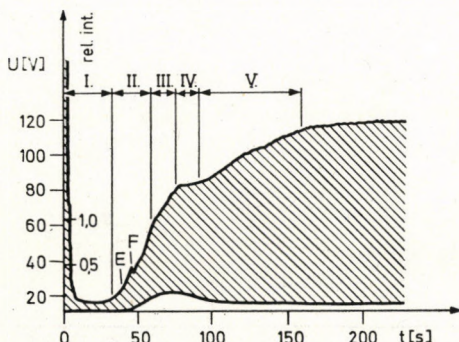
Fig. 4. Build up characteristic of the effective voltage $\bar{U}(t)$ and of the Hg 4358,3 Å wavelength lines, as functions of time: 1 — voltage characteristic; 2 — line intensity
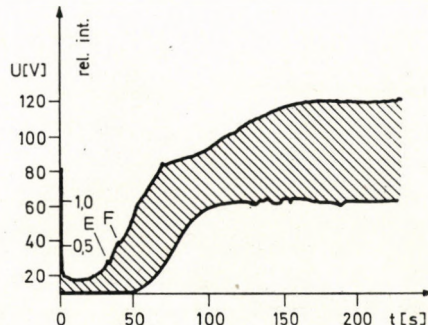
Fig. 5. Build up characteristic of the effective voltage $\bar{U}(t)$ and of the Tl 5350,46 Å wavelength line, as functions of time: 1 — voltage characteristic; 2 — line intensity

II. In the second interval begins the evaporation of the Hg into the discharge arc — this is proved by the rapid intensity increase of the Hg lines. In the sensibility range of our measurement equipment neither the Tl, nor the Dy lines appear with measurable intensity, therefore the voltage rise is caused by the increase of the n_{Hg} mercury vapour concentration. The input energy is used to cover the heat conduction losses and, above that, for covering the excitation and ionization of the Hg atoms.

III. As a consequence of the gradual increase of the wall temperature (at ~ 300 °C) begins the evaporation of the TlI into the system, but at the same time the Hg concentration further increases. For a time the voltage rise is moderated, the rise of the intensity curve of the Hg lines is reduced. This is the consequence of the cross sections being changed by the influence of the low mean excitation and ionization potential (6,3 eV) of Tl.

IV. In the initial period of this range parallel with the increasing wall temperature, as a consequence of evaporating phenomen the n_{Hg} final concentration is attained, n_{τ_1} gets into the saturation range and at the same time starts the rise of the n_{Dy} concentration (approx. from $450-500$ °C).

V. The further increase of the voltage can be ascribed to the complete vapourization of DyI_3 and to the radiation losses appearing therein. It lasts until the equilibrium state is reached.

The rise of the spectral lines emitted by the atoms of the various additives well explains qualitatively every distinctive point of the voltage characteristic $\overline{U}(t)$, except the point F marked on Figs 4, 5, 6. It is quite likely that this point is due to the participation in the cycle of the iodine compounds of the Zr, introduced into the tube as a getter material. Similarly the monochromator investigations did not explain the action of the electronegative gases, such as iodine, on the build up characteristics.
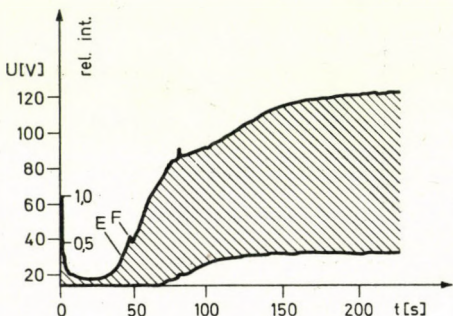
Fig. 6. Build up characteristic of the effective voltage $\overline{U}(t)$ and of the Dy 4211,2—4213,2 wavelength line group, as functions of time: 1 — voltage characteristic; 2 — line intensity
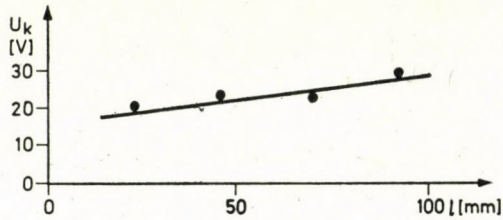
Fig. 7. Dependence of the terminal voltage of the discharge on electrode distance at 20 °C wall temperature

For a further investigation of the mentioned problems spectral photographs of 5 sec exposure time were taken with a PGS-2 spectrograph suitable for separating the Zr lines in the surroundings of point F. On the inlet slit of the spectrograph the central part of the positive discharge column was projected with the slit normal to the axis of the discharge. As an example, a part of the spectrum situated in the 4226···4242 Å range is shown in Fig. 8, together with the Fe spectrum used for calibration.

The spectrograms show that in the vicinity of point E (Fig. 4) no lines of any metallic component appear beside the atomic lines of the Hg. But in the surroundings of point F already the atomic lines of Zr dominate and also an intensive continuous radiation appears which is due to the electronaffinity effects of the iodine atoms.

At a relatively low wall temperature (100—150 °C) intensively starts the evaporation of the ZrI_4 into the arc where it dissociates into metallic Zr and atomic iodine, i.e.

$$ZrI_4 \Rightarrow Zr + 4I . \tag{2}$$

The electronegative iodine atoms emit a continuous radiation during the electron capture and the transition into the basic energy state corresponding to the new electron configuration [7], the wavelength of which depends on
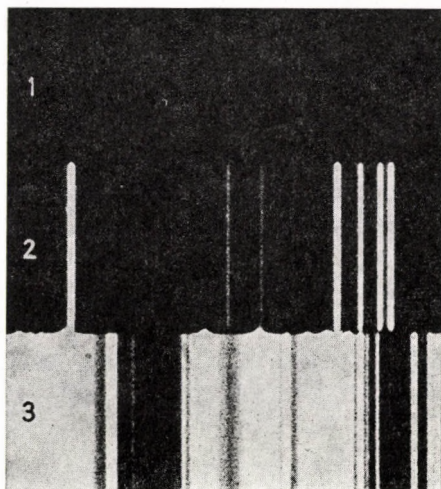
Fig. 8. Recorded spectrum in the range 4243 Å—4226 Å: 1 — Spectrum of the discharge in the surroundings of the characteristic point E; 2 — Zr lines recorded in the surroundings of point F; 3 — Spectrum of the Fe calibration arc
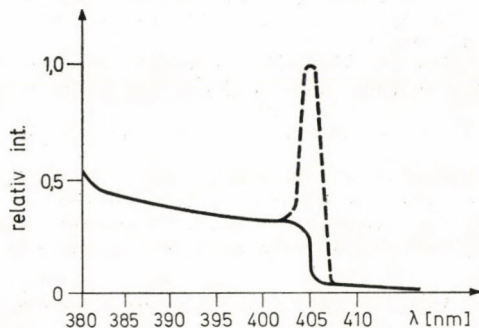
Fig. 9. The electron affinity continuum of the $J(^2P_{3/2})$ atoms. — — — — — 4046,5 Å line of Hg

the kinetic energy of the captured electron. Its wavelength threshold is given by

$$e(v = 0) + I(^2P_{3/2}) = I^-(^1S_0) + \frac{hc}{\lambda_k} \tag{3}$$

where

$hc/\lambda_k =$ the electron affinity energy of the

$I(^2P_{3/2})$ atom = 3,06 eV .

The wavelength determined by (3) is therefore $\lambda_k = 4048$ Å. From this threshold value the continuous spectrum stretches towards the shorter wavelengths, depending on the value of the electron energy. In the investigated discharge system of the spectra, recorded in the point F of the characteristic $\overline{U}(t)$, (Fig. 9) the affinity continuum can be quite well identified. Thus, the jump of the characteristic in F is due to the ZrI_4 dissociation phenomena and can be attributed to the effects of the electron capture on the free iodine.

It is to be remarked that in a.c. wall-stabilized discharges the role of the electronegative gases in the build up period as well as in the equilibrium state is of basic importance. In the build up period it is the iodine in the first line that determines the re-ignition characteristics of the discharge, while in the equilibrium state it is of basic importance for particle transport. In the future the intention is to study the influence of the iodine on the re-ignition peak characteristic $U(t)$ and through this on the frequent arc instability problems following the break down.

Acknowledgements

REFERENCES

1. GRIEM, H. R.: Plasma Spectroscopy, McGraw-Hill Book, New-York 1964
2. WAYMOUTH, J. F.: Electric Discharge Lamps, M.I.T. Press, London 1971
3. ROMPE, R.–STEENBECK, M.: Ergebnisse der Plasmaphysik und der Gaselektronik, Akademie Verlag, Berlin 1967
4. BITÓ, J. F.: Az oxidkatódos kisülések katódoldali jelenségeiről, Kandidátusi értekezés (On the cathode side phenomena of oxyde-cathode discharges, Thesis for Candidate degree), 1966
5. ELENBAAS, W.: High Pressure Mercury Vapour Lamps, N. V. Philips Eindhoven 1965, p. 149
6. CONWAY, J. G.–WARDEN, E. F.: Preliminary Level Analysis of the First and Second Spectra of Dysprosium, DyI and DyII, *J. of the Opt. Soc. of Am.*, **61**, (1974) 704.
7. NEIGER, M.: Quantitative Investigations on the Radiation of the Negative Iodine Ion, 11*th Int. Conf. on Phenomena in Ionized Gases*, Prague 1973, p. 410

Untersuchung der Anlaufcharakteristik von wandstabilisierten Hochdruckentladungen. — Die physikalischen und chemischen Vorgänge während der Anlaufperiode von Hochdruckgasentladungsystemen mit Hg: TlI : DyI$_3$ Zusätzen wurden durch gleichzeitige Messung der Klemmenspannung der Entladung und ihrer spektralen Charakteristiken untersucht. Der Einfluß der einzelnen Zusätze auf die elektrischen Charakteristiken im Verlauf der zum Anlauf der Wandtemperatur der Versuchsröhre parallelen Eindämpfungsvorgänge wurde bestimmt. Die Ergebnisse wurden vom Standpunkt der Energiedissipationsvorgänge in der Entladung — Ionisation, Rekombination, Fotonemission/Absorption, Dissipation — ausgewertet.

Исследование характеристики нарастания разрядов высоких довлениях. Исследованы физические и химические процессы, происходящие на этапах нарастания. газоразрядных систем при высоких давлениях с добавками Hg : TlI : DyI$_3$. при одновременном измерении напряжения на зажиме разряда и спектральных характеристик разряда. Определено воздействие добавок на электрические характеристики во время процессов выпарки, параллельных нарастанию температуры стенки разрядной трубки. Полученные результаты оценены с точки зрения процессов рассева энергии, возникающей при разряде, а именно процессов ионизации (рекомбинации, фотонной эмиссии), абсорбции, рассева.

DETERMINATION OF THE PIRN SHAPE

B. GREGA*

CAND. OF TECH. SCI.

On the basis of mathematical considerations the author gives a solution for the determination of the pirn shape by the use of which weft breakages due to variations in yarn force can be considerably reduced. It is shown that the meridian section of the initial surface of such a pirn has always the form of a hyperbola.

Weaving efficiency is considerably influenced by machine stops, i.e. by the number of breakages occurring in the weft yarn. Yarn breakages, in addition to reducing production, also impair the quality of the fabric produced. In modern large scale production when using similar material, yarn counts, furthermore temperature and relative humidity, the number of weft yarn breakages exponentially increases with higher machine speeds. Thus, it appears advisable to so choose the shape of pirns as to reduce the number of weft breakages, i.e. machine speed is to be increased only up to that measure at which the number of yarn breakages can be kept within reasonable limits.

In the following a method for determining the pirn shape is described, by which a considerable decrease in weft yarn breakages can be achieved.

In yarns, winding-off from the pirn with a constant velocity v a tensioning force arises. Let p be the yarn force depending on the momentary place of the winding-off process. On the one hand, the force p is due to the unbending of the yarn, winding-off from the pirn, on the other hand, it arises in balloon formation as a counterbalance of the centrifugal force, furthermore, in overcoming the yarn weight, and in eliminating the friction and medium resistance during winding-off.

Thus, the force p depends partly on the curvature of the yarn, partly on the distance of the momentary winding-off point, measured from the guide eye, i.e.

$$p = p(g, m - x) = p(g, \xi),$$

where

$$\xi = m - x$$

* B. GREGA, Németvölgyi út 22, H-1126 Budapest, Hungary

and x is the abscissa of the momentary running point,
       g —   the curvature of the yarn at the running point, and
       m —   the distance measured from the base of the pirn covered by yarn, to the place
                 of the guide eye (Fig. 1.)

   In order to be able to establish the variation in the tensioning force
during processing, let us expand in Taylor series the function with the two
independent variables $p(g, m-x) = p(g, \xi)$ for a place in the surrounding of
$(g, m-x) = (g, \xi)$.
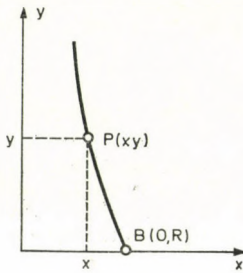
Fig. 1

   The index 0 expresses the initial point of the expansion in series, is the
point $(g, m-x) = (g, \xi)$. For small variations of the curvature g and for that
of the distance x, the second and higher order terms of the series can be ignored
and, thus,

$$p(g, m - x) = p(g, \xi) \approx p_0 + \frac{1}{1!} \left\{ \left(\frac{\partial p}{\partial g} \right)_0 dg + \left(\frac{\partial p}{\partial \xi} \right)_0 dx \right\} ,$$

i.e. briefly

$$p = p_0 + \left(\frac{\partial p}{\partial g} \right)_0 dg + \left(\frac{\partial p}{\partial \xi} \right)_0 d\xi ,$$

$$p = p_0 + \left(\frac{\partial p}{\partial g} \right)_0 dg + \left(\frac{\partial p}{\partial x} \right)_0 \frac{dx}{d\xi} d\xi .$$

Since $x = m - \xi$ and $dx/d\xi = -1$, i.e. $d\xi = -dx$, therefore, the variation of
the tensioning force

$$p - p_0 = dp = \left(\frac{\partial p}{\partial g} \right)_0 dg + \left(\frac{\partial p}{\partial x} \right)_0 (-1)(-dx) = \left(\frac{\partial p}{\partial g} \right)_0 dg + \left(\frac{\partial p}{\partial x} \right)_0 dx .$$

Introducing for the the partial differential quotients $(\partial p/\partial g)_0$ and $(\partial p/\partial x)_0$ the
following notations

$$\left(\frac{\partial p}{\partial g} \right)_0 = \varkappa$$

and

$$\left(\frac{\partial p}{\partial x} \right)_0 = \lambda ,$$

the variation of the tensioning force is given by the expression

$$dp = \varkappa dg + \lambda dx .$$

Let $\varkappa$ be the factor of the change in the curvature, and
λ the factor of the change in the distance.
The method for determining the factors $\varkappa$ and λ is as follows.

Experimental determination of the factor $\varkappa = \partial p/\partial g$

Let the yarn be wound-on to a cylinder with radius r, covered by yarn and consider the section s of the unbending yarn. Let P be the smallest force just to straighten the considered yarn section. Even if the yarn is straightened by some other force and owing to some other reason, the same yarn force will arise in the yarn. Now, be the yarn wound-on to a cylinder with different radius r' covered by yarn, and be the force P' just high enough to straighten the chosen yarn section s'.

For calculating the differential quotient $\varkappa = \partial p/\partial g$ let us determine the tensioning forces p_1 and p_1' falling on the unit length. Since

$$p_1 = \frac{P}{s}$$

and

$$p_1' = \frac{P'}{s'} ,$$

therefore, the change in the tensioning force for the unit length is

$$\Delta p = p_1' - p_1 .$$

For the determination of the differential quotient, also the change in the curvature has to be established. The curvature of the circle with radius r

$$g = \frac{1}{r} ,$$

while that of the circle with radius r'

$$g' = \frac{1}{r'} .$$

The change in the curvature

$$\Delta g = g' - g = \frac{1}{r'} - \frac{1}{r} .$$

Be its approximation value considered as sufficient, then use can be made of the differential quotient $\Delta p/\Delta g$.

Thus, in that case

$$\frac{\partial p}{\partial g} \approx \frac{\Delta p}{\Delta g} = \frac{p_1' - p_1}{\dfrac{1}{r'} - \dfrac{1}{r}} \;.$$

We shall show that in the instant $\Delta g \to 0$ the exact value of $\varkappa$ is given by the limit value of the differential quotient. In that case

$$\varkappa = \frac{\partial p}{\partial g} = \lim_{\Delta g \to 0} \frac{\Delta p}{\Delta g} = \lim_{\Delta g \to 0} \frac{p_1' - p_1}{\dfrac{1}{r'} - \dfrac{1}{r}} = \frac{dp}{-\dfrac{dr}{r^2}} = -r^2 \frac{dp}{dr} \;.$$

Namely, in the nominator

$$\lim_{\Delta g \to 0} \left(\frac{1}{r'} - \frac{1}{r} \right) = \lim_{\Delta r \to 0} \left(\frac{1}{r + \Delta r} - \frac{1}{r} \right) = \lim_{\Delta r \to 0} \frac{r - (r + \Delta r)}{(r + \Delta r)} = \lim_{\Delta r \to 0} \frac{\Delta r}{r(r + \Delta r)} \;.$$

Since dr as compared to r is rather small, it can be neglected and thus

$$\lim_{\Delta g \to 0} \left(\frac{1}{r'} - \frac{1}{r} \right) \to -\frac{dr}{r^2} \;.$$

Thus, for determining $\varkappa$ experimentally, the following equation is obtained:

$$\varkappa = \left(-r^2 \frac{dp}{dr} \right)_0 \;.$$

For calculating the value of $\varkappa$ the original radius r, the change in the yarn force falling on the unit length dp and the changes in the radii have to be measured and from these measurable quantities the value of $\varkappa$ can be determined.

Experimental determination of the factor $\lambda = \partial p/\partial x$

The differential change in the yarn force corresponding to the differential movement dx of the yarn along its axis x is also to be determined (Fig. 2). For this purpose the yarn should be carried over a pulley and its end fixed to a dynamometer. The dynamometer has to be operated with the maximum speed v the highest speed the machine is able to attain. (The reason for applying maximum winding-off speed is to obtain such a corresponding value λ, at which the weft yarn cannot break.) The maximum yarn force corresponding to the movement of maximum velocity v of the dynamometer is registered

by the pointer of the dynamometer. This measurement is repeated for different values of x with winding yarn lengths of about $2 \div 3$ m at two places of the rotation surface and then winding these yarns off at a maximum velocity v. The quotient of the differential change in tension measured at the two neighbouring places p_2 and p_2', and the corresponding change in distance dx gives $\lambda = \partial p / \partial x$ (Fig. 3). However, it is essential also to know the value of λ for
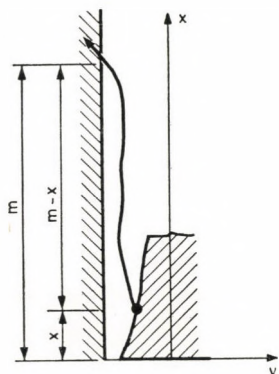
Fig. 2
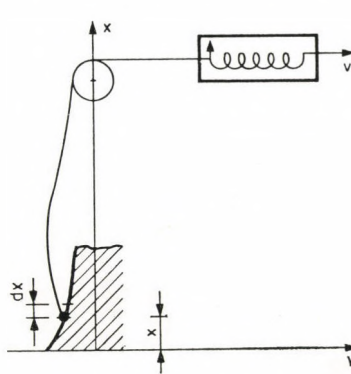
Fig. 3
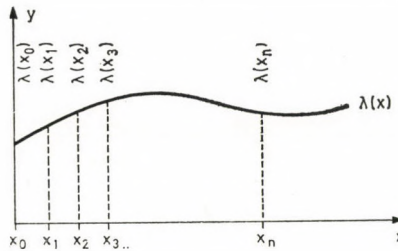
Fig. 4

different values of x, i.e. for the base and top of the pirn. By representing the values of λ corresponding to the different distances (x, λ) in a rectangular coordinate system, the function curve $\lambda(x)$ is obtained. In this way λ can be defined graphically as the variable function of x having the form

$$\lambda(x) = \lambda_0 + \lambda_1 x + \lambda_2 x^2 + \lambda_3 x^3 + \ldots$$

The unknown coefficients $\lambda_0, \lambda_1, \lambda_2 \ldots$ can be calculated by means of the corresponding and measured values of the abscissa and those of the ordinate (Fig. 4).

Let us now return to the consideration of the original equation in further detail. In succeeding to eliminate the variations in pulling caused by the yarn

force along the whole initial surface of the pirn, then no weft yarn breakages can occur. To be able to eliminate the pulling variations responsible for weft breakages along the initial surface of the pirn, the most favourable pirn shape has to be determined. To this effect we shall calculate the equation of the curve cut out from the end of the pirn by the plane passing through the axis of the pirn. The equation of the curve determines the optimum shape of the pirn.

The shape of the pirn will be correct if the yarn force p remains constant at any place and for the whole period of the winding-off process, i.e. if the change in the yarn force is zero everywhere, thus $dp = 0$. Is there no change in the yarn force, then the cause of yarn breakages is eliminated and a pirn of the described shape ensures trouble-free winding-off of the yarn.

However, when $dp = 0$, then the equation takes the form

$$\varkappa dg + \lambda(x)\, dx = 0 \ .$$

Since at the point of winding-off the curvature

$$g = \frac{1}{y} \, ,$$

therefore

$$dg = -\frac{dy}{y^2} \, ,$$

thus

$$-\varkappa \frac{dy}{y^2} + \lambda(x)\, dx = 0 \ .$$

This is a homogeneous, linear differential equation to be solved by the separation of the variables. Separating the variables

$$\varkappa \frac{dy}{y^2} = \lambda(x)\, dx$$

and integrating on both sides

$$\varkappa \int \frac{dy}{y^2} = \int \lambda(x)\, dx \ ,$$

thus

$$-\varkappa \frac{1}{y} = \int \lambda(x)\, dx + C \ .$$

The general solution of the differential equation takes the form

$$y = \frac{\varkappa}{\int^x \lambda(x) dx + C} \ .$$

The integration constant C is to be determined from the initial condition. According to the initial condition at $x = 0$ $y = R$, thus the equations

$$R = - \frac{\varkappa}{\int^0 \lambda(x)\, dx + C} \, ,$$

and

$$C = - \frac{\varkappa}{R} - \int^0 \lambda(x)\, dx \, .$$

The required particular solution of the differential equation is thus as follows:

$$y = - \frac{\varkappa}{\int^x \lambda(x)\, dx - \int^0 \lambda(x)\, dx - \dfrac{\varkappa}{R}} = - \frac{\varkappa}{\int^x \lambda(x)\, dx - \dfrac{\varkappa}{R}} \, .$$

i.e.

$$y = \frac{\varkappa}{\dfrac{\varkappa}{R} - \displaystyle\int_0^x \lambda(x)\, dx} \, .$$

Hence, the solution of the differential equations leads to an equation of a (higher order) hyperbola. This means that the elimination of weft breakages requires the use of a pirn of the form of a (higher order) hyperboloide of revolution of one sheet.

Approaching the function $\lambda(x)$ on the basis of the diagram by a higher order parabola

$$\lambda(x) = \lambda_0 + \lambda_1 x + \lambda_2 x^2 + \lambda_3 x^3 + \ldots$$

and closing the expansion in series after the linear term, we obtain

$$\lambda(x) \approx \lambda_0 + \lambda_1 x \, .$$

Using this latter expression of the function $\lambda(x)$ in the solution of the differential equation, we arrive at the solution

$$y = \frac{\varkappa}{\dfrac{\varkappa}{R} - \displaystyle\int_0^x (\lambda_0 + \lambda_1 x)\, dx} = \frac{\varkappa}{\dfrac{\varkappa}{R} - \lambda_0 x - \dfrac{\lambda_1}{2} x^2} \, .$$

Retaining but the linear term, in the nominator the solution takes the form

$$y \approx \frac{\varkappa}{\dfrac{\varkappa}{R} - \lambda_0 x} \, .$$

Accordingly, for achieving the correct shape of the pirn it is sufficient to determine the value of λ measured at the point x_0, i.e. at the initial point of the revolution surface. By retaining also the second order term of the nominator, a (higher order) hyperboloide of revolution of one sheet is obtained, the shape of which hardly differs from the surface containing only a linear term in the nominator.

In practice it is expedient to develop the initial surface of the pirn in the form of a hyperboloide of revolution, from which the yarn coils do not slip-off. In accordance with this requirement, let us take the measurements of the base and cover circles of the old initial cone, furthermore the previous height of the initial surface. In this way, the new initial surface of the pirn can be established without experimentally determining the values of $\varkappa$ and λ.

Let R be the base radius of the frustrated cone, r the radius of its cover circle and m its length. Since $A(m, r)$ is a point of the meridian of the revolution surface, its coordinates satisfy the equation of the curve, hence

$$r = \frac{\varkappa}{\dfrac{\varkappa}{R} - \lambda_0 x} \, .$$

Dividing by $\varkappa$ the numerator and the nominator of the fraction, we obtain

$$r = \frac{1}{\dfrac{1}{R} - \dfrac{\lambda_0}{\varkappa} m} \, .$$

From the latter equation

$$\frac{1}{r} = \frac{1}{R} - \frac{\lambda_0}{\varkappa} m$$

or,

$$\frac{\lambda_0}{\varkappa} m = \frac{1}{R} - \frac{1}{r}$$

and

$$\frac{\lambda_0}{\varkappa} = \frac{\dfrac{1}{R} - \dfrac{1}{r}}{m} \, .$$

Substituting the value of $\lambda_0/\varkappa$ into the equation of the meridian hyperbola, we have

$$y = \frac{\varkappa}{\dfrac{\varkappa}{R} - \lambda_0 x} = \frac{1}{\dfrac{1}{R} - \dfrac{\lambda_0}{\varkappa} x} = \frac{1}{\dfrac{1}{R} - \dfrac{(1/R) - (1/r)}{m} x} =$$

$$= \frac{1}{\dfrac{(1/r) - (1/R)}{m} x + \dfrac{1}{R}} = \frac{1}{\dfrac{R - r}{m \cdot r \cdot R} + \dfrac{1}{R}} \, .$$

By multiplying by $m \cdot r \cdot R$ the numerator and nominator of the fraction on the right side is

$$y = \frac{m \cdot r \cdot R}{(R - r) x + mr} .$$

From the equation obtained, the meridian hyperbola of the initial surface can be constructed (Fig. 5).
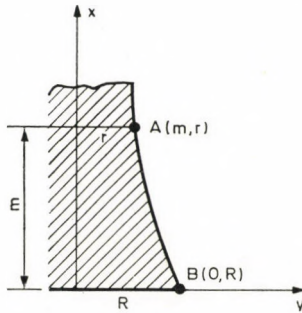
Fig. 5

The simplest way of constructing the meridian hyperbola is to transform the equation to an isosceles hyperbola taking the form

$$y_1 = \frac{c}{x_1} .$$

The initial point of the coordinate system, $O(u_1, v_1)$ be in the centre of the hyperbola. Are x and y the coordinates of a running point of the curve with respect to the axes of the old system, furthermore x_1 and y_1 the coordinates of the same point with respect to the new axes, then between the old and new coordinates the following relations exist

$$x = x_1 + u_1 ,$$
$$y = y_1 + v_1 .$$

By substituting these values of x and y into the equation of the hyperbola, the curve is transformed to the new coordinate system, Thus, the transformed equation can be written as

$$y_1 + v_1 = \frac{m \cdot r \cdot R}{(R - r)(x_1 + u_1) + mr} = \frac{m \cdot r \cdot R}{(R - r) x_1 + (R - r) u_1 + mr} .$$

As the values u_1 and v_1 can temporarily be arbitrary ones, the value of u_1 is to be chosen so as to obtain

$$(R - r)\ u_1 + mr = 0\ .$$

However, this is only then the case, if

$$u_1 = -\frac{m \cdot r}{R - r} = \frac{m \cdot r}{r - R}\ .$$

As for the equation

$$y_1 + v_1 = \frac{m \cdot r \cdot R}{(R - r)\ x_1} = \frac{c}{x_1}$$

where

$$c = \frac{m \cdot r}{R - r}\ R = -\ u_1 \cdot R\ .$$

In order to obtain the equation in the form $y_1 = c/x$ the similarly arbitrary value of v_1 is to be chosen, so as to get $v_1 = 0$, and then we arrive indeed at an isosceles meridian hyperbola

$$y_1 = \frac{c}{x_1}\ .$$

The equations of the straight lines

$$u_1 = \frac{m \cdot r}{R - r}$$

and

$$v_1 = 0$$

are at the same time the end tangents of the transformed hyperbola

$$y_1 = \frac{c}{x_1}\ \ .$$

For constructing the curve $y_1 = c/x_1$ also the half length of the real axis has to be determined. The end point c of the real axis lies on the hyperbola, hence for the new coordinate axes the equation

$$x_1^2 = c$$

is valid. On the other hand, denoting by a_t the half length of the real axis,

$$a_t^2 = 2x_1^2 = 2c\ ,$$

whence

$$a_t = \sqrt{2|c|} = \sqrt{2\left|\frac{m \cdot r}{R - r} \cdot R\right|} \quad .$$

After having calculated the coordinates of the center of the hyperbola and by that the equation of the end tangents, furthermore the half length
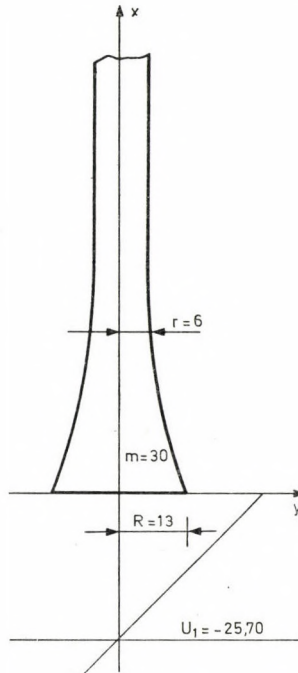
Fig. 6

of the real axis, the meridian curve can be constructed. By that also the form of the pirn end as a hyperboloide of revolution is completely determined.

In the following example the determination of the pirn shape is described.

Be
$$r = 6 \text{ mm}, \ R = 13 \text{ mm}, \ m = 30 \text{ mm}.$$
Since

$$y = \frac{m \cdot r \cdot R}{(R - r)x + m \cdot r},$$

hence the equation of the curve

$$y = \frac{30 \cdot 6 \cdot 13}{7x + 30 \cdot 6} = \frac{2340}{7x + 180} \ .$$

The equation of the end tangents

$$u_1 = \frac{m \cdot r}{r - R}$$

and

$$v_1 = 0$$

Thus,

$$u_1 = -\frac{180}{7} = -25{,}70\,,$$

$$v_1 = 0.$$

The half of the real axis

$$a_t = \sqrt{2\left|\frac{m \cdot r}{R - r} \cdot R\right|}\,,$$

$$a_t = \sqrt{2 \cdot \frac{180}{7} \cdot 13} = \sqrt{\frac{4680}{7}} \approx 25{,}85\,.$$

The manner of constructing the pirn end is represented in Fig. 6.

REFERENCES

1. STEIN, W.—HOBE, I.: *Textil Praxis* (1969) 2
2. STEPANOW, G. V.: *Text. Prom.* (1973) 2
3. GREGA, B.: *Periodica Polytechnica*, 1 (1973) No. 2.

Bestimmung der Form von Webspulen. — Aufgrund von mathematischen Überlegungen gibt der Verfasser eine Lösung für eine Form der Schußspulen bekannt, welche die durch Fadenkraftschwankungen verursachten Kettenrisse weitgehend verringert. Er zeigt, daß der Meridianschnitt der Anfangsoberfläche einer solchen Schußspule immer eine Hyperbel ist.

Определение формы ткацкого початка. Автор на основе математического соображения дает решение определения такой формы ткацкого початка, которая в большой мере уменьшает разрыв утка, который происходит от колебания усилия нити. В работе показано, что в случае такого початка утка разрез по меридиане начальной поверхности всегда является гиперболой.

ANALYSIS OF AXISYMMETRICALLY DEFORMED SHELLS BY THE FINITE ELEMENT DISPLACEMENT METHOD

B. HERPAI* and I. PÁCZELT**

CAND. OF TECHN. SCI

The elements adopted follow the actual geometry of the shell. The minimum degree of freedom of the elements is 12. In concluding the calculation an opportunity offers for supervising at each element the degree of non-satisfaction of the equilibrium equations "a priori" non-satisfied. If the degree of non-satisfaction at each element is below a predetermined value, so the calculation can be considered to be accomplished. If not, by maintaining the subdivision and increasing the degree of freedom of the elements in question, with repeated calculations more exact results may be obtained. The efficiency of the procedure is well demonstrated by a number of numeric examples.

1. Introduction

The axisymmetrical shells are elements of structures having diversified functions, widely spread in the practice of mechanical engineering and architecture. In order to be able to precisely estimate the durability and reliability of the structures it is necessary to clearly understand the behaviour (displacement and state of stress) of the parts of constructions under the effect of load.

The strength analysis of axisymmetrical shells of a complicated construction, geometry and load conditions, represents a rather serious problem for the structural engineer. Even in applying the engineering shell theory, to be built up on Kirchhoff—Love's hypothesis used in the calculation of thin shells, notwithstanding the publication of a great number of works [1 to 7] which transformed the basic differential equation of the shell in different ways, producing exact solutions, one frequently meets in the engineering practice such geometrical, support and load conditions to the treatment of which the aforementioned "classic" methods are unsuitable.

Consequently different approximate methods applying also digital computers, have been developed [8 to 11]. Recently those procedures have been continuously increasing which approximate the fields to be found over a finite number of regions (finite element) with the aid of arbitrarily selected

* Dr. B. HERPAI Melinda u. 18, H-3530 Miskolc, Hungary
** Dr. I. PÁCZELT Győri Kapu 37, H-3531, Miskolc, Hungary

approximate functions. A part of the coefficients of the approximating series (in general, power series) are expressed by the finite number of points (nodal point, nodal circle) values, derivatives of the unknown functions. By fitting the fields above each element together (subregion), all the fields interpreted above, the whole region analysed may be produced.

The function values of unknown nodal points, their derivatives and the remaining part of the coefficients in approximating series, in a function associated with an error principle, (for example, method of the weighted residues, least error squares minimum principle, Bubnov—Galjorkin's method), with different principles of variation (for example, Lagrange, Castigliano, Reissner, etc.), by making use of its steady state, are obtained by solving an algebraic set of equations.

In case of axisymmetrical shells, by applying the engineering shell theory, the first finite element method built up on Lagrange's variation principle approximated the geometry of the shell by elements having the form of a truncated cone (single curved elements) [12]. This procedure has been found by numerous followers [13 to 15]. Later on also doubly curved elements were applied [16 to 19]. From among these latter, with respect to efficiency, the [18] and [19] were outstanding, where the displacement and the rotation of the normal to the shell middle surface were approximated by high degree polynomes (the geometric equations were not established on the basis of Kirchhoff—Love's hypothesis).

As is known, in case of Lagrange's variation principle, the potential energy of the elastic system will be minimized by assuming a kinematically admissible displacement field. In order to have the potential energy furnished for the whole structure by the sum of the potential energies calculated separately for each element, it is necessary and sufficient that, in case of Kirchhoff—Love's hypothesis, on the transition from one element to another, the displacement of the middle surface and the rotation of the normal be the same. To fulfil this condition it causes no trouble in case of axisymmetrical deformation. However, at the same time, in case of a compatible displacement model built up on Lagrange's variation principle, the force and moment components of the stress resultants[1] caused by the kinematically admissible displacement field, do not generally satisfy either the equilibrium equations, nor the dynamic boundary and joint conditions. If they are not satisfied, the errors caused by the approximation of the displacement field, appear with an increased magnitude.

With the method discussed in this paper, by assuming an axisymmetrical deformation, applying a kinematically admissible displacement field, treating

---

[1] Besides the denominations "stress resultants" in the literature on the subject also the names "normal middle surface forces, shear force and bending moment" or "the forces and moments per unit middle surface length" are used.

it as a supplementary condition, dynamic boundary conditions as well as the continuity of stress resultants can be fulfilled, discontinuities of a given magnitude and their prescribing as dynamic joint conditions. In this way, the potential energy of the shell structure is minimized by the fulfilment of the supplementary conditions. Hereby, in carrying out the calculations, an opportunity is offered for supervising the degree of non-satisfaction of the "a priori" non-satisfied equilibrium equations and thereby for the estimation and also for the improvement of the accuracy of the calculation. The closer the exact solution, the lower the degrees of the non-satisfaction will be. Be these degrees lower than a predetermined value, thus the calculation may be considered to be completed. Be they higher, so by maintaining the subdivision and augmenting the degree of the freedom of the elements, i.e., by increasing the number of degrees of the approximation series, and making use of some results obtained in the earlier calculation, by a repeated calculation, more exact results may be obtained. This successive approximation should be continued until the degree of non-satisfaction of the equilibrium equations becomes lower than the value given preliminarily. The technique of increasing the number of degrees was first applied to the solution of plate problems discussed in [20].

2. Basic relationships

In case of an axisymmetrical deformation the displacement of the points on the middle surface of the shell is definitely determined by the displacements u and w, the tangential and normal directions respectively (Fig. 1). The specific strains and curvature changes related to the middle surface of the shell, may be calculated from the relationships

$$\varepsilon_1 = \frac{1}{R_1}\left(\frac{du}{d\theta} + w\right), \qquad \varepsilon_2 = \frac{u\cos\theta + w\sin\theta}{r}, \qquad (1a, b)$$

$$\varkappa_1 = \frac{1}{R_1}\frac{d\vartheta}{d\theta}, \qquad \varkappa_2 = \frac{\cos\theta}{r}\,\vartheta, \qquad (1c, d)$$
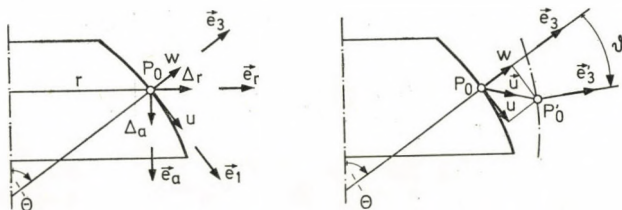
Fig. 1. Interpretation of the displacement vector in the system of coordinates defined by the base vectors $(\vec{e}_1, \vec{e}_2, \vec{e}_3)$ or $(\vec{e}_a, \vec{e}_2, \vec{e}_r)$: $\vec{u} = u\vec{e}_1 + w\vec{e}_3$; $\vec{u} = \varDelta_r\vec{e}_r + \varDelta_a\vec{e}_a$; ϑ — rotation of the normal of the middle surface

and the rotation of the normal from the relationship

$$\vartheta = \frac{1}{R_1}\left(u - \frac{dw}{d\theta}\right) \tag{1e}$$

where ϑ is the angle formed by the normal of the middle surface of the shell and with the axis of revolution,

    r is the radius measured on the parallel plane, and

    R_1 is the radius of the curvature of the meridional curve (Fig. 2).
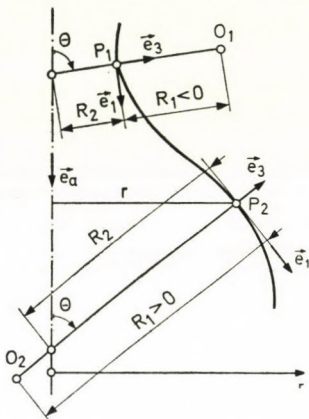
Fig. 2. Interpretation of the radii R_1, R_2 of the principal curvature at points P_1 and P_2, the Θ and of the elementary length of arc $ds = R_1 \cdot d\Theta$

Fig. 3. Positive directions of the force components of the stress resultants and moment components of the stress resultants
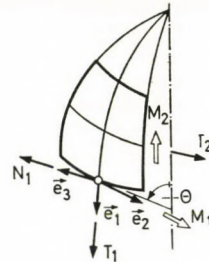
The force components of the stress resultants [N/cm] and moment components of the stress resultants [cmN/cm] (Fig. 3) may, in case of homogeneous, isotropic, linearly elastic material, be calculated as follows

$$T_1 = B(\varepsilon_1 + \mu\varepsilon_2), \qquad T_2 = B(\varepsilon_2 + \mu\varepsilon_1), \tag{2a, b}$$

$$M_1 = D(\varkappa_1 + \mu\varkappa_2), \qquad M_2 = D(\varkappa_2 + \mu\varkappa_1), \tag{2c, d}$$

and

$$N_1 = \frac{1}{rR_1}\left[\frac{d}{d\theta}(rM_1) - M_2R_1\cos\theta\right], \tag{2e}$$

where:

$$\begin{aligned}
B &= Eh/(1 - \mu^2), \\
D &= Eh^3/12(1 - \mu^2), \\
E &= \text{Young's elasticity modulus,} \\
h &= \text{thickness of shell,} \\
\mu &= \text{Poisson's ratio.}
\end{aligned}$$

As is known, in case of an axisymmetrical deformation three equilibrium equations may be established. Expressing the first two of these (the equilibrium equations involving the stress resultants H and V, Fig. 4 [6]) interpreted in the global system of coordinates $\vec{e}_a$, $\vec{e}_2$, $\vec{e}_r$ and integrating them, the following equations are obtained

$$rV - r_0V^\circ + \int_{s_0}^s p_a r\, ds = 0 \,, \tag{3a}$$

$$rH - r_0H^0 - \int_{s_0}^s (T_2 - p_e r)\, ds = 0 \,, \tag{3b}$$
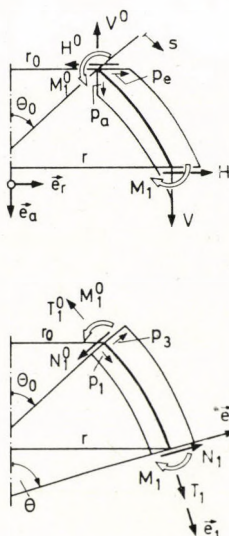
Fig. 4. Representation of the stress resultants and load in the global and local systems of coordinates defined by $(\vec{e}_a, \vec{e}_2, \vec{e}_r)$ and $(\vec{e}_1, \vec{e}_2, \vec{e}_3)$, respectively

wherein:
   s is arc coordinate measured along the meridional curve of shell;
quantities with zero subscripts and superscripts designate values assumed at fixed $s = s_0$ while those without subscripts (superscripts) denote values assumed at arbitrary loci of s;
   p_a and p_e are axial and radial coordinates, respectively, of intensity [N/cm²] of external load of shell reduced to the middle surface of shell.

The third equilibrium equation is furnished by expression (2e).

3. Assumption of the generalized displacement vector of the nodal circle. Building up of the approximation matrix

As was mentioned in the beginning, the purpose is to assure, beside maintaining the continuity of the displacement field and rotation field, the discontinuity of predetermined value or continuity of the stress resultants.

In the following it will be pointed out that these requirements can only be fulfilled with the aid of elements of at least twelve or higher degrees of freedom, except the case where the element contains the point $r = 0$ (this question is treated in [27]).

At the joints of the elements, at the nodal circles of the shell divided by a series of planes of finite number, normal to the axis of revolution, into *elements* (subregions), their jointment (the displacement fields u and w assumed locally and the rotation of the normal ensuing on Kirchhoff—Love's hypothesis) should be carried out on the basis of the joint conditions applied in the shell theory; i.e., the kinematic and dynamic joint conditions should be taken into account.

Let us introduce the rules of notation according to which a quantity belonging to an element is designated by the superscript (symbol of the element) is designated by the superscript (symbol of the element) while those belonging to a nodal circle is designated by the subscript (symbol of the nodal circle).

In case of the elements denoted by the superscripts e and $e + 1$ adjoining the nodal circle denoted by the subscript i, the *kinematic joint conditions*[2] relating to the ith nodal circle, expressed by the displacements Δ_r, Δ_a and the rotation of the normal ϑ represented in Fig. 1 may be written in the form

$$\Delta_{r,i}^e = \Delta_{r,i}^{e+1} = \Delta_{r,i}^0 , \tag{4a}$$

$$\Delta_{a,i}^e = \Delta_{a,i}^{e+1} = \Delta_{a,i}^0 \tag{4b}$$

$$\vartheta_i^e = \vartheta_i^{e+1} = \vartheta_i^0 \tag{4c}$$

wherein:
  $\Delta_{r,i}^0$, $\Delta_{a,i}^0$ and ϑ_i^0 are the (unknown) displacements and rotation of the points on the nodal circle i.

The kinematic prescriptions and boundary conditions are derived on the basis of the kinematic joint conditions. Be, in the expressions (4a, b, c), one of the values $\Delta_{r,i}^0$, $\Delta_{a,i}^0$, ϑ_i^0 a given quantity, so with respect to the given quantity (quantities) they are called *kinematic boundary conditions* or *kinematic prescriptions* depending on whether one or more elements are adjoining the ith nodal circle.

Using the symbols of Fig. 5, the *dynamic joint conditions* representing the equilibrium of the ith nodal circle may be written as follows:

$$H_i^e - H_i^{e+1} = H_{0,i} , \tag{5a}$$

$$V_i^e - V_i^{e+1} = V_{0,i} , \tag{5b}$$

$$M_{1,i}^e - M_{1,i}^{e+1} = M_{1,0,i} \tag{5c}$$

[2] For the sake of an easier understanding in writing down the kinematic and later the dynamic joint equations we must be content with the case where only two elements meet at the nodal circle (i.e., the shell has no branch). In case of branching structures the respective formal extension of the equations is needed.

wherein:

V_i^α, H_i^α and $M_{1,i}^\alpha (\alpha = e, \ e + 1)$ are components of internal force components of the stress resultants (V_i being the parallel, H_i the normal component to the axis of revolution) and internal meridional bending moment respectively;

$H_{0,i}$, $V_{0,i}$ and $M_{1\,0,i}$ are symbols of values affecting nodal circle i caused by a given external load (known) or support (unknown).
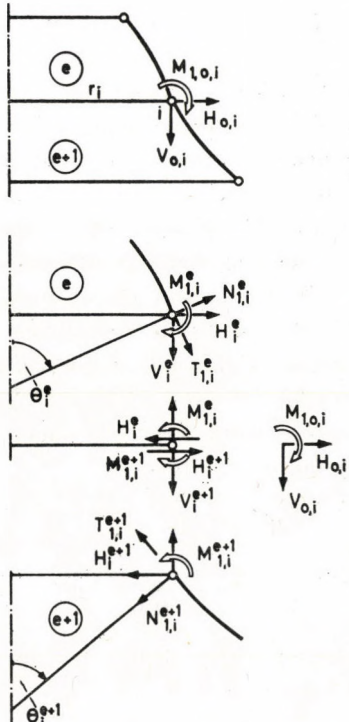
Fig. 5. Dynamic joint conditions on the ith nodal circle $M_{1,i}^e - M_{1,i}^{e+1} = M_{1,0,i}$; $H_i^e - H_i^{e+1} = H_{0,i}$; $V_i^e - V_i^{e+1} = V_{0,i}$; a) External load: $H_{0,i}$, $V_{0,i}$, $M_{1,0,i}$ applied at the joint of nodal circle i of the elements e and $e + 1$. b) Stress resultants induced on the common nodal circle i of the elements e and $e + 1$ in the global and local system of coordinates and internal and external loads acting on the nodal circle i

In case where only a single element is associated with the nodal circle i, from among the conditions (5a, b, c) those, at whose right-hand side known values are involved, these are called *dynamic boundary conditions*. As a matter of course, in this case, at the left hand side of the conditions (5a, b, c) only the quantities which are associated with the elements e or $e + 1$ enter.

It is obvious that the conditions (4a), (5a); (4b), (5b); (4c), (5c) by pairs cannot be applied, at the same time, at any of the nodal circles as kinematic boundary conditions, prescriptions or dynamic boundary or joint conditions.

In establishing the joint equations associated with the common nodal circles of the adjoining elements concerning the displacement field, rotation

field and the derivatives of the displacement field, the satisfaction or non-satis-
faction of the following *condition A* should be taken as a starting basis.

Condition A: on the common nodal circles of the adjoining elements, the thickness, curvature and material characteristics of the shell are identic; with the nodal circle neither kinematic prescriptions, nor external concentrated (distributed along the circle) load is associated; at the nodal circle only two elements meet.

Be the condition A fulfilled, so by considering the relationships (1a to 1e), (2a to 2e) it can be seen that beside assuring the continuities of the displace-
ments and rotation, the necessary and sufficient condition for realizing the continuities of the stress resultants, is that on the nodal circle the radial and axial displacements (Δ_r) and (Δ_a) respectively, the rotation of the normal (ϑ), the first derivative of the tangential displacement (u) with respect to the arc coordinate s ($u_{,s}$), the first ($\vartheta_{,s}$) and a second ($\vartheta_{,,s}$) derivatives of the rota-
tion ϑ with respect to the arc coordinate s should be identic.[3] The vector prod-
uced from these quantities will be called *generalized displacement vector* of the nodal circle.

The generalized displacement vector associated with the nodal circle i of the element e is designated as follows:[4]

$$\mathbf{q}_i^{eT} = [\mathring{\mathbf{q}}_i^{e,T} \mid \tilde{\mathbf{q}}_i^{e,T}] , \tag{6}$$

where

$$\mathop{\mathring{\mathbf{q}}_i^{e,T}}_{(1,3)} = [\Delta_r \, \Delta_a \, \vartheta]_i^e , \quad \mathop{\tilde{\mathbf{q}}_i^{e,T}}_{(1,3)} = [u_{,s} \, \vartheta_{,s} \, \vartheta_{,,s}]_i^e . \tag{7a, b}$$

If the elements denoted with e and $e + 1$ meet at the ith nodal circle then, for the validity of condition A is true that

$$\mathring{\mathbf{q}}_i^e = \mathring{\mathbf{q}}_i^{e+1} , \quad \tilde{\mathbf{q}}_i^e = \tilde{\mathbf{q}}_i^{e+1} , \tag{8a, b}$$

thus,

$$\mathbf{q}_i^e = \mathbf{q}_i^{e+1} , \tag{8c}$$

i.e., at the joint (attachment) of both elements in question, the generalized displacement vectors belonging to the common nodal circle i, are the same.

From Fig. 1 may be seen that by introducing the transformation matrix

$$\mathop{\mathbf{T}_i^e}_{(3,3)} = \left[\begin{array}{ccc} \cos\theta & \sin\theta & 0 \\ -\sin\theta & \cos\theta & 0 \\ 0 & 0 & 1 \end{array} \right]_i^e$$

between the vector

$$\mathop{\mathring{\mathbf{q}}_i^{e,T}}_{(1,3)} = [uw\theta]_i^e$$

[3] Here and in the following the notations
$d(.)/ds = 1/R_1 \, d(.)/d\Theta = (.)_{,s}, \quad d^2(.)/ds^2 = (.)_{,,s}$ are used.
[4] T is the symbol of transposition.

defined in the local system of coordinates $(\vec{e}_1, \vec{e}_2, \vec{e}_3)$ and $\mathbf{\mathring{q}}_i^e$, defined in the global system of coordinates $(\vec{e}_a, \vec{e}_2, \vec{e}_r)$ the relationship

$$\mathbf{\mathring{q}}_i^{\circ e} = \mathbf{T}_i^e \, \mathbf{\mathring{\tilde{q}}}_i^e$$

is valid. Therefore,

$$\mathbf{q}_i^e = \left[\begin{array}{cc} \mathbf{T}_i^e & \mathbf{0} \\ \mathbf{0} & \mathbf{E} \end{array} \right] \left[\begin{array}{c} \mathbf{\mathring{\tilde{q}}}_i^e \\ \mathbf{\tilde{q}}_i^e \end{array} \right] = \overline{\mathbf{T}}_i^e \, \overline{\mathbf{q}}_i^e , \tag{9}$$

wherein $\mathbf{E}$ is a unit matrix of type 3×3.

If any of the conditions A does not exist, then only the part realizing the continuity of the displacement field and rotation field of the generalized displacement vector associated with the common nodal circle i of the successive elements e, $e + 1$ may be fitted together according to (4a, b, c), i.e.,

$$\mathbf{\mathring{q}}_i^e = \mathbf{\mathring{q}}_i^{e+1} \tag{10}$$

while by virtue of the relationships (5a, b, c), (2a, c, e), (7a, b) between the vectors $\mathbf{q}_i^e$ and $\mathbf{q}_i^{e+1}$, also in this case, an unambiguous connection exists. By considering the definition (6) of the generalized displacements as well as the relationships (2a to 2e) and (1a to 1d) it may be observed that the stress resultants belonging to any nodal circle may be expressed as the functions of the generalized displacements associated with the very same nodal circle. Therefore, the dynamic joint equations (5a, b, c) relating to the common nodal circle of the elements e and $e + 1$ may be written in the following concise form:

$$\mathbf{A}_i \left[\begin{array}{c} \mathbf{q}_i^e \\ \\ \mathbf{q}_i^{e+1} \end{array} \right] = \left[\begin{array}{c} H_0 \\ V_0 \\ M_{1,0} \end{array} \right]_i = \mathbf{d}_i , \tag{11}$$

in which the coefficient matrix $\mathbf{A}_i$ may, according to the partition of the generalized displacement vector (7a, b), be partitioned as follows

$$\mathbf{A}_i = [\mathbf{\mathring{A}}_i^e \, \mathbf{\tilde{A}}_i^e \, \mathbf{\mathring{A}}_i^{e+1} \, \mathbf{\tilde{A}}_i^{e+1}] .$$

In case of a dynamic boundary condition at the left-hand side of relationship (11) only the quantities belonging either, only to the element e or only to the element $e + 1$, are included.

At all the nodal circles where kinematic prescriptions, boundary conditions are not given, the number of equations (11) is three, otherwise it is three, minus the number of the kinematic constraints. The rows corresponding to the non-prescribable dynamical joint or boundary conditions, in the matrix $\mathbf{A}_i$ and vector $\mathbf{d}_i$ for reasons of calculation technique, it is recommended to be filled in with zeros.

Since an element has two nodal circles, and at each of these the generalized displacement vector has six elements, thus, the generalized displacement vector of element e bounded by the ith and jth nodal circles, takes the following form:

$$\mathbf{q}^{e,T}_{(1,12)} = [\mathbf{q}^{e,T}_i \; \mathbf{q}^{e,T}_j] = [\mathring{\mathbf{q}}^{e,T}_i \; \widetilde{\mathbf{q}}^{e,T}_i \; \mathring{\mathbf{q}}^{e,T}_j \; \widetilde{\mathbf{q}}^{e,T}_j] \,, \tag{12}$$

Therefore, the generalized displacement vector is of the type 12×1.

The displacement field (u, w) is to be sought for each element as a linear combination of approximate functions made up of unknown constants. The number of unknown constants represents the *degree of freedom* of the element.
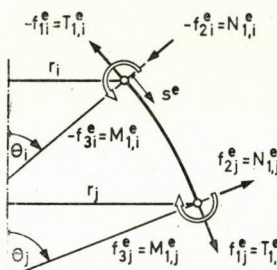
Fig. 6. The load applied at the edges of the element e and interpretation of the arc coordinate s^e

Since the purpose is to assure the continuity of the displacement field and rotation field, further, the continuity or the predetermined discontinuity of the stress resultants and the satisfaction of the dynamic boundary conditions, where to the assumption of twelve generalized displacements defined by (6) is necessary, therefore, a definite relationship between the constants and generalized displacements can only be established by making use of elements of twelve or higher degrees of freedom.

An empirical fact is that in case of approximation with polynomes of high degrees the displacement and state of stress of the shell may be determined at a significantly lower number of unknown quantities involved in the final set of equations, contrarily to the approximation with polynomes of lower number of degrees, however, in case of an algebraic set of equations obtained necessarily by assuming for more elements. Accordingly, the use of elements of higher than twelve degrees of freedom, is justified.

In accordance with that said above the *displacement vector $u^e(s^e)$ within the element* formed of the displacement vector $\vec{u} = u\vec{e}_1 + w\vec{e}_3$ interpreted in the local system of coordinates is approximated in the following form:

$$\mathbf{u}^e(s^e) = \begin{bmatrix} u(s) \\ w(s) \end{bmatrix}^e = \mathbf{\Phi}^e(s^e)\,\mathbf{a}^e + \hat{\mathbf{\Phi}}^e(s^e)\,\hat{\mathbf{a}}^e \,, \tag{13}$$

$$\underset{(2,1)}{}$$

wherein, in case of a single curved shell element ($R_1 = \infty$; cylinder, cone, plate, disc)

$$\underset{(2,12)}{\boldsymbol{\Phi}^e} = \begin{bmatrix} 1 & s & s^2 & s^3 & 0 & 0 & 0 & 0 & 0 & 0 & 0 & 0 \\ 0 & 0 & 0 & 0 & 1 & s & s^2 & s^3 & s^4 & s^5 & s^6 & s^7 \end{bmatrix}^e \tag{14}$$

$$\underset{(2,p')}{\boldsymbol{\hat{\Phi}}^e} = \begin{bmatrix} s^4 & s^5 & \ldots & s^{f_u} & 0 & 0 & \ldots & 0 \\ 0 & 0 & \ldots & 0 & s^8 & s^9 & \ldots & s^{f_w} \end{bmatrix}^e \tag{15}$$

and in case of a doubly curved shell element

$$\boldsymbol{\Phi}^e = \begin{bmatrix} 1 & s & s^2 & s^3 & \sin\theta & 0 & 0 & 0 & 0 & 0 & 0 & 0 \\ 0 & 0 & 0 & 0 & -\cos\theta & 1 & s & s^2 & s^3 & s^4 & s^5 & s^6 \end{bmatrix}^e, \tag{16}$$

$$\boldsymbol{\hat{\Phi}}^e = \begin{bmatrix} s^4 & s^5 & \ldots & s^{f_u} & 0 & 0 & \ldots & 0 \\ 0 & 0 & \ldots & 0 & s^7 & s^8 & \ldots & s^{f_w} \end{bmatrix}^e \tag{17}$$

where

$\left.\begin{matrix} f_u^e \\ f_w^e \end{matrix}\right\}$ means to the function $\begin{Bmatrix} u \\ w \end{Bmatrix}$ applied number of degrees,

$\underset{(12,1)}{\mathbf{a}^e}$, $\underset{(p^e,1)}{\mathbf{\hat{a}}^e}$ are the vectors of the constants

wherefrom it follows that the degree of freedom of the element is

$$l^e = 12 + p^e = f_u^e + f_w^e + \begin{Bmatrix} 2 \\ 3 \end{Bmatrix} \text{ if the shell is } \begin{Bmatrix} \text{single} \\ \text{doubly} \end{Bmatrix} \text{ curved}$$

where $p^e \geq 0$, the number of plus constants.

From the basic function matrices (14) and (16) it can be seen that the terms originating from the motion as a rigid body (from the displacement parallel to the direction of the axis of revolution) has been taken into consideration both in case of single curved and doubly curved shell elements (a_1^e, a_5^e) and ($a_5^e \sin\theta$, $- a_5^e \cos\theta$) respectively. With the aid of the relationships (1a to 1d) it may be proved that the values of the deformations associated with these displacements are equal to zero. The application of the polynomes is partly justified by the fact that every continuous function can be approximated by polynomes [21], partly by the easy numerical treatment.

The efficiency of the finite element method is basically determined by assuming the displacement field. Numerous works treat the problem of the convergence of the method; by the refinement of the division in the sense of energy by what conditions the assumed displacement field tends towards the actual value.

Here can be only referred to [22] where the critical analysis of several earlier works is to be found. By summarizing the results reported in [22] the assumed displacement field should satisfy the following conditions: within the element and at its boundary, i.e., at the transition to the neighbouring element it should be continuous; the displacement field should be the linear function of the generalized displacement vector of the element, it is desirable but not necessary, that the displacement field should contain the displacement caused by the motion as a rigid body. Are the interpolation functions used for the approximation in the sense of the energy complete, so the procedure converges to the actual solution. According to [23] the presence of the terms of the rigid body-like displacement significantly augments the numeric effectiveness of the method. Owing to this, it is convenient to take these terms in connection with the matrix $\boldsymbol{\Phi}^e$ into account.

The continuity of the displacement field and the normal rotation is assured by the generalized displacement vector of the nodal circle defined by (6) through the kinematic joint equations (8a) or (10).

In order to be able to realize the connection, the vector $\mathbf{u}^e(s^e)$ should be expressed through the vectors $\overline{\mathbf{q}}^e$ and $\hat{\mathbf{a}}^e$. Expressing the generalized displacement vector $\overline{\mathbf{q}}^e$ of the element e by its constant vectors $\mathbf{a}^e$, $\hat{\mathbf{a}}^e$ by making use of (11), (12) yields:

$$
\overline{\mathbf{q}}^e_{(12,1)} = \left[\begin{array}{c} \overline{\mathbf{q}}_i \\ \hline \overline{\mathbf{q}}_j \end{array} \right]^e = \mathbf{G}^e_{(12,12)} \, \mathbf{a}^e_{(12,1)} + \hat{\mathbf{G}}^e_{(12,p^e)} \, \hat{\mathbf{a}}^e_{(p^e,1)} \tag{18}
$$

where

$\mathbf{G}^e$ = quadratic matrix containing coordinates of a generalized displacement vector related to vector $\mathbf{a}^e$ and involving geometric parameters, while

$\hat{\mathbf{G}}^e$ = matrix containing coordinates of generalized displacement the displacement vector related to vector $\hat{\mathbf{a}}^e$.

Since in case in question ensuing from (14), (16) and (18), det $\mathbf{G}^e \neq 0$, with the aid of (18) one obtains

$$
\left[\begin{array}{c} \mathbf{a}^e \\ \hat{\mathbf{a}}^e \end{array} \right] = \mathbf{V}^e \left[\begin{array}{c} \overline{\mathbf{q}}^e \\ \hat{\mathbf{a}}^e \end{array} \right] , \tag{19}
$$

where

$$
\mathbf{V}^e_{(l^e, l^e)} = \left[\begin{array}{c|c} (\mathbf{G}^e)^{-1} & -(\mathbf{G}^e)^{-1} \, \hat{\mathbf{G}}^e \\ \hline \mathbf{0} & \mathbf{E} \end{array} \right]
$$

and $\mathbf{E}$ is a unit matrix of the type $p^e \times p^e$. To express the displacement vector (13) by taking (19) into consideration the following equation may be written

$$
\mathbf{u}^e(s^e) = \left[\boldsymbol{\Phi}(s) \mid \hat{\boldsymbol{\Phi}}(s) \right]^e \mathbf{V}^e \left[\begin{array}{c} \overline{\mathbf{q}} \\ \hat{\mathbf{a}} \end{array} \right] . \tag{20}
$$

4. Strain, state of stress and potential energy of the element

The vector

$$\underset{(1,4)}{\boldsymbol{\varepsilon}^{e,T}} = [\varepsilon_1\ \varepsilon_2\ \varkappa_1\ \varkappa_2]^e \tag{21}$$

associated with the element denoted by e combined of the specific elongations and changes of curvature introduced by (1a to 1d) is called the *generalized strain vector* of the element which, by using the displacement vector (20) and introducing the matrix operator

$$\underset{(4,2)}{\boldsymbol{\partial}} = \begin{bmatrix} \dfrac{d(.)}{ds} & \dfrac{1}{R_1} \\[2ex] \dfrac{\cos\theta}{r} & \dfrac{\sin\theta}{r} \\[2ex] \dfrac{d}{ds}\left(\dfrac{(.)}{R_1}\right) & -\dfrac{d^2(.)}{ds^2} \\[2ex] \dfrac{\cos\theta}{rR_1} & -\dfrac{\cos\theta}{r}\dfrac{d(.)}{ds} \end{bmatrix}$$

may be written in the form

$$\boldsymbol{\varepsilon}^e = {}'\mathbf{u}^e = \left[\mathbf{W}(s)\ \vdots\ \hat{\mathbf{W}}(s)\right]^e \mathbf{V}^e \begin{bmatrix} \bar{\mathbf{q}} \\ \hat{\mathbf{a}} \end{bmatrix}^e \tag{22}$$

wherein

$$\mathbf{W}^e = \boldsymbol{\partial}\boldsymbol{\Phi}^e\,, \quad \hat{\mathbf{W}}^e = \boldsymbol{\partial}\hat{\boldsymbol{\Phi}}^e\,.$$

From the stress resultants the generalized displacement vector of the element is formed in the following way

$$\underset{(1,4)}{\boldsymbol{\sigma}^{e,T}} = [T_1\ T_2\ M_1\ M_2]^e$$

which expressed through the matrix of the material law $\mathbf{D}^e$ and interpretable on the basis of (22) and (22a to 22d) yields:

$$\boldsymbol{\sigma}^e(s) = \mathbf{D}^e(s)\,\boldsymbol{\varepsilon}^e(s) = \mathbf{D}^e(s)\left[\mathbf{W}(s)\ \vdots\ \hat{\mathbf{W}}(s)\right]^e \mathbf{V}^e \begin{bmatrix} \bar{\mathbf{q}} \\ \hat{\mathbf{a}} \end{bmatrix}^e\,. \tag{23a}$$

Are there also present initial deformations (for example, caused by thermal load) so by collecting them into the vector $\boldsymbol{\varepsilon}_0^e$, the generalized stress vector may be found with the aid of the relationship[5]

$$\boldsymbol{\sigma}^e = \mathbf{D}^e(\boldsymbol{\varepsilon}^e - \boldsymbol{\varepsilon}_0^e)\,. \tag{23b}$$

[5] For the simplification of the discussion the investigation of the initial deformation will be omitted.

The potential energy of the element may be calculated from the deformation energy and from the potential of the external load according to the formula

$$\Pi^e = \frac{1}{2} \int\limits_{(A^e)} \boldsymbol{\sigma}^{e,T} \, \boldsymbol{\varepsilon}^e \, dA - \int\limits_{(A^e)} \mathbf{u}^{e,T} \, \mathbf{p}^e \, dA - \overline{\mathbf{q}}^{e,T} \, \mathbf{f}^e \tag{24}$$

wherein $\mathbf{p}^{e,T} = [p_1 \; p_3]^e$ is the vector of the external load distributed on the middle surface A^e of the element interpreted in the local system of coordinates (Fig. 4),

$$\mathbf{f}^{e,T}_{(1,12)} = [\mathbf{f}^{e,T}_i \; \vdots \; \mathbf{f}^{e,T}_j]_{(1,6)}$$

is the vector of the resultant of the external load distributed on a circular line, acting on the nodal circles i and j of the shell element (as a matter of course, the potential of the load distributed along the nodal circle should always be considered only for one element),

$$\mathbf{f}^{e,T}_n = 2\pi r_n [f_{1n} f_{3n} f_{2n} \; 0 \; 0 \; 0]^e, \quad (n = i, j) \, .$$

Replacing the quantities (23a), (22), (20) into (24) gives

$$\Pi^e = \Pi^e(\overline{\mathbf{q}}^e, \hat{\mathbf{a}}^e) = \frac{1}{2} \, [\overline{\mathbf{q}}^T \, \vdots \, \hat{\mathbf{a}}^T]^e \, \mathbf{Q}^e \left[\frac{\mathbf{q}}{\hat{\mathbf{a}}} \right]^e - [\overline{\mathbf{q}}^T \, \hat{\mathbf{a}}^T]^e \, \mathbf{h}^e \, , \tag{25}$$

where

$$\mathbf{Q}^e_{(l^e, l^e)} = \mathbf{V}^{e,T} \int\limits_{(A^e)} \left[\frac{\mathbf{W}^T}{\hat{\mathbf{W}}^T} \right]^e \mathbf{D}^e [\mathbf{W} \, \vdots \, \hat{\mathbf{W}}]^e \, dA \mathbf{V}^e = \left[\begin{array}{cc} \mathbf{K}_{qq} & \mathbf{K}_{qa} \\ \mathbf{K}_{aq} & \mathbf{K}_{aa} \end{array} \right]^e \tag{26}$$

is the stiffness matrix extention of the element, while its partitioned parts are

$$\mathbf{K}^e_{qq} = [\mathbf{G}^e]^{-1,T} \int\limits_{(A^e)} \mathbf{W}^{e,T} \, \mathbf{D}^e \, \mathbf{W}^e dA [\mathbf{G}^e]^{-1} \, , \tag{27}$$

$$\mathbf{K}^e_{qa} = (\mathbf{K}^e_{aq})^T = -\mathbf{K}^e_{qq} \hat{\mathbf{G}}^e + [\mathbf{G}^e]^{-1,T} \int\limits_{(A^e)} \mathbf{W}^{e,T} \, \mathbf{D}^e \, \hat{\mathbf{W}}^e dA \, , \tag{28}$$

$$\mathbf{K}^e_{aa} = \hat{\mathbf{G}}^{e,T} \, \mathbf{K}_{qq} \, \hat{\mathbf{G}}^e - \hat{\mathbf{G}}^{e,T} [\mathbf{G}^e]^{-1,T} \int\limits_{(A^e)} \mathbf{W}^{e,T} \, \mathbf{D}^e \, \hat{\mathbf{W}}^e dA - $$

$$- \int\limits_{(A^e)} \hat{\mathbf{W}}^{e,T} \, \mathbf{D}^e \, \mathbf{W}^e \, dA [\mathbf{G}^e]^{-1} \, \hat{\mathbf{G}}^e + \int\limits_{(A^e)} \hat{\mathbf{W}}^{e,T} \, \mathbf{D}^e \, \hat{\mathbf{W}}^e \, dA \, , \tag{29}$$

further the vector from the load

$$\mathbf{h}^e_{(l^e, 1)} = \mathbf{V}^{e,T} \int\limits_{(A^e)} \left[\frac{\boldsymbol{\Phi}^T}{\hat{\boldsymbol{\Phi}}^T} \right]^e \mathbf{p}^e dA + \tilde{\mathbf{f}}^e = \left[\frac{\mathbf{b}_q}{\mathbf{b}_a} \right]^e \, , \tag{30}$$

where

$$\underset{(1,\,l^e)}{\widetilde{\mathbf{f}}^{e,T}} = [\mathbf{f}^{e,T} \mathbin{\vrule height 8pt} \mathbf{0}] \tag{31}$$

$$\underset{(12,1)}{\mathbf{b}_q^e} = [\mathbf{G}^e]^{-1,T} \int_{(A^e)} \boldsymbol{\Phi}^{e,T} \, \mathbf{p}^e \, dA + \mathbf{f}^e$$

$$\underset{(p^e,1)}{\mathbf{b}_a^e} = \hat{\mathbf{G}}^{e,T}(\mathbf{b}_q^e - \mathbf{f}^e) + \int_{(A^e)} \hat{\boldsymbol{\Phi}}^{e,T} \, \mathbf{p}^e \, dA \; . \tag{32}$$

From formulae (27 to 32) it can readily be seen that in case of an element of a degree of freedom higher than twelve, the stiffness matrix $\mathbf{K}_{qq}$ associated with the element of twelve degrees of freedom and the generalized force vector $\mathbf{b}_q$ also appears with the element of increased degree of freedom, further, they will be also used in calculating the quantities $\mathbf{K}_{qa}^e$, $\mathbf{K}_{aa}^e$ and $\mathbf{b}_a^e$. That is, the repeated calculation of the numerous terms associated with the element of twelve degrees of freedom which may only be produced by numeric integration, and as such, requiring long computer time, may be eliminated by the convenient organization of the computer program.

5. Establishment of the set of algebraic equations to be solved

Let us rearrange the generalized displacement vectors defined by Eq. (6) associated with all the elements of the shell divided into n elements and the vectors of the surplus constants $\hat{\mathbf{a}}^e(e = 1, 2, \ldots, n)$ into a vector each, as follows:

$$\mathbf{q}_*^T = [\overset{\circ}{\mathbf{q}}{}^{1,T} \mathbin{\vrule height 8pt} \widetilde{\mathbf{q}}_1^{1,T} \mathbin{\vrule height 8pt} \overset{\circ}{\mathbf{q}}_2^{1,T} \mathbin{\vrule height 8pt} \ldots \mathbin{\vrule height 8pt} \overset{\circ}{\mathbf{q}}_m^{n,T} \mathbin{\vrule height 8pt} \widetilde{\mathbf{q}}_m^{n,T}] \tag{33}$$

where m denotes the number of the nodal circles and

$$\hat{\mathbf{a}}^T = [\hat{\mathbf{a}}^{1,T} \mathbin{\vrule height 8pt} \hat{\mathbf{a}}^{2,T} \mathbin{\vrule height 8pt} \ldots \mathbin{\vrule height 8pt} \hat{\mathbf{a}}^{n,T}] \tag{34}$$

Writing down the kinematic prescriptions given in the formulae (4a, b, c), the joint and boundary conditions, to the nodal circles number m, and summarizing them into a matrix equation yields

$$\underset{(3m,\,12n)}{\mathbf{A}_k} \, \mathbf{q}_* = \underset{(3m,\,1)}{\mathbf{k}} \; . \tag{35}$$

Eq. (35) corresponds for each nodal circle to three equations, in such a way that they express the equality of the generalized displacement vectors $\overset{\circ}{\mathbf{q}}_i^r$ of $t + 1$ elements designated with $r = e, e + 1, \ldots, e + t$ adjoining each nodal circle i or, in case of a given kinematic prescription, in the boundary condition they express their prescribed value. If dynamic boundary conditions

are pertaining to the edges, the number of the kinematic boundary conditions is three minus the number of the dynamic conditions; then, in these rows of the matrix $\mathbf{A}_k$ zeros are entered. The elements of the vector $\mathbf{k}$ associated with those nodal circles to which no boundary condition, no prescription is given, are equal to zero; all other element of the vector involve the displacement and rotation values defined by the boundary conditions and kinematic prescription. The matrix $\mathbf{A}_k$, as results from its interpretation, is built up of the numbers $0, 1, -1$, in case of shells without branching, it is of quasi-diagonal structure.

Let us sum up the dynamic boundary and joint conditions type (11) and the dynamic joint conditions of type (8b) established for all the nodal circles (of number m) into one single matrix equation

$$\mathbf{A}_d \quad \mathbf{q}_* = \mathbf{d} \ . \tag{36}$$
$$\underset{(3m,12n)}{\mathbf{A}_d} \underset{(12n,1)}{\mathbf{q}_*} \underset{(3m,1)}{\mathbf{d}}$$

Eqs (35) and (36) may also be written in the concise form:

$$\mathbf{A}^*\mathbf{q}_* = \mathbf{i} \tag{37}$$

where

$$\underset{(6m,12n)}{\mathbf{A}^*} = [\mathbf{A}_k^T \, \mathbf{A}_d^T]^T \ , \quad \underset{(6m,1)}{\mathbf{i}} = [\mathbf{k}^T \, \mathbf{d}^T]^T \ .$$

By making use of the formulae (25), (9), (33) and (34), the potential energy of the loose system may be produced as the quadratic functions of the vectors $\mathbf{q}$ and $\hat{\mathbf{a}}$

$$\Pi = \Pi(\mathbf{q}, \hat{\mathbf{a}}) = \sum_{e=1}^{n} \Pi^e(\mathbf{q}^e, \hat{\mathbf{a}}^e) \ . \tag{38}$$

Considering the aforesaid the following mathematical problem may be established: let us try to find the minimum of the potential energy of the loose system by satisfying the supplementary conditions (37), i.e., the programming problem is

$$\min \left\{ \Pi(\mathbf{q}, \hat{\mathbf{a}}) \mid \mathbf{A}^*\mathbf{q}_* = \mathbf{i} \right\} \ .$$

The Lagrange-function belonging to the given problem is

$$L_* = \Pi(\mathbf{q}, \hat{\mathbf{a}}) + \boldsymbol{\lambda}_*^T(\mathbf{A}^*\mathbf{q}_* - \mathbf{i}) \ , \tag{40}$$

where $\boldsymbol{\lambda}_*$ is the vector of the Lagrange-multiplicators.

The necessary and sufficient condition of the minimum is

$$\frac{\partial L_*}{\partial \mathbf{q}_*} = \mathbf{0} \ , \quad \frac{\partial L_*}{\partial \hat{\mathbf{a}}} = \frac{\partial \Pi}{\partial \hat{\mathbf{a}}} = \mathbf{0} \ , \quad \frac{\partial L_*}{\partial \boldsymbol{\lambda}_*} = \mathbf{0} \ , \tag{41a, b, c}$$

which, with respect to the elements of the unknown vectors $\mathbf{q}_*, \hat{\mathbf{a}}, \boldsymbol{\lambda}_*$ constitute a linear set of algebraic equations.

By making use of its properties given under (41b), $\hat{\mathbf{a}}$ may be expressed through $\mathbf{q}$ which results in reducing the number of unknown quantities involved in the final set of algebraic equations.

When calculating actual problems the great advantage is that from the independence of the supplementary constants of each element (24) ensues

$$\frac{\partial \Pi}{\partial \hat{\mathbf{a}}^e} = \frac{\partial \left(\sum_s \Pi^s \right)}{\partial \hat{\mathbf{a}}^e} = \frac{\partial \Pi^e}{\partial \hat{\mathbf{a}}^e} = \mathbf{0}, \quad (e = 1, 2, \ldots, n)$$

i.e., by taking into account the relationships (25), (26) and (30) to (32) the vector $\hat{\mathbf{a}}^e$ may be expressed for each element. As a result, partly

$$\hat{\mathbf{a}}^e = [\mathbf{K}^e_{aa}]^{-1} (\mathbf{b}^e_a - \mathbf{K}^e_{aq} \mathbf{q}^e) \tag{42}$$

is obtained, partly, by replacing $\hat{\mathbf{a}}^e$ into (25), the potential energy of the element e may be expressed through $\mathbf{q}^e$ as follows:

$$\Pi^e = \frac{1}{2} \mathbf{q}^{e,T} \mathbf{K}^e \mathbf{q}^e - \mathbf{q}^{e,T} \mathbf{b}^e \tag{43}$$

where

$$\underset{(12, 12)}{\mathbf{K}^e} = \mathbf{K}^e_{qq} - \mathbf{K}^e_{qa} [\mathbf{K}^e_{aa}]^{-1} \mathbf{K}^e_{aq} \tag{44}$$

is the *reduced stiffness matrix of the element* and

$$\mathbf{b}^e = \mathbf{b}^e_q - \mathbf{K}^e_{qa} [\mathbf{K}^e_{aa}]^{-1} \mathbf{b}^e_a \tag{45}$$

is the *reduced generalized force vector of the element*.

Hereafter, using Eq. (43) also the potential energy expressed by (38) may be rewritten and in lieu of the problem formulated by (39)

$$\min \left\{ \Pi(\mathbf{q}_*) \mid \mathbf{A}^* \mathbf{q}_* = \mathbf{i} \right\} \tag{46}$$

may be written.

Let us now, by taking into consideration the kinematic joint equations (35) as well as the dynamic joint equations type (8b), following from the validity of *condition A*, rearranging the generalized displacement vectors *differing* from each other, associated with all the nodal circles into a single vector.[6]

$$\mathbf{q}^T = [\overset{\circ}{\mathbf{q}}_1^{1,T} \; \tilde{\mathbf{q}}_1^{1,T} \; \overset{\circ}{\mathbf{q}}_2^{1,T} \; \tilde{\mathbf{q}}^{1,T} \; \ldots \; \overset{\circ}{\mathbf{q}}_m^{n,T} \; \tilde{\mathbf{q}}_m^{n,T}] \tag{47}$$

---

[6] If there are K elements altogether and the number of nodal circles at them is $\check{N}$, to which the dynamic joint and boundary conditions (11) are calid, then, in case of structures without branching, the number of the vector $\mathbf{q}$ is: $3(2K + \check{N})$

Here n and m are the serial numbers of the last element and nodal circle, respectively.

Let us denote the dynamic boundary and joint conditions type (11) which were not as yet taken into account, as follows:

$$\mathbf{Aq} = \mathbf{r} \, . \tag{48}$$

Using the notation adopted in lieu of (46) the following problem may be established: let us try to find the minimum of the potential energy $\Pi = \Pi(\mathbf{q})$ of the shell structure by satisfying the supplementary condition equations (48), i.e.,

$$\min \left\{ \Pi = \Pi(\mathbf{q}) = \frac{1}{2}\,\mathbf{q}^T\mathbf{Kq} - \mathbf{q}^T\mathbf{b} \mid \mathbf{Aq} = \mathbf{r} \right\}. \tag{49}$$

The problem formulated by (49) is equivalent to the condition of stationariness relating to the functional

$$L = \frac{1}{2}\,\mathbf{q}^T\mathbf{Kq} - \mathbf{q}^T\mathbf{b} + \boldsymbol{\lambda}^T(\mathbf{Aq} - \mathbf{r}) \tag{50}$$

thus

$$\delta L = \delta\mathbf{q}^T\,\frac{\partial L}{\partial \mathbf{q}} + \delta\boldsymbol{\lambda}^T\,\frac{\partial L}{\partial \boldsymbol{\lambda}} = 0 \tag{51}$$

where $\delta\mathbf{q}$, $\delta\boldsymbol{\lambda}$ mean the possible variations of the vectors $\mathbf{q}$, $\boldsymbol{\lambda}$. Namely, vector $\mathbf{q}$ in (47) has also to satisfy the kinematic boundary conditions and prescriptions, therefore, some elements of the $\mathbf{q}$ vector are of prescribed magnitude, i.e., the variation of the elements of given values (fixed variables) of $\mathbf{q}$ disappear. The same is the case with vector $\boldsymbol{\lambda}$ where, due to the kinematic constraints in the dynamic boundary and joint equations which are not prescribable, the elements of vector $\boldsymbol{\lambda}$ are of prescribed (for example zero) values.

Let $\mathbf{E}_1^q$ be a diagonal matrix whose dimension is the same as that of matrix $\mathbf{K}$ and in its principal diagonal, besides the units stand zeros at all the places where the elements of the vector $\mathbf{q}$ have prescribed values, further, be $\mathbf{E}_1^\lambda$ a diagonal matrix of such a $j \times j$ type as is multipliable by the vector $\boldsymbol{\lambda}$ entering in (50) and in its principal diagonal besides the unit at all the places zeros are entering, where neither dynamic boundary nor joint conditions may be prescribed. Then, according to the aforesaid it is true that

$$\delta\mathbf{q} = \mathbf{E}_1^q\tilde{\delta}\mathbf{q}; \quad \delta\boldsymbol{\lambda} = \mathbf{E}_1^\lambda\tilde{\delta}\boldsymbol{\lambda} \tag{52a, b}$$

where $\tilde{\delta}\mathbf{q}$, $\tilde{\delta}\boldsymbol{\lambda}$ designate the change of all elements of the vectors $\mathbf{q}$ and $\boldsymbol{\lambda}$.

Owing to the independence and the arbitrary value of the variations $\delta\mathbf{q}$, $\delta\lambda$ involved in (51), by considering the relationship (52a, b) one can write

$$\mathbf{E}_1^q \frac{\partial L}{\partial \mathbf{q}} = \mathbf{E}_1^q (\mathbf{K}\mathbf{q} - \mathbf{b} + \mathbf{A}^T\lambda) = \mathbf{0} \tag{53a}$$

$$\mathbf{E}_1^\lambda \frac{\partial L}{\partial \lambda} = \mathbf{E}_2^\lambda (\mathbf{A}\mathbf{q} - \mathbf{r}) = \mathbf{0}. \tag{53b}$$
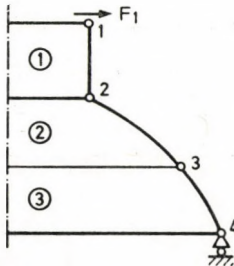

Fig. 7. Example for the establishment of the set of equations (56)

The coefficient matrix of the linear set of equations obtained is not symmetrical but may be made to be such. Let us interprete the diagonal matrices $\mathbf{E}_2^q$, $\mathbf{E}_2^\lambda$ by the following relationships

$$\mathbf{E}_2^q = \mathbf{E}^q - \mathbf{E}_1^q ; \qquad \mathbf{E}_2^\lambda = \mathbf{E}^\lambda - \mathbf{E}_1^\lambda \tag{54a, b}$$

where $\mathbf{E}^q$, $\mathbf{E}^\lambda$ are unit matrices. By making use of the identities

$$\mathbf{q} = (\mathbf{E}_1^q + \mathbf{E}_2^q)\,\mathbf{q}, \qquad \lambda = (\mathbf{E}_1^\lambda + \mathbf{E}_2^\lambda)\,\lambda \tag{55a, b}$$

and adding the known vectors $\mathbf{E}_2^q\mathbf{q}$ and $\mathbf{E}_2^\lambda\lambda = \mathbf{0}$ to each side of the equations (53a) and (53b), respectively, the following set of symmetrical coefficient matrix equations are obtained

$$\begin{bmatrix} \mathbf{E}_2^q + \mathbf{E}_1^q\,\mathbf{K}\,\mathbf{E}_1^q & \mathbf{E}_1^q\,\mathbf{A}^T\,\mathbf{E}_1^\lambda \\ \mathbf{E}_1^\lambda\,\mathbf{A}\,\mathbf{E}_1^q & \mathbf{E}_2^\lambda \end{bmatrix} \begin{bmatrix} \mathbf{q} \\ \lambda \end{bmatrix} = \begin{bmatrix} (\mathbf{E}_2^q - \mathbf{E}_1^q\,\mathbf{K}\,\mathbf{E}_2^q)\,\mathbf{q} + \mathbf{E}_1^q\mathbf{b} \\ \mathbf{E}_1^\lambda(\mathbf{r} - \mathbf{A}\,\mathbf{E}_2^q\,\mathbf{q}) \end{bmatrix}. \tag{56}$$

The coefficient matrix of the set of equations (56) is symmetrical, of non quasi-diagonal structure, however, by placing the equations of the dynamic boundary and joint conditions (i.e., by the convenient partitioning of the matrix $\mathbf{A}$ or by the appropriate rearrangement of the unknown quantities) the coefficient matrix *may be transformed into a band matrix*.

In order to demonstrate this, the establishment of the set of equations is presented on a structure consisting of three elements, in Fig. 7. The procedure is the same, even in more intricate cases.

$$(57)$$
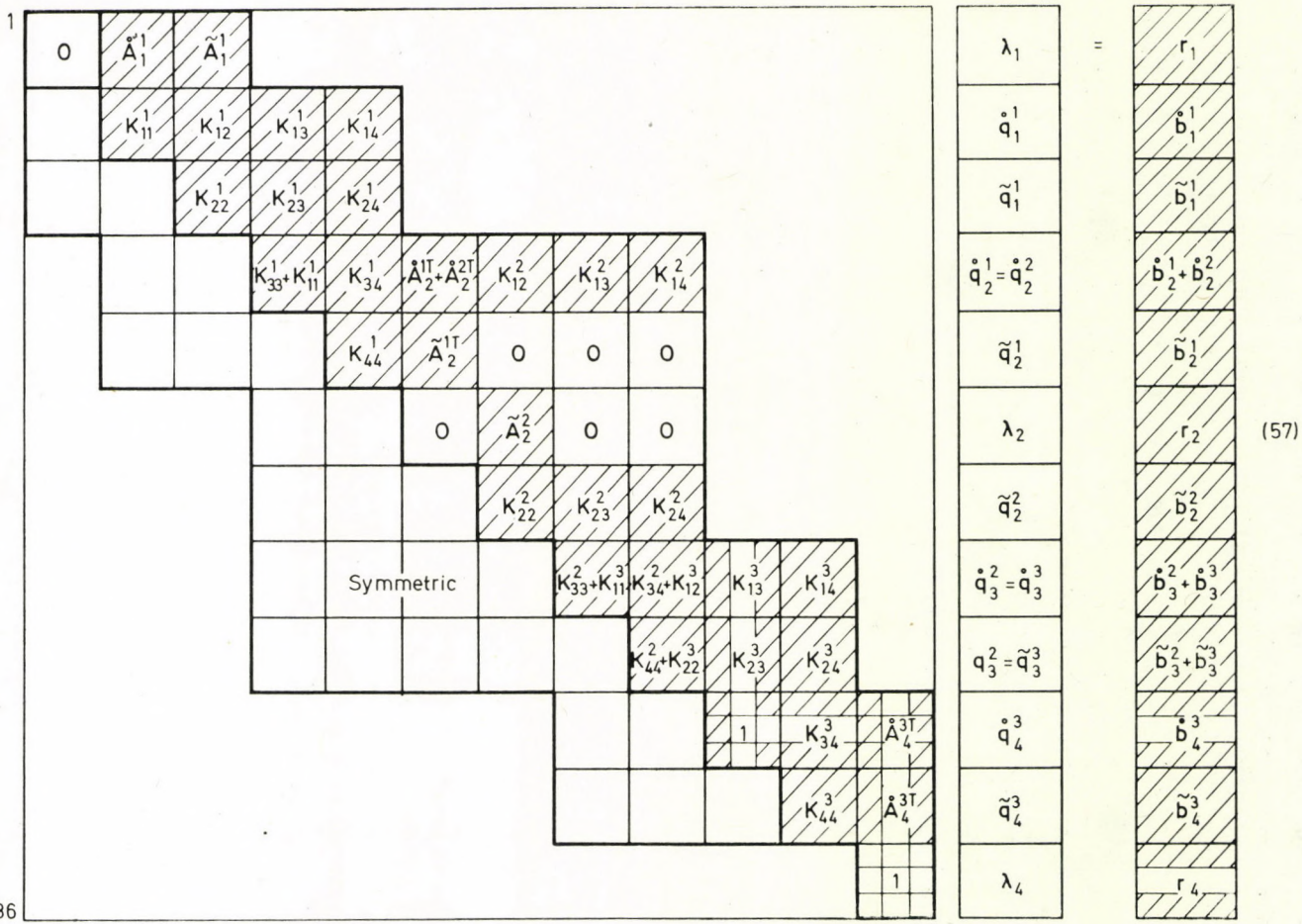
Fig. 16

After making allowance for (6), (43) to (45), the stiffness matrix, the generalized force vector of the element e may be partitioned. With the nodal circle 3 no constraint equation is associated because the *condition A* is valid. If one the nodal circle denoted with 3, kinematic prescription or a load of a given value should be applied, when $\mathbf{q}_3^2 \neq \mathbf{q}_3^3$, the establishment of a constraint equation would be necessary. For the nodal circles 1 and 4 dynamic and kinematic boundary conditions might be written (for the nodal cicles 1: $M_1 = 0$, $T_1 = 0$, $N_1 = -F_1$; for the nodal circles 4: $M_1 = 0$, $N_1 = 0$, $\Delta_a = 0$) while for the circle 2 only the fitting of the vectors $\overset{\circ 1}{\mathbf{q}}_2 = \overset{\circ 2}{\mathbf{q}}_2$ may be prescribed. Consequently, the appearance of the set of equations is the same as that of (57) where after carrying out the operations with the matrices $\mathbf{E}_1^\alpha$, $\mathbf{E}_2^\alpha$ $(\alpha = q, \lambda)$ the remaining blocks of matrices (differing from zero) are designated by shading.

The solution to the set of equations obtained is carried out by a special algorithm based on the Gaussian elimination method with the aid of which both the utilization of the memory unit and the number of the operations to be carried out is optimized [27].

6. Supervising and upgrading the accuracy of the calculation

In the procedure described above the displacement field assumed satisfies both the dynamic boundary conditions, prescriptions and even at the transition between the elements, the prescribed discontinuity or continuity of the internal forces and moments. If the calculated fields satisfy the equilibrium equations at any value of the arc coordinates s, the exact solution to the problem is obtained.

The degree of non-satisfaction of equations (3a, b) offers an opportunity to estimate the accuracy of the solution.

In case of a given subdivision of the shell the calculation should be begun by making use of the elements of twelve degrees of freedom then, with the aid of the displacement field resulted, the equilibrium equations (3a, b) should be supervised. For the elements, at which the degree of non-satisfaction is higher than the number ε preliminarily given, the degree of freedom of the element should be increased and with unchanged subdivision, by using certain results of the preceeding calculation [see (25) to (31)] the calculation should be repeated. One should proceed in this way until the degree of non-satisfaction of all the elements is below a predetermined value.

7. Calculation results

For the application of the procedure described in the foregoing a Fortran source language program has to be established. In connection with the assembly and operation of the program is to be noted that it automatically; carries out the subdivision of the shell structure into elements to the solution of the set of linear equations an algorithm based on the Gaussian elimination method is applied, the integrations required are carried out by the Gaussian quadrature method. For the purpose of the calculations the computer of the Hungarian Academy of Sciences, type CDC 3300 was used.
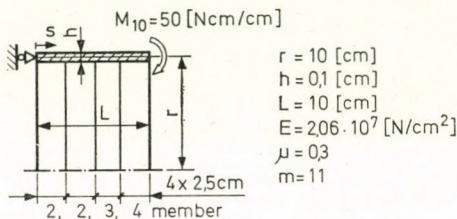

Fig. 8. Subdivision into elements of the circular cylindrical shell loaded at its edge

In the following some of the calculations carried out are presented to demonstrate the numeric efficiency of the procedure worked out by the authors. The results obtained in solving the problems were always compared with those found by the calculations carried out according to other calculation methods, and their close agreement has been experienced. The procedure proved to be convergent both for the refinement of the subdivision and for increasing the degree of freedom of the elements. In comparing it to the finite element method to be found in the literature on the subject, the rate of convergence of the procedure discussed is far more favourable (in working with lower number of elements and in reaching higher accuracy). In calculating the different problems it has been experienced that if the maximum of the degree of non-satisfaction of the mechanical equilibrium equations (3a, b) was below one [N], so the *stress* values calculated agreed by two cyphers with the results obtained with the aid of the analytic method.

7.1. The investigations were begun on the circular cylindrical shell depicted in Fig. 8. In the figure, besides the geometric dimensions and material constants also the subdivision and maximum number (m) of the elements are represented. The degree of freedom of the elements were twelve.

The results have been printed in to four digits; both the displacements and rotations as well as stress resultants agreed in their values to four places of the digits with the exact solution. The degree of non-satisfaction of the equilibrium equations (3a) and (3b) was for all the elements 10^{-4} order of

magnitude. The problem was also calculated with the aid of the procedure reported in [12]. The elements used here are single curved elements; u and w are linear and cubic functions, respectively, of the arc coordinates s, i.e., the element is of six degrees of freedom which does still not assure the continuity of the stress resultants. It is worthwhile mentioning that with the choice of *eighty elements* only (approximately) could the same result be attained as was furnished by the procedure described in points 2 to 4 with the assumption of *eleven elements*, moreover, even the use of three elements of 20 degrees of freedom, each yielded the exact solution.

In this connection, the results concerning the loaded edge of the cylinder are listed and compared in Table 1.

Table 1

	Number of elements	Number of unknown quantities	T_1 [N/cm]	T_2 [N/cm]	M_1 [Ncm/cm]
Points 2 to 4 (exact)	11 (12 df*)	78	10^{-22}	413,1	$-50,00$
	3 (20 df)	30	10^{-24}	413,1	$-50,00$
According to ref. [12]	80	243	10,6	419,1	$-50,20$

* df = degree of freedom

7.2. The cylindrical shell represented in Fig. 9 is submitted to a load linearly changing along the longitudinal axis. For the same number (4) of elements the results obtained by changing the number of degrees of the approximate polynomes are listed in Table 2. The lengths of the elements chosen surpass the length l_0 dying out.

Table 2

No. of degrees		N_1 [N/cm]	M_1 [Ncm/cm]	Degree of nonsatisfaction of	
f_u	f_w			(3a) [N]	(3b) [N]
3	7	$-81,3$	$-29,12$	115,4	16,6
3	10	$-76,22$	$-28,73$	46,5	2,1
3	13	$-76,11$	$-28,73$	36,0	0,01
7	13	$-75,78$	$-28,69$	1,1	0,0098
9	13	$-75,78$	$-28,69$	0,072	0,0097
Exact solution		$-75,78$	$-28,69$	—	

From the results it is to be seen that the index-number of non-satisfaction of the equilibrium equations decreases with the increase of the number of degrees of the polynomes. The table contains the index-numbers appearing at the element near the clamped edge, namely, the maximum values were always obtained at this element. The case 4 already furnishes a result which, from the viewpoint of the stress resultants equals that of the exact solution. It is to be remaked that the augmentation of the number of degrees of the polynome approximating the displacement of axial (u) direction (see cases 3 and 4) influences the accuracy of the calculation more strongly than (in cases 2 and 3) the augmentation of the number of degrees of the polynome approximating w.
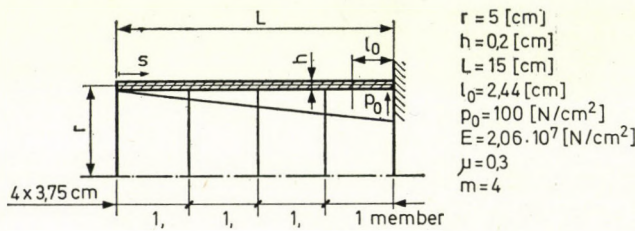

Fig. 9. Function of the circular cylindrical shell under linearly changing distributed load

7.3. From among the finite element solutions concerning the axisymmetrical shells to be found in the literature on the subject, from the viewpoint of numeric effectiveness the procedures treated in [18, 19] are the most outstanding, however, neither these procedures assure the continuity between the elements with the predetermined discontinuity of the stress resultants and the satisfaction of the dynamic boundary conditions. The calculation results reported in these papers persuasively show the advantages of the application of the elements of a high degree of freedom. For the cylindrical problem depicted in Fig. 10a, also numeric results are to be found. By uniform subdivision and applying six elements it was investigated how the augmentation of the degree of freedom affects the exactitude of the results. In Fig. 10b the change of the meridional bending moment M_1 published in [18] depending on the arc coordinate is shown. The different curves denoted by $d = 8, 10, 14$ represent the values obtained by the application of elements of d-degree of freedom (the curve drawn with full line renders the exact solution). For comparison, the problem was calculated by making use of six elements of fourteen degrees of freedom. In Fig. 10b the ● signs designate the results of the procedure discussed in the present paper, wherefrom it might be stated that even the effectiveness of the method reported in [18] falls behind that of the procedure worked out by the authors.
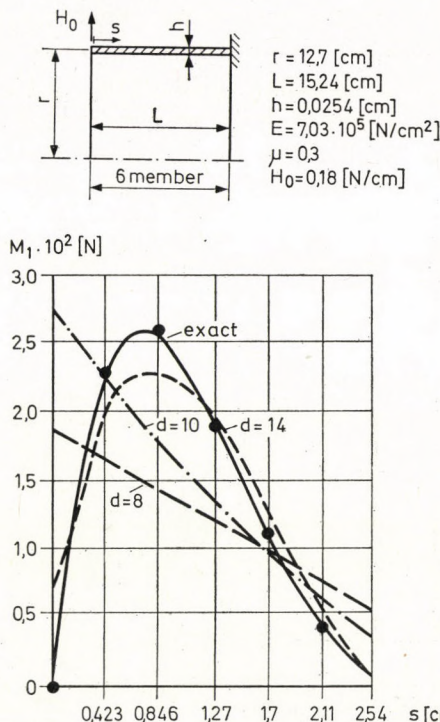
Fig. 10. a) circular cylindrical shell loaded at its edge; b) change of the meridional bending moment $M_1 = M_1(s)$. On the basis of the method discussed in points 2 to 4 by applying elements of 14 degrees of freedom denoted by ●, the curves denoted by d represent according to the ref. [18] the results obtained by using the elements having $d =$ 8, 10, 14 degrees of freedom
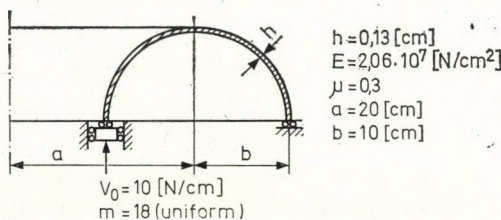

Fig. 11. Torus-formed shell subjected to a force parallel to the axis of revolution

7.4. To the strength analysis of a shell having a torus-like form depicted in Fig. 11 doubly curved elements have been applied. The calculation results were compared with those of the approximate analytic solution to be found in [6].

Using in solving the problem of uniform subdivision, the number of the elements obtained was 18 and their degree of freedom twelve. In Fig. 12
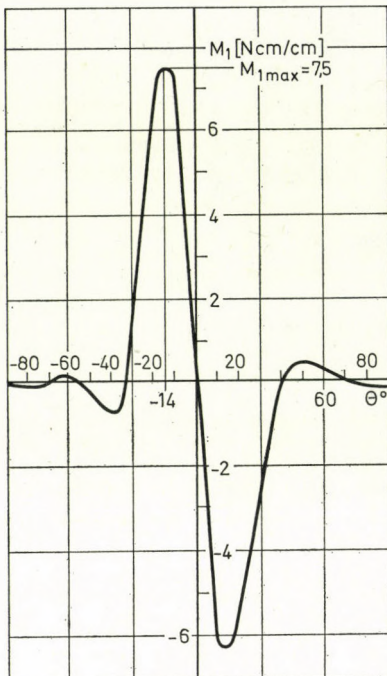
Fig. 12. Variation of the meridional bending moment M_1 depending on Θ induced in the torus-shell depicted in Fig. 11
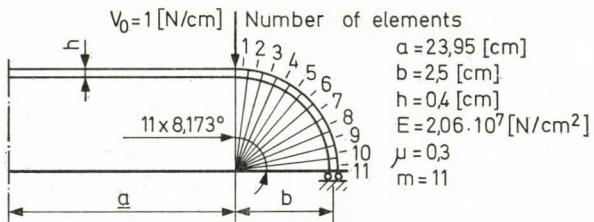

Fig. 13. Torus-formed shell loaded at its edge subdivided into elements $(0 \leq \Theta \leq \pi/2)$

the change of the meridional bending moment M_1 versus θ is shown. By applying the approximate relationships reported in [6], p. 395, the maximum value of M_1 occurs at $\theta = -13.9°$, being 7,49 Ncm/cm, while the vertical displacement of the edge at $\theta = -90°$ is $\varDelta_a = 0.2924$ cm in comparison with the value $\varDelta_a = 0.2927$ cm calculated with the method described above. In Fig. 12 a close agreement with the moments calculated at $\theta = 13.9°$ is to be seen. The index-number of the non-satisfaction of the equilibrium equations did not attain one [N].

7.5. The geometric proportions of the torus shell shown in Fig. 13 are such as, according to the knowledge of the authors, no solution of closed

(asymptotic) form exists [6]. In solving the problem by using a uniform subdivision, eleven elements were applied. For the degree of freedom of the elements fifteen was selected, thus, it was in (17) $f_u = 5, f_w = 7$, the maximum degree of the non-satisfaction of the equilibrium equations occurred at element No. 4, and its values were 0,0066N and 0,018N.

Using the compatible displacement model elements worked out by the authors, the calculation results obtained at the angles $\theta = 0$, $\pi/2$, are to be found in the first line of Table 3, while in the second line the values calculated according to [28][7] are entered. The deviation of the stress values obtained on

Table 3

|	σ_1 [N/cm²]			σ_2 [N/cm²]		
	$z = -h/2$	$z = 0$	$z = h/2$	$z = -h/2$	$z = 0$	$z = h/2$
According to points 2 to 4	−65,82	−2,263	61,2	−0,9125	18,15	37,21
According to ref. [28]	−65,299	−2,264	59,825	−0,9162	17,502	35,99
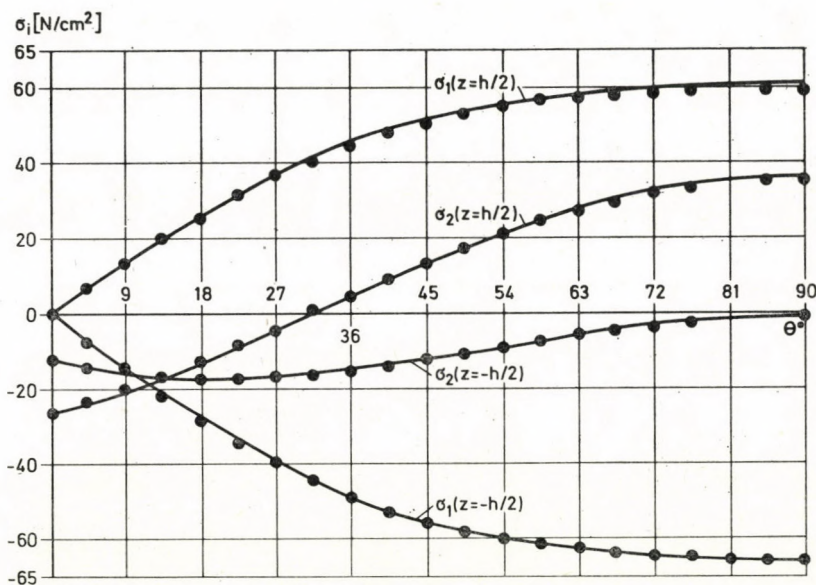
Fig. 14. Change of the stresses induced in the shell depicted in Fig. 13 at the middle surface of the shell as well as at the bounding surfaces of the shell wall $z = h/2$ and $z = -h/2$: ● according to the ref [28]; continuous curves according to points 2 to 4

[7] The program assembled for the procedure based on the method of the influence coefficients established at the Technical University of Dresden have been run on the request of the authors.
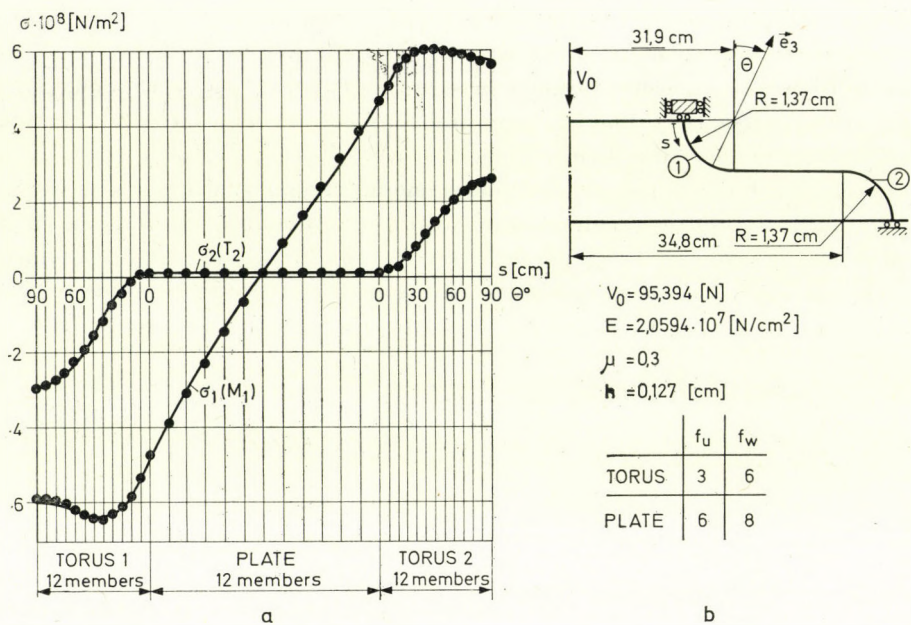
Fig. 15. An example to the thermocompensator: a) geometry; b) change of the functions $\sigma_1(M_1, z = h/2)$ and $\sigma_2(T_2)$ depending on the arc coordinate s

Table 4

	Θ	$\sigma_1(M_1)$ 10^{-4} [N/cm²]	$\sigma_2(T_2)$ 10^{-4} [N/cm²]	Ref.
Torus 1		$-6,058$	$-2,992$	[10]
	$\pi/2$	$-6,031$	$-3,017$	[26]
		$-5,848$	$-2,949$	
		$-5,142$	$0,074$	[10]
	0	$-4,848$	$0,075$	[26]
		$-4,832$	$0,073$	
		$4,920$	$0,074$	[10]
	0	$4,744$	$0,072$	[26]
		$4,606$	$0,079$	
Torus 2		$5,973$	$2,780$	[10]
	$\pi/2$	$5,743$	$2,526$	[26]
		$5,677$	$2,544$	

the internal $(z = -h/2)$, middle $(z = 0)$ and external $(z = + h/2)$ surface of the shell with both methods of calculation may be neglected.

In Fig. 14 the change of the stresses found on the external and internal surface of the shell according the angle θ is represented. The full line shows the results obtained according to the method worked out by the authors, the plus signs represent those found by the application of the method dealt with in [28].

7.6. One of the problems concerning the shell structures of an intricate construction, consisted in trying to clarify the state of stress of the thermo-compensator depicted in Fig. 15b. The number of the adopted elements and the number of their degree of freedom, as well as the distribution of the stresses are shown in Fig. 15a. The fully drawn line shows the (approximate) results reported in [10], the ● signs designate those obtained with the application of the authors' method.

Table 4 contains the stresses caused by the moment M_1 and force T_2 applied on the torus surface defined by the positive direction $\vec{e}_3$ at the angles $\theta = 0$ and $\pi/2$ of the tori No. 1 and No. 2.

In column R the references to the literature on the subject may be found. In the rows where no reference is entered, the results obtained by the authors are given.

The maximum of the index-number of the non-satisfaction of the equilibrium equations did not attain the value one [N].

REFERENCES

1. НОВОЖИЛОВ, В. В.: Теория тонких оболочек, Судпромгиз, Ленинград, 1962
2. ВЛАСОВ, В. З.: Общая теория оболочек, ГИТТЛ, М., 1953
3. ГОЛЬДЕНВЕЙЗЕР, А. Л.: Теория упругих тонких оболочек, ГИТТЛ, М., 1953
4. ЧЕРНЫХ, К. Ф.: Линейная теория оболочек, т. 1., т. 2., ЛГУ, Ленинград, 1962, 1964
5. TIMOSHENKO, S.— WOINOWSKY-KRIEGER, S.: Theory of Plates and Shells (in Hungarian), Műszaki Könyvkiadó, Budapest 1966
6. ЧЕРНИНА, В. С.: Статика тонкостенных оболочек вращения, Наука, М., 1968
7. ПРОЧНОСТЬ, УСТОЙЧИВОСТЬ, КОЛЕБАНИЯ: Справочник в трех томах, Машиностроение, М., 1968
8. ВАЙНБЕРГ, Д. В., ЖДАН, В. З.: Матриные алгоритмы в теории оболочек вращения, Изд. Киевского Университета, Киев, 1967
9. СВИРСКИЙ, И. В.: Методы типа Бубнова-Галёркина и последовательных приближений, Наука, М., 1968
10. ФИЛИППОВ, А. П., БУЛГАКОВ, В. Н., ВОРОБЬЕВ, Ю. С., КАНТОР, Б. Я., МАРЧЕНКО, Г. А.: Численные методы в прикладной теории упрогости, Наукова думка, Киев, 1968
11. ОГИБАЛОВ, П. М., КОЛТУНОВ, М. А.: Оболочки и пластины, Изд. Московского университета, М., 1969
12. GRAFTON, P. R.—STROME, D. R.: Analysis of Axisymmetrical Shells by the Direct Stiffness Method, *AIAA Jnl.*, **1**, 10 (1962), 2342—2357
13. POPOV, E. P.—PENZIEN, J.—LU, Z. A.: Finite Element Solution for Axisymmetrical Shells, *ASCE Eng. Mech. Div.* (1964), 119—145
14. KLEIN, S.: A Study of the Matrix Displacement Method as Applied to Shells of Revolution, Paper presented at the Conference on Matrix Methods in Structural Mechanics, Wright-Patterson Air Force Base Ohio, 26—28, October, 1965

15. PERCY, J. H.—PIAN, T. H. H.—KLEIN, S.—NAVARATNA, D. R.: Application of Matrix Displacement Method of Linear Elastic of Shells of Revolution, *AIAA Jnl.*, **3** (1965) 2138—2145
16. STICKLIN, J. A.—NAVARATNA, D. R.—PIAN, T. H. H.: Improvement on the Analysis of Shells of Revolution by the Matrix Displacement Method, *AIAA, Jnl.*, **4** (1966), 2069—2072
17. JONES, R. E.—STROME, D. R.: Direct Stiffness Method of Shells of Revolution Utilizing Curved Elements, *AIAA Jnl.* **4** (1966), No. 9
18. BROMBOLICH, L. J.—GOULD, P. L.: A High-Precision Curved Shell Finite Element, *AIAA Jnl.*, **10** (1972), 277—228
19. SEN, K. S.—GOULD, P. L.: Criteria for Finite Element Discretization of Shells of Revolution, *Int. J. num. Meth. Engng.* **6** (1973) 265—274
20. SZABÓ, B. A.—CHUNG-TA TSAI: The Quadratic Programming Approach to the Finite Element Method, *Int. J. Num. Meth. Engng.*, **5** (1973), 375—381
21. RALSTON, A.: A First Course in Numerical Analysis McGraw-Hill, 1965
22. ODEN, J. T.: Finite Element of Nonlinear Continua, McGraw-Hill, 1972
23. MURRAY, K. H.: Comments on the Convergence of Finite Element Solution, *AIAA Jnl.*, **8** (1970), 815—816
24. PIAN, T. H. H.: Derivation of Stiffness Matrices, *AIAA. Jnl.*, **2**, March 1964, 1333—1336
25. ZIENKIEWICZ, O. C.: The Finite Element Method in Engineering Science, McGraw-Hill 1972
26. ЛАУПА, А., ВЕЙЛ, Н.: Расчет компензаторов с U образными гофрами, Прикладная механика, 29, 1., 1962
27. HERPAI B.—PÁCZELT I.: Some Comments on Calculation of Axisymmetrical Shells by Applying Finite Element Method Compatible Displacement Model, (Manuscript in Hungarian), Heavy Industries Polytechnic University, Miskolc 1976
28. LANDGRAF, G.: Information by letter, Technische Universität, Dresden, 1975

Berechnung Flächentragwerke rotationssymmetrischer Verformung mit Hilfe der Methode der endlichen Elemente. — Ausser der Kontinuität des Verschiebungsfeldes und Normalenverdrehungsfeldes sichert die von den Autoren ausgearbeitete Methode auch die Kontinuität oder die vorgeschriebene Diskontinuität der Flächenspannungen und Flächenspannungspaare, sowie die Befriedigung der dynamischen Randbedingungen. Die angenommenen Elemente folgen der warhaften Geometrie der Schale. Der niedrigste Freiheitsgrad der Elemente ist 12. Am Ende der Berechnung ergibt sich eine Möglichkeit bei jedem Element zur Überprüfung des Grades der Nichtbefriedigung der "a priori" nicht befriedigten Gleichgewichtsbedingungen. Bleibt der Grad der Befriedigung bei jedem Element unter einem vorangegebenen Wert, so kann die Berechnung als beendigt betrachtet werden. Gegenfalls, kann man bei Beibehaltung der Aufteilung durch Erhöhung des Freiheitsgrades der zur Frage stehenden Elemente, mit wiederholter Rechnung genauere Ergebnisse erhalten. Die Wirksamkeit des Verfahrens ist durch numerische Beispiele demonstriert.

Расчет оболочек вращения при осеимметричной деформации с помощью метода конечных эмементов. Разработанный метод обеспечивает непрерывность поля перемещений срединной поверхности оболочек вращения и поля угла поворота нормали к поверхности, далее непрерывность внутренних усилий и моментов или их заданный скачок, а также заботится об удовлетворении динамическим граничным условиям.

Выбранные элементы и форма меридиального сечения совпадают. Минимальная степень свободы элементов равна 12.

В конце рассчета имеется возможность по элементам определить меру неудовлетворенности уравнений равновесия, которые «a priori» не были учтены в процессе расчёта.

Поскольку при каждом элементе мера неудовлетворенности меньше зафиксированной заранее величины, то расчёт считается законченным. Если нет, то при неизменном разбиении оболочки на элементы, увеличиваем степень свободы проблематичных элементов и повторяем расчет (ы). Таким образом можно уточнить результаты.

Множество приведенных примеров хорошо показывают эффективность метода.

НАХОЖДЕНИЕ ОПТИМАЛЬНОГО ЧИСЛА, МЕСТА И ОКРЕСТНОСТИ ТРАНСФОРМАТОРОВ В НИЗКОВОЛЬТНОЙ ЭЛЕКТРИЧЕСКОЙ СЕТИ С ПОМОЩЬЮ ПРОБЛЕМЫ ПОКРЫТИЯ МНОЖЕСТВА

М. ГРОС*

Реконструкция низковольтных электрических сетей, а также построение новых сетей, снабжающих электроэнергией новые кварталы, в настоящее время является очень частой задачей. Уже и ранее были сделаны попытки частичной механизации большого числа числовых рассчетов [1]. На первой стадии механизации можно было определить только поперечное сечение проводов и цепей трансформатора, сформированных на основе субъективного решения. Увеличение числа таких задач поставило на повестку дня необходимость автоматизации проектирования. Для этого необходимо, в первую очередь, определить расположение трансформаторов в сети и алгоритм построения цепи трансформатора. Как всякий технологический процесс, заходящий за традиционные рамки, решение данной задачи требует новой математической модели. В настоящей работе методы прикладной математики применены таким образом, чтобы они подходили при решении подобных технических проблем. Разработанные на основе данной модели программы используются в институте «САМГЕП».

Инженерная формулировка задачи

Пусть дана трехфазная электрическая сеть с её техническими данными, потребителями, а также техническими и экономическими параметрами трансформаторов.

Нужно найти оптимальное число и место трансформаторов в сети, причем такое месторасположение, которое обеспечивает минимальные потери мощности в сети, а также для каждого трансформатора непересекающиеся электрические цепи, в которых напряжение больше некоторой наперед заданной величины.

В ходе рассуждений не учитывается влияние низковольтной сети на высоковольтную (вывод при постоянном потенциале) и допускается

$$\cos \varphi = 0,$$

а также предполагается постоянное сопротивление и величина тока на выводе:

$$I[\text{Ампер}] = \frac{1}{3} W[\text{Ватт}]/220[\text{Вольт}].$$

* M. Grósz Csalit u. 9, H-1025 Budapest, Hungary.

Предположение о постоянной величине сопротивления необходимо только до построения непересекающихся деревьев, так как неизвестно месторасположения трансформаторов в сети и структура деревьев и поэтому по техническим причинам нельзя учитывать действительное сопротивление в сети только после окончательного построения деревьев.

Математическая формулировка задачи

2.1 Общее описание

Из четырех проводов трехфазной электрической сети рассматривается только один, таким образом, электрическая сеть может быть представлена в виде связного графа C. Из чисто технических соображений в дальнейшем предполагаем, что локальная степень произвольной вершины графа C не превышает четырех:

$$\varrho(x) \leq 4 \quad x \in S,$$

где S — множество вершин графа C. Места расположения трансформаторов представляют собой источники, обладающие определенной интенсивной величиной (непряжением), а потребители являются поглотителями текущей в сети экстенсивной величины (заряда) [3]. Под окрестностью трансформатора подразумеваем такое дерево, корнем которого является вышеупомянутый источник. При таком подходе законы Кирхгофа могут быть сформулированы следующим образом:

I. В любой точке сумма экстенсивных количеств равна нулю (I [заряд/время]);

II. Интеграл интенсивных количеств (напряжений Δu) по замкнутой кривой равен нулю.

Пусть число проектируемых или уже действующих трансформаторов равно m, а места их расположения вершины k_i графа C ($i = 1, 2, \ldots, m$). На графе C построим максимальное дерево C'_{k_i}, корнем которого является вершина k_i ($i = 1, 2, \ldots, m$). Под максимальным деревом подразумеваем такое дерево, которое получается исключением простых циклов графа C. Однозначное построение такого дерева возможно на основе следующей теоремы:

Теорема 1. Пусть k_i будет некоторая фиксированная вершина графа C. Тогда существует такое максимальное дерево C_{k_i} с корнем k_i, при котором произвольная вершина графа C соответствует тому ребру простой цепи, выходящей из k_i, на котором максимальна соответствующая экстенсивная величина.

Доказательство. Так как C связный граф, то любые две вершины графа могут быть соединены простой цепью, поэтому длины их являются положительными целыми числами. Таким образом, всегда существует найкратчайшая цепь, между вершинами x и y; её длину незываем расстоянием между вершинами x и y и обозначаем через $d(x, y)$. Для произвольного числа n существует такое множество вершин A_n, для элементов которого справедливо

$$d(k_i, x) = n \quad x \in A_n.$$

Таким образом, с помощью непересекающихся подмножеств A_n множество можно записать в виде:

$$S = k_i \cup A_1 \cup A_2 \cup \cdots$$

Вершины, относящиеся к подмножеству A_n, могут быть соединены только с вершинами, относящимися к подмножествам A_{n-1}, A_n, A_{n+1}. В противном случае, если существует ребро, связывающее элементы множеств A_n и A_{n+l} ($l \geq 2$), то в подмножестве A_{n+l} существовал бы элемент z, для которого

$$d(k_i, z) \leq n + 1 \quad z \in A_{n+l}.$$

Максимальное дерево C'_{k_i} получим таким образом, что из ребер, связывающих вершину $z \in A_n$ с элементами подмножества A_{n-1}, выберем ребро с наибольшей экстенсивной величиной, остальные исключим из графа. Легко видеть, что полученный подграф C'_{k_i} связный и не имеет простых циклов, а также добавлением любого ребра получим простой цикл. Значит, C'_{k_i} максимальное дерево, покрывающее все вершины графа C, и каждая вершина соответствует тому ребру простой цепи, выходящей из корня дерева k_i, которому соответствует наибольшая экстенсивная величина.

Теперь рассмотрим возможный метод построения максимального дерева C'_{k_i}. Для вершин связного графа C запишем закон Кирхгофа

$$\sum_y i_{xy} + I_x = 0, \qquad (1)$$

где x — фиксированная вершина, а y пробегает все соседние с x вершины,

$\quad i_{xy}$ — интенсивные величины, относящиеся к ребрам с вершиной x,

$\quad I_x$ — величина тока, потребляемая в вершине x.

Используя связь между градиентом интенсивных количеств и экстенсивными количествами, на основе уравнения (1) можно записать следующую систему линейных уравнений:

$$\left[-\frac{1}{R_{xy_1}} \ \cdots \ \sum_{i=1}^{\tau} \frac{1}{R_{xy_i}} \ \cdots \ -\frac{1}{R_{xy_\tau}} \right] \times \begin{bmatrix} U_{y_1} \\ \vdots \\ \hline U_x \\ \hline \vdots \\ U_{y_\tau} \end{bmatrix} + \begin{bmatrix} \\ \\ I_x \\ \\ \\ \end{bmatrix} = 0$$

где τ — число ребер в вершине x,

    R_{xy_i} — сопротивление на ребре (x, y_i),

    U_{y_i} — интенсивное количество в вершине y_i.

Решив систему линейных уравнений, которые автоматически обеспечивают выполнение II-го закона Кирхгофа, получим значения U_{y_i}, с помощью которых вычислим значения экстенсивных количеств, соответствующих отдельным ребрам.

Найдем те вершины графа C, которые соответствуют нескольким ребрам Из них в каждой вершине выберем то ребро, которому соответствует наибольшее интенсивное количество, а остальные ребра исключим из графа. Согласно теоремы 1 полученный подграф C'_{k_i} будет максимальным деревом.

Исключение ребер может быть выполнено также с помощью задачи Кэли [8]. Для этого каждому ребру ставится в соответствие некоторая мера. В нашем случае это может быть интенсивное количество.

2.2 Модель первичной оптимизации

В нашей задаче требуется минимизировать затраты на капиталовложения при минимальных потерях электроэнергии, т. е. задаче является многоцелевой. Пименим к ней правило преференции: сначала оптимизируем затраты — первичная оптимизация, а потом оптимизируем потери электроэнергии — вторичная оптимизация.

Обозначим множество вершин, в которых проектируется или действует трансформатор, через K ($K \subseteq S$). Для всех источников можно построить такие деревья C_{k_i} с помощью процедуры, рассмотренной ниже, что интенсивные количества в любой вершине этого дерева будут больше некоторой наперед заданной величины. Покрытию q графа C деревьями C_{k_i} должно соответствовать такое подмножество K_q, для которого выполняется следующее:

$$C = \bigcup_{k_i \in K_q} C_{k_i}$$

Рассмотрим вектор $\delta = (\delta_{k_1}, \ldots, \delta_{k_m})$,

$$\text{где } \delta_{k_i} = \begin{cases} 0, & \text{если } k_i \notin K_q \\ 1, & \text{если } k_i \in K_q \end{cases}.$$

Требуется найти такие покрытия графа C деревьями C_{k_i}, для которых выполняется:

$$\sum_{i=1}^{m} \delta_{k_i} \cdot T_{k_i} \rightarrow \min \tag{2}$$

$$C = \bigcup_{k_i \in K_q} C_{k_i} \tag{3}$$

$$U_{k_i x} \geq \alpha \quad x \in S_{k_i}, \tag{4}$$

где T_{k_i} — капитальные затраты k_i-ого источника,
 $U_{k_i x}$ — интенсивное количество в вершине x дерева C_{k_i},
 S_{k_i} — множество вершин дерева C_{k_i},
 α — заданная постоянная величина (минимальное напряжение).

2.3 Процедура построения деревьев C_{k_i}

Рассмотрим построение деревьев C_{k_i}, удовлетворяющих условию (4), из максимальных деревьев C'_{k_i} ($C'_{k_i} \supseteq C_{k_i}$). Вычислим интенсивные количества $U_{k_i x}$ в вершинах дерева C'_{k_i}. Функция является строго убывающей функцией в направлении от корня дерева к концевой точке. Из множества концевых точек дерева C'_{k_i} найдем ту, в которой $U_{k_i x}$ минимальна и не удовлетворяет условию (4). Эту вершину вместе с соответствующим ребром исключим из дерева. Снова вычислим интенсивные количества $U_{k_i x}$ и повторим наши рассуждения до тех пор, пока не будет удовлетворено условие (4). Таким образом, можем сформулировать следующую лемму:

Лемма. Дерево C_{k_i} покрывает все те вершины графа C, в которых выполняется условие (4), и каждая вершина дерева C_{k_i} принадлежит той простой цепи графа C, состоящей из ребер с наибольшими экстенсивными количествами.

Вершины, упускаемые при построении дерева C_{k_i} из дерева C'_{k_i}, должны принадлежать хотя бы одному дереву C_{k_i} ($x \in S_{k_i}$). В противном случае, как это будет показано в следующем пункте, не удовлетворятся необходимое и достаточное условие существования решения задачи. Поэтому вводятся дополнительные источники до тех пор, пока каждая вершина графа C не будет принадлежать хотя бы одному дереву C_{k_i}.

2.4 Метод решения задачи

Построим такую матрицу инциденций A, в которой каждому столбцу однозначно будет соответствовать некоторое дерево C_{k_i}, а каждой строке матрицы — вершина:

$$A = \{a_{ji}\} = \begin{cases} 0, & \text{если } x_j \notin S_{k_i} \quad i = 1, 2, \ldots, m \\ 1, & \text{если } x_j \in S_{k_i} \quad j = 1, 2, \ldots, n \end{cases} \tag{5}$$

где m — количество возможных источников,

n — количество вершин графа C.

Таким образом, задача (2)—(4) может быть сведена к следующей задаче о покрытии множества:

$$\sum_{i=1}^{m} \delta_{k_i} \cdot T_{k_i} \to \mathbf{min} \tag{6}$$

$$\sum_{i=1}^{m} a_{ji} \cdot \delta_{k_i} \geq 1 \quad j = 1, 2, \ldots, n \tag{7}$$

Для решения задачи (6)—(7) известны эффективные алгоритмы (4)—(7), так как матрица инциденций A является довольно редкой. С помощью любого из этих алгоритмов найдем множество решений данной задачи:

$$\{\delta^q\} = Q.$$

Если число возможных источников m выбрано таким образом, что каждая вершина графа C принадлежит хотя бы одному дереву C_{k_i}, то

$$\sum_{i=1}^{m} a_{ji} \geq 1, \quad (j = 1, 2, \ldots, n),$$

что является необходимым и достаточным условием существования решения задачи (6)—(7). Таким образом, если это условие выполняется, то множество Q не будет пустым.

Деревья, входящие в покрытие q, будем обозначать через $C_{k_i}^q$. Отметим, что деревья, входящие в покрытие q, могут пересекать друг друга. Однозначное построение непересекающихся деревьев $D_{k_i}^q$ будет приведено ниже.

2.5 Вторичная оптимизация

Пусть даны множество решений и однозначно определенные непересекающиеся деревья $D_{k_i}^q \subseteq C_{k_i}^q$ ($k_i \in K_q$). Каждому дереву $C_{k_i}^q$ поставим в соответствие некоторую меру $F_{k_i}^q$ (в случае электрической сети — потери электроэнергии).

Найдем такое покрытие q, которому соответствует минимальная сумма мер и удовлетворяются следующие условия:

$$\sum_{i=1}^{m} F_{k_i}^{q} \cdot \delta_{k_i}^{q} \to \min \tag{8}$$

$$D_{k_i}^{q} \subseteq C_{k_i}^{q} \qquad \delta^{q} \in Q, \ k_i \in K_q \tag{9}$$

В случае электрической сети мера $F_{k_i}^{q}$ будет иметь следующий вид:

$$F_{k_i}^{q} = \sum_{l=1}^{l_{k_i}^{q}} \frac{(U_{k_ie})^2}{R_e} \ ,$$

где $l_{k_i}^{q}$ — число ребер дерева $D_{k_i}^{q}$,

R_l — сопротивление ребра l дерева $D_{k_i}^{q}$.

U_{k_il} — падение напряжение на ребре l дерева $D_{k_i}^{q}$. Если выполняется условие (9), то заведомо выполняется и (4).

2.5 Построение деревьев $D_{k_i}^{q}$

Рассмотрим покрытие q $(\delta^{q} \in Q)$. Допустим, что вершина x принадлежит одновременно нескольким деревьям $C_{k_i}^{q}$, т. е.

$$x \in \bigcap_{i=1}^{\tau} S_{k_i}^{q}. \tag{10}$$

Чтобы получить непересекающиеся деревья необходимо, чтобы вершина x принадлежала единственному множеству, которое будем обозначать через $Z_{k_i}^{q}$. Теперь рассмотрим правило, согласно которому такие вершины x однозначно будут принадлежать тому или иному множеству $Z_{k_i}^{q}$:

$$\begin{cases} x \in Z_{k_i}^{q}, \text{ если } \max U_{k_ix} = U_{k_ix} \ (i = 1, 2, \ldots, \tau) \\ x \in Z_{k_l}^{q}, \text{ если } U_{k_ix} = U_{k_jx} \text{ и они максимальны,} \\ \qquad \text{а также } k_l < k_j \end{cases} \tag{11}$$

Правило (11) сформулировано таким образом, чтобы при его использовании потери электроэнергии в сети были минимальны. Применяя правило (11) для общих вершин деревьев $C_{k_i}^{q}$, получим такие множества $Z_{k_i}^{q}$, для которых выполняется следующее:

$$Z_{k_i}^{q} \subseteq S_{k_i}^{q} \tag{12}$$

$$Z_{k_i}^{q} \cap Z_{k_j}^{q} = \varnothing \quad i \neq j \tag{13}$$

$$\bigcup_{k_i \in K_q} Z_{k_i}^{q} = \bigcup_{k_i \in K_q} S_{k_i}^{q} \tag{14}$$

Для применения правила (11) достаточно знать множество $S_{k_l}^q$ и соответствующие вершинам и деревьям величины U_{k_ix}, и несущественно знать топологию деревьев $C_{k_i}^q$. Рассмотрим следующую теорему.

Теорема 2. Для каждого покрытия q графа C деревьями $C_{k_i}^q$ существует такое покрытие из непересекающихся дерaвьев $D_{k_i}^q$ после применения правила (11), для которых справедливо следующее:

$$D_{k_i}^q \subseteq C_{k_i}^q \quad k_i \in K_q \tag{15}$$

$$D_{k_i}^q \cap D_{k_j}^q = \varnothing \quad \forall i \neq j \tag{16}$$

$$\bigcup_{k_i \in K_q} C_{k_i}^q = \bigcup_{k_i \in K_q} D_{k_i}^q \tag{17}$$

Доказательство. Сначала покажем, что подграф $D_{k_i}^q$ на множестве $Z_{k_l}^q$, полученном после применения правила (11), является связным, в таком случае $D_{k_l}^q$ обязательно будет деревом, так как $C_{k_l}^q$ является также деревом. На произвольном дереве $C_{k_l}^q$ выберем те концевые точки x, где на маршруте $L = L (k_l, \ldots, y, x)$ есть общие вершины с деревьями $C_{k_i}^q$. Рассмотрим маршрут L, отправляясь из точки x в направлении корня дерева k_i. Покажем, что если $x \in Z_{k_l}^q$, то для соседней вершины также $y \in Z_{k_l}^q$. Допустим противное, что $x \in Z_{k_l}^q$, а $y \in Z_{k_t}^q$. Тогда согласно правилу (11)

$$U_{k_lx} \geq U_{k_ix} \quad k_i \in I_1 \tag{18}$$

$$U_{k_ly} \geq U_{k_iy} \quad k_i \in I_2, \tag{19}$$

где I_1 — множество деревьев, к которым принадлежит вершина x,

I_2 — множество деревьев $C_{k_i}^q$, к которым принадлежит вершина y.
Возможны следующие *три случая:*

1. Концевое ребро (x, y) дерева $C_{k_l}^q$ принадлежит также дереву $C_{k_t}^q$. В дальнейшем под направлением будем подразумевать направление от концевой точки в сторону корня дерева. В данном случае направление на ребре (x, y) или совпадает или нет, но в обоих случаях ребро (x, y) должно быть концевым ребром дерева $C_{k_t}^q$. В противном случае для дерева $C_{k_l}^q$ не выполняется утверждение леммы, так как существует по крайней мере одна такая вершина z, что

$$U_{k_lz} \geq U_{k_tz} \geq \alpha \, u \, z \in S_{k_l}.$$

Последнее неравенство получено из (18) с учетом, того, что U_{k_l} и U_{k_t} строго убывающие функции на том же самом ребре (x, y).

1.1 Если направление на ребре (x, y) совпадают (рис. 1) и выполняется условие (18), то запишем закон Кирхгофа для вершины x для обоих деревьев:

$$U_{k_lx} = U_{k_ly} - R_{xy} \cdot I_x \tag{20}$$

$$U_{k_tx} = U_{k_ly} - R_{xy} \cdot I_x \tag{21}$$

Применяя неравенство (19), получим, что

$$U_{k_t x} \geq U_{k_t x} ,$$

а это противоречит условию (18).
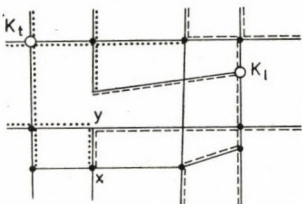
Рис. 1
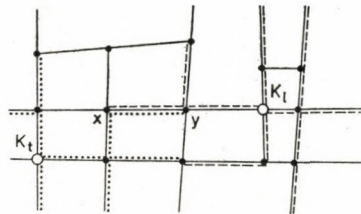

Рис. 2

1.2 Если направления на ребре (x, y) не совпадают (рис. 2) и выполняются (18)—(19), то

$$U_{k_t x} > U_{k_t y} \ u \ U_{k_t y} > U_{k_t x} ,$$

так как U_{k_t} и U_{k_t} — убывающие в противоположном направлении функции. В результате этого получаем

$$U_{k_t x} > U_{k_t y} \geq U_{k_t y} > U_{k_t x} ,$$

что опять-таки противоречит неравенству (18).

2. Вершины x и y принадлежат дереву $C_{k_t}^q$, но ребро (x, y) уже нет. В этом случае концевая точка дерева $C_{k_t}^q$ будет также концевой и для $C_{k_t}^q$. В противном случае для дерева $C_{k_t}^q$ не выполняются утверждения леммы, так как существует такая вершина z, что

$$U_{k_t z} \geq U_{k_t z} \geq \alpha \ u \ z \notin S_{k_t}^q .$$

Последнее неравенство получено с учетом того, что выполняется условие (18) и U_{k_t} и U_{k_t} являются строго убывающими функциями. Таким образом, вершина x является концевой точкой дерева $C_{k_t}^q$. Здесь также возможны два случая.

2.1 Допустим, что $d(k_t, x) = n$ и $d(k_t, y) = n-1$ (рис. 3) Запишем закон Кирхгофа в вершине x обоих деревьев $C_{k_t}^q$ и $C_{k_t}^q$:

$$U_{k_t x} = U_{k_t y} - R \cdot I_x , \tag{22}$$

$$U_{k_t x} = U_{k_t z} - R \cdot I_x . \tag{23}$$

Покажем, что

$$U_{k_t z} \geq U_{k_l y}$$

Согласно лемме

$$U_{k_t z} \geq U_{k_l y} ,$$

а согласно условию (19)

$$U_{k_l y} \geq U_{k_l y}$$

то есть

$$U_{k_t z} \geq U_{k_l y} .$$

Таким образом, из уравнений (22)—(23) получим, что

$$U_{k_t x} \geq U_{k_l x} ,$$

а это противоречит неравенству (18).

2.2 Допустим, что $d(k_t, x) = n-1$ и $d(k_l, y) = n$ (рис. 4).
Согласно (19)

$$U_{k_l y} \geq U_{k_l y}$$

и по построению дерева $C^q_{k_t}$ и $C^q_{k_l}$

$$U_{k_l y} \geq U_{k_l x} \quad u \quad U_{k_l x} \geq U_{k_l y} .$$

Таким образом, опять получено противоречие:

$$U_{k_l x} \geq U_{k_l y} \geq U_{k_l y} \geq U_{k_l x} .$$
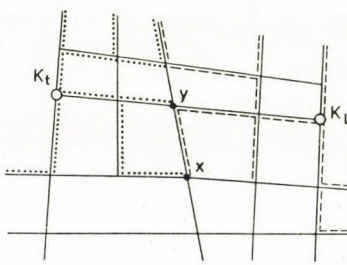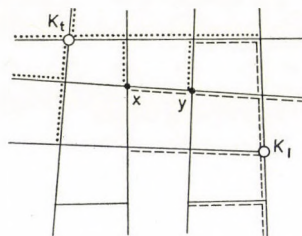
Рис. 3   Рис. 4

3. Вершина x не принадлежит дереву $C^q_{k_t}$, только вершина y, т. е. $x \notin S^q_{k_t}$, $y \in S^q_{k_t}$. Согласно условию (19)

$$U_{k_t y} \geq U_{k_l y} ,$$

а согласно лемме

$$U_{k_t y} \geq U_{k_t x} \geq \alpha ,$$

т. е. U_{k_tx} должно быть больше, чем U_{k_tx} и α, так как U_{k_t} и U_{k_t} являются строго убывающими функциями на ребре (x, y). Таким образом, для дерева $C^q_{k_t}$ не выполняется утверждение леммы, так как существует такая вершина x, что

$$U_{k_tx} \geq \alpha,$$

но в то же время x не принадлежит дереву $C^q_{k_t}$. Этим самым мы доказали, что $y \in Z^q_{k_t}$, если $x \in Z^q_{k_t}$. Если $x \in S^q_{k_t}$, но $x \notin Z^q_{k_t}$, то эту вершину с соответствующим ребром (x, y) опускаем из дерева $C^q_{k_t}$. Если вершина y в результате этого стала концевой точкой, то повторим вышеприведенные рассуждения. Из всего сказанного выше видно, что подграф $D^q_{k_t}$ будет связным.

Повторив все вышеприведенные рассуждения для каждого покрытия q, получим непересекающиеся деревья $D^q_{k_i} \subseteq C^q_{k_i}$. Легко видеть, что условия (16)—(17) являются следствием условий (14)—(13). Этим самым доказательство теоремы завершено.

После построения деревьев $D^q_{k_i}$ поперечное сечение проводов выбирается таким образом, чтобы оно не убывало в любом направлении от корня дерева и удовлетворялось условие (4).

Таким образом, получим конечное множество покрытий непересекающихся деревьев $D^q_{k_i}(\delta^q \in Q)$. Из этого конечного множества Q выберем то покрытие, которому соответствуют минимальные потери электроэнергии.

3. Выводы

В данной статье в общем виде сформулирована проблема оптимального проектирования сетей часто встречающаяся в практике, которые могут быть представлены в виде связного графа. Ищем такое оптимальное разбиение графа на непересекающиеся деревья, при котором сумма капитальных вложений и потери электроэнергии достигают минимума. В статье рассматривается также вопрос построения деревьев из связного графа, удовлетворяющих некоторым условиям. В связи с этим доказано две теоремы. С помощью матрицы инциденций решение задачи может быть сведено к решению задачи о покрытии множества. На конечном множесте решений этой задачи выберем то, которому соответствуют минимальные потери энергии.

Согласно первого опыта можно сэкономить приблизительно 10% числа трансформаторов по сравнению с традиционными методами проектирования электрических сетей. Программа на языке ФОРТРАН для ЭВМ «СИМЕНС 4004/151» разработана в «САМГЕП»-е по заказу проектного института «ЭВИТЕРВ».

Finding of Optimal Number, Place and District Ovetransformes in Low-Voltage Electric Networks by a "0−1" Linear Programming. In this paper the even more frequent problem of optimum networking is formulated in a general form. The essential of the problems is to search for the optimum location and number of those sources which satisfy the limiting conditions in every network point and secure minimum network losses. To source is ordered a tree, for which two therorems are proved. By introducing an incidence matrix the problem can be reduced to a zero-one linear programming problem, for the solution of which several efficient methods are known from literature. From the finite set of solutions, one is selected which provides minimum network losses. According to the first experiences with practical problems about 10% of the transformes could be saved, which gives the same savings for the investment costs as compared with earlier plans. The computer program has been elaborated on a commission from ÉVITERV for a SIEMENS 4004/151 comuter, using FORTRAN language.

Bestimmung der optimalen Anzahl, Versorgungsbereiche und der Placierung von Transformatoren in Niederspannungsnetzen mittels einer »0−1« Programmierung. In der vorliegenden Arbeit wird ein häufiges Problem, das der optimalen Projektierung von Netzen, in allgemeiner Form abgefaßt. Das Wesentliche des Problems ist, daß die optimale Anzahl und Placierung jener Quellen gesucht wird, welche die beschränkenden Bedingungen in jedem Netzpunkt erfüllen und dabei minimale Netzverluste ergeben. Jeder Qielle wird ein Baum zugeordnet, für dessen Aufbau zwei Sätze bewiesen werden. Durch Einführung einer Inzidenz-Matrix kann das Problem auf eine lineare 0−1 Programmierungsaufgabe zurückgeführt werden, für deren Lösung aus der Literatur mehrere wirksame Methoden bekannt sind. Aus der endlichen Menge der Lösungen wird diejenige ausgewählt, welche einen minimalen Netzverlust ergibt. Nach den bisherigen ersten Erfahrungen kann bei den in der Praxis vorkommenden Aufgaben ca. 10% der Transformatoren erspart werden, was verglichen mit den früheren Plänen eine Verringerung der Investkosten im gleichen Verhältnis ergibt. Das Rechenprogramm wurde im Auftrag von ÉVITERV für einen SIEMENS 4004/141 Rechner in FORTRAN ausgearbeitet.

VELAROIDAL SHELLS
FOR COVERING UNIVERSAL INDUSTRIAL HALLS

M. MIHAILESCU* and Miss I. HORVÁTH*

In order to cover large column-free square areas a new type of shell structure is proposed. Considering its shape and its way of generation, the surface belongs to the family of velaroidal ones. Choosing the generatrix as an ellipse, advantageous geometrical and mechanical properties are obtained. Membrane stress analysis and a numerical example are presented.

1. Introduction

It is well known that large span industrial halls of 18×18 to 40×40 m draw great attention. They provide large functional possibilities, housing various technological processes of a character continually changing and developing.

The thin shell structure is a rational solution to cover quadratic areas owing to its spatial manner of work and being able to satisfy a great number of functional requirements concerning natural lighting, ventilation, a smooth ceiling, as well as the hanging of a series of overhead light — duty transporting equipments.

In this paper a structure, made of thin shells, proposed for the use of universal industrial halls, which best meets the multiple functional needs as well as those of mechanical behaviour and execution technology, is presented.

2. Velaroidal shells. Some important geometrical properties

In establishing the shape of the middle surface of the shell we first took into account the functional requirements of cover in a square area, and then (using a bisymmetrical surface) to avoid discontinuities which might disturb the membrane stress state in the shell.

From the surfaces satisfying the two requirements, the velaroidal one was chosen, due to its characteristic of having straight edges to simplify the requirement of contour elements.

* Polytechnical Institute of Cluj-Napoca, Romania.

The velaroidal surface (Fig. 1) is generated by a variabile curve (1) which is translated on another curve (2) degenerating into straight lines on the boundaries. The generating profile can be any plane curve, consequently resulting in surfaces of different geometrical peculiarities.

For parabolic profiled velaroids BALLESTEROS [1], BREBBIA's and FERRANTE's [2] and L. KOLLÁR's [3] papers are known.

The velaroidal shells with parabolic directrix have also been studied by the authors in designing an exhibition hall in the city of Cluj-Napoca (Fig. 2) [4].

Fig. 1

LINES OF PARABOLICAL POINTS IF THE DIRECTRIX IS ① PARABOLA ② CIRCLE ③ ELLIPSE
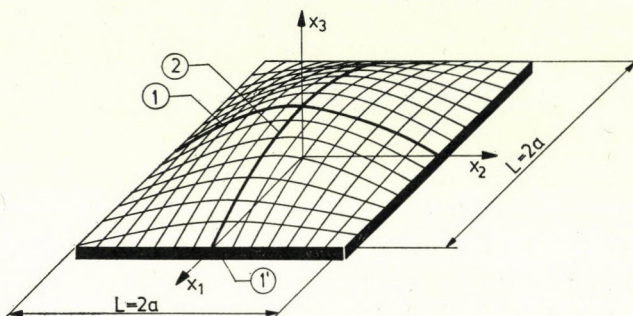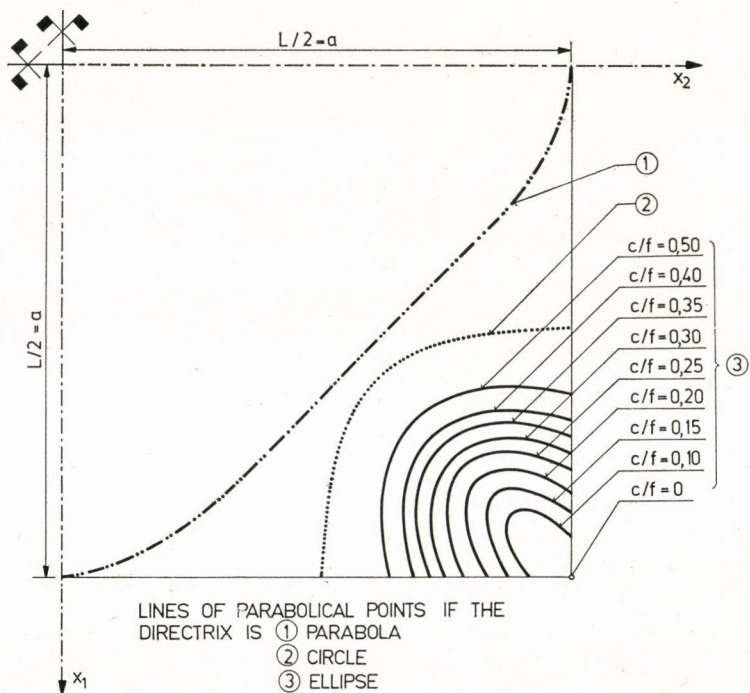
Fig. 2

In proceeding with the study of universal industrial hall coverings we have chosen a new form of velaroidal surface, that generated by an ellipse, the one we shall call *elliptical velaroid*. The reason for this choice is to reduce the region of hyperbolic points as much as possible on the surface (in the corner zones), that might disturb the stress state of the shell.

We have also taken into consideration the more advantageous mechanical behaviour of the superelevated profiles with respect to the circle and parabola shape, thus extending DISCHINGER's [5] and JAKOBSEN's [6] consideration from cylindrical shells to velaroidal ones.
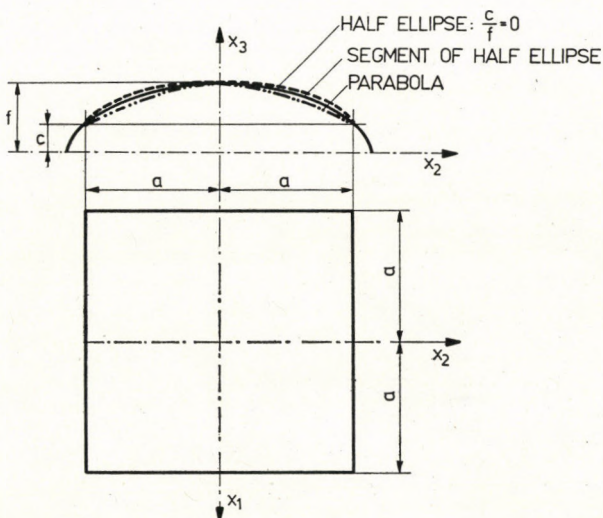
Fig. 3

The comparative study, made for velaroidal surfaces with parabolic, circular and elliptical directrix having the same height/span ratio, on the trajectories of parabolic type of points which separate the elliptical surface zones from those of hyperbolic ones shows that the smallest hyperbolic zones are obtained in the case of elliptical velaroid. It is possible in extreme situations, that these zones be completely eliminated, namely, for a semi-elliptical directrix with a slope of 90° at each boundary point (Fig. 3). In this latter case the corner point is not an inflexional point but rather a singular one, the diagonal-directed cross-section of the surface being a second degree parabola.

It is to be noticed that while in the case when the directrix curve is a parabola or a circle, the velaroidal surface is geometrically determined by a single adimensional parameter (for example the height/span ratio), for defining the shape of an elliptical velaroid there are two free parameters which may be: the height/span ratio, that is $\lambda = (f-c)/2a$, and the slope of the directrix

on the boundary which can be replaced by the ratio $k = c/f$ (Fig. 4), as follows from the surface equation:

$$x_3 = \sqrt{f^2 - \frac{f^2 - c^2}{a^2}(x_1^2 + x_2^2) + \frac{f^2 - c^2}{a^4} x_1^2 x_2^2} \quad ,$$

or denoting $k = c/f$:

$$x_3 = \frac{f}{a^2}\sqrt{a^4 - a^2(1 - k^2)(x_1^2 + x_2^2) + (1 - k^2) x_1^2 x_2^2} \ . \tag{2}$$
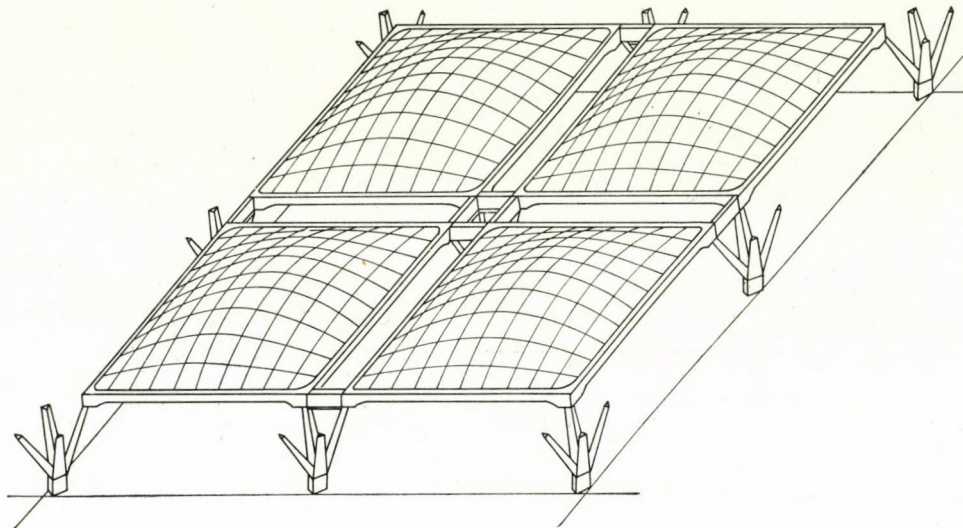
Fig. 4

The elliptical velaroid generated by semiellipses, described by equation

$$x_3 = \frac{f}{a^2}\sqrt{a^4 - a^2(x_1^2 + x_2^2) + x_1^2 x_2^2} \ , \tag{3}$$

thus appears as a particular case ($c = k = 0$) of a more general class of surfaces described by equation (1) and (2), further these latter ones are especially insisted upon.

From the point of view of stress state and boundary conditions two geometrical characteristics are of interest:

— the surface tangent variation along the boundary $x_1 = \pm a$ (Fig. 4):

$$\tan \alpha_1 = \partial_1 x_3 = \frac{f^2 - c^2}{ac}\left(\frac{x_2^2}{a^2} - 1\right) = 2\lambda \frac{1 + k}{k}\left(\frac{x_2^2}{a^2} - 1\right) \tag{4}$$

- the curvature radius variation, with the greatest values in the central zones of the surface, which are of interest from the point of view of thin shell stability; for $x_1 = x_2 = 0$ the curvature radius has the value:

$$\varrho = -\frac{a}{f-c}\frac{a}{1+k}.\qquad(5)$$

From relation (5) as well as from Fig. 4 it can be observed that the greatest curvature radii are obtained for small values of k (at the limit $k = 0$) in the central zone, a disadvantageous situation for thin shell's stability.

3. Edge conditions. Solution for the state of stresses

The state of stresses was determined with the aid of the membrane theory, considering the problem as a Dirichelet problem. The stress function was specified along the edges, in concordance with the type and constructive achievement of the supports.
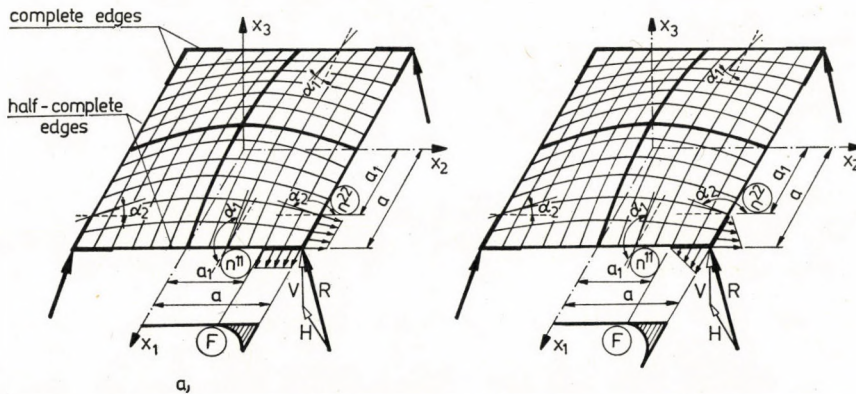

Fig. 5

For structure (Fig. 5) supported at the corner points, with their edge beams working as ties, strengthened towards the corners, zones where some horizontal stiffenings are also provided, the following boundary conditions are established: half-complete edges capable of taking over only tangential stresses; complete edges capable of taking over both tangential and normal stresses at the corner zones (Fig. 6).

In order to have the variation of normal stress n^{11}, respectively n^{22} as close to reality as possible, two variants were selected on the complete edge zone:

a) the normal stress is constant, $n^{11} = K$ (Fig. 6a), or b) linearly variable, $n^{11} = m\,(x_2 - a_1)$ (Fig. 6b).

In these two cases, from the overall equilibrium condition, the boundary stress values are deduced for symmetrical loadings as follows:

$$4 \int_{a_1}^{a} n^{11} \tan \alpha_1 \cos \alpha_2 dx_2 + 4 \int_{a_1}^{a} n^{22} \tan \alpha_2 \cos \alpha_1 dx_1 = 4V ,$$

or

$$8 \int_{a_1}^{a} n^{11} \tan \alpha_1 \cos \alpha_2 dx_2 = 4V \tag{6}$$
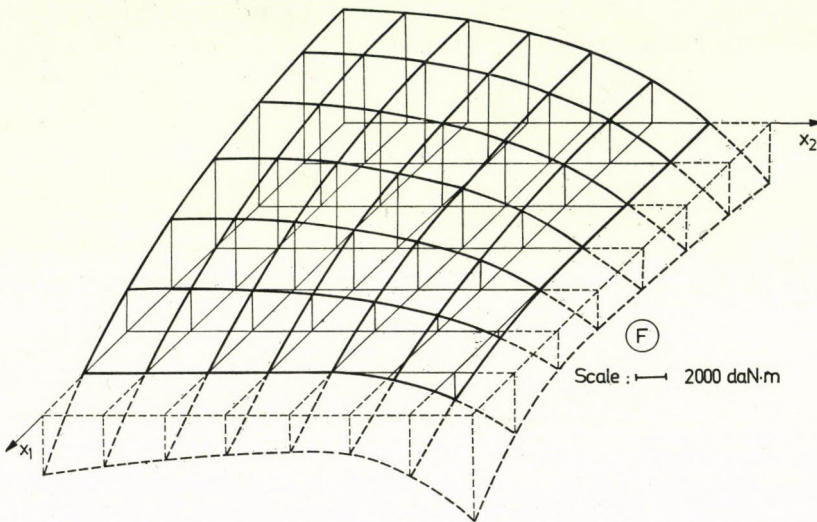
Fig. 6

where α_1 and α_2 are the angles of the surface slope along the edges $x_1 = \pm$ a, respectively, $x_2 = \pm$ a, V is the vertical projection of the oblique reactive force, $n^{11} = N^{11} \cos \alpha_1 / \cos \alpha_2 = \cos \alpha_1 N^{11}$ ($\cos \alpha_1 = 1$ along the edges $x_1 = \pm a$); $\tan \alpha_1$ is achieved by the relation (4), or denoting

$$b = \frac{f^2 - c^2}{a^2} \quad \text{and} \quad d = \frac{f^2 - c^2}{a^4}$$

it can be expressed by the formula

$$\tan \alpha_1 = \frac{a}{c} \left(-b + dx_2^2 \right) . \tag{7}$$

In order to describe the state of stresses of the shell a stress function of Airy type "F" is introduced from which the stress resultants are obtained by the formulae:

$$n^{11} = \partial_{22} F ; \quad n^{12} = - \partial_{12} F ; \quad n^{22} = \partial_{11} F . \tag{8}$$

This stress function has to satisfy the governing differential equation

$$r\partial_{22}F - 2s\partial_{12}F + t\partial_{11}F = I \tag{9}$$

where r, s and t are the curvature coefficients of the middle surface, I is the loading.

The boundary conditions converted into the stress function are: along the half-complete edges $F = 0$, and facing the complete edge zones, F should be determined by integrating the expression of $\partial_{22}F$, after replacing n^{11}, obtained from relation (6) in equation (8). Thus, for the two assumed cases (Fig. 6a and b) the variation of the stress function along the edge $x_1 = a$, follows from the relations:

$$F = \frac{n^{11}}{2}(x_2 - a_1)^2 , \tag{10}$$

respectively,

$$F = \frac{m}{6}(x_2 - a_1)^3 . \tag{11}$$

It is to be noticed that the variation of F given by relation (11) is more suitable for assuring the continuity of the solution at the connection point between the half-complete and complete edge zones.

4. Numerical example

As an application, the state of stresses for an elliptical velaroid with a ground area of 24×24 m, for a height/span ratio equal to $1/6$ and $c/f = 1,5/5,5$ was determined.

The integration of the differential equation (9) was carried out by the finite difference method taking as a quarter of the base surface a lattice of 64 points. The calculations were carried out with a FORTRAN programme on a FELIX C 256 computer, for a loading of 25 daN/m² deadweight, and "a" type boundary conditions. For the stress function and stress resultants the diagramms as shown in Figs 7, 8 and 9 have resulted. Finally, the values as well as the trajectories of the principal stress resultants have been determined.

5. Conclusions

Analysing the state of stresses, the following conclusions can be drawn:
— The prevailing stresses are of compression type in inverse relation to surface curvature (Figs 8 and 9).
— The principal compressive stresses are directed towards the corners.
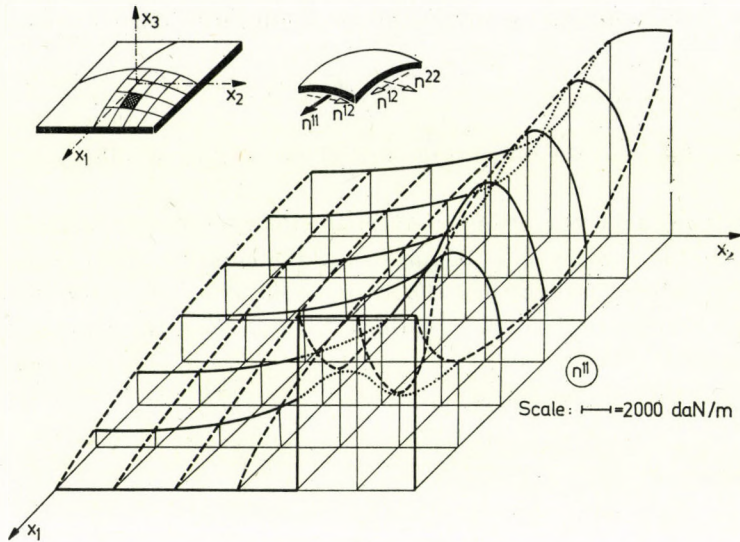
Fig. 7
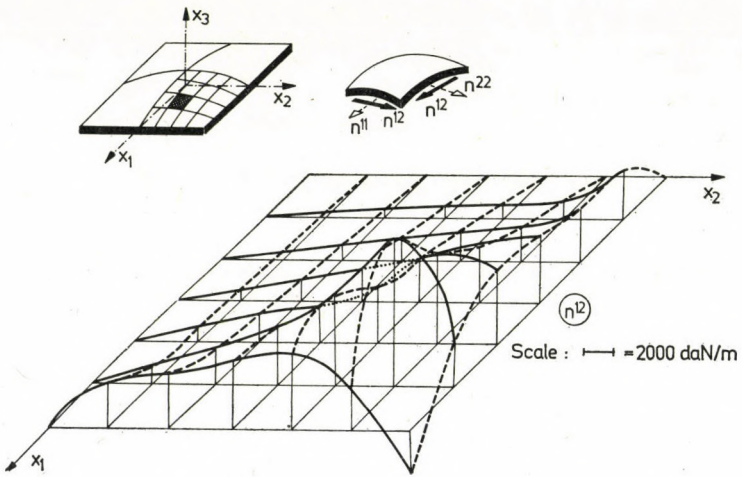
Fig. 8

— Small tensile stresses occur in the vicinity of the half-complete edges.
— Tensile stresses also occur in a small zone in the vicinity of the corner points. They are perpendicular to the diagonal and require a proper reinforcement.
— The stress resultant n^{12} acting along the edge lines as well as the horizontal components of the reactive forces can be easily taken over by prestressing the rectilinear edge beams.
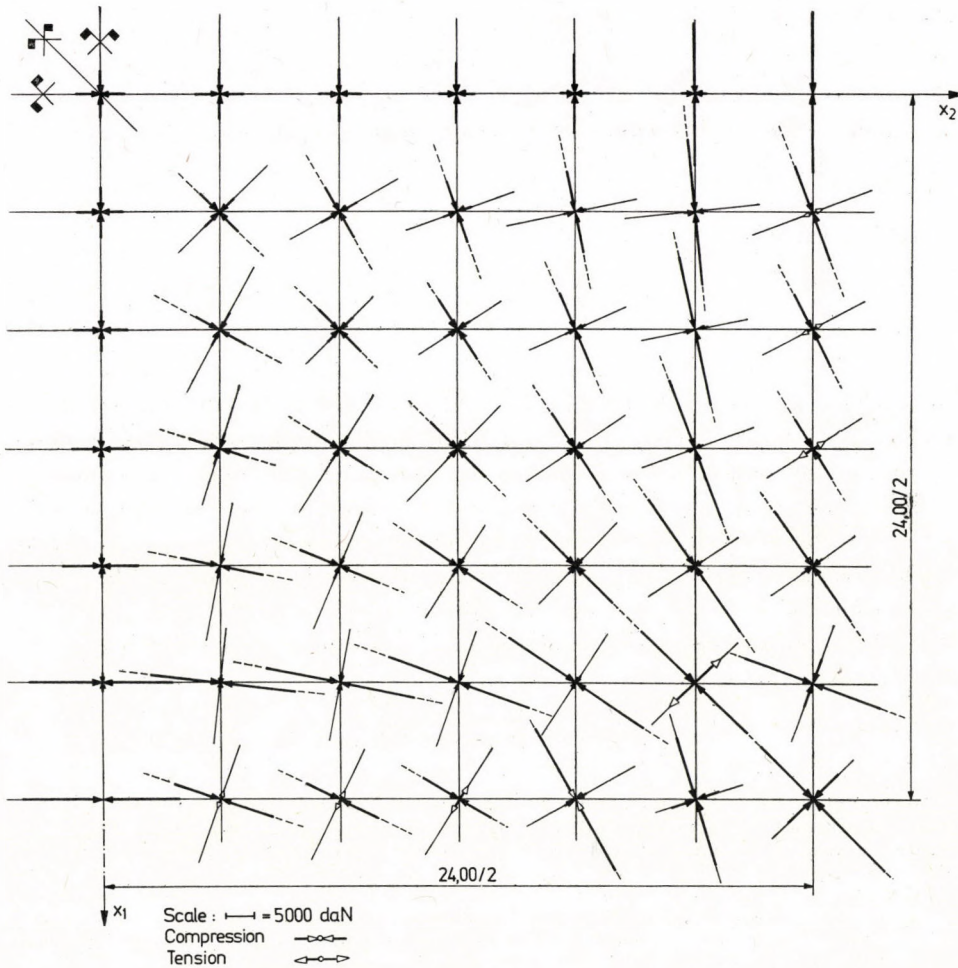
Fig. 9

6. The stability of the velaroidal shells

Problems concerning the stability of the elliptical velaroid are still to be studied. In paper [2] the stability of a velaroid with parabolic directrix is approximated with that of a similar elliptical paraboloid. It seems that reality is closer to the approximation offered by a funicular-type shell, resembling the shape of the velaroidal one better, theoretically and experimentally dealt with in papers [7], respectively [8]. The relation for the critical loading proposed in the last paper (used also in [9]) is:

$$p_{cr} = c \cdot E \cdot \left(\frac{\delta}{a} \cdot \frac{f_1}{a} \right)^2 \tag{12}$$

where

$$c = 0,40 \cdot e^{-\frac{a}{12,2}}$$

in which "δ" is the thickness, "a" the halfspan, and "f_1" the total height of the shell.

Considering relation (5), that means $\varrho \cong a^2/f_1$, from formula (12), the critical loading can be expressed by

$$p_{cr} \cong c \cdot E \cdot \left(\frac{\delta}{\varrho} \right)^2 , \qquad (13)$$

an equation known from the linear theory of local stability. Lacking a proper calculating relation for elliptical velaroidal shells supported at corner points, the use of formula (13) can be recommended, taking as curvature radius the greatest one, that is, the curvature of the center of the elliptical velaroid.

For checking the calculated state of stresses and the general behaviour of the structure under load, as well as the behaviour of joints in the case of precasting the shell a 1 : 8 scaled, reinforced mortar model was tested.

Aspects concerning experimental results will be presented later on.

REFERENCES

[1] BALLESTEROS, P.: Parabolic Velaroidal Shell. *International Symposium on Shell Structures in Engineering Practice*, Budapest, Hungary, 31st Aug. to 3rd. Sept. 1965
[2] BREBBIA, C. A.—FERRANTE, A. J.: On the Parabolic Velaroidal Shell. *Bulletin of the IASS* Nr. 38, June 1969
[3] KOLLÁR, L.: Negyedrendű felületű, egyenes peremű hajlított héj számítása szimmetrikus és antimetrikus teherre. (Bending Analysis of a Symmetrically or Antimetrically Loaded Straight-Edge Shell with a Surface of Fourth Order). *Műszaki Tudomány* **43**, 1970 (In Hungarian)
[4] MIHAILESCU, M.—HORVÁTH, I.—POCANSCHI, A.: Invelitoare velaroidală prefabricată pentru sala de expoziție Cluj. (Precast Velaroidal Shell for an Exhibition Hall in Cluj). *Conferinţa a IV-a de Betoane*, Braşov, Romania, 1972.
[5] DISCHINGER, FR.: Der Spannungszustand in affinen Schalen und Raumfachwerken. *Der Bauingenieur* 17 (1936)
[6] JAKOBSEN, A. A.: Zylinderschalen mit veränderlichem Krümmungshalbmesser und veränderlicher Schalenstärke. *Der Bauingenieur* 18 (1973)
[7] DAYARATNAM, P.: Buckling of Funicular Shell of Square Plane. The Institution of Engineers (India), March 1965
[8] ADELLO, R. I.—ALGOOD, I. R.: Shells for Standard Floor and Roof Elements. *Journal of the Structural Division.* ST 10, 1973.
[9] GIONCU, V.: Studii teoretice şi experimentale privitoare la stabilitatea învelitorilor subţiri pe contur patrat (Theoretical and Experimental Analysis on Stabiliy of Thin Shells of Square Plane). Institutul Politehnic "Traian Vuia" Timişoara martie 1975

Velaroidschalen zur Abdeckung universaler Industriehallen. — Zur Abdeckung grosser quadratischer Räume wird eine neuartige Schalenkonstruktion vorgeschlagen. Nach der Form und Herstellungsweise gehört diese Fläche zur Familie der Velaroidflächen. Wählt man eine Ellipse als Leitkurve, so erhält man vorteilhafte geometrische und mechanische Eigenschaften. Es werden die Methode der Membranspannungszustandsanalyse der behandelten Schale und eine numerisches Beispiel dargestellt.

Веляроидные оболочечные конструкции для покрытия универсальных промышленных корпусов. Веляроидные оболочки являются новой формой оболчек, рекомендуемых для покрытия больших площадей четырехугольной формы, не имеющих опор на колоннах. Вследствие имеющейся формы и способа геометрического построения поверхность оболочка может быть отнесена к группе веляроидных поверхностей. Если в качестве основной кривой выбрать эллипс, тогда получаются выгодные геометрические и механические условия, здесь идет речь об анализе мембранных напряжений оболочечной конструкции при одновременной иллюстрации числового примера.

VARIATION METHOD GIVING THE SOLUTION TO THE TORSION PROBLEM OF PRISMATIC BARS OF COMPOSITE MATERIAL

I. ECSEDI*

The author deals with the problem of free torsion of prismatic bars having a solid cross section, built up of composite materials. In Chapter 2 of the paper, methods of the variation calculus are presented which may be used for the solution to quasi-static boundary-value problems of linearly elastic continua of composite materials. This chapter sums up and generalizes the conditions of stationariness and minimum principles of the theory of elasticity connected with the *potential energy* and *complementary work*. The third chapter reports on the basis of the literature on the subject, on what should be known in connection with the elastic free torsion of bars with an inhomogeneous cross section, the so-called prismatic bars made up of composite materials. Chapters 4 to 7 report on some new achievements concerning the free torsion of composite prismatic bars which may be obtained by the application of the theorems described in different chapters of the paper. It is emphasized that according to a given formula the torsional stiffness may be estimated from below and according to another from above. Chapter 6 treats the torsional problem of prismatic bars reinforced with a thin layer. Chapter 7 comprises three examples.

1. Introduction

1.1 *Preliminaries*

In this paper the free torsion problem of prismatic bars having a solid cross section, produced from composite material, is dealt with. The shear modulus of elasticity of the analysed material of the bar has discontinuity in the plane of the cross section. This discontinuity follows from the fact that the prismatic bar is built up from several different homogeneous isotropic materials. The elastic free torsion of prismatic bars has been treated of by several authors. Their method was based on the direct integration of the equations related to the problem of continuum mechanics. Thus, for example, MUSKHE-LISHVILI [2] resolved the torsion problem of the inhomogeneity embedded into homogeneous field by applying the theory of integral equations. ELY and ZIENKIEWICZ [6] endeavoured to find a solution according to the grid method frequently applied in the field of mathematical physics to the

* Dr. I. ECSEDI, Vászonfehérítő u. 24, H-3531 Miskolc, Hungary.

boundary-value problem defining the stress function. Other authors, such as for example, ARUTJUJÁN and ABRAMJAN [1], LEHNICKIJ [8] and SEIDE [5] gave an analytic solution by separating the Fourier variables. The present paper describes the solution to the above problem by the method of variation.

1.2 *Notations*

The following symbols of major significance as used in this paper:

B_1, B_2, B	space regions
A_1, A_2, A_{12}, A_n, A_p	bi-dimensional surfaces
i	subscript designating elastic body of material constants G_i, v_i ($i = 1, 2$)
G_i	shear elastic modulus
v_i	Poisson's ratio
$\bar{p}$	given surface load
$\bar{q}$	given volume load
$\bar{u}$	given displacement vector
$\mathbf{u}_i = \mathbf{u}_i(\mathbf{P})$	displacement vector
$\mathbf{A}_i = \mathbf{A}_i\,(\mathbf{P})$	deformation tensor
$\mathbf{F}_i = \mathbf{F}_i\,(\mathbf{P})$	stress tensor
$(i = 1, 2)$	
$P \in B_i$ ($i = 1, 2$);	P is point of region B
$P \in A$	P is point of surface A
$P \in g$	P is point of curve g
$\cdot$	denotes scalar multiplication
$\cdot\cdot$	denotes double scalar multiplication
$\triangledown$	Hamilton's differential operator
$\operatorname{tr} \mathbf{A}_i$	first scalar invariant of tensor $\mathbf{A}_i$
$\operatorname{tr} \mathbf{F}_i$	first scalar invariant of tensor $\mathbf{F}_i$
$\mathbf{I}$	second order unit tensor

$$\operatorname{def} \mathbf{u}_i = \frac{1}{2}\,(\triangledown u_i + u_i \triangledown)$$

$\triangledown u_i$, $u_i \triangledown$	diadic product of vectors $\triangledown$ and $\mathbf{u}_i$
$\mathbf{C}_i$, $\mathbf{K}_i$	fourth order symmetric tensors of elastic material constants
α	designation of state
ε	state of equilibrium
"$\wedge$"	designation of kinematically permissible quantity (variable)
"$\sim$"	designation of statically permissible quantity (variable)
P	designation of example
T	symbol of theorem, statement
$\hat{e}_i\ \tilde{e}_i$	density of energy
$=:$	"by definition be equal to"
$R \equiv (-\infty, \infty)$	set of real numbers
π_L, π_C	functionals
δ	operation symbol of forming variation
x, y, z	coordinates of the Cartesius orthogonal system of coordinates
i, j, k	unit vectors of system of coordinates xyz
$\mathbf{R} = \mathbf{x}\,\mathbf{i} + \mathbf{y}\,\mathbf{j}$	
$u^{(i)}, v^{(i)}, w^{(i)}$	scalar coordinates of displacement vector u_i in system of coordinates xyz
$\varepsilon_x^{(i)}, \varepsilon_y^{(i)}, \gamma_{xy}^{(i)},$	
$\varepsilon_z^{(i)}, \gamma_{xz}^{(i)}, \gamma_{yz}^{(i)}$	scalar coordinates of deformation tensor in system of coordinates xyz
$\sigma_x^{(i)}, \sigma_y^{(i)}, \sigma_z^{(i)},$	scalar coordinates of stress tensor $\mathbf{F}_i$ in system of coordinates xyz
$\tau_{xy}^{(i)}, \tau_{yz}^{(i)}, \tau_{xz}^{(i)}$	scalar coordinates of stress tensor $\mathbf{F}_i$ in system of coordinates xzy
u_0, v_0, w_0 $\left.\right\}$ $\omega_1, \omega_2, \omega_3$	constants related to the stiff-body motion
ϑ	relative rotation
$\Phi_i = \Phi_i(P) = \Phi_i(\mathrm{x,y})$	stress function
$\varphi_i = \varphi_i(\mathrm{x,y})$	function characterizing warping of cross section

T_1, T_2, T_{12} regions in plane xy
g_1, g_2, g_{12} curves in plane xy
t tangent unit vector
n normal unit vector
τ_{nz} shear stress
M_c twisting moment
I_c twisting stiffness
$I_{C,L}$, $I_{C,C}$ approximate values of twisting stiffness
I_1, I_2 polar second order moments
l length of prismatic bar
$\partial/\partial s$ derivate calculated in t direction
$\partial/\partial n$ derivate calculated in n direction

$\square = \partial/\partial x\, \mathbf{i} + \dfrac{\partial}{\partial y}\, \mathbf{j}$ Hamilton's bi-dimensional differential operator

$\triangle = \square \cdot \square = \partial^2/\partial x^2 + \partial^2/\partial y^2$ Laplace's operator

2.1 Setting up the problem

The body depicted in Fig. 2.1 is composed of two different homogeneous isotropic, linearly elastic materials. The materials in volume B_1 and B_2 are characterized by Lamé's material constants G_1, ν_1 and G_2, ν_2, respectively.
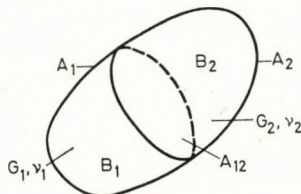
Fig. 2.1. Composite-material body
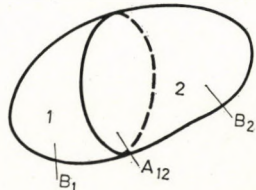
Fig. 2.2a. Body of inhomogeneity a Fig. 2.2b. Body of inhomogeneity b
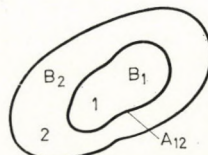
The even (at least even in some sections) surface A_{12} separating the different materials may be situated so (see Fig. 2.2a) that B_1 and B_2 should simply be coherent but may be positioned also in the way that B_1 be simply and B_2 doubly coherent (see Fig. 2.2b). In the first case the inhomogeneity will be called *type a* and in the second *type b*.

The following simplification will be applied:

1. Displacements and deformations are small;
2. The problem is quasi-static;

3. Thermal effects are negligible;

4. The intensity $\bar{q}$ of the system of volume forces acting in the volume $B = B_1 + B_2$ of the body is a given value;

5. The displacement vector $\bar{u}$ on the surface section A_u of the surface A bordering the region $B = B_1 + B_2$ is given;

6. The intensity $\bar{p}$ of the surface load on the surface section A_p of the surface A bordering the region $B = B_1 + B_2$ is familiar;

7. A_u and A_p are, with respect to the whole body complementary, i.e., $A = A_u + A_p$;

8. Stability problems are disregarded;

9. The external field of force (that of volume and surface loads) is conservative, the law of conservation of mechanical energy is valid;

10. The continuum problem has a solution.

To the solution to the continuum problem the basic system of elasticity equations established for the regions B_1 and B_2 have yielded boundary conditions at the sections A_p and A_u, however, for the section A_{12} one tries to find a solution satisfying certain fitting conditions.

Let us introduce the following designations

$$
\begin{aligned}
\mathbf{u}_i &= \mathbf{u}_i(P) &&= \text{displacement vector,} \\
\mathbf{A}_i &= \mathbf{A}_i(P) &&= \text{deformation tensor,} \\
\mathbf{F}_i &= \mathbf{F}_i(P) &&= \text{stress tensor,}
\end{aligned}
$$

at point P of the region B_i $(i = 1, 2)$. The parts of surface sections A_p and A_u being on the boundary of B_i let then be denoted by A_{pi} and A_{ui} $(i = 1, 2)$. The continuum problem leads to the following boundary-value problem:

The fields of displacement vector, deformation tensor and stress tensor

$$\mathbf{u}_i = \mathbf{u}_i(P), \quad \mathbf{A}_i = \mathbf{A}_i(P) \quad \text{and} \quad \mathbf{F}_i = \mathbf{F}_i(P) \qquad (i = 1, 2)$$

should be determined to satisfy the equilibrium equation of mechanics

$$\mathbf{F}_i \cdot \nabla + \bar{q} = \mathbf{0}, \quad P \in B_i \qquad (2.1)$$
$$(i = 1, 2)$$

the geometric equation

$$\mathbf{A}_i = \operatorname{def} \mathbf{u}_i, \quad P \in B_i \qquad (2.2)$$
$$(i = 1, 2)$$

the material equation

$$\mathbf{F}_i = \mathbf{C}_i \ .. \ \mathbf{A}_i, \quad P \in B_i \qquad (2.3)$$
$$(i = 1, 2)$$

further, at the surface section A_p the static boundary condition

$$\mathbf{F}_i \cdot \mathbf{n} - \bar{\mathbf{p}} = 0 , \quad P \in A_{pi} \tag{2.4}$$
$$(i = 1, 2)$$

and at the surface section A_u the geometric boundary condition

$$u_i - \bar{u} = 0 , \quad P \in A_{ui} \tag{2.5}$$
$$(i = 1, 2)$$

on the surface A_{12} the fitting condition

$$\mathbf{u}_1(P) - \mathbf{u}_2(P) = 0 , \quad P \in A_{12} \tag{2.6}$$

associated with the continuity of the displacement vector, further the fitting condition

$$\mathbf{p}_1(P) - \mathbf{p}_2(P) = 0 , \quad P \in A_{12} \tag{2.7}$$

associated with the continuity of the internal set of forces, wherein

$$\mathbf{p}_i(P) = \lim \mathbf{F}_i(Q_i) \cdot \mathbf{n} , \tag{2.8}$$
$$B_i \ni Q \to P \in A_{12}$$
$$(i = 1, 2) .$$

In Eq. (2.3) $\mathbf{C}_i$ $(i = 1, 2)$ denotes the fourth order symmetric tensor of the elastic material constants (see, for example, [14], [15], [20]) and accordingly,

$$\mathbf{C}_i \cdot\cdot \mathbf{A}_i = 2G_i \left[\mathbf{A}_i + \frac{v_i}{1 - 2v_i} (tr\mathbf{A}_i) \mathbf{I} \right] \tag{2.9}$$
$$(i = 1, 2) .$$

Furthermore, in Eq. (2.4) $\mathbf{n}$ denotes the normal unit vector pointing outwards from the material at point P of the surface A_p; in Eq. (2.8) $\mathbf{n}$ denotes the normal unit vector pointing to the point P of the surface A_{12} from the material of the body "1" to the material of the body "2".

In Eq. (2.8) Q_i may tend to the point P of the surface A_{12} at any plots assumed in the region B_i $(i = 1, 2)$.

2.2 *Variation principles and minimum theorems*

For the discussion of the stationary principles and minimum theorems it is convenient to introduce the following concepts.

D.1. The ordered triad defined by the vectorfield of the displacements, the tensorfield of deformation and tensorfield of stress is called *state*. The state is denoted by greek small letter, as for example:

$$\alpha = \left(u_i(P), \ \mathbf{A}_i(P), \ \mathbf{F}_i(P) \ i = 1, 2 \right) \tag{2.10}$$

D.2. The state defined by the triad $\mathbf{u}_i$, $\mathbf{A}_i$, $\mathbf{F}_i$ ($i = 1, 2$) satisfying the basic Eqs (2.1), (2.2), (2.3), the boundary conditions (24), (25) concerning the surface sections A_u and A_p, as well as the fitting condition prescribed on the surface A_{12} by the Eqs (2.6), (2.7), is called equilibrium state.

The symbol of the equilibrium state is: ε.

D.3. Statically possible (permissible) stress tensor field $\mathbf{F}_i$ ($i = 1, 2$) satisfies the equilibrium field (Eq. (2.1), the static boundary condition (2.4) and the fitting condition prescribed on the surface A_{12} by the Eq. (2.7).

D.4. Kinematically possible (permissible) displacement vector field $\hat{u}_i$ ($i = 1, 2$) satisfies the geometric boundary condition (2.5) and the fitting condition prescribed on the surface A_{12} by the Eq. (2.6), in addition, one can be derived from it in the region B_i with the aid of the geometric field equation

$$\hat{\mathbf{A}}_i = \operatorname{def} \hat{\mathbf{u}}_i \,, \tag{2.11}$$

$$(i = 1, 2)$$

the deformation tensor field $\hat{\mathbf{A}}_i$ ($i = 1, 2$).

D.5. Statically possible (permissible) state

$$\tilde{a} = (\tilde{\mathbf{u}}_i, \tilde{\mathbf{A}}_i, \tilde{\mathbf{F}}_i \,; \ i = 1, 2) \tag{2.12}$$

wherein

  I. $\mathbf{F}_i$ ($i = 1, 2$) statically possible,
 II. $\tilde{\mathbf{A}}_i = \mathbf{K}_i \, .. \, \tilde{\mathbf{F}}_i$, ($i = 1, 2$)   (2.13)
III. $\tilde{\mathbf{u}}_i$ ($i = 1, 2$) in the region B_i ($i = 1, 2$)
    is derivable, at least twice, otherwise it is an arbitrary vector.

Eq. (2.13) established with the aid of the fourth order symmetrical tensor $\mathbf{K}_i$ ($i = 1, 2$) including the material constants (G_i, v_i, $i = 1, 2$) of the elastic body involved in the definition *D.5.* in a detailed form appears as follows:

$$\tilde{\mathbf{A}}_i = \frac{1}{2G_i} \left[\tilde{\mathbf{F}}_i + \frac{v_i}{1 + v_i} \, (tr\tilde{\mathbf{F}}_i) \, \mathbf{I} \right] \,, \tag{2.14}$$

$$(i = 1, 2) \,.$$

It should be noted that we do not prescribe on the surface A_{12} in connection with $\tilde{\mathbf{u}}_i$ $(i = 1, 2)$ that

$$\tilde{\mathbf{u}}_1(P) - \tilde{\mathbf{u}}_2(P) = 0 , \qquad P \in A_{12} \tag{2.15}$$

should be fulfilled !

D.6. *Kinematically possible (permissible) state*

$$\hat{\alpha} = (\hat{\mathbf{u}}_i, \hat{\mathbf{A}}_i, \hat{\mathbf{F}}_i, \quad i = 1, 2) , \tag{2.16}$$

wherein

I. $\hat{\mathbf{u}}_i$ $(i = 1, 2)$ kinematically is possible, its consequence is that

$$\hat{\mathbf{A}}_i = \operatorname{def} \hat{\mathbf{u}}_i , \quad (i = 1, 2) , \tag{2.17}$$

II. $\hat{\mathbf{F}}_i = \mathbf{C}_i \, .. \, \hat{\mathbf{A}}_i, \quad (i = 1, 2) . \tag{2.18}$

The following statement is evident:

T.1. The equilibrium state

$$\varepsilon = (\mathbf{u}_i, \mathbf{A}_i, \mathbf{F}_i; \quad i = 1, 2) \tag{2.19}$$

is both statically and kinematically a possible (permissible) state.

D.7. *Kinematically possible deformation energy density*

$$\hat{e}_i = \frac{1}{2} \hat{\mathbf{F}}_i \, .. \, \hat{\mathbf{A}}_i = \frac{1}{2} \hat{\mathbf{A}}_i \, .. \, \mathbf{C}_i \, .. \, \hat{\mathbf{A}}_i , \tag{2.20}$$

$$(i = 1, 2).$$

D.8. *Statically possible stress (complementary, conjugated) energy density*

$$\tilde{e}_i = \frac{1}{2} \tilde{\mathbf{F}}_i \, .. \, \tilde{\mathbf{A}}_i = \frac{1}{2} \tilde{\mathbf{F}}_i \, .. \, \mathbf{K}_i \, .. \, \tilde{\mathbf{F}}_i , \tag{2.21}$$

$$(i = 1, 2) .$$

D.9. *Kinematically possible potential energy* at the function π_L interpreted by the following prescription

I. Its interpretation region is the set of kinematically permissible states,

$$\pi_L : \hat{\alpha} \to R \equiv (-\infty, \infty) , \tag{2.22}$$

II. $\pi_L = : \displaystyle\sum_{i=1}^{2} \left(\int_{B_i} \hat{e}_i dB - \int_{B_i} \bar{\mathbf{q}} \cdot \hat{\mathbf{u}}_i dB - \int_{A_{pi}} \bar{\mathbf{p}} \cdot \hat{\mathbf{u}}_i dA \right) . \tag{2.23}$

D.10. The statically possible complementary work in connection with the function π_C interpreted by the following prescription:

I. Its interpretation region is the set of statically permitted states

$$\pi_C : \tilde{\alpha} \to R \equiv (-\infty, \infty) \tag{2.24}$$

II. $\pi_C = : \sum_{i=1}^{2} \left(\int_{B_i} \tilde{e}_i dB - \int_{A_{ui}} (\widetilde{\mathbf{F}}_i \cdot n) \cdot \bar{u}_i dA \right).$ $\tag{2.25}$

Stationariness statements

T.2. In equilibrium state π_L is stationary, i.e.,

$$\delta\pi_L = 0 \,. \tag{2.26}$$

T.3. In equilibrium state π_C is stationary, i.e.,

$$\delta\pi_C = 0 \,. \tag{2.27}$$

Only the verification of *T.2.* will be outlined for a body having an inhomogeneity type *a*.

In the course of evolution of the first variation of π_L it is assumed that

1. The functions appearing are through their region of interpretation derivable to the order required.

2. The following two identities derivable by the simultaneous application of the product integration and the Gaussian theorem concerning the integral transformation are valid:

$$\int_{B_1} \delta\hat{e}_1 dB = -\int_{B_1} (\widehat{\mathbf{F}} \cdot \nabla) \cdot \delta\hat{\mathbf{u}}_1 dB +$$

$$+ \int_{A_1} (\widehat{\mathbf{F}}_1 \cdot \mathbf{n}) \cdot \delta\hat{\mathbf{u}}_1 dA + \int_{A_{12}} (\widehat{\mathbf{F}}_1 \cdot \mathbf{n}) \cdot \delta\hat{\mathbf{u}}_1 dA \,, \tag{2.28}$$

$$\int_{B_2} \delta\hat{e}_2 dB = -\int_{B_2} (\widehat{\mathbf{F}}_2 \cdot \nabla) \cdot \delta\hat{\mathbf{u}}_2 dB +$$

$$+ \int_{A_2} (\widehat{\mathbf{F}}_2 \cdot \mathbf{n}) \cdot \delta\hat{\mathbf{u}}_2 dA - \int_{A_{12}} (\widehat{\mathbf{F}}_2 \cdot \mathbf{n}) \cdot \delta\hat{\mathbf{u}}_2 dA \,. \tag{2.29}$$

3. The sequence of the derivation and forming variation may be changed.

4. The sequence of the integration and forming variation may be changed. Taking into account that said above we obtain:

$$\delta\pi_L = \sum_{i=1}^{2} \left(-\int_{B_i} (\widehat{\mathbf{F}}_i \cdot \nabla + \bar{\mathbf{q}}) \cdot \delta\hat{\mathbf{u}}_i dB + \right.$$

$$\left. + \int_{A_{pi}} (\widehat{\mathbf{F}}_i \cdot \mathbf{n} - \bar{\mathbf{p}}) \cdot \delta\hat{\mathbf{u}}_i dA \right) +$$

$$+ (\hat{\mathbf{p}}_1 \cdot \delta\hat{\mathbf{u}}_1 - \hat{\mathbf{p}}_2 \cdot \delta\hat{\mathbf{u}}_2) \, dA \,. \tag{2.30}$$

By making use of the fact that in the region B_i and on the surface section A_{pi} $\delta\hat{\mathbf{u}}_i$ $(i = 1, 2)$ is arbitrary, and on the surface section A_{12} the $\delta\hat{u}_i = \delta u_2 = \delta u_{12}$ is arbitrary, from the assumption of stationariness the mechanical equilibrium equation

$$\mathbf{F}_i \cdot \nabla + \bar{\mathbf{q}} = 0 , \qquad P \in B_i \tag{2.31}$$
$$(i = 1, 2)$$

the static boundary condition

$$\mathbf{F}_i \cdot \mathbf{n} - \mathbf{p} = 0 , \qquad P \in A_{pi} \tag{2.32}$$

and the equation of fitting

$$\hat{\mathbf{p}}_1 - \hat{\mathbf{p}}_2 = 0 , \qquad P \in A_{12} \tag{2.33}$$

may be derived. Their validity *for the kinematically permissible state* assures the existance of the *equilibrium state*.

D.11. The kinematically permissible variation of the equilibrium state is

$$\delta\hat{\varepsilon} = (\delta\hat{\mathbf{u}}_i , \quad \delta\hat{\mathbf{A}}_i, \quad \delta\mathbf{F}_i ; \quad i = 1, 2) \tag{2.34}$$

wherein:

I. $\delta\hat{\mathbf{u}}_i$ is continuous, derivable at least twice in the region B_i $(i = 1, 2$

II. $\delta\hat{\mathbf{A}}_i = \operatorname{def} \delta\hat{\mathbf{u}}_i , \quad P \in B_i$ $\hspace{2cm}$ (2.35))

III. $\delta\hat{\mathbf{u}}_i = 0 , \quad P \in A_u$ $\hspace{2cm}$ (2.36)

IV. $\delta\mathbf{F}_i = \mathbf{C}_i \cdot\cdot \delta\mathbf{A}_i , \quad P \in B_i$ $\hspace{2cm}$ (2.37)

D.12. Statically permissible variation of the equilibrium state is

$$\delta\tilde{\varepsilon} = (\delta\tilde{\mathbf{u}}_i , \quad \delta\tilde{\mathbf{A}}_i , \quad \delta\mathbf{F}_i ; \quad i = 1, 2) \tag{2.38}$$

wherein:

I. $\delta\mathbf{F}_i \cdot \nabla = 0 , \quad P \in B_i$ $\hspace{2cm}$ (2.39)

II. $\delta\mathbf{F}_i \cdot \mathbf{n} = 0 , \quad P \in A_{pi}$ $\hspace{2cm}$ (2.40)

III. $\delta\tilde{\mathbf{p}}_1 - \delta\tilde{\mathbf{p}}_2 = 0 , \quad P \in A_{12}$ $\hspace{2cm}$ (2.41)

$$\delta p_i = \lim_{B_i \ni Q_i \to P \in A_{12}} \delta\mathbf{F}_i(Q_i) \cdot \mathbf{n} , \tag{2.42}$$
$$(i = 1, 2) ,$$

IV. $\delta\tilde{\mathbf{A}}_i = \mathbf{K}_i \cdot\cdot \delta\mathbf{F}_i , \quad P \in B_i$ $\hspace{2cm}$ (2.43)

V. $\delta\hat{\mathbf{u}}_i$ $(i = 1, 2)$ is at least twice derivable in the region B_i $(i = 1, 2)$, otherwise it is an arbitrary vector.

The $\delta\tilde{\mathbf{u}}_i$ involved in the definition *D.11.* does not need to fulfil the condition on the surface A_{12}

$$\delta\tilde{\mathbf{u}}_1(P) - \delta\tilde{\mathbf{u}}_2(P) = 0 , \qquad P \in A_{12} . \tag{2.44}$$

The result of the definitions *D.11.* and *D.12.* is that

$$\hat{\delta} = : \varepsilon + \delta\hat{\varepsilon} = : (\mathbf{u}_i + \delta\hat{\mathbf{u}}_i , \quad \mathbf{A}_i + \delta\hat{\mathbf{A}}_i ,$$
$$\mathbf{F}_i + \delta\hat{\mathbf{F}}_i ; \quad i = 1, 2) \tag{2.45}$$

is kinematically permissible state and

$$\tilde{\delta} = : \varepsilon + \delta\tilde{\varepsilon} = : (\mathbf{u}_i + \delta\tilde{\mathbf{u}}_i , \quad \mathbf{A}_i + \delta\tilde{\mathbf{A}}_i ,$$
$$\mathbf{F}_i + \delta\mathbf{F}_i ; \quad i = 1, 2) \tag{2.46}$$

is a statically permissible state.

Minimum principles

   T.4. In the equilibrium state π_L is minimum,

$$\pi_L(\varepsilon) \le \pi_L(\hat{\delta}) . \tag{2.47}$$

   T.5. In the equilibrium state π_C is minimum,

$$\pi_C(\varepsilon) \le \pi_C(\tilde{\delta}) . \tag{2.48}$$

Only the verification of *T.4.* will be outlined. Let us investigate the change of π_L in case of the kinematically permissible variation $\delta\varepsilon$ of the equilibrium state! Carrying out the detailed evolution, yields

$$\Delta\pi_L = \pi_L(\varepsilon + \delta\hat{\varepsilon}) - \pi_L(\varepsilon) = \frac{1}{2} \sum_{i=1}^{2} \int_{B_i} (\delta\hat{\mathbf{A}}_i \cdot\cdot \mathbf{C}_i \cdot\cdot \delta\tilde{\mathbf{A}}_i) \, dB . \tag{2.49}$$

Considering that $\mathbf{C}_i$ $(i = 1, 2)$ is a fourth order positive definite symmetrical tensor* (see [15], [20]) on the basis of Eq. (2.49) may be written:

$$\Delta\pi_L \ge 0 , \tag{2.50}$$

i.e.,

$$\pi_L(\varepsilon + \delta\hat{\varepsilon}) = \pi_L(\hat{\delta}) \ge \pi_L(\varepsilon) , \tag{2.51}$$

from which follows

$$\min \pi_L(\hat{\delta}) = \pi_L(\varepsilon) . \tag{2.52}$$

---

* $\mathbf{C}_i$ $(i = 1,2)$ is in the following sense a positive definit (see, for ex., [20]):
I. The symmetric second order tensor of every $\mathbf{X} \ne \mathbf{0}$ is $\mathbf{X} \cdot\cdot \mathbf{C}_i \cdot\cdot \mathbf{X} > 0$.
II. $\mathbf{X} \cdot\cdot \mathbf{C}_i \cdot\cdot \mathbf{X} = 0$ only in case, when $\mathbf{X} = \mathbf{0}$.

With the aid of the following proposition the relationship between $\pi_L(\varepsilon)$ and $\pi_C(\varepsilon) = \min \pi_C(\tilde{\delta})$ may be established.

T.6. With an arbitrary statically possible (permissible stress tensor field $\tilde{\mathbf{F}}_i$ ($i = 1, 2$) and kinematically possible (permissible) displacement field $\hat{u}_i$ ($i = 1, 2$) the following equality is valid:

$$\sum_{i=1}^{2} \int_{B_i} (\tilde{\mathbf{F}}_i \cdot\cdot \hat{\mathbf{A}}_i)\, dB = \sum_{i=1}^{2} \left(\int_{B_i} \bar{q} \cdot \hat{u}_i dB + \right.$$

$$\left. + \int_{A_{pi}} \bar{p} \cdot \hat{u}_i dA + \int_{A_{ui}} (\tilde{\mathbf{F}}_i \cdot n) \cdot \bar{u}_i dA \right), \tag{2.53}$$

$$\hat{\mathbf{A}}_i = \operatorname{def} \hat{u}_i\,, \tag{2.54}$$

$$(i = 2, 1)\,.$$

The verification of the statement may be carried out similarly to the analogous statement [17], [9] concerning the continua of a homogeneous linearly elastic material having undergone a small deformation.

T.7. In equilibrium state

$$\pi_L(\varepsilon) + \pi_C(\varepsilon) = 0\,. \tag{2.55}$$

To verify *T.7.* let us apply the statement *T.6.* to the equilibrium state

$$\varepsilon = (\mathbf{u}_i, \quad \mathbf{A}_i, \quad \mathbf{F}_i;\quad i = 1, 2) \tag{2.56}$$

which yields

$$\sum_{i=1}^{2} \left(\int_{B_i} (\mathbf{F}_i \cdot\cdot \mathbf{A}_i)\, dB = \sum_{i=1}^{2} \int \bar{\mathbf{q}} \cdot \mathbf{u}_i dB + \right.$$

$$\left. + \int_{A_{pi}} \bar{\mathbf{p}} \cdot \mathbf{u}_i dA + \int_{A_{ui}} (\mathbf{F}_i \cdot n) \cdot \bar{\mathbf{u}}_i dA \right). \tag{2.57}$$

From Eq. (2.57) by elementary transformation the equation

$$\sum_{i=1}^{2} \left(\frac{1}{2} \int_{B_i} (\mathbf{F}_i \cdot\cdot \mathbf{A}_i)\, dB - \int_{B_i} \bar{\mathbf{q}} \cdot \mathbf{u}_i dB - \int_{A_{pi}} \bar{\mathbf{p}} \cdot \mathbf{u}_i dA \right) +$$

$$+ \sum_{i=1}^{2} \frac{1}{2} \int_{B_i} \mathbf{F}_i \cdot\cdot \mathbf{A}_i dB - \int_{A_{ui}} (\mathbf{F}_i \cdot \mathbf{n}) \cdot \bar{\mathbf{u}}_i dA = 0 \tag{2.58}$$

is obtained wherefrom, by taking into account the interpretation of π_L and π_C, the statement of *T.7.* resulted. The consequence of *T.7.* is *T.8.*

T.8. To kinematically permissible arbitrary state $\hat{\alpha}$ and statically permissible state $\tilde{\beta}$ the following inequality is true:

$$\pi_L(\hat{\alpha}) + \pi_C(\tilde{\beta}) \geq 0\,. \tag{2.59}$$

For the verification let us start with the equalities:

$$\pi_L(\hat{\alpha}) \geq \pi_L(\varepsilon) , \tag{2.60}$$

$$\pi_C(\tilde{\beta}) \geq \pi_C(\varepsilon) \tag{2.61}$$

which may be established on the basis of the statements *T.4.* and *T.5.* To the inequality obtained by additioning Eqs (2.60) and (2.61) the use of *T.7.* results in the inequality (2.59).

Equivalence of the state of equilibrium T.9. Only a single state of equilibrium can exist.

In order to verify this statement, consider the identity

$$\sum_{i=1}^{2} \int_{B_i} (\widetilde{\mathbf{F}}_i \, .. \, \operatorname{def} \mathbf{v}) \, dB = \sum_{i=1}^{2} \left(\iint_{A_{pi}} \mathbf{p} \cdot \mathbf{v} dA + \right.$$

$$\left. + \int_{A_{ui}} (\widetilde{\mathbf{F}}_i \cdot \mathbf{n}) \cdot \mathbf{v} dA + \int_{B_i} \mathbf{q} \cdot \mathbf{v} dB \right) \tag{2.62}$$

which may be deduced by the simultaneous application of the rules of the product integration and the Gaussian integral transformation to statically possible (permissible) arbitrary stress field $\widetilde{\mathbf{F}}_i$ $(i = 1, 2)$ and in the region B_i $(i = 1, 2)$ derivable at least twice, in the region deductable to continuous v-vector field. Let us assume the two equilibrium states to be, ε_1 and ε_2:

$$\varepsilon_1 = (\mathbf{u}_i^{(1)}, \; \mathbf{A}_i^{(1)}, \; \mathbf{F}_i^{(1)}; \quad i = 1, 2) , \tag{2.63}$$

$$\varepsilon_2 = (\mathbf{u}_i^{(2)}, \; \mathbf{A}_i^{(2)}, \; \mathbf{F}_i^{(2)}; \quad i = 1, 2) . \tag{2.64}$$

Let us apply the identity (2.62) to the statically possible (permissible) stress fields $\mathbf{F}_i^{(1)}$ $(i = 1, 2)$ and $\mathbf{F}_i^{(2)}$ $(i = 1, 2)$ and, for the moment, to the arbitrary vector v. By forming the difference of the two equations the following is obtained:

$$\sum_{i=1}^{2} \int_{B_i} (\mathbf{F}_i^{(1)} - \mathbf{F}_i^{(2)}) \, .. \, \operatorname{def} \mathbf{v} \, dB = \sum_{i=1}^{2} \int_{A_{ui}} (\mathbf{F}_i^{(1)} \cdot \mathbf{n} - \mathbf{F}_i^{(2)} \cdot \mathbf{n}) \cdot \mathbf{v} \, dA . \tag{2.65}$$

Be

$$\mathbf{v} = \mathbf{u}_i^{(1)} - \mathbf{u}_i^{(2)} , \quad P \in B_i , \tag{2.66}$$

$$(i = 1, 2) .$$

The consequence of Eq. (2.66) is

$$\mathbf{v}(P) = 0 \quad \text{if} \quad P \in A_u = A_{u1} + A_{u2} . \tag{2.67}$$

Use of the material laws (2.67) and (2.13) and the consideration of Eq. (2.65) allows us to write down:

$$\sum_{i=1}^{2} \left(\int_{B_i} \Delta \mathbf{F}_i \ldots \mathbf{K}_i \ldots \Delta F_i \, dB \right) = 0 \tag{2.68}$$

wherein:

$$\Delta \mathbf{F}_i = \mathbf{F}_1^{(1)} - \mathbf{F}_i^{(2)}, \tag{2.69}$$
$$(i = 1, 2).$$

Due to the positive definiteness of $\mathbf{K}_i$ $(i = 1, 2)$, the Eq. (2.69) may only be valid with the symmetrical tensors $\Delta \mathbf{F}_i$ $(i = 1, 2)$ if $\mathbf{F}_i = \mathbf{0}$ $(i = 1, 2)$, i.e.,

$$\mathbf{F}_i^{(1)} = \mathbf{F}_i^{(2)}, \tag{2.70}$$
$$(i = 1, 2).$$

From this last equality, by applying Hooke's law (Eq. 2.3), the following equality is obtained

$$\mathbf{A}_i^{(1)} = \mathbf{A}_i^{(2)}. \tag{2.71}$$

The consequence of (2.71) (see, for example, [9], [12], [13]), disregarding the rigid body displacement of the displacement fields $u_i^{(1)}$ and $u_i^{(2)}$, that is:

$$\mathbf{u}_i^{(1)} = \mathbf{u}_i^{(2)} + \mathbf{a} + \mathbf{b} \times \mathbf{r}, \tag{2.72}$$
$$(i = 1, 2).$$

From Eqs (2.70), (2.71) and (2.72) it is to be seen (the rigid body motion disregarded which is characterized by a, b) that, indeed, *only a single state of equilibrium may exist.*

The described stationariness theorems and variation principles allow the approximate solution of the boundary value problems associated with the continuum of composite material without the direct integration of the basic system of equations (2.1), (2.2), (2.3). For seaking the approximate solution the method Ritz [19], the Kantorovich method [19] and the method of successive approximation developed by Kerr [18] might be applied.

3. Free torsion of prismatic bars with inhomogeneous cross section

In connection with the prismatic bar with an inhomogeneous cross section depicted in Fig. 3.1 it should be assumed that
1. the mantle of the bar is unloaded,
2. the end faces are subjected to a torsional moment of a given M_c value.
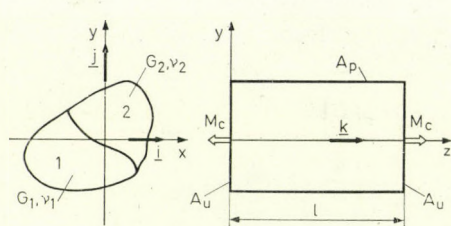
**Fig. 3.1.** Prismatic bar of composite material with a solid cross section
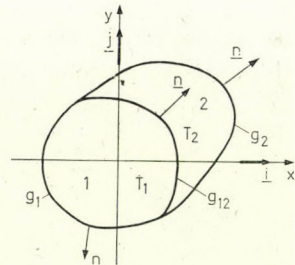
Fig. 3.2. Cross section of torsioned prismatic bar

Some symbols and denominations (Fig. 3.2)

T — region defined by cross section
g — curve bordering region T
g_{12} — curve separating different materials in plane of cross section being smooth (or at least in some sections)
T_1 — part of region T belonging to material denoted by "1"
T_2 — part of region T belonging to material denoted by "2"
g_1 — part of border of region T along g
g_2 — part of border of region T along g
n — unit vector of normal, directed outwards from material $g(g_1, g_2)$
n — normal unit vector on curve g_{12} pointing from material "1" to material "2"
s — arc length measured along curve $g(g_1, g_2)$. Along curve g in the direction of increasing s, the cross section lies to the left-hand side; direction of s along curve g_{12} is understood by going along curve g_{12} in the sense of increasing s and material "1" lies at the lefthand side
$\partial/\partial n$ derivative calculated in direction of n
$\partial/\partial s$ — derivative calculated along curve $g(g_1, g_2)$ or g_{12}
$a.$ — type of inhomogeneity where T_1 and T_2 are *simply* coherent (see Fig. 3.3a)
$b.$ — type of inhomogeneity where T_1 is *simply* and T_2 doubly coherent (Fig. 3.3b)
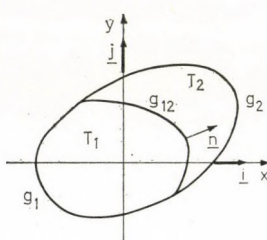
Fig. 3.3a. Cross section of bar of inhomogeneity *a*
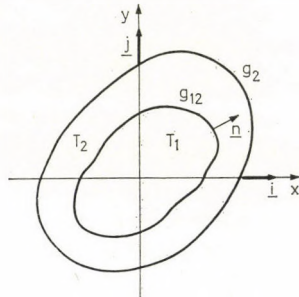
Fig. 3.3b. Cross section of bar of inhomogeneity *b*

It is known that in case of pure torsion the displacement vector of the prismatic bar is

$$\mathbf{u}_i = u^{(i)}\mathbf{i} + v^{(i)}\mathbf{j} + w^{(i)}\mathbf{k} , \qquad (3.1)$$

wherein:

$$u^{(i)} = u^{(i)}(x, y) = -\vartheta yz + \omega_2 z - \omega_3 y + u_0 , \qquad (3.2)$$

$$v^{(i)} = v^{(i)}(x, y) = \vartheta xz + \omega_3 z - \omega_1 z + v_0 \,, \tag{3.3}$$

$$w^{(i)} = w^{(i)}(x, y) = \vartheta \varphi_i(x, y) + \omega_1 y - \omega_2 x + w_0 \,, \tag{3.4}$$

$$(i = 1, 2) \,.$$

In the above set of equations u_0, v_0, w_0, ω_1, ω_2, ω_3 denote the constants associated with the rigid body displacement of the bar and ϑ is the relative torsion per unit length. By applying the *geometric equation* and the general Hooke's law, from the equations (3.2), (3.3), (3.4) we obtain:

$$\varepsilon_x^{(i)} = \varepsilon_y^{(i)} = \varepsilon_z^{(i)} = \gamma_{xy}^{(i)} = 0 \,, \tag{3.5}$$

$$\sigma_x^{(i)} = \sigma_y^{(i)} = \sigma_z^{(i)} = \tau_{xy}^{(i)} = 0 \,, \tag{3.6}$$

$$(i = 1, 2) \,.$$

Eq. (2.1) of the mechanical equilibrium is identically satisfied if the shear forces $\tau_{xz}^{(i)}$, $\tau_{yz}^{(i)}$, differing from zero, are produced in the following form

$$\tau_{xz}^{(i)} = G_i \vartheta \, \frac{\partial \Phi_i}{\partial y} \,, \tag{3.7}$$

$$\tau_{yz}^{(i)} = - G_i \vartheta \, \frac{\partial \Phi_i}{\partial x} \,, \tag{3.8}$$

$$(i = 1, 2)$$

Here $\Phi_i = \Phi_i(P) = \Phi_i(x, y)$ $(i = 1, 2)$ is the stress function of the composite cross section. With detailed evolution of the static boundary condition relating to the mantle of the bar

$$\mathbf{F}_i \cdot \mathbf{n} = 0 \,, \quad (i = 1, 2) \tag{3.9}$$

the homogeneous boundary condition

$$\Phi_i = 0 \,, \quad P \in g_i \,, \quad (i = 1, 2) \tag{3.10}$$

valid at the border of the cross section, may be deduced to the stress function. From the compatibility equation

$$\frac{\partial \gamma_{xz}^{(i)}}{\partial y} - \frac{\partial \gamma_{yz}^{(i)}}{\partial x} = -2\vartheta \tag{3.11}$$

11

which may be derived from the Eqs (3.2), (3.3), (3.4) with the replacements

$$\gamma_{xz}^{(i)} = \frac{1}{G_i}\,\tau_{xz}^{(i)} = \vartheta\,\frac{\partial \Phi_i}{\partial y}\,, \tag{3-12a}$$

$$\gamma_{yz}^{(i)} = \frac{1}{G_i}\,\tau_{yz}^{(i)} = -\vartheta\,\frac{\partial \Phi_i}{\partial x}\,, \tag{3.12b}$$

$$(i = 1, 2)$$

one obtains for the $\Phi_i = \Phi_i(x, y)$ function Poisson's partial differential equation

$$\Delta\Phi_i = -2\,, \quad P \in T_i \quad (i = 1, 2). \tag{3.13}$$

From the equation

$$\tau_{n2}^{(1)} = \tau_{n2}^{(2)}\,, \quad P \in g_{12}$$

corresponding to the fitting equation (2.7) relating to the curve g_{12}, for the function (see [1], [6], [8]) we obtain the prescription

$$G_1\frac{\partial \Phi_1}{\partial s} = G_2\,\frac{\partial \Phi_2}{\partial s}\,, \quad P \in g_{12}\,. \tag{3.14}$$

This might be fulfilled if (see [1], [6])

$$G_1\Phi_1 = G_2\Phi_2\,. \tag{3.15}$$

The continuity of the displacement vector field is assured at the points of the curve g_{12} (see [1], [6]) by satisfying the equation

$$\frac{\partial \Phi_1}{\partial n} = \frac{\partial \Phi_2}{\partial n}\,, \quad P \in g_{12}\,. \tag{3.16}$$

The value of the torsional moment M_c attacking the cross section (see [1]) may be calculated from the equation

$$M_c = \vartheta I_c \tag{3.17}$$

wherein

$$I_c = 2 \sum_{i=1}^{z} G_i \int_{T_i} \Phi_i dT \tag{3.18}$$

is the torsional stiffness of the cross section.

The verification made in the foregoing might be summarized as follows: The free elastic torsion problem of a prismatic bar of a composite cross section leads to the following boundary conditions [1]:

$$\Delta\Phi_i = -2 , \quad P \in T_i ,$$ (3.19)

$$\Phi_i = 0 , \quad P \in g_i ,$$ (3.20)

$$(i = 1, 2) ,$$

$$G_1\Phi_1 = G_2\Phi_2 , \quad P \in g_{12} ,$$ (3.21)

$$\frac{\delta\Phi_1}{\partial n} = \frac{\partial\Phi_2}{\partial n} , \quad P \in g_{12} .$$ (3.22)

The free elastic torsion problem of a prismatic bar of a composite cross section may also be treated as a boundary value problem associated with the function $\varphi_i = \varphi_i(P) = \varphi_i(x, y)$ $(i = 1, 2)$. Starting out from the equations (3.2), (3.3), (3.4), by making use of the geometric equation and the general Hooke's law the following equations are obtained

$$\tau_{xz}^{(i)} = G_i\vartheta \left(\frac{\partial\varphi_i}{\partial x} - y \right) ,$$ (3.23)

$$\tau_{yz}^{(i)} = G_i\vartheta \left(\frac{\partial\varphi_i}{\partial y} + x \right) ,$$ (3.24)

$$(i = 1, 2) .$$

Replacement of the above results into the non-identically satified equation of the mechanical equilibrium

$$\frac{\partial\tau_{xz}^{(i)}}{\partial x} + \frac{\partial\tau_{yz}^{(i)}}{\partial y} = 0$$ (3.25)

$$(i = 1, 2)$$

yields that $\varphi_i = \varphi_i(P)$ is harmonic in the region $T_i(i = 1, 2)$. The consequence of the boundary condition

$$\tau_{nz}^{(i)} = 0 , \quad P_i \in g$$ (3.26)

$$(i = 1, 2)$$

relating to the bordering curve of the cross section that

$$\frac{\partial\varphi_i}{\partial n} - \frac{\partial}{\partial s} \left(\frac{x^2 + y^2}{2} \right) = 0, \quad P_i \in g_{12} .$$ (3.27)

The displacement field is continuous on the curve g_{12} if

$$\varphi_1 = \varphi_2 , \qquad P \in g_{12} . \tag{3.28}$$

The consequence of the fitting condition

$$\tau_{n2}^{(1)} = \tau_{n2}^{(2)} , \qquad P \in g_{12} \tag{3.29}$$

prescribed for the curve g_{12} (see [1], [2]) that

$$G_1 \left[\frac{\partial \varphi_1}{\partial n} - \frac{\partial}{\partial s} \left(\frac{x^2 + y^2}{2} \right) \right] = G_2 \left[\frac{\partial \varphi_2}{\partial n} - \frac{\partial}{\partial s} \left(\frac{x^2 + y^2}{2} \right) \right] . \tag{3.30}$$

Starting from the equation

$$M_c = \sum_{i=1}^{2} \int_{T_i} \left[x \tau_{xz}^{(i)} - y \tau_{yz}^{(i)} \right] dT \tag{3.31}$$

by making use of the equations (3.23) and (3.24) and Stoke's theorem the equation

$$M_c = \vartheta \left[G_1 I_1 - G_2 I_2 - G_1 \int_{T_1} (\Box \varphi_1)^2 \, dT - G_2 \int_{T_2} (\Box \varphi_2)^2 \, dT \right] \tag{3.32}$$

may be deduced to the torsional moment equally valid for the inhomogeneities both $a.$ and $b.$

Herein:

$$I_i = \int_{T_i} (x^2 + y^2) \, dT , \tag{3.33}$$

$$(i = 1, 2) .$$

From Eq. (3.32) results that the torsional stiffness of the cross section may be expressed by the function φ in the following form:

$$I_c = G_1 I_1 + G_2 I_2 - G_1 \int_{T_1} (\Box \varphi_1)^2 \, dT - G_2 \int_{T_2} (\Box \varphi_2)^2 \, dT . \tag{3.34}$$

By additioning the prescriptions related to the function $\varphi_i = \varphi_i(x, y) = \varphi_i(P)$ one can state that the elastic free torsional problem of a prismatic bar of composite material leads, in connection with the function $\varphi_i = \varphi_i(x, y) = \varphi_i(P)$ $(i = 1, 2)$ to the following boundary value problem:

$$\Delta \varphi_i = 0 , \qquad P \in T_i , \tag{3.35}$$

$$\frac{\partial \varphi_i}{\partial n} - \frac{\partial}{\partial s} \left(\frac{x^2 + y^2}{2} \right) = 0 , \qquad P \in g , \tag{3.36}$$

$$(i = 1, 2) ,$$

$$\varphi_1 = \varphi_2, \quad P \in g_{12}, \tag{3.37}$$

$$G_1 \left[\frac{\partial \varphi_1}{\partial n} - \frac{\partial}{\partial s} \left(\frac{x^2 + y^2}{2} \right) \right] = G_2 \left[\frac{\partial \varphi_2}{\partial n} - \frac{\partial}{\partial s} \left(\frac{x^2 + y^2}{2} \right) \right], \quad P \in g_{12}. \tag{3.38}$$

4. Application of the principle of complementary work minimum for the approximate determination of torsional stiffness

In the cross sections defined by the coordinates $z = 0$ and $z = l$ the displacement vector is assumed to be known:

$$\mathbf{u}_i = u_i^{(i)}(x, y, z)\,\mathbf{i} + v^{(i)}(x, y, z)\,\mathbf{j} + w^{(i)}(x, y, z)\,\mathbf{k}, \tag{4.1}$$

$$u^{(i)}(x, y; 0) = v^{(i)}(x, y, 0) = 0, \tag{4.2}$$

$$w^{(i)}(x, y, 0) = \vartheta \varphi_i(x, y), \tag{4.3}$$

$$u^{(i)}(x, y, l) = -\vartheta l y, \tag{4.4}$$

$$v^{(i)}(x, y, l) = \vartheta l x, \tag{4.5}$$

$$w^{(i)}(x, y, l) = \vartheta \varphi_i(x, y), \tag{4.6}$$

$$(i = 1, 2).$$

In this problem the cross sections defined by the coordinates $z = 0$ and $z = l$ mean the surface section A_u and the unloaded mantle of the bar represents the surface section A_p. The statically possible (permissible) state will be built up with the aid of the stress function $\Phi_i = \Phi_i(P)$. Thus we have:

$$\tilde{\tau}_{xz}^{(i)} = G_i \vartheta \frac{\partial \Phi_i}{\partial y}, \tag{4.7}$$

$$\tilde{\tau}_{yz}^{(i)} = -G_i \vartheta \frac{\partial \Phi_i}{\partial x} \tag{4.8}$$

wherein the function

$$\Phi_i = \Phi_i(x, y) = \Phi_i(P) \quad (i = 1, 2)$$

has only to satisfy, besides the necessary conditions of derivability, the homogeneous boundary condition

$$\Phi_i = 0, \quad P \in g \tag{4.9}$$

and the fitting condition

$$G_1 \Phi_1 = G_2 \Phi_2, \quad P \in g_{12}. \tag{4.10}$$

Substituting Eqs (4.7), (4.8) and (4.2), (4.3), ..., (4.6) into Eq. (2.25) and integrating with respect to z for the statically possible complementary work yields

$$\pi_c = \pi_c(\Phi_i) = \frac{\vartheta^2 l}{2} \sum_{i=1}^{2} G_i \int_{T_i} [(\square\Phi_i)^2 +$$
$$+ 2\mathbf{R} \cdot (\square\Phi_i)] \, dT \,, \quad (R = xi + yj) \,. \tag{4.11}$$

This equation may also be written in the form

$$\pi_c = \frac{\vartheta^2 l}{2} \sum_{i=1}^{2} G_i \int_{T_i} [(\square\Phi_i)^2 - 4\Phi_i] \, dT \,. \tag{4.12}$$

The verification of this transformation will only be carried out to the inhomogeneity type a.

Let us consider the following two equations

$$\int_{T_1} \square \cdot (\mathbf{R}\Phi_1) \, dT = \int_{g_1} \mathbf{n} \cdot \mathbf{R}\Phi_1 \, ds + \int_{g_2} \mathbf{n} \cdot \mathbf{R}\Phi_1 ds \,, \tag{4.13}$$

$$\int_{T_2} \square \cdot (\mathbf{R}\Phi_2) \, dT = \int_{g_2} \mathbf{n} \cdot \mathbf{R}\Phi_2 ds - \int_{g_{12}} \mathbf{n} \cdot \mathbf{R}\Phi_2 ds \tag{4.14}$$

which may be written by making use of the identity

$$\square \cdot (\mathbf{R}\Phi_i) = 2\Phi_i + \mathbf{R} \cdot (\square\Phi_i) \,, \tag{4.15}$$
$$(i = 1, 2)$$

and Stokes's theorem.

Using further that

$$\Phi_i = 0 \,, \quad P \in g_i \tag{4.16}$$

and applying the equations (4.13), (4.14), (4.15) yields

$$\int_{T_1} \mathbf{R} \cdot \square\Phi_1 dT = \int_{g_{12}} \mathbf{n} \cdot \mathbf{R}\Phi_1 ds \,, \tag{4.17}$$

$$\int_{T_2} \mathbf{R} \cdot \square\Phi_2 dT = -\int_{g_{12}} \mathbf{n} \cdot \mathbf{R}\Phi_2 ds \,. \tag{4.18}$$

Substitution of these last results into Eq. (4.11) already results in the shape (4.12) of π_C, if one considers that

$$G_1\Phi_1 = G_2\Phi_2 \,, \quad P \in g_{12} \,. \tag{4.19}$$

Since in the state of equilibrium the first variation of π_C is equal to zero, it is only enough to investigate the following functional p_C proportional to π_C:

$$p_c = p_c(\Phi_i) = : \frac{1}{2} \sum_{i=1}^{2} G_i \int_{T_i} [(\Box\Phi_i)^2 - 4\Phi_i] \, dT \ . \tag{4.20}$$

By the use of

$$I_c = 2 \sum_{i=1}^{n} G_i \int_{T_i} \Phi_i \, dT \tag{4.21}$$

p_c may be written also in the form

$$p_c = \frac{1}{2} \sum_{i=1}^{2} G_i \int_{T_i} [(\Box\Phi_i)^2 - 2\Phi_i] \, dT - \frac{I_c}{2} \tag{4.22}$$

and in the state of equilibrium:

$$\sum_{i=1}^{2} \int_{T_i} G_i [(\Box\Phi_i)^2 - 2\Phi_i] \, dT = 0 \ . \tag{4.23}$$

The truth of the above statement, by carrying out the verification also in this case, only in respect to the inhomogeneity type a., may be recognized as follows. From the identity

$$\Box \cdot [\Phi_i \Box \Phi_i] = \Phi_i \Delta\Phi_i + (\Box\Phi_i)^2 = (\Box\Phi_i)^2 - 2\Phi_i \quad (i = 1, 2) \tag{4.24}$$

by using Stokes's theorem we obtain

$$\int_{T_1} (\Box\Phi_1)^2 \, dT = 2 \int_{T} \Phi_1 \, dT + \int_{g_1} \mathbf{n} \cdot (\Box\Phi_1) \, \Phi_1 \, dS +$$

$$+ \int_{g_{12}} \Phi_1 (\Box\Phi_1) \cdot \mathbf{n} \, ds \ , \tag{4.25}$$

and

$$\int_{T_2} (\Box\Phi)^2 \, dT = 2 \int_{T_2} \Phi_2 \, dT + \int_{g_2} \mathbf{n} \cdot (\Box\Phi_2) \, \Phi_2 \, ds -$$

$$- \int_{g_{12}} \Phi_2 (\Box\Phi_2) \cdot \mathbf{n} \, ds \ . \tag{4.26}$$

From the equations obtained by the addition of Eqs (4.25) and (4.26) one can deduce the inequality to be verified if one applies the boundary condition (4.9) and fitting condition (4.10). Thus, it can be written that in the state of equilibrium

$$p_c = - \frac{I_c}{2} \ . \tag{4.27}$$

From the theorem of minimum it follows that the value p_{CK} of p_C is higher than that of min $p_C = -I_C/2$ associated with the state of equilibrium, i.e.:

$$\min p_c = -\frac{I_c}{2} \leq p_{ck} = -\frac{I_{c,c}}{2} \, . \tag{4.28}$$

In turn, from the inequality (4.28) the following conclusion may be deduced:

By applying the approximate procedure based on the principle of complementary work, for the torsional stiffness we obtain a lower value than that of the actual torsional stiffness,

$$-2p_{ck} = I_{c,c} \leq I_c \, . \tag{4.29}$$

5. Application of the principle of the minimum potential energy for the approximate determination of the torsional stiffness

The surface section where the load has a given value, is represented by the mantle of the bar. Accordingly in the present case we have

$$\pi_L = \sum_{i=1}^{2} \int_{B_i} \hat{e}_i dB \, . \tag{5.1}$$

The kinematically possible state will be built up from the displacement vector defined by Eqs (3.2), (3.3), (3.4), where the function $\varphi_i = \varphi_i(x, y) = = \varphi_i(P)$ is considered to be unknown. Further, the values of the constants u_0, v_0, w_0, ω_1, ω_2, ω_3 characterizing the rigid body motion are selected to be equal to zero. The scalar coordinates, (wich are different from zero) of the stress tensor associated with the kinematically possible state are as follows

$$\hat{\tau}_{xz}^{(i)} = G_i \vartheta \left(\frac{\partial \varphi_i}{\partial x} - y \right) \, , \tag{5.2}$$

$$\hat{\tau}_{yz}^{(i)} = G_i \vartheta \left(\frac{\partial \varphi_i}{\partial y} + x \right) \, , \tag{5.3}$$

wherein the function $\varphi_i = \varphi_i(P)$ (i = 1, 2), besides the necessary conditions of derivability, satisfies also the fitting conditions

$$\varphi_1 = \varphi_2 \, , \quad P \in g_{12} \tag{5.4}$$

valid along curve g_{12}.

After substituting (5.2), (5.3) into Eq. (5.1) and carrying out the integration with respect to z, the following result is obtained to π_L:

$$\pi_L = \pi_L(\varphi_i) = \frac{1}{2}\,\vartheta^2 l \sum_{i=1}^{2} G_i \int_{T_i} \left([\Box\varphi_i]^2 - 2\Box\varphi_i \cdot (\mathbf{R}\times\mathbf{k})\right) dT +$$

$$+ \frac{1}{2}\,\vartheta^2 i(I_1 G_1 + I_2 G_2)\,. \tag{5.5}$$

Since our task is the investigation of the equation $\delta\pi_L = 0$ characterizing the state of equilibrium, instead of the investigation of π_L, it would be enough to investigate the following functional only:

$$p_L = p_L(\varphi_i) =: \frac{1}{2}\sum_{i=1}^{2}\left[G_i \int_{T_i}\left((\Box\varphi_i)^2 - 2\Box\varphi_i(\mathbf{R}\times\mathbf{k})\,dT\right) + I_i G_i\right] \tag{5.6}$$

which is proportional to π_L.

By using Stoke's theorem and the rule of integration of a product may be justified in that the value of p_L is in the state of equilibrium (if the function $\pi_i = \pi_i(P)$ is a solution to the boundary-value problem defined by (3.35), (3.36), (3.37), (3.38)), the half of the torsional stiffness of the cross section, and accordingly, on the basis of the propriety of the potential energy minimum can be written*

$$\min p_L = \frac{I_c}{2}\,. \tag{5.7}$$

And to p_{LK} defined by kinematically possible states approximating the state of equilibrium: the inequality

$$\min p_L = \frac{I_c}{2} \leq p_{LK} = \frac{I_{C,L}}{2} \tag{5.8}$$

follows. From this it is to be seen that for the actual torsional stiffness, by applying the approximate method based on p_L, a higher value is obtained than the actual, i.e.,

$$I_C \leq I_{C,L} = 2p_{LK}\,. \tag{5.9}$$

---

* The validity of Eq. (5.7) may readily be recognized by considering Eq. (2.55), because $\pi_L(\varepsilon) + \pi_C(\varepsilon) = \vartheta^2 l\,(\min p_C + \min p_L) = 0$, wherefrom follows that $\min p_L = -\min p_C = I_C/2$.

6. Torsion of a prismatic bar with a solid cross section
reinforced with a thin layer

Let us consider the torsional problem of a prismatic bar having a solid cross section reinforced with a thin layer (Fig. 6.1). To investigate the cross section having inhomogeneity type *b.* a system of curvilinear coordinates should be introduced (s, ζ) in the plane x, y (Fig. 6.2):

$$\mathbf{R} = x\mathbf{i} + y\mathbf{j} = \rho(s) + \zeta\mathbf{n}(s),\qquad\qquad(6.1)$$

wherein:

$\rho = \rho(s)$ — equation of curve g_{12}
s — arc coordinate measured along curve g_{12},
$\mathbf{n}$ — unit normal vector on curve g_{12} pointing outwards from the material of body "1",
ζ — coordinate measured in direction $\mathbf{n}$.
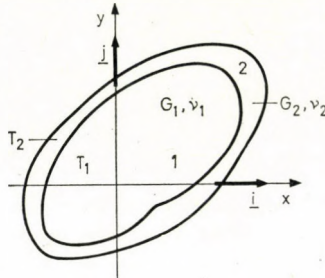
Fig. 6.1. Cross section reinforced with a thin layer
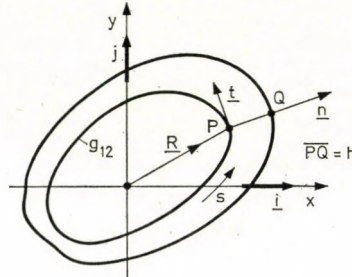
Fig. 6.2. System of curvilinear coordinates (s, ζ)

The surface element

$$dT = dx\, dy\qquad\qquad(6.2)$$

may be defined in the system of curvilinear coordinates (s, ζ) by using the equation

$$dT = (1 + \gamma\zeta)\, ds\, d\zeta\qquad\qquad(6.3)$$

wherein ζ is the curvature of curve g_{12} at point P.

In the following, will be investigated that from the stationariness condition of $p_C\, \delta p_C = 0$, what problem of boundary value might be deduced. The function $\Phi_i = \Phi_i(P)$ $(i = 1, 2)$ has to satisfy the boundary and fitting conditions

$$\Phi_2 = 0, \qquad\qquad P \in g_2\qquad\qquad(6.4)$$

and

$$G_1\Phi_1 = G_2\Phi_2, \qquad\qquad P \in g_{12}\qquad\qquad(6.5)$$

respectively. By satisfying the function $\Phi_2 = \Phi_2(P)$ interpreted in region T_2, the prescriptions (7.4) and (7.5) are assumed to take the form

$$\Phi_2 = \Phi_2(s, \zeta) = \frac{G_1}{G_2}\left(1 - \frac{\zeta}{h}\right)\Phi_1(s) \tag{6.6}$$

wherein $\Phi_1 = \Phi_1(s)$ is the value of the function $\Phi_1 = \Phi_1(P)$ at the point P defined by the arc coordinate s of curve g_{12}. The investigation will be limited to a cross section where

$$C \gg Dh^2 \;, \tag{6.7}$$

(C and D being the given functions of s),

$$\gamma h \approx 0 \;. \tag{6.8}$$

By using (6.7) and (6.8)

$$\int_{T_2} [(\Box\Phi_2)^2 - 4\Phi_2]\, dT = \int_{g_{12}}\int_{\zeta=0}^{h}\left[\frac{G_1^2}{G_2^2}\frac{\Phi_1^2(s)}{h^2} - 4\frac{G_1}{G_2}\left(1 - \frac{\zeta}{h}\right)\Phi_1(s)\right]\cdot$$
$$\cdot\, ds d\zeta = \frac{G_1}{G_2}\int_{g_{12}}\left[\frac{G_1}{G_2}\frac{\Phi_1^2(s)}{h} - 2\Phi_1(s)\,h\right]ds \tag{6.9}$$

is obtained if one applies the approximation

$$(\Box\Phi_2)^2 \approx \frac{G_1}{G_2}\frac{\Phi_1^2(s)}{h^2}\;. \tag{6.10}$$

Finally, calculating with the approximation obtained by neglecting the term $2h\Phi_1(s)$ the following may be written

$$\int_{T_2}[(\Box\Phi_2)^2 - 4\Phi_2]\, dT = \frac{G_1^2}{G_2^2}\int_{g_{12}}\frac{\Phi_1^2}{h}\, ds. \tag{6.11}$$

Application of the above approximation yields the final formula to p_C:

$$p_c = \frac{G_1}{2}\left\{\int_{T_1}[(\Box\Phi_1)^2 - 4\Phi]\, dT + \frac{G_1}{G_2}\int_{g_{12}}\frac{\Phi_1^2}{h}\, ds\right\}. \tag{6.12}$$

The equation $\delta p_C = 0$ evolved in detail means the following equation:

$$\delta p_c = G_1\left[\int_{T_1}[(\Box\Phi_1)\cdot(\Box\delta\Phi_1) - 2\delta\Phi_1]\, dT + \frac{G_1}{G_2}\int_{g_{12}}\frac{\Phi_1}{h}\,\delta\Phi_1 ds\right]\;. \tag{6.13}$$

By making use of the identities

$$\square \cdot (\delta\Phi_1 \square \Phi_1) = (\square \delta\Phi_1) \cdot \square \Phi_1 + (\varDelta\Phi_1)\, \delta\Phi_1) \,, \tag{6.14}$$

$$\int_{T_1} \square \cdot (\delta\Phi_1 \square \Phi_1)\, dT = \int_{g_{12}} \mathbf{n} \cdot (\square \Phi_1)\, \delta\Phi_1 ds \,, \tag{6.15}$$

δp_C may be written in the form:

$$\delta p_c = -G_1 \int_{T_1} (\varDelta\Phi_1 + 2)\, \delta\Phi_1 dT + \int_{g_{12}} \left(G_1 \frac{\partial\Phi_1}{\partial n} + \frac{G_1^2}{hG_2}\Phi_1\right) \delta\Phi_1 ds \,. \tag{6.16}$$

Since in the region T_1 and on the curve $g_{12}\,\delta\Phi_1$ is arbitrary, the equation $\delta p_C = 0$ may only be true if (see for example [16]) the function $\Phi_1 = \Phi_1(P)$ is the solution for the following boundary-value problem

$$\varDelta\Phi_1 + 2 = 0 \,, \qquad P \in T_1 \,, \tag{6.17}$$

$$\frac{\partial\Phi_1}{\partial n} + \frac{G_1}{G_2}\frac{1}{h}\Phi_1 = 0 \,, \quad P \in g_{12} \,. \tag{6.18}$$

ARUTJUJAN and ABRAMJAN derived the boundary condition (6.18) with the aid of another method [1].

7. Examples

7.1. *Example* 1

Let us consider the solid square cross section depicted in Fig. 7.1. In the regions T_1 and T_2 materials have a shear elasticity moduli G_1 and G_2, respectively. Be $\alpha = G_2/G_1$. The functions defining the statically possible state are assumed to be as follows:

$$\Phi_1 = \Phi_1(x, y) = -\alpha C(x - l)\,(y^2 - l^2)$$
$$0 \leq x \leq l; \quad -l \leq y \leq l;$$
$$\Phi_2 = \Phi_2(x, y) = C(x + l)\,(y^2 - l^2) \tag{a}$$
$$-l \leq x \leq 0; \quad -l \leq y \leq l;$$
$$L = 2l \,.$$

These functions satisfy the boundary and fitting conditions (4.9) and (4.10), respectively, at any value of C, and the stresses calculated from them according to (4.7) and (4.8) also satisfy the equilibrium equation

$$\frac{\partial\tilde{\tau}_{xz}}{\partial x} + \frac{\partial\tilde{\tau}_{yz}}{\partial y} = 0 \,. \tag{b}$$

The constant C may be determined from the necessary condition of the minimum of

$$p_c = \frac{G_1}{2} \int_{T_1} [(\Box \Phi_1)^2 - 4\Phi_1] \, dT + \frac{G_2}{2} \int_{T_2} [(\Box \Phi_2)^2 - 4\Phi_2] \, dT. \qquad (c)$$

Replacement of the assumed functions $\Phi_i = \Phi_i(x, y)$ $(i = 1, 2)$ into the expression of p_C, then after integration and some reduction, yields

$$p_{CK} = G_1 \left(\frac{11}{720} C^2 \alpha^2 L^6 + \frac{1}{24} C\alpha L^5 \right) + G_2 \left(\frac{11}{720} C^2 L^6 + \frac{1}{24} CL^5 \right) . \qquad (d)$$
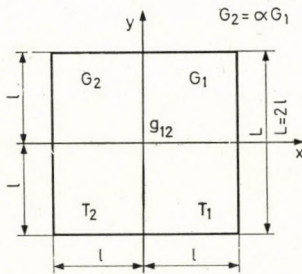
Fig. 7.1. Solid square cross section of composite material

From the condition of stationariness

$$\delta p_{CK} = \frac{\partial p_{CK}}{\partial C} \delta C = 0$$

the equation

$$\frac{\partial p_{CK}}{\partial C} = 0$$

follows. This is true if

$$C = -\frac{30}{11} \frac{1}{\alpha + 1} \frac{1}{L} . \qquad (e)$$

With the above constant C, one obtains for a possible lower limit of the torsional stiffness of the composite cross section, the following result:

$$I_{C,c} = -2p_{CK} = \frac{5}{22} \frac{\alpha}{\alpha + 1} GL^4 . \qquad (f)$$

In case of $\alpha = 2$ from the above formula

$$I_{c,c} = 0,1565 GL^4 .$$

ELY and ZIENKIEWICZ [6] found for $\alpha = 2$ and for the above cross section that

$$I_c = 0{,}1941 L^4 G .$$

7.2. *Example 2*

In connection with the cross section shown in Fig. 7.1 a possible upper limit of the torsional stiffness should be determined with the aid of Eq. (5.9). The function $\varphi_i = \varphi_i(x, y)$ $(i = 1, 2)$ defining the kinematically possible state is assumed to take the form

$$\varphi_i = \varphi_i(x, y) = cxy , \qquad P \in T_i , \qquad (i = 1, 2) . \tag{g}$$

The above function satisfies the fitting condition (5.4) at any value of the constant C. The value of the constant C may be assumed from the necessary condition of the minimum of

$$p_L = \frac{1}{2} \sum_{i=1}^{2} \left(G_i \int_{T_i} [(\Box \varphi_i)^2 - 2(\Box \varphi_i) \cdot (\mathbf{R} \times \mathbf{k})] \, dT + G_i I_i \right) . \tag{h}$$

With the assumed functions $\varphi_i = \varphi_i(x, y)$ $(i = 1, 2)$ for p_{LK} the following result is found

$$p_{LK} = (c^2 + 1) \frac{\alpha + 1}{24} GL^4 , \qquad \left(\alpha = \frac{G_2}{G_1} , \quad G_1 = G \right) . \tag{i}$$

From the condition of stationariness

$$\delta p_{LK} = \frac{\partial p}{\partial c} \, \delta c = 0$$

follows the equation

$$\frac{\partial p_{CK}}{\partial c} = 0 .$$

This is true if

$$c = 0 .$$

With this value of the constant c

$$I_{C,L} = 2 p_{LK} = \frac{\alpha + 1}{12} GL^4 \tag{j}$$

will be a possible upper limit of the torsional stiffness of the "composite" square cross section. This gives for $\alpha = 2$ the result

$$I_{C,L} = 0{,}25 GL^4 .$$

7.3. *Example 3*

In the next problem the stress function of the solid circular cross section reinforced with a thin layer is treated (Fig. 7.2). The stress function of the cross section should be determined according to the Ritz method. Be

$$\Phi_1 = \Phi_1(r) = A_0 + A_1 r^2,$$

(A_0, A_1 being arbitrary constants).
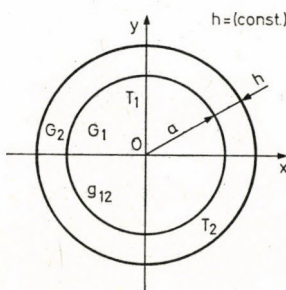
Fig. 7.2. Circular cross section reinforced with a thin layer

For the above function we have

$$(\Box\Phi_1)^2 = 4A_1^2 r^2, \quad \int_{T_1} \Phi_1 dT = 2\pi\left(A_0 \frac{a^2}{2} + A_1 \frac{a^4}{4}\right)$$

$$\int_{g_{12}} \Phi_1^2 ds = 2\pi a (A_0 + A_1 a^2)^2, \quad \int_{T_1} (\Box\Phi_1)^2 \, dT = 2\pi A_1^2 a^4. \tag{k}$$

From this for p_c (see Eq. 6.12)

$$p_c = G_1 \pi \left[A_1 a^4 - 2A_0 a^2 - A_1 a^4 - \frac{G_1}{hG_2}(A_0 + A_1 a^2)^2 \, a \right] \tag{l}$$

is obtained. The solution to the system of equations

$$\frac{\partial p_c}{\partial A_0} = 0, \quad \frac{\partial p_c}{\partial A_1} = 0$$

following from the condition of stationariness

$$\delta p_c = \frac{\partial p_c}{\partial A_0}\delta A_0 + \frac{\partial p_c}{\partial A_1}\delta A_1 = 0 \tag{n}$$

is

$$A_0 = \frac{a^2}{2} + \frac{G_2}{G_1}ha, \quad A_1 = -\frac{1}{2}. \tag{o}$$

Accordingly, the stress function will be

$$\Phi_1 = \Phi_1(r) = \frac{G_2}{G_1} ha + \frac{1}{2}(a^2 - r^2) \, . \tag{p}$$

It may be pointed out that in this case the equations

$$\Delta\Phi_1 = -2 \, , \qquad P \in T_1 \, ,$$

$$\frac{\partial \Phi_1}{\partial n} + \frac{G_1}{hG_2}\Phi_1 = 0 \, , \quad P \in g_{12} \tag{r}$$

are valid. Thus, $\Phi_1 = \Phi_1(r)$ presents the exact solution to the present problem.

REFERENCES

1. АРУТЮИЯН Н. Х., АБРАМЯН Б. Л.: Кручение упругих тел. Физматгиз, Москва 1963
2. MUSHKELISHVILI, N. J.: Sur le problème de torsion de poutres élastiques composées. *Compte rendu*. **194** (1932), 1435—1437
3. MITRA, N. D.: Torsion of Composite Sections of Different Isotropic Materials. *Bull. of the Calcutta Math. Soc.* **47** (1955), 191—197
4. WITRIC, H. N.: Torsion of Multiwebbed Rectangular Tube. *Aircraft Engineering* **25** (1958), 372
5. SEIDE, P.: On the torsion of Rectangular Sandwich plates. *Journ. Appl. Mech.* **23** (1956), No 2
6. ELY, I. F.—ZIENKIEWICZ, O. C.: Torsion of Compound Bars (a relaxation solution). *Intern. Journ. of Mech. Sci.* **1** (1960), 356—365
7. KUO, H.—CONWAY, M. D.: Torsion of Composite Rhombus Cylinder. *Journ. Appl. Mech.* March (1974) p. 103
8. ЛЕХНИШКИЙ С. Г.: Кручение анизотропных и неоднородных стержней. Изд. Наука, Москва 1971
9. ЛУЬЕ. А. И.: Теория упругости. Изд. Наука Москва, 1970.
10. LANGHAR, H. L.: Energy Methods in Applied Mechanics. John Wiley and Sons. Inc. New York, London 1962
11. KYIOICHIO WASHIZU: Variational Methods in Elasticity and Plasticity. Pergamon Press. Oxford, London, New York, Toronto, Sidney, Paris, Braunschweig 1968
12. СЕДОВ, А. И.: Механика сплотной среды. Том. I. Изд. Наука Москва 1973
13. СЕДОВ, А. И.: Механика стлочиной среды. Том II. Изд. Яаука Москва 1973
14. MASE, G. E.: Theory and Problems of Continuum Mechanics. McGraw-Hill Book Company, New York. London. Toronto 1970
15. MILNE, L. M.—THOMSON: Antiplane Elastic System. Springer-Verlag. Berlin—Göttingen—Heidelberg 1962
16. WEIWSTOCK, E.: Calculus of Variations, McGraw-Hill Book Company. New York—Toronto—London 1952
17. LEIPHOLZ, H.: Theory of Elasticity. Noordhof. International Publishing Leyden. 1974
18. KERR, A. D.: An Extension of the Kantorovich Method. Quarterly Applied Math. **26** (1968), 219—229
19. KANTOROVITSCH L. W.—KRYLOW W.: Näherungsmethoden der höheren Analysis. Deutscher Verlag der Wissenschaften, Berlin 1956.
20. TRUESDELL, C.— NOLL, W.: The Nonlinear Field Theories of Mechanics. Handbuch der Physik. Bd. III/3. (S. Flügge ed.) Berlin—Heidelberg. Springer Verlag, New York 1965

Variationsmethode zur Lösung des Verdrehungsproblems eines aus verschiedenen Stoffen Zusammengesetzten prismatischen Stabes. — Behandelt wird das Verdrehungsproblem von aus verschiedenen Stoffen zusammengesetzten prismatischen Stäben mit vollem Querschnitt. Im Abschnitt 2 der Abhandlung sind Variationsrechnungsmethoden beschrieben, die zur Lösung quasistatischer Randwertaufgaben von aus verschiedenen Stoffen zusammengesetzten linearisch elastischen Kontinua geeignet sind. In diesem Abschnitt werden die mit der *Potentialenergie* und *Ergänzungsarbeit* zusammenhängenden Stationäritätsbedingungen und Minimumprinzipien der Elastizitätslehre zusammengefasst und verallgemeinert. Im Abschnitt 3 werden aufgrund der einschlägigen Literatur die mit der freien Verdrehung der Stäbe mit inhomogenem Querschnitt — der sog. aus zusammengesetzten Stoffen hergestellten prismatischen Stäbe — zusammenhängenden Kenntnisse erörtert. In den Abschnitten 4 bis 7 werden einige neue Resultate im Zusammenhang mit der freien Verdrehung der zusammengesetzten Stäbe vorgeführt, die mit Hilfe der in der Abhandlung hergeleiteten Sätze erhalten werden können. Es wird betont, daß die Drehsteifigkeit sowohl von unten, als von oben mit Hilfe der angegebenen Abhängigkeitenabgeschätzt werden kann. Abschnitt 6 behandelt die Verdrehungsaufgabe des durch eine dünne Schicht verstärkten Stabes. Abschnitt 7 enthält drei Beispiele.

Вариационный метод реяшени задачи кручения призматического стержня из комбинированного материала. Работа посвящена вопросу свободного кручения призматических стержней сплошного сечения, изготовленных из комбинированных материалов. Во второй главе описываются вариационные методы, пригодные для решения квазистатических задач краевых значений линейно упругих упругих континуумов из комбинированных материалов. В указанной выше главе подытоживается и обобщается стационарные условия и минимальные принципы теории упругости, связанные с потенциальной энергией и дополнительной работой. В 3-ей главе на основе литературных данных [1, 6, 8] излагаются сведения по упругому ссвободному кручению призматических стержней из комбинированных материалов, обладающих негомогенностью по своему сечению. В 4, 5, 6 и 7 главах излагаются некоторые новые результаты по свободному кручению призматических стержней из комбинированных материалов, которые модно получить с помощью позиций Т. 2 (2,26); Т. 3 (2,27) и Т. 4 (2,47); Т. 5 (2,48) главы 2. Следует особо подчеркнуть, что жесткость кручения можно оценить снизу на основе (4,29), а на основе (5,9) — сверху. Глава 6 посвящена задаче кручения призматического стержня, укрепленного тонким слоем. В главе 7 излагается три примера.

LATERAL BUCKLING OF PLANE TRUSSES WITH PARALLEL CHORDS AND HINGED JOINTS

T. TARNAI*

An approximate investigation of the lateral buckling of plane trusses with parallel chords is dealt with on the basis of the continuum method. The truss is modelled by I-beam with non-torsioning flanges, the web of which is connected to the flanges with the aid of hinges. The differential equations of such a beam are deducted for the lateral-buckled state. The relationships between the equations obtained and the lateral-buckling equations of thin-walled beams having non-deformable cross section are presented.

Notation

The following symbols are used in this paper:

x, y	horizontal and vertical coordinates, respectively, related to axis point on a bottom flange cross section,
z, ζ	coordinate along longitudinal axis,
h	distance between axes of top and bottom flanges,
e	distance to point of application of axial load from bottom flange axis,
e_N	distance to point of application of concentrated axial force N from bottom flange axis in cross section,
e_S	distance to centroid of cross section from bottom flange axis,
s	distance to point of application of transverse load from bottom flange axis,
y_M	distance to shear center of cross section from bottom flange axis,
r_x	radius of cross section,
w_1, w_2, ξ_1, ξ_2	displacements of arbitrary points of axes of top and bottom flanges, respectively, in x direction,
u	displacement of shear center in x direction,
φ	angle of rotation of cross section,
F	area of cross section,
F_1, F_2	cross-sectional areas of top and bottom flange respectively,
J_y	moment of inertia of beam cross section about y-axis,
J_1, J_2	moments of inertia of cross sections of top and bottom flanges, respectively, about y-axis,
$k = J_1/J_2$,	
J_c	torsional constant of cross section of beam,
J_ω	warping constant of cross section of beam,
E	modulus of elasticity,
S	centroid of cross section,
M	shear center of cross section,
Q, q	concentrated and distributed tranverse loads respectively,
q_1, q_2	parts of distributed transverse load divided to top and bottom flanges respectively,
P, p_n	concentrated and distributed axial loads respectively,
p_{n1}, p_{n2}	parts of axial load divided to top and bottom flanges respectively,

* Dr. T. TARNAI, Kolostor u. 17, H-1037 Budapest, Hungary.

t_1, r_1, p_1; t_2, r_2, p_2 forces induced by transverse loads on top and bottom flanges respectively,
N resultant of axial forces being to the left of cross section (its value is the same as that of normal force acting on cross section),
$\overline{N}_1$, $\overline{N}_2$ normal forces in top and bottom flanges respectively,
$\hat{N}_1$, $\hat{N}_2$ normal forces in top and bottom flanges, respectively, from a transverse load,
N_1, N_2 normal forces in top and bottom flanges, respectively, from an axial load,
T_x, T_y shearing forces in x and y directions, respectively, generated in cross section,
$\overline{M}_x$ bending moment in x direction acting on cross section,
M_x part of bending moment $\overline{M}_x$ from transverse load,
M_{xN_1}, M_{xN_2} moments of axial forces being to the left of cross section around top and bottom flange axis points, respectively, of the same cross section,
M_y bending moment in y direction acting on cross section,
T_{x1}, M_{y1}; T_{x2}, M_{y2} shearing forces and bending moments in top and bottom flanges respectively,
$(.)' = d/dz$ symbol of derivation,
$(.)_1$ (1 in subscript) quantity relating to top flange,
$(.)_2$ (2 in subscript) quantity relating to bottom flange.

For other symbols see also Figs 3 and 4.

1. Introduction

The problem of lateral buckling of plane trusses with parallel chords is, in general, rather intricate. For approximate investigations, the problem may significantly be simplified by replacing the truss with continuum. For the case, where the warping rigidity of the truss was neglectable, in comparison to the torsional rigidity, the substituting continuum was determined by CSONKA [4]. The contrary case, where the torsional rigidity was low compared to the warping rigidity, was dealt with by WINTER [9]. The truss was modelled by WINTER as an I-beam having a non-deformable cross section which had no torsional rigidity. However, in case of an I-beam with a non-deformable cross section (Fig. 1a), contrary to the original truss, boundary conditions for the top and bottom flanges cannot be given independently of each other. This might be done only in the case where the I-beam could be considered as having a deformable web (Fig. 1b). However, the lateral buckling of such beams, according to the knowledge of the author, is solved only for the case of a symmetrical and constant cross section.

The torsional rigidity of steel trusses can also be neglected due to the fact, that if the bars of the latticework are relatively stiff, the lattice bars are connected by very flexible gussets to the chords. These gussets behave like hinges. The cross section of such a truss will change its shape already in the state of lateral buckling. For this type of truss, the replacing continuum might be constituted by an I-beam with non-torsioning flanges where the web is connected by hinges to the flanges (Fig. 1c). With this model the same boundary conditions may be assured as those of the original truss. For the analysis of trusses modelled in such a way DULÁCSKA and the author of the the present paper [5] developed on the basis of the method of successive

approximation worked out by KOVÁCS and FABER [7] for some actual problems an approximate analytic method.

This method is generalized in this paper. With the aid of the continuum method a set of differential equations is deduced for the investigation of the lateral buckling of the truss which is valid even in cases where

— the cross sections of the chords of the truss vary independently of each other,

— the magnitude and point of application of the axial and transverse loads applied to the truss freely vary along its length in its plane,

— the boundary conditions for the top and bottom chords may be prescribed independently of each other.
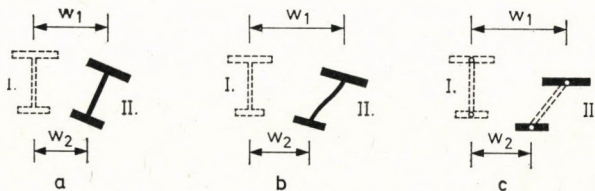
Fig. 1. Different cases of lateral buckling of I-beams: a) non-deformable cross section, b) cross section with deforming web, c) hinged cross section with non-torsioning flanges. (I — A cross section of the unloaded beam. II — The same cross section of the laterally buckled beam)

The set of equations obtained has a very simple form. This can be assigned to the fact that in lieu of the variables customarily used in the literature on the subject (displacement of the shear center and rotation of the cross section) the displacements of the axis points on the flanges are taken into account as variables.

2. Assumptions and constraints

For the investigations the following assumptions and constraints are adopted:

1. The material of the truss is ideally elastic, it follows Hooke's law.

2. Both the top and bottom chords are continuous bars of rectilinear axis through the whole length of the truss for which the Bernoulli—Navier hypothesis is true.

3. The truss is a plane girder, i.e., the axes of the chord and lattice bars lie in the very same plane. This plane is, at the same time the symmetry plane of the truss.

4. The axes of the chords of the truss are parallel to each other.

5. The lattice bars are connected to the chords by ball-and-socket joints and the axes of the lattice bars and chord members intersect at one point at all the joints.

6. The latticework of the truss is statically determined. The net of the primary latticework is, in the general case, identical with that which is to be seen in Fig. 2. If in the latticework there are also ties and a secondary grid then their influence on the lateral buckling of the truss may be neglected.

7. The latticework of the truss is so dense that it can be considered as being continuous. At the transition of the discrete latticework into the continuous one (i.e., in the course of $(\overline{AB}) \to 0$, where $(\overline{AB})$ designates the length of the segment $\overline{AB}$), the properties $\overline{CC'} \perp \overline{AB}$, $\overline{BB'} \perp \overline{CD}$ and $(\overline{AC'})/(\overline{C'B}) = (\overline{DB'})/(\overline{B'C}) = constant$ are maintained (Fig. 2).
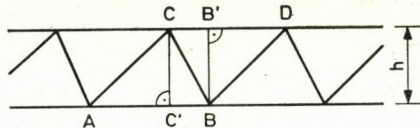
Fig. 2. Network of the truss

8. However, the continuous web developed in this way has neither torsional rigidity, nor longitudinal strain and flexural rigidities. The transverse strains of the web can be neglected.

9. The form of the truss is geometrically perfect and the deformations preceding the occurrence of the lateral buckling as well as the deformations taking place in the plane of the truss are negligible.

10. In the course of lateral buckling the chords are not twisted.

11. The magnitude of the displacements taking place during lateral buckling is such that at the rotations of the cross section the effect of the application of the approximation

$$\psi \approx \sin \psi \approx \tan \psi ; \qquad \cos \psi \approx 1 \tag{1}$$

remains below the permissible error limit.

12. The loads q and p_n applied in the transverse and axial directions, respectively, to the truss, act before the lateral buckling takes place, in the plane of the truss, and after lateral buckling has occurred, they retain their original directions, and their points of application remain unchanged.

3. Deduction of the set of differential equations of lateral buckling

Let us first define the signs of the quantities entering the discussion.

The applied orthogonal, left-spin system of coordinates x, y, z is fitted to the truss in such a way, that previous to lateral buckling the z-axis lies in the axis of the bottom chord of the truss and the y-axis is directed downwards in the symmetry plane of the truss (Fig. 3).
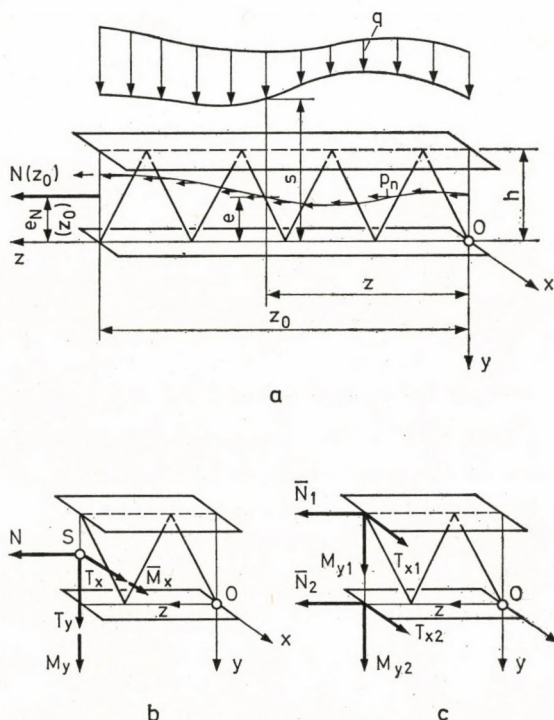
Fig. 3. a) Loads applied to the truss. b) Forces and bending moments in the truss. c) Forces and bending moments in the chords of the truss

Let the truss be submitted to the loads q and p_n of transverse (y) and axial (z) directions respectively. The forces and moments induced in one of the cross sections of the truss are, as is customary, interpreted by the reduction of the forces being to the left of the cross section to the centroid S of the cross section. To the bending moment, vectors are coordinated in such a way that by looking in front of the arrow of the vector the rotation of the moment should show in the clockwise direction (Fig. 3b). The forces and moments are interpreted in each of the chord cross sections in the very same way (Fig. 3c).

All of the externally applied forces (the loads q and p_n acting in the transverse and axial directions respectively) and all of the internal forces, moments (the normal forces N; $\bar{N}_1$, $\bar{N}_2$, shearing forces T_x, T_y; T_{x1}, T_{x2}, T_{y1}, T_{y2} and bending moments $\bar{M}_x$, M_y; M_{y1}, M_{y2}) are considered to be positive if their sense of acting coincides with the positive sense of the respective axes of coordinates. In Fig. 3, all loads, forces and moments are depicted with a positive direction.

The displacements w_1, w_2 and u are positive if they take place in the positive direction of the x-axis. The rotation φ is positive if looking in front of the positive direction of the z-axis it is of clockwise direction.
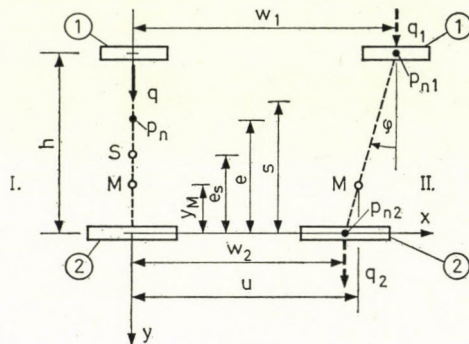
Fig. 4. Data of the beam cross section. I) The cross section prior to lateral buckling. II) The cross section after lateral buckling. (① Top flange, ② Bottom flange)

The distances h, e, e_N, e_S, s, y_M are positive if they can be measured in the *negative direction* of the y-axis starting from the axis of the bottom chord (Figs 3a and 4).

The bending moment $\bar{M}_x$ of the cross section is composed corresponding to the transverse and axial forces having two parts: $\bar{M}_x = M_x + (e_S - e_N)N$. Similarly, the normal forces acting on the chords are: $\bar{N}_1 = \hat{N}_1 + N_1$, $\bar{N}_2 = \hat{N}_2 + N_2$.

With respect to the above sign rules the following relationships will be true:

$$q = -T_y', \tag{2}$$

$$T_y = M_x', \tag{3}$$

and from (2), (3)

$$q = -M_x''. \tag{4}$$

Further, on the basis of the assumption of Chapter 2:

$$M_{y1} = EJ_1 w_1''; \qquad\qquad M_{y2} = EJ_2 w_2'', \tag{5a, b}$$

$$T_{x1} = -(EJ_1 w_1'')'; \qquad\qquad T_{x2} = -(EJ_2 w_2'')'. \tag{6a, b}$$

In deducting the equations of the lateral buckling one sets out from the fundamental idea applied in ref. [5].

Let us consider the bottom view of a segment of the truss laterally buckled, i.e., its projection to the plane xz (Fig. 5a), and also two neighbouring lattice bars. Their point of intersection is on the axis of one of the chords. These two lattice bars, under the effect of transverse loads applied to the truss, transmit a concentrated force F to the chord, acting at the point of intersection and in the plane of the bars, if the externally applied load also lies in the plane of the lattice bars. In this case, the line of action of force F will be parallel to the straight line connecting the end points of the two lattice bars lying on the axis of the other chord. This statement follows from the
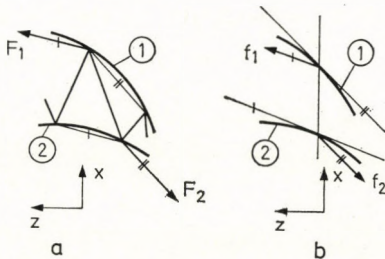
Fig. 5. Bottom view of the laterally buckled truss. a) wide-meshed lattice, b) dense lattice. (① Top chord, ② Bottom chord)

assumptions 4, 9 and 11 in Chapter 2, and from the equilibrium of the forces acting on the point of intersection of the neighbouring lattice bars. Namely, owing to the neglection of deformations in the vertical plane and small displacements, the axes of the chords of the laterally buckled truss may be considered, as lying in two planes parallel to each other. Due to the equilibrium of the forces acting on the intersection point of the neighbouring lattice bars the force F must lie on the one hand in the plane of the chord axis including the point of intersection of the lattice bars, on the other hand in the plane of the lattice bars; i.e., on the line of intersection of the two planes.

However, this straight line is parallel to that connecting the end points of the two lattice bars lying on the axis of the other chord being the planes of chords parallel to each other and by intersecting both of these planes with a third plane (with the plane of the lattice bars), parallel straight lines are obtained. The projections of these parallel straight lines to any arbitrary plane, as also to the plane xz, are parallel as well. The signs of the forces F depend on whether they are looked at on the top or bottom chord. If the latticework is densified according to the assumption 7 of Chapter 2 (and assuming that the latticework is infinitely dense), than the latticework transmits distributed forces f to the flanges. The action line of the forces will, in a fixed point

of the flanges defined by common z-abscisse, always be parallel to the tangent of the curved axis of the other flange. On the top flange with that of the bottom flange and on the bottom flange with that of the top flange (Fig. 5b).

These f-forces may be decomposed into two components, one (t) of which is parallel to the z-axis and the other (r) to the x-axis (Fig. 6).

Since the angle in question is small,

$$t = f \cos \varepsilon \approx f, \tag{7}$$

$$r = t \cdot \tan \varepsilon \approx t \cdot \varepsilon. \tag{8}$$

The forces t and r are positive if their senses of action are the same as those of the axes z and x, respectively.
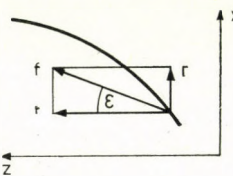
Fig. 6. Decomposition of force f applied to the flange of the laterally buckled beam

The forces f and t are normal force increments attacking the flanges of the beam. Since the normal forces acting in the flanges caused by the transverse loads are

$$\widehat{N}_1 = -\frac{M_x}{h}, \qquad \widehat{N}_2 = \frac{M_x}{h},$$

the forces t will be as follows:

$$t_1 = -\widehat{N}_1' = \frac{M_x'}{h}, \tag{9}$$

$$t_2 = -\widehat{N}_2' = -\frac{M_x'}{h}. \tag{10}$$

The forces r may be calculated from the relationship (8). The $\tan \varepsilon$ is the slope of the tangent of the axis of the other flange, i.e., the derivative of the axis function. Accordingly, the values of the r-forces with the right signs are as follows:

$$r_1 = w_2' t_1 = w_2' \frac{M_x'}{h}, \tag{11}$$

$$r_2 = w_1' t_2 = -w_1' \frac{M_x'}{h}. \tag{12}$$

Let us now decompose the transverse load attacking the laterally buckled beam to the components acting on the top and bottom flanges (Fig. 4). Then

$$q_1 = q\,\frac{s}{h}, \tag{13}$$

$$q_2 = q\left(1 - \frac{s}{h}\right). \tag{14}$$

The transverse forces q_1 and q_2 attacking the top and bottom flanges, respectively, may be decomposed into a force component lying in the web
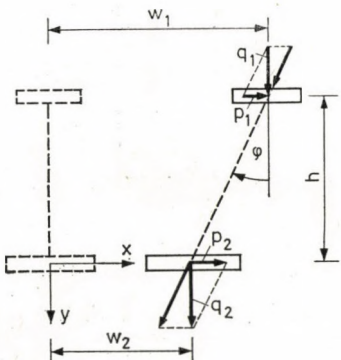
Fig. 7. Decomposition of the transverse loads on the laterally buckled beam

line of the cross section of the beam and to another component p bending the flange and acting in the x direction (Fig. 7). These p-forces are, in case of a distributed q-load, as a matter of course, distributed, while in case of a concentrated Q-load they will be concentrated. The p-forces are considered to be positive if they are directed to the positive direction of the x-axis.

The forces p will be tan φ times the load q. The angle φ being small, considering the relationships (1) for the p forces, the following values are obtained on the top and the bottom flanges, respectively:

$$p_1 = q_1\,\frac{w_1 - w_2}{h}, \tag{15}$$

$$p_2 = q_2\,\frac{w_1 - w_2}{h}. \tag{16}$$

Also the axial loads applied to the beam should be decomposed into two components, one loading the top and the other the bottom flange

$$p_{n1} = \frac{e}{h}\cdot p_n, \tag{17}$$

$$p_{n2} = \frac{h - e}{h} \cdot p_n.$$ (18)

In the cross section $z = z_0$ of the beam the following forces and moments act in the top flange: the normal force $\bar{N}_1(z_0) = N_1(z_0) + \hat{N}_1(z_0) = N_1(z_0) - M_x(z_0)/h$, the shearing force $T_{x1}(z_0)$ and the bending moment $M_{y1}(z_0)$.

In the bottom flange: the normal force $\bar{N}_2(z_0) = N_2(z_0) + \hat{N}_2(z_0) = N_2(z_0) + M_x(z_0)/h$, the shearing force $T_{x2}(z_0)$ and the bending moment $M_{y2}(z_0)$. After decomposition into components, the top flange is submitted
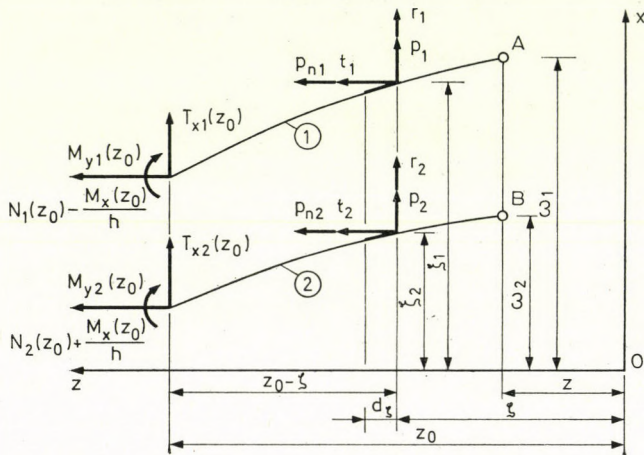
Fig. 8. Forces acting on the flanges of the laterally buckled beam (① Top flange ② Bottom flange)

to forces p_1, r_1, t_1 and p_{n1}, the bottom flange to the forces p_2, r_2, t_2 and p_{n2}. The flanges of the laterally buckled beam are, on the effect of the above forces, in equilibrium.

Let us now determine in the top and bottom flanges the bending moments of y direction in a point of arbitrary abscisse z of the beam. For that purpose the moment equations of the forces attacking the flanges should be written down at point A for the top flange and at point B for the bottom flange (Fig. 8).

Accordingly, the bending moment in point A is:

$$M_{y1} = M_{y1}(z_0) + \left(N_1(z_0) - \frac{M_x(z_0)}{h} \right) (w_1 - w_1(z_0)) +$$

$$+ T_{x1}(z_0) (z_0 - z) + \int_z^{z_0} (p_{n1} + t_1) (w_1 - \xi_1) \, d\zeta +$$

$$+ \int_z^{z_0} (r_1 + p_1) (\zeta - z) \, d\zeta$$ (19)

and in point B:

$$M_{y2} = M_{y2}(z_0) + \left(N_2(z_0) + \frac{M_x(z_0)}{h} \right) (w_2 - w_2(z_0)) +$$

$$+ T_{x2}(z_0)(z_0 - z) + \int_z^{z_0} (p_{n2} + t_2)(w_2 - \xi_2) d\zeta +$$

$$+ \int_z^{z_0} (r_2 + p_2)(\zeta - z) d\zeta . \tag{20}$$

Let us substitute into Eq. (19) the expressions (5a), (9), (11), (13), (15) and (17), and into Eq. (20) the expressions (5b), (10), (12), (14), (16) and (18), then, differentiate the so obtained equations twice with respect to the variable z. Consideration of

$$N_1(z_0) = \frac{e_N(z_0)}{h} N(z_0) , \tag{21}$$

$$N_2(z_0) = \frac{h - e_N(z_0)}{h} N(z_0) , \tag{22}$$

$$p_n = -N' , \tag{23}$$

$$\left(h - e_N(z_0) \right) N(z_0) + \int_z^{z_0} (h - e) p_n d\zeta = M_{xN1} , \tag{24}$$

$$e_N(z_0) \cdot N(z_0) + \int_z^{z_0} e p_n d\zeta = -M_{xN2} \tag{25}$$

yields the following equations:

$$(EJ_1 w_1'')'' + \frac{1}{h}(M_{xN2} + M_x) w_1'' - \frac{1}{h}(eN' - M_x') w_1' -$$

$$- q \frac{s}{h^2} w_1 - \frac{1}{h} M_x' w_2' + q \frac{s}{h^2} w_2 = 0 , \tag{26}$$

$$(EJ_2 w_2'')'' - \frac{1}{h}(M_{xN1} + M_x) w_2'' - \frac{1}{h}\left[(h - e) N' + M_x' \right] w_2' +$$

$$+ q \frac{h - s}{h^2} w_2 + \frac{1}{h} M_x' w_1' - q \frac{h - s}{h^2} w_1 = 0 . \tag{27}$$

The set of Eqs (26), (27) is the lateral buckling set of equations of the substituting continuum of plane trusses of hinged joints and parallel chords. This set of equations describes the equilibrium of flanges of the laterally buckled beam.

4. The boundary conditions

Equations (26), (27) are fourth order ordinary differential equations wherein, similarly to the bent bars of the straight axis, the perpendicular to the axis displacement of the cross sections is unknown. Accordingly both at the top and bottom flange boundary conditions also occurring in case of bent bars may be established, for each there are four in number.

The boundary conditions of the trusses are for the most frequent supporting modes as follows:

4.1 *Fork-like supported truss end*

In this type of supports both the top and bottom flange is supported on hinges. The flange cross sections above the supports can rotate round the y-axis but cannot be displaced and in the support cross section no bending moment in the y direction can take place.

The boundary conditions on the basis of (5a, b) are:

$$w_1 = 0, \qquad\qquad\qquad\qquad w_2 = 0,$$
$$M_{y1} = 0, \quad \text{i.e.,} \quad w_1'' = 0, \qquad M_{y2} = 0, \quad \text{i.e.,} \quad w_2'' = 0.$$

4.2. *Fixed truss end*

In this case both the top and bottom flange is rigidly supported, neither the displacements nor rotation of either flanges can occur. The boundary conditions are

$$w_1 = 0, \qquad\qquad\qquad w_2 = 0,$$
$$w_1' = 0, \qquad\qquad\qquad w_2' = 0.$$

4.3. *Free truss end*

In case of the free truss end both the top and bottom flanges may freely be displaced and rotated. In the end cross section neither bending moment in the y direction nor shearing force in the x direction can occur. The boundary conditions according to the formulae (5a, b), (6a, b) are

$$M_{y1} = 0, \text{ i.e., } w_1'' = 0, \ M_{y2} = 0, \text{ i.e., } w_2'' = 0,$$
$$T_{x1} = 0, \text{ i.e., } (EJ_1 w_1'')' = 0, \ T_{x2} = 0, \text{ i.e., } (EJ_2 w_2'')' = 0,$$

or, these latter two in case of constant cross sections:

$$w_1''' = 0, \ w_2''' = 0.$$

Besides those mentioned above elastic support and elastic fixation may also occur.

The boundary conditions discussed so far were the same for both the top and bottom flange. However, also such boundary conditions can be established, as differing from each other on the two flanges. Thus, for example, it may be prescribed that the end of the top flange of the beam should be fixed and the bottom flange simply supported. For this kind of support the following boundary conditions are coordinated:

$$w_1 = 0, \qquad\qquad w_2 = 0,$$
$$w_1' = 0, \qquad\qquad w_2'' = 0.$$

The fact that boundary conditions can independently be prescribed, separately for the top and bottom flanges, this is made possible by the introduction of the variables w_1 and w_2.

5. Relationship between the substituting continua of the non-deformable cross section and hinged cross section of the truss

In the following it will be analysed what relationship there is between the substituting continuum of the non-deformable cross section and that of hinged cross section with non-torsioning flange. What connection is between the familiar lateral buckling equations of the thin-walled I-beams with non-deformable cross section without torsional rigidity and the equations (26) and (27) deduced above, will be investigated.

5.1. *Equations of the beam with proportionately changing cross section*

In the literature on the subject the lateral buckling of beams of I-cross section is discussed depending on the rotation φ of the cross section and the displacement u of the shear center in direction x. In order to compare the lateral buckling equations of the two types of substituting continua, also the equations (26) and (27) should be rewritten with the variables φ and u in lieu of w_1 and w_2.

The distance y_M defining the position of the shear center of the cross section (Fig. 4) is given by the relationship

$$y_M = \frac{J_1}{J_y} h, \tag{28}$$

wherein

$$J_y = J_1 + J_2. \tag{29}$$

With the consideration of Fig. 4 and the relationship (1) relating to small angles, it can be written:

$$w_1 = u + (h - y_M)\,\varphi\,, \quad \bullet \tag{30}$$

$$w_2 = u - y_M\varphi\,. \tag{31}$$

Substitution of the expressions (30) and (31) into the differential equations (26) and (27) would result in a rather intricate set of equations rather difficult to survey. But, it is much simpler to treat beams with only the moment of inertia of the cross section of whose both top and bottom flange changes in exactly the same proportion. Such beams will be called beams with proportionately changing cross section. Thus, at this beam the quotient of the moments of inertia of the flange cross sections

$$k = \frac{J_1}{J_2}$$

is constant. However, in this case also the position of the shear center remains constant throughout the length of the beam i.e.,

$$y = const. \tag{32}$$

The warping constant of the I cross section is given by the known relationship

$$J_\omega = \frac{J_1 J_2}{J_1 + J_2}\,h^2\,. \tag{33}$$

Let us introduce the notion of the radius of cross section denoted by r_x. This is defined as a longitudinal quantity measuring the asymmetry of the cross section:

$$r_x = \frac{J_1 - J_2}{J_1 + J_2}\,h\,. \tag{34}$$

In the following, the modulus of elasticity E is assumed to be constant. Hereafter, let us replace the expressions (30) and (31) into the set of differential equations (26), (27) and let us consider the property (32). In addition of the so obtained two equations and making use of the relationships (4) and (29) as well as that

$$N = N(z_0) + \int_z^{z_0} p_n d\zeta\,,$$

the following equation is yielded

$$E(J_y u'')'' - (Nu')' + y_M(N\varphi')' - eN'\varphi' +$$
$$+ M_{xN2}\varphi'' + (M_x\varphi)'' = 0\,. \tag{35}$$

If one multiplies the first of the two equations with $(h - y_M)$ and the second one with $(-y_M)$ and adds them, and considering the expressions (28), (29), (33) and (34), so the following equation is obtained:

$$E(J_\omega\varphi'')' - y_M^2(N\varphi')' + r_x e N'\varphi' - r_x M_{xN2}\varphi'' - r_x(M_x\varphi')' +$$
$$+ (y_M - s)\, q\varphi + y_M(Nu')' - eN'u' + M_{xN2}u'' + M_x u'' = 0\,. \qquad (36)$$

The set of equations (35), (36) of the lateral buckling of the I-beams with non-torsioning flanges proportionately changing hinged cross section this is already suitable for a direct comparison with the lateral buckling equations of the I-beams with a non-deformable cross section.

To equations (35), (36) a more simplified form might be given by making further assumptions.

If $e_N = e = constant$, so the equations appear in the following form

$$E(J_y u'')' - \{N[u' + (e - y_M)\,\varphi']\}' + (M_x\varphi)'' = 0\,, \qquad (37)$$

$$E(J_\omega\varphi'')' - \{[(y_M^2 - e r_x)\, N + r_x M_x]\varphi'\}' -$$
$$- (e - y_M)\,(Nu')' + M_x u'' + q(y_M - s)\,\varphi = 0\,. \qquad (38)$$

And even the cross section is assumed to be constant, so we obtain

$$EJ_y u'''' - \{N[u' + (e - y_M)\varphi']\}' + (M_x\varphi)'' = 0\,, \qquad (39)$$

$$EJ_\omega\varphi'''' - \{[(y_M^2 - e r_x)\, N + r_x M_x]\,\varphi'\}' -$$
$$- (e - y_M)\,(Nu')' + M_x u'' + q(y_M - s)\,\varphi = 0\,. \qquad (40)$$

5.2. Boundary conditions in case of a proportionately changing cross section and the variables u and φ

If one considers the set of equations (35), (36) or its shapes written for simpler cases in lieu of (26), (27), so the boundary conditions should be formulated with the use of the variables u and φ in lieu of w_1 and w_2. All the boundary conditions which were prescribed in Chapter 4 at the top and bottom flanges to the same derivatives of the variables w_1 and w_2, can now be specified also for the variables u and φ, these variables being easily expressible from the equations (30) and (31). Thus, for example, in case of a fork-like support of the beam end from the conditions

$$w_1 = 0, \quad w_1'' = 0\,, \quad w_2 = 0\,, \quad w_2'' = 0$$

the conditions

$$u = 0, \qquad\qquad \varphi = 0,$$
$$u'' = 0, \qquad\qquad \varphi'' = 0$$

follow.

However, if for the top and bottom flanges derived conditions which differ from each other are prescribed, the conditions formulated with the variables w_1 and w_2 will not have equivalents to be expressed with the variables u and φ. This may easily be recognized after expressing u and φ from (30), (31). Thus, for example, in case of a constant cross section the conditions $w_1 = 0$, $w_1' = 0$, $w_2'' = 0$, $w_2''' = 0$ of the beam end which is fixed on top and free at the bottom, this cannot be prescribed by using the variables u and φ.

It is to be noted that also to the variables u and φ such boundary conditions may be prescribed which cannot be expressed with the variables w_1 and w_2, however, such conditions are of no interest in case of trusses.

5.3. *Relationship between the equations of lateral buckling of the thin-walled I-beam with a non-deformable cross section but without torsional rigidity and those of thin-walled I-beam with non-torsioning flanges and hinged cross section*

The investigations in this field are carried out in connection with I-beams, considering that in most cases in the literature on the subject only for such beams which have constant cross sections, are equations of lateral buckling to be found.

The ordinary set of differential equations (39), (40) will be compared to the equations of three authors who carried out their deductions in more or less different ways (VLASOV [8], BÜRGERMEISTER *et al.* [2], BLEICH [1]).

1. VLASOV's *equations*

Be $e = e_S = constant$. If $J_c = 0$ having no effect on x direction occurs, so from VLASOV's set of equations ([8] page 302, (1.28)) the first equation is identical with the equilibrium equation (39) of the present study. The third equation, with the symbols of the present paper is:

$$EJ_\omega \varphi''' - \left\{ \left[\left(y_M^2 - e_S r_x + \frac{J_y}{F} \right) N + \left(\frac{1}{h} \left(\frac{J_2}{F_2} - \frac{J_1}{F_1} \right) + r_x \right) M_x \right] \varphi' \right\}' -$$
$$- (e_S - y_M)(Nu')' + M_x u'' + q(y_M - s)\,\varphi = 0\,.$$

Compared to Eq. (40), deduced by the author of the present paper, deviations may be found only in the coefficients of $(N\varphi')'$ and $(M_x\varphi')'$.

2. BÜRGERMEISTER's *equations*

Be $e = e_S = constant$ and $N = -P$ a constant compressive force, further, $J_c = 0$. In this case BÜRGERMEISTER's equation [2] (787a) agrees with Eq. (39) deduced by the author of the present paper while BÜRGER-

MEISTER's Eq. (790a), after some rearrangement with the symbols of the present study reads as follows:

$$EJ_\omega \varphi'''' + P\left[\left(y_M^2 - e_S r_x + \frac{J_y}{F}\right)\varphi'' + (e_S - y_M)u''\right] -$$

$$-\left[\frac{1}{h}\left(\frac{J_2}{F_2} - \frac{J_1}{F_1}\right) + r_x\right](M_x \varphi')' + M_x u'' + q(y_M - s)\varphi = 0.$$

This equation similarly to that of VLASOV differs from Eq. (40) deduced here only with its coefficients of $P\varphi''$ and $(M_x\varphi')'$. It is to be noted that KOLL-BRUNNER and MEISTER [6] established equations which are similar to BÜRGER-MEISTER's equation (see [6], equations (IV. 405), (IV. 406)) which in case of $P = 0$ are identical with the equations (22) of CHWALLA [3]. But CHWALLA also takes the effect of the lateral continuous elastic support into account.

3. BLEICH's *equations*

Let e be an arbitrary constant, $N = -P$ a constant compressive force and $J_c = 0$. For these constants BLEICH's [1] Eq. (308a) is the same as Eq. (39) of the present paper but BLEICH's equation (308b) with the symbols of the present paper reads as follows

$$EJ_\omega \varphi'''' + P\left\{\left[e_S(h - e_S) + \frac{J_y}{F} - (e - e_S)\left(\frac{1}{h}\left(\frac{J_2}{F_2} - \frac{J_1}{F_1}\right) + r_x\right)\right]\varphi'' + \right.$$

$$+ (e - y_M)u''\Big\} + M_x u'' + q(y_M - s)\varphi = 0.$$

It can be observed that this equation significantly differs from Eq. (40) of this paper, and in case of $e = e_S$ even from VLASOV's and BÜRGER-MEISTER's similar equations. A significant difference is in the coefficients of $P\varphi''$, further, the term is missing which contains $(M_x\varphi')'$.

Since VLASOV and CHWALLA (and following this latter, also BÜRGER-MEISTER) obtained the very same result independent of each other, therefore, their equations can be considered to be the equations of lateral buckling of the thin-walled beams and at the same time of the I-beams.

Accordingly comparing VLASOV's third equation mentioned above with Eq. (40) deduced in the present paper, it can be stated that between a thin-walled I-beam (Fig. 1a) having no torsional rigidity but non-deformable cross section, and an I-beam with non-torsioning flanges and hinged cross section (Fig. 1c) a significant difference exists if the cross sections of the flanges strongly differ from each other, i.e., if the beam is also submitted to

an axial force. If no axial force is applied to the beam, and its flanges are
the same (i.e., the cross section has two symmetry axes) so, from the view-
point of lateral buckling, there is no difference between an I-beam having
no torsional rigidity with non-deformable cross section and that with non-
torsioning flanges and hinged cross section.

It should be noted that the difference between the two models is caused
by the fact that the normal stresses σ_z, arising in the thin flanges, give
distributed torsional couple resultants if the flanges twist. In case of a
compressive force N this always diminishes the critical load, in case of a
bending moment M_x, however, this can increase or decrease the critical load,
depending on whether the couple resultants of the tension or compression
stresses prevail.

REFERENCES

1. BLEICH, F.: Buckling Strength of Metal Structures. McGraw-Hill Book Comp. New York—
    Toronto—London 1952
2. BÜRGERMEISTER, G.—STEUP, H.—KRETZSCHMAR, H.: Stabilitätstheorie. Teil I. 3. Auf-
    lage. Akademie-Verlag, Berlin 1966
3. CHWALLA, E.: Kippung von Trägern mit einfach-symmetrischen, dünnwandigen und offenen
    Querschnitten. *Sitzungsberichte der Akademie der Wissenschaften Wien* IIa, **153** (1944),
    47—60
4. CSONKA P.: Stiffness Characteristics of Rigid Warren Girders. *Acta Techn. Hung.* **20** (1958),
    103—118
5. DULÁCSKA E.—TARNAI T.: Stability of Trusses. *Magyar Építőipar* **23** (1974), 207—218.
    (In Hungarian)
6. KOLLBRUNNER, C. F.—MEISTER, M.: Knicken, Biegedrillknicken, Kippen. Springer-Verlag,
    Berlin—Göttingen—Heidelberg 1961
7. KOVÁCS O.—FABER G.: Manual of Elastic Stability. Műszaki Könyvkiadó, Budapest 1963.
    (In Hungarian)
8. ВЛАСОВ, В. З.: Тонкостенные упругие стержни. Избранные труды. Том II. Издатель-
    ство Академии Наук СССР, Москва, 1963
9. WINTER, G.: Lateral Stability of Unsymmetrical I-Beams and Trusses in Bending. *Trans-
    actions of ASCE* (1943), 247—268

Kippen von ebenen Fachwerkträgern mit Gelenkquerschnitt und Parallelflanschen
— Behandelt wird eine Näherungsanalyse von parallelgeflanschten ebenen Fachwerkträgern
aufgrund der Kontinuummethode. Der Fachwerkträger wird als ein Träger modelliert, dessen
Flanschen drillungsfest und steggelenkig den Flanschen angeschlossen ist. Die Gleichgewichts-
Differentialgleichungen werden für diesen Fachwerkträger in ausgekipptem Zustand abgeleitet.
Es wird der Zusammenhang zwischen den erhaltenen Gleichungen und den Kippungsgleichun-
gen von dünnwandigen Trägern mit formbeständigem Querschnitt behandelt.

**Устойчивость плоской формы изгиба плоскостных ферм с параллельными поя-
сами и шарнирными узловыми точками.** Работа занимается устойчивостью плоской формы
изгиба плоскостных ферм с параллельными поясами и шарнирными узловыми точками.
Ферма моделируется в карестве такой двутавровой балки с не работающим на кручение
поясом, в случае которой хребет соединяется с поясами шарнирно. Выведено диффе-
ренциальное уравнение равновесия такой балки в состоянии после кручения. Показана
связь между уравнениями устойчивости плоской формы изгиба тонкостенных соформных
балок и полученными уравнениями.

DETERMINATION OF THE EQUATION OF THE CURVE OF THE PLANE BALLOON IN RING SPINNING

B. GREGA*

CAND. OF TECH. SCI.

[Manuscript received June 12, 1976]

The author determines the equation of the balloon curve for ring spinning by neglecting the Coriolis force and air resistance. The solution of the system of differential equations of the equilibrium of forces acting on the yarn element shows that for that case the equation of the balloon plane curve cannot be set up in a closed form. The equation of the balloon plane curve is given by the Legendre-type elliptical integral of the first kind.

The exact analysis of the phenomena occurring in the balloon requires the consideration of all the acting forces. However, experiments have proved that in practical spinning the weight of the yarn element, the Coriolis force, furthermore the centrifugal force arising due to the comparatively slow motion of the yarn along the yarn curve, can be neglected. Though air resistance — because of the high rotational velocity — can be fairly high, it hardly exerts any influence on balloon tension and only effects the shape of the balloon.

We shall set up the equation of the balloon curve by neglecting the technically admissable forces.

Geometrically, the neglection of air resistance and the Coriolis force means that the yarn curve is considered as a plane curve. In that case the plane of force

$$S(x) \, \frac{ds}{\varrho}$$

of the resultant of the tensioning forces $S(x)$ and $S'(x)$ coincides with the plane of the curve (Fig. 1).

Denoting by α the angle formed by the tangent pertaining to the point $P(x, y)$ of the curve and the positive half of the axis x, the direction tangent

* B. Grega, Németvölgyi út 22, 1126 Budapest, Hungary

being $y' = \tan \alpha$, the direction cosine of the tensioning force $S(x)$ takes the form

$$\cos \alpha = \frac{1}{\sqrt{1 + y'^2}} \, ,$$

$$\sin \alpha = \frac{y'}{\sqrt{1 + y'^2}} \, .$$
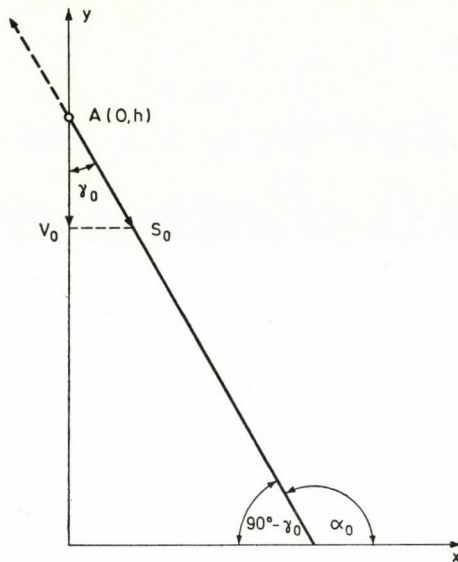
Fig. 1

The arc element ds of the yarn curve is in equilibrium, if the resultant of all the forces acting on it is always zero, i.e. $\Sigma\, X_i = 0$ és $\Sigma\, Y_i = 0$, or in detail

$$\sigma.ds.x.\omega^2 - S(x). \cos \alpha + S'(x). \cos \alpha' = 0 \, ,$$

$$-\sigma.ds.g - S(x) \sin \alpha + S'(x) \sin \alpha' = 0 \, .$$

The latter system of equations is the system of differential equations of the balloon plane curve loaded by its weight.

The quantities contained in the system of equations are as follows: ds — length of the arc element considered, ω — angular velocity of the running point of the balloon rotating around the spindle axis, g — gravitational acceleration, σ — linear density of the yarn, $S(x)$ and $S'(x)$ — tangential tensioning forces arising at the two end points of the yarn element. This ordinary system of equations also follows from the system of equations of the space curve of the yarn previously given, with the technically acceptable neglections.

For the solution of the system of differential equations we shall extend the functions $S'(x) \cos \alpha'$ and $S'(x) \sin \alpha'$ in series; and as ds is very small, we shall close the series after the terms of first order. Thus,

$$S'(x) \cos \alpha' = S(x) . \cos \alpha + \frac{d\{S(x) \cos \alpha\}}{dx} \, dx + \dots ,$$

$$S'(x) \sin \alpha' = S(x) . \sin \alpha + \frac{d\{S(x) \sin \alpha\}}{dx} \, dx + \dots .$$

Hence, the equations of the equilibrium:

$$\sigma . ds . x . \omega^2 - S(x) \cos \alpha + S(x) \cos \alpha + \frac{d\{S(x) \cos \alpha\}}{dx} \, dx = 0 ,$$

$$- \sigma . ds . g - S(x) \sin \alpha + S(x) \sin \alpha + \frac{d\{S(x) \sin \alpha\}}{dx} \, dx = 0$$

i.e.

$$\sigma . ds . x . \omega^2 + \frac{d}{dx} \{S(x) \cos \alpha\} \, dx = 0 ,$$

$$- \sigma . ds . g + \frac{d}{dx} \{S(x) \sin \alpha\} \, dx = 0 .$$

Taking into consideration the length of the yarn element, integrating after rearrangement

$$S(x) . \cos \alpha = - \sigma . \omega^2 \left(\int_0^x \sqrt{1 + y'^2} dx + c \right) ,$$

$$S(x) . \sin \alpha = \sigma . g \left(\int_0^x \sqrt{1 + y'^2} dx + c_1 \right) .$$

Multiplying the first equation by $-\sin \alpha$, and the second one by $+\cos \alpha$ and summing up

$$0 = \sigma . \omega^2 . \sin \alpha \left(\int_0^x x \sqrt{1 + y'^2} dx + c \right) + \sigma . g . \cos \alpha \left(\int_0^x \sqrt{1 + y'^2} dx + c_1 \right) ,$$

whence

$$0 = \frac{\omega^2}{g} \tan \alpha \left(\int_0^x x \sqrt{1 + y'^2} dx + c \right) + \left(\int_0^x \sqrt{1 + y'^2} dx + c_1 \right) ,$$

with

$$\tan \alpha = y'$$

$$\frac{\omega^2}{g} y' \left(\int_0^x x \sqrt{1 + y'^2} dx + c \right) + \int_0^x \sqrt{1 + y'^2} dx + c_1 = 0$$

Differentiating both sides of the equation with respect to x and arranging, we obtain

$$\int_0^x x\sqrt{1+y'^2}dx + c = -\frac{\left(y'x+\dfrac{g}{\omega^2}\right)\sqrt{1+y'^2}}{y''} \; .$$

Again differentiating with respect to the variable x

$$x\sqrt{1+y'^2} = \frac{d}{dx}\left\{-\frac{\left(y'x+\dfrac{g}{\omega^2}\right)\sqrt{1+y'^2}}{y''}\right\} \; .$$

This latter is a common third order non-linear differential equation, the differential equation of the yarn curve loaded by its weight. The solution of the equation can be determined in the form of an infinite series. Instead of this, however, it is to be considered that the weight of the yarn is very small as compared to the centrifugal force, thus, it can be ignored, and hence from the second equation of the system of differential equations (1)

$$\frac{d}{dx}\{S(x)\sin\alpha\} = 0 \; ,$$

i.e.

$$S(x)\sin\alpha = c_2 \; .$$

From the first integration

$$S(x).\cos\alpha = -\sigma.\omega^2\left\{\int_0^x x\sqrt{1+y'^2}dx + c\right\} \; .$$

Dividing the equations by each other

$$\frac{\cos\alpha}{\sin\alpha} = \cot\alpha = \frac{1}{y'} = -\frac{\sigma.\omega^2}{c_2}\left(\int_0^x x\sqrt{1+y'^2}dx + c\right) .$$

Rearranging and differentiating with respect to x on both sides

$$\frac{d}{dx}\left(-\frac{c_2}{\sigma.\omega^2}\cdot\frac{1}{y'}\right) = x\sqrt{1+y'^2}$$

i.e.

$$\frac{c_2}{\sigma.\omega^2}\cdot\frac{1}{y'^2}\cdot y'' = x\sqrt{1+y'^2}$$

whence

$$y'' = \frac{\sigma.\omega^2}{c_2}\cdot x.y'^2\sqrt{1+y'^2} \; .$$

The equation of the balloon curve obtained is a second order, deficient and non-linear one. We can arrive at its solution by the transformation $y' = p$. With that

$$\frac{dp}{dx} = \frac{\sigma.\omega^2}{c_2} xp^2 \sqrt{1 + p^2} \ .$$

This equation can be integrated after separating the variables

$$\int \frac{dp}{p^2 \sqrt{1 + p^2}} = \frac{\sigma.\omega^2}{c_2} \int x \, dx \ .$$

The left side after substitung $p = \sinh u$

$$\int \frac{\cosh u \, du}{\sinh^2 u \sqrt{1 + \sinh^2 u}} = \frac{\sigma\omega^2}{c_2} \int x \, dx$$

or

$$\int \frac{du}{\sinh^2 u} = \frac{\sigma\omega^2}{2c_2} x^2 + B \ ,$$

i.e.

$$-\coth u = \frac{\sigma\omega^2}{2c_2} x^2 + B \ .$$

By transforming the left side

$$-\frac{\cosh u}{\sinh u} = -\frac{\sqrt{1 + \sinh^2 u}}{\sinh u} = \frac{\sigma\omega^2}{2c_2} x^2 + B$$

i.e.

$$\frac{\sqrt{1 + y'^2}}{y'} = \frac{\sigma\omega^2}{2c_2} x^2 + B$$

or

$$\frac{1}{y'^2} + 1 = \left(\frac{\sigma\omega^2}{2c_2} x^2 + B \right)^2 \ .$$

Be

$$\frac{\sigma\omega^2}{2c_2} = A$$

then

$$\frac{1}{y'^2} = (Ax^2 + B)^2 - 1$$

$$y'^2 = \frac{1}{(Ax^2 + B)^2 - 1}$$

whence by integration

$$y = \int^x \frac{dx}{\sqrt{(Ax^2 + B)^2 - 1}} + K.$$

At the point $A(O, h)$ of the balloon curve

$$h = \int^0 \frac{dx}{\sqrt{(Ax^2 + B)^2 - 1}} + K.$$

From the difference of the two integrals

$$y = \int_0^x \frac{dx}{\sqrt{(Ax^2 + B)^2 - 1}} + h.$$

Since the polynom under the root is the biquadratic expression of x, the integral is elliptic. Thus, the expression of the balloon plane curve is given by this last formula, in which the elliptical integral has to be transformed into a canonical form. The determination of the modulus of the elliptical integral requires the determination of the values of the integral constants c_2 and B.

Denoting by S_0 the tensioning force pertaining to the point $A(O, h)$ of the balloon curve and by V_0 the component with direction y of S, then at the point $A(O, h)$, i.e. if $x = 0$ and $y = h$, $y'_0 = \tan \alpha_0$, where α_0 is the angle formed by the tensioning force S_0 and the positive half of the axis x (Fig. 2).

With the initial conditions, the equation

$$-\frac{\sqrt{1 + y'^2}}{y'} = \frac{\sigma \omega^2}{c_2} \frac{x^2}{2} + B$$

takes the form

$$-\frac{\sqrt{1 + \tan^2 \alpha_0}}{\tan \alpha_0} = B.$$

whence

$$B = -\frac{1}{\sin \alpha_0}.$$

Being, however, $\alpha_0 = 90° + \gamma_0$,

$$\sin \alpha_0 = \sin (90° + \gamma_0) = \cos \gamma_0,$$

$$B = -\frac{1}{\cos \gamma_0} = -\frac{S_0}{V_0}.$$

With equal initial conditions, also the value of the integration constant c_2 can be determined from the equation $S(x) \cdot \sin \alpha = c_2$. Namely, for the point $A(O, h)$

$$S_0 \sin \alpha_0 = c_2,$$

or, by substituting $\alpha_0 = 90° + \gamma_0$

$$c_2 = S_0 \sin(90° + \gamma_0) = S_0 \cos \gamma_0 = S_0 \frac{V_0}{S_0} = V_0 \,.$$

Substituting the values of the constants B and c_2 into the elliptical integral

$$y = \int_0^x \frac{dx}{\left(\frac{\sigma\omega^2}{2V_0} \cdot x^2 - \frac{S_0}{V_0}\right)^2 - 1} + h \,.$$
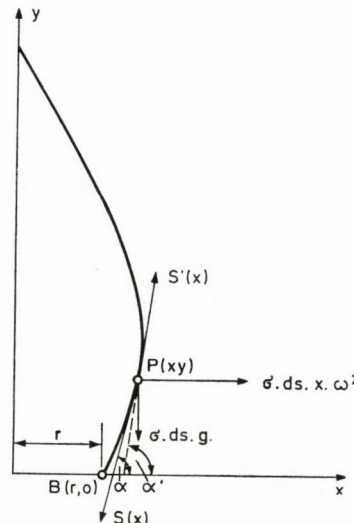
Fig. 2

Reducing the biquadratic polinom under the root to its product

$$y = \int_0^x \frac{dx}{\sqrt{\left\{\frac{\sigma\omega^2}{2V_0} \cdot x^2 + \left(1 - \frac{S_0}{V_0}\right)\right\} \left\{\frac{\sigma\omega^2}{2V_0} \cdot x^2 - \left(1 + \frac{S_0}{V_0}\right)\right\}}} + h \,.$$

By eliminating the constants

$$y = \int_0^x \frac{dx}{\sqrt{\left(1 - \frac{S_0^2}{V_0^2}\right)\left(\frac{\sigma\omega^2}{2V_0\left(1 - \frac{S_0}{V_0}\right)} x^2 + 1\right)\left(\frac{\sigma\omega^2}{2V_0\left(1 + \frac{S_0}{V_0}\right)} x^2 - 1\right)}} + h \,,$$

or

$$y = \int_0^x \frac{dx}{\sqrt{-\dfrac{S_0^2 - V_0^2}{V_0^2}\left(-\dfrac{\sigma\omega^2}{2(S_0 - V_0)}x^2 + 1\right)\left(\dfrac{\sigma\omega^2}{2(S_0 + V_0)}x^2 - 1\right)}} + h \; .$$

Eliminating the constant from that

$$y = \sqrt{\frac{V_0^2}{S_0^2 - V_0^2}}\int_0^x \frac{dx}{\sqrt{\left(1 - \dfrac{\sigma\omega^2}{2(S_0 - V_0)}x^2\right)\left(1 - \dfrac{\sigma\omega^2}{2(S_0 + V_0)}x^2\right)}} + h \; .$$

For obtaining the canonical form of the elliptical integral let us use the transformation

$$x = \sqrt{\frac{2(S_0 - V_0)}{\sigma\omega^2}}\sin\varphi \; ,$$

thus

$$dx = \sqrt{\frac{2(S_0 - V_0)}{\sigma\omega^2}}\cos\varphi d\varphi \; ,$$

$$\varphi = \arcsin\sqrt{\frac{\sigma\omega^2}{2(S_0 - V_0)}} \cdot x \; ,$$

$$y = \sqrt{\frac{V_0^2}{S_0^2 - V_0^2}} \times$$

$$\times \int_0^x \frac{\sqrt{\dfrac{2(S_0 - V_0)}{\sigma\omega^2}}\cos\varphi d\varphi}{\sqrt{(1 - \sin^2\varphi)\left(1 - \dfrac{\sigma\omega^2}{2(S_0 + V_0)} \cdot \dfrac{2(S_0 - V_0)}{\sigma\omega^2} \cdot \sin^2\varphi\right)}} + h \; .$$

Eliminating the constants under the integral and by simplification

$$\varphi = \arcsin\sqrt{\frac{\sigma\omega^2}{2(S_0 - V_0)}}x \; .$$

$$y = \sqrt{\frac{2V_0^2}{\sigma\omega^2(S_0 + V_0)}}\int_0^{\varphi} \frac{d\varphi}{\sqrt{1 - \dfrac{S_0 - V_0}{S_0 + V_0}\sin^2\varphi}} + h$$

and finally, applying the notation

$$k^2 = \frac{S_0 - V_0}{S_0 + V_0} \; ,$$

we obtain the canonical form of the elliptical integral

$$\varphi = \arcsin \sqrt{\frac{\sigma\omega^2}{2(S_0 - V_0)}}\, x\,,$$

$$y - h = \sqrt{\frac{2V_0^2}{\sigma\omega^2(S_0 + V_0)}} \int_0^{} \frac{d\varphi}{\sqrt{1 - k^2 \cdot \sin^2\varphi}}\,.$$

This integral is a Legendre-type elliptical integral of the first kind. Using the notation

$$\Delta\varphi = \Delta amu = \sqrt{1 - k^2 \sin^2 amu} = \sqrt{1 - \frac{S_0 - V_0}{S_0 + V_0} \cdot \sin^2\left(\arcsin\sqrt{\frac{\sigma\omega^2}{2(S_0 - V_0)}}\, x\right)}$$

$$\varphi = \arcsin \sqrt{\frac{\sigma\omega^2}{2(S_0 + V_0)}}$$

$$y - h = \sqrt{\frac{2V_0^2}{\sigma\omega^2(S_0 + V_0)}} \int_0^{} \frac{d\varphi}{\Delta\varphi}$$

we get obtain

$$y - h = \sqrt{\frac{2V_0^2}{\sigma\omega^2(S_0 + V_0)}} \cdot F(k, \varphi) =$$

$$= \sqrt{\frac{2V_0^2}{\sigma\omega^2(S_0 + V_0)}} \cdot F\left(\sqrt{\frac{S_0 - V_0}{S_0 + V_0}}\,,\ \arcsin\sqrt{\frac{\sigma\omega^2}{2(S_0 - V_0)}}\right).$$

The equation obtained if the Legendre-type form of the equation of the balloon plane curve. Thus, on the basis of the Table F of elliptical integrals, the balloon curve can be constructed.

REFERENCES

1. DITHELM, A.: *L'Industrie Textile*, **9** (1960) No. 883. 611—614
2. GRISHIN, P. F.: Optimum Spinning. *Platts Bulletin*, **9**, 219—236
3. VALOTY, M.: *L'Industrie Textile*, **11** (1954) 780—785
4. GREGA, B.: Thesis for candidature. Budapest 1973

Bestimmung der Gleichung der ebenen Ballonkurve beim Ringspinnen unter Berücksichtigung des Fadengewichts. — Der Verfasser stellt ein System von Differentialgleichungen der ebenen Ballonkurve auf, unter Berücksichtigung der entgegengesetzten Zugkräfte an den beiden Enden des Fadenelements, der Zentrifugalkraft und des Fadenelementgewichts. Da es keine Möglichkeit für eine Lösung in geschlossener Form gibt, wird die Gleichung der Ballonkurve durch Reihenentwicklung berechnet.

Определение уравнения плоской кривой баллона при кольцепрядении. Автор определяет уравнение баллонной кривой кольцепрядения для случая, когда не принимаются во внимание усилие Coziolis-а и сопротивление воздуха. При решении системы дифференциальных уравнений равновесия усилий, действующих на элемент нити, выясняется, что уравнение плоскостной кривой баллона также в данном случа нельзя получить в закрытой форме. Уравнение плоской кривой баллона можно дать с помощью элиптического интеграла первого рода.

ESTIMATE OF THE TORSIONAL STIFFNESS OF PRISMATIC BARS OF HETEROGENEOUS MATERIAL

I. ECSEDI*

The free torsional problem of prismatic bars of heterogeneous, isotropic, linearly elastic material is treated. On the basis of the literature on the subject, the knowledge of the torsion of prismatic bars made of heterogeneous materials is summed up with some completion, such as for example, a formula for the determination of torsional stiffness. Certain statements of DIAZ and WEINSTEIN are extended. According to the inequalities deduced by the author for the determination of the torsional stiffness of prismatic bars of heterogeneous, however isotropic material, upper and lower limiting values may be defined. By choosing suitable auxiliary functions the limits defined from the inequalities deduced for this purpose by the author, may arbitrarily be narrowed. A numerical example is also presented.

Symbols of major importance which are used in this paper

$G = G(x, y)$	shear modulus of elasticity
$v = v(x, y)$	Poisson's ratio
x, y, z	Cartesian orthogonal coordinates
O	origin of system of coordinates xy lying in the plane of the cross section
$\mathbf{i}, \mathbf{j}, \mathbf{k}$	unit vectors of the system of coordinates xyz
$\mathbf{r} = x\mathbf{i} + y\mathbf{j} + z\mathbf{k}$	position vector
$\mathbf{R} = x\mathbf{i} + y\mathbf{j}$	position vector in the plane of the cross section
T	region coherent $(p + 1)$-times in plane xy, cross section of the twisted prismatic bar
$g = g_0 + g_1 + g_2 \ldots \ldots + g_p$	border of region T
$g \ (i = 0, 1, 2, \ldots \ldots p)$	closed smooth curves at each section without conjugate point
T_i	surface area closed by curve g_i
ϑ	relative torsion
$\varphi = (x, y)$	warping function of cross section
$\nabla = \partial/\partial_x \mathbf{i} + \partial/\partial_y \mathbf{j}$	Hamilton's differential operator
" . "	symbol of scalar multiplication
" $\times$ "	symbol of vectorial multiplication
$\varepsilon_x, \varepsilon_y, \varepsilon_z$	specific elongations
$\gamma_{xy}, \gamma_{yz}, \gamma_{xz}$	specific rotations
$\sigma_x, \sigma_y, \sigma_z,$	normal stresses
$\tau_{xy}, \tau_{xz}, \tau_{xz},$	shear stresses
$\tau_z = \tau_{xz}\mathbf{i} + \tau_{yz}\mathbf{j}$	
$\mathbf{n} = n_x\mathbf{i} + n_y\mathbf{j}$	normal unit vector of limit curve g directed outwards from
T	(Fig. 2.1)
$\mathbf{t}$	tangential unit vector of limit curve; going round the limit curve in direction $\mathbf{t}$, the region defined by cross section lies at the left-hand side (Fig. 2.1)
s	arc coordinate interpreted on limit curve g

* Dr. I. ECSEDI, Vászonfehéritő u. 24. IV/1, H-3531 Miskolc, Hungary.

$\partial/\partial n$	derivative calculated in direction n
$\partial/\partial s$	derivative calculated in direction t
$\mathbf{F} = \mathbf{F}_x\mathbf{i} + \mathbf{F}_y\mathbf{j}$	shear force
M	torsional moment
I_c	torsional stiffness

Other values and variables are interpreted in the text.

1. Introduction

In this paper the upper and lower limiting values (3,6), (3,14), (3,34), (3,42) are deduced for the prismatic bar of heterogeneous, isotropic and linearly elastic material. For this purpose first of all the generalization of DIAZ' and WEINSTEIN' results may be used [2], [3].
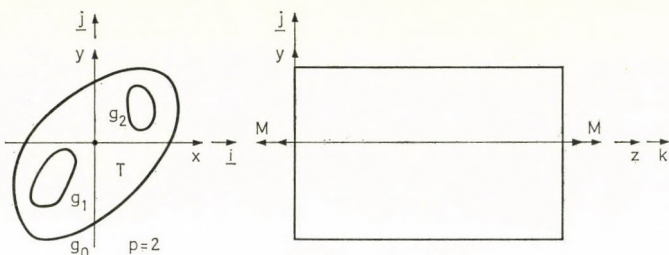
Fig. 1.1. The twisted prismatic bar

The material constants G and v are constant along the length of the axis of the bar, however, their values change in the plane of the cross section vertical to the axis of the bar. Thus, if the axis z of the system of coordinates xyz is the axis of the prismatic bar, the planes of the cross sections of the bar will be parallel to the plane xy and accordingly, the heterogeneity is characterized by the given functions

$$G = G(x, y), \qquad\qquad v = v(x, y). \qquad (1.1)$$

In connection with the prismatic bar depicted in Fig. 1.1 it is assumed that

1. the mantle of the bar is unloaded,

2. the end faces are subjected to a torsional moment M,

3. rotation of the cross section defined by the coordinate $z = 0$ is equal to zero,

4. the displacements and deformations are small.

2. Basic principles of the theory of elasticity

It is known [1] that in the case of pure torsion the displacement vector of the point P of the prismatic bar may be represented by the formula

$$\mathbf{t} = u(x, y, z)\,\mathbf{i} + v(x, y, z)\,\mathbf{j} + w(x, y, z)\,\mathbf{k}\,, \tag{2.1}$$

where

$$
\begin{aligned}
u &= u(x, y, z) = -\vartheta yz\,, \\
v &= v(x, y, z) = \vartheta xz\,, \\
w &= w(x, y, z) = \vartheta\varphi(x, y)\,.
\end{aligned}
\tag{2.2}
$$

In the above formulae $\varphi = \varphi(x, y)$ is the warping function of the cross section, ϑ is the angle of relative torsion. Considering the geometric equation and Hooke's general law, it can be understud that the consequence of Eqs (2.1) and (2.2), is the validity of the equations

$$\varepsilon_x = \varepsilon_y = \varepsilon_z = 0\,, \qquad \gamma_{xy} = 0\,, \tag{2.3}$$

$$\sigma_x = \sigma_y = \sigma_z = 0\,, \qquad \tau_{xy} = 0 \tag{2.4}$$

in an arbitrary point P of the prismatic bar. For the scalar coordinates of the stress tensor, differing from zero, by making use of the geometric equation and Hooke's general law the following equations may be deduced

$$\tau_{xz} = G\vartheta\left(\frac{\partial\varphi}{\partial x} - y\right)\,, \tag{2.5}$$

$$\tau_{yz} = G\vartheta\left(\frac{\partial\varphi}{\partial y} + x\right)\,. \tag{2.6}$$

We have

$$\boldsymbol{\tau}_z = \tau_{xz}\mathbf{i} + \tau_{yz}\mathbf{j}\,. \tag{2.7}$$

By replacement of (2.5) and (2.6) into (2.7) one obtains

$$\boldsymbol{\tau}_z = G\vartheta(\nabla\varphi - \mathbf{R}\times\mathbf{k})\,, \tag{2.8}$$

$$(\mathbf{R} = x\mathbf{i} + y\mathbf{j})\,.$$

Replacement into the non-identically satisfied equation of the mechanical equilibrium

$$\frac{\partial\tau_{xz}}{\partial x} + \frac{\partial\tau_{yz}}{\partial y} = \nabla\cdot\boldsymbol{\tau}_z = 0 \tag{2.9}$$

14

the terms (2.5), (2.6) and (2.8) yields the partial differential equations

$$\frac{\partial}{\partial x}\left[G\left(\frac{\partial \varphi}{\partial x} - y\right)\right] + \frac{\partial}{\partial y}\left[G\left(\frac{\partial \varphi}{\partial y} + x\right)\right] = 0 \tag{2.10}$$

and

$$\nabla \cdot [G(\nabla \varphi - \mathbf{R} \times \mathbf{k})] = 0 . \tag{2.11}$$

The consequence of the unloadedness of the mantle of the bar is that $\tau_{nz} = \tau_z \cdot \mathbf{n} = 0$, i.e.,

$$G\vartheta\left[\frac{\partial \varphi}{\partial n} - \frac{\partial}{\partial s}\left(\frac{x^2 + y^2}{2}\right)\right] = 0 . \tag{2.12}$$

Thus, at the boundary, the function $\varphi = \varphi(x, y)$ should satisfy the boundary condition

$$\frac{\partial \varphi}{\partial n} = \frac{\partial}{\partial s}\left(\frac{x^2 + y^2}{2}\right) . \tag{2.13}$$

This latter equation, by using a vector symbol, may also be written in the form

$$\mathbf{n} \cdot (\nabla \varphi - \mathbf{R} \times \mathbf{k}) = 0 . \tag{2.14}$$

In the following it will be verified that the system of the forces of shear stresses distributed through the plane of the cross section and derived by the equations (2.5) and (2.6) from the function satisfying the equilibrium equation (2.10) and boundary condition (2.13) is equivalent to a couple of forces. For the verification the following identities will be used

$$\frac{\partial}{\partial x}\left[xG\left(\frac{\partial \varphi}{\partial x} - y\right)\right] + \frac{\partial}{\partial y}\left[xG\left(\frac{\partial \varphi}{\partial y} + x\right)\right] = G\left(\frac{\partial \varphi}{\partial x} - y\right) , \tag{2.15}$$

$$\frac{\partial}{\partial x}\left[yG\left(\frac{\partial \varphi}{\partial x} - y\right)\right] + \frac{\partial}{\partial y}\left[yG\left(\frac{\partial \varphi}{\partial y} + x\right)\right] = G\left(\frac{\partial \varphi}{\partial y} + x\right) , \tag{2.16}$$

wherein $\varphi = \varphi(x, y)$ satisfies the differential equation (2.10). The projection of the x-direction of the resultant of shear stresses distributed through the plane of the cross section is

$$F_x = \int_T \tau_{xz} dT = \vartheta \cdot \int_T G\left(\frac{\partial \varphi}{\partial x} - y\right) dT . \tag{2.17}$$

Transformation of Eq. (2.17) with the aid of Eq. (2.15) yields:

$$F_x = \vartheta\left\{\int_T \left(\frac{\partial}{\partial x}\left[xG\left(\frac{\partial \varphi}{\partial x} - y\right)\right] + \frac{\partial}{\partial y}\left[xG\left(\frac{\partial \varphi}{\partial y} + x\right)\right]\right) dT\right\} . \tag{2.18}$$

By transforming this surface integral and making use of the Gaussian integral transformation theorem

$$\int_T \left(\frac{\partial P}{\partial x} + \frac{\partial Q}{\partial y} \right) dT = \int_g (Pn_x + Qn_y)\, ds \qquad (2.19)$$

the following equation is obtained

$$F_x = \vartheta \int_g x \left[G \frac{\partial \varphi}{\partial n} - \frac{\partial}{\partial s} \left(\frac{x^2 + y^2}{2} \right) \right] ds \;. \qquad (2.20)$$
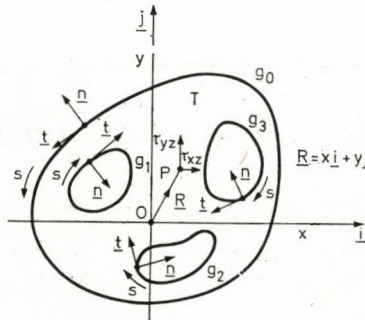
Fig. 2.1. Calculation of the torsional moment attacking the cross section

Since for the boundary curve $g = g_0 + g_1 + g_2 + \ldots \ldots + g_p$ (2.13) is valid, from Eq. (2.20) it already follows that $F_x = 0$. By making use of Eq. (2.16) it can similarly be verified that

$$F_y = \int_T \tau_{yz} dT = \vartheta \int_T G \left(\frac{\partial \varphi}{\partial y} + x \right) dT = 0 \;. \qquad (2.21)$$

The torsional moment applied to the cross section may be determined from the following equation (Fig. 2.1)

$$M = \mathbf{k} \cdot \int_T \mathbf{R} \times \tau_z dT = \mathbf{k} \cdot \int_T \mathbf{R} \times \left[G\vartheta(\nabla\varphi - \right.$$

$$\left. - \mathbf{R} \times \mathbf{k}) \right] dT = \vartheta \int_T G[R^2 - (\mathbf{R} \times \mathbf{k}) \cdot \nabla\varphi]\, dT \;, \qquad (2.22)$$

$$(R^2 = x^2 + y^2) \;.$$

With the aid of the following identities the expression of the torsional moment can be transformed:

$$\int_T \nabla \cdot [G(\mathbf{R} \times \mathbf{k})\, \varphi]\, dT = \int_g G(\mathbf{R} \times \mathbf{k}) \cdot \mathbf{n}\varphi ds \;, \qquad (2.23)$$

and at the boundary curve g:

$$\mathbf{n} \cdot G(\mathbf{R} \times \mathbf{k})\, \varphi = G\mathbf{R} \cdot \mathbf{t}\varphi = G\varphi \frac{\partial}{\partial s}\left(\frac{x^2 + y^2}{2}\right) = G\varphi \frac{\partial \varphi}{\partial n} = G(\varphi \nabla \varphi) \cdot \mathbf{n} \,. \quad (2.24)$$

By applying the Gaussian integral transformation theorem we obtain

$$\int_g G \frac{\partial \varphi}{\partial n}\, \varphi ds = \int_g G(\varphi \nabla \varphi) \cdot \mathbf{n} ds = \int_T \nabla \cdot (G \nabla \varphi)\, dT = \int_T G(\nabla \varphi)^2\, dT +$$

$$+ \int_T \varphi \nabla \cdot (G\nabla \varphi)\, dT \,. \quad (2.25)$$

The left-hand side of Eq. (2.23) is, in a detailed form

$$\int_T \nabla \cdot [G(\mathbf{R} \times \mathbf{k})\, \varphi]\, dT = \int_T \varphi \nabla \cdot [G(\mathbf{R} \times \mathbf{k})]\, dT + \int_T G(\mathbf{R} \times \mathbf{k}) \cdot \nabla \varphi dT \,. \quad (2.26)$$

Use of the form

$$\nabla \cdot \big[G(R \times k)\big] = \nabla \cdot (G\nabla \varphi) \qquad \cdot \quad (2.27)$$

of the equilibrium equation and combination of Eqs (2.23), (2.25) and (2.26) gives

$$\int_T G(\mathbf{R} \times \mathbf{k}) \cdot \nabla \varphi dT = \int_T G(\nabla \varphi)^2\, dT \,. \quad (2.28)$$

Replacement of (2.28) into Eq. (2.22) results in

$$M = \vartheta \int_T G(R^2 - (\nabla \varphi)^2\, dT \,. \quad (2.29)$$

Thus, on the basis of Eq.

$$I_c = \frac{M}{\vartheta} \quad (2.30)$$

the torsional stiffness to be coordinated to the cross section may be given in the following forms

$$I_c = \int_T G[R^2 - (\mathbf{R} \times \mathbf{k}) \cdot \nabla \varphi]\, dT \,, \quad (2.31)$$

$$I_c = \int_T G[R^2 - (\nabla \varphi)^2]\, dT \,. \quad (2.32)$$

3. Some inequalities in connection with the torsional stiffness

Let $v_i = v_i(x, y)$ $(i = 1, 2)$ be in the region T and at the boundary of the region T a continuous, and in T (except for the points of the finite smooth curves running in region T) a continuously derivable function of two variables. Be further

$$D(v_1, v_2) = \int_T G\nabla v_1 \cdot \nabla v_2 dT , \qquad (3.1)$$

$$D(v_1) = D(v_1, v_1) = \int_T G(\nabla v_1)^2 \, dT . \qquad (3.2)$$

Since $G > 0$, from the above interpretation it follows that

$$D(v_1) \geq 0 , \qquad (3.3)$$

$$\big(D(v_1, v_2)\big)^2 \leq D(v_1) \, D(v_2) . \qquad (3.4)$$

The second of the above inequalities is the Schwarz inequality. Starting from Eq. (2.32) it may be written

$$I_c = J - D(\varphi) \qquad (3.5)$$

wherein

$$J = \int_T G(x^2 + y^2) \, dT . \qquad (3.6)$$

By making use of the inequality $D(\varphi) \geq 0$ one obtains from Eq. (3.5) the generalization of the result found by DIAZ and WEINSTEIN [2]

$$I_c \leq J . \qquad (3.7)$$

A more precise estimate may be made by applying Schwartz's inequality (3.4). Be

$$v_1 = \varphi , \qquad\qquad v_2 = v \qquad (3.8)$$

(is not constant within the range T). With the functions (3.8) of v_1 and v_2 it may be written:

$$D(\varphi, v) = \int_T G\nabla\varphi \cdot \nabla v dT = \int_T \nabla \cdot (G\nabla\varphi v) \, dT - \int_T v[\nabla \cdot (G\nabla\varphi)] \, dT . \qquad (3.9)$$

By using the Gaussian integral transformation theorem and the equation

$$\nabla \cdot [G(\mathbf{R} \times \mathbf{k})] = \nabla \cdot [G(\nabla\varphi)] \qquad (3.10)$$

which follows from the equilibrium equation, Eq. (3.9) may be written in the form

$$D(\varphi, v) = \int_T G(R \times k) \cdot \nabla v dT . \qquad (3.11)$$

With the comparison of the inequality (3.4) and Eq. (3.11) we have

$$D(\varphi) \geq \frac{\left(\int_T G(\mathbf{R} \times \mathbf{k}) \cdot \nabla v dT \right)^2}{\int_T G(\nabla v)^2 \, dT} \, . \tag{3.12}$$

Equality in (3.12) occurs in the case, and only in the case where

$$v = a\varphi + b \, , \tag{3.13}$$

wherein a, b ($a \neq 0$) are arbitrary real constants. The inequality (3.12) may be considered to be the generalization of [2]. By combining (3.12) and (3.5) for the upper limit of the torsional stiffness

$$I_C \leq J - \frac{\int_T G(\mathbf{R} \times \mathbf{k}) \cdot \nabla v dT \Big)^2}{\int_T G(\nabla v)^2 \, dT} \tag{3.14}$$

may be given.

A possible lower limit may be deduced for the torsional stiffness if one estimates $D(\varphi)$ from above. To establish this estimate one should start out from Schwarz's inequality

$$\left(\int_T G\mathbf{u} \cdot \mathbf{v} dT \right)^2 \leq \left(\int_T G\mathbf{u}^2 dT \right) \left(\int_T G\mathbf{v}^2 dT \right) , \tag{3.15}$$

where

$$\mathbf{u} = u_x \mathbf{i} + u_y \mathbf{j} \, , \qquad \mathbf{v} = v_x \mathbf{i} + v_y \mathbf{j} \tag{3.16}$$

are functions of two variables interpreted in the region and at the border of the region wherein the integrals entering in the inequality (3.15) exist and are finite. Be

$$\mathbf{u} = \nabla \varphi \qquad P \in T + g \, , \tag{3.17}$$

$$\nabla \cdot \left[G(\mathbf{v} - \mathbf{R} \times \mathbf{k}) \right] = 0 \qquad P \in T \, , \tag{3.18}$$

$$\mathbf{n} \cdot \mathbf{v} = \frac{\partial \varphi}{\partial n} \qquad P \in g \, . \tag{3.19}$$

With the vector functions u and v of properties (3.17), (3.18), (3.19) it may be written

$$\int_T G\nabla \varphi \cdot \mathbf{v} dT = \int_T \nabla \cdot (G\varphi \mathbf{v}) \, dT - \int_T \varphi \nabla \cdot [G\mathbf{v}] \, dT =$$

$$= \int_g \mathbf{n} \cdot (G\varphi \mathbf{v}) \, ds - \int_T \varphi \nabla \cdot \left[G(\mathbf{R} \times \mathbf{k}) \right] dT = \int_g G(\varphi \nabla \varphi) \cdot \mathbf{n} ds -$$

$$- \int_T \varphi \nabla G \cdot \left[(\mathbf{R} \times \mathbf{k}) \right] dT = \int_T \left[G(\varphi \nabla \varphi) \right] \cdot \nabla dT -$$

$$- \int_T \varphi \nabla \cdot (G\nabla \varphi) \, dT = \int_T G(\nabla \varphi)^2 \, dT \, . \tag{3.20}$$

In the deduction the Gaussian integral transformation theorem and Eqs (2.11), (2.14) being related to the function φ were applied. Use of Eq. (3.20) and inequality (3.15) — leaving the case $D(\varphi) = 0$ out of consideration — yields the estimate

$$D(\varphi) \leq \int_T G\mathbf{v}^2 dT \,. \tag{3.21}$$

Equality only occurs in (3.21) if

$$\mathbf{v} = \nabla\varphi \,. \tag{3.22}$$

Let us choice for the vector $\mathbf{v} = \mathbf{v}\,(x, y) = v_x \mathbf{i} + v_y \mathbf{j}$ the following

$$\mathbf{v} = \mathbf{v}(x, y) = \frac{1}{G}\nabla A + \mathbf{R}\times\mathbf{k} \,. \tag{3.23}$$

The vector $\mathbf{v} = \mathbf{v}\,(x, y)$, in case of a scalar function $A = A\,(x, y)$ arbitrarily derivable, satisfies the Eq. (3.18). Replacement of the above function $\mathbf{v} = \mathbf{v}(x,y)$ into Eq. (3.19) results in the condition

$$\frac{\partial\varphi}{\partial n} = \frac{1}{G}\frac{\partial A}{\partial s} + \frac{\partial}{\partial s}\left(\frac{x^2 + y^2}{2}\right) \tag{3.24}$$

at the boundary curve.
Considering

$$\frac{\partial\varphi}{\partial n} = \frac{\partial}{\partial s}\left(\frac{x^2 + y^2}{2}\right) \quad P \in g \tag{3.25}$$

one may write

$$\frac{\partial A}{\partial s} = 0 \quad P \in g \tag{3.26}$$

i.e., $A = A(x, y)$ is constant at the boundary curve, thus

$$A = B_i = \text{const}\,. \qquad P \in g_i \,, \tag{3.27}$$
$$(i = 0, 1, 2, \ldots p)\,.$$

Therefore, from the inequality (3.21), with the aid of the function v of (3.23) the upper limit

$$D(\varphi) \leq \int_T \frac{(\nabla A)^2}{G}\,dT + \int_T GR^2 dT + 2\int_T \mathbf{R}\cdot\nabla A\,dT \tag{3.28}$$

may be deduced for $D(\varphi)$. The inequality (3.28) may be reduced again, because

$$\int_T \mathbf{R} \cdot \nabla A dT = \int_T \nabla \cdot (\mathbf{R}A)\, dT - \int_T A(\nabla \cdot \mathbf{R})\, dT =$$

$$= \int (\mathbf{n} \cdot \mathbf{R})\, A ds - 2 \int_T A dT = 2B_0 T_0 -$$

$$- 2 \sum_{k=1}^{p} B_k T_k - 2 \int_T A dT \,. \tag{3.29}$$

We have

$$\int_g \mathbf{n} \cdot \mathbf{R} A ds = B_0 \int_{g_0} \mathbf{n} \cdot \mathbf{R} ds + \sum_{k=1}^{p} B_k \int_{g_k} \mathbf{R} \cdot \mathbf{n} ds \tag{3.30}$$
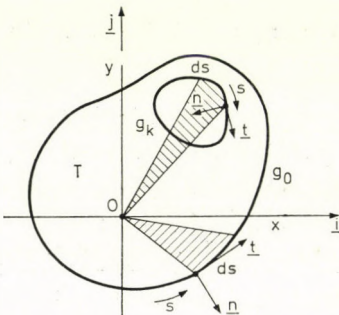
Fig. 3.1. Geometrical meaning of $\int_g \mathbf{R} \cdot \mathbf{n}\, ds$ and $\int_{g_k} \mathbf{R} \cdot \mathbf{n}\, ds$

because the integrals extended to the curves g_0 and g_k $(k = 1, 2, \ldots \ldots, p)$ (Fig. 3.1) are values proportional to the surface areas bordered by the curves g_0 and g_k. Considering the concept of the integration the following might be written:

$$\int_{g_0} \mathbf{R} \cdot \mathbf{n} ds = \mathbf{k} \int_{g_0} (\mathbf{R} \times \mathbf{t})\, ds = 2T_0 \,, \tag{3.31}$$

$$\int_{g_k} \mathbf{R} \cdot \mathbf{n} ds = \mathbf{k} \int_{g_k} (\mathbf{R} \times \mathbf{t})\, ds = -2T_k \,, \tag{3.32}$$

$$(k = 1, 2, \ldots p) \,.$$

Finally, by replacing Eq. (3.29) into inequality (3.28) we arrive at the result

$$D(\varphi) \leq \int_T \frac{(\nabla A)^2}{G}\, dT + \int_T GR^2 dT + 4B_0 T_0 - 4 \int_T A dT - 4 \sum_{k=1}^{p} B_k T_k \,. \tag{3.33}$$

Considering the inequality (3.33), from Eq. (3.5) the lower limit follows

$$I_c \geq - \int_T \frac{(\nabla A)^2}{G}\, dT - 4B_0 T_0 + 4 \int_T A dT + 4 \sum_{k=1}^{p} B_k T_k \tag{3.34}$$

for the torsional stiffness. Be

$$p(A) = -\int_T \frac{(\nabla A)^2}{G}\,dT - 4B_0 T_0 + 4\int_T A\,dT + 4\sum_{k=1}^{p} B_k T_k\,. \qquad (3.35)$$

In the following the refinement of the estimate

$$I_c \geq p(A) \qquad (3.36)$$

will be discussed. In case of a fixed function $A = A\,(x, y) \neq 0$ we establich the quantity

$$q(\alpha) = p(\alpha A) \qquad (3.37)$$

by using an arbitrary constant. It is obvious that

$$I_c \geq q(\alpha) = p(\alpha A)\,. \qquad (3.38)$$

From (3.38) the best estimate for I_c — in case of the fixed function $A = A(x, y)$ — will be furnished by the maximum value of $q(\alpha)$. From the equation

$$q(\alpha) = p(\alpha A) = -\alpha^2 \int_T \frac{(\nabla A)^2}{G}\,dT + \alpha\left(-4B_0 T_0 + 4\int_T A\,dT + 4\sum_{k=1}^{p} B_k T_k\right)$$

$$(3.39)$$

it is to be seen that $q(\alpha)$ is a second order integer rational function of the variable α, and since the coefficient of α^2 is negative, and $q(\alpha) = 0$, if $\alpha = 0$, the function $q(\alpha)$ has at

$$\alpha^* = \frac{2\left(\int_T A\,dT + \sum_{k=1}^{p} B_k T_k - B_0 T_0\right)}{\int_T \frac{(\nabla A)^2}{G}\,dT} \qquad (3.40)$$

a maximum, and the value of this maximum is

$$q(\alpha^*) = \max_{\alpha} q(\alpha) = \max_{\alpha} p(\alpha A) =$$

$$= \frac{4\left(\int_T A\,dT + \sum_{k=1}^{p} B_k T_k - B_0 T_0\right)^2}{\int_T \frac{(\nabla A)^2}{G}\,dT}\,. \qquad (3.41)$$

It is to be noted that the lower limit for the torsional stiffness

$$I_c \geq \frac{4\left(\int_T A\,dT + \sum_{k=}^{p} B_k T_k - B_0 T_0\right)^2}{\int_T \frac{(\nabla A)^2}{G}\,dT} \tag{3.42}$$

is, in the literature on the subject, established in connection with the prismatic bar of homogeneous material by the introduction and use of Prandtl's stress function [3].

4. An example for the estimation of the torsional stiffness

Let us consider the solid square cross section depicted in Fig. 4.1. The modulus of elasticity for the material of the bar is

$$G = \begin{cases} y + 1 & \text{if} \quad y \geq 0\,, \\ -y + 1 & \text{if} \quad y \leq 0 \end{cases} \tag{4.1}$$

With the help of the formula $I_c \leq I$, for the torsional stiffness the upper limit

$$I_c \leq 4{,}3333 \tag{4.2}$$

may be given. From the inequality (3.14) the use of the function

$$v = xy \tag{4.3}$$

permits the deduction of the upper limit

$$I_c < 4{,}3016\,. \tag{4.4}$$

And if we calculate with the function in (3.14)

$$v = x^3 y - y^3 x\,, \tag{4.5}$$

so the upper limit

$$I_c < 3{,}806 \tag{4.6}$$

is obtained. From the inequality (3.42) by selecting $B_0 = 0$, and by calculating with the function $A = A\,(x, y)$ depicted in Fig. 4.2 by a pyramid of K height, the lower limit

$$I_c > 2{,}563 \tag{4.7}$$
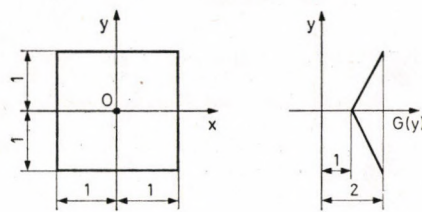
Fig. 4.1. Solid square cross section
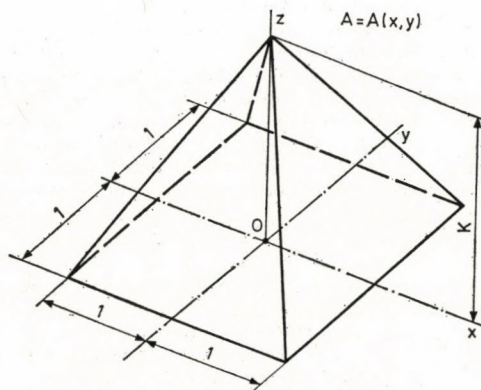
Fig. 4.2. The "pyramid of height K" function

can be established. And, if one uses the assumption

$$A = A(x, y) = (x^2 - 1)(y^2 - 1) \qquad (4.8)$$

so, from the inequality (3.42) the lower limit

$$I_c > 3,1604 \qquad (4.9)$$

can be deduced. The exact value of I_c is not known, however, the arithmetic mean I_c^* of (4.9) and (4.6),

$$I_c^* = 3,483 \qquad (4.10)$$

may diverge at most by 10 per cent from the exact value of I_c.

REFERENCES

[1] ЛЕХНИЦКИЙ С. Г.: Кручение анизотропных и неоднородных стержней, Изд. Наука Москва 1971. 83—126
[2] DÍAZ, J. B.—WEINSTEIN, A.: The Torsional Rigidity and Variational Methods, *American Journal of Math.* **70** (1948), 107—116
[3] WEINSTEIN, A.: New Method for the Estimation of Torsional Rigidity. *Proceedings of Symposium in Applied Mathematics.* **3** (1950), 141—161

Abschätzung der Verdrehungssteifheit der aus heterogenem Material hergestellten prismatischen Stäbe. — Das Problem der freien Verdrehung der aus heterogenem, isotropem, linear-elastischem Material hergestellten prismatischen Stäbe wird behandelt. Aufgrund der einschlägigen Literatur werden die mit der Verdrehung von prismatischen, aus heterogenem Material gefertigten Stäben zusammenhängende Kenntnisse zusammengefaßt, jedoch mit gewissen Ergänzungen, wie z. B. eine Formel zur Ermittelung der Verdrehungssteifigkeit. Die Gültigkeit einiger Ergebnisse von J. B. DÍAZ und A. WEINSTEIN wird auf neuen Bereich erstreckt. Aufgrund der Ungleichungen, die von dem Autor zur Ermittelung der Verdrehungssteifheit der aus heterogenem, jedoch isotropem Material hergestellten Stäbe abgeleitet wurden, können obere und untere Grenzen definiert werden. Durch die Auswahl von geeigneten Hilfsfunktionen können die vom Autor für diesen Zweck aus den Ungleichungen ermittelten Grenzen nach Belieben eingeengt werden. Schließlich wird ein numerisches Beispiel vorgeführt.

Об оценке жесткости кручени призматических стержней из гетерогенных материалов. Данная работа посвящена задаче свободного кручения гетерогенных призматических стержней из изотропных и линеарно упругих материалов. Во второй главе работы на основе литературных данных [1] дается обобщение сведений по кручению призматических стержней из гетерогенных материалов. И данная глава содержит определенное дополнение по отношению к литературным сведениям, например, формулу (2,31) жесткости кручения. В третей главе дается распространение некоторых результатов Й. Б. Диаза и А. Вейнштейна [2], [3]. На основе главы 3 данной работы в отношении жесткости кручения призматического гетерогенного стержня из изотропного материала на основе неравенств (3,6), (3,14) можно образовать верхние границы, а на основе неравенств (3,34) и (3,42) — нижние. При подходящем выборе соответствующих вспомогательных функций — A = A(x, y), § = §(x, y) — границы, образованные на основе неравенств (3,7) и (3,34), (3,42), можно сузить в любых масштабах.

INDEX

O. Haszpra:

MODELLING HYDROELASTIC VIBRATIONS

Dangerous vibrations may occur when hydraulic structures (movable weirs, locks) are partially opened due to the hydrodynamic effect of water flowing through or around them. This effect can be avoided by means of suitable design. A major problem, however, is that in many cases these vibration phenomena cannot be determined by calculations. To overcome these difficulties model experiments are needed. After summarizing the results obtained in the field of modelling aero- and hydroelastic vibrations of aircrafts, bridges, buildings, and ships, the author discusses the hydroelastic similarity, giving emphatic consideration to the viewpoints emerging in hydraulic structures. A number of the practical applications are presented, the instrumental and model technological questions of major importance are surveyed, and the future tasks related to hydroelastic modelling research are outlined. A special merit of the book is that the theoretical results are presented in such form that makes it possible for the modelling engineer to use them directly in practice.

Printed in Hungary

Acta Techn. Hung. **85** (1978), pp. 11—28

ALPAN, I.—BAKER, R.: *The Speed Effect in Pavement Deflection*

The influence of vehicle speed on pavement deflection is a problem of obvious importance related to the evaluation of pavement performance. The fact that the deflections diminish with increasing speed implies a dissipative component in the system. A simple visco-elastic model is analysed which furnishes results in good agreement with empirical evidence and may be used in assessing the distortion pattern of pavements under idealized service conditions. Furthermore, relatively simple experimental procedures may be used to determine the required material parameters.

Acta Techn. Hung. **85** (1978) pp. 29—52

PETHŐ, SZ.—PATVAROS, J.: *Mathematical Statistical Analysis of the Exploitability Functions*

The exploitability functions can be derived from the distribution function of one of the components of the mineral occurrence (e.g. its metal content). With the aid of the distribution function the mean component of the two truncated functions and its variance can be determined for any mass proportion. One truncated function refers to the exploited part, the other one to the part left back. Exploitability functions are called the distribution function and the continuous variations, as functions of the constituent of the mean component of the two truncated functions and their variances as well as the losses of the valuable constituent.

Acta Techn. Hung. **85** (1978) pp. 53—70

GOSCHY, B.: *Combined Strength Pattern of Thin-Walled Box-Griders in Torsion*

In this paper the theory of torsion of thin-walled box girders is extended to the general case of combined torsion by taking also into account the effects of the shear deformations. The purpose of the paper is to formulate mathematically the mechanical phenomenon of combined torsion for the engineering practice as well as to demonstrate the application of the formulae presented in the framework of a numerical example. In addition, besides the more familiar procedures WANNSLEBEN, URBAN, etc. also the significance of the secondary shear deformation is emphasized in the paper.
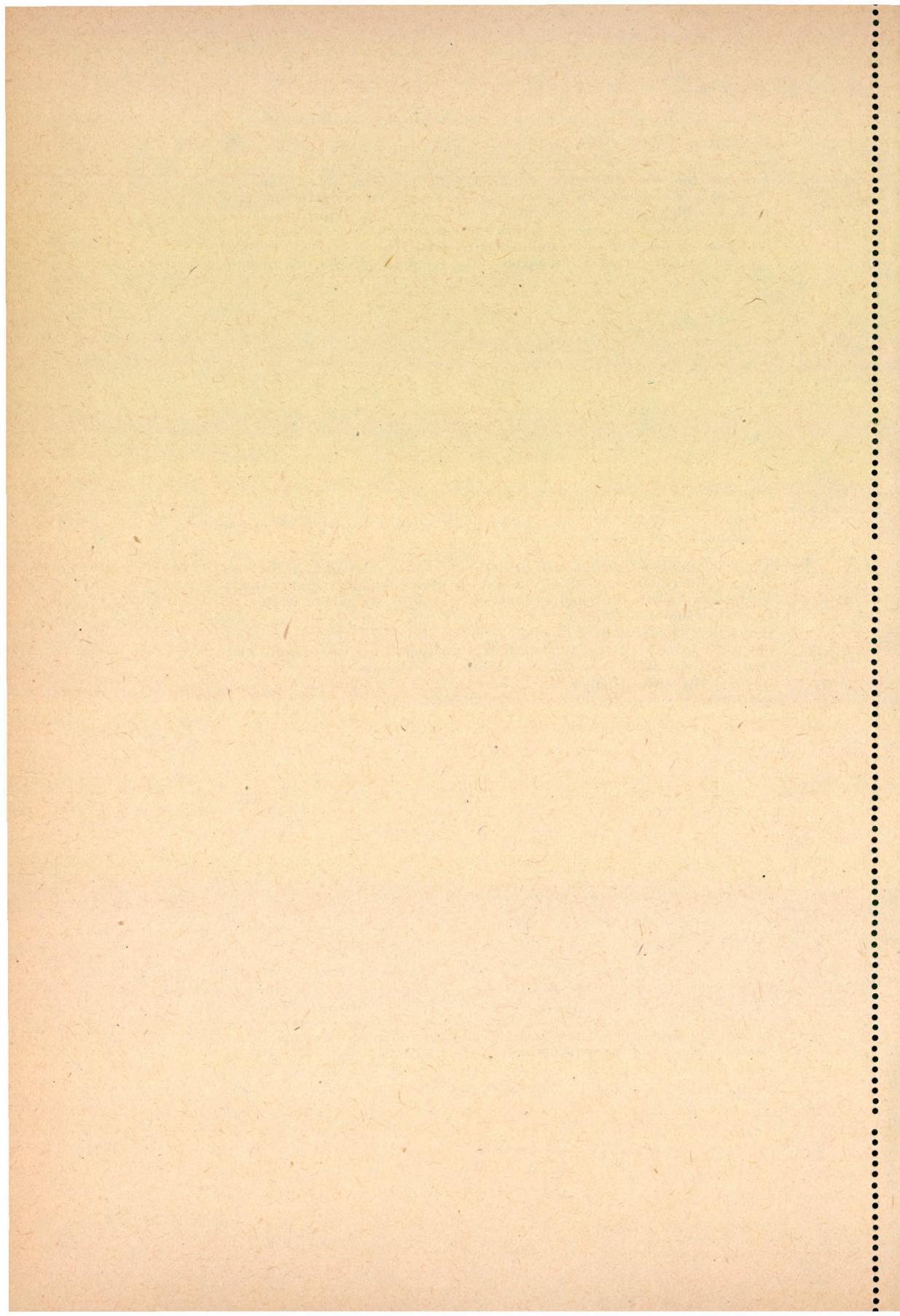
Acta Techn. Hung. **85** (1978) pp. 71—80

BOLLA, I.—CSÁNYI, I.: *Examination of the Build up Characteristics of Highpressure Wall-Stabilized Discharges*

The physical and chemical phenomena during the build-up period of high-pressure gas discharge systems with $Hg : TII : DyI_3$ additives were investigated by simultaneously measuring the terminal voltage and the spectral characteristics of the discharge. The influence of each additive on the electrical characteristics during the evaporation processes, which are parallel to the build-up of the discharge tube wall temperature, was determined. The results were evaluated from the point of view of the energy dissipation phenomena — ionization/recombination, photoemission/absorption, dissociation — in the discharge.

Acta Techn. Hung. **85** (1978) pp. 81—92

GREGA, B.: *Determination of the Pirn Shape*

On the basis of mathematical considerations the author gives a solution for the determination of the pirn shape by the use of which weft breakages due to variations in yarn force can be considerably reduced. It is shown that the meridian section of the initial surface of such a pirn has always the form of a hyperbola.

Acta Techn. Hung. **85** (1978) pp. 93—122

HERPAI, B.—PÁCZELT, I.: *Analysis of Axisymmetrically Deformed Shells by the Finite Element Displacement Method*

The elements adopted follow the actual geometry of the shell. The minimum degree of freedom of the elements is 12. In concluding the calculation an opportunity offers for supervising at each element the degree of non-satisfaction of the equilibrium equations "a priori" non-satisfied. If the degree of non-satisfaction at each element is below a predetermined value, so the calculation can be considered to be accomplished. If not, by maintaining the subdivision and increasing the degree of freedom of the elements in question, with repeated calculations more exact results may be obtained. The efficiency of the procedure is well demonstrated by a number of numeric examples.
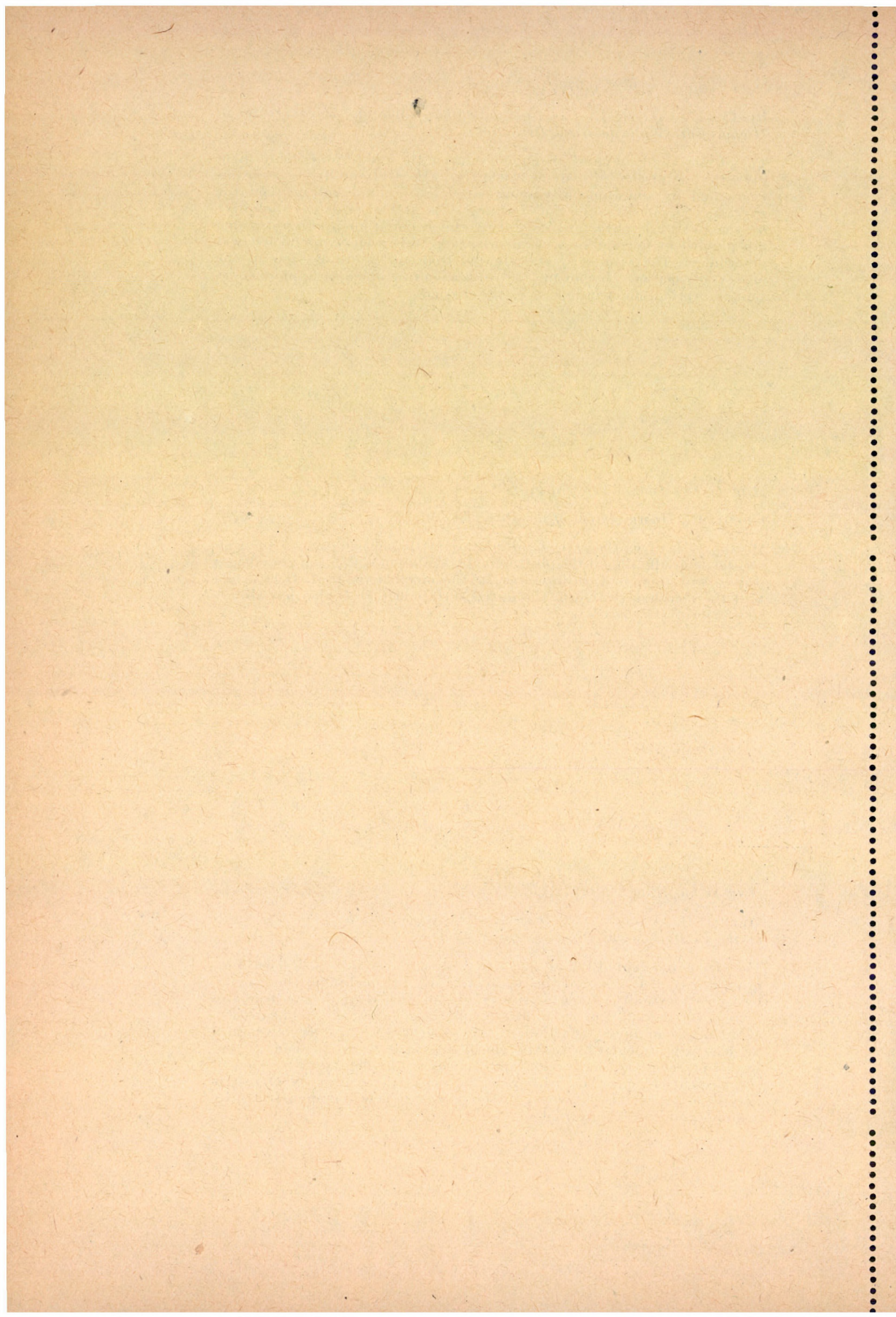
Acta Techn. Hung. **85** (1978) pp. 123—134

GRÓSZ, M.: *Automated Designing with Integer Programming*

In this paper the author presents a possible model for the general solution of automated designing. The design problems is defined as follows: a design of a structure with given geometry and composed from a given stock of elements is looked for, where for the elements the equilibrium compatibility and limiting conditions are fullfiled and where the structure is optimum from some point of view (weight, cost, or their ratio). For the problem thus defined the mathematical model for linear limiting conditions is established and then it is extended to the case of non-linearity. In both cases the problems are reduced to that of a "0—1" integer programming task to which the enumeratio method can be applied. For this method the inversion of a large matrix would be necessary. A solution method is shown for avoiding this.

Acta Techn. Hung. **85** (1978) pp. 135—145

MIHAILESCU, M.—MISS. HORVÁTH, I.: *Velaroidal Shells for Covering Universal Industrial Halls*

In order to cover large column-free square areas a new type of shell structure is proposed. Considering its shape and its way of generation, the surface belongs to the family of velaroidal ones. Choosing the generatrix as an ellipse, advantageous geometrical and mechanical properties are obtained. Membrane stress analysis and a numerical example are presented.

Acta Techn. Hung. **85** (1978) pp. 147—177

ECSEDI, I.: *Variation Method Giving the Solution to the Torsion Problem of Prismatic Bars of Composite Material*

The author deals with the problem of free torsion of prismatic bars having a solid cross section, built up of composite materials. In Chapter 2 of the paper, methods of the variation calculus are presented which may be used for the solution to quasistatic boundary-value problems of linearly elastic continua of composite materials. This chapter sums up and generalizes the conditions of stationariness and minimum principles of the theory of elasticity connected with the *potential energy* and *complementary work*. The third chapter reports on the basis of the literature on the subject, on what should be known in connection with the elastic free torsion of bars with an inhomogeneous cross section, the so-called prismatic bars made up of composite materials. Chapters 4 to 7 report on some new achievements concerning the free torsion of composite prismatic bars which may be obtained by the application of the theorems described in different chapters of the paper. It is emphasized that according to a given formula the torsional stiffness may be estimated from below and according to another from above. Chapter 6 treats the torsional problem of prismatic bars reinforced with a thin layer. Chapter 7 comprises three examples.

TARNAI, T.: *Lateral Buckling of Plane Trusses with Parallel Chords and Hinged Joints*

An approximate investigation of the lateral buckling of plane trusses with parallel chords is dealt with on the basis of the continuum method. The truss is modelled by I-beam with non-torsioning flanges, the web of which is connected to the flanges with the aid of hinges. The differential equations of such a beam are deducted for the lateral-buckled state. The relationships between the equations obtained and the lateral-buckling equations of thin-walled beams having non-deformable cross section are presented.

GREGA, B.: *Determination of the Equation of the Curve of the Plane Balloon in Ring Spinning*

The author determines the equation of the balloon curve for ring spinning by neglecting the Coriolis force and air resistance. The solution of the system of differential equations of the equilibrium of forces acting on the yarn element shows that for that case the equation of the balloon plane curve cannot be set up in a closed form. The equation of the balloon plane curve is given by the Legendre-type elliptical integral of the first kind.

ECSEDI, I.: *Estimate of the Torsional Stiffness of Prismatic Bars of Heterogeneous Material*

The free torsional problem of prismatic bars of heterogeneous, isotropic, linearly elastic material is treated. On the basis of the literature on the subject, the knowledge of the torsion of prismatic bars made of heterogeneous materials is summed up with some completion, such as for example, a formula for the determination of torsional stiffness. Certain statements of J. B. DIAZ and A. WEINSTEIN are extended. According to the inequalities deduced by the author for the determination of the torsional stiffness of prosmatic bars of heterogeneous, however isotropic material, upper and lower limiting values may be defined. By choosing suitable auxiliary functions the limits defined from the inequalities deduced for this purpose by the author, may arbitrarily be narrowed. A numerical example is also presented.

The *Acta Technica* publish papers on technical subjects in English, French, German and Russian.

The *Acta Technica* appear in parts of varying size, making up one volume.

Manuscripts should be addressed to

Acta Technica
1051 Budapest
Münnich Ferenc u. 7
Hungary

Correspondence with the editors and publishers should be sent to the same address, Subscription rate: $ 36.00 a volume.

Orders may be placed with "Kultura" Foreign Trading Company (1389 Budapest 62, P. O. B. 149. Account No. 218-10990) or its representatives abroad.

Les *Acta Technica* paraisent en français, allemand, anglais et russe et publient des travaux du domaine des sciences techniques.

Les *Acta Technica* sont publiés sous forme de fascicules qui seront réunis en volumes. On est prié d'envoyerales manuscrits destinés à la rédaction à l'adresse suivante:

Acta Technica
1051 Budapest
Münnich Ferenc u. 7.
Hongrie

Toute correspondance doit être envoyée à cette même adresse.

Le prix de l'abonnement: $ 36.00 par volume.

On peut s'abonner à l'Entreprise du Commerce Extérieur «Kultura» (1389) Budapest 62, P. O. B. 149. Compte courant No. 218-10990) ou chez représentants à l'étranger.

«*Acta Technica*» публикуют трактаты из области технических наук на русском, немецном, английском и французском языках.

«*Acta Technica*» выходят отдельными выпусками разного объема. Несколько выпусков составляют один том.

Предназначенные для публикации рускописи следует направлять по адресу:

Acta Technica
1051 Budapest,
Münnich Ferenc u. 7.
Венгрия

По этому же адресу направлять всякую корреспонденцию для редакции и администрации.

Подписная цена — $ 36.00 за том. Заказы принимает предприятие по внешней торговле «Kultura» (1389 Budapest 62, P. O. B. 149 Текущий счет № 218-10990) или его заграничные представительства и уполномоченные.

Reviews of the Hungarian Academy of Sciences are obtainable at the following addresses:

AUSTRALIA
C.B.D. LIBRARY AND SUBSCRIPTION SERVICE,
Box 4886, G.P.O., *Sydney N.S.W. 2001*
COSMOS BOOKSHOP, 135 Ackland Street, *St. Kilda (Melbourne), Victoria 3182*

AUSTRIA
GLOBUS, Höchstädtplatz 4, *1200 Wien* XX

BELGIUM
OFFICE INTERNATIONAL DE LIBRAIRIE,
30 Avenue Marnix, *1050 Bruxelles*
LIBRAIRIE DU MONDE ENTIER, 162 Rue du Midi, *1000 Bruxelles*

BULGARIA
HEMUS, Bulvar Ruszki 6, *Sofia*

CANADA
PANNONIA BOOKS, P.O. Box 1017, Postal Station "B", *Toronto, Ontario M5T 2T8*

CHINA
CNPICOR, Periodical Department, P.O. Box 50, *Peking*

CZECHOSLOVAKIA
MAD'ARSKÁ KULTURA, Národní třida 22, *115 66 Praha*
PNS DOVOZ TISKU, Vinohradská 46, *Praha 2*
PNS DOVOZ TLAČE, *Bratislava 2*

DENMARK
EJNAR MUNKSGAARD, Norregade 6, *1165 Copenhagen*

FINLAND
AKATEEMINEN KIRJAKAUPPA, P.O. Box 128, *SF-00101 Helsinki 10*

FRANCE
EUROPERIODIQUES S. A., 31 Avenue de Versailles, *78170 La Celle St. Cloud*
LIBRAIRIE LAVOISIER, 11 rue Lavoisier, *75008 Paris*
OFFICE INTERNATIONAL DE DOCUMENTATION ET LIBRAIRIE, 38 rue Gay-Lussac, *75240 Paris Cedex 05*

GERMAN DEMOCRATIC REPUBLIC
HAUS DER UNGARISCHEN KULTUR, Karl-Liebknecht-Strasse 9, *DDR-102 Berlin*
DEUTSCHE POST ZEITUNGSVERTRIEBSAMT, Strasse der Pariser Kommüne 3—4, *DDR-104 Berlin*

GERMAN FEDERAL REPUBLIC
KUNST UND WISSEN ERICH BIEBER,
Postfach 46, *7000 Stuttgart 1*

GREAT BRITAIN
BLACKWELL'S PERIODICALS DIVISION, Hythe Bridge Street, *Oxford OX1 2ET*
BUMPUS, HALDANE AND MAXWELL LTD., Cower Works, *Olney, Bucks MK46 4BN*
COLLET'S HOLDINGS LTD., Denington Estate, *Wellingborough, Northants NN8 2QT*
W.M. DAWSON AND SONS LTD., Cannon House, *Folkestone, Kent CT19 5EE*
H. K. LEWIS AND CO., 136 Gower Street,
London WC1E 6BS

GREECE
KOSTARAKIS BROTHERS, International Booksellers, 2 Hippokratous Street, *Athens-143*

HOLLAND
MEULENHOFF-BRUNA B.V., Beulingstraat 2, *Amsterdam*
MARTINUS NIJHOFF B.V., Lange Voorhout 9—11, *Den Haag*

SWETS SUBSCRIPTION SERVICE, 347b Heereweg, *Lisse*

INDIA
ALLIED PUBLISHING PRIVATE LTD., 13/14 Asaf Ali Road, *New Delhi 110001*
150 B-6 Mount Road, *Madras 600002*
INTERNATIONAL BOOK HOUSE PVT. LTD., Madame Cama Road, *Bombay 400039*
THE STATE TRADING CORPORATION OF INDIA LTD., Books Import Division, Chandralok 36 Janpath, *New Delhi 110001*

ITALY
EUGENIO CARLUCCI, P.O. Box 252, *70100 Bari*
INTERSCIENTIA, Via Mazzé 28, *10149 Torino*
LIBERIA COMMISSIONARIA SANSONI,
Via Lamarmora 45, *50121 Firenze*
SANTO VANASIA, Via M. Macchi 58, *20124 Milano*
D. E. A., Via Lima 28, *00198 Roma*

JAPAN
KINOKUNIYA BOOK-STORE CO. LTD., 17-7 Shinjuku-ku 3 chome, Shinjuku-ku, *Tokyo 160-91*
MARUZEN COMPANY LTD., Book Department, P.O. Box 5056 Tokyo International, *Tokyo 100-31*
NAUKA LTD. IMPORT DEPARTMENT, 2-30-19 Minami Ikebukuro, Toshima-ku, *Tokyo 171*

KOREA
CHULPANMUL, *Phenjan*

NORWAY
TANUM-CAMMERMEYER, Karl Johansgatan 41—43, *1000 Oslo*

POLAND
WĘGIERSKI INSTYTUT KULTURY, Marszalkowska 80, *Warszawa*
CKP I W ul. Towarowa 28 *00-958 Warsaw*

ROMANIA
D. E. P., *Bucureşti*
ROMLIBRI, Str. Biserica Amzei 7, *Bucureşti*

SOVIET UNION
SOJUZPETCHATJ — IMPORT, *Moscow*
and the post offices in each town
MEZHDUNARODNAYA KNIGA, *Moscow G-200*

SPAIN
DIAZ DE SANTOS, Lagasca 95, *Madrid 6*

SWEDEN
ALMQVIST AND WIKSELL, Gamla Brogatan 26, *101 20 Stockholm*
GUMPERTS UNIVERSITETSBOKHANDEL AB Box 346, *401 25 Göteborg 1*

SWITZERLAND
KARGER LIBRI AG, Petersgraben 31, *4011 Basel*

USA
EBSCO SUBSCRIPTION SERVICES, P.O. Box 1943, *Birmingham, Alabama 65201*
F. W. FAXON COMPANY, INC., 15 Southwest Park, *Westwood, Mass, 02090*
THE MOORE-COTTRELL SUBSCRIPTION AGENCIES, *North Cohocton, N. Y. 14838*
READ-MORE PUBLICATIONS, INC., 140 Cedar Street, *New York, N. Y. 10003*
STECHERT-MACMILLAN, INC., 7250 Westfield Avenue, *Pennsauken N. J. 08110*

VIETNAM
XUNHASABA, 32, Hai Ba Trung, *Hanoi*

YUGOSLAVIA
JUGOSLAVENSKA KNJIGA, Terazije 27, *Beograd*
FORUM, Vojvode Mišića 11, *21000 Novi Sad*

ACTA TECHNICA

TECHNICA

ACTA TECHNICA

SZERKESZTŐ BIZOTTSÁG

BARTA ISTVÁN, | BÖLCSKEI ELEMÉR, | GESZTI P. OTTÓ,
HELLER LÁSZLÓ

Az *Acta Technica* angol, francia, német és orosz nyelven közöl értekezéseket a műszak. tudományok köréből.

Az *Acta Technica* változó terjedelmű füzetekben jelenik meg, több füzet alkot egy kötetet.

A közlésre szánt kéziratok a következő címre küldendők:

Acta Technica
1051 Budapest, Münnich Ferenc u. 7.

Ugyanerre a címre küldendő minden szerkesztőségi és kiadóhivatali levelezés.

Megrendelhető a belföld számára az „Akadémiai Kiadó"-nál (1363 Budapest Pf. 24. Bankszámla 215 11448), a külföld számára pedig a „Kultura" Külkereskedelmi Vállalatnál (1389 Budapest 62, P. O. B. 149 Bankszámla: 218 10990) vagy annak külföldi képviseleteinél és bizományosainál.

Die *Acta Technica* veröffentlichen Abhandlungen aus dem Bereiche der technischen Wissenschaften in deutscher, englischer, französischer und russischer Sprache.

Die *Acta Technica* erscheinen in Heften wechselnden Umfanges. Vier Hefte bilden einen Band.

Die zur Veröffentlichung bestimmten Manuskripte sind an folgende Adresse zu senden:

Acta Technica
1051 Budapest,
Münnich Ferenc u. 7.
Ungarn

An die gleiche Anschrift ist auch jede für die Schriftleitung und den Verlag bestimmte Korrespondenz zu richten.

Abonnementpreis pro Band: $ 36.00.

Bestellbar bei »Kultura« Außenhandelsuntelsunternehmen (1389 Budapest 62, P. O. B 149 Bankkonto Nr. 218 10990) oder seinen Auslandsvertretungen.

S. VITÁLIS

1900—1976

Die wissenschaftliche und technische Welt Ungarns nahm traurigen Herzens Abschied vom Universitätsprofessor im Ruhestand und Präsidenten der Ungarischen Hydrologischen Gesellschaft Dr. Sándor VITÁLIS, der am 11. April 1900 in Selmecbánya geboren und am 21. Juni 1976 in Budapest verschieden ist. Während eines halben Jahrhunderts diente er uneigennützig seinem geliebten Vaterland mit seiner Tätigkeit auf dem Gebiet der geologischen Wissenschaft und mit deren Fortentwicklung, sowie mit der Förderung des gesellschaftlichen Fortschritts.

Der zu Arbeit und Schöpfung bestimmte Mensch ließ schon in früher Jugend seine individuellen Werte erkennen. Sándor VITÁLIS beteiligte sich bereits als 17 jähriger Schüler an der Arbeit der Hydrologischen Sektion der Ungarischen Geologischen Gesellschaft. Bald wurde er aktives Mitglied dieser Sektion und des Ungarischen Landesvereins für Bergbau und Hüttenwesen.

Seine Reifeprüfung legte er in der traditionsreichen Stadt, Selmecbánya ab und brachte von dort sein Wissen, und seine Arbeitsfreudigkeit, Ehrenhaftigkeit und seinen kristallklaren menschlichen Charakter mit nach Budapest, wo er an der philosophischen Fakultät der Budapester Eötvös Loránd Universität 1922 das Schlußzeugnis erhielt und 1923 zum Doktor der geologischen Wissenschaft promoviert wurde. Hier nimmt seine stets steigende wissenschaftliche Laufbahn ihren Anfang. In ununterbrochener Reihenfolge erscheinen seine nahezu hundert im Druck und mehrere hundert in Manuskripten veröffentlichten wertvollen, selbständigen Abhandlungen.

Im Jahre 1942 erlangt er mit seinem Werk »Die Hydrologie Ungarns« den Titel eines Privatdozenten an der Universität von Szeged. Als hervorragender Lehrer und Pädagog fördert er in hohem Maße die Ausbildung der künftigen Generation von Fachleuten und Wissenschaftlern. Selbstlos und bescheiden übergibt er sein Wissen den jüngeren Kollegen und seinen Hörern, in deren Kreis er ungemein beliebt ist.

Seine Arbeitsfreudigkeit und Selbstlosigkeit tritt im Rahmen seiner gesellschaftlichen Tätigkeit, an der er sich während seines ganzen Lebens be-

teiligt, noch markanter in Erscheinung. 1939 wird er Ausschußmitglied und 1944 Ausschußvorstand der Hydrologischen Sektion. Nach der Befreiung Ungarns im Jahre 1945 reorganisiert er mit einigen Mitgliedern der Sektion diese aus eigenen Mitteln und schreitet an die Fortsetzung ihrer Arbeit. Im Jahre 1949 wird er der erste Vorstand der Hydrologischen Gesellschaft, die dem Verband Ungarischer Wissenschaftlicher Vereine METESZ angehört. Diesen Posten bekleidet er vorerst bis 1950, dann von 1960 bis zu seinem Ableben, also während 17 Jahre.

Er war ein, auch seitens der Ungarischen Akademie der Wissenschaften anerkannter Wissenschaftler und wurde in Anerkennung seiner auf dem Gebiet des Mineralienabbaues geleisteten Arbeit bleibenden Wertes und großer volkswirtschaftlicher Bedeutung zum Doktor der geologischen und mineralogischen Wissenschaften promoviert. Einen fast unschätzbaren volkswirtschaftlichen Wert bedeuten für Ungarn die von ihm vorgenommenen Erforschungen von mineralischen Rohstoffen und seine hydrologischen Forschungen. Er war einer jener wenigen Professoren und Wissenschaftler, deren theoretisches Wissen, auf persönlich durchgeführter und geleiteter, Jahrzehnte währender Arbeit und Erfahrung beruhte. Seiner pädagogischen Arbeit ist der Ausbau international anerkannter Schulen ungarischer Geologen zu verdanken. Bis 1970 — als er in den Ruhestand trat — leitete er den Lehrstuhl für angewandte Geologie der Budapester Eötvös Lóránd Universität. Wohlverdient wurde ihm 1951 der Kossuthpreis und die Dr. Ferenc Schafarzik-Erinnerungsmedaille, in den Jahren 1967 und 1971 der goldene Orden der Arbeit, 1969 der Titel des Bestarbeiters im Unterrichtswesen und 1970 der, der Wasserwirtschaft verliehen.

Sein ausgedehntes Blickfeld, seine gründlichen theoretischen Kenntnisse und sein eingehendes praktisches Wissen benützte er um die der Hydrologischen Gesellschaft angehörenden Fachleute zur Teilnahme an der Lösung großer, komplexer, volkswirtschaftlicher Probleme zu veranlassen.

Die Triebkraft solcher gesellschaftlicher Arbeit setzt sich aus Vaterlandsliebe, Humanismus und aus dem Hang am Fachgebiet zusammen. Seine edle Selbstlosigkeit hat Sándor VITÁLIS gerade dadurch unter Beweis gestellt, daß er neben seiner berufsmäßigen Tätigkeit seine Freizeit stets gesellschaftlicher Arbeit opferte.

Er hielt eine Reihe interessanter und wertvoller Vorträge und spielte eine leitende Rolle in der komplexen Entwicklung des Balaton Sees und der Bewässerung bzw. in der frühzeitigen Erkenntnis der diesen Themen innewohnenden mächtigen volkswirtschaftlichen Werte. Sein weites Blickfeld bezeugen seine wissenschaftlichen und organisatorischen Arbeiten, die er hinsichtlich der Verwertung des Grubenwassers, der Wasserwirtschaft von Bergbaurevieren, des Aufschlußes von Tiefenwassern und Interesse der Verwertung der geothermischen Energie leistete. Besondere Aufmerksamkeit wid-

mete er den steten Erhöhung des Niveaus der Fachzeitschrift »Hydrologische Mitteilungen« der Hydrologischen Gesellschaft und dem Ausbau ihrer internationalen wissenschaftlichen Verbindungen.

Es bereitete Freude und bot ein Erlebnis sich mit Sándor VITÁLIS zu unterhalten. Freude, weil seine Individualität reinste Menschenliebe, Warmherzigkeit und Güte ausstrahlte und ein Erlebnis, weil seine Sprache einfach und weise war, sich stets auf das Wesentliche und allein auf die Wahrheit beschränkte und von Bescheidenheit erfüllt war.

Sándor VITÁLIS wurde von der Ungarischen Hydrologischen Gesellschaft, der Budapester Eötvös Lóránd Universität und vom Staatlichen Geologischen Institut am 5. Juli 1976 am 5. Juli 1976 am Budapester Friedhof Farkasrét zu Grabe geleitet. An der Bahre hielten seitens der Ungarischen Hydrologischen Gesellschaft deren Generalsekretär Árpád BERCZIK, seitens des Ungarischen Staatlichen Geologischen Instituts József KONDA, im Namen der ehemaligen Mitschüler Jenő MOLNÁR und am Grabe seitens der Eötvös Lóránd Universität und des Ungarischen Geologischen Verbandes der Dozent Viktor DANK, Vorsitzender des Ungarischen Geologischen Verbandes Abschiedsreden.

Miklós Kozák

H. LAMPL

1883—1976

Hugo LAMPL ist am 10. April 1883 in Budapest geboren und im Alter von 93 Jahren am 14. Juni 1976 verschieden.

Er war eine außerordentliche Persönlichkeit, die ihre außergewöhnlichen Fähigkeiten während sieben Jahrzehnte selbstlos in den Dienst seines Vaterlandes stellte. Es ist eine besondere Gabe des Schicksals jemandem während sieben Jahrzehnte eine so hervorragende und erfolgreiche Tätigkeit zu ermöglichen, wie sie Hugo LAMPL beschieden war.

Am Anfang seiner Laufbahn unterstand die Leitung des Wasserbaus in Ungarn Jenő KVASSAY, dem hervorragende Mitarbeiter, wie Ödön BOGDÁNFY, Sámuel HAJÓS, Zsigmond FEKETE, József BENEDEK, und Ede VICZIÁN zur Seite standen. KVASSAY und BOGDÁNFY begannen zu dieser Zeit einen neuen Abschnitt des ungarischen Wasserbaues, das Programm der Wasserverwertung — vornehmlich der Flußregulierung — vorzubereiten, während sich KOLOZSVÁRY und BOGDÁNFY den Problemen der Bewässerung, VICZIÁN in bahnbrechender Weise der Ermittlung der Wasservorräte Ungarns widmeten und BENEDEK sich mit der Entwicklung von Wasserbauten befaßte.

Hugo LAMPL begann seine Laufbahn fast gleichzeitig mit seinem Zeitgenossen — dem großen Organisator und seinem besten Freund — Elemér SAJÓ, der bereits vor vierzig Jahren verstorben ist. Vor fast anderthalb Jahrzehnten verschied auch der andere Freund und Mitarbeiter Árpád TRUMMER, der in Gemeinschaft mit Hugo LAMPL, und Endre NÉMETH, die Arbeit von Elemér SAJÓ fortsetzte und sein Vermächtnis weiterentwickelte. Der um acht Jahre jüngere Endre NÉMETH, ein hervorragender Betreuer des Vermächtnisses von SAJÓ, verschied zwei Wochen vor LAMPLs Tod.

Die Namen dieser Großen und die Aufgaben, die sie zu bewältigen hatten, wurden nicht nur zwecks Veranschaulichung des historischen Hintergrundes angeführt, sondern weil sie LAMPLs technische Laufbahn, ja sogar die Entfaltung seiner Persönlichkeit und seines menschlichen Charakters maßgeblich beeinflußten. Die ihn kannten, wissen, welch große Rolle die klare Erkenntnis der Aufgaben, das Pflichtgefühl, die unermüdliche Aktivität und nicht weniger die schwungvolle schöpferische Atmosphäre spielten, die nur außergewöhnliche Führer und Mitarbeiter einem erfolgreichen Leben bieten können.

Die sieben Jahrzehnte der Geschichte des ungarischen Wasserbaus sind reich an Fortschritten auf diesem Gebiet. Sie umfassen die Beendigung der Wasserschutzanlagen und der Flußregulierungen, die Vorbereitung der in der Wasserwirtschaft notwendigen größeren Bauten und schließlich die Ausführung von Großbauwerken, die den verschiedenen Zwecken der modernen Wasserwirtschaft dienen. Diese Zeitspanne war eine historisch entscheidende Epoche hinsichtlich der Fortentwicklung der Flußregulierung, sowie der Vorbereitung und Durchführung der planmäßigen Wasserwirtschaft. Es gibt kaum ein Arbeitsgebiet in dieser ereignisreichen Epoche, auf dem sich Hugo LAMPL nicht betätigt hätte und wo sein Name nicht mit einer bahnbrechenden, in die Zukunft weisenden Schöpfung oder mit einer, das ganze Land betreffenden organisatorischen Arbeit verbunden wäre.

Seine praktische Tätigkeit begann Hugo LAMPL bei der Wasserschutzgesellschaft der Insel Csepel und setzte sie bis 1968 als Sachverständiger im wissenschaftlichen Forschungsinstitut für Wasserwesen VITUKI, sowie bei der Landesbehörde für Wasserbau OVH fort, wobei er sich vornehmlich mit den Problemen der Instandhaltung von Wasserbauten befaßte.

Es wäre schwer, die sich auf alle Gebiete der Wasserwirtschaft erstreckende Tätigkeit LAMPLs detailliert zu behandeln, da dies mit der Geschichte eines halben Jahrhunderts der ungarischen Wasserwirtschaft und des Wasserbaues gleichbedeutend wäre.

Hugo LAMPL machte sein Abiturium 1901 in Budapest und erlangte 1905 sein Ingenieurdiplom an der Budapester Technischen Universität.

In seiner Tätigkeit standen Wissenschaft und Praxis in enger Wechselwirkung zueinander. Einige Werke seiner wissenschaftlichen Tätigkeit sind die 1908 erstmalig in Ungarn auf dem Gebiet des Wasserbaues durchgeführten — auch im Mosaikbild des VITUKI dargestellten — Modellversuche, sowie die den Beton behandelnde Monographie, für die ihm der Großpreis des Ungarischen Architekten- und Ingenieurvereins im Jahre 1914 zugesprochen wurde. Beide Werke schuf er gemeinsam mit Elemér SAJÓ. Sein Buch »Entwässerung von Baugruben durch Grundwasserabsenkung« erschien im Jahre 1954, wird aber heute noch vielfach gebraucht. Die den Zusammenhang zwischen der Kornzusammensetzung und Wasserdurchlässigkeit der Böden behandelnde Arbeit war bahnbrechend. Im Rahmen seiner wissenschaftlichen Tätigkeit gelang es ihm in mustergültiger Weise die ungeduldige Neugier des Forschers, der die Geheimnisse des Materials zu enthüllen bestrebt ist, mit der seitens der Praxis erforderten Nüchternheit, Maßhaltung und Verständlichkeit zu vereinen.

Die handgreiflichen Ergebnisse seiner Tätigkeit sind allbekannt, wenn es auch nicht jeder weiß, daß diese Werke mit seinem Namen verknüpft sind. Zwischen 1905 und 1955 (die beiden Jahreszahlen bedeuten die offiziellen Grenzen seines Wirkens) entstand in Ungarn kaum ein Bauwerk im Wasserbau

mit dessen Konzeption, Planung oder Leitung der Name Hugo Lampls nicht organisch verbunden gewesen wäre. Die Kvassay-Schleuse, die 1956 leider beschädigte Staustufe von Tass, die Häfen von Balatonboglár, Alsóörs und Balatonfüred, der Freihafen von Csepel, die Staustufe von Békésszentandrás, der fertiggestellte Abschnitt des Donau—Theiß-Kanal, die Bewässerungs-anlagen von Tiszalök, Tiszafüred und Hódmezővásárhely zeugen beredter und wirkungsvoller für seine Tätigkeit und bewahren nachdrücklicher die Erinnerung an sein Wirken, als ein Denkmal jedweder Art.

Neben seiner fachmännischen Arbeit beteiligte er sich auch am öffent-lichen Leben. Seit 1954 war er Mitglied des wissenschaftlichen Ausschusses für Wasserwirtschaft der Ungarischen Akademie der Wissenschaften. Im Jahre 1943 wurde er in die Rigorosenkommission der Budapester Technischen Uni-versität berufen, 1952 wurde ihm der wissenschaftliche Grad eines C. sci. zu-erkannt und 1955 erfolgte seine Promotion zum Doktor der technischen Wis-senschaften. 1954 wurde Hugo Lampl die Verdienstmedaille für sozialistische Arbeit und 1965 der goldene Orden der Arbeit verliehen.

Hugo Lampl war gründendes Mitglied der Ungarischen Hydrologischen Gesellschaft, wurde 1954 zum Ehrenmitglied der Gesellschaft gewählt und 1973 mit dem Zeichen höchster Anerkennung seitens der Gesellschaft, mit dem Vásárhelyi Pál-Preis ausgezeichnet. Er empfand diese Auszeichnungen als Ansporn zu einer noch hingebungsvollere Tätigkeit für diese Gesellschaft.

Sein geistiges Vermächtnis bildet einen unvergänglichen Schatz, dessen wir im Moment des schmärzlichen Abschieds eingedenk sein müssen. Die gesamte Körperschaft der ungarischen Wasserbau-Ingenieure bewahrt mit größter Achtung, Dankbarkeit und Ehrfurcht das Andenken an Hugo Lampl.

J. Bogárdi

Bücher und bedeutendere Abhandlungen von Hugo Lampl

1. Gróf Széchenyi István emlékhajóút a Tiszán (Graf István Széchenyi Gedenkschiffahrt auf der Theiß). 1933, 56 Seiten
2. Wasserwirtschaftliche Fragen in Ungarn mit besonderer Berücksichtigung der Wasser-straßen. 1935, 9 Seiten
3. Az öntözésügy kormányzati, közigazgatási és műszaki kérdései (Die regierungsseitigen, administrativen und technischen Fragen der Bewässerung). 1943, 21 Seiten
4. Az öntözéses termelés szerepe az ország újjáépítésének munkájában (Die Rolle der Pro-duktion durch Bewässerung im Wiederaufbau des Landes). 1945, 11 Seiten
5. A Duna—Tisza csatorna (Der Donau—Theiß-Kanal). 1947, 318 Seiten
6. Vízépítkezések organizációs feladatai (Organisatorische Aufgaben bei Wasserbauten). 1953, 69 Seiten
7. Munkagödrök viztelenítése talajvízszintsüllyesztéssel (Entwässerung von Baugruben durch Grundwasserabsenkung). 1954, 152 Seiten
8. A cementhabarcs besajtolási eljárás (Verfahren zur Einpressung von Zementmörtel). 1947, 28 Seiten
9. Modell (Tetszésszerinti keverésű betonok szilárdsága . . .) Használati utasítás (Modell , Festigkeit von Betonen beliebiger Zusammensetzung . . . Gebrauchsanweisung). 1914, 25 Seiten

10. Időszerű vízépítési közmunkák a munkanélküliség leküzdésének szolgálatában (Zeitgemäße öffentliche Wasserbauarbeiten zwecks Vermeidung der Arbeitslosigkeit). 1938, 19 Seiten
11. Az alföldi altalajok osztályozása és gyakorlati meghatározása a mérnök szempontjából (Die Klassifizierung und praktische Bestimmung des Untergrundes der Tiefebene vom Standpunkt des Ingenieurs). 1933, 47 Seiten
12. Balatoni kikötők (Häfen am Balaton). 1938, 52 Seiten
13. A Tiszavölgy szerepe a mezőgazdaságunk újjáép'tésében (Die Rolle des Theißtales im Wiederaufbau unserer Landwirtschaft). 1946, 18 Seiten
14. A beton (Der Beton). 1914, 553 Seiten
15. Új eljárás (Neues Verfahren). 1914, 38 Seiten
16. A csepelszigeti cementkísérleti és anyagvizsgáló állomás (Die Zementversuchs- und Materialprüfungsanstalt auf der Insel Csepel). 1912, 18 Seiten
17. Vasszádfalak (Stahlspundwände). 1917, 143 Seiten
18. Vasszádpallók és vasszádlemezek (Stahlspundbohlen und Stahlspundplatten). 1948, 60 Seiten
19. Agyagszádfalak készítése öblítéses eljárással lesüllyesztett acélhüvelyek segítségével (Herstellung von Tonspundwänden im Spühlverfahren mit versenkten Stahlhülsen). Mélyépítéstudományi Szemle, (1954), 570—678
20. Vízépítési munkáink fejlődése (Entwicklung unserer Wasserbauarbeiten). Vízügyi Közlemények, (1954), 373—404
21. A talaj szemösszetétele és fizikai tulajdonságai közötti összefüggések (Zusammenhang zwischen der Kornzusammensetzung und den physikalischen Eigenschaften des Bodens). Vízügyi Közlemények, (1955), 360—366
22. Vízzáró függöny előállítása fúrási eljárással (Herstellung eines wasserdichten Vorhanges im Bohrverfahren). Vízügyi Közlemények, (1957), 336—346
23. A mai eszközökkel végzett talajkutató fúrások megbízhatósága a vízépítés szempontjából (Die Zuverlässigkeit der mit den heutigen Mitteln vorgenommenen Bodenuntersuchungen durch Bohrungen vom Gesichtspunkt des Wasserbaues). Hidrológiai Közlöny (1958), 92—93
24. Buzgár-képződés és talajtörés (Entstehung von Sandaufbrüchen und Grundbruch). Vízügyi Közlemények, (1959), 25—49
25. Javaslat a cementbesajtolás technológiájának fejlesztését célzó rendszeres kutató kísérletek elvégzésére (Vorschlag zur systematischen Durchführung von Forschungsversuchen zwecks Fortentwicklung der Technologie der Zementeinpressung). Vízgazdálkodási Műszaki Szemle, (1960), 25—30
26. Árvízvédelmi töltéseken épült műtárgyak munkagödre visszatöltésének kérdése (Probleme der Rückfüllung der Baugrube von auf, dem Hochwasserschutz dienenden Deichen ausgeführten Bauten). Vízgazdálkodás, (1963), 23—24
27. A tiszafüredi szivattyutelepnél besajtolt cementfüggöny hatékonyságának vizsgálata (Untersuchung des bei der Pumpstation in Tiszafüred eingepreßten Zementvorhanges). Vízügyi Közlemények, (1965), 226—236
28. A siófoki hajózsilip helyreállítása (Rekonstruktion der Schiffahrtsschleuse bei Siófok). Vízügyi Közlemények, (1965), 237—241.
29. Források keletkezésének és buzgárok képződésének törvényszerűségei (Gesetzmäßigkeiten des Entstehens von Quellen und Sandaufbrüchen). Vízgazdálkodás, (1967), 65—68

L. GILLEMOT
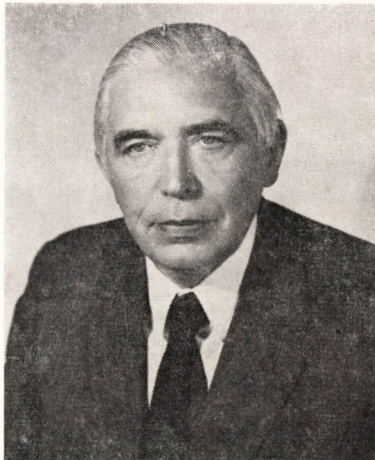
1917—1977

The death of Dr. L. GILLEMOT, member of the Hungarian Academy of Sciences is indeed a very great loss for the Hungarian Academy of Sciences and its Section of Technical Sciences. With his death, the Hungarian and international science of engineering has lost an inexhaustible scholar extremly rich in ideas, whose during more than 40 years of activity was governed fundamentally by the objectives of our contry, taking the road for building up socialism, in need of great engineering achievements. His achievements, comprising the milestones of his career, have been highly appreciated everywhere, always reminding his contemporaries as well as the next generations the unforgottable merits of this outstanding scientist.

Dr. L. GILLEMOT was born in Budapest, in 1912. In 1930, after an eminent high-school graduation, he was admitted to the Faculty of Mechanical Engineering of the "József Nádor" Technical University, predecessor of the present Technical University of Budapest. To satisfy his wide range of interest, parallel to his Technical University studies he attended the lectures of the philosophy faculty as well, taking mathematics, physics, and philosophy, each as major, during four semesters. He obtained a degree as a mechanical engineer in 1935.

In the same year he was appointed as a demonstrator to the Mechanical Technology Institute of the Technical University. In practice, this was both

his very first and, thereafter, permanent working place until his death, and this was where he worked in every and each stage of the university educational line, up tell to the position of Department Head university professor and Institute Director.

In 1947 he was appointed to the post of University Professor, when he had already been for more than 6 months, Department Head of the Heavy Industry Centre, an institution established to control our nationalized heavy industry, in charge of the technological resarch activities. He carried on this dual work up to the end of his life, never interrupting his university job but frequently changing his secondary activity according to the objectives set by the competent state authorities. Thus, in 1948, the State Council of Economics entrusted him with the organization and management of the Hungarian Aluminium and Light Metal Research Institute, whose director he remained until 1959. Only one year thereafter he was commisioned to organize and lead the Research Institute of the Iron Industry, which he had in the meantime directed parallelly until 1952. From 1970 on he was Executive Vice-President of the Technical Research Co-ordination Council of the State Office of Technical Development.

Similarly in the meantime, he was Rector of the Budapest Technical University from 1954 to 1957, then scientific Deputy Rector between 1965 and 1967.

Besides these comprehensive governmental duties he hade an outstanding creative role in our technical-scientific life. His very first steps in the field of sciences have already been successful. Thus, in 1940 he was awarded with the Carnegie Prize for his paper "Fatigue of Wire Ropes", Six years after obtaining his degree, his paper "X-ray examination of welds" was appreciated by the Technical University with the Doctor's degree. In 1945 he was commissioned, together with some others, to construct the Kossuth bridge whereby the two parts of the Capital, left without permanent brides after the Second World War, could be connected again. In this project he introduced welding, an entirely new technique in the construction of such large-size bridges and never used for this purpose in Hungary before, to connect the iron structural elements, whereby completion could be reduced by several months. His efforts in this project was awarded by the government with the Kossuth Prize in 1949. Furthermore, he combined this practical work with scientific research, and, on the basis of his achievements in testing welded bridges, he was appointed to the Technical University as "Private Professor" (honorary lecturer).

He was an enthusiastic and successful advocate of welding all through his whole life, in the fields of both theory and practice. His practical results are verified by a number of relevant patents, while his theoretical success was best evidenced by the fact that, with respect to his research results, the International Institute of Welding had not only elected him into its Governing

Council, but also appointed him to the position of Vice-President for the 1971—1974 period.

His technical-scientific activity will always be remembered when we realize that the Research Institutes for the Metal and Iron Industries, respectively, whose organization and provisional direction also belonged to his duties, have not only became the bases of Hungarian non-ferrous metal and ferrous metallurgical research, but also the scientific workshops having international reputation.

In addition to these two institutes, the main area of his scientific activities was always the Mechanical Technology and Material Structure Institute of the Budapest Technical University. There he had actually created a school in which many young professionals could take their very first steps towards their scientific career. His success in this field is attested by the fact that many of his former associates have already won several scientific degrees and some of them, as university professors, now follow the road along which he has started them. Moreover, the young proffesionals always considered it as a privilege if them were given an opportunity to work on the staff of Prof. GILLEMOT.

With a great number of associates he has created everlasting results in the fields of welding, metallurgy, plastic formation, heat treatment, and material testing. The present review of his activities simply cannot cover everything. However, his achievements are clearly reflected by his 156 papers, 24 books and chapters in comprehensive volumes, and 22 patents. In these publications he has reported, among others, on the twin-electrode welding technique he himself designed, on easily weldable high-strength steels, and on the test methods adaptable for such weldable steels.

He was the one to initiate and elaborate the production technology of metal titanium, for which he was awarded for the second time with the Kossuth Prize in 1957.

He insisted on the design and construction of then actually designed an equipment suitable for high-speed formation whereby, in addition to studies on the extremely high-speed plastic formation technique, he achieved together with some of his associates, new results partly on the time and energy requirement of such a formation process, and partly on the effect of high-speed formation leading to significant changes in the material properties. In this topic he delivered lectures which were followed with great interest at a number of international congresses.

In the field of material testing he elaborated new measurement methods, and conducted remarkable experiments on the causes of metal fracture. His research efforts in fracture mechanics proved to be particularly successful, and attracted much interest as well as fully justified appreciation from among the professionals both home and abroad.

The above instances do not only characterize his theoretical activities, but that he always combined the scientific problems with investigations on the possibilities of routine applications as well. He only talked about national economy interests, but took there into consideration whatever he did, and demanded the same from his associates. This is why his activities have always been highly appreciated not only by scientific circles but also by practical professionals, as attested by innumerable acknowledgements. He was the most proud of the fact that, on the basis of his scientific achievements, the Hungarian Academy of Sciences elected him to a corresponding member at the age of only 37, then as regular member in 1965.

His wide field of interest is clearly evidenced by the interesting fact that he delivered an inauguration lecture on globular cast irons after his election to corresponding member, and the one following his election to regular membership on the correlation between the properties of metals on one hand, and a new material testing parameter he himself had introduced, the contraction energy, on the other.

Appreciation of his activities is clearly shown by his membership and position as an official in a number of international scientific organizations. The Yugoslavian Academy of Sciences and Art had elected him to be corresponding member, the French Scientific Academy honored him with the highest degree of the "Ordre du Mérite pour la Recherche et l'Invention". He was member of the International Congress on Fracture and of the "Collège International pour l'Étude Scientifique des Techniques de Production Mechanique", and was engaged in the editorial committee of two international periodicals, the International Journal of Mechanical Sciences, and the Journal of Mechanical Working Technology.

As a university professor, he taught thousands of mechanical engineering students the fundamental principles and love of technology. His lectures had always been colorful, so the students simply had to pay attention and enjoyed the magic of his personality, too.

As Rector, then Deputy Rector of the Budapest Technical University he could successfully centrol and direct all the research projects under progress.

His science organization efforts, too, have always been exemplary in character. As chairman of the Mechanical Engineering and Metallurgical Scientific Working Group of the Section of Technical Sciences of the Academy he led and controlled research for many years in the various relevant disciplines. In addition, he was also chairman of the Committee for Theoretical Technology in the Hungarian Academy of Sciences.

One of the most important roles of his scientific organization work was what he performed as the Executive Vice-President of the Technical Research Co-ordination Council of the State Office for Technical Development. In this function he elaborated a number of scientific policy principles, both

alone and together with his associates in the SOTD. Another immortal merit of his was the lion's share he had in creating increasingly strong connections between the two top-reputation bodies of the country, responsible for engineering sciences, the Section of Technical Sciences at the Academy, and the State Office of Technical Development.

He was one of the founders and, in various official positions, similarly one of the most active leaders of the Scientific Society of Mechanical Engineers, where he was first awarded with "Pattantyús Á. Géza" commemorative medal, then later with the one named after "Bánki Donát".

He served scientific and technical development in many other functions as well, such as in the College of the Minister of Culture, and in the Technical Council of the Ministry of Metallurgy and Machine Industry, as well as that of the Ministry of Heavy Industry.

Beside his innumerable technical-scientific membership duties and official positions, he had enough vigour to participate in the social and political public life as well. Thus, he was Presidium Member in the Budapest Committee of the Patriotic People's Front and of the National Peace Council, and acted as Technical Assessor for the Supreme Court.

The life and career of Prof. L. GILLEMOT, member of the Hungarian Academy of Sciences, has inseparably been intertwined with the road the Hungarian engineering science has followed. His scientific and technical activities should present an example to all those who are engaged in similar fields.

J. Prohászka

The literary work of L. Gillemot

I. Papers

1. The X-ray Examination of Welding. *Technika* (1938), No. 7, pp. 1—4. (In Hungarian)
2. The Fatigue of Steel Cable Lines. *Bányászati és Kohászati Lapok* (1940), Nos 21, 22, 23. (In Hungarian)
3. The X-Ray Examination of Welding. Doctorate Thesis. Edition of Magyar Anyagvizsgálók Egyesülete. Budapest 1941. (In Hungarian)
4. The Non-destructive Testing of Welding. *Rimagil Közlemények* (1941). (In Hungarian)
5. Determination of Measures by X-Rays in the Technical Testing of Materials. *Anyagvizsgálók Közlönye* (1938). (In Hungarian)
6. The Accuracy of the Strength Examination of Fibrous Materials. *Magyar Textiltechnológusok Lapja* (1937), No. 9. (In Hungarian)
7. The Examination of Bearings. *Technika* (1942), No. 6 (In Hungarian)
8. The Replacement of Cast Bearing Bronzes with Aluminium Alloys. *Technika* (1942), No. 6. (In Hungarian)
9. The Strenth Characteristics of Aluminium Alloys Replacing Cast Tin Bronzes. (Co-author: F. NAGY). *Technika* (1942), No. 7. (In Hungarian)
10. A High-Precision Tensile Strength Testing Machine for the Examination of Paper and Fabrics. *Technika* (1943), No. 2. (In Hungarian)
11. A New Type Fatigue Machine. *Technika* (1943), No. 2. (In Hungarian)
12. Tests for Unifying the Strength Examination of Light Metal Castings. (Co-author: F. NAGY). *Technika* (1943), No. 5. (In Hungarian)

13. A New Type Tensile Strength Testing Machine for Fabrics. *Magyar Textiltechnológusok Lapja* (1943), No. 3. (In Hungarian)
14. The Problems of Scientific Research in Hungary. *Bányászati és Kohászati Lapok* (1949), No. 3. (In Hungarian)
15. New Ways in the Use of Aluminium. *Bányászati és Kohászati Lapok. Aluminium* (1949), p. 265—270. (In Hungarian)
16. The New Trends of Production Technology. Separatum. (Ministry of Heavy Industries, Budapest). (In Hungarian)
17. Experiments for a Better Utilization of the Hungarian Bauxites. *Bányászati és Kohászati Lapok* (1950, No. 2—3. (In Hungarian)
18. Use of Ultrasonics for Technical Purposes. *Természet és Technika* (1950). (In Hungarian)
19. Methods of Speeded-up Metal Machining. *Szovjet Kultúra* (1950), III. (In Hungarian)
20. Speeded-up Machining of Metals. *Természet és Technika* (1950). (In Hungarian)
21. The Problems of Higher Technical Education. *Népszava* (1950), VIII. 13. (In Hungarian)
22. Science and Practice. *Élet és Tudomány* (1950), IX. (In Hungarian)
23. Science and Innovation. *Újítók Lapja* (1950),·X. 9. (In Hungarian)
24. Patentierung von Stahldraht mittels Hochfrequenzerhitzung. *Acta Techn. Hung.* 1 (1950), 50—77. Co-author: I. KONCZ.
25. New Ways for the Processing of Hungarian Bauxite. *Kohászati Lapok* (1951), No. 2. (In Hungarian)
26. Powder Metallurgy and Precision Casting. Academic Lecture, 1951. Separatum. (In Hungarian)
27. The Crystallization of Spherical Graphite. *Kohászati Lapok* (1951), No. 3. (In Hungarian)
28. Meßeinrichtung zur Untersuchung wahrer Spannungen. *Acta Techn. Hung.* 1 (1951), 191—197
29. New Methods in the Welding Industry. *Élet és Tudomány* (1951), X. (In Hungarian)
30. Technical X-Ray Examination. *Élet és Tudomány* (1951), X. (In Hungarian)
31. Isledovaniye sferoidalnovo (globulyarnovo) grafita. *Acta Techn. Hung.* 3 (1951), 79—96
32. Theory of the Crystallization of Spherical Graphite. *MTA VI. Oszt. Közl.* 3 (1952), 35—75. (In Hungarian)
33. Methods for the Production of Titanium in Hungary. *MTA VI. Oszt. Közlem.* 3 (1952) 229—248. (In Hungarian)
34. The Theory of the Crystallization of Spherical Graphite. *Kohászati Lapok, Öntőde* (1952), No. 2. (In Hungarian)
35. The Problems of the Education of Technical Aspirants. *Felsőoktatási Szemle* (1953), III. (In Hungarian)
36. Structural Steels Alloyed with Titanium. *MTA VI. Oszt. Közl.* 10 (1953), 231—269. (In Hungarian)
37. A New Method for the Speeding-up of Manual Arc Welding. *GÉP* (1953), No. 4. (In Hungarian)
38. Calculation of the Characteristics of Two-rod Rapid Welding. *GÉP* (1953), No. 6. (In Hungarian)
39. A New Method for the Speeding-up of Manual Arc Welding. *Acta Techn. Hung.* 7 (1953), 277—292. (In Russian)
40. Steels Produced with Hungarian Alloy Components. *Magyar Technika* (1953), 481—483. (In Hungarian)
41. University Examination Regulation. *Felsőoktatási Szemle* (1954), No. 1. (In Hungarian)
42. The Titanium. *Magyar Technika* (1954), 362—371. (In Hungarian)
43. The Production of Metallic Titanium from Bauxite. *MTA VI. Oszt. Közl.* 14 (1954), 303—341. (In Hungarian)
44. Some More Important Social Problems of the Academie Youth. *Felsőoktatási Szemle* (1954), No. 11. (In Hungarian)
45. The Titanium. *Természet és Technika* (1954), No. 12 (In Hungarian)
46. Design and Operation of Reactors for Titanium Production. *Acta Techn. Hung.* 10 (1955), 221—245.
47. The Actual Problems of the Education of Engineers. *GÉP* (1955), July (In Hungarian)
48. Non-destructive Material Testing in the Iron and Metal Industries. *MTA VI. Oszt. Közl.* 16 (1955), 173—184. (In Hungarian)
49. The Education of Mechanical Engineers. *Műszaki Élet* (1955), No. 16. (In Hungarian)
50. Some Experiences in the Soviet Higher Education. *Felsőoktatási Szemle* (1955), 412—413. (In Hungarian)
51. Opening Speech for the Academic Year at Budapest Technical University. *Műszaki Élet* (1955), Nov. 5. (In Hungarian)

52. The Processing of Metallic Titanium. *Koháraszati Lapok.* (1955), 548—553. (In Hungarian)
53. Die Verarbeitung von metallischem Titan. *Acta Techn. Hung.* 15 (1956, 155—167
54. The Titanium. *Néphadsereg* (1956), III. No. 3. (In Hungarian)
55. Stand und Entwicklungsrichtlinien der Titanmetallurgie. *Neue Hütte* 2 (1957), 84—91
56. The Present Situation of the Titanium Industry and the Trends of its Development. *Magyar Kémikusok Lapja* 12 (1957), February. 45—52. (In Hungarian)
57. Nitrierbare Titanstähle. *Periodica Polytechnica, Engineering,* 2 (1958), No. 1. Co-author: Mrs. T. TÖMÖRY
58. The Contraction Work as a Material Characteristic. *MTA VI. Oszt. Közl.* (1958), 22, 344—366. Co-author: G. SINAY G. (In Hungarian)
59. Die Brucharbeit als Werkstoffkenngröße. *Acta Techn. Hung.* 22 (1958) 149—173. Co-author: G. SINAY
60. Über die Rolle der Werkstoffprüfung bei der zeitgemäßen Maschinenbemessung. *Periodica Polytechnica, Maschinen- und Bauwesen,* 2 (1958), 251—273
61. Nitrateable Titanium Steels. *GÉP* 10, 177—184. Co-author: Mrs. T. TÖMÖRY. (In Hungarian)
62. The Contraction Work as a Material Characteristic. *GÉP* 10 (1958), 237—246. Co-author: G. SINAY. (In Hungarian)
63. Erfahrungen mit der neuen Art von Diplomarbeiten. *Periodica Polytechnica,* Maschinen- und Bauwesen, 3 (1959), 117—122
64. Einfluß der Oberflächenbehandlung auf Ermüdung und Sprödbruch. *Freiberger Forschungshefte,* B 50, 1960 Mai, p. 123—135. Co-author: Mrs. T. TÖMÖRY.
65. The Influence of the Multiaxial State of Stress on the Contraction Work, *GTE Kongreszszusi Kiadványsorozat* (1960), 203—214 (In Hungarian)
66. The Role of Material Testing in the Modern Dimensioning of Machines. *GTE Kongresszusi Kiadványsorozat* (1960), 178—202. (In Hungarian)
67. Experiments for the Further Development of Welding Rods for the CO_2-protected Welding. Lecture delivered at the Conference on Welding Technology. Budapest 1960, XII. 1—3. (In Hungarian)
68. Critical Examination of the Quality of Welding Rods Based on the Contraction Work. Lecture delivered at the Conference on Welding Technology. Budapest 1960, XII. 1—3. (In Hungarian)
69. Increased Use of Welded Structures in Mechanical Engineering. Complete Proceedings of the Conference on Modern Prefabrication Technologies in Mechanical Engineering. Budapest 1960, Jan. 18—20 (Editor: M. DÉNES). Budapest 1960, Országos Tervhivatal, Kohó- és Gépipari Minisztérium, Gépipari Tud. Egyesület, Terv nyomda, p. 243. (In Hungarian)
70. Einfluß der Schweißfehler auf die Sprödbruchneigung der Schweißnähte. Lecture delivered at the Warsaw Conference on Welding Technology, 1961, May
71. Zur rechnerischen Ermittlung der Brucharbeit. *Materialprüfung* 3 (1961), Düsseldorf, pp. 330—336
72. Die Spannungsverteilung in Drahtseilbahn-Tragseilen in der Nähe der Verbindungsmuffe. *ATTI Abhandlungen,* Papers, 2ter. p. 9—18 (in German, with a Summary in Italian). International Colloque on the Fatigue Strength of Wire Ropes (Torino)
73. The Present Situation of Protective Gas Weldings. Lecture delivered at the National Welding Conference of the GTE at Győr, 1961. Nov. 13. (In Hungarian)
74. Recent Research Results in the Field of Material Fatigue. Lecture delivered at the Session of the "Material Fatigue" Working Committee of the Gépipari Tudományos Egyesület, 1961. Dec. 13. (In Hungarian)
75. Grundlagen von Stählen, in denen die Sprödbruchneigung durch Kaltverformung nur wenig beeinflußt wird. Lecture delivered at the Conference on Modern Dimensioning. *Acta Techn. Hung.* 35—36 (1961), 185—195. Co-author: M. RÓNAY
76. Schlag-Zerreißversuch an gekerbten Proben. Lecture delivered at the Conference on Modern Dimensioning. *Acta Techn. Hung.* 35—36 (1961), 197—209. Co-author: S. NADASAN
77. Der Einfluß mehrachsiger und ungleichmäßig verteilter Spannungszustände auf die Werkstoffeigenschaften. Lecture delivered at the Conference on Modern Dimensioning. *Acta Techn. Hung.* 35—36 (1961), 165—184
78. The Examination of Weldability. Lecture delivered at the 2nd Congress on Testing Materials, Budapest, 1961, July. *GÉP* (1961), 403—412. (In Hungarian)
79. Experiments on the Further Development of the Wires for CO_2-protected Welding. Lecture delivered at the Congress on Welding Technology in Temesvár, 1962. Oct. 12—14. (In Hungarian)

80. Beiträge zur Frage der Sprödbruchneigung von Schweißverbindungen. Lecture delivered at the »Sprödbruch« Conference in Prague. *Periodica Polytechnica, Maschinen- und Bauwesen,* **6** (1962), 97—113.
81. A New Type of Steel Suitable for Cold Working. *Gépgyártástechnológia,* **3** (1963), 201—204 and 219. Lecture delivered at the Conference on Cold Pressing, Budapest, 1962. Nov. 15—17. (In Hungarian)
82. Die Beurteilung der Schweißarbeit an Hand der Brucharbeit. Conference at the III. International Colloque »Schweißbarkeit der Stähle«, Weimar, 1963. Febr. 28—March 1. *Schweißtechnik,* **13** (1963), 305—311
83. Die Beurteilung der Werkstoffe auf Grund der Brucharbeit. Lecture delivered at the XIII. Berg- und Hüttenmännischer Tage in Freiberg, 1961. May 27. *Freiberger Forschungshefte* B **76,** 1963 Sept. pp. 5—18
84. Some New Development Trends in Material Testing. Conference delivered at th II. Assembly on Material Testing, Székesfehérvár, 1963. Sept. 5—7. (In Hungarian)
85. The Investigation of Material in Multiaxial Stress State. Conference delivered at Election Session of the Department of Material Testing of the Gépipari Tudományos Egyesület. Budapest, 1963. Dec. 2. (In Hungarian)
86. Eine neue Methode zur Bestimmung der Sprödbruchgefahr. *Periodica Polytechnica, Maschinen- und Bauwesen* **8** (1964) 1—14
87. Determination of Some Characteristic Points of the Wöhler Diagram. Lectures of the III. Congress on Material Testing, Section I, Mechanical Technology. Published by GTE, Budapest 1964, 5—24. (In Hungarian)
88. The Determination of the Velocity Constant of Metals and Alloys Based on Tensile Tests. Lectures at the III. Congress on Material Testing, ClassI: Mechanical Technology. *GÉP* **17** (1965), 81—85. Co-author: E. MIHÁLYI. (In Hungarian)
89. Some Remarks on the Development of Socialist Man. *Társadalmi Szemle* **19** (1964), 72—76. (In Hungarian)
90. Einfluß der Dehngeschwindigkeit auf die wahre Spannungskurve. *Freiberger Forschungshefte* B **109,** 1965 Juli, 79—94. Co-author: E. CZOBOLY
91. Simplified Method to Plot Haigh and/or Smith Graphs. *Acta Techn. Hung.* **50** (1965), 81—92
92. Low-Cycle Fatigue by Constant Amplitude True Mean Stress. International Conference on Fracture (1965) Sendai, Japan No. 3. D. I. 47—80
93. New Trends in Natural and Technical Sciences. *Magyar Tudomány* **10** (1965), 409—412 (In Hungarian)
94. Determination of Fatigue Limit Scatter by the Increasing Amplitude Method. *Proceedings of the Second Conference on Dimensioning and Strength Calculations.* Budapest 5—10. Oct. 1975. Akadémiai Kiadó, Budapest 1965, p. 287-301. Co-author: E. CZOBOLY
95. Brittle Fracture of Welded Materials. Commonwealth Welding Conference, 1965. Session VIII—XI. C. 7.1—6. (London)
96. Science, University, Industry — on Academic Research Work. Communicated by E. SZLUKA. *Népszabadság* 23 (1965), No. 168, p. 7. (In Hungarian)
97. The Characterization of Metals by the Specific Deformation Work. *MTA VI. Oszt. Közl.* **37** (1966), 9—31. (In Hungarian)
98. Determination of the Scattering of the Fatigue Limit by Step-wise Loading. *GÉP* **18** (1966), 289—295. Co-author E. CZOBOLY (In Hungarian)
99. Low-cycle Fatigue by Constant Amplitude True Mean Stress. *Periodica Polytechnica, Engineering,* **10** (1966), 77—94
100. Organization Problems of Scientific Work. *Felsőoktatási Szemle* (1966), 641—646. (In Hungarian)
101. Network Planning Methods in Scientific Research Work. *Magyar Tudomány* **11** (1966), 92—98. (In Hungarian)
102. The Influence of the Strain Rate on Metal Characteristics. *Periodica Polytechnica, Engineering — Maschinen- und Bauwesen,* **10** (1966), 427—436
103. From the Economic Decision to the Organization of Research. A conversation, Reporter: N. J. *Magyar Nemzet* **22** (1966), No. 67, p. 8. (In Hungarian)
104. The Rare Metals and the Pure Metals. *Népszabadság* **24** (1966), No. 109, p. 9. To the article by E. SAVICKIY: The Vitamins of Metallurgy. (In Hungarian)
105. Report on the Work of the Technical Sciences Department of the Hung. Academy of Sci. Reporter: G. BOGNÁR (Co-report). *MTA Műsz. Oszt. Közl.* 37 (1966), 243—289. (In Hungarian)
106. Die Ermittlung des Zusammenhanges zwischen der wahren Spannung und der Einschnürung an Zugproben. *Archiv für das Eisenhüttenwesen,* **37** (1966), 591—598

107. Report on the book of L. G. Johnson: Theory and Technique of Variation Research, p. 105, Elsevier Publ. Co. Amsterdam—London New York and the book of L. G. Johnson: The Statistical Treatment of Fatigue Experiments, Elsevier Publ. Co. Amsterdam—London—New York, 1964, p. 114. *Acta Techn. Hung.* **57** (1967), 429

108. The Variation of the Fracture Work of Heat Treatment Carbon Steels as a Function of the Treatment Parameters. Papers of the IV. Congress on Material Testing, II. Mechanical-Technological Investigations. Edited by Gépipari Tudományos Egyesület, Budapest 1967, 445—450. Co-author: Mrs. E. Kristyák. (In Hungarian)

109. The Fatigue Phenomenon and Dimensioning for Fatigue. *GÉP* **19** (1967), 360—369. (In Hungarian)

110. The Results of Technical Mechanics in Hungary and the Future Tasks in Engineering and Metallurgy. *MTA VI. Oszt. Közl.* **38** (1967), 399—409. (In Hungarian)

111. Transformation des métaux à grande vitesse. *Journées Scientifiques et Techniques Hongroises*, Paris, 1968 No. 3, pp. 1—28

112. Stefan Nadasan, 1901—1967, Obituary. *Magyar Tudomány* **13** (1968), 300—303. (In Hungarian)

113. The Forming of Metals by Pneumo-Mechanical Methods. *Gépgyártástechnológia* **8** (1968), 201—205 (In Hungarian)

114. Equipment for High Speed Forming. *Hungarian Heavy Industries*, 2nd Quarter 1968. Vol. 8, pp. 18—26

115. Contribution to the Report of The Department Secretary. *Műszaki Tudomány* **41**, (1968), 42—43. (In Hungarian)

116. The Design of High-Speed Impact Hammers. *GÉP* **20** (1968), p. 297—307. Co-authors: J. Morzál, L. Gillemot jun. (In Hungarian)

117. Science and Practice. *Magyar Tudomány* **13** (1968), 554—561. (In Hungarian)

118. High-speed Metal Forming. *Hungarian Scientific and Technical Days*, Helsinki 1968, No. 7, pp. 1—12

119. The Influence of Tensile Testing Machine Hardness on the Flow Curve. Proceedings of the Third Conference on Dimensioning and Strength Calculation. Akadémiai Kiadó, Budapest 1968, pp. 427—443

120. Die technische Erziehung in Ungarn. *Die Deutsche Universitätszeitung* **23** (1968), No. 3, pp. 26—29

121. High-speed Metal Forming. *Konepajamies* **22** (1969), 4—9. (In Finnish)

122. Les outils utilisés pour le forgeage à grande vitesse. *La Métallurgie* **10** (1969), 333—340

123. Some Problems of Technical Development. *GÉP* **21** (1969), 209—216. *Gépgyártástechnológia* **9** (1969), 289—296. *Járművek, Mezőgazdasági Gépek* **16** (1969), 201—208. (In Hungarian)

124. The Present Situation of Technical Higher Education in Hungary. *Hungarian Heavy Industries*, 1st Quarter 1969, Vol. 19, pp. 25—30

125. High-speed Impact Design. *Acta Techn. Hung.* **64** (1969), 259—285. Co-authors: J. Morzal, L. Gillemot jun.

126. The Expected Role of the Academy in the New System of Science Direction. *Magyar Tudomány* **14** (1969), 734—738. (In Hungarian)

127. Transformation des métaux ó grande vitesse. *Mécanique Électricité* **52** (1969), 20—24

128. The Law of Proportionality of the Notched Tensile Tests. Conferences at the V. Conference on Material Testing, Dept. I., p. 1—13. Edition of GTE, Budapest 1970. (In Hungarian)

129. Some Experiences of High-energ-rate Forging. *Metal Forming* **37** (1970), 137—144. (England)

130. The Development of Technologies from the Point of View of the Modernization of the Hungarian Machine Park. *Budapesti Műszaki Egyetem Jubileumi Tudományos Ülésszak* 1970. Ápr. 23—24. Gépészmérnöki Kari Szekció, 9—16, Budapest 1970. (In Hungarian)

131. Entwicklungsrichtlinien der hochfesten Stähle und Aluminiumlegierungen in Schweißkonstruktionen. *Zavarivanje* **13** (1970), 146—149

132. Generalized Theory of Fracture. Lectures at the VI. Conference on welding Technology. Budapest 1970. VI. 8—13. *MTESZ* Vol. 5 p. 338. Co-author E. Czoboly (In Hungarian)

133. Generalized Theory of Fracture. *Proceedings of the Second Symposion on Fracture.* Marianské Lázně: 1970. Co-author: E. Czoboly

134. Pneumo-mechanical Forming. *Technos* 1970. Scientific conference Budapest 1970 March 2—6. 1st Section: Prefabrication. Budapest 1970, *GTI*, p. 561. (In Hungarian)

135. Proceedings of the Research Institute for Non-Ferrous Metals. 9. Papers of the Anniversary Congress of the Institute. Akadémiai Nyomda, Budapest 1971. p. 501

136. Pneumo-mechanical Forming. *Gépgyártástechnológia* **11** (1971) 16—18. (In Hungarian)

137. Experiments with High-speed Forming Machine. *Proceedings of the Research Institute for Non-Ferrous Metals.* Akadémiai Kiadó, Budapest 1971, p. 359—364. Co-authors: G. SINAY, K. R. VASSEL

138. Twenty Years of the Research Institute for Non-Ferrous Metals. *Proceedings of the Research Institute for Non-Ferrous Metals.* Akadémiai Kiadó, Budapest 1971, pp. 29—40

139. The Expected Development of the Steel and Metal Structures. *Magyar Építőipar* **30** (1971), 327—332. (In Hungarian)

140. Modern Dimensioning on the Base of the Probability Theory. Editor J. SVÁB Notes of the Instruction Course of GTE. Budapest 1971; reproductions. Gépipari Tudományos Egyesület műszaki kiadványsorozat 80. Co-authors: P. BAJCSAY, K. KÁDAS (In Hungarian)

141. Material Testing Laboratories. Engineering Laboratories 1. UNESCO 1960, Paris. (Printed in Belgium SC. 68. (XXII. 1) (1) pp. 1—38

142. Dimensioning and Material Testing. *GÉP* **23** (1971), 328—332. (In Hungarian)

143. Die Technologie der Hochgeschwindigkeits-Umformung in Osteuropa. *Naturwissenschaft und Technik* **15** (1971), 2. pp. 103—118

144. High Energy Rate Forging. SME Technical Paper, Material Forming. Society of Manufacturing Engineers (USA, Dearborn, Michigan), 1971. MF 71—200, pp. 1—17

145. Investigation of Die Steels. *Periodica Polytechnica, Mechanical Engineering* **16** (1972), 3—11

146. The Dimensioning Conferences. *Magyar Tudomány* (1972), 251—252. (In Hungarian)

147. Some Design Principles of Work Pieces Produced by HERF. *Acta Techn. Hung.* **75** (1973), 161—176

148. Einfluß einer vorangegangenen Dauerbeanspruchung auf die Übergangstemperatur von Stählen. Co-author: I. HAVAS *Materialprüfung* **15** (1973), 206—209

149. M. CONSTANT—M. CAUBO—L. GILLEMOT et al.: Stress Relief Heat Treatments and their Affection of Mechanical Properties of Welded Joints. Doc. IIS/IIW X. 707/1973. International Institute of Welding, X. Commission

150. The Newer Development Trends of Welding. *Műszaki Élet* (1974), July. (In Hungarian)

151. ERDEY-GRÚZ, T.—KULCSÁR, K.: Science and Scholarship in Hungary. Chapter "Technical Sciences (L. GILLEMOT—F. CSÁKI) Corvina Press, Budapest, 1975, pp. 158—186

152. Some Problems of the Central Research Program of the Aluminium Industry. *Műszaki Tudomány* **50** (1975), 129—151. (In Hungarian)

153. KATOR Lajos — 1932—1974 (obituary). *Acta Techn. Hung.* **81** (1975), 195—196
    KATOR Lajos (1932—1974) (Obituary). *Műszaki Tudomány* **50** (1975), 283—284. (In Hungarian)

154. GILLEMOT L.—RÉTPALVI F.—DOMANOVSZKY, S. et al.: The Welding Problems of Increase Yield Limit Structural Steels. Országos Műszaki Fejlesztési Bizottság, 2—7104 It. p. 1—67. 1976 Jan., OMKDK Reproduction Shop. (In Hungarian)

155. Some Basic Principles for the Dimensioning of Welded Constructions. *GÉP* **28** (1976), 433—441. (In Hungarian)

156. Criterion of Crack Initiation and Spreading. *Engineering Fracture Mechanics* **8** (1976), 239—253. Appeared also in LIEBOWITZ H.: Progress in Fatigue and Fracture. Freudenthal Anniversary Volume, Pergamon Press, 1976, pp. 239—253

157. The Present Situation of Engineering Technology Research and its Future Tasks. *Műszaki Tudomány* **53**, No. 3—4 (In Hungarian)

II. Books, Parts of Books

1. Technical X-Ray Examination. The Subject Matter of the 1941 Course of the Mérnöki Továbbképző Intézet. Budapest 1942. Királyi Magyar Egyetemi Nyomda, 80 p., 67 Figs. (In Hungarian)

2. The Technology of Metals, Vol. I: The Forming of Metals by Heat Action. 1st edition: Egyetemi Nyomda 1047, 265 p., 195 Figs., 17 photos. 2nd edition: Nehézipari Könyv- és Folyóiratkiadó V. 1950. 270 p., 196 Figs. (In Hungarian)

3. Wood as a Building Material (part of book). Editor: L. PALOTÁS, L. GILLEMOT: Strength and Physical Properties of Wood, p. 64—85. Edition of the Budapesti Építőmesterek Ipartestülete, Budapest 1949. (In Hungarian)

4. Aluminium Handbook. Edited by S. GELEJI Chapter on Welding of Aluminium: pp. 368—391. Subject Matter of the 1948 course of the Mérnöki Továbbképző Intézet, Budapest 1949. (In Hungarian)

5. Testing of Materials. Printed as Manuscript. Budapest 1949. Műegyetemi Jegyzetkiadó. 72 p. (In Hungarian)
6. Aluminium. Chapter on Newer Developments of Aluminium Technology, pp. 116—119. Edition of Aluminiumipari és Kereskedelmi Propaganda Biz., Budapest 1950. (In Hungarian)
7. Metallography and Material Testing. University Text Book, Tankönyvkiadó Váll., Budapest 1952, 558 p., 270 Figs. (In Hungarian)
8. Iron and Metal Industries Material Sciences L. GILLEMOT— K. KERPELY). Népszava Kiadó, Budapest 1952, 598 p., 215 Figs. (In Hungarian)
9. Technology of Structural Materials, Vol. I. Tankönyvkiadó Váll., Budapest 1954. 272 p., 210 Figs. (In Hungarian)
10. High-Speed Welding Methods. Mérnöki Továbbképző Intézet, Lecture Notes, 1954. 46 p. (In Hungarian)
11. The Non-Ferrous Metals — Important Engineering Materials. A Guide for Lecturers in Towns and Villages. Művelt Nép Kiadó, Budapest 1954. 60 p. (In Hungarian)
12. Ten Years of Hungarian Science. 1945—1955. Chapters on Non-Ferrous Metallurgy, Metal Industries, Alumina Industry, Aluminium Smelting, Light Metal Semi-finished and Finished Products Production, Magnesium Smelting. p. 302—308. Akadémiai Kiadó, Budapest. (In Hungarian)
13. Chapter on the Characterization of Structural Steels by the Contraction Work in "Sovremenniye problemi metallurgii", published at the occasion of the 70th anniversary of Academician BARDIN. Published by the Acad. of Sci. of the SU. Moscow 1958, p. 572— 582. (In Russian)
14. Technology of Structural Materials II. Welding. University Textbook. Tankönyvkiadó Váll. Budapest 1980. 292 p. (2nd edition 1966). (In Hungarian)
15. Technical Explanatory Dictionary. Vol. 11: Mechanical Technology Part I. Material Structure and Material Testing. Edited by L. GILLEMOT Budapest 1960. Terra, 167 p. Index of Words in four languages. Vol. 12.: Mechanical Technology Part 2. Technological operations, 212 p. (In Hungarian)
16. L. GILLEMOT— J. PROHÁSZKA— L. KATOR: Complementary Notes to the Textbook on Metallography and Material Testing. Tankönyvkiadó Budapest, 1963. 77 p. J 4—366. (In Hungarian)
17. Chapter "A New Type of Steel for Cold Forming" in the Book: Ksiega jubileuszowa dla uczczenia zaslug naukowych Aleksandra Krupowskiego. Polska Akademia Nauk, Warszawa 1965, pp. 193—203
18. Material Structure and Material Testing, Part I. University Lecture Notes, Tankönyvkiadó Budapest 1965, 143 p. (In Hungarian)
19. Material Structure and Material Testing, Part II. University Lecture Notes, Tankönyvkiadó Budapest 1965, 101 p. (In Hungarian)
20. Material Structure and Material Testing, Part III. University Lecture Notes. Tankönyvkiadó Budapest 1966, 263 p. (In Hungarian)
21. Introduction to Industrial Research Work. Editors: L. GILLEMOT and S. MÉSZÁROS Conference series of the Mérnöki Továbbképző Intézet. Budapest 1967. (In Hungarian)
22. Material Structure and Material Testing. University Text Book. Tankönyvkiadó, Budapest 1967, 429 p. (In Hungarian)
23. L. GILLEMOT— Gy. ZIAJA: The Plastic Forming of Metals. University Notes. Tankönyvkiadó, Budapest 1968, J 4—586, 386 p. (In Hungarian)
24. Proceedings of the Research Institute for Non Ferrous Metals. Editor: L. GILLEMOT Akadémiai Kiadó, Budapest 1971
25. ARTINGER I.— KATOR L.— ROMVÁRI P.: Technology of Metals. Editor: L. GILLEMOT Műszaki Könyvkiadó, Budapest 1971. 400p. (In Hungarian)

PLANNING OF OPTIMAL INVESTMENT CAPACITIES FOR INTERCONNECTED POWER SYSTEMS USING PROBABILISTIC CONSTRAINED PROGRAMMING

K. SZENDY*

CORR. MEMBER OF THE HUNG. AC. OF SCI.

By means of probabilistic constrained programming the paper gives a useful tool for determining the optimal enlargement of generating and transfer capacities in an interconnected system. In the described method the instantaneous transfer powers are eliminated. The admissibility and reliability of the power supply are investigated by generation and interconnection constraints. The available generating and transfer capacities, as well as the peak load deviations are considered as random variables. In addition to technical constraints the optimization process contains the prescribed reliability level as a lower limit. Furthermore, the cost of load shedding can also be taken into consideration. The method is illustrated by a simple example.

Introduction

The complexity of the interconnection of several power systems led the planning engineers to the simulation methods for finding the most appropriate structure for the investments and for a future system operation. The selection of optimal solution has also been found to be a tiresome work in spite of appropriate engineering judgement. The available generating capacities, the load demands as well as the transfer capacities of the interconnection are random variables. At the first glance a probabilistic constrained programming model can be chosen as a direct method to recommend the optimal investment of new generating and transfer capacities for an increased load demand satisfying at a given reliability level of the power supply under a simplified condition [1, 2]. To overcome the obstacles caused by the transfer powers, a special probabilistic model is presented in the following. In this model only a future peak period of one year is investigated as significant for the power supply, assuming that the hydro-energy takes a less important role in the system. The model has a *static* character, the electromechanic transients are not considered.

The task is the determination of the optimal extension state for a future peak demand condition, starting out from an original interconnected system state. This is rather complicated if beside the random nature of some parameters, the Kirchhoff's 2nd law (voltage law) is taken into consideration.

---

* Prof. Dr. K. SZENDY Ábrányi E. 1, H-1026 Budapest, Hungary

Therefore, in some papers the emergency help, by means of tie line interconnections, is considered by an assumed dispatching logic [3]. In formulae of the present optimization process, these instantaneous power transfers are eliminated, thus making the solution of the problem easier.

The interconnected systems consists of subsystems. Our probabilistic model was developed from a deterministic one. The formulation changes as soon as certain parameters become random values. The random character of the probabilistic model is expressed by individual outcomes. An *outcome* is declared *successful* if the power supply is not restricted, and if this condition is not met, the outcome is *unsuccessful*. The reliability index p of the power supply is the probability of successful outcomes; the reliability level p_S is the lower boundary of the reliability indices. In practice this lower boundary has to be near unity.

The objective function to be optimized is the investment cost of the generating and interconnection extension. The network power loss in an optimization process is not considered with the aspect of the short duration of the deviation from the scheduled power values. The deterministic constraints of an individual outcome are the loading limits of available generation and tie lines. The probability constraints are expressed by the probability of satisfying the successful outcomes.

The random variables can be characterized by their distribution and density functions. The sum of density of two random variables μ, δ can be derived by an auxiliary variable ω, e.g.

$$\xi = \mu + \delta - \bar{\mu} \qquad (\bar{\mu} = \text{const})$$
$$\omega = \delta \tag{0.1}$$

Denoting the joint density function of μ, and δ by $f_{\mu\delta}$ the new density function is [4]:

$$f_\xi = \int\limits_{-\infty}^{\infty} f_{\mu\delta}(\xi - \omega - \bar{\mu}, \omega)d\omega . \tag{0.2}$$

If the μ and δ random variables are independent of each other, the density of their sum equals the convolution of their respective densities.

The random variables are estimated from the past history of the system and its new possibilities. Therefore, the random variables are investigated as known values. The mathematical symbols utilized in this paper are summarized in Appendix A., the formulae and terms in Appendix **B**.

The outcome can be considered successful if the following two conditions are satisfied without load shedding:

1. the power balances of each subsystems,
2. the transfer constraints of the interconnections.

1. Power balance of a subsystem

The power balance in a subsystem is considered satisfactory if the available generation capacity is higher than the generation demand consisting of the total demand d and the overall power transfer to other subsystems which will be considered as positive bus power i.

The available generation capacity is the difference of the installed generation capacity is the difference of the installed generation capacity h and the capacity deficiency μ as a random variable due to forced outage, main-
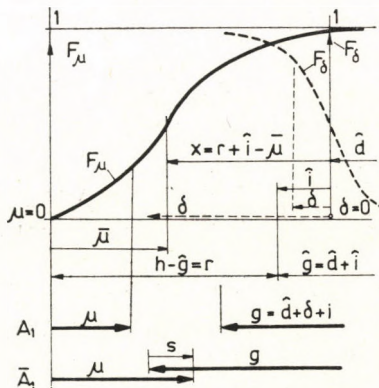
Fig. 1

tenance, etc. The reserve generation capacity r can be defined as the difference of installed capacity h and the scheduled generation power $\hat{g}$. The load demand is composed by the scheduled demand $\hat{d}$ and the random demand deviation δ, the positive value of the latter corresponds with the increased demand. The scheduled demand is determined by taking the mean of demand deviation equal to zero. The outgoing bus power i to the other subsystems (export is positive) contains the scheduled $\hat{i}$ and the emergency bus power.

In Fig. 1 the random character of the capacity deficiency μ and the load demand deviation δ is shown, furthermore an A_1 successful and $\bar{A}_1$ unsuccessful outcome. In case of insufficient available generating capacity (unsuccessful outcome), the power balance can be restored by load shedding s preventing further, and eventually greater cascading disturbances.

Thus for maintaining the power balance, the following condition has always to be satisfied:

$$h - \mu \geq \hat{d} + \delta + i - s \tag{1.1}$$

where

$$h = \hat{g} + r = \hat{d} + \hat{i} + r.$$

Introducing the resultant capacity vector as shown in Fig. 1

$$x = r + \hat{\imath} - \bar{\mu} \tag{1.2}$$

where $\bar{\mu}$ is the mean value of the capacity deficiency, furthermore the sub-system random variable

$$\xi = \mu + \delta - \bar{\mu}.$$

Obviously the mean of load demand deviation is zero ($\bar{\delta} = 0$), and considering the above-mentioned relations, the balance condition can be written as follows:

$$\xi + i \leq x + s,$$
$$s \geq 0. \tag{1.3}$$

If (1.3) can be satisfied;

$$\left. \begin{array}{l} \text{by } s = 0 \text{ the outcome is successful } (A_1 \text{ in Fig. 1);} \\ s > 0 \text{ the outcome is unsuccessful } (\bar{A}_1 \text{ in Fig. 1)} \end{array} \right\} \tag{1.4}$$

The reliability index of $i - th$ subsystem is defined as

$$p_i = P\{s_i = 0\}, \quad \text{or}$$
$$\bar{p}_i = 1 - p_i = P\{s_i > 0\}. \tag{1.5}$$

The reliability index of a system containing n subsystems is:

$$p = P\{s_i = 0; \quad i = 1, \ldots, n\}. \tag{1.6}$$

Obviously

$$p \leq \text{Min}(p_i),$$
$$i = 1, \ldots, n. \tag{1.7}$$

The reliability level prescribes the exceptable reliability condition. Denoting the reliability level for subsystem i as p_{Li}, as well as for the whole system p_S, it can be written that:

$$p_i \geq p_{Li}, \quad (i = 1, \ldots, n) \tag{1.8}$$
$$p \geq p_S. \tag{1.9}$$

The system unreliability index can be defined as the complement of the reliability index and noted by $\bar{p}$. This value shows the probability of unsuccessful outcomes, when the power supply is disturbed. Obviously

$$\bar{p} = 1 - p. \tag{1.10}$$

2. Technical constraints of interconnections

This model investigation assumes, that the generations, the load demands and the bus powers are concentrated in one point for each subsystem. The transfer power can be expressed by the bus powers. Figure 2 shows an interconnected system consisting of three subsystems. The system interconnections are indicated by thick lines. In the simplified model each subsystem is mapped into a node point. These node points are interconnected by branches shown in the left side of Fig. 3. The transfer powers of each branch are limited by trans-
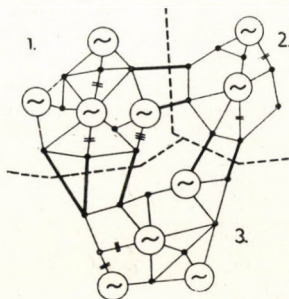
Fig. 2
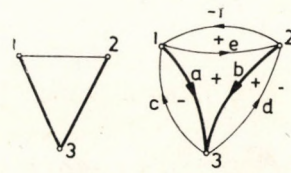
Fig. 3
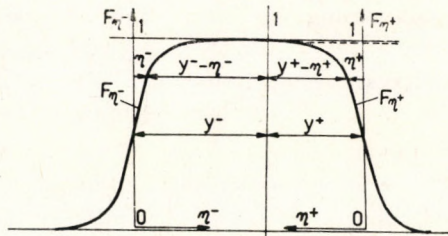
Fig. 4

fer capacities in both directions, which can be different from each other. The right side of Fig. 3 presents the same interconnections, but by directed edges corresponding to the power flow direction.

The transfer capacity $(\mathbf{y}^+, \mathbf{y}^-)$ in each direction and the transfer power distribution matrix $\mathbf{K}$ is changed by the variation of network configuration, due to outages or the line capacity is modified by the weather conditions, etc. An uncertainty was also resulted by the concentration of the subnetworks into equivalent node points, and by equivalent network branches. These uncertainties can be added to the above-mentioned random character of transfer capacities, but the coefficients of the transfer distribution matrix are kept unchanged for the sake of simplicity. Thus equivalent transfer capacity is the difference of the nominal installed transfer capacity (y^+, y^-) and the random deviation (η^+, η^-), respectively, shown in Fig. 4.

For further simplification the equivalent network is represented by *dc* state, i.e. the vector and matrix components are real numbers, and the active powers are proportional with the currents. If it is necessary, the variation of the transfer power distribution can be considered in the iterative process of probabilistic optimization.

The technical constraints can be expressed by the following relation

$$\mathbf{K}\,\mathbf{i} \leqq \mathbf{y} - \eta \qquad (2.1)$$

where

$$\mathbf{y} = \begin{vmatrix} \mathbf{y}^+ \\ \mathbf{y}^- \end{vmatrix}, \qquad \eta = \begin{bmatrix} \eta^+ \\ \eta^- \end{bmatrix}$$

containing the transfer capacities and their deviations in positive and negative directions.

Furthermore, $\mathbf{i}^T = [i_1, \ldots, i_{n-1}]$ is the independent bus power vector, from which the reference bus power is

$$i_n = -\mathbf{l}_{n-1}^T\,\mathbf{i}. \qquad (2.2)$$

3. The admissible range of interconnected system states

The interconnected system consisting of n equivalent nodes subsystems and q equivalent branches can be optimized with respect to unknown variable vectors $(\mathbf{x}, \mathbf{y})$ for given distributions of random variables (ξ, η). The explicit form of $\mathbf{i}$ bus power vector is not desirable in this process. The elimination of $\mathbf{i}$ vector in the above-mentioned inequality relation can be performed by equality relations and introducing the auxiliary variables $\alpha \geqq \mathbf{0}$, and $\beta \geqq \mathbf{0}$ as generating, and transfer surplus power vectors.

The outcome is *admissible* if the subsystem balances and the technical constraints are satisfied, eventually by means of load shedding.

The *subsystem balances* can be written from (1.3) and (2.2) in the following vectorial form completed by α generating surplus vector:

$$\xi + \mathbf{I}'\mathbf{i} + \alpha = \mathbf{x} + \mathbf{s} \qquad (3.1)$$

where

$$\mathbf{I}' = \begin{bmatrix} \mathbf{I}_{n-1} \\ -\mathbf{l}_{n-1}^T \end{bmatrix}.$$

The *technical constraints* given in (2.1) can be completed by β transfer surplus vectors as

$$\eta + \mathbf{K}\,\mathbf{i} + \beta = \mathbf{y}. \qquad (3.2)$$

For a particular choise of tree, the branches on the tree are called "tree branches", whereas these that are not on the tree are called "chords". The **i** bus power vector can be expressed from the equation (3.2) by its partition into a tree branch block with positive direction and chord block consisting of all chords and the negative-directed part of tree branches.

In accordance

$$\eta_t + \mathbf{K}_t \,\mathbf{i} + \beta_t = \mathbf{y}_t,$$

$$\eta_c + \mathbf{K}_c \,\mathbf{i} + \beta_c = \mathbf{y}_c$$

(3.3)

where

$$\eta_t = \eta_t^+, \beta_t = \beta_t^+, \mathbf{y}_t = \mathbf{y}_t^+,$$

$$\eta_c = \begin{bmatrix} \eta_t^- \\ \eta_c^+ \\ \eta_c^- \end{bmatrix}, \quad \beta_c = \begin{bmatrix} \beta_t^- \\ \beta_c^+ \\ \beta_c^- \end{bmatrix}, \quad \mathbf{y}_c = \begin{bmatrix} \mathbf{y}_t^- \\ \mathbf{y}_c^+ \\ \mathbf{y}_c^- \end{bmatrix}.$$

Obviously $\mathbf{K}_t$ regular matrix has an $\mathbf{K}_t^{-1}$ inverse, thus from (3.1) and (3.3) can be written

$$\gamma = -\begin{bmatrix} \alpha \\ \beta_c \end{bmatrix} + \begin{bmatrix} \mathbf{I}' \\ \mathbf{K}_c \end{bmatrix} \mathbf{K}_t^{-1} \beta_t = \begin{bmatrix} \xi \\ \eta_c \end{bmatrix} - \begin{bmatrix} \mathbf{x} \\ \mathbf{y}_c \end{bmatrix} - \begin{bmatrix} \mathbf{s} \\ \mathbf{0}_c \end{bmatrix} - \begin{bmatrix} \mathbf{I}' \\ \mathbf{K}_c \end{bmatrix} \mathbf{K}_t^{-1}(\eta_t - \mathbf{y}_t). \quad (3.4)$$

Let us consider the convex polyhedral cone of γ vector in $2q + 1 = 2n + 2c - 1$ dimensional space:

$$\Gamma = \left\{ \gamma : \gamma = \begin{bmatrix} -\mathbf{I}_{n+c}, \begin{bmatrix} \mathbf{I}' \\ \mathbf{K}_c \end{bmatrix} \cdot \mathbf{K}_t^{-1} \end{bmatrix} \cdot \begin{bmatrix} \begin{bmatrix} \alpha \\ \beta_c \\ \beta_t \end{bmatrix} \end{bmatrix}; \begin{array}{l} \alpha \le \mathbf{0} \\ \beta_c \le \mathbf{0} \\ \beta_t \le \mathbf{0} \end{array} \right\}. \quad (3.5)$$

According to Weyl's theorem [1] there exist vectors $\mathbf{d}_1', \ldots, \mathbf{d}_v'$ for which

$$\Gamma = \{ \gamma : [\mathbf{d}_{Ni}^T, \mathbf{d}_{ci}^T] \gamma \le 0; \quad i = 1, \ldots, v \} \quad (3.6)$$

and

$$\mathbf{d}_i'^T = [\mathbf{d}_{Ni}^T, \mathbf{d}_{ci}^T]$$

assuming that no pair of $\mathbf{d}_1', \ldots, \mathbf{d}_v'$ is linearly dependent.

From (3.4) and (3.6)

$$[\mathbf{d}_{Ni}^T, \mathbf{d}_{ci}^T] \begin{bmatrix} \mathbf{I}' \\ \mathbf{K}_c \end{bmatrix} \mathbf{K}_t^{-1} \le \mathbf{0}_{n-1}^T \text{ and } \mathbf{d}_{Ni}^T \ge \mathbf{0}_n^T, \mathbf{d}_{ci}^T \ge \mathbf{0}_c^T.$$

Introducing $\mathbf{d}_{Ti}^T \ge \mathbf{0}_{n-1}^T$ the inequality can be substituted by the following equality

$$[\mathbf{d}_{Ni}^T, \mathbf{d}_{ci}^T] \begin{bmatrix} \mathbf{I}' \\ \mathbf{K}_c \end{bmatrix} \cdot \mathbf{K}_t^{-1} + \mathbf{d}_{Ti}^T = \mathbf{0}_{n-1}^T. \quad (3.7)$$

Then the outcome is admissible if and only if $\gamma \in \Gamma$. Thus, the condition of admissibility is from (3.4), (3.6) and (3.7)

$$[\mathbf{d}_{Ni}^T, \mathbf{d}_{ci}^T]\left\{\begin{bmatrix}\xi\\\eta_c\end{bmatrix} - \begin{bmatrix}\mathbf{x}\\\mathbf{y}_c\end{bmatrix} - \begin{bmatrix}\mathbf{s}\\\mathbf{O}_c\end{bmatrix}\right\} + \mathbf{d}_{Ti}^T\begin{bmatrix}\mathbf{I}'\\\mathbf{K}_c\end{bmatrix} \cdot \mathbf{K}_t^{-1}(\eta_t - \mathbf{y}_t) \lesseqgtr 0 \,. \qquad (3.8)$$

The vectors $\mathbf{d}_{Ni}^T, \mathbf{d}_{ci}^T, \mathbf{d}_{Ti}^T$ can be determined from (3.7). For sake of placing the positive tree edge before other branch edges, an interconnection matrix is:

$$\mathbf{J}^T = [(\mathbf{K}_t^{-1})^T \mathbf{I}'^T \,\vdots\, \mathbf{I}_{n-1} \,\vdots\, (\mathbf{K}_t^{-1})^T \cdot \mathbf{K}_c^T] \qquad (3.9)$$

and can be used for further investigation.

The external directions $\mathbf{d}$ of the $2n + 2c - 1$ dimensional polyhedral cone of Γ are given by the basic solution of $\mathbf{J}^T$:

$$\mathbf{J}^T\mathbf{d}_i = \mathbf{O}_{r-1},$$

$$\mathbf{d}_i = \begin{bmatrix}\mathbf{d}_{Ni}\\\mathbf{d}_{Ti}\\\mathbf{d}_{ci}\end{bmatrix} \geq \mathbf{O}_{n+2q}\,. \qquad (3.10)$$

Obviously, the *upper limit of non-zero components* of $\mathbf{d}_i$ vectors are the n number of nodes (subsystems). Let $\mathbf{d}_i$ column vectors of $\mathbf{D}$ matrix be decomposed into three blocks. The first $\mathbf{D}_\xi$ block corresponds to the equivalent nodes, the second $\mathbf{D}_\eta$ block to the branch edges with random deviations and the third block to the branch edges without deviations. The condition of the admissible outcomes of an interconnected system can be expressed from (3.8), as

$$\mathbf{D}_\xi^T(\xi - \mathbf{s}) + D_\eta^T\eta \leq \mathbf{u} \qquad (3.11)$$

where

$$\mathbf{u} = \mathbf{D}^T\mathbf{z}\,,$$

$$\mathbf{z} = \begin{bmatrix}\mathbf{x}\\\mathbf{y}\end{bmatrix}. \qquad (3.12)$$

The columns of $\mathbf{J}^T$ determine the sequence in $\mathbf{D}$ in order of ξ, η_t and η_c. The first block of $\mathbf{J}^T$ has n columns, if all branches with both directions are investigated the other two blocks have altogether twice the branch number q. Obviously the v number of the possible extremal solutions is generally less has than the total combination of branches into the blocks of the same number as the nodes, on account of the following:

— the optimization is not necessarily extended over all equivalent branches, and often the power flows are not considered in both directions,

— many combinations of basic column of $\mathbf{J}^T$ matrix have no admissible solution ($\mathbf{d}_i \geq \mathbf{O}$ is not valid),

— omitted are those solutions which have no basic column of at least one equivalent node.

Therefore, if more than 6 or 8 subsystems exist, the decomposition procedure can be utilized or the investigation is extended to those subsystems which effectively influence the subject.

Obviously the first solution is always

$$\mathbf{d}_1^T = [\mathbf{l}_n^T, \mathbf{O}_{2m}^T].$$

Therefore, condition

$$\mathbf{l}_n^T(\boldsymbol{\xi} - \mathbf{x} - \mathbf{s}) \leq \mathbf{O} \tag{3.13}$$

in each case is satisfied, but this does not contain the technical constraints of the interconnections.

4. Reliability level

The *reliability index* of the *interconnected system* can be determined more easily than a one subsystem index. The probability of the successful outcomes of the interconnected system without load shedding ($\mathbf{s} = \mathbf{O}$) from (3.11)

$$p = P\{\boldsymbol{\zeta} \leq \mathbf{u}\} = F_{\xi}(\mathbf{u}) \tag{4.1}$$

where the transformed random vector:

$$\boldsymbol{\xi} = \mathbf{D}_{\zeta}^T\boldsymbol{\zeta} + \mathbf{D}_{\eta}^T\boldsymbol{\eta}, \tag{4.2}$$

and $\mathbf{F}_{\xi}$ is the distribution function of $\boldsymbol{\xi}$ transformed random variable vector.

Then the probabilistic constraint expressed by the system, reliability level is:

$$F_{\zeta}(\mathbf{u}) \geq p_S. \tag{4.3}$$

The *subsystem reliability index* can be determined in a more difficult way. The necessary condition of a successful outcome for i-th subsystem is the satisfaction of relation (3.11) ($s_i = 0$), and that of a further general system condition. E.g. this latter condition can be determined by minimizing the total load shedding if the outcome is unsuccessful from the system's viewpoint. In that case the following χ_i convex polyeder has to be determined from (3.11)

$$\chi_i = \left\{ \begin{array}{ll} \boldsymbol{\xi}_i, \boldsymbol{\eta}_i : \mathbf{D}_{\xi}^T(\boldsymbol{\xi}_i - \mathbf{s}) + \mathbf{D}_{\eta}^T\boldsymbol{\eta}_i \leq \mathbf{u} & s_i = 0 \\ \text{Max } \mathbf{l}_n^T(-\mathbf{s}) & \begin{array}{l} s_j \geq 0 \\ j \neq i \end{array} \end{array} \right\}. \tag{4.4}$$

Then the probabilistic constraint expressed by the i-th subsystem reliability level is:

$$p_i = P\{(\xi, \eta) \quad \in \chi_i\} \leq p_{Li} \, . \tag{4.5}$$

The χ_i range can be determined by relation (4.4) if only a few subsystems are interconnected, otherwise detailed simulation of individual outcomes can be used.

5. Optimization model

The objective function to be minimized is the investment cost of a new generating equipment and transmission extension of the interconnected system. For the sake of simplicity it can be assumed that the investment costs are linear functions of the $\mathbf{x}$ resultant generating capacity vector and the $\mathbf{y}$ transfer capacity vector.

The cost of load shedding can be considered if the optimization is analysed as a *two-stage* problem, where in the *second stage* the objective function to be minimized is:

$$l = \mathbf{b}^T \mathbf{s} \tag{5.1}$$

where $\mathbf{b}^T$ is the unit cost vector of load shedding. The constraints are the relation (3.11), (3.12), (4.3), and

$$\mathbf{z} \geq \mathbf{z}(0) \tag{5.2}$$

which shows that the $\mathbf{z}$ extension vector starts out from an initial position of $\mathbf{z}(0)$ vector.

The *first-stage problem* can be formulated in the following manner.

The objective function is:

$$f_0 = \mathbf{a}^T \mathbf{z} + E\{l\} \tag{5.3}$$

where $\mathbf{a}$ is the specific generation and transmission cost vector, $E\{l\}$ is the expectation of l. The objective function to be minimized is subjected to the (5.2) initial condition and to the p_S prescribed reliability level given in (4.3).

As a first approximation we shall neglect $E\{l\}$ and this seems to be admissible because we usually choose p_S very high in practice. The random variables can be considered as interdependent with logarithmic concave measure properties. Therefore, the gradient of system reliability index gives a quasi-concave probability constraint, and thus the first-stage problem can be solved by stochastic programming discussed in Section 8 of reference [1].

The procedure starts with an arbitrary feasible vector $\mathbf{z}(1)$. If $\mathbf{z}(1), \ldots, \mathbf{z}(k)$ are already determined, then we solve the linear program with an arbitrary fixed positive number Θ from (4.1), (4.2), (4.3), (5.2) and (5.3) in the following manner:

Minimize ν subject to

$$\mathbf{a}^T[\mathbf{z} - \mathbf{z}(k)] \leq \nu$$

$$F_\zeta[\mathbf{u}(k)] + \nabla \mathbf{u}\{F_\zeta[\mathbf{u}(k)]\}\mathbf{D}^T[\mathbf{z} - \mathbf{z}(k)] + \Theta\nu \geq p_S. \qquad (5.4)$$

$$\mathbf{z} \geq \mathbf{z}(0)$$

Let us denote the optimal solution of (5.4) $\mathbf{z}^*(k)$ and minimize $\mathbf{a}^T\mathbf{z}$ on the feasible part of ray $\mathbf{z}(k) + \lambda\mathbf{z}^*(k)$, $\lambda \geq 0$, and finally define the minimizing point as $\mathbf{z}(k + 1)$. The convergence proof is shown in reference [2]. Let us substitute the minimizing solution of $\mathbf{z}^0$ in the second-stage program and evaluate the expection of l load shedding cost $E\{l\}$, which can influence the expression (5.3) of the first-stage program published in [1]. It can be noticed that in several cases the first-stage optimization is sufficient alone.

6. Evaluation of J interconnection matrix

Denote in the equivalent network shown in Fig. 3.:
— the partition of the node-branch incidence matrix into tree branches and chords on the basis of positive flow directions as: $\mathbf{A}_t$, $\mathbf{A}_c$;
— similarly the partition of the mesh-branch incidence matrix as: $\mathbf{B}_t$, $\mathbf{I}_c$;
— the diagonal branch admittance and impedance matrices as: $\mathbf{Y}_t$, $\mathbf{Y}_c$ and $\mathbf{Z}_t$, $\mathbf{Z}_c$, respectively;
— the node admittance and impedance matrices as $\mathbf{Y}$ and $\mathbf{Z}$, respectively.
The reference point of the equivalent network is selected in such a manner that to this no chord (with positive direction) is connected. E.g. in Fig. 3. the tree branches are $1-3$ and $2-3$, the chord is $1-2$. So generally

$$\mathbf{I}_{n-1}^T\mathbf{A}_c = \mathbf{O}^T. \qquad (6.1)$$

Obviously

$$\mathbf{B}_t = -\mathbf{A}_c^T(\mathbf{A}_t^{-1})^T. \qquad (6.2)$$

The transfer matrix block of tree defined in paragraph 3. by (3.3) is

$$\mathbf{K}_t = \mathbf{Y}_t\mathbf{A}_t^T\mathbf{Z} \qquad \mathbf{K}_t^{-1} = \mathbf{Y}(\mathbf{A}_t^{-1})^T\mathbf{Z}_t$$

the remaining transfer matrix block

$$\mathbf{K}_c = \begin{bmatrix} -\mathbf{Y}_t\mathbf{A}_t^T \\ \mathbf{Y}_c\mathbf{A}_c^T \\ -\mathbf{Y}_c\mathbf{A}_{c1}^T \end{bmatrix}\mathbf{Z}.$$

Furthermore,

$$\mathbf{Y} = \mathbf{A}_t\mathbf{Y}_t\mathbf{A}_t^T + \mathbf{A}_c\mathbf{Y}_c\mathbf{A}_c^T.$$

From (3.9)

$$\mathbf{J} = \begin{bmatrix} \mathbf{I}'\mathbf{K}_t^{-1} \\ \mathbf{I}_{n-1} \\ \mathbf{K}_c\mathbf{K}_t^{-1} \end{bmatrix} \begin{matrix} 1) = \\ 2) = \\ 3) \end{matrix} \left. \begin{bmatrix} \mathbf{A}_t \; - \; \mathbf{A}_c\mathbf{L} \\ - \; \mathbf{I}_{n-1}^T\mathbf{A}_t \\ \mathbf{I}_{n-1} \} \text{ tree block} \\ - \; \mathbf{I}_{n-1} \\ \mathbf{L} \\ - \; \mathbf{L} \end{bmatrix} \right\} \begin{matrix} \} \text{nodes} \\ \\ +\} \\ -\} \text{tree branches} \\ +\} \\ -\} \text{chords} \end{matrix} \qquad (6.3)$$

chord block

where

$$\mathbf{L} = \mathbf{Y}_c\mathbf{B}_t\mathbf{Z}_t . \qquad (6.4)$$
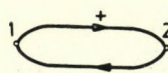
Fig. 5

Example

The equivalent network of two interconnected systems shown in Fig. 5. At first the transfer capacity deviation is not considered. Obviously $A_t = 1$, $B_t = 0$, $L = 0$.

$$\mathbf{J}^T = \begin{bmatrix} x_1 & x_2 & y^+ & y^- \\ 1 & -1 & 1 & -1 \end{bmatrix}$$

furthermore

$$\mathbf{D}^T = \begin{bmatrix} x_1 & x_2 & y^+ & y^- \\ 1 & 1 & 0 & 0 \\ 1 & 0 & 0 & 1 \\ 0 & 1 & 1 & 0 \end{bmatrix} .$$

$$\underbrace{\qquad\qquad}_{\mathbf{D}_\xi^T}$$

From (3.11)

$$(\xi_1 - s_1) + (\xi_2 - s_2) \leq x_1 + x_2 ,$$
$$\xi_1 - s_1 \qquad\qquad \leq x_1 + y^- ,$$
$$\xi_2 - s_2 \leq x_2 + y^+ .$$

These constraints can be seen in Fig. 6. The shaded areas show the different states of load shedding in case of minimum system load shedding.

Now

$$\text{Max} \, (-s_1 - s_2) .$$

Obviously

$$\chi_1 = A_0 \cup A_2 \cup [\text{possible partly} \, (A_2' \cup A_3)]$$
$$\chi_2 = A_0 \cup A_1 \cup [\text{possible partly} \, (A_1' \cup A_3)]$$

The load shedding in A_1', A_2' and A_3 areas can be shared between 1 and 2 subsystem, so that the probability index of both system does not differ significantly from each other.
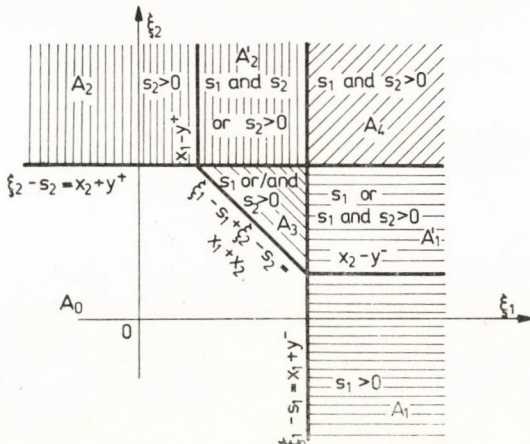
Fig. 6
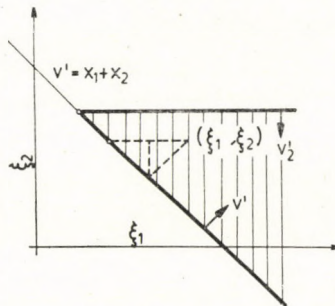
Fig. 7

If the transfer deviation is not neglected from (3.11) then

$$\xi_1 - s_1 + \xi_2 - s_2 \qquad \leq x_1 + x_2,$$
$$\xi_1 - s_1 \qquad + \eta^- \leq x_1 + y^-,$$
$$\xi_2 - s_2 + \eta^+ \leq x_2 + y^+.$$

7. Unreliability index $\bar{p}$ and expected load shedding $S = E\,\{\mathbf{1}_n^T \mathbf{s}\}$ in two interconnected systems

Assuming the ξ_1, ξ_2 random variables with normal distribution to be independent and let η be neglected. Let us determine the unreliability index corresponding to the shaded area shown in Fig. 7.

Introducing the transformation

$$\zeta' = \begin{bmatrix} \zeta' \\ \zeta'_2 \end{bmatrix} = \begin{bmatrix} 1 & 1 \\ 0 & 1 \end{bmatrix} \begin{bmatrix} \xi_1 \\ \xi_2 \end{bmatrix} = \mathbf{D}_{i1}^T \boldsymbol{\xi}.$$
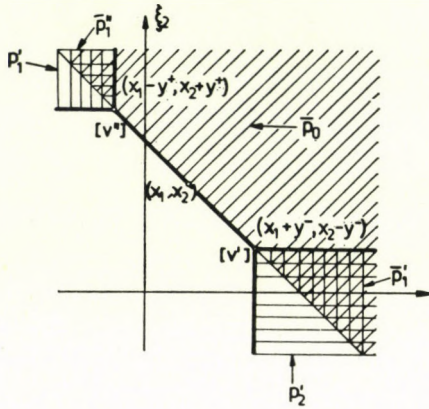
Fig. 8

The unreliability index corresponding to vertically lined area of v' point is

$$\bar{p}'_1 = \int_{\xi'=v'}^{\infty} \varphi\left(\frac{\zeta'}{\sigma_r}\right) \Phi\left(\frac{\sigma_r}{\sigma_1\sigma_2} v'_2 - \frac{\sigma_2}{\sigma_1\sigma_r} \zeta'\right) d\left(\frac{\zeta'}{\sigma_r}\right) \tag{7.1}$$

where φ, Φ the density and distribution function of standardized normal distribution, and

$$\sigma_r^2 = \sigma_1^2 + \sigma_2^2, \quad v' = v'_1 + v'_2, \text{ and from Fig. 8.}$$

$$v'_1 = x_1 + y^-, \quad v'_2 = x_2 - y^-.$$

Without transfer restriction $v'_2 = \infty$, the unreliability index

$$\bar{p}_0 = 1 - \Phi\left(\frac{x_1 + x_2}{\sigma_r}\right). \tag{7.2}$$

The unreliability index corresponding to horizontally lined area of $[v']$ point is

$$\bar{p}'_2 = \left[1 - \Phi\left(\frac{v'_1}{\sigma_1}\right)\right]\Phi\left(\frac{v'_2}{\sigma_2}\right). \tag{7.3}$$

Similarly for $[v'']$ point in Fig. 8 $v'' = v''_1 + v''_2$, $v''_1 = x_2 - y^+$, $v''_2 = x_2 + y^+$.

So

$$\bar{p}_1'' = \int_{\zeta''=v''=v}^{\infty} \varphi\left(\frac{\zeta''}{\sigma_r}\right) \Phi\left(\frac{\sigma_r}{\sigma_1\sigma_2} v_1'' - \frac{\sigma_1}{\sigma_2\sigma_r} \zeta''\right) d\left(\frac{\zeta''}{\sigma_r}\right), \tag{7.4}$$

and

$$\bar{p}_2'' = \Phi\left(\frac{v_1''}{\sigma_1}\right)\left[1 - \Phi\left(\frac{v_2''}{\sigma_2}\right)\right]. \tag{7.5}$$

The resultant unreliability index is from (7.1) to (7.5)

$$\bar{p} = \bar{p}_0 - \bar{p}_1' + \bar{p}_1'' - \bar{p}_2' + \bar{p}_2''. \tag{7.6}$$

The expected load shedding corresponding to the vertically lined are a shown in Fig. 7. and 8. as

$$S_1' = \sigma_r \int_{\zeta'=v'=0}^{\infty} \left(\frac{\zeta'}{\sigma_r} - \frac{v}{\sigma_r}\right) \varphi\left(\frac{\zeta'}{\sigma_r}\right) \Phi\left(\frac{\sigma_r}{\sigma_1\sigma_2} v_2' - \frac{\sigma_2}{\sigma_1\sigma_r} \zeta'\right) d\left(\frac{\zeta'}{\sigma_r}\right). \tag{7.7}$$

Without transfer restriction the expected load shedding is

$$S_0' = \sigma_r \left\{ \varphi\left(\frac{x_1 + x_2}{\sigma_r}\right) - \left(\frac{x_1 + x_2}{\sigma_r}\right)\left[1 - \Phi\left(\frac{x_1 + x_2}{\sigma_r}\right)\right]\right\}. \tag{7.8}$$

The unreliability index corresponding to horizontally lined area in Fig. 8. can be expressed as

$$S_2' = \sigma_1 \left\{ \varphi\left(\frac{v_1'}{\sigma_1}\right) - \frac{v_1'}{\sigma_1}\left[1 - \Phi\left(\frac{v_1'}{\sigma_1}\right)\right]\right\} \Phi\left(\frac{v_2'}{\sigma_2}\right), \tag{7.9}$$

$$S_1'' = \sigma_r \int_{\zeta''=v''=v}^{\infty} \left(\frac{\zeta''}{\sigma_r} - \frac{v}{\sigma_r}\right) \varphi\left(\frac{\zeta''}{\sigma_r}\right) \Phi\left(\frac{\sigma_r}{\sigma_1\sigma_2} v_1'' - \frac{\sigma_1}{\sigma_2\sigma_i} \zeta''\right) d\left(\frac{\zeta''}{\sigma_r}\right), \tag{7.10}$$

$$S_2'' = \sigma_2 \left\{ \varphi\left(\frac{v_2'}{\sigma_2}\right) - \frac{v_2'}{\sigma_2}\left[1 - \varphi\left(\frac{v_2'}{\sigma_2}\right)\right]\right\} \Phi\left(\frac{v_1'}{\sigma_1}\right). \tag{7.11}$$

The resultant expected load shedding from (7.7) to (7.11)

$$S = S_0 - S_1' + S_1'' - S_2' + S_2''. \tag{7.12}$$

Example:

Generating and transfer powers and capacities in p.u. are

$$\hat{g}^T = [20\ 20], \quad \hat{d}^T = [18.4\ 21.6], \quad \hat{\imath} = -1.6,$$
$$r^T = [3.2\ 3.2], \quad \bar{\mu}^T = [1.6\ 1.6],$$
$$\sigma_1 = 1, \quad \sigma_2 = 1 \quad \text{so} \quad x^T = [0\ 3.2].$$

The unreliability indices and the expected load sheddings are shown in Table 1.

Table 1

x_1	$y^+=y^-$	v_1'	v_2'	$\bar{p}\cdot 10^3$				$S\cdot 10^3$		
				1 & 2	1	Σ		1 & 2	1	Σ
				system				system		
0,2	2,2	2,2	1	10,3	11,7	22,0		5,31	4,14	9,45
	2,4	2,4	0,8	10,9	6,5	17,4		5,57	2,14	7,71
	2,6	2,6	0,6	11,4	2,5	13,9		5,65	1,00	6,65
	2,8	2,8	0,4	11,6	1,7	13,3		5,73	0,41	6,14
	3	3	0,2	11,8	0,8	12,6		5,76	0,16	5,96
	∞			11,9		11,9				5,81
0,2	2,2	2,4	1	7,3	6,9	14,2		3,58	2,29	5,87
	∞			8,2		8,2				3,81

$(x_2 = 3,2)$

Obviously, the extension of interconnection is the optimum for obtaining the reliability level of 0,985. However, for the boundary $S = 6 \cdot 10^{-3}$ of expected load shedding the generation extension of the 1st subsystem shows a more favourable solution.

Conclusion

The presented probabilistic constrained programming, the discussed admissibility requirements, the reliability and load shedding evaluations can give useful tools for the decisions of new generating and transfer capacity investments and for some operational standpoints in a power pool.

The technical feasibility of the derived global optimum has to be checked by means of a detailed investigation, e.g. short circuit, stability conditions. The integer optimum solution is approached by the presented programming.

Acknowledgements

REFERENCES

1. PRÉKOPA, A.: Contribution to the Theory of Stochastic Programming. *Mathematical Programming* 4 (1973), 202—211, North-Holland Publication Co.
2. PRÉKOPA, A.: On Probabilistic Constrained Programming, held in Princeton 1967. Princeton University Press, Princeton, N. J. 1970, pp. 113—131
3. SPEARS, H. T.—KENNETH, L.—HICKS, STEPHEN—LEE, T. V.: Probability of Loss of Load for Three Areas, *IEEE* Vol. PAS-80 (1970), 521—526
4. PAPOULIS, A.: Probability, Random Variables and Stochastic Processes. McGraw-Hill Kogakusha Ltd., Tokio, 1965

Appendix A

Mathematical symbols for an interconnected system containing n subsystems, which are the nodes (buses) of an equivalent network with q branches (partitioned into t tree branches and c chords) are the following:

h, r, and **x**   installed, reserve and resultant capacity vectors, respectively, (n dimensional, in MW); *unknown variables to be determined,*

g, and **d**   generation, and demand power vectors resp. (n dimensional, in MW's),
i   real net power injection of each bus of the equivalent network denoted as bus power (n-dimensional, in MW),

ĝ, d̂, î   scheduled value vectors of **g, d,** i,

$\delta = \mathbf{d} - \hat{\mathbf{d}}$ demand deviation vector with estimated probability distribution having a zero mean value ($\bar{\delta} = \mathbf{0}$, n dimensional, in MW),

μ capacity deficiency vector with estimated (joint) probability distribution (n dimensional, in MW),

$\xi = \mu + \nu + \bar{\mu}$ subsystem's *random vector*, defined by (0.1) and (0.2) (n dimensional, in MW),

$\bar{\mu}, \bar{\xi}$ mean value vectors of μ, ξ resp.,

s   load shedding vector (n dimensional, in MW),

α generating surplus power vector (n dimensional, in MW),

$\mathbf{y} = \begin{bmatrix} \mathbf{y}^+ \\ \mathbf{y}^- \end{bmatrix}$ transfer capacity vector (partitioned to $\mathbf{y}^+$ positive direction vector, and $\mathbf{y}^-$ negative direction vector, both q dimensional; **y** is $2q$ dimensional; all vectors in MW); *unknown variables to be determined,*

$\mathbf{y}_t \ \mathbf{y}_c$ transfer capacity vector partitioned to a tree branch block with positive direction ($n - 1$ dimensional in MW, and chord block containing all chords and the negative-directed part of tree branches ($n - 1 + 2c$ dimensional; in MW),

$\beta = \begin{bmatrix} \beta_t \\ \beta_c \end{bmatrix}$ transfer surplus power vector (partitioned to tree and chord blocks; $2q$, $n - 1$, $n - 1 + 2c$ dimensional, resp.; in MW),

$\eta = \begin{bmatrix} \eta^+ \\ \eta^- \end{bmatrix} = \begin{bmatrix} \eta_t \\ \eta_c \end{bmatrix}$ transfer capacity deviation vector (partitioned to positive and negative direction, or to tree and chord blocks $2q$; q, q; $n - 1$, $n - 1 + 2c$ dimensional, resp; in MW); *random vector* having a zero mean value ($q = n - 1 + c$),

$\mathbf{A} = \begin{bmatrix} \mathbf{A}_t \\ \mathbf{A}_c \end{bmatrix}$ node-branch incidence matrix (partitioned to tree and chord blocks; $2q \times (n - 1)$, $(n - 1) \times (n - 1)$, $(n - 1 + 2c) \times (n - 1)$ dimensional, resp.),

$\mathbf{B} = [\mathbf{B}_t, \mathbf{I}_c]$ mesh-branch incidence matrix (partitioned to tree and chord blocks; $2c \times 2q$; $2c \times (n - 1)$, $2c \times 2c$ dimensional, resp.),

$\mathbf{Y}_t, \mathbf{Y}_c$ and $\mathbf{Z}_t, \mathbf{Z}_c$ diagonal branch admittance, and impedance matrices (for tree blocks $(n - 1) \times (n - 1)$ dimensional, for chord blocks $(n - 1 + 2c) \times (n - 1 + 2c)$ dimensional),

Y, and **Z**   node admittance, and impedance matrices resp. (both $(n - 1) \times (n - 1)$ dimensional),

$\mathbf{K} = \begin{bmatrix} \mathbf{K}_t \\ \mathbf{K}_c \end{bmatrix}$ transfer power distribution matrix relating branch flows to net bus injection partitioned to tree and chord blocks ($2b \times (n-1)$, $(n-1) \times (n-1)$, $(n - 1 + 2c) \times (n-1)$ dimensional, their variation by system interconnection is neglected,

γ auxiliary vector $2q + 1$ dimensional composed by (3.4),
Γ region of γ,

$\mathbf{d}_i = \begin{bmatrix} \mathbf{d}_{Ni} \\ \mathbf{d}_{Ti} \\ \mathbf{d}_{ci} \end{bmatrix}$ $n + 2q$ dimensional vector partitioned to node, tree, and chord blocks (n, $n - 1$, and $n - 1 + 2c$ dimensional) as a basic solution of (3.8),

J $(n + 2q) \times (n - 1)$ dimensional interconnection matrix. Its transposed J^T matrix is given by (3.9),

$\mathbf{D} = [\mathbf{d}_1, \ldots, \mathbf{d}_i, \ldots, \mathbf{d}_v]$ $(n + 2q) \times v$ dimensional transformation matrix. Its transposed $\mathbf{D}^T$ matrix is partitioned to node $\mathbf{D}_\xi$ block and $\mathbf{D}_\eta$ branch block.

Latter contains branches random capacity deviation. Index v is the number of basic solutions of $\mathbf{d}_i$ on the basis of 3.8),

z   composed system capacity vector consisting of a generation and transfer capacity vector as unknown variables to the optimized ($n + 2q$ dimensional),

u   transformed system vector (v dimensional),

ζ transformed random vector (v dimensional),

F_μ F_δ, F_ξ, F_η, F_ζ joint distribution functions of μ, δ, ξ, η, ζ random vectors resp.,

f_μ, f_δ, f_ξ, f_η f_ζ joint density functions of μ, δ, ξ, η, ζ, random vectors, resp.,

a   specific generation and transmission cost vector ($n + 2q$ dimensional, in monetary units / MW),

b   unit cost vector of load shedding (n dimensional, in monetary units / MW),

l load shedding cost (in monetary units),

f_0 objective function to be minimized (in monetary units),

Φ and φ Gaussian distribution and density functions,

σ_i standard deviation of i component (in MW),

p reliability index of the interconnected system,

$\bar{p} = 1 - p$ unreliability index of the interconnected system,

p_i reliability index of i-th subsystem,

p_S reliability level of the interconnected system,

p_{Li} reliability level of the i-th subsystem,

$\mathbf{1}_{n-1}$ $n - 1$ dimensional vector, each component is 1,

$\mathbf{I}_{n-1}$ $n - 1$ dimensional unit matrix (diagonal matrix with components of value 1),

$\mathbf{\Gamma} = \begin{bmatrix} \mathbf{I}_{n-1} \\ \mathbf{1}_{n-1} \end{bmatrix}$ $n \times (n - 1)$ dimensional matrix,

$\nabla_u F = \left[\dfrac{\partial}{\partial u_1} F, \ldots, \dfrac{\partial}{\partial u_j} F, \ldots, \dfrac{\partial}{\partial u_v} F \right]$ is the gradient (in form of a v dimensional row vector) of scalar F with respect to the v dimensional vector **u**,

$\mathbf{z}(o)$, $\mathbf{u}(o)$ the vector variables of **z**, **u** resp. in the original state (before expansion) of the interconnected system,

$\mathbf{z}(k)$, $\mathbf{u}(k)$ the vector variables of **z**, **u** resp. in k-th state of the optimization process.

Appendix B

Mathematical formulae and terms utilized in this paper are the following:

$\mathbf{a}^T$, and $\mathbf{A}^T$ the transposed **a** vector, and **A** matrix, resp; i.e. the i row and j column component of $\mathbf{A}^T$ corresponds to j row and i column component of **A**,

$\mathbf{A} = \begin{bmatrix} \mathbf{A}_t \\ \mathbf{A}_c \end{bmatrix}$ $(n' + n'') \times m$ hypermatrix composed by $\mathbf{A}_t$ $n' \times m$ matrix and $\mathbf{A}_c$ $n'' \times m$ matrix (the transposed hypermatrix can be similarly formed)

$\chi =$ $(\mathbf{x} : \mathbf{x} = \mathbf{A}\mathbf{y}; \mathbf{y} \geq \mathbf{0})$ a region determined in n dimensional vector space by the relation of $\mathbf{x} = \mathbf{A}\mathbf{y}$

$$\mathbf{y} \geq \mathbf{0}, \text{ where}$$

x, **y** and **A** are $n \times 1$, $m \times 1$, and $n \times m$ dimensional, resp.

$a \in A$ a is an element of region A

$A \cup B = C$ union of regions A and B

$a \in A$, $b \in B$
$\quad c \in C$ if $c = a$ or b

$A \cap B = D$ intersection of regions A and B

$a \in A, \; b \in B$
$\quad d \in D \quad$ if $d = a$ and b

$P(\Re)$ $\qquad$ the probability of an event $\Re$ consisting of outcomes specified by ξ ramdom variable. E.g. $\Re = \{\xi : \xi \leq x\}$ than $P(\Re) = P(\xi \leq x)$

$\bar{\xi} = E(\xi) = \int\limits_{-\infty}^{\infty} \xi f(\xi)\, d\xi \quad$ mean value of ξ random variable,

$\sigma^2 = E\{(\xi - \bar{\xi})^2\} = \int\limits_{-\infty}^{\infty} (\xi - \bar{\xi})^2 f(\xi) d\xi \quad$ variance or dispersion σ^2, where its positive square root σ is called standard deviation,

$F_\zeta(u) = \int\limits_{-\infty}^{u} f(\zeta) d\zeta \quad$ the distribution function of ζ continuous random variable can be expressed by the integral of $f(\zeta)$ density function,

$\varphi\left(\dfrac{\xi}{\sigma}\right) = \dfrac{1}{\sigma\sqrt{2\pi}}\, e^{-\frac{1}{2}\left(\frac{\xi}{\sigma}\right)^2} \quad$ density function of ξ normally distributed random variable with σ standard deviation,

$\varphi(\xi)$ $\qquad$ density function of ξ normally distributed standardized random variable $(\sigma = 1)$

$\Phi(x) = \dfrac{1}{2} + erf\, \dfrac{x - \bar{\xi}}{\sigma} \quad$ where $\quad erf = \dfrac{1}{\sqrt{2\pi}} \int_0^x e^{-y^2/2}\, dy$

$E\{g(\xi)\} = \int\limits_{-\infty}^{\infty} \ldots \int\limits_{-\infty}^{\infty} g(\xi_1, \ldots, \xi_m) d\xi_1 \ldots d\xi_m$

expectation of $g(\xi)$ scalar-vector function, ξ is m-dimensional random vector with $f(\xi_1, \ldots, \xi_m) = f(\xi)$ joint distribution function,

$c_{ij} = E\{(\xi_i - \bar{\xi}_i)(\xi_j - \bar{\xi}_j)\}$ covariance of ξ_i, ξ_j random components of ξ.

Planung der optimalen Investitionen von elektrischen Verbundnetzen unter Verwendung der durch Wahrscheinlichkeitsvariable begrenzten Programmierung. — Mit Hilfe der durch Wahrscheinlichkeitsveränderliche begrenzten Programmierung wurde ein verwendbares Verfahren für die Bestimmung der optimalen Vergrößerung der Kraftwerks- und Übertragungskapazität in einem Verbundsystem ausgearbeitet. Die Methode eliminiert die fallweise auftretenden Übertragungsleistungen. Die Zulässigkeit und die Zuverlässigkeit der Leistungsabweichungen werden durch die Erzeugungs- und die Übertragungsbegrenzungen bestimmt. Die verfügbaren Produktions- und Übertragungskapazitäten sowie die Abweichungen der Spitzenlasten treten als Wahrscheinlichkeitsvariable auf. Im Optimierungsprozeß ergänzt das vorgeschriebene Zuverlässigkeitsniveau als untere Grenze die technischen Schranken. Im weiteren Verlauf können auch die Kosten der Lastbeschränkung in Betracht gezogen werden. Ein einfaches Beispiel demonstriert die Methode.

Проектирование оптимальных мощностей капитального строительства для объединенных электроэнергетических сетей, используя при этом программирование, ограниченное переменными вероятности. В статье с помощью программирования, ограниченного переменными вероятности, излагается применимое на практике средство, пригодное для определения оптимального увеличения мощностей электростанций и передачи. Излагаемый метод ликвидирует периодически возникающие мгновенные мощности передачи. Допустимость и надежность отклонений мощности определяют ограничения передачи. Имеющиеся в распоряжении мощности по выработке и передаче, а также пиковые нагрузки фигурируют в качестве переменных вероятности. Предписанный уровень надежности дополняет технические ограничения в процессе оптимизации, а именно в качестве нижней границы. В дальнейшем можно учитывать также расходы по ограничению нагрузки. Метод демонстрируется на простом примере.

PRELIMINARY STUDY OF THE INTERACTIONS OF LOW ENERGY OXYGEN IONS WITH SOLID CARBON AND PLATINUM TARGETS

J. LUKÁCS*,

CORR. MEMBER OF THE HUNG. AC. SCI.

and

P. GADÁNYI**

The aim of this study was to show the possibility of measuring the energy distribution of charged particles produced by the interaction of low energy oxygen ions with carbon. The oxygen ions were produced by a Kistemaker-ionsource working with a hot cathode Penning-discharge. In a first step the beam was not mass-analyzed and the measurements were made only in the pressure range of 10^{-5}—10^{-6} torr. Authors succeeded in producing an oxygen ion beam having, first about 45 eV and now about 15 eV kinetic energy, with 20—30 nA intensity. They made preliminary measurements with an 45 eV oxygen ion beam. The targets were outgassed on the temperature of about 1000 °C for several hours in high vacuum. Short discussion of the results of the calculated energy distributions of the backscattered charged particles from carbon and platinum targets, and of the possible reaction mechanisms will be given.

The aim of this study is to investigate the additional translational energy of CO^+ ions derived by the $C + O^+$ combustion process. In the frame of this work we measured the energy distribution of ionized products of the gas phase–solid state reaction of ionized oxygen with solid carbon, in comparison with the energy distribution of the incident oxygen ion beam.

For this purpose we developed an apparatus. This apparatus consists of a Kistemaker-ion source, [1] working with a hot-cathode Penning-discharge an electrostatic lens for the focussing and forming of the ion beam, a heatable target, a sphere-shaped detecting electrode enveloping the target for the detection of the charged particles leaving the target, a Faraday cage shielding the detector sphere from spurious ions, the target heater and the pumping and measuring sections. We had decided to build a Kistemaker-source, and for building the source it seemed to be simpler than to build a duoplasmatron, having little experience in ion sources. On the other hand the Kistemaker-ion source gives a relatively large intensity beam, with little ion energy and little ion energy spread.

We built the Kistemaker-ion source as large as possible, to get enough ion intensity with little extraction voltages.

Therefore the hot-cathode: a 1 mm diameter tungsten wire, wound in a plane-spiral was heated with 50 A DC current. The anode voltage was about 40—50 V. The extraction voltage was 100 V. The reflector plate was on cathode

* Dr. J. Lukács ⎫
** P. Gadányi, ⎬ Cservenka M u. 86. H-1158 Budapest. Hungary

potential. The potential of the bottom-plate electrode will be discussed in detail later.

The ion source was pumped by a 100 l/sec capacity oil diffusion pump with a water-cooled baffle. The cylindrical anode was made of copper and was water-cooled. The housing of the ion-source and all the other metal components were made of stainless steel. The isolation was made of teflon and of glass re-inforced epoxide. The bottom-plate electrode, the housing of the ion source, and especially the cathode current feed throughs were water-cooled. All water cooling circuits were isolated from each other.
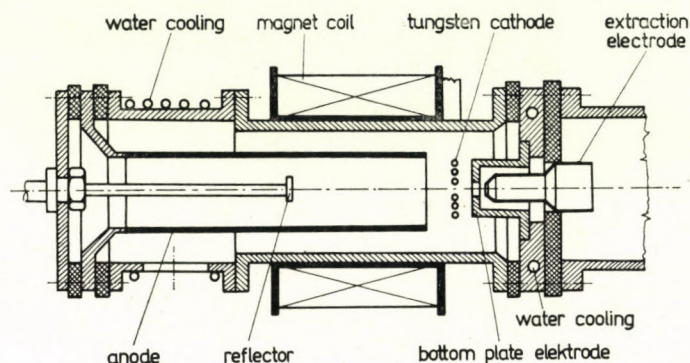
Fig. 1. Complete scheme of ion source

In Fig. 1. the structure and the details of the ion source are shown. Our aim was to produce a large intensity, low energy oxygen–ion beam.

During the experimental work, we obtained the following results. We could not decrease the anode voltage below 40 V, because the discharge current became diminishingly low. To decrease the extraction voltage below 100 V was impossible too, on similar grounds. Because of this we could extract from the ion source positive oxygen ions with about 150 eV energy.

As is known, the electrons, emitted by the hot cathode, fly towards the cylindrical anode and will start to go on spiral paths around an axis which lies parallel with the axis of the cylindrical anode, due to the axial magnetic field. Because of this a potential well is formed for the positive ions, which are generated in the gas by the impact ionization of the electrons, in the axis of the device.

It is possible to focus the ions in a beam which goes into the extraction electrode, by selecting suitable potentials for the anode, the bottom-plate electrode and the extraction electrode.

When the anode voltage is 40 V, the extraction voltage is −100 V, the voltage of the bottom-plate electrode was selected experimentally so, that the

extracted ion beam intensity should be the highest. The optimum bottom-plate voltage was found to be about $+5 - 10$ V with respect to the cathode. (All voltages are given with respect to the cathode.) In this case rather high electron current flows to the bottom-plate electrode.

The total electrical circuit diagram of the ion source is shown in Fig. 2.[2]

With the electrostatic lens, which was behind the extraction electrode, we could focus the ion beam to the target, possibly so, that the incident beam did not arrive to the detector sphere. This was achieved by a metal-box sur-
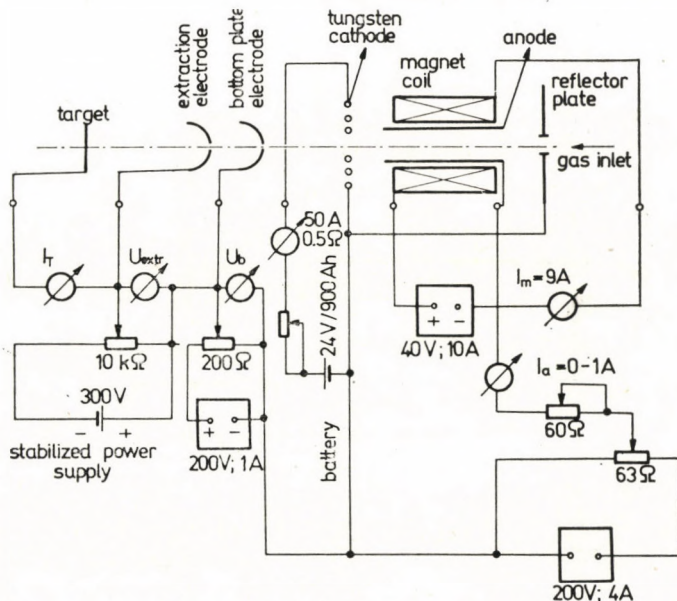
Fig. 2. Circuit diagram of ion source

rounding the detector sphere (Faraday cage), and which was electrically connected to the target. The maximum ion beam intensity achieved by us on a 20 mm diameter target was about $50-100$ nA with 45 eV kinetic energy.

The geometrical arrangement of the bottom-plate electrode of the ion source, the electrodes of the electrostatic focussing lens, the target, the detector-sphere and the Faraday box of the detector, are all shown in Fig. 3.

The main vacuum chamber, which contains the detector and target etc., was pumped by an oil-diffusion pump of 1200 l/sec capacity and with a water-cooled baffle.

The total measuring circuit diagram, and the heater-circuit diagram for outgassing of the target are shown in Fig. 4.

We could produce 45 eV kinetic energy positive oxygen ions by connecting on to the target a retarding potential of 100 V.

We have tried to apply the 11-element retardation lens of Gustafsson and Lindholm too [3] but we experienced a significant decrease of the total ion beam current, as the kinetic energy of the ions decreased below the anode voltage of the ion source. Notwithstanding we have succeeded in producing a positive oxygen ion beam of 15 eV kinetic energy and 20—30 nA intensity.
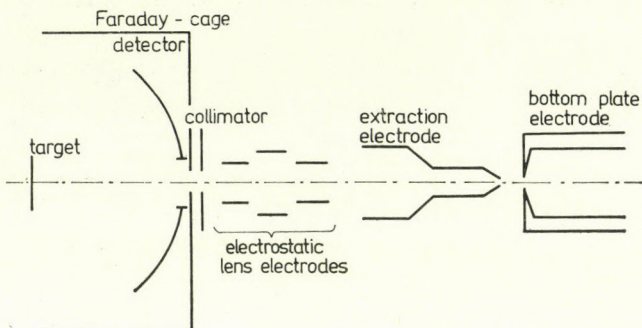
Fig. 3. Geometrical arrangement
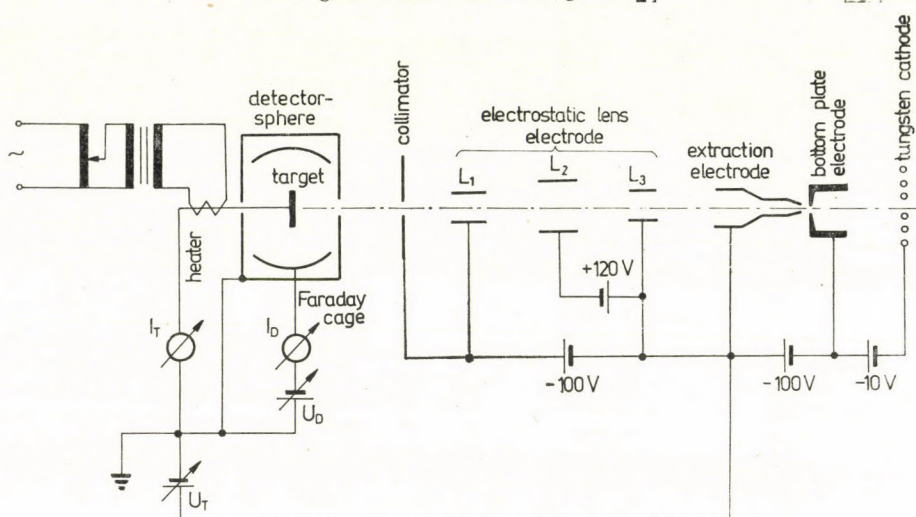
Fig. 4. Circuit diagram of the measuring apparatus

But we did not succeed in getting useful results with this low energy ion beam, because in this case, the ratio of the positively charged particles to the negatively charged ones was less than 1, in the detected current scattered from the target, and without mass-separation we could not apply our calculation method for the determination of the energy distribution of scattered positive ions.

Therefore, in the present state of activities we had to use the 45 eV energy ion beam.

Since the target has to be outgassed, which was done by heating the target, therefore, the target was made hollow, and in the hole was placed the heater, a coil wound of 1 mm diameter tungsten wire, and which was heated with an AC current of 100 A.

Due to the electron emission of the tungsten, and the alternating magnetic stray field of the very high heater currents, the measurements of the
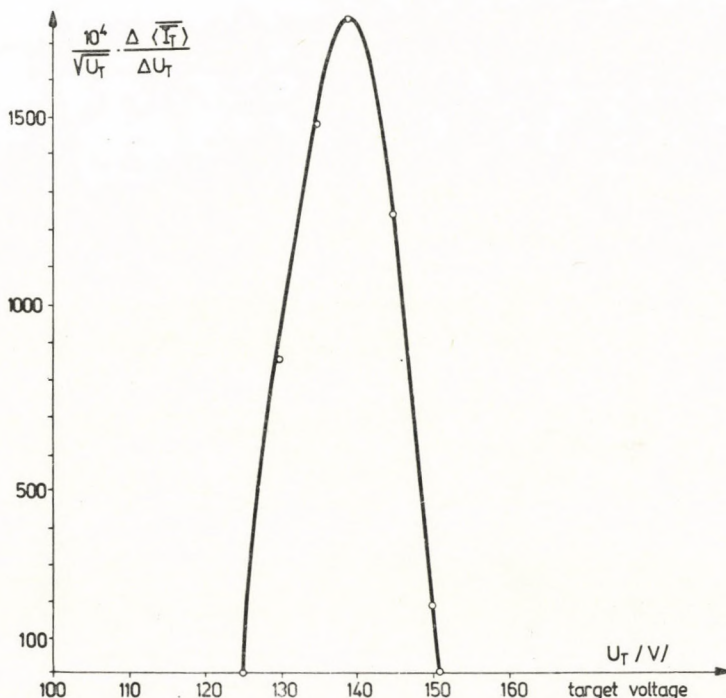
Fig. 5. Incident ion energy distribution

very low ion currents, were disturbed, so we acted in the following way: before the measurement of ion-scattering, the target was heated at 1000°C temperature for 3 hours. After this heat-cycle, we switched off the heater current and after cooling down, when the target reached 5 — 600°C temperature, and the electron emission of the heater was totally nil, we started to measure the scattered ion currents.

All high temperature measurements were made between 600 and 300°C.

The measured results are shown in the following Figures. Figures 5 — 9. were evaluated according to dr. J. ANTAL's theory [4].

Figure 5 shows the energy distribution of the incident ion beam averaged over warm and cold platinum and solid carbon targets.

The averaging process was the following:

We measured I_T target current and I_D detector current, as the functions of U_T target voltage, in the cases of room temperature carbon target, warm carbon target, room temperature platinum target and warm platinum target, respectively, when U_D detector voltage was zero.

These groups of measurements, which were determined under similar conditions, were averaged. So we got $\bar{I}_T$ and $\bar{I}_D$ values in the four main cases. Then we added the two values in each group. So we obtained those values, which are written in brackets:

$$\bar{I}_T + \bar{I}_D = \langle \bar{I}_T \rangle$$
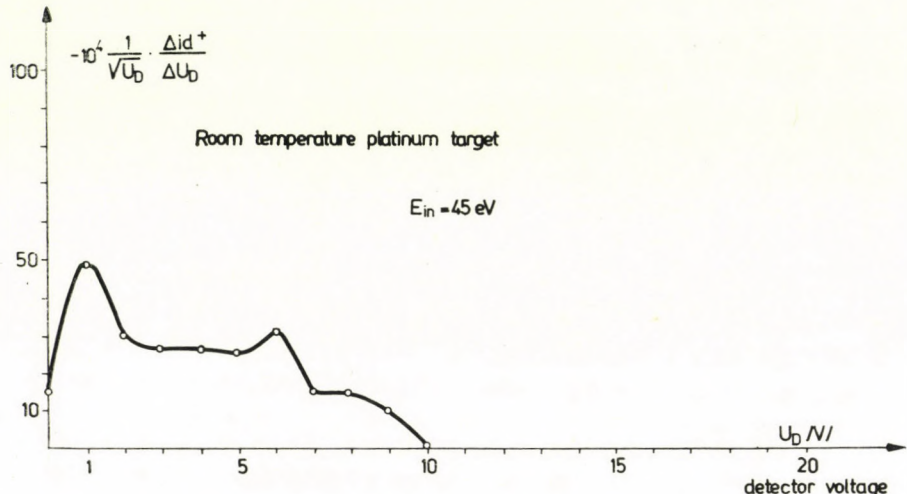
Fig. 6. Measured energy distribution of scattered positive ions

Now, in all four main cases, we averaged those I_T values, which correspond to the same U_T value.

So we averaged this values, over the four main cases, when U_T was constant. Thus we got another average value, which was denoted by $\langle \bar{I}_T \rangle$.

Hence it was clear, that this $\langle \bar{I}_T \rangle$ value was a function of U_T. Figure 5 shows the derivative of this quantity divided by $\sqrt{\overline{U_T}}$ and multiplied by 10^4. So we brought to the same form, the incident ion energy distribution, as was the backscattered ion energy distributions.

By comparison we show Fig. 6 and Fig. 7, which were measured in cold condition, on platinum and solid carbon targets, respectively. Before each measurements, naturally the targets were outgassed at 1000°C for 3 hours.

As is known, the derivative of the ion current by the retardation voltage of the collecting electrode, multiplied by $(-e)$, (the elementary charge) gives information about the energy distribution of the incident ions. (If, and only if the ion current contains only positive, or only negative charge carriers.)

In case of a good ion source, the $\blacktriangle E$ energy-spread of the ions is small, relative to the maximal value E_{max}.

Unfortunately, this was the main problem of the experiment, because we could diminish E_{max} arbitrarily with a retardation lens, but the $\blacktriangle E$ energy-spread could not be lessened, so the relative energy-spread $\blacktriangle E/E_{max}$ increased, and at 10 eV incident ion energy, the $\blacktriangle E$ energy-spread was greater than E_{max}.
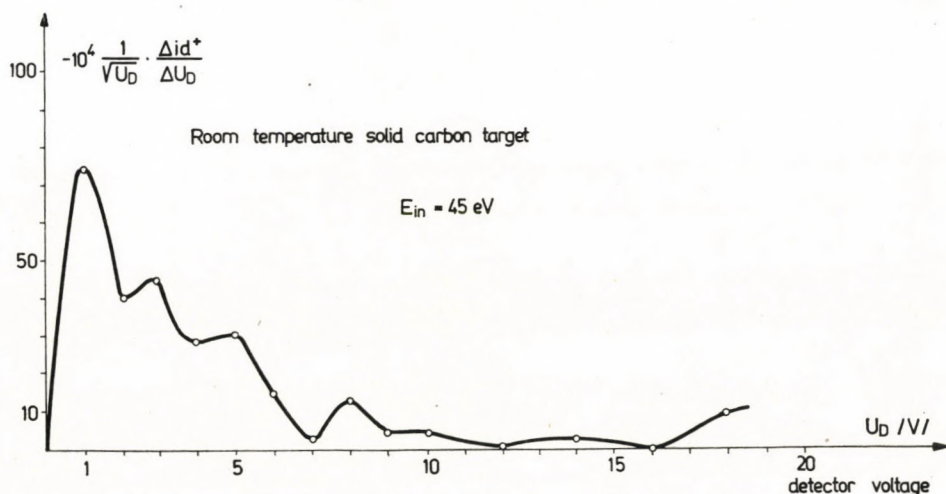
Fig. 7. Measured energy distribution of scattered positive ions

Therefore, all the above measurements were made without retardation lens, with $U_T = +100$ V retardation voltage.

The interpretation of the measured energy peaks is quite difficult. Finally in Fig. 8. and Fig. 9. in high temperature condition, we presented the energy distribution of the scattered positive ions from platinum and solid carbon targets, respectively.

These scattered ion energy distributions show that the energy distribution of ion backscattering from the platinum target can be explained only by the assumption, that the ion source emits O^+ oxygen atomic ions.

We assumed that on platinum, no chemical reaction takes place. On the other hand, we got a well determined backscattered ion energy peak of 32 eV from the platinum.

As is known from the literature the backscattered ion energy distribution of $100-200$ eV energy incident ions may be well explained by the simple binary collision theory of free atoms.

On this ground the measured energy peak can be explained with the assumption, that the target particle is a free platinum atom, with atomic

mass number 196, and the bombarding particle is a particle with atomic mass number 16, i.e. an oxygen atomic ion. (cf. formulae in Figs 6—9.) Because the working conditions of the ion source were the same in cases of
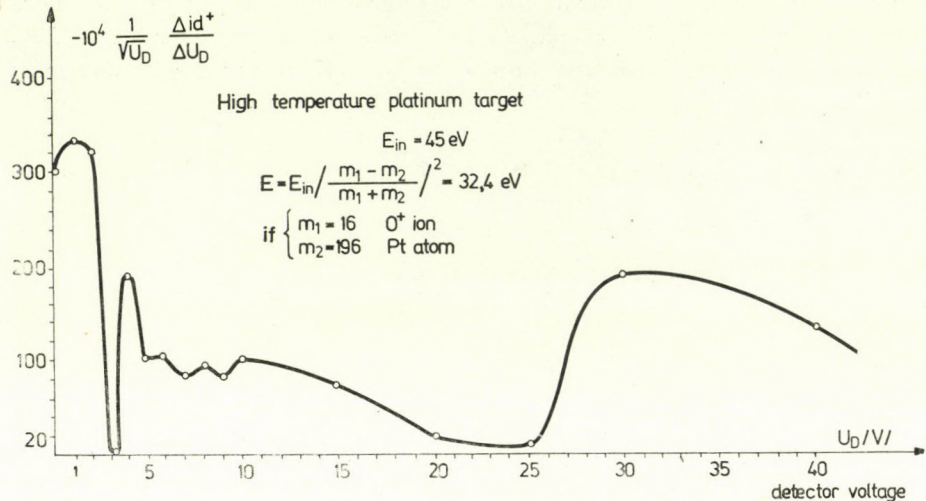
Fig. 8. Measured energy distribution of scattered positive ions
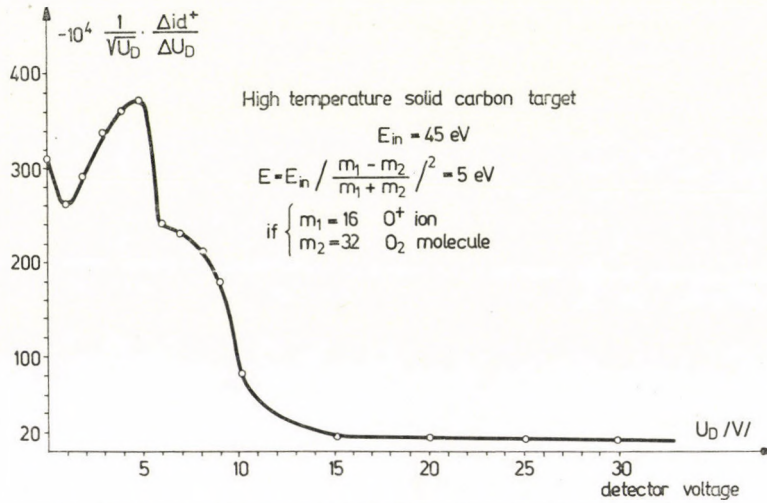
Fig. 9. Measured energy distribution of scattered positive ions

bombarding platinum and solid carbon targets, we had to assume that in both cases, the incident ions were O^+ oxygen atomic ions.

In this case, the results of the scattered ion energy distribution from the solid carbon target can be explained only with a target particle of an atomic mass of 32, that is, the mass of an oxygen molecule. This means that

either we were unable to outgas the solid carbon, that is graphite target, or we had to assume, that a chemical reaction takes place, that is:

$$C + O^+ = CO^+$$
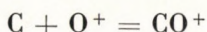
and the ionized reaction product, the CO^+, (or the product of some other reactions) leaves the solid carbon target, with 5 eV kinetic energy.

Acknowledgments

LITERATURE

1. Kistemaker, J., Douwes Dekker, H. L.: Physica, **16,** 198, 209, 1950.
2. Academy of Sciences Institute of Electronics, Uzbek Soviet Socialist Republic, Publisher "FAN" Uzbek SSR Taskhent 1972. Atomic collisions on solid surfaces. Arifov, U. A., Gruich, D. D., Jermakov, G. E., Halmirzajev Z., Second chapter p. 28—55
3. Atomic and molecular processes. Ed. by D. R. Bates 1962. Academic Press. New York and London. p. 705.
4. Unpublished theory and private communications of Dr. J. Antal

Anfängliche Untersuchung der Wechselwirkung von Oxygenionen niedriger Energie mit festen Karbon- und Platintargeten. Zweck der Untersuchung war, die Möglichkeit für die Messung der Energieverteilung der bei der Wechselwirkung von Sauerstoffionen und fester Kohle entstehenden geladenen Teilchen nachzuweisen. Die Sauerstoffionen wurden durch eine mit Penning-Entladung arbeitende Kistemaker-Ionenquelle erzeugt. Als erster Schritt wurde das Strahlbündel nicht massenanalysiert und die Messungen wurden nur im Druckbereich $10^{-5} \ldots 10^{-6}$ Torr durchgeführt. Es gelang zuerst einen Ionenstrahl mit 45 eV Energie, später einen solchen mit 15 eV kinetischer Energie und $20 \ldots 30$ nA Intensität zu erzeugen. Die anfänglichen Untersuchungen wurden mit dem 45 eV Sauerstoffionenbündel durchgeführt. Die Targetes wurden mehrere Stunden lang im Hochvakuum entgast. Die Verfasser werden demnächst aufgrund der Auswertung der Versuchsergebnisse über die berechnete Energieverteilung der von der Kohle und dem Platin zurückgestreuten geladenen Teilchen und die möglichen Reaktionsmechanismen berichten.

Начальные исследования взаимодействия кислородных ионов низкой энергии с на графитовыми и платиновыми мишенвями. Данными исследованиями была поставлена цель — показать возможность измерения распределения энергии частиц, образующихся при взаимодействии кислорода и графит. Кислородные ионы вырабатывались ионным источником типа Кистемакер, работающим Пеннинговым разрядом с накальным катодом. В качестве первого шага пучок не был подвергнут массовому анализу и только при давлениях в пределах 10^{5}—10^{6} Торр были выполнены соответствующие измерения. Удалось получить сперва ионный пучок кислорода с кинетической энергией в 45 эВ, а позднее с кинетической энергией в 15 эВ с интенсивностью 20—30 А. Начальные исследования проводились при использовании ионного пучка кислорода с энергией 45 эВ. Использованные при исследованиях мишени подвергались процессу обезгаживания при температуре 1000° С в течение нескольких часов. На основе оценки полученных при измерениях данных приведены заключения относительно расчетных распределений энергии заряженных частиц, отраженных с графита платины, и возможных механизмах реакции.

BODENMECHANISCHE UNTERSUCHUNGEN FÜR EINE WIRTSCHAFTLICHE TECHNOLOGIE ZUM SCHÜTTEN UND VERDICHTEN VON DÄMMEN

M. KINZE*

Staudämme müssen für alle Bau- und Betriebszustände eine ausreichende Standsicherheit aufweisen. Außerdem dürfen die unter Eigengewicht und Wasserdruck auftretenden Verformungen die Funktion des Dammes, insbesondere von Dichtung, Dichtungsanschlüssen und Schutzschichten nicht in Frage stellen. Der Aufsatz befasst sich mit diesen Problemen auf Grund von Labor- und Feldversuchen.

1. Veranlassung und Zielstellung

Es ist erforderlich, den Spannungs- und Verformungszustand eines Dammes in allen Bau- und Betriebsphasen hinreichend genau zu kennen, um zwei entscheidende Fragen beantworten zu können:

1. Welche Verformungen können im Hinblick auf die vorgesehene Dichtung und die Bauaufgaben zugelassen werden?
2. Welche Güteforderungen ergeben sich daraus für die Schüttung?

Die Beantwortung dieser Fragen soll ermöglichen, Dämme mit dem im Steinbruch oder an anderen Gewinnungsstellen anfallenden Material bei einem möglichst wirtschaftlichen Schüttbetrieb und geringem Verdichtungsaufwand zu bauen. Der bei zahlreichen Staudämmen praktizierte Grundsatz, eine maximale Verdichtung der Schüttlagen in allen Dammbereichen anzustreben, widerspricht einer optimalen Bauweise und berücksichtigt nicht die Erkenntnisse über Größe und zeitlichen Ablauf der Dammverformungen.

In der DDR sind in den letzten Jahren zahlreiche Dämme mit einer bituminösen Außenhautdichtung errichtet worden. Für diese Dichtungsart wird die Dichtungshaut praktisch nach Fertigstellung des gesamten Dammkörpers aufgebracht, so daß hinsichtlich der Verformungen und der damit verbundenen Beanspruchung der Dichtung lediglich die während des Aufbringens der Dichtung auftretenden sowie die sich während der Schonzeit und beim Anstau ergebenden Anteile interessieren.

* Dr. Ing. habil. MICHAEL KINZE, Institut für Wasserwirtschaft, Otto Wagner-Str. 3, 806 Dresden, DDR

Der aus Eigengewicht resultierende Hauptanteil der Dammverformung ist — wie zahlreiche Messungen bei Dämmen aus nichtbindigem Schüttstoff nachgewiesen haben — bereits während der Bauzeit des Dammes abgeklungen. Ausgehend von diesen grundsätzlichen Überlegungen wurden für den derzeit höchsten Steinschütt-Damm der DDR, die Talsperre Schönbrunn, in der Vorbereitungsphase Untersuchungen und Berechnungen mit dem Ziel durchgeführt, eine dem Spannungs- und Verformungszustand des Dammes angemessene Schütt- und Verdichtungsart zu ermitteln, die von der derzeitigen »maximalen« Verdichtung in allen Dammbereichen abweicht.

2. Labor- und Feldversuche

Zur Kennwertbestimmung des Schüttmaterials, einem Tonschiefer der Katzhütter Schichten, wurden neben den üblichen Spreng- und Klassierungsversuchen zusätzliche Großversuche durchgeführt (Durchführung der Versuche durch den VEB Geologische Forschung und Erkundung Halle, BT Jena). Dabei handelte es sich zunächst um Kompressionsversuche mit verhinderter Seitendehnung ($D = 120$ cm, $h = 30$ cm), bei denen die Abhängigkeit des
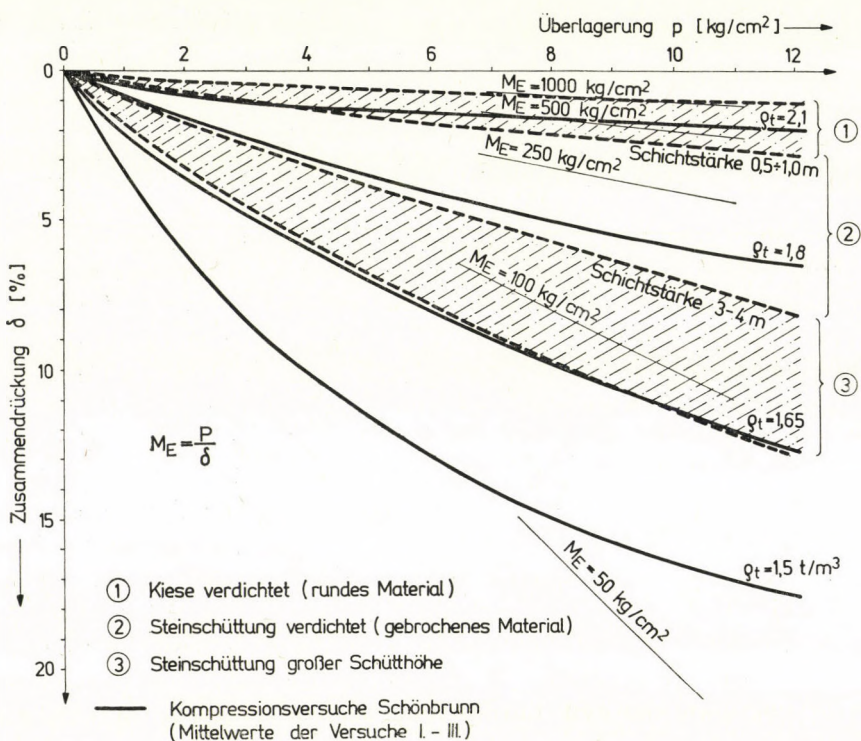
Bild 1. Druck-Setzungs-Kurven von grobkörnigen Schüttungen

Spannungs-Stauchungsverhaltens des Schüttmaterials von Einbaudichte und Wassergehalt sowie die Veränderung der Trockenrohdichte unter der Verdichtungsspannung bestimmt wurde.

Die Bilder 1 und 2 zeigen typische Versuchsergebnisse. Auf Bild 1 ist außerdem der Zusammenhang zwischen Setzungen und dem Überlagerungsdruck angegeben, wie er sich aus der Auswertung von Setzungsbeobachtungen ergibt. Aus diesen Darstellungen läßt sich der für die Berechnung erforderliche
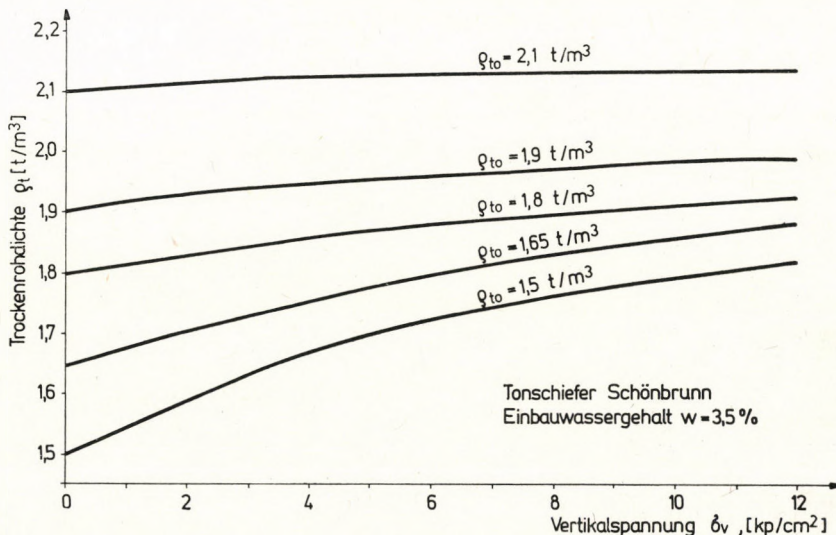
Bild 2. Veränderung der Trockenrohdichte infolge der Vertikalspannung

Kompressionsbeiwert M_e bestimmen. Aus Bild 1 kann ein Zusammenhang zwischen Kompressibilität, Dichte, Einbautechnologie und Art des Schüttmaterials konstruiert werden, wie er auf Bild 3 dargestellt ist. Die praktische Anwendung demonstriert Bild 4 an einem Beispiel.

Aus diesem Diagramm läßt sich bei Kenntnis der Einbaudichte bzw. des für die statischen Verhältnisse erforderlichen M_e und bei bekanntem Überlagerungsdruck die mögliche maximale Schütthöhe bestimmen, mit der der Einbau zu erfolgen hat. Umgekehrt läßt sich für bestimmte zulässige Dehnungen z. B. der Oberflächendichtung die erforderliche Dichte bzw. Schütthöhe ermitteln.

Zur Festlegung der praktischen Maßnahmen für die Anwendung dieser Erkenntnisse macht sich die Durchführung von Messungen auf der Baustelle erforderlich. Dabei ist mittels der vorgesehenen Einbaugeräte deren Verdichtungswirkung sowie eine evtl. Entmischung bei den vorgesehenen Schütthöhen zu überprüfen. Bei den in Schönbrunn durchgeführten Versuchen sollte vor allem die Dichteverteilung bei Schütthöhen, die für die kleine Walze (WVW

550) an und für sich zu hoch sind, geprüft werden. Bild 5 zeigt das **Ergebnis.** Die Dichtebestimmung erfolgte mit Oberflächennivellement und **hydro**statischer Höhenmessung in verschiedenen Tiefen.
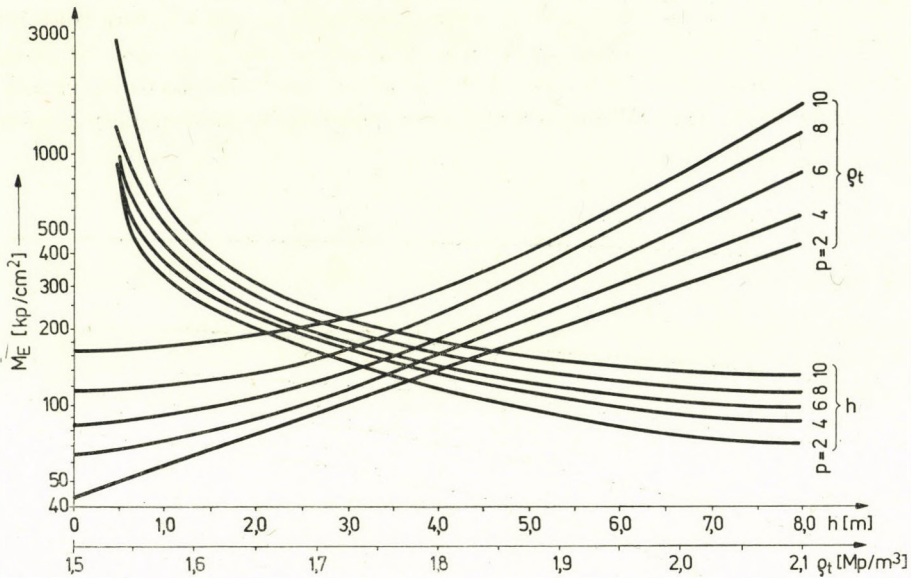
Bild 3. Zusammenhang zwischen Kompressibilität, Dichte C_t und Schütthöhe h bzw. Überlagerungsdruck p
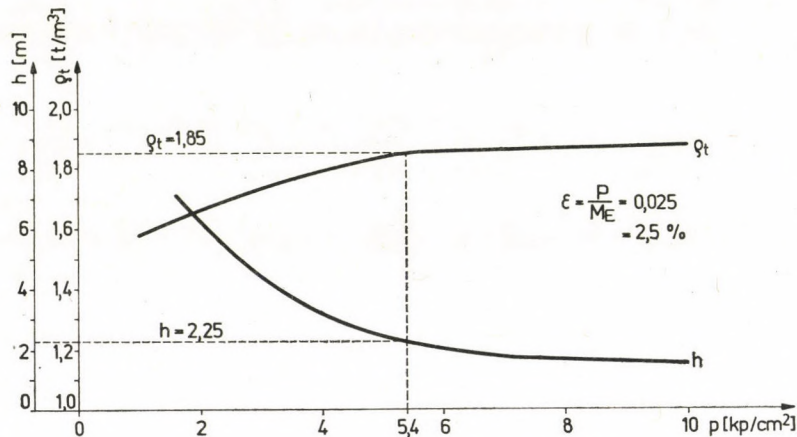
Bild 4. Beispiel: Überlagerungsdruck $p = 5,4$ kp/cm²; $h = 2,25$ m; $\varrho_t = 1,85$ t/m³

Die erreichte mittlere Dichte ist auf Bild 6 dargestellt. Eine detaillierte Interpretation der Versuchsergebnisse soll an dieser Stelle nicht erfolgen.

Aus dem Dichteverlauf von Bild 5 bzw. 6 kann in Verbindung mit Bild 1 eine Aussage über die unterschiedliche Kompressibilität der Schüttung in
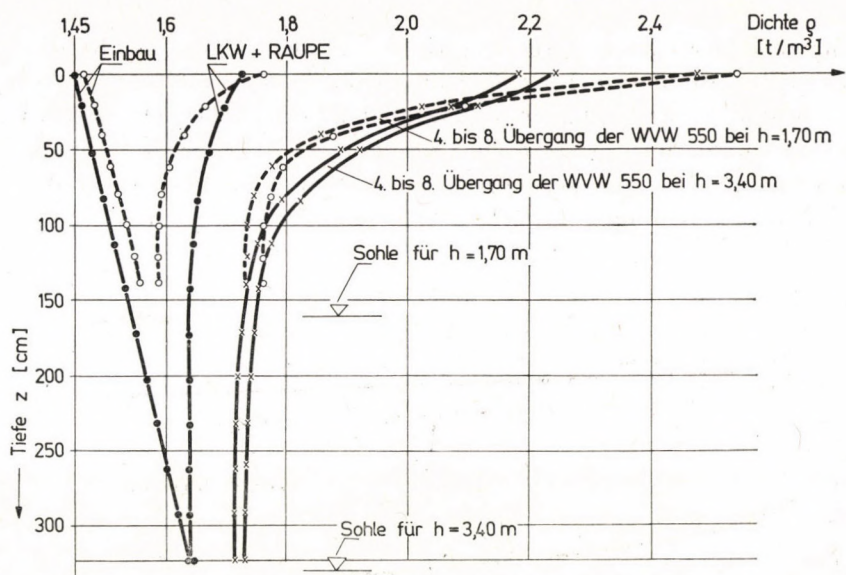
Bild 5. **Dichteverteilung über die Tiefe**
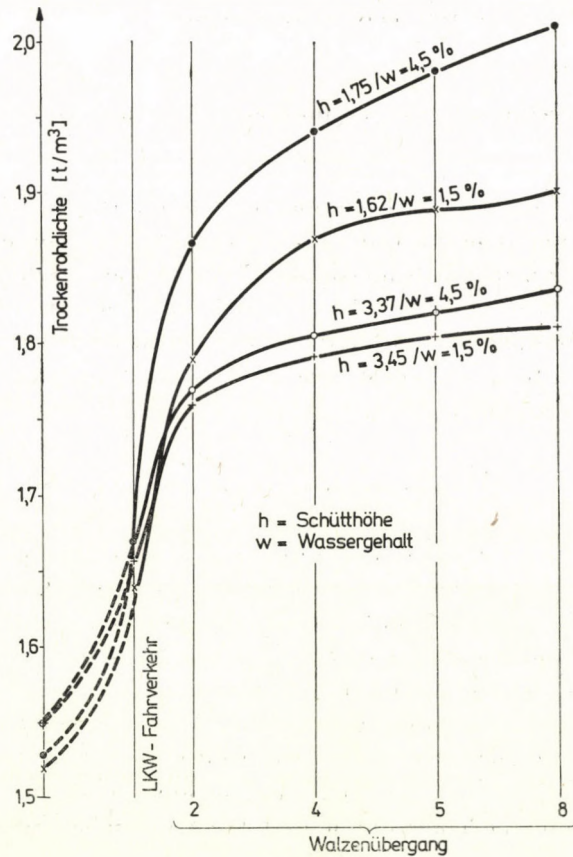
Bild 6

Abhängigkeit der Einbaumethode getroffen werden. Damit ist die wichtigste Voraussetzung für die analytische Untersuchung des Problems gegeben.

Erwähnt werden soll auch, daß der Schönbrunner Tonschiefer bei Durchfeuchtung und Belastung zusätzliche Setzungen, sogenannte Sackungen erleidet (Bild 7). Wie in speziellen Kompressionsversuchen ermittelt wurde, betragen diese Sackungen zwischen 22% und 36% der Setzungen, die vor
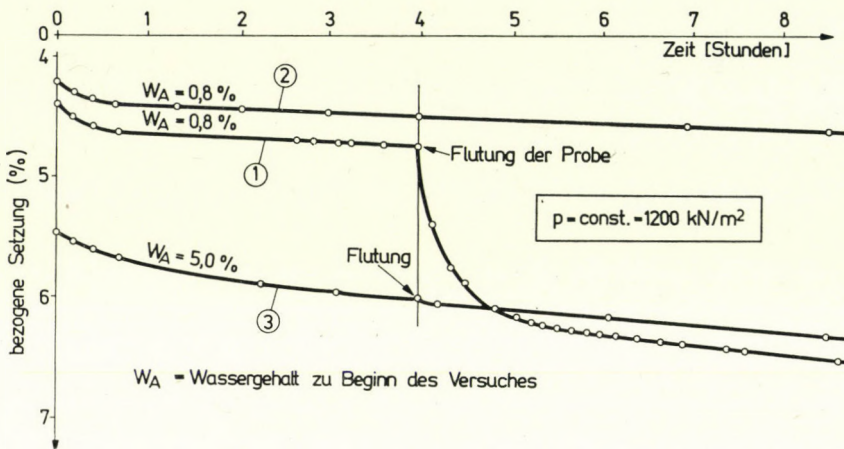
Bild 7. Zeit-Setzungs-Verlauf im trockenen, nassen bzw. gefluteten Zustand

der Wasserzugabe bei der Erstbelastung aufgetreten waren. Die Vorwegnahme der Sackungen vor dem Lastfall »Betriebsstau« bzw. vor dem Aufbringen bituminöser Oberflächendichtungen durch Nässen des Schüttmaterials und sorgfältige Verdichtung der oberflächennahen Bereiche ist eine wichtige bautechnologische Maßnahme, um spätere Setzungsschäden zu vermeiden. Das gilt übrigens auch für andere grobkörnige Schüttstoffe, wie sie für Steinschüttdämme in Frage kommen.

3. Rechnerische Untersuchung

Mit Hilfe eines FEM-Rechenprogrammes läßt sich das Verformungsverhalten für die unterschiedlichsten Kombinationen der Dichteverteilung im gesamten Dammquerschnitt untersuchen. Bild 8 zeigt ein Beispiel, bei dem die Eigenverdichtung unter dem aufgehenden Schüttkörper optimal ausgenutzt werden soll. In den Bereichen hoher Vertikalspannungen werden niedrige Dichten geschüttet und umgekehrt. Aus Vergleichsrechnungen mehrerer solcher Fälle lassen sich Diagramme wie Bild 9 konstruieren.

Solche analytischen Vergleichsuntersuchungen lassen sich für jeden beliebigen Dammbereich ausführen und können sich auf den Vergleich der
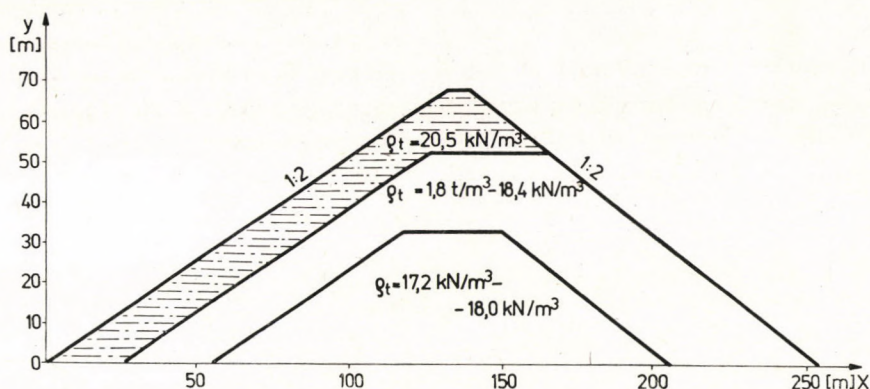
Bild 8. Einbaudichten im Dammkörper
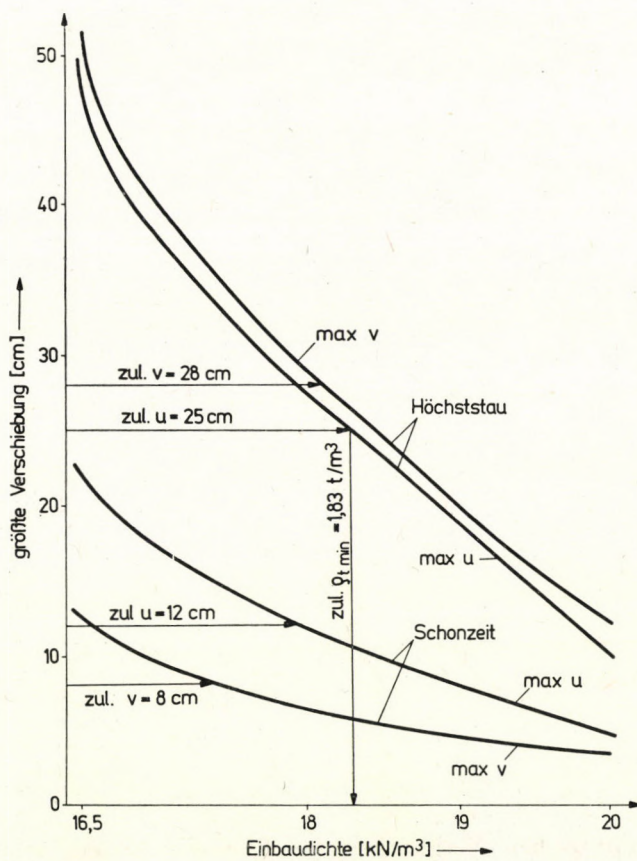
Bild 9

Verschiebungen, der Verzerrungen, Spannungen oder auch der Sicherheit
gegen Bruch erstrecken. In Abhängigkeit der entsprechenden zulässigen
Werte kann man die erforderlichen Einbaudichten ermitteln. An dieser Stelle
sei darauf hingewiesen, daß bezüglich der Scherfestigkeit des Schönbrunner
Schiefers keine wesentliche Veränderung in Abhängigkeit der Dichte im Labor
festgestellt wurde.
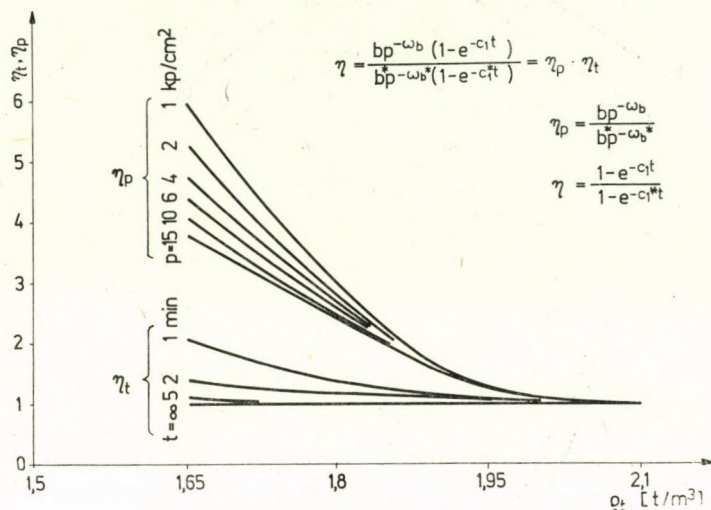
Bild 10. Faktoren für die Änderung der zeitlichen Deformationen bei Abnahme der Einbau-
dichte

Sofern der zeitliche Verlauf der Deformationen von Interesse ist, kann
man diesen durch Ansatz rheologischer Gleichungen (vergl. KÉZDI: Handbuch
der Bodenmechanik I) ermitteln. Für den Tonschiefer der Talsperre Schön-
brunn wurden spezielle Kompressionsversuche auf diese Weise ausgewertet.
Bild 10 zeigt die Veränderung der rheologischen Beiwerte mit der Dichte.
Eine Verringerung der Dichte von 2,1 auf 1,85 t/m³ würde z. B. eine Verdop-
pelung der zeitabhängigen Setzungen zur Folge haben.

4. Schlußfolgerungen

Mit den genannten Ergebnissen ist man in der Lage, die Schüttung
nach den unter 1. genannten Grundsätzen bei Gewährleistung der Funktions-
und Standsicherheit durchzuführen. Die ökonomische Bedeutung einer solchen
Verfahrensweise liegt auf der Hand, wenn man die Einsparung an Verdich-
tungsenergie, die Verringerung der benötigten Schüttmassen und die mögliche
Bauzeitverkürzung betrachtet.

Für die erfolgreiche Einführung dieser Erkenntnisse in die Praxis ist es erforderlich, die Versuchseinrichtungen so zu verbessern, daß Verformungskennwerte an Steinschüttmaterial ermittelt werden können, die in ihrer Aussagekraft den umfangreichen Möglichkeiten elektronischer Berechnungen des Verformungsverhaltens von Staudämmen entsprechen. Weiterhin sind Festlegungen über die Zulässigkeit der Beanspruchungen von bituminösen Oberflächendichtungen zu treffen.

Schließlich ist durch ausreichende Maßeinrichtungen im Dammbauwerk zu sichern, daß während des Baues und in der Probestauphase die Gültigkeit der Deformationsprognosen überprüft werden kann.

Soil Mechanic Investigation on an Economical Technique for Filling and Compaction of Rockfill Dams. Earth and rockfill dams must have a sufficient stability in all phases of construction and operation. Additional deformations due to dead load and water pressure must not impair the function of bituminous facing and watertight joints at the foot wall. The paper deals with these problems on the basis of laboratory and field tests.

Грунтомеханические исследования по экономичной технологии сооружения заградительных дамб. Заградительные дамбы при процессе строительства и во время их эксплуатации должны иметь соответствующий запас прочности. Кроме сказанных выше существенным является то, чтобы деформации насыпи, возникающие под воздействием собственного веса и давления массы воды, не влияли бы вредно на эксплуатацию, плотность, водозапирающую способность насыпи и не воздействовали бы вредно на сохранность защитных слоев заградительной дамбы. Данная работа посвящена исследованию перечисленных выше вопросов на основе данных исследований в лабораторных условиях и по месту.

LARGE SIGNAL PROPERTIES OF INJECTION LOCKED DIODE OSCILLATORS

T. BERCELI*

DR. OF TECHN. SCI.

A large signal model is used to investigate the properties of injection locked diode oscillators. Relations between the input and output signals are derived and used, to determine the locking band. It is shown that the locking band is shifted to lower frequencies as the diode susceptance non-linearity is increased. Transmission characteristics such as output power and phase, further group delay time, AM-to-PM conversion and AM compression are determined. Frequency dependence of the parameters is investigated at different values of input power, load and diode susceptance non-linearity. This latter parameter has the effect of causing unsymmetry, resulting in the lowest distortion at a frequency which is higher than the band centre.

1. Introduction

Injection locked diode oscillators are now widely used, and application fields are steadily widening as an increasing number of microwave diode types are becoming available. Gunn and IMPATT diodes are primarily used as active elements.

The frequency of diode oscillators in the vicinity of the free running oscillation frequency may be controlled by the injection of a locking signal. For the case of a modulated locking signal, transmission characteristics will be important because they will be responsible for the distortion introduced.

The analysis of injection locked oscillators has been presented by several authors. The small signal locking band was determined by ADLER [1]. Noise problems were treated by KUROKAWA [2], further by HINES, COLLINET and ONDRIA [3]. Amplification properties were investigated by HINES [4], relations for stability criteria have been derived by HANSSON and LUNDSTRÖM [5], further by KUROKAWA [6]. There are also several papers dealing with experimental results.

In most of the papers dealing with injection locked oscillators, a small signal approximation is used to investigate circuit behaviour, and for large signal operation, only qualitative treatments are presented. However, the small signal approximation may not be applied in the usual case when the input power of injection locked oscillators is appr. 10 dB below the output power.

* T. BERCELI, Research Institute for Telecommunication, Gábor Áron-u. 65, H-1026, Budapest, Hungary

In this paper, a large signal model is used to investigate the properties of injection locked diode oscillators, and quantitative transmission characteristics are presented. These show a significant departure compared to the small signal case. Both the conductance and the susceptance of diodes are level dependent which are characterized by the describing function, assuming a quasi-stationary state. This is used for deriving relations between input and output signals for a single frequency operation. These relations are numerically evaluated by a computer, and transmission characteristics, such as output power and phase, further group delay, AM-to-PM conversion and AM compression are presented in diagrams.

Frequency dependence of the parameters are investigated at different values of input power, load and non-linearity of diode susceptance. The characteristics are symmetrical with respect to the resonant frequency in the case of linear diode susceptance. However, non linearity of diode susceptance results in unsymmetrical characteristics, and the band centre is shifted from the resonant frequency to a lower value. Unsymmetry has the effect of displacing the point of lowest distortion from the band centre to a higher frequency.

Calculation of the locking band shows that the locking band increases with loading and input power. The locking band is also slightly influenced by the non-linearity of susceptance. A larger locking band will introduce less distortion.

2. Large signal circuit model

The analysis of injection locked diode oscillators is based on the model of Fig. 1. The diode is represented by a non-linear conductance G_d and non-linear capacitance C_d. The circuit comprising the diode is substituted by a parallel resonant circuit $L_p - C_p$. Internal conductance of the generator driving the input and the load terminating the output is G. Input and output are separated by a circulator which is considered to be ideal. Wave admittance
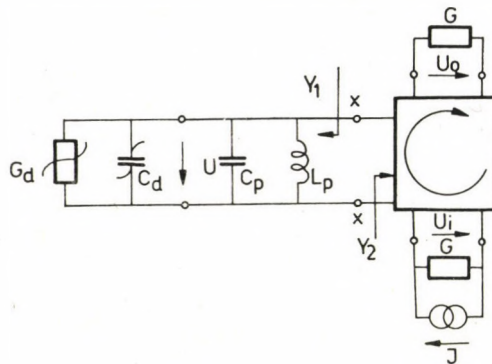
Fig. 1. Equivalent circuit

of the circulator in all parts is also G. The oscillator is analyzed in the steady-state condition by using the method of the describing functions [7, 8].

The diode is considered to be voltage driven and it is assumed that only a single frequency voltage component is present across the diode terminals. In this case, the following expression is selected for describing the non-linear diode admittance:

$$Y_d = -G_0(1 - \alpha U^2) + j\omega C_{d0}(1 + \beta U^2) \, . \tag{1}$$

Here the following notations are used:

ω angular frequency,
U r.m.s. value of voltage across diode terminals,
G_0 small signal negative conductance,
C_{d0} small signal diode capacitance,
α, β coefficients representing the diode non-linearity which are determined by measurement.

The sign of α is always positive, the sign of β, is in most cases positive too, but can also be negative as the diode capacity usually increases with voltage and rarely decreases [9, 10].

Let us introduce normalized quantities. The diode admittance will then be

$$y_d = -1 + \frac{1}{2} u^2 + j \frac{\omega}{\omega_0} (Q_{d0} + b_n u^2) \tag{2}$$

where

$$u = \frac{U}{U_m}, \quad y_d = \frac{Y_d}{G_0}, \tag{3}$$

$$U_m = \frac{1}{\sqrt{2\alpha}}, \tag{4}$$

$$\omega_0 = \frac{1}{\sqrt{L_p(C_p + C_{d0})}}, \tag{5}$$

$$Q_{d0} = \frac{\omega_0 C_{d0}}{G_0}, \tag{6}$$

$$b_n = Q_{d0}\beta U_m^2 \, . \tag{7}$$

The voltage has been normalized to the voltage U_m pertaining to maximum free running oscillator power (Appendix A−1), and the admittance has been normalized to G_0. Further notations are:

ω_0 small signal angular frequency of the oscillator,
Q_{d0} diode small signal Q-factor,
b_n susceptance non-linearity factor.

The latter may be readily determined by the measurement in the amplifier mode (Appendix A—4).

According to the equivalent circuit of Fig. 1, the relation between input and output signals of the injection locked oscillator is given by the reflection coefficient at terminals $x-x$ in the direction of the diode. This method of approach seems to be simple but actually turns out to be difficult, because the diode admittance is dependent on the diode voltage, and this is the resultant of the input and output signal voltages. We thus arrive at a non-linear complex equation of high degree, the solution of which is a lengthy procedure, generally yielding several roots. The selection of the root having a physical meaning presents an extra problem.

In order to arrive at relations which may be evaluated better, the concept of operating input admittance will be introduced in the analysis of the injection locked oscillator (Appendix A—2). The operating input admittance may be applied for the steady state condition or in the case of slow changes. Looking in the direction of the circulator from terminals $x-x$, the operating input admittance is given by the following expression:

$$y_2 = \frac{u_0^2 - u_i^2 - j2u_0u_i \sin \Theta}{u_0^2 + u_i^2 + 2u_0u_i \cos \Theta} \, g \, .$$
(8)

Here u_i and u_0 are the normalized voltages of the input and output signals, respectively, Θ is the phase difference between these voltages, and g is the normalized value of the load conductance.

This means that at the operating frequency, an admittance differing both in magnitude and phase from the conductance g will be present looking in the direction of the circulator. However, this is only valid at the operating frequency. At all other frequencies, $u_i = 0$, as no input signal is present, so the admittance value towards the circulator is g.

Looking in the direction of the diode, the operating input admittance is identical with the large signal admittance y_1 which will be, taking the diode admittance formula (2) into account, the following:

$$y_1 = -1 + \frac{1}{2} u^2 + j(2Q_0\delta + b_n u^2)$$
(9)

where

$$Q_0 = \frac{\omega_0(C_{d0} + C_p)}{G_0},$$
(10)

$$\delta = \frac{\omega - \omega_0}{\omega_0}.$$
(11)

Here Q_0 denotes the small signal Q-factor of the oscillator and δ is the relative frequency deviation.

3. Relation between input and output signals

The operating input admittance in one direction should be the negative of the admittance in the other direction:

$$y_2 = -y_1. \tag{12}$$

Substituting Eqs (8) and (9) we have a complex equation which may be split into the real and the imaginary part:

$$\frac{u_0^2 - u_i^2}{u^2} g = 1 - \frac{1}{2} u^2, \tag{13}$$

$$\frac{2u_0 u_i \sin \Theta}{u^2} g = 2Q_0 \delta + b_n u^2. \tag{14}$$

The diode voltage u is the resultant of the input signal voltage and the output signal voltage:

$$u^2 = u_0^2 + u_i^2 + 2u_0 u_i \cos \Theta. \tag{15}$$

The voltages are vector-additive as shown by Fig. 2.
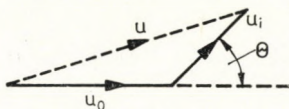
Fig. 2. The resultant of voltages

The relation between input and output signals is given by the set of non-linear equations (13) and (14). There are two unknowns, u_0 and Θ, which may be determined from the two equations. However, suitable rearrangements are needed, introducing powers instead of voltages, by using the following relations:

$$p_0 = 2g u_0^2, \tag{16}$$

$$p_i = 2g u_i^2. \tag{17}$$

Let us introduce the power generated by the diode which is the difference between the output and input power:

$$p_d = p_0 - p_i, \tag{18}$$

5

The following cubic equation is derived for determining the diode power p_d (see Appendix A—3):

$$\frac{1}{4} A^2 p_d^3 + 2g(2gB^2 - gAC - AB)p_d^2 + 4g[A(gC - p_i) - 2gB(gC - 2p_i) +$$
$$+ g^3C^2]p_d + 16g^2(p_i^2 - gCp_i) = 0 , \tag{19}$$

where

$$A = 1 + 4b_n^2 ,$$

$$B = 1 + (Q_0\delta + b_n)\frac{4b_n}{g} , \tag{20}$$

$$C = 1 + (Q_0\delta + b_n)^2\frac{4}{g^2} .$$

Equation (19) gives three values for p_d but only one real solution may have a physical meaning. At the upper limit of the frequency range, always a single real root only is present if $b_n \geq 0$. Should more than one real root be present at some frequency, the correct solution can be selected by demanding that no abrupt power change or phase change may occur when decreasing the frequency in small steps, starting from the upper limit of the frequency range.

The following two expressions are derived for the phase (see Appendix A—3):

$$\tan \Theta = \frac{2}{g} \frac{p_d(Q_0\delta + b_n)(4g^2C - Ap_d) - 2gb_np_d(2gC - 2p_i - Bp_d)}{p_d(4g^2C - Ap_d) - 2(p_d + 2p_i)(2gC - 2p_i - Bp_d)} , \tag{21}$$

$$\cos \Theta = \frac{1}{2\sqrt{(p_d + p_i)p_i}}\left[\frac{1}{2}\frac{4g^2C - Ap_d}{2gC - 2p_i - Bp_d} p_d - p_d - 2p_i\right]. \tag{22}$$

Equations (21) and (22) are both needed for the phase computation, as the phase may be between π and $-\pi$. If $\cos \Theta > 0$, than $-\pi/2 < \Theta < \pi/2$ so the phase may be computed from Eq. (21) by using the arctan operation. If $\cos \Theta < 0$ and $\tan \Theta > 0$, then π should be subtracted from the value computed from Eq. (21) in order to get the correct value of Θ. And if $\cos \Theta < 0$ and $\tan \Theta < 0$, then π should be added to the value computed from Eq. (21) in order to get the correct value of Θ.

4. Locking band

The locking band is defined as the frequency band in which the frequencies of the oscillator input and output signals are identical. This means that within the locking band, the oscillator output signal frequency may not differ from the input frequency, so the condition for oscillation may not be fulfilled at

other frequencies. These considerations allow the determination of the locking band limits.

According to the equivalent circuit of Fig. 1 and to Eq. (8), the diode sees a load of normalized value g at all frequencies differing from the input signal frequency. Thus, oscillation at other frequencies may not take place if the negative value of the diode conductance g_d is less than g. Within the locking band, at the input signal frequency, the diode conductance is determined by the voltage across the diode terminals. Thus, according to the previous considerations, the locking band limits are characterized by the relation

$$-g_{ds} = g \, . \tag{23}$$

Subscript s refers to the band limit, and g_{ds} is determined by the input signal.

Substituting Eqs (15), (16) and (17) into Eq. (2), the diode conductance will be the following:

$$-g_d = 1 - \frac{1}{4g} (p_0 + p_i + 2 \sqrt{p_0 p_i} \cos \Theta) \, . \tag{24}$$

Substituting (24) into (23) we have a relation for the phase at the band limits:

$$\cos \Theta_s = \frac{1}{2\sqrt{p_{0s} p_i}} [4g(1 - g) - p_{0s} - p_i] \, . \tag{25}$$

For calculating the phase band-limit value, the output power band-limit value p_{0s} should be known. This may generally be calculated from Eq. (19) by using Eq. (18). However, this equation may have three real roots in some cases. Let us first investigate the case with a single real solution for the output power.

At the upper end of the locking band, if $b_n \geq 0$, we always have a single real solution for the output power, and this may be simply determined: substituting (23) into (13) and taking into account that the right-hand side of (13) is now equal to $-g_{ds}$, we arrive at the following relation:

$$u_1^2 = u_{01}^2 - u_i^2 \, . \tag{26}$$

Subscript 1 refers to the upper end of the locking band. Substituting now Eqs (26), (16) and (17) into (13), we get the output power at the upper end of the band:

$$p_{01} = 4g(1 - g) + p_i \, . \tag{27}$$

Substituting (27) into (25) we have the phase at the upper end:

$$\cos \Theta_1 = -\sqrt{\frac{p_i}{p_{01}}} = -\sqrt{\frac{p_i}{4g(1-g)+p_i}} \,. \tag{28}$$

As $\cos \Theta_1$ is negative, the phase Θ_1 is between $\pi/2$ and π.

The frequency of the locking band upper end may be determined from (14). Substituting into this equation (26), (27) and (28) and taking into account (16) and (17), we have the following result:

$$Q_0 \delta_1 = \frac{1}{2} \sqrt{\frac{gp_i}{1-g}} - (1-g)b_n \,. \tag{29}$$

The power, phase and frequency pertaining to the lower limit of the locking band may only be determined by numerical analysis for the general case. Exceptions are those cases when we have a single real value for the power, when

$$\begin{aligned} p_{02} &= p_{01}, \\ \Theta_2 &= -\Theta_1 \,. \end{aligned} \tag{30}$$

Subscript 2 refers to the lower band limit. In this case, the frequency at the lower band limit, similarly as the previous one is given by

$$Q_0 \delta_2 = -\frac{1}{2} \sqrt{\frac{gp_i}{1-g}} - (1-g)b_n \,. \tag{31}$$

However, a separate investigation is necessary to make sure that actually a single solution is only available. If $b_n = 0$, there is always a single solution at the lower band limit only.

The width of the locking band, using (29) and (31), is given by

$$B_L = f_1 - f_2 = \frac{f_0}{Q_0} \sqrt{\frac{gp_i}{1-g}}, \tag{32}$$

or

$$B_L = \frac{2f_0}{Q} \sqrt{\frac{p_i}{p_0}} \,. \tag{33}$$

Here Q means the loaded Q-factor:

$$Q = \frac{\omega_0(C_{d0} + C_p)}{G} \,. \tag{34}$$

Further, the free-running oscillator power, as computed in Appendix A—1, is given by

$$p = 4g(1 - g).$$ \hfill (35)

According to Eq. (33), the locking band width is proportional to the square root of the ratio of the input power to the free running oscillator power.
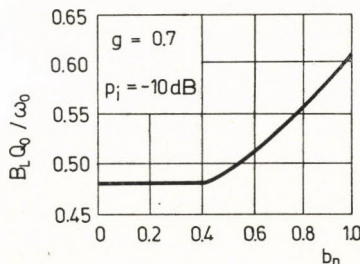
Fig. 3. Locking band as a function of susceptance non-linearity
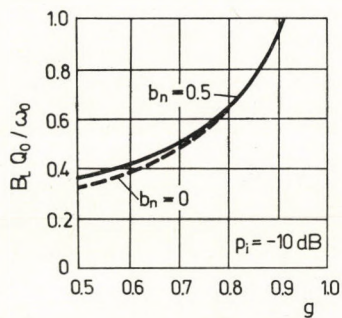
Fig. 4. Locking band as a function of loading
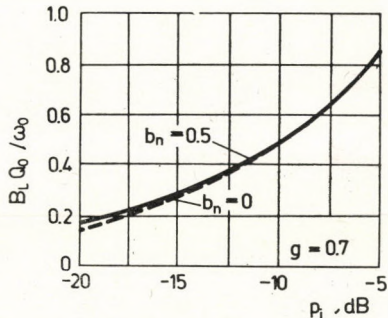
Fig. 5. Locking band as a function of input power

If we have several solutions for the output power at the lower band limit, the relations (31), (32) and (33) will not give correct results, though they are useful as approximations. The locking band width may be determined more precisely by using numerical analysis as shown by some diagrams.

The effect of susceptance non-linearity is shown by Fig. 3 for the case when the input power is lower by 10 dB than the maximum output power of the free running oscillator. In the Figure, the quantity $B_L Q_0/\omega_0$ is plotted as a function of b_n; this quantity is proportional to the relative width of the locking band. If b_n is small, the locking bandwidth is constant, i.e. b_n has no effect. However, at higher b_n values, the locking bandwidth is substantionally increased.

The effect of load is shown in Fig. 4 for the case of $p_i = -10$ dB. Increasing of the loading, i.e. the value g, will substantially increase the locking bandwidth. Values of $b_n = 0.5$ and $b_n = 0$ pertain to the solid and dotted curve, respectively. At higher loads we have two identical curves.

Dependence of the locking bandwidth on the input power is shown in Fig. 5 for two b_n values with $g = 0.7$. The locking bandwidth increases with increasing input power. At higher powers we have two identical curves.

5. Transfer properties

The transfer properties of the injection locked oscillator have been numerically determined too by using the relations between the input and output signal, and are shown in diagrams. In the diagrams, the independent
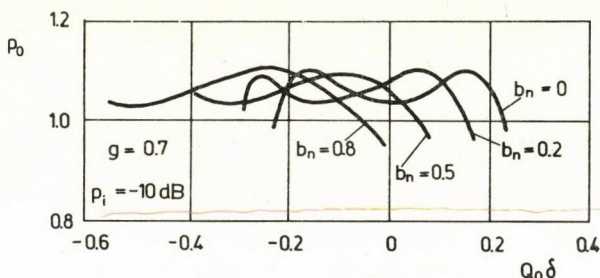
Fig. 6. Output power frequency response for different values of susceptance non-linearity

variable is generally the product of the relative detuning and the quality factor Q_0. The value $\delta = 0$ corresponds to the small signal resonant frequency of the circuit. b_n, g and p_i are used as parameters from which two are fixed and the third is variable. The following fixed values are used: $b_n = 0.5$, $g = 0.7$, $p_i = -10$ dB. Curves are plotted along the whole locking band, thus the ends of the curves denote the ends of the locking band.

Output power frequency characteristics are presented in Fig. 6 for different susceptance non-linearity factors. The characteristic is symmetrical for $b_n = 0$, unsymmetry will be more pronounced with higher b_n, and the locking band is shifted in the direction of lower frequencies.

The output power frequency characteristic is dependent on the input power, too, as shown in Fig. 7. Increasing the input power will introduce higher output power fluctuation, and simultaneously the bandwidth is considerably increased.

Let us now investigate the dependence of output power band centre value on the various parameters. The output power band centre value is independent of the susceptance non-linearity factor.

The dependence of output power band centre value on the input power for different g values is given in Fig. 8. For g values between 0,5 and 1, the output power band centre value has a maximum value at some input power value.
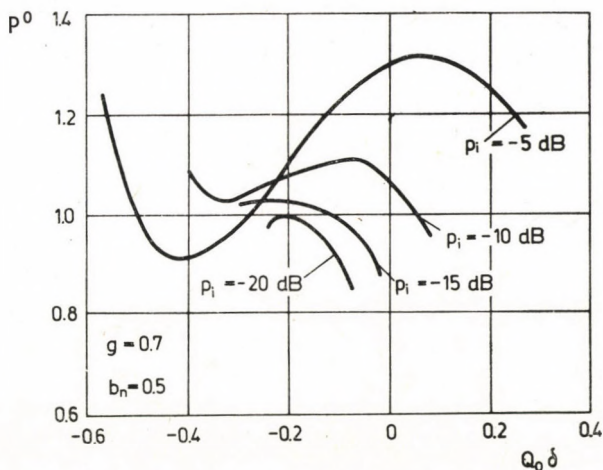
Fig. 7. Output power frequency response for different values of input power
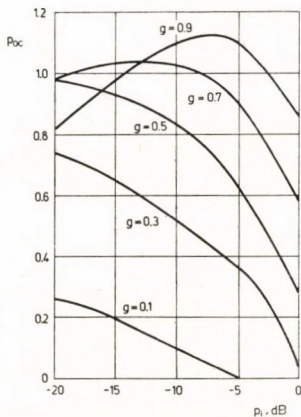
Fig. 8. Band centre output power as a function of input power for different loadings

The position and value of the maximum is dependent on g. Higher maximum values are attained with higher g values but also require higher input power. Output power may be higher than unity which means that the injection locked oscillator output power may be higher than the free running oscillator output power.

At $g = 0,5$, the free running oscillator has a maximum output power. For an injection locked oscillator, the adjustment corresponding to $g = 0,5$

always results in a lower output power than the free running oscillator power. For injection locked operation, g should be chosen to give a near maximum output power at the given input power, thus g should be between 0,5 and 1. If $g < 0,5$, then p_{0c} shows a monotonous decrease with increasing input power, so this adjustment is practically useless. Therefore no investigations will be conducted for values $g < 0,5$.
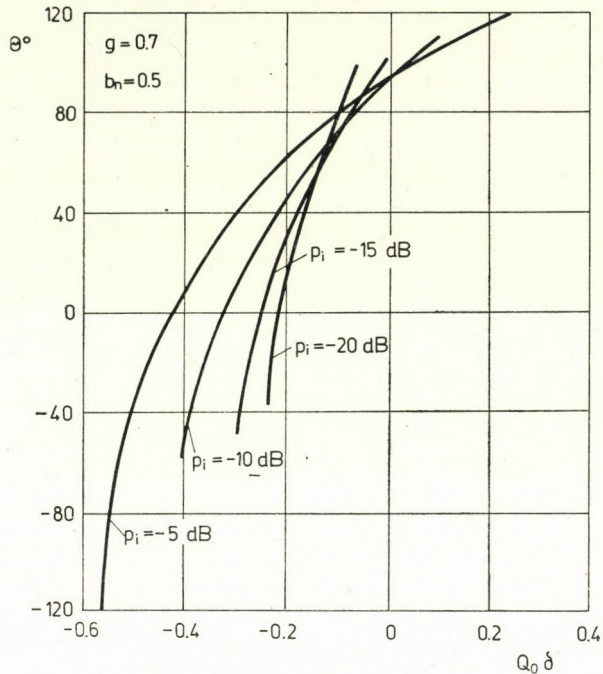
Fig. 9. The phase characteristic for different input powers

The phase-frequency dependence for different input powers is shown in Fig. 9. For increasing input power, the slope of the phase characteristic decreases and the zero-phase point is shifted to lower frequencies.

The phase characteristic is dependent on the susceptance non-linearity, too, as is shown in Fig. 10. For $b_n = 0$, the curve is symmetrical with respect to the zero-phase point. Increasing susceptance non-linearity will introduce higher unsymmetry, and the zero-phase point is shifted to lower frequencies. For instance, for $b_n = 0,8$, the zero-phase point is shifted to the end of the locking band. Thus the zero-phase point is not at locking band centre for $b_n \neq 0$. Increasing susceptance non-linearity will shift the locking band to lower frequencies.

The effect of load on the phase characteristic is given in Fig. 11. Increasing the load, i.e. g, will lower the slope of the characteristic and the locking band is shifted to higher frequencies.
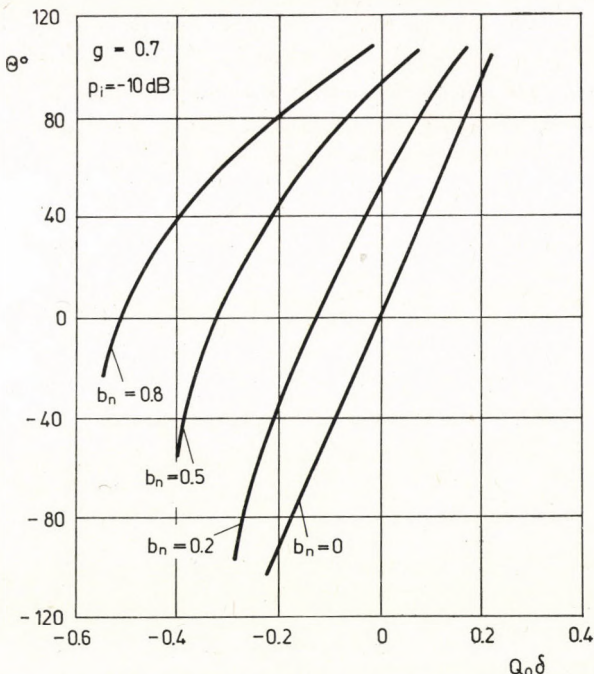
Fig. 10. The phase characteristic for different susceptance non-linearities
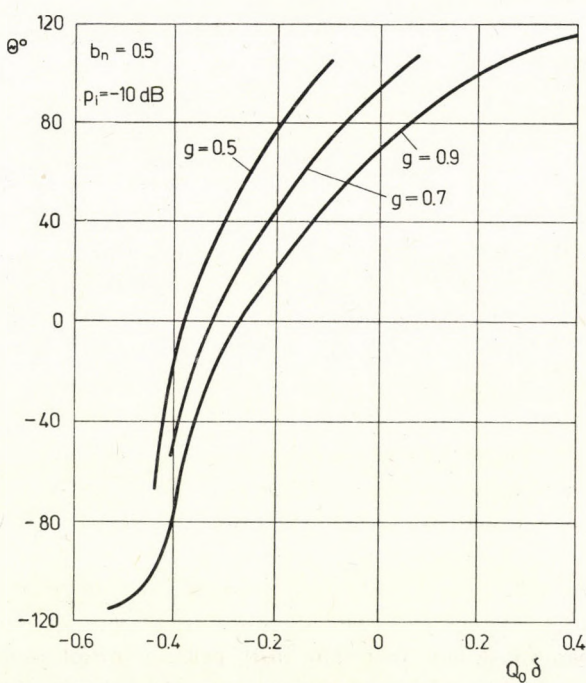
Fig. 11. The phase characteristic for different loadings

6. Curves of derivated characteristics

In the transmission of frequency or phase modulated signals, distortion is primarily determined by the derivated characteristics which are defined in Appendix A—5. Derivated characteristics are determined by numerical differentiation, and their dependence on the parameters is plotted in diagrams.
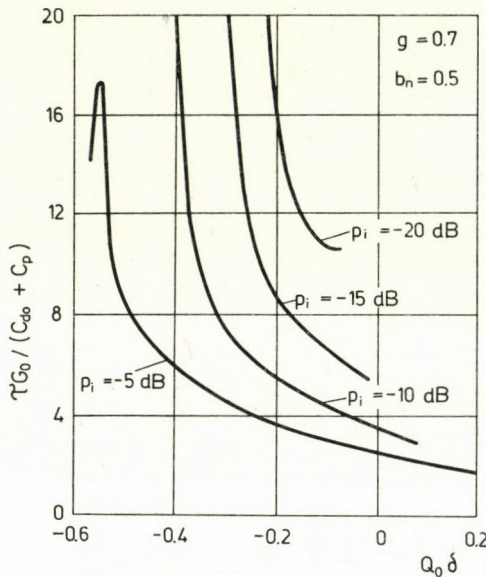
Fig. 12. The group delay time characteristic for different input powers

The quantity $\tau G_0/(C_{d0} + C_p)$ which is proportional to group delay time is shown in Fig. 12 as a function of $Q_0\delta$ for different input powers. Higher input power introduces less group delay time and less group delay time fluctuation in a given band.

Figure 13 shows the dependence of the group delay time characteristic on the susceptance non-linearity. If the susceptance is linear, i.e. $b_n = 0$, then the characteristic is symmetrical with respect to the small signal resonant frequency, and the fluctuation in the centre range of the locking band is very small. Susceptance non-linearity has the effect of shifting the characteristic to lower frequencies, make it unsymmetrical, and considerably increase its slope, introducing higher group delay fluctuation in a given band. However, the latter quantity is rather small.

The group delay characteristic is only slightly dependent on the load as shown by Fig. 14. On the other hand, group delay time is considerably effected by the total capacity, $(C_{d0} + C_p)$ and the small signal negative conductance of the diode G_0.
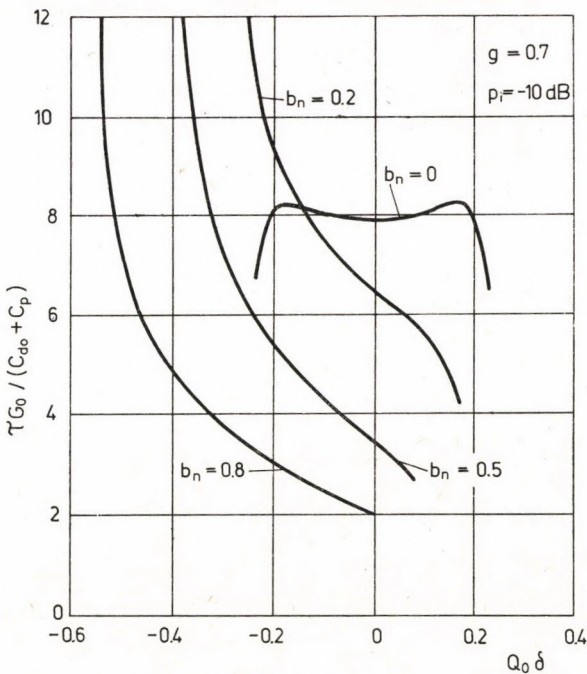
Fig. 13. The group delay time characteristic for different susceptance non-linearities
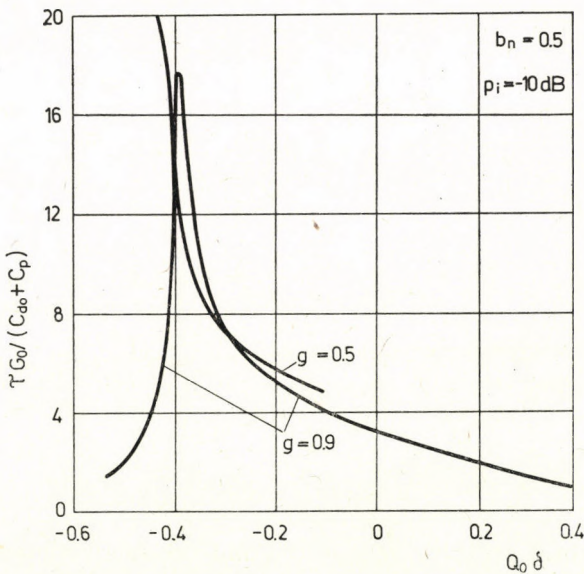
Fig. 14. The group delay time characteristic for different loadings

AM-to-PM conversion as a function of $Q_0\delta$ for different values of input power is shown in Fig. 15. Increasing input power will have little effect on conversion in the middle range of the band, but conversion is substantially decreased in other parts of the band, especially in the low-frequency part.
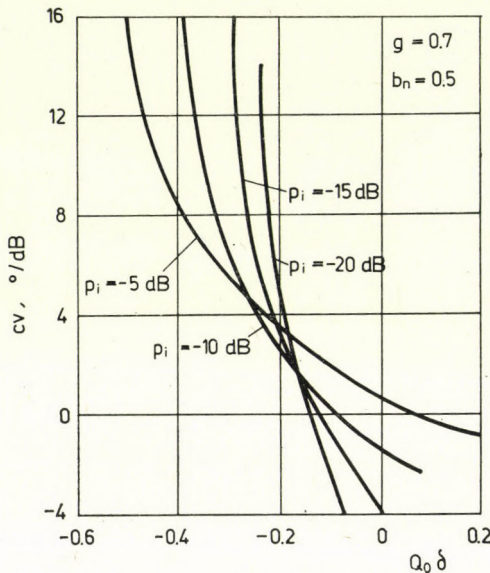

Fig. 15. AM-to-PM conversion frequency response for different input powers
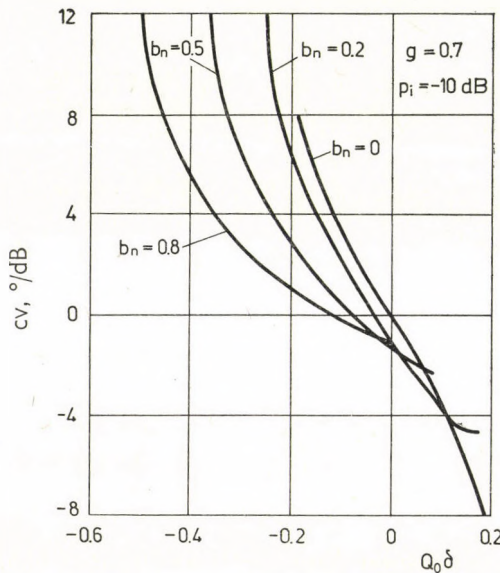
Fig. 16. AM-to-PM conversion frequency response for different susceptance non-linearities

AM-to-PM conversion is dependent on susceptance non-linearity as well as is shown in Fig. 16. If the susceptance is linear, i.e. $b_n = 0$, then the characteristic is symmetrical with respect to the small signal resonant frequency. Susceptance non-linearity results in a shift to lower frequencies and higher conversions and in the appearance of unsymmetry.
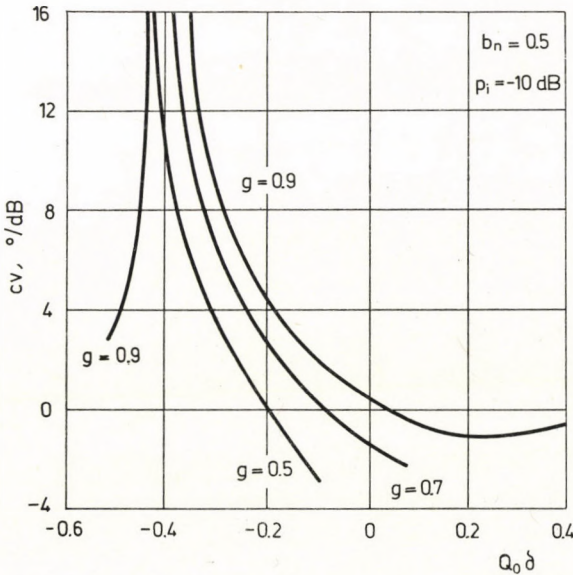
Fig. 17. AM-to-PM conversion frequency response for different loadings
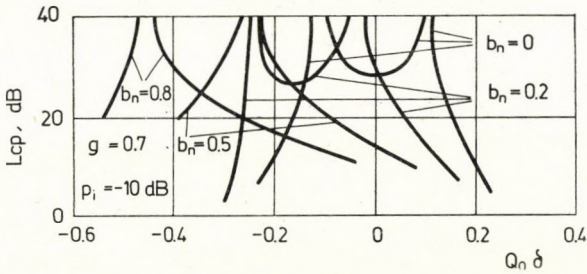
Fig. 18. AM compression frequency response for different susceptance non-linearities

Dependence of AM-to-PM conversion on load is shown in Fig. 17. The curve $g = 0,9$ has a maximum at $Q_0\delta = -0,4$ (the maximum does not appear within the range shown in the Figure). With increasing load, the locking bandwidth is increased, and the AM-to-PM conversion around the band centre is decreased.

It may be concluded from Figs 15, 16 and 17 that in the case of $b_n \neq 0$, zero conversion occurs not in the locking band centre but at higher frequencies,

and the zero-conversion point is shifted to higher frequencies with increasing p_i and g, and with decreasing b_n.

The dependence of AM compression on susceptance non-linearity is shown in Fig. 18. Compression has poles at one or two frequencies. If b_n is small, the curve has two poles but only a single pole occurs with high b_n. At the pole the AM compression is infinite, i.e. output power does not depend on input power.

7. Dual circuit

In the previous part, the injection locked oscillator has been investigated by assuming a voltage controlled active element. However, a current controlled rather than a voltage controlled active element may also be assumed, introducing an equivalent circuit and element values which are duals of those given in Fig. 1.

The relations derived for the voltage controlled case may be rewritten according to the dual concept, thus describing the current controlled case which does not require separate treatment. All results valid for the voltage controlled case may be directly applied for the current controlled circuit after formal rewriting. Some parameters such as power, frequency and phase are duals of themselves and thus require no rewriting. In the final expressions, only the following two quantities should generally be rewritten:

$$
\begin{aligned}
g &\rightarrow r, \\
b_n &\rightarrow x_n.
\end{aligned}
\tag{36}
$$

Here r denotes the normalized load resistance, and x_n denotes the non-linearity factor of the diode reactance.

8. Conclusions

Properties of injection locked diode oscillators have been investigated according to the large signal model. Relations have been derived between the input and the output signal, and these have been used to determine the locking band. The locking band becomes substantially wider with increasing load and increasing input power, and is shifted to lower frequencies with increasing susceptance non-linearity.

Transfer properties such as output power, phase, group delay time, AM-to-PM conversion and AM compression have been determined. The frequency dependence of some parameters at different values of input power, load and diode susceptance non-linearity has been investigated. The charac-

teristis are symmetrical with respect to the resonant frequency if the diode susceptance is linear, but susceptance non-linearity introduces unsymmetry. Due to this unsymmetry, the lowest distortion is attained at higher than the band centre frequency.

<div align="center">Appendix</div>

$A-1$. Free-running oscillator

The free-running oscillator is treated according to Fig. 1. Diode admittance is given by Eq. (1). In the stable state, the admittance as seen in one of the directions at terminals $x-x$, has to be the negative value of the admittance as seen in the other direction. As admittances are complex quantities, this relation should separately hold for the real and for the imaginary parts as given by the following equations:

$$G_0(1 - \alpha U^2) = G\,, \tag{A-1}$$

$$- \omega C_{d0}(1 + \beta U^2) = \omega C_p - \frac{1}{\omega L_p}\,. \tag{A-2}$$

From these equations, two quantities, the amplitude and the frequency of the oscillation may be determined.

The power in the load is given by

$$P = GU^2 = G_0(1 - \alpha U^2)U^2. \tag{A-3}$$

Let us take the derivative of power with respect to U^2 and equate it to zero. From this relation we have

$$\alpha = \frac{1}{2U_m^2} \tag{A-4}$$

where U_m denotes the voltage at maximum power. Voltages will be normalized with respect to this quantity.

Let us normalize the admittances with respect to G_0. Substituting (A-4) into (1), the diode admittance will be according to Eq. (2).

Power is normalized with respect to the maximum value:

$$p = \frac{P}{P_m}\,. \tag{A-5}$$

Substituting (A-4) into (A-3) we get the maximum power:

$$P_m = \frac{1}{2}\,G_0 U_m^2\,. \tag{A-6}$$

Substituting (A-3) and (A-6) into (A-5), we have the normalized power:

$$p = \frac{GU^2}{\frac{1}{2}G_0 U_m^2} = 2gu^2. \tag{A-7}$$

Here g denotes the normalized value of the load conductance:

$$g = \frac{G}{G_0}. \tag{A-8}$$

According to (A-1) and (A-4), this may be written as follows:

$$g = 1 - \frac{1}{2} u^2. \tag{A-9}$$

Expressing u^2 and substituting it into (A–7), we have

$$p = 4g(1 - g). \tag{A-10}$$

The power is maximum ($p = 1$) if $g = 1/2$.

Oscillation frequency is determined from Eq. (A-2). At low voltages, the oscillation frequency is given by

$$\omega_0 = \frac{1}{\sqrt{L_p(C_p + C_{d0})}}. \tag{A-11}$$

This is identical with the small signal resonant frequency of the oscillator.

A—2. Operating input admittance

The operating input admittance may be defined in the case of operating circuits, for terminals at which both current and voltage is present at a given frequency. After specifying the positive directions of current and voltage, the operating input admittance for this side will be the ratio of these quantities:

$$Y_{0p} = \frac{I_{0p}}{U_{0p}}. \tag{A-12}$$

Here I_{0p} denotes the operating (actual) current flowing through the terminal at the given frequency, and U_{0p} is the operating (actual) voltage across the terminal at the same frequency.

The positive direction of the operating input admittance points to that side of the terminal pair at which the positive directions of the current and voltage are identical. In the direction of the other side, the operating input admittance will be $-Y_{0p}$ as the positive direction of the current is pointing in the opposite direction at this side, and the positive direction of the voltage is unchanged.

The operating input admittance may also be called operating admittance or input admittance. The operating output admittance may also be defined, being the negative value of the operating input admittance. Further, the operating input impedance may also be determined instead of the operating input admittance.

The concept of operating input admittance may be applied for steady state conditions or for the case of slow changes. It is dependent on the operating conditions of the circuit, and may only be defined by taking into account the complete circuit, including the driving and terminating conditions.

According to the previous considerations, the sum of the operating admittances taken in the two directions at a terminal pair is zero. This statement is valid at all frequencies at which current and voltage are simultaneously present.

Two reflection coefficients may also be determined for a terminal pair by regarding the propagating wave as entering into the terminal from the given side and the reflected wave as coming from the terminal in the opposite direction. The product of the reflection coefficients in the two directions is unity.

Let us apply these considerations for the circuit of Fig. 1. Let us determine the reflection coefficient at terminal $x-x$ looking in the direction of the circulator. Let u_0 be the voltage of the propagating wave and u_i the voltage of the reflected wave, thus the reflection coefficient is given by

$$\Gamma_c = \frac{u_i}{u_0} e^{j\Theta} . \tag{A-13}$$

From the known reflection coefficient, the operating input admittance y_2 in the direction of the circulator may be determined:

$$y_2 = \frac{1 - \Gamma_c}{1 + \Gamma_c} g . \tag{A-14}$$

Substituting into this equation (A-13) and making suitable rearrangements, we have

$$y_2 = \frac{u_0^2 - u_i^2 - j2u_0u_i \sin \Theta}{u_0^2 + u_i^2 + 2u_0u_i \cos \Theta} g . \tag{A-15}$$

6

A—3. *Relation between input and output signals*

The relation between input and output signals is implicitly contained in the set of non-linear equations (13) and (14). However, suitable rearrangements are necessary to separate the unknown variables.

Let us multiply (13) by u^2, and expressing u^4 from the equation thus formed, let us substitute it into (14) which is also multiplied by u^2. The following relation is then attained:

$$2u_0 u_i \sin \Theta = \frac{2}{g}(Q_0\delta + b_n)u^2 - 2b_n(u_0^2 - u_i^2). \tag{A-16}$$

Further, from (15) we obtain

$$2u_0 u_i \cos \Theta = u^2 - (u_0^2 - u_i^{..}) - 2u_i^2. \tag{A-17}$$

Squaring Eqs (A-16) and (A-17) and summing these equations, further expressing u^4 from (13) and substituting it into this sum, we have the following relation for u^2:

$$u^2 = \frac{1}{2}\frac{2gC - A(u_0^2 - u_i^2)}{C - B(u_0^2 - u_i^2) - 2u_i^2}(u_0^2 - u_i^2). \tag{A-18}$$

Here the notations as given in (20) are applied.

The diode voltage u as given by Eq. (A-18) does not depend on Θ. Substituting thus (A-18) into (13), u^2 is eliminated, leaving a single unknown, $(u_0^2 - u_i^2)$ in the equation. Rearranging this equation, and introducing powers instead of voltages by utilizing (16), (17) and (18), we arrive at the cubic equation (19).

The tangent of the phase is given by the quotient of (A-16) and (A-17)

$$\tan \Theta = \frac{\dfrac{2}{g}(Q_0\delta + b_n)\,u^2 - 2b_n(u_0^2 - u_i^2)}{u^2 - (u_0^2 - u_i^2) - 2u_i^2}. \tag{A-19}$$

Substituting into this equation the formulas (A-18), (16), (17) and (18), we arrive at Eq. (21).

Further, substituting into (A-17) formulas (A-18), (16), (17) and (18) we have Eq. (22) which is the cosine of the phase.

A—4. *Measurement of the susceptance non-linearity factor*

The susceptance non-linearity factor can be measured in the amplifying operating mode in the following way. First, the band centre frequency f_0, the band centre power gain G_{p0} and the half power bandwidth B_s are measured

with the given diode at a low level. Following this, the band centre frequency f_c and the band centre power gain G_{pc} are measured at a higher level. From these measured values, the susceptance non-linearity factor is calculated according to the following equation:

$$b_n = \frac{2Q_0}{\sqrt{1 - p_{dc}} - 1} \left(\frac{f_c}{f_0} - 1 \right) \tag{A-20}$$

where

$$Q_0 = \frac{f_0}{B_s} \frac{g^2 - 1}{\sqrt{4g - (g-1)^2}} \ , \tag{A-21}$$

$$p_{dc} = \frac{\sqrt{G_{pc}} - 1}{(\sqrt{G_{pc}} + 1)^2} \ [8g^2 - 4g(g-1)(\sqrt{G_{pc}} + 1)] \ , \tag{A-22}$$

$$g = \frac{\sqrt{G_{p0}} + 1}{\sqrt{G_{p0}} - 1} \ . \tag{A-23}$$

The relations between input and output signal are valid not only for injection locked oscillators but also for reflection type amplifiers, the only difference being that for oscillators, $g \leq 1$, and for amplifiers, $g > 1$. Applying the relations for low level and band centre, the previous formulae for the susceptance non-linearity factor may be derived. As b_n is a quantity which is characteristic for the diode only, the value measured in the amplifying mode will be valid for oscillator mode, as well.

A—5. Derivated characteristics

The group delay time is the derivative of the phase shift with respect to angular frequency:

$$\tau = \frac{d\Theta}{d\omega} \ . \tag{A-24}$$

AM-to-PM conversion is defined as the phase change in degrees introduced by a 1 dB input power change. This is computed by taking the derivative of the phase with respect to the input power and multiplying this by the 1 dB change of the input power. In the following, a 1 dB increase, i.e. 26% change of the input power will be taken, thus the formula for AM-to-PM conversion is the following:

$$cv = 0{,}26 \frac{180}{\pi} \ p_i \ \frac{d\Theta}{dp_i} \ [^\circ/dB] \ . \tag{A-25}$$

The derivative value reflects the circuit behaviour in the vicinity of the working point, as at an input power increased by 1 dB, the function $\Theta(p_i)$ may deviate somewhat from the tangent.

6*

AM compression is defined as the ratio of input signal relative amplitude change to output signal relative amplitude change. Assuming a differential change, the formula for AM compression is the following:

$$cp = \frac{du_i/u_i}{du_0/u_0} = \frac{u_0}{u_i}\frac{du_i}{du_0}.$$

(A-26)

Computing the du_i/du_0 derivative by using the chain rule, we have

$$\frac{du_i}{du_0} = \frac{du_i}{dp_i}\frac{dp_i}{dp_0}\frac{dp_0}{du_0} = \frac{u_0}{u_i}\frac{dp_i}{dp_0}.$$

(A-27)

Substituting (A-27) into (A-26) and taking into account Eqs (16) and (17), the AM compression will be expressed as follows:

$$cp = \frac{p_0}{p_i}\frac{dp_i}{dp_0}.$$

(A-28)

The AM compression may have a negative sign, meaning that the phase of the amplitude modulation is shifted by π.

AM compression may also be expressed in dB:

$$Lcp = 20 \lg \mid cp \mid, \ [dB].$$

(A-29)

The sign of the compression is then lost. The amplitude modulation is decreased when $\mid cp \mid > 1$, and increased when $\mid cp \mid < 1$.

REFERENCES

1. ADLER, R.: A Study of Locking Phenomena in Oscillators, *Proc. IRE*, **34**, (1946) 351—357
2. KUROKAWA, K.: Noise in Synchronized Oscillators, *IEEE Trans. MTT*, Vol. MTT-16, (1968) 234—240
3. HINES, M. E.—COLLINET, J. R.—ONDRIA, J. G.: FM Noise Suppression of an Injection Phase-locked Oscillator, *IEEE Trans. MTT*, Vol. MTT-16, (1968) 738—742
4. HINES, M. E.: Negative-resistance Diode Power Amplification, *IEEE Trans. ED.*, Vol. ED-17, (1970) 1—8
5. HANSSON, G. H. B.—LUNDSTRÖM, K. I.: Stability Criteria for Phase-locked Oscillators, *IEEE Trans. MTT*, Vol. MTT-20, (1972), 641—645
6. KUROKAWA, K.: Injection Locking of Microwave Solid-state Oscillators, *IEEE Trans. MTT*, Vol. MTT-21, (1973), 1386—1410
7. BERCELI, T.: Analysis of Microwave Tunnel-diode Oscillators, *XII. Internationales Wissenschaftliches Kolloquium (Ilmenau)*, Heft 9, *Mikrowellentechnik*, Teil II, (1967), 33—40
8. GUSTAFSSON, L.—HANSSON, G. H. B.—LUNDSTRÖM, K. I.: On the Use of Describing Functions in the Study of Non-linear Active Microwave Circuits, *IEEE Trans. MTT*, Vol. MTT-20, (1972), 402—409
9. GREILING, P. T.—HADDAD, G. I.: Large-signal Equivalent Circuits of Avalanche Transit-time Devices, *IEEE Trans.*, *MTT*, Vol. MTT-18, (1970), 842—853

10. Eisenhart, R. L.: An X-band GaAs Impatt Power Amplifier, 1975, *IEEE International Solid-State Circuits Conference*, Digest of Technical Papers, 132—133.
11. Hines, M. E., Large-signal Noise, Frequency Conversion, and Parametric Instabilities in Impatt-diode Networks, *Proc. IEEE*, **60** (1972), 1534—1548
12. Van der Pol, B., Forced Oscillations in a Circuit, with Non-linear Resistance, *Phil. Mag.*, (1927), 65—80
13. Tager, A. S.—Bold, Petrov, V. M.: Avalanche Diodes and their Application in Microwave Techniques, (in Russian), Sovietskoe Radio, Moscow 1968
14. Berceli, T.: Nonlienar Effects in Impatt-diode Amplifiers, *Conference Proceedings of the 5th European Microwave Conference/Microwave 75*, (1975) 705—709
15. Gustafsson, L.—Lundström, K. I.—Hansson, G. H. B.: Basic Properties of Subharmonic Injection Locking, *IEEE Trans. MTT*, Vol. MTT-21, (1973), 28—34
16. Haddad, G. I.: Avalanche Transit-time Devices, Artech House Inc, Dedham, Mass. 1973.
17. Gustafsson, L.—Lundström, K. I.—Hansson, G. H. B.: Maximum Phase-locking Bandwidth Obtainable by Injection Locking, *IEEE Trans. MTT*, Vol. MTT-21, (1973), 353—355
18. Bulman, P. J.—Hobson, G. S.—Taylor, B. C.: Transferred Electron Devices, Academic Press, New York 1972
19. Hobson, G. S.: The Gunn Effect, Clarendon Press, Oxford 1974.

Eigenschaften von durch Signalinjektion gesteuerten Dioden bei großen Signalen. Die Eigenschaften der mittels Signalinjektion gesteuerten Diodenoszilllatoren werden aufgrund eines Modells mit großem Signal untersucht. Für den Zusammenhang des Ein- und des Ausgangssignals werden Zusammenhänge abgeleitet und hieraus wird der Steuerbereich bestimmt, der sich bei Vergrößerung der Nichtlinearität der Suszeptanz in Richtung von niedrigeren Frequenzen verschiebt. Die Übertragungscharakteristiken werden bestimmt, und zwar die Ausgangsleistung und -phase, die Gruppenlaufzeit, die AM-PM-Konversion und die AM-Kompression. Die Frequenzabhängigkeit der einzelnen Charakteristiken wird bei verschiedenen Werten der Eingangsleistung, der Belastung und der Nichtlinearität der Diodensuszeptanz untersucht. Als Folge der Nichtlinearität der Diodensuszeptanz zeigt sich Asymmetrie. Wegen derselben erhält man die kleinste Verzerrung nicht in der Bandmitte, sondern bei höheren Frequenzen.

Свойства при больших сигналах диодных осцилляторов, управляемых введением сигнала. Свойства диодных осцилляторов, управляемых введением сигнала, исследованы на основе модели с большим сигналом. Выведены зависимости относительно связи между сигналами на входе и выходе. На основе этой зависимости определена полоса управления. Эта полоса при повышении нелинейности сусцептанции сдвигается в сторону меньших частот. Определены характеристики переноса, а именно выходную мощность и фазу, далее время группового пробега, конверсию АМ—РМ и компрессию АМ. Исследована зависимость от частоты отдельных характеристик при различных значениях мощности, нагрузки и нелинейности сусцептанции диода. В результате нелинейности сусцептанции диода имеет место асимметрия. Наименьшее искажение из-за асимметрии получается не по середине полосы, а при частоте, превышающей частоту середины полосы.

A COMPARATIVE EXPERIMENTAL STUDY OF THE ACCURACY AND PRECISION OF MEASUREMENTS OF EXTERNAL SCREW THREADS BY DIFFERENT METHODS

ABDEL-MONEIM M. HAMOUDA*

The main objective of this paper is to compare experimentally among three methods applied for measuring the effective diameter of external screw threads namely, the optical, the optical with knife edge and the three wire method regarding — a) the degree of accuracy and b) the degree of precision of the result computed from the measurements taken by each method on a screw thread plug gauge. The three methods are different and each has its own cause system of errors, both the controllable and uncontrollable errors inherent in the measuring system of each method.

Symbols

F = Effective or flank diameter, on which the thickness of the thread is equal to half the pitch [mm]
M = Measurements over the wire [mm]
P = Linear pitch [mm]
α = Profile angle
β = Mean helix angle given by the formula $\tan \beta = P/(\pi F)$
d = Wire diameter [mm]
c = Correction term compensating for the obliquity of the wire in the thread, and equal to $1/2\, d \tan{}^2\beta \cos \alpha/2 \cot \alpha/2$
σ_T = Total precision of measurements μm
σ_m = Precision of measuring machine μm
σ_c = Precision of the operator μm
σ_{os} = Precision of the operator due to the setting process μm
σ_{or} = Precision of the operator due to the reading process μm

1. Introduction

The screw threads are widely used for the purpose of locating, transmitting motion, force or torque and providing an easy method for the assembly and disassembly of machine parts.

To obtain a high quality performance, specially in fine precise motion, the screw thread dimensions should be accurate.

There is a wide range for the degree of accuracy of the measurements of screw threads that interest the metrologist, varying from the wide tolerance limits applicable to commercial nuts and bolts to the very close limits set for reference screw gauges.

* Dr. ABDEL-MONEIM, M. HAMOUDA, Assistant Professor Production Engineering Dept. Faculty of Engineering, Alexandria University, Egypt

The statistical characteristics of a measurement process can be assessed and used only when it can be verified that this particular process is generated by the specified method with the assigned system of causes and is capable of a state of statistical control, two statistical characteristics of a measurement process here are of importance, precision and accuracy.

The words precise and accurate as well as precision and accuracy have acquired a relative or comparative sense when applied to the statistical properties of a measurement process. "Precision" of a measurement process refers to the natural agreement between the individual measurements from the process, while "Accuracy" refer to the degree of agreement of measurements with an accepted reference level of the property in the material measured.

2. Experimental work

Specimen:

A standard screw thread plug gauge made of hardened steel having the following dimensions according to (SI) standard was used: —

outer diameter = 20 [mm],
pitch   = 2,5 [mm]

nominal effective diameter = 18,37 [mm]

Apparatus and measuring techniques

1. *The Optical Method*

The universal measuring microscope (Fig. 1) was used. The screw thread is clamped between centres and the goniometer ocular eye-piece head is focused. and then one of the lines in the dial templet is to be set coincident with
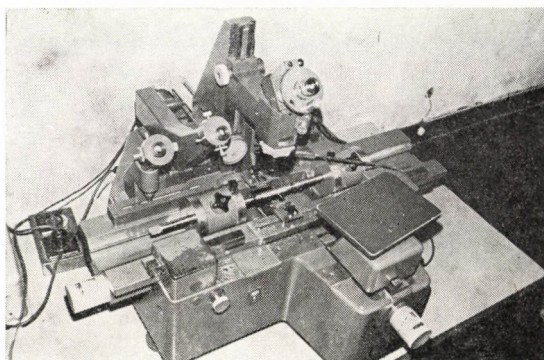
Fig. 1. An Universal Measuring Microscope

the thread flanks, as shown in Fig. 2. Then the difference of the traverse direction readings (I and II) determines the value of the effective diameter.

2. *The Optical Method Using Knife Edge Technique*

The universal measuring microscope previously described was also used. Knife edges make it possible to produce images of sectional planes without damaging the specimen (Fig. 3). The lines of intersection are represented by
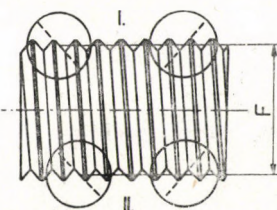
Fig. 2. Measuring effective Diameter by Optical Method
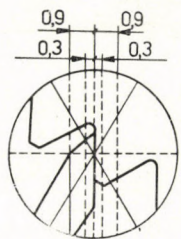
Fig. 3a. Measuring effective diameter by knife edge
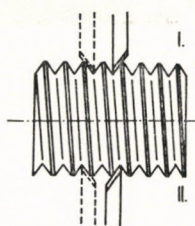
Fig. 3b. Knife edge setting

a hair line, at a distance of 0,3 or 0,9 mm from the edge of the knife-edge. This line is engraved on the top surface of each knife edge and it must be brought to coincide with the corresponding line of the goniometer ocular, previously described.

The knife edges are fixed in their holders and each of them is brought into contact with each flank of the screw thread.

The readings are taken when the hair line on the knife edge coincides with one of the outer dotted lines on the goniometer ocular as shown in Fig. 3.

3. *The Three Wire Method*

The effective diameter of plug screw thread was measured by the well-known three wire method using the Abbe Horizontal Metroscope (Fig. 4).

The experimental work was carried out at constant measuring load of 125 gms. The best wire diameter was determined from tables at $\alpha = 60°$ and pitch $= 2,5$ mm to be 1,35 mm

The effective diameter can be calculated from the following formula (see Fig. 5 and Appendix)

$$F = M + (P/2 \tan (\alpha/2) - d \left(1 + \frac{1}{\sin \alpha/2}\right) - c .$$
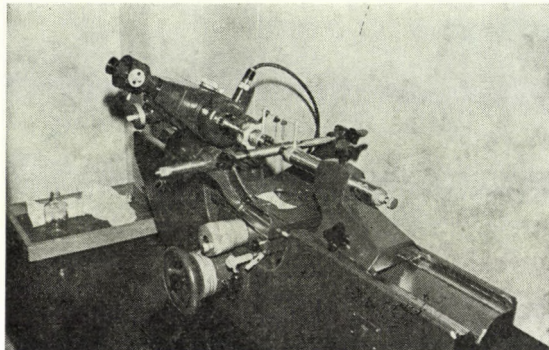

Fig. 4. Abbe Horizontal Metroscope
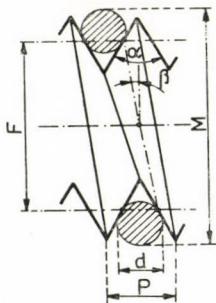
Fig. 5. Measuring Effective diameter using three wire

Operators

Four operators (A, B, C and D) carried out the experimental work after being given sufficient training on the measuring equipment used.

Each of them measured the effective diameter of the standard screw thread plug gauge of the known standard value 100 times in a well kept thermal environment of $20 \pm 1\ °C$ following the procedure set for each of the three methods investigated.

Error computation

The frequency distribution curve for each group of 100 readings was plotted.

The deviation of the mean value of the 100 readings from the standard value of the plug gauge was considered as a measure of the degree of accuracy, while the standard deviation of the 100 readings was considered as a measure of the degree of precision.

3. Results

A) Optical method

The frequency distribution curves Figs 6, 7, 8 and 9 were plotted for operators A, B, C and D.

It can be seen from the Figures that they conform the normal distribution characteristics, A normality test was carried out to find out whether the confidence level for all plotted histograms lies between 80 and 90%.

This means that the standard deviation (σ) can be taken to represent the index of the overall precision of the measuring operation (both the equip-
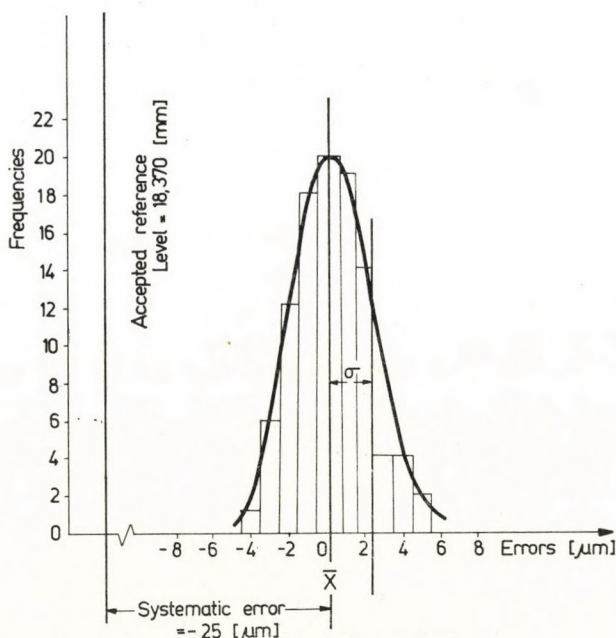
Fig. 6. Frequency Curve of Person (A)

ment and the operators) and the difference between the mean value and the standard value can be taken to represent the index of the accuracy of the operation.
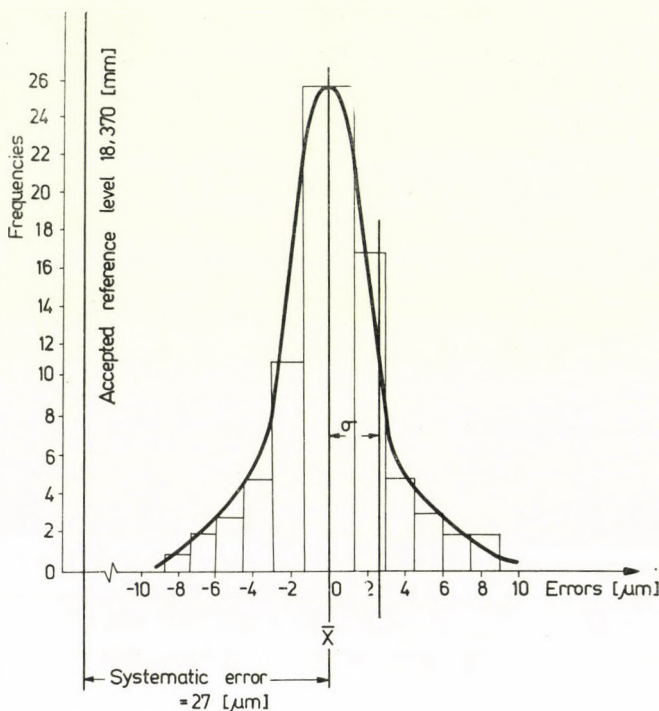
Fig. 7. Frequency curve of person (B)

The following results were obtained:

Operator	Index of overall precision [μm]	Index of accuracy [μm]
A	2,4	—25
B	2,5	—27
C	2,4	—22
D	2,7	—30
Average	2,5	—28
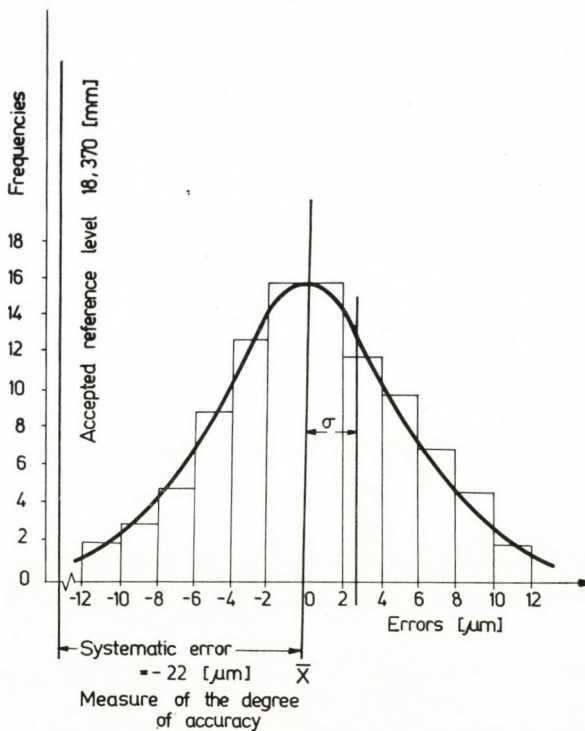
Fig. 8. Frequency curve of person (C)
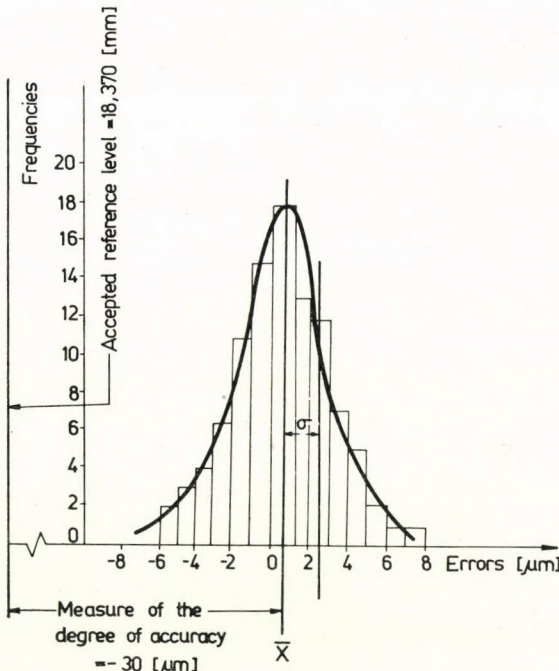
Fig. 9. Frequency curve of person (D)
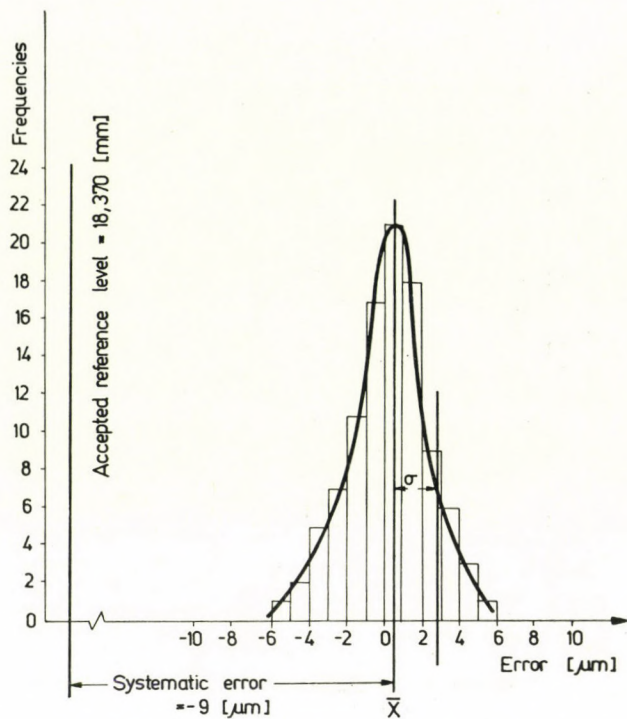
Fig. 10. Frequency curve of person (D)

B) Knife edge method

Figure (10) shows one of the obtained results for operator *D* while the results for the four operators were obtained as follows:

Operator	Index of precision [μm]	Index of accuracy [μm
A	2,3	−10
B	2,2	− 8
C	2,4	−11
D	2,3	− 9
Average	2,3	− 9,5

C) Three wire method

Figure (11) shows one of the obtained results for operator *A* while the results for the four operators were obtained as follows:

Operator	Index of precision [μm]	Index of accuracy [μm]
A	0,6	22
B	0,7	24
C	1,0	22
D	0,9	20
Average	0,8	22
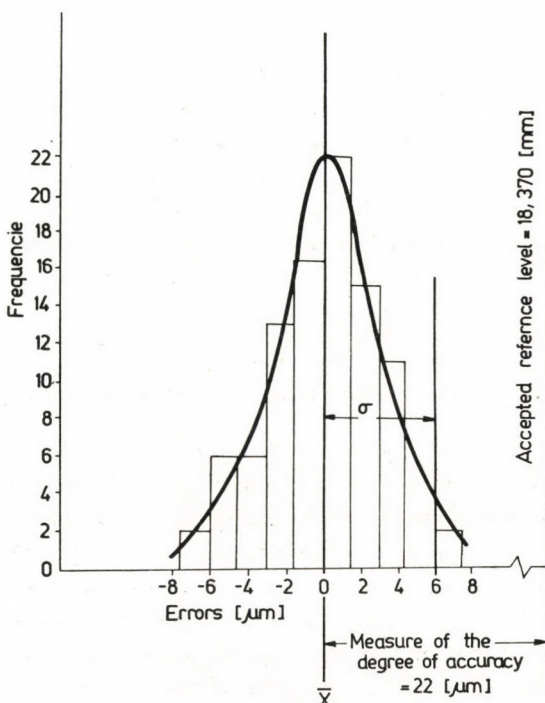
Fig. 11. Frequency curve of person (A)

4. Discussion

From the results obtained for the three different methods we can see that the degree of accuracy varies from one operator to the other for each of the three methods especially in the optical one. This can be explained as due to the relatively large values of error incorporated in the setting of the hair lines in the occular tangent to the profile of the flank of the screw thread while in the knife edge method the error of coinciding the lines on the knife edge with the line in the goniometer occular is much less.

The degree of accuracy obtained by the four operators in each of the three methods cannot be considered consistent, e.g. the most accurate operator was C in the optical method while operator B in the knife edge method and D in the three wire method. This means that every operator has his own degree of skillness, excellence and judgement incorporated with the specific method of measurement.

Regarding the index of the total precision for each method they can be graded according to the following order:

1. Three wire method
2. Knife edge method
3. Optical method

This is significant since in the three wire method the value of the total precision depends only on the inherent precision of the horizontal metroscope and the estimation error of the operator while reading on the spiral vernier scale, while in the case of the knife edge method the total precision is a result of the inherent precision of the universal tool-makers' microscope, reading off the scale and the process of the setting of the two hair lines to be concident with the engraved lines on the knife edge which can be more precisely done than in the case of the optical method.

Operator precision as a cause system of measuring errors

The total precision (σ_T) of measurements is a resultant of both the inherent precision of the measuring machine (σ_m) and the precision of the operator (σ_o), the latest precision can be divided into two types,

a) Setting precision for each operator, which depends on the individual skill applied to the setting process for the hair lines in both optical and knife edge methods not occuring in the case of three wire method (contact type).

b) Reading precision for each operator, which depends on the degree of skill in the estimation of the fraction of the last digit.

Evaluation of the overall total precision

The overall total precision can be expressed as follows:

$$\sigma_T = \sqrt{\sigma_o^2 + \sigma_m^2} \ .$$

The above equation illustrates the so-called "Component variance Model" in which σ_0 and σ_m are the standard deviations associated with operator and inherent precision of the measuring machine, respectively.

Also we can express the standard deviation of the operator σ_0 by the following equation:

$$\sigma_o = \sqrt{\sigma_{os}^2 + \sigma_{or}^2}$$

where

σ_{os} = standard deviation due to the setting process
σ_{or} = standard deviation due to the reading process

and the following epuations can be applied for the three methods:

$$\sigma_o(\text{optical}) = \sigma_{oop} = \sqrt{\sigma_{os}^2 + \sigma_{or}^2}\,,$$

$$\sigma_o(\text{knife edge}) = \sigma_{ok} = \sqrt{\sigma_{os}^2 + \sigma_{or}^2}\,,$$

$$\sigma_o(\text{three wire}) = \sigma_{orw} = \sqrt{\sigma_{or}^2}$$

From the previous results the equations of the total coverage overall precision for each method produced from four persons are:

$$\sigma_{mop}^2 + \sigma_{0op}^2 = 6{,}25\,, \tag{1}$$

$$\sigma_{mk}^2 + \sigma_{0k}^2 = 5{,}29\,, \tag{2}$$

$$\sigma_{mrw}^2 + \sigma_{0rw}^2 = 0{,}64\,, \tag{3}$$

since $\sigma_m\,op = \sigma_m k$ (the same measuring machine) and assuming that

$$\sigma_{mk} = \sigma_{mrw} = \sigma_m$$

in case of three wire-method which is a very acceptable assumption, then

$$\sigma_m^2 + \sigma_{or}^2 + \sigma_{os'} = 6{,}25\,, \tag{4}$$

$$\sigma_m^2 + \sigma_{or}^2 + \sigma_{os}^2 = 5{,}29\,, \tag{5}$$

$$\sigma_m^2 + \sigma_{or}^2 = 0{,}64\,. \tag{6}$$

Since the spiral vernier scales are the same for each method, so the standard deviation resulting from the reading process and the machine, can be considered identical for all methods and persons.

Then from Eqs 4, 5 and 6

$$\sigma_{os'}^2 = 5{,}61\,, \qquad \sigma_{os}^2 = 4{,}65\,,$$

$$\sigma_{os'}^2 = 2{,}37\,\mu\text{m} \qquad \sigma_{os} = 2{,}16\,\mu\text{m}$$

i.e. the standard deviation produced from the setting process for the optical method $(\sigma_{os'})$ is larger than that produced from the knife edge method (σ_{os}).

To find out each value of σ_m and σ_{or} we have to make the following assumption.

7

For any machine its precision (i.e.) the ability of the machine to repeat and regain its position should not exceed normally 0,1 of the least devision of its scale.

Then we can say $6\sigma_m = 0,1$ μm and if we can consider that the precision of the machines under investigation have deteriorated by 100% since their purchase 15 years ago, then

$$6\,\sigma_m = 0,2$$

$$\sigma_m = 0,03\ \mu\text{m}$$

substituting in Eq. (7)

$$\sigma_{or}^2 = 0,631$$

then $\sigma_{or} = 0,8$ μm. it is clear that the value of σ_m^2 is negligible compared with σ_{or}^2.

5. Conclusion

We can conclude the following:

1. The precision of any measurement is mainly governed and highly affected by the operator.

2. The precision of any measurement should be analyzed to determine the value of the precision of the operator at each step (e.g.)

a) The setting precision which depends whether it is a contact method or contactless, it greatly affects the total measuring precision especially in the contactless type, in case of optical method $(\sigma_{os'})$ was 2,37 μm, in case of knife edge method (σ_{os}) was 2,16 μm. The setting precision can be neglected in case of a contact type of three wire method under constant measuring load (125 gms).

b) The reading precision, which depends on the designed scale, has small effect on the total measuring precision than the setting precision. On the spiral vernier scale it was 0,7 μm.

3. The degree of accuracy in the contact type is lower than in the contactless type because the deformation effects are the same of working conditions!

4. The inherent precision of the measuring machine can be neglected compared with both setting and reading precision of the operator.

5. Comparing the values of the index of accuracy obtained for each method they can be graded according to the following order:

Knife edge method,
Three wire method,
Optical method.

Regarding the index of precision the following order was obtained

Three wire method,
Knife edge method,
Optical method.

Appendix

Theoretical formulae for the measurement of effective diameter using three wire method

Theoretical formulae of the measurement of effective diameter using the 3-wire method

The general formula is:

$$F = M + \frac{P}{2.\tan \alpha/2} - d - \frac{d}{\sin \alpha/2} - C .$$

It remains valid for whatever wire diameter and profile angle, even when bissectrix of this angle is not accurately pendicular to the thread axis. In this case the effective diameter refers to equal thickness of thread and notch, whereas the apparent diameter is larger.

The single condition for the validity of the above formula is that the wires take contact on the flanks and that same are straight Fig. (5) For curved flanks the effective diameter has no sense.

The correction C compensates for the obliquity of the wires in the thread according to the mean helix angle β.
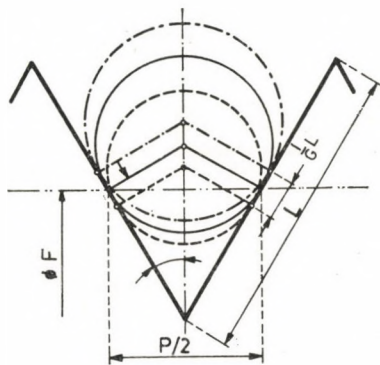
Fig. 12

The term C is given by the formula

$$C = \frac{1}{2} d \tan^2 \beta \cdot \cos \frac{\alpha}{2} \cot \alpha/2 .$$

For standard threads, C is equal to about 0,002 mm and it is, therefore, necessary to be taken into account. For fine pitches, C can mostly be neglected

Best wire diameter

The general formula given is valid for any pitch and diameter of wires, on condition to introduce the actual profile angle and so for as the contact takes place on the flanks. As the actual profile angle α is never accurately equal to the nominal angle, it will be of advantage to use wires of "best diameter" with which the contact is obtained exactly on the effective diameter the error of angle α taken will have no noticeable influence on the measurement of the effective diameter F.

As the great variety of pitches and the manufacturing tolerances of the wires do not allow the performance of the measurement with the absolute best diameter d_{nom}, the influence of the angle α and the diameter d on F was to be negligible when the contact between wire and thread flank is obtained within the medium eighth of the flank length (Fig. 12), i.e. when

$$d_{max} = d_{nom} \left(1 + \frac{1}{8}\right) = 1,124 \ d_{nom} ,$$

$$d_{min} = d_{nom} \left(1 - \frac{1}{8}\right) = 0,876 \ d_{nom} ,$$

where d_{nom} is the wire diameter which contacts exactly on the effective diameter F according to the formula:

$$d_{nom} = \frac{P}{2 \cos \alpha/2}$$

when using wire of the best diameter d_{nom} or at least between d_{max} and d_{min} the error of α as was practically realized, will have no noticeable influence on F. The errors in P can also be neglected.

Acknowledgments

Eine vergleichende experimentelle Studie über Genauigkeit und Präzision von Außengewindemessungen mit verschiedenen Methoden. Hauptzweck der Arbeit ist drei Verfahren für die Messung des Flankendurchmessers von Außengewinden zu vergleichen, und zwar das optische Verfahren, das optische Verfahren mit einer Messerschneide und die Dreidrahtmethode. Untersucht wurden a) die Genauigkeit und b) die Präzision der Resultate mit jeder Methode, berechnet aus den Messungen an einem Gewindelehrdorn. Die drei Verfahren sind verschieden und jedes hat sein eigenes System von Fehlerursachen, sowohl was die beherrschbaren als auch die nicht beherrschbaren Fehler betrifft.

Сравнительное экспериментальное исследование точности и прецизности измерения внешних нарезок, выполненного при помощи различных методов. Основной целью данной работы является экспериментальное сравнение трех различных методов измерения среднего диаметра внешней нарезки, а именно оптического метода, далее очень резкого оптического метода и метода с помощью трех измерительных проволок в отношении *а)* степени точности и *б)* степени прецизионности. Результаты вычислены на основе данных измерений, выполненных с помощью всех трех методов на калибре «пробке» для измерения внутренней нарезки. Все три метода являются различными и каждая из этих методов имеет собственную ингерентную систему погрешностей, как в отношении доминируемых, так и в отношении недоминируемых погрешностей.

THE EXCITATION MECHANISM OF THE 6¹D₂ LEVEL OF Hg ATOMS IN THE POSITIVE COLUMN OF A LOW-PRESSURE MERCURY-ARGON-DISCHARGE

K. G. ANTAL,* E. GÁTI**

In the paper the radial structure of the positive column of a discharge in $6 \cdot 10^{-7}$ Torr Hg vapour and 2,5 Torr Ar working gas is investigated experimentally and theoretically. The assumed plasma model is checked by probe measurements, and by a spectroscopic method, the radial distribution of the intensity of the 579,1 nm wavelength line is determined. As an evaluation of the obtained profile the ratio of the direct and the indirect processes is determined using a simple population model. The dependence of this ratio from the microparameters of the discharge and the integrated transition probabilities has been calculated.

1. Introduction

In the radiation mechanism of low-pressure vapour discharges with an Ar working gas a fundamental role is played by the 6^3P_1 and 6^1P_1 resonance levels. As is known from the point of view of light generation the transition $6^3P_1 - 6^1S_0$ (253,6 nm) can be considered of prime importance, as it provides 90% of the ultraviolet flux easily converted into visible. For this reason the population of the metastable levels 6^3P_1 and of 6^3P_0 and 6^3P_2 forming with it a triplet, have been theoretically and experimentally investigated by numerous authors [1, 2]. Assuming that the $6^3P_{0,1,2}$ system can be considered as being relatively independent of the higher levels, already knowing the eaerlier measured excitation functions [3, 4] a theoretical model could be elaborated which agrees well with the experiments.

Less attention is paid by authors to the transition $6^1P_1 - 6^1S_0$ (184,9 nm) which, although of secondary importance for light generation, plays an important role in the reduction during the life of the efficiency of some discharge light sources (e.g. the photolysis of halophosphate luminescent powders).

It is well shown on the energia diagram of the Hg atom (Fig. 1) that besides the direct excitation which can be considered as a first approximation with the population of the 6^1P_1 level, in the finer approximation, nearer to the experimental results, the transitions from the levels 7^1S_0 and 6^1D_2 must be considered too. These levels are much higher than the $6^3P_{0,1,2}$ system and so

* K. G. ANTAL, Ritka u. 3 H-1204 Budapest, Hungary
** E. GÁTI, Bajcsy Zs. köz 3, H-1065 Budapest, Hungary

it can be assumed that during their excitation the two-stage phenomena provides a non-negligible contribution. The more complicated equations describing the one- and two-stage processes are naturally no longer linear.
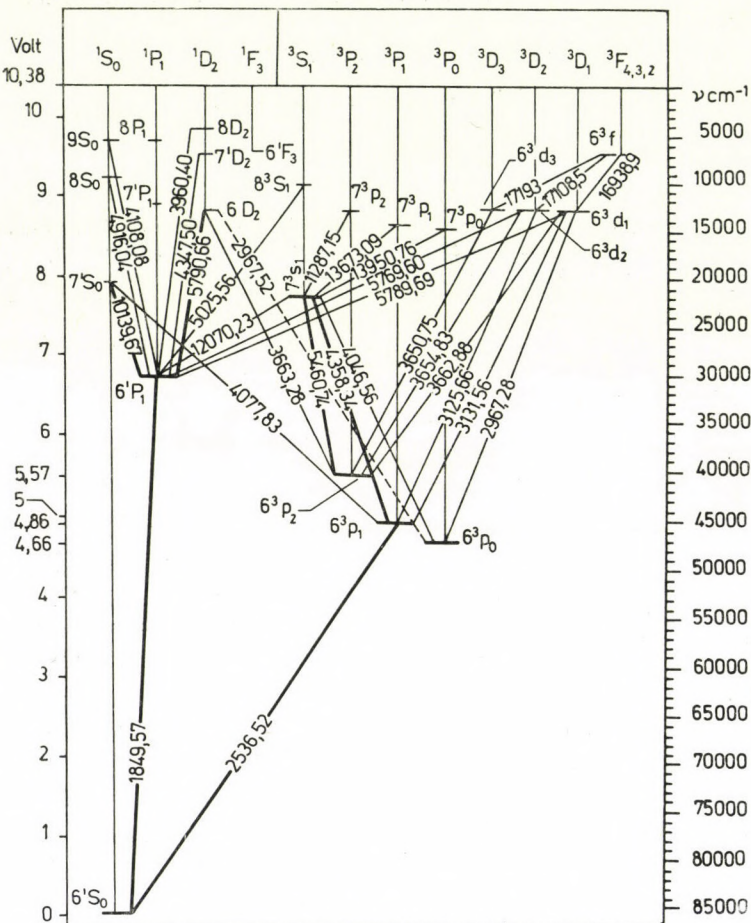

Fig. 1. The energy level system of the Hg atom [5]

The population of the higher excited levels as a function of the electron concentration can be described in the well-known generalized form

$$n_s = An_e + Bn_e^2 \tag{1}$$

where

n_s — the population of the excited level,
n_e — the electron concentration,
A, B — factors containing the integrated excitation probabilities.

The value of the parameters A and B naturally depends on the concrete discharge conditions.

In the present paper the radial structure of the intensity of the 579,1 nm line belonging to the transition $6^1D_2 - 6^1P_1$, and through this the population and the excitation mechanism of the 6^1D_2 level, will be investigated. (We will not investigate the transition $7^1S_0 - 6^1P_1$ which can be dealt with in a similar way as the transition $6^1D_2 - 6^1P_1$). The measurements were made on the positive column of a 36 mm inner dia., 1200 mm long glass discharge tube with oxide cathodes of equal construction. The principal characteristics of the examined discharge are the following: 2,5 Torr argon; saturated Hg vapour pressure corresponding to 40 °C wall temperature ($6 \cdot 10^{-3}$ Torr); in a d.c. operation the discharge current was 430 mA, the burning voltage 104 V.

2. Experimental results

The experimental tube was operated with the system shown in Fig. 2 where the switch K_1 permitted to change from the a.c. operation facilitating the ignition to the d. c. operation used for the measurements. In d.c. operation the switch K_2 serves for changing polarity. The discharge current was measured on the poles 7—8, the burning voltage on the poles 5—6.

For determining two characteristic microparameters of the discharge — its electron temperature and its electron concentration — the probe circuit shown in Fig. 3 was employed. The radially moveable probe was placed in the centre of the tube, the A_1 stabilized d.c. supply unit with the 10 kOhm
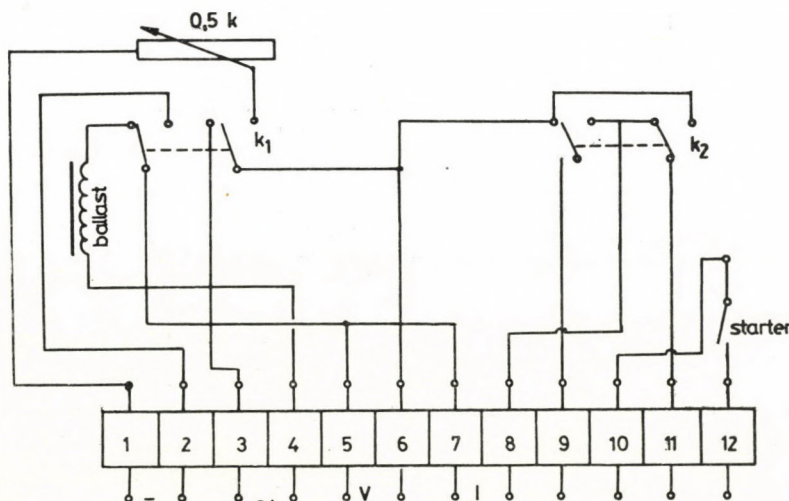

Fig. 2. Supply unit. fojtó = V, 2 A); 3—4 a.c. stabilized supply unit (0 ... 250 V, 2 A, 50 Hz); 5—6 voltmeter, 7—8 ammeter, 9—10, 11—12 to electrodes

rheostat belonging to it were used for adjusting the probe voltage, galvano-
meter G measured the working current. Measurement of the probe voltage was
made more accurate by compensating the plasma potential referred to the
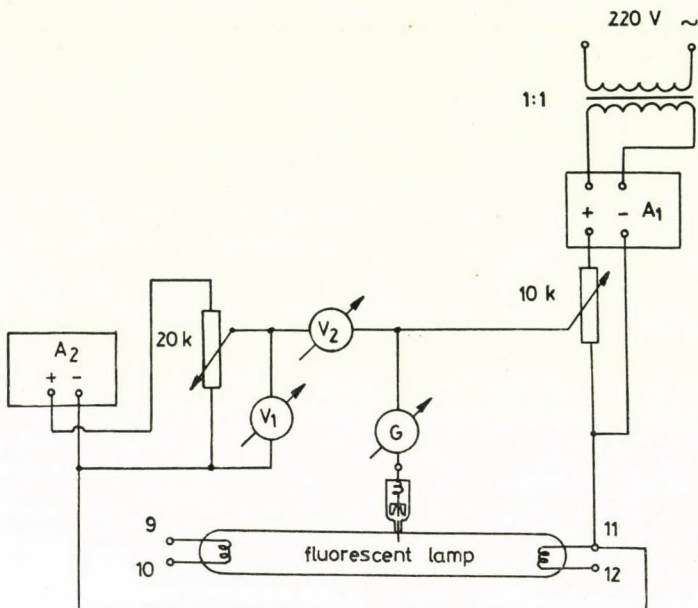
*Fig. 3.* d. c. probe circuit; discharge tube
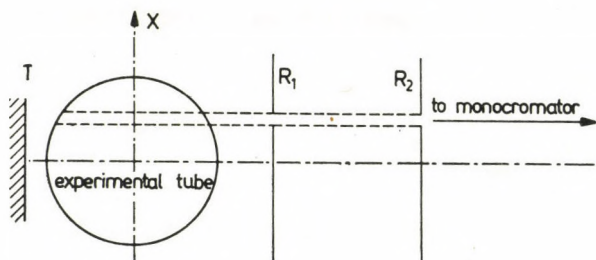
Fig. 4. Optical arrangement for measuring the intensity distribution along the X axis; discharge
tube; to monochromator

cathode (approx. 50 V) with the stabilized supply unit A_2 and the deviation
from this was measured with the instrument V_2. The cylindrical probe used
was made of molybdenum, its dia. was 0,50 mm, its length 2,20 mm — the
geometry and the measuring arrangement are the same as described in ref. [7].

With the optical arrangement shown in Fig. 4 the distribution along the
X axis of the 579,1 nm Hg line was measured with the aid of an UM-2 type
monochromator. The X—Y coordinate system was fixed in a plane normal

to the axis of the discharge tube. The height of the slits R_1 and R_2 was 10,0 mm, their width 0,20 mm. Mirror T served for checking any self-absorption. Measuring the intensity with and without the mirror, the radial distribution of the self-absorption was determined and thus it was ascertained that for the 579,1 nm line the plasma can be considered as a thin one.

3. The radial distribution of the electron concentration and the electron temperature

When modelling the positive column, for a start the following assumptions were made, which are generally accepted and experimentally confirmed for similar discharges [8, 9]:

— the argon working gas does not take part directly in the excitation and ionization phenomena, due to its action in the first approximation the mean free paths are negligible as compared with the characteristic dimensions of the tube;

— the ionization of the Hg atoms and the excitation of the non-resonant levels is by electron collision, in one or two stages;

— recombination takes place only on the wall of the tube, where the charge carriers get by through ambipolar diffusion;

— in the column the density of the atoms in basic state and the electron temperature do not change radially;

— the longitudinal and radial drift velocities are small compared with the random velocity, the velocity of the electrons follows the Maxwellian distribution.

Considering these assumptions the electron concentration profile determined by the radial diffusion is given by the solution of the following equation:

$$\Delta_r n_e(r) = -C^2(\alpha)n_e^\alpha(r) \tag{2}$$

where

$\alpha = 1$ — if the ionization is direct
$\alpha = 2$ — if the ionization takes place in two stages,
$C(\alpha)$ — a constant containing the ionization frequency and the ambipolar diffusion factor,
r — distance from the axis of the discharge tube, $0 < r < R$.

The solution of Eq. (2) is, with the following normalized boundary conditions

$$\left. \frac{n_e(r)}{n_0} \right|_{r=0} = 1 , \qquad \left. \frac{n_e(r)}{n_0} \right|_{r=R} = 0$$

where

n_0 — the electron concentration measured on the axis,
R — the radius of the discharge tube (in the following is taken as equal to unity), given by the following plasma balance conditions:

$$C(\alpha = 1) = \frac{2{,}40}{R} , \qquad C(\alpha = 2) = \frac{2{,}92}{R} .$$

The solutions of Eq. (2) [10, 11], the radial profile of the electron concentration for $\alpha = 1$ and $\alpha = 2$ are shown in Fig. 5 (broken lines).

As is known, from the ascending section of the probe current vs. probe voltage characteristic the electron temperature is

$$T_e = \frac{e}{k} \cdot \frac{d(U_{sz} - U_p)}{d \ln I_e} \tag{3}$$
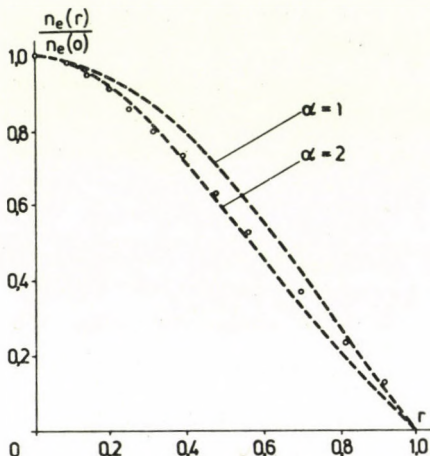
Fig. 5. The relative electron concentration as function of the tube radius. o — measured values; $\alpha = 1$ calculated distribution function for one-stage ionization; $\alpha = 2$ calculated distribution function for two-stage ionization

where

T_e — the electron temperature,
e — the electron charge,
k — the Boltzmann constant,
U_{sz} — the probe voltage,
U_p — the plasma potential measured on the emplacement of the probe,
I_e — the electron component of the probe current;

while from the current belonging to the saturation point, the mean random velocity of the electrons and the probe voltage, the electron concentration is

$$n_e = 4 \frac{I_e(U_{sz} = U_p)}{e v_e S} \tag{4}$$

where

$v_e = \left(\dfrac{8kT_e}{\pi m} \right)^{\frac{1}{2}}$ — the mean random velocity of the electron,
m — the mass of the electron,
S — the surface of the probe.

On the base of the above relations and with the measuring method and arrangement used here [7] the radial distributions of the electron temperature and of the electron concentration can also be determined. The measured electron temperature is shown in Fig. 6, and the electron concentration is characterized by the measured points shown besides the theoretical curves of Fig. 5 (the absolute concentration $n_0 = 2,71 \cdot 10^{11}$ cm^{-3} measured in the axis of the plasma at $r = 0$). Within the errors generally permitted with probe measurements the assumptions are considered as being proved that
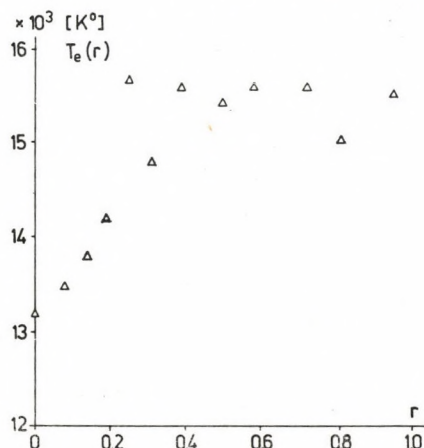

Fig. 6. Radial distribution of the electron temperature

— the electron temperature is constant on a considerable part of the tube radius,
— in the examined plasma the overwhelming majority of the ionization processes takes place in two stages.

These partial results are the base of the further considerations and it is accepted that the radial distribution of the electron density is provided by the solution of Eq. (2) for $\alpha = 2$ [10, 11].

4. The radial intensity distribution of the 579,1 nm Hg line

With the arrangement shown in Fig. 4 the intensity distribution $I(x)$ along the X axis of the 579,1 nm line belonging to the transition $6^1D_2 - 6^1P_1$ was measured in relative units. The result is shown in Fig. 7. The normalized measuring points shown in the figure are connected by the continuous function

$$\frac{I(x)}{I(O)} = \sum_{k=1}^{4} c_k (1 - x^2)^{\frac{2k+1}{2}} \tag{5}$$

($c_1 = 0{,}2614$, $c_2 = 0{,}8017$, $c_3 = -1{,}0549$, $c_4 = 0{,}9918$).

In a cylindrico-symmetrical case there is a mutually univocal relation between the emissivity of the plasma (light energy radiated per unit time by the volume element dV situated at distance r from the tube axis) and the intensity distribution measured along the X axis:

$$\varepsilon(r) = -\frac{1}{\pi} \int_r^1 \frac{I'(x)}{\sqrt{x^2 - r^2}}\, dx, \quad I(x) = 2 \int_x^1 \frac{\varepsilon(r)r}{\sqrt{r^2 - x^2}}\, dr. \qquad (6)$$
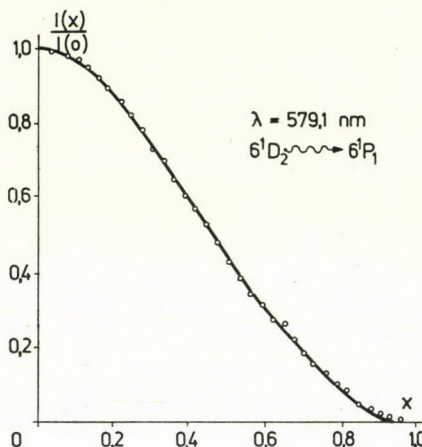
Fig. 7. Distribution of the intensity along the X axis. o measured points; ——— fitting curve

The shape of the approximated function defined by (5) agrees with the empirical fact that the intensity distribution along the line has, at the points $x = 0$ and $x = 1$ a zero tangent, on the other hand the inversion prescribed by Eqs (6) is analytically feasible. Thus, the radial distribution of the emissivity can be written in the form

$$\frac{\varepsilon(r)}{\varepsilon(O)} = \sum_{k=1}^{4} d_k(1 - r^2)^k. \qquad (7)$$

For this distribution it is characteristic that — similar to the distribution of the electron concentration derived from the diffusion model — in point $r = 1$ its derivative is zero and in point $r = 1$ it has a finite derivative.

Figure 8 shows the normalized radial distribution $\varepsilon(r)/\varepsilon(0)$ ($d_1 = 0{,}1933$, $d_2 = 0{,}7411$, $d_3 = -1{,}376$, $d_4 = 1{,}2033$) calculated by the above inversion from the intensity distribution shown in Fig. 7. In the same figure are also shown curves characterizing the real structure of the electron concentration and its square.

Starting out from the proportionality between the emissivity and the population of the upper energy level belonging to the given line, in a way

similar to relation (1) — assuming direct and two-stage excitation processes — the normalized emissivity can be characterized by the dimensionless expression

$$\frac{\varepsilon(r)}{\varepsilon(O)} = \frac{n_s(r)}{n_s(O)} = a\,\frac{n_e(r)}{n_e(O)} + b\,\frac{n_e^2(r)}{n_e^2(O)} \tag{8}$$

where a and b — dimensionless proportionality factors, for the general case their values being determined by the local plasma parameters.
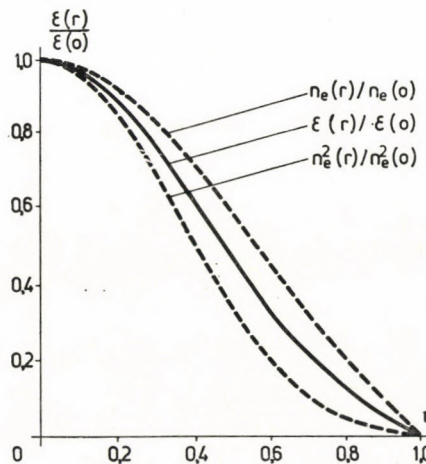

Fig. 8. Radial distribution of emissivity. - - - - - relative electron concentration distribution; ———— relative emissivity distribution; —.—. the quadrate of relative electron concentration distribution

From Fig. 8 it is possible to determine, by using these relations — considering that from the definition of the relative distributions $a + b = 1$ — the radial dependence of the ratio b/a:

$$\frac{b}{a}(r) = \frac{\dfrac{n_e(r)}{n_e(O)} - \dfrac{\varepsilon(r)}{\varepsilon(O)}}{\dfrac{\varepsilon(r)}{\varepsilon(O)} - \dfrac{n_e^2(r)}{n_e^2(O)}} . \tag{9}$$

In the sense of the above definition the ratio b/a can be determined for the surroundings of points $r = 0$ and $r = 1$ only as limit values. In Fig. 8 — taking into consideration the error limits of the basic curves — the radial dependence of the ratio b/a is given for $0{,}1 \leq r \leq 0{,}8$.

Subsequently the obtained experimental results will be interpreted within the frame of a simple model.
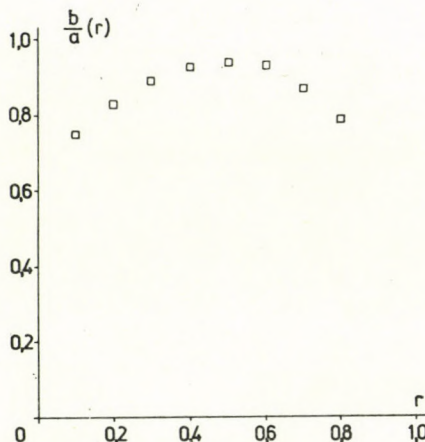
Fig. 9. Radial dependence of the quotient b/a characterizing the excitation mechanism

5. Discussion

In order to interpret the spectroscopically obtained intensity distribution along r and to derive from this the radial distribution of the population of the 6^1D_2 level, the assumptions made in para. 3 are completed as follows:

— it is assumed that in the two-stage excitation of the 6^1D_2 level the intermediate step is the triplet $6^3P_{0, 1, 2}$ (Fig. 10);

— the 6^3P system is reduced to one single level (m) which can be excited from its basic state in one step by electron collision and which is depopulated passing through the 6^1P_1 resonance level by the emission of the 253,7 nm ultraviolet line;

— the 6^1D_2 level (s) can be excited from the (g) basic state directly or passing through the (m) level in two stages by electron collision and this level is emptied during spontaneous radiation of the 579,1 nm line.

In case of equilibrium it holds for (s) as well as for (m) that the number of states originating during unit time is equal to the number of disappearing states. With symbolic notations

$(g, m) =$ light radiation

$(g, s) + (m, s) =$ light radiation.

In detail

$$k_{gm}n_e n_g = \frac{n_m}{\tau_m}, \tag{10}$$

$$k_{gs}n_e n_g + k_{ms}n_e n_m = \frac{n_s}{\tau_s} \tag{11}$$

where

k_{gm}, k_{gs}, k_{ms} — the integral probabilities of the respective levels,
n_g, n_m, n_s — the populations of the respective levels,
τ_m, τ_s — the mean life of the (m) and (s) levels, respectively.

The probabilities of the transitions k_{ij} can be expressed by the cross-sections of the respective phenomena:

$$k_{ij} = v_e \int_{\epsilon_i}^{\infty} \sigma_{ij}^2(\epsilon)\epsilon e^{-\epsilon} d\epsilon \tag{12}$$
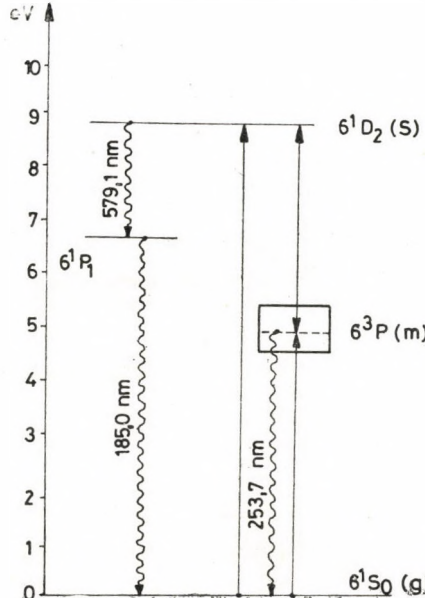
Fig. 10. Simplified model of the energy level system of the Hg atom

where

$\epsilon_i = E_i/(kT_e)$ — (E_i is the energy of level i)
$\sigma_{ij}(\epsilon)$ — the active action radius referring to the $i-j$ transition as a function of the energy of the colliding electron.

Expressing n_m from Eq. (10) and placing it into (11),

$$\frac{n_s}{\tau_s} = k_{gs}n_g \cdot n_e + k_{ms}k_{gm}\tau_m n_g \cdot n_e^2 \tag{13}$$

is obtained. Comparing Eq. (13) with formula (1), the parameters A and B defined there can be explained within the limits of the model and their quotient is given by the following relation containing the microparameters of the plasma:

$$\frac{B}{A} = \frac{k_{ms}k_{gm}}{k_{gs}} \tau_m. \tag{14}$$

The quotient b/a which can directly be determined from the measurements can also be expressed as a combination of the microparameters of the plasma by Eqs (1), (8) and (13):

$$\frac{b}{a} = \frac{B}{A}\, n_e(O) = \frac{k_{ms}k_{gm}}{k_{gs}}\, \tau_m n_e(O)\,. \tag{15}$$

The radial distribution of the population of the radiating level, considering that it is proportional to the emissivity, can be written in the form

$$n_s(r) = n_s(O)\,\frac{\varepsilon(r)}{\varepsilon(O)} = n_s(O)\,\frac{\dfrac{n_e(r)}{n_e(O)} + \dfrac{n_e^2(r)}{n_e^2(O)}\,\dfrac{b}{a}\,(r)}{1 + \dfrac{b}{a}\,(r)} \tag{16}$$

For calculating the absolute value of the population one can calculate from (13)

$$n_s(O) = f\big(k_{gm},\, k_{gs},\, k_{ms},\, \tau_m,\, \tau_s,\, n_g,\, n_e(O)\big) \tag{17}$$

while by measuring the ratio b/a the following simpler relation is obtained:

$$n_s(O) = \left[1 + \frac{b}{a}\,(O)\right] k_{gs}\tau_s n_g n_e(O)\,. \tag{18}$$

6. Summary

In the paper an experimental method for investigating the light generating mechanism in the positive column of the low-pressure Hg-Ar-Discharge has been described. The radial distribution of the emissivity of the 579,1 nm Hg line belonging to the transition $6^1D_2 - 6^1P_1$ has been examined experimentally. With the aid of a simplified model the experimentally obtained parameter b/a has been explained.

The results can be summed up in the following:

— in the sense of Eq. (8) the ratio b/a gives the proportion of the stepped and of the direct processes in the excitation mechanism of the level — in our case, not considering the radial dependence of b/a, calculating with 0,866 average value, 53,6% of the excitation is direct, 46,4% is in two-stages;

— in the sense of Eq. (15) b/a is a function of five parameters depending on the discharge; by measuring b/a, and knowing four parameters, the fifth can be determined — e.g. the integrated probabilities k_{ms} of the transition from the intermediate level m to the radiating level r, which it is difficult to evaluate by other methods;

— on the base of expression (13) the absolute value of $n_s(0)$ can be calculated knowing the seven parameters listed in (17), but by measuring the quotient b/a on the base of (18) it can directly be determined without knowl-

edge of the parameters characterizing the parameters of the intermediate level;

— Eq. (16) characterizes the radial distribution of the population of the excited level r. The normalized form of the relation stems directly from measurement and defines the radial dependence of the parameter b/a (Fig. 9). In the initial model it has been assumed that the electron temperature is radially constant and as a consequence of the model the local value of b/a depends on the local electron temperature by way of the integrated transition probabilities. By comparing this dependence with the radial structure of the electron temperature gained from probe measurements a possibility opens from further refining the model.

Acknowledgments

REFERENCES

1. Kenty, C.: *J. Appl.* Phys., **21**, (1950), 1309
2. Penkin, N. P.—Redko, T. P.: Optika i spectroscopiya, **36** (1974), 446
3. Waymouth, J. F.—Bitter, F.: *J. Appl. Phys.*, **27**, (1956), 122
4. Cayless, M. A.: *Proc. V. International Conference on Ionization Phenomena in Gases*, Münich 1962, p. 262
5. Spolskiy, E. V.: Atomfizika, Akadémiai Kiadó, Budapest 1958, p. 249
6. Klarfield, B. N.: Electronniye i ionniye pribori, Trudi Vsesoyusnogo Electrotekhnitcheskogo Instituta, T. 41, *Gosenergoizdat*, Moscow (1940)
7. Bitó, J.: Doctor thesis, 1971
8. Schottky, W. Z.: *Z. Physik* **25** (1924), 342
9. Verweij, W.: *Philips Research Repts.* Suppl., **2**, (1961)
10. Johnson, P. C.—Antal, K. G.—Allen, J. E.: Symposium of Plasma Physic Group, Institute of Physics, Bangor, UK, 1974
11. Johnson, P. C.—Antal, K. G.—Allen, J. E.: The International Conference on Gas Discharges, London 1974

Der Erregungsmechanismus des 6^1D_2 Niveaus der Hg-Atome in der positiven Säule einer Niederdruck-Hg-Ar-Entladung. In der Arbeit wird die radiale Struktur der positiven Säule einer Entladung in $6 \cdot 10^{-3}$ Torr Hg-Dampf und 2,5 Torr Ar Arbeitsgas experimentell und theoretisch untersucht. Mittels Sondenmessungen wird das angenommene Plasmamodell kontrolliert und dann wird die radiale Verteilung der Intensität der zum $6^1D_2 - 6^1P_1$ Übergang gehörenden 579,1 nm Linie bestimmt. Als Auswertung des erhaltenen Profils wird unter Verwendung eines einfachen Populationsmodells das Verhältnis der direkten und der mehrstufigen Vorgänge bestimmt. Die Abhängigkeit dieses Verhältnisses von den Mikroparametern der Entladung sowie von den integrierten Übergangswahrscheinlichkeiten wird angegeben.

Механизм возбуждения уровня 6^1D_2 атома Hg на положительном столбике ртутно-аргонового разряда низкого давления. В данной работе экспериментально и теоретически исследуются радиальная структура положительного столбика разряда, созданного в рабочем газе (аргоне) давлением 2,5 Торр и в парах ртути давлением $6 \cdot 10^{-3}$ Торр. Измерением с помощью зонда проконтролированная предполагаемая плазмовая модель, после чего с помощью спектроскопического метода определяется радиальное распределение интенсивности линии длины волны 579,1 нм, соответствующей переходу $6^1D_2 - 6^1P_1$ атомов ртути. В качестве оценки полученного профиля путем использования простой популяционной модели определяется отношение между прямыми и ступенчатыми процессами, далее дается зависимость этого отношения от микропараметров разряда, а также от интегрированных переходных вероятностей.

DETERMINATION OF THE EQUATION OF THE BALLOON PLANE CURVE IN RING SPINNING TAKING THE WEIGHT OF THE YARN INTO CONSIDERATION

B. GREGA*

CAND. OF TECHN. SCI

The author set up the system of differential equations of the plane balloon by taking into consideration the tensioning forces of opposite directions acting at the two end points of the yarn element. As there is no possibility for a solution in a closed form, expansion in series is suggested for defining the equation of the plane balloon.

In a previous paper when analyzing the phenomena occurring in the balloon, the yarn forces of opposite directions acting at the two end points of the yarn element, furthermore the centrifugal force have been considered. Now, in addition, also taking into account the weight of the yarn element, for the system of differential equations of the equilibrium of the arc element of the yarn we have

$$\Sigma X_i = \sigma \cdot ds \cdot x \cdot \omega^2 - S(x) \cdot \cos \alpha + S'(x) \cdot \cos \alpha' = 0\,,$$
$$\Sigma Y_i = -\sigma \cdot ds \cdot g - S(x) \sin \alpha + S'(x) \sin \alpha' = 0$$

where σ — is the linear density of the yarn, $S(x)$ and $S'(x)$ — tangential tensioning forces arising at the two end points of the yarn element, ω — angular velocity of the running point of the balloon rotating around the spindle axis, α and α' angles, formed by the tangential yarn forces and the coordinate axis x.

By the transformation of the system of differential equations we have already shown that the differential equation of the balloon plane curve taking the yarn weight into consideration

$$x\sqrt{1+y'^2} = -\frac{d}{dx}\left(\frac{\left(xy' + \dfrac{g}{\omega^2}\right)\sqrt{1+y'^2}}{y''}\right).$$

If

$$\frac{g}{\omega^2} = a$$

then

$$x\sqrt{1+y'^2} = -\frac{d}{dx}\left(\frac{(xy' + a)\sqrt{1+y'^2}}{y''}\right).$$

* B. Grega, Némtvölgyi út 22, H-1126 Budapest, Hungary

Introducing the transformation

$$p = \frac{dy}{dx} \quad \text{i.e.} \quad p' = \frac{dp}{dx}$$

the differential equation takes the form

$$p'^2 x \sqrt{1 + p^2} = -\left\{ p'(xp' + p)\sqrt{1 + p^2} + p'(xp + a)\frac{p \cdot p'}{\sqrt{1 + p^2}} - \right.$$
$$\left. - p''(xp + a)\sqrt{1 + p^2} \right\}.$$

Since there is no possibility for

$$\sqrt{1 + p^2} = 0,$$

because from the point of view of spinning it does not lead to a real solution, hence dividing by that

$$p'^2 x = -\left\{ p'(xp' + p) + p'(xp + a)\frac{p \cdot p'}{1 + p^2} - p''(xp + a) \right\},$$

$$-p'^2 x = pp' + xp'^2 + \frac{xp^2 p'^2}{1 + p^2} + a\frac{p \cdot p'^2}{1 + p^2} - xpp'' - ap'',$$

$$-p'^2 x = pp' + xp'^2 + xp'^2 - x\frac{p'^2}{1 + p^2} + a\frac{pp'^2}{1 + p^2} - xpp'' - ap''.$$

After reducing and arranging

$$pp' + 3xp'^2 - \frac{xp'^2}{1 + p^2} + a\frac{pp'^2}{1 + p^2} - xpp'' - ap'' = 0,$$

$$pp' + 3xp'^2 - \frac{xp'^2}{1 + p^2} + a\frac{pp'^2}{1 + p^2} - (xp + a)p'' = 0.$$

Thus, we have obtained for p an ordinary second order non-linear differential equation with a non-constant coefficient. Solving the equation for p''

$$p'' = f(x, p, p'),$$

i.e. the differential equation is non-deficient.

    With the initial conditions $x = x_0$; $y = y_0$, $p = y' = y_0'$ and $p' = y'' = y_0''$ we may arrive at the solution as follows: (Fig. 1.).

    If

$$x_0 = 0, y_0 = h, y_0' = \tan \alpha_0 = \tan(90° + \gamma_0) = -\cot \gamma_0 = -\frac{1}{\tan \gamma_0}.$$

Observations have shown that due to the centrifugal force the angle of inclination formed at the apex of the balloon is of the order $\gamma_0 = 26,5°$, hence

$$x_0 = 0 \, ,$$

$$y_0 = h = 12 \text{ cm} \, ,$$

$$y_0' = - \frac{1}{\tan 26,5°} \approx -2 \, ,$$

$$y_0'' = -0,001 \, ,$$
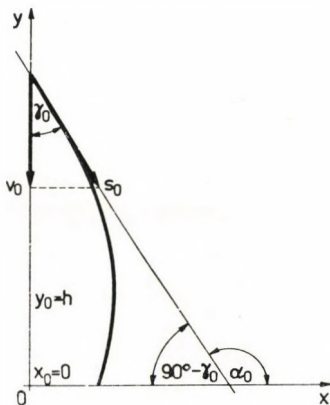
Fig. 1

with the aid of these, the value of $y''' = p''$ can be determined from the latter differential equation

$$p_0'' = f(x_0, p_0, p_0') \, .$$

Now, we shall define the third differential quotient of p with respect to x and since on the right side of

$$y_0^{(IV)} = p_0''' = (f_x')_0 + (f_p' \cdot p')_0 + (f_{p'}' \cdot p'')_0$$

all the terms are known,
$y_0^{(IV)} = p_0'''$ can be determined. At the initial place the values of the higher order differential quotients $y_0^{(V)}$, $y_0^{(VI)}$ ... can be calculated in a similar way. Knowing the values of the differential quotients of the function at the initial place, the equation of the balloon curve is obtained by expansion into Taylor series in the form

$$y = y_0 + \frac{y_0'}{1!} x + \frac{y_0''}{2!} x^2 + \frac{y_0'''}{3!} x^3 + \ldots$$

For verifying the principle of our statement we have determined the equation of the balloon for the neighbourhood of the apex on a ring spinning machine. With the previous initial conditions, with the balloon height of 120 mm, and with $\gamma_0 = 26.5°$, i.e. with the angles $\alpha_0 = 116.5°$, measured at the moment of observation, furthermore by taking into consideration the value of $a = = 0.912 \cdot 10^{-3}$,

$$p_0'' = \frac{0.002}{0.912} \cdot 10^3 + \frac{0.000002}{5} = 2.19 \,.$$

Thus, in the neighbourhood of the apex the equation of the balloon curve is

$$y = 12 - \frac{2}{1!} x - \frac{0.001}{2!} x^2 + \frac{2.19}{3!} x^3 + \dots ,$$

or approximately

$$y \approx -0.0005x^2 - 2x + 12 \,.$$

In order to know to what extent the approximate balloon equation can be made use of, the order of the error committed has to be determined. Since the yarn force is measured in the range of $0.1 - 2.25$, and within that interval the maximum value of the third derivative

$M = p_{\xi=0,1}'' = -0.01005$, the maximum error committed is

$$\delta_n = \frac{|M|}{3!} |x|^3 = \frac{|-0.01005|}{3!} \cdot 2.15^3 = 0.0166 \,,$$

i.e. negligibly small, and thus, the equation can be applied for the determination of the yarn force.

REFERENCES

1. DE BARR, A. E.: *Textile Manufacturer* **87** (1961), No. 1036, pp. 135—138
2. GRISHIN, P. F.: *Balloon Control. Platts Bulletin.* **8,** 161—191
3. GRISHIN, P. F.: Control of the Collapsing Balloon. *Platts Bulletin* **8,** 240—260
4. GREGA, B.: Thesis for candidature, Budapest 1973
5. GREGA, B.: *Periodica Polytechnica,* **1,** No. 2 (1973)

Bestimmung der Gleichung der ebenen Ballonkurve beim Ringspinnen. Der Verfasser berechnet die Gleichung der Ballonkurve beim Ringspinnen für den Fall, daß die Corioliskraft und der Luftwiederstand außer acht gelassen werden. Bei der Lösung des Differentialgleichungssystems für das Gleichgewicht der auf das Fadenelement wirkenden Kräfte wird ersichtlich, daß die ebene Ballonkurve auch in diesem Fall nicht in geschlossener Form dargestellt werden kann. Die Gleichung der ebenen Ballonkurve kann durch ein Legendresches elliptisches Integral erster Art dargestellt werden.

Определение уравнения плоской кривой баллона с учетом веса пряжи. Автор выводит систему дифференциальных уравнений для плоского баллона при учете растягивающих усилий противоположного направления, действующих в двух конечных точка пряжи, при учете центробежных сил и веса элемента пряжи. Решение этой системы дифференциальных уравнений невозможно в закрытой форме, поэтому путем разложения в ряд дается решение с целью определения уравнения плоского баллона.

THE ERROR FUNCTIONS AND THE MOST FAVOURABLE MEASURING CONDITIONS FOR MASS YIELD AND COMPONENT YIELD

SZ. PETHŐ*

DOCTOR OF TECHN. SCI.

[Manuscript received 11 March, 1976]

The main parameters for evaluating the separation operations are the mass yield, the component yield and the efficiency. Their error functions can be calculated by using the law of error propagation. By fixing the errors of the parameters the accuracy of product analysis can also be deduced.

1. Introduction

The main parameters for the evaluation of mineral separation operations, the mass yield m, the component yield k and the efficiency η are calculated with the following relations [4]:

$$m = \frac{a - c}{b - c} = \frac{F_a(x) - F_c(x)}{F_b(x) - F_c(x)}, \tag{1}$$

$$k = \frac{b}{a} \frac{a - c}{b - c} = \frac{F_b(x)}{F_a(x)} \frac{F_a(x) - F_c(x)}{F_b(x) - F_c(x)}, \tag{2}$$

$$\eta = \frac{k - m}{1 - m_0} = \frac{(a - c)(b - a)}{(b - c)a(1 - a/A_0)} = \frac{[F_a(x) - F_c(x)][F_b(x) - F_a(x)]}{(F_b(x) - F_c(x))F_a(x)[1 - F_a(x)]}. \tag{3}$$

In these equations a is the average quality of the raw material, b and c are those of the separation product (e.g. metal content); $F_a(x)$, $F_b(x)$ and $F_c(x)$ are the distribution values of the same products — (e.g. the mass proportion of a part of specific weight below a given limit). Therefore a, b, c, $F_a(x)$, $F_b(x)$ and $F_c(x)$ are all component contents. Let there be $b > a > c$, then $b - c > a - c$ and $b - c > b - a$, but $b - a \gtreqless a - c$ and the same inequalities hold for the corresponding distribution values.

In the following on the base of the law of error propagation the determination of the variances μ_m^2, μ_k^2 and μ_η^2 of the mass yield, the component yield and the efficiency and the optimization of the measuring conditions are dealt with ([1], [2]).

* Dr. Sz. Pethő, Miskolc Egyetemváros, Ásványelőkészítő Tanszék H-3515, Hungary

2. The error functions of the parameters

The partial derivatives of the mass yield are

$$\frac{\partial m}{\partial a} = \frac{1}{b - c}, \tag{4}$$

$$\frac{\partial m}{\partial b} = -\frac{a - c}{(b - c)^2} = -\frac{m}{b - c}, \tag{5}$$

$$\frac{\partial m}{\partial c} = \frac{a - b}{(b - c)^2} = -\frac{1 - m}{b - c}. \tag{6}$$

The variance of the mass yield, if μ_a^2, μ_b^2 and μ_c^2 are the standard deviations for the determination of mean quality, is ([2])

$$\mu_m^2 = \left(\frac{\partial m}{\partial a}\right)^2 \mu_a^2 + \left(\frac{\partial m}{\partial b}\right)^2 \mu_b^2 + \left(\frac{\partial m}{\partial c}\right)^2 \mu_c^2 =$$

$$= \frac{1}{(b - c)^4} [(b - c)^2 \mu_a^2 + (a - c)^2 \mu_b^2 + (a - b)^2 \mu_c^2]. \tag{7}$$

Amongst these difference $b - c$ is the largest, therefore, the reduction of the numerator and with it of the variance of the mass yield is best obtained by a more accurate determination (μ_a^2) of the average raw material quality (a) · · $|a - c| \gtrless |a - b|$, accordingly accuracy of average quality (μ_b^2 and μ_c^2) must be strived for. The denominator of the error function is independent of the accuracy of the analyses, the standard deviation of the mass yield is inversely proportional to the square of the foregoing maximum difference.

If $\mu_a = \mu_b = \mu_c = \mu$, i.e. the accuracies of the analyses are equal — a fact which also occurs in practice — then

$$\mu_m^2 = \frac{1}{(b - c)^2} [1 + m^2 + (1 - m)^2] \mu^2. \tag{8}$$

According to those relation the standard deviation of the mass yield is proportional to the analyzing errors assumed as being equal and inversely proportional to the maximum difference $b - c$. The magnitude of the standard deviation is still influenced by the mass yield: for $m = 0$ or $m = 1$ the expression within the square brackets has a maximum, its value is 2, for $m = 1/2$ there is a minimum: 3/2. Its mean value is ([3])

$$\int_0^1 [1 + m^2 + (1 - m)^2] \, dm = \frac{5}{3}. \tag{9}$$

The function $1 + m^2 + (1 + m)^2$ is shown on Fig. 1. The horizontal line for the mean variance, $5/3$, is also shown it intersects the function at $1/2 + 1/2\sqrt{1/3}$ and $1/2 - 1/2\sqrt{1/3}$ mass yields. The mean variance of the mass yield is

$$\mu_m^2 = \frac{5}{3(b-c)^2} \mu^2 \,. \tag{10}$$

$$y = 1 + m^2 + (1-m)^2$$
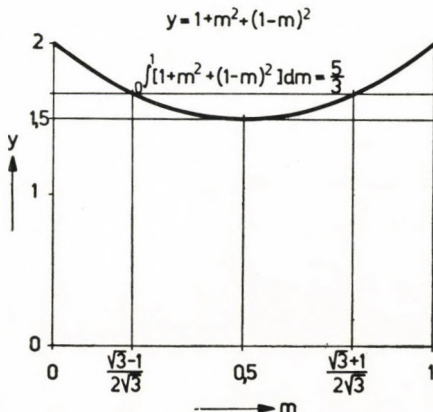
$$\int_0^1 [1 + m^2 + (1-m)^2] \, dm = \frac{5}{3}$$

Fig. 1

The standard deviation of the mass yield is

$$\mu_m = \frac{1}{b-c} [1 + m^2 + (1-m)^2]^{1/2} \mu \,. \tag{11}$$

The maximum of that part of the function which is connected to the mass yield is $\sqrt{2}$, its minimum is $\sqrt{3/2}$. Its mean value is ([3])

$$\int_0^1 [1 + m^2 + (1-m)^2] \, dm = \sqrt{2} \int_0^1 (m^2 - m + 1)^{1/2} \, dm =$$
$$= \sqrt{2} \int_0^1 \left[\left(m - \frac{1}{2} \right)^2 + \frac{3}{4} \right]^{1/2} dm = \frac{3}{2\sqrt{2}} \left(Ar \, sh \frac{1}{\sqrt{3}} + \frac{2}{3} \right) = 1{,}2897 \,. \tag{12}$$

The mean standard deviation is

$$\bar{\mu}_m = \frac{1{,}2897}{b-c} \mu \,. \tag{13}$$

Comparing (10) and (13) shows that $\mu_m > \bar{\mu}_m \cdot (\sqrt{5/3} = 1{,}2910 > 3$
(Ar sh $1/\sqrt{3} + 2/3)/2\sqrt{2} = 1{,}2897)$.

The variance μ_k^2 of the component yield is

$$\mu_k^2 = \frac{1}{a^4(b-c)^4}\left[(bc)^2(b-c)^2\mu_a^2 + (ac)^2(a-c)^2\mu_b^2 + (ba)^2(b-a)^2\mu_c^2\right]. \quad (14)$$

The standard deviation is inversely proportional to the square of $a(b-c)$ appearing in the nominator of the component yield $[a(b-c) > c(b-a)]$. For the products in the square brackets according to the initial conditions only the inequality $bc(b-c) > ac(a-c)$ can be stated, correspondingly the determination of raw material quality must be carried out with a greater accuracy than that of the concentrate.

The variance of the efficiency is

$$\mu_\eta^2 = \left[\frac{a^2\left(\dfrac{b-c}{A_0} - 1\right) + bc\left(1 - \dfrac{2a}{A_0}\right)}{(b-c)a^2\left(1 - \dfrac{a}{A_0}\right)^2}\right]\mu_a^2 +$$

$$+ \left[\frac{(a-c)^2}{(b-c)^2 a\left(1 - \dfrac{a}{A_0}\right)}\right]^2\mu_b^2 + \left[\frac{(a-b)^2}{(b-c)^2 a\left(1 - \dfrac{a}{A_0}\right)}\right]^2\mu_c^2. \quad (15)$$

3. Determination of the optimum measuring conditions

The optimum measuring conditions can be obtained by equalizing the expressions in the square brackets of Eqs (7) and (14).

If the sum in the expression for the variance of the mass yield is fixed,

$$(b-c)\mu_a + (a-c)\mu_b + (a-b)\mu_c = x_1 + x_2 + x_3 = K,$$

then the sum of squares $x_1^2 + x_2^2 + x_3^2$ is minimum if $x_1 = x_2 = x_3 = x$:

$$x = (b-c)\,\mu_{am} = (a-c)\,\mu_{bm} = (a-b)\,\mu_{cm},$$

$$\mu_m = \pm\frac{\sqrt{3x}}{(b-c)^2}. \quad (16)$$

From this equation by fixing μ_m the following analyzing errors can be calculated:

$$\mu_{am} = \pm\frac{b-c}{\sqrt{3}}\,\mu_m, \quad (17)$$

$$\mu_{bm} = \pm\frac{b-c}{\sqrt{3}\,m}\,\mu_m = \pm\frac{\mu_{am}}{m}, \quad (18)$$

$$\mu_{cm} = \pm \frac{b - c}{\sqrt{3(1 - m)}} \quad \mu_m = \pm \frac{\mu_{am}}{1 - m} \, . \tag{19}$$

The last three Eqs give the determination error of the product quality as being inversely proportional to the mass yield of the products. Hence, the analysing error of the product with a small mass yield can be relatively large as compared to the error of the raw material or to that of the other separation product.
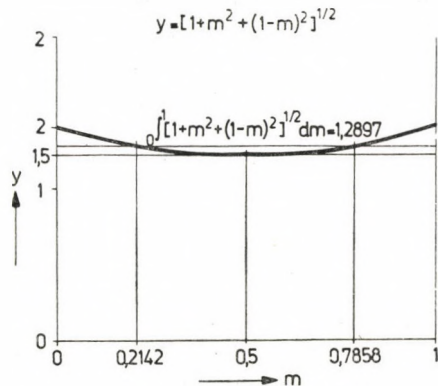

Fig. 2

The products of the variances of the component yields, which in the interest of optimization are made equal, are denoted by z:

$$z = (bc)(b - c)\mu_{ak} = (ac)(a - c)\mu_{bk} = (ba)(b - a)\mu_{ck} \, .$$

With this,

$$\mu_k = \pm \frac{\sqrt{3z}}{a^2(b - c)^2} \, . \tag{20}$$

With a preliminary fixing of μ_k the accuracy of the determination of the quality of individual products is

$$\mu_{ak} = \pm \frac{a^2(b - c)}{\sqrt{3bc}} \, \mu_k \, , \tag{21}$$

$$\mu_{bk} = \pm \frac{b(b - c)}{\sqrt{3}\, ck} \, \mu_k \, , \tag{22}$$

$$\mu_{ck} = \pm \frac{c(b - c)}{\sqrt{3b(1 - k)}} \, \mu_k \, . \tag{23}$$

In these error functions $a^2/bc \gtreqless 1$, $b/c > 1$. The accuracy of the determination is proportional to the corresponding component yields. In case of a very good

preparation efficiency ($k \to 1$, $c \to 0$), the quality of the concentrate can be determined inaccurately, that of the other separation product should be determined with great accuracy ($1 - k = 1 - m)c/a$; $(1- m)/a > 1$; $c/(1 - k) \to$ $\to 0$; $\mu_c \to 0$). In such a case the accuracy of raw material quality measurement should be between that of the two separation products ($\mu_{ak} : \mu_{bk} =$ $= a^2 : b^2$).

If the errors of the component yield and of the mass yield are assumed as being inequal the ratios of the corresponding analyzing errors are

$$\frac{\mu_{ak}}{\mu_{am}} = \frac{a^2}{bc} \gtrless 1 , \tag{24}$$

$$\frac{\mu_{bk}}{\mu_{bm}} = \frac{a}{c} > 1 , \tag{25}$$

$$\frac{\mu_{ck}}{\mu_{cm}} = \frac{a}{b} < 1 . \tag{26}$$

Let there be $a = 0{,}04$, $b = 0{,}74$, $c = 0{,}002$, then $m = 0{,}0515$, $k = 0{,}9526$. If $\mu_k = 0{,}001$, $\mu_{ak} = 0{,}00046$, $\mu_{bk} = 0{,}1655$, $\mu_{ck} = 0{,}00002$. If $\mu_m = 0{,}001$, $\mu_{am} = 0{,}00043$, $\mu_{bm} = 0{,}0083$, $\mu_{cm} = 0{,}00045$. If the analysis were carried out with $\mu_a = 0{,}00043$, $\mu_b = 0{,}0083$ and $\mu_c = 0{,}00002$ errors, then μ_k and μ_m would both be reduced by $0{,}001$.

In the numerator of each function for product quality there appears the difference $b - c$. Subsequently for a given operation that value of the parameter (grain size, specific weight, etc.) is determined for which the difference of distributions $F_b(x) - F_c(x)$ has a maximum. If the analysis is made for the parameter belonging to this maximum the accuracy of determination of the mass yield will be the largest possible.

In the upper part of Fig. 3 the distribution functions $F_a(x)$, $F_b(x)$ and $F_c(x)$ are shown, in the lower part the density functions $f_a(x)$, $f_b(x)$ and $f_c(x)$. The abscissae show that the physical quality of the products to be separated, ($x_{\min} \le x \le x_{\max}$) for the difference of which the separation is carried out.

The three density functions have a common point of intersection, its abscissa $x_{r1/2}$ is the relative median of the separation [5]. It is easy to see that the sum of the area parts determined by the density functions of the two separation products

$$\int_{x_{\min}}^{x} f_c(x)dx + \int_{x}^{x_{\max}} f_b(x)dx = F_c(x) + [1 - F_b(x)] \tag{27}$$

has a minimum for the relative median. These area parts are on the distribution function the ordinates marked:

$$\int_{x_{\min}}^{x r^{1/2}} f_c(x)dx + \int_{x r^{1/2}}^{x_{\max}} f_b(x)dx = F_c(x_{r_{1/2}}) + [1 - F_b(x_{r_{1/2}})] \to \min . \tag{28}$$
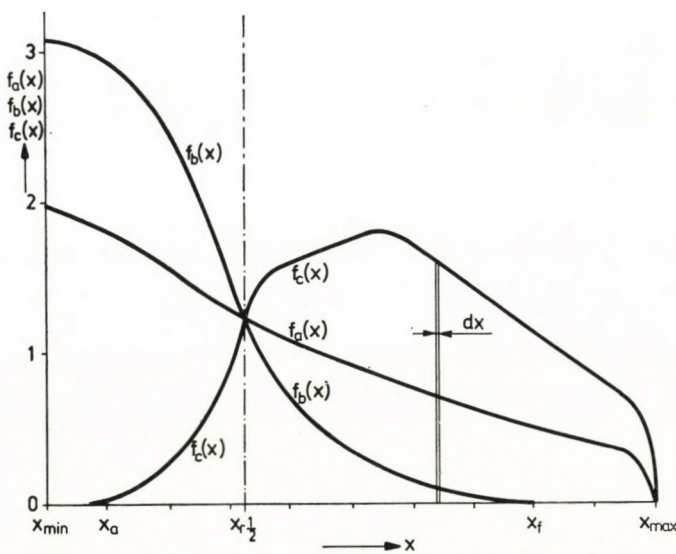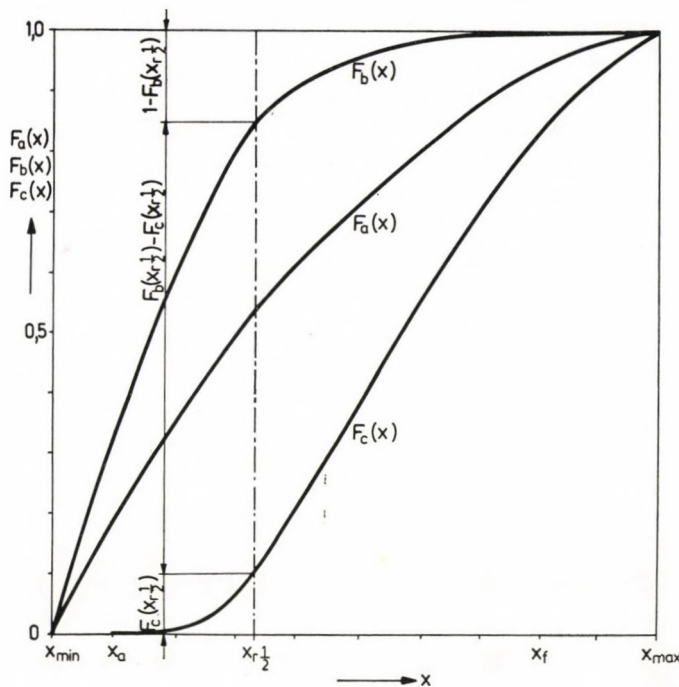
Fig. 3

From this equation it follows that at the relative median the $F_b(x) - F_c(x)$ distribution differences have a maximum:

$$F_b(x_{r_{1/2}}) - F_c(x_{r_{1/2}}) \rightarrow \max.$$ (29

Because of the common point of intersection the direction tangents of the three distribution functions are equal at the relative median.

4. Conclusions

In the paper the error functions of the three basic measures for the evaluation of the separation operations: the mass yield, the component yield and the efficiency have been deduced and the measuring conditions have been optimized.

The standard deviation of the mass yield is inversely proportional to the difference of the component contents of the separation products. This deviation depends only little on the size of the mass yield, if the qualities of the products have been determined with equal accuracies. In that case the error of the mass yield is the quotient of $\approx 1,3x$ the analyzing error and the difference of the aforesaid component contents. If the error of the mass yield is fixed according to the most favourable conditions of error propagation, the error of determination of the component contents of the products is inversely proportional to their mass yield, while being directly proportional to the difference of the component contents of the two separation products. For a concrete separation operation the difference of the distributions of the two separation products has a maximum at the relative median. The optimum measuring conditions are satisfied if for the determination of the mass yield the necessary analyses are made at this parameter.

The error of the component yield depends — besides on the analyzing errors — mainly on the product of the differences of component contents of the raw material and the two separation products; it is inversely proportional to the square of the latter product. If the error of component yield is adequately fixed, the errors of the component are inversely proportional to their component yields. If the component yield of one product is large, the analyzing error of this product may be large, but the component content of the other product must be analyzed with great accuracy.

REFERENCES

1. Mayer, F. W.: Streuungsfortpflanzung in Form von Vertrauensbereichen in häufig verwendeten Formeln der Aufbereitungstechnik. *AT* (1974), 194—200
2. Pethő, S.—Smirnow, S.: Untersuchungen über das wahrscheinliche Mengenausbringen, *Glückauf-Forschungshefte* **36** (1975), 205—208
3. Pethö, S.: Über die Fehler der in Glüh- und Trockenöfen feststellbaren Gütekennwerte, *Acta Techn. Hung.*, **70** (1971) 133—141
4. Tarján, G.: Ásványelőkészítés (Mineralaufbereitung). Tankönyvkiadó, Budapest, 1974 (in Hungarian)
5. Pethő, Sz.: Újabb adatok a szétválasztási műveletek értékeléséhez (Weitere Angaben zur Auswertung der Separationsoperationen), *Bányászati és Kohászati Lapok — Bányászat* **107** (1974), 50—52. (in Hungarian)

Fehlerfunktionen und optimale Meßbedingungen für Massenausbringen und Bestandteilausbringen. Die hauptsächlichsten Parameter für die Auswertung der Trennvorgänge sind die Massenausbringen, die Bestandteilausbringen und der Wirkungsgrad. Ihre Fehlerfunktionen können aufgrund des Fehlerfortpflanzungsgesetzes bestimmt werden. Bei Festlegung der Parameterfehler kann auch die Genauigkeit der Produktanalyse abgeleitet werden.

Функции погрешности и наиболее выгодные условия измерения массового выхода и выхода компонентов. Основными параметрами оценки процессов разделения являются массовый выход, выход компонентов и коэффициент полезного действия. Функции погрешности этих факторов можно определить при использовании закономерности распространения погрешности. Фиксированием погрешностей параметров можно вывести также точность анализа продуктов.

MEMBRANKRÄFTE UND MEMBRANFORMÄNDERUNGEN VON FLACHEN ELLIPTISCHEN PARABOLOIDSCHALEN MIT GLEICHFÖRMIG VERTEILTER HORIZONTALER BELASTUNG

E. DULÁCSKA*

KAND. DER TECHN. WISS.

und

L. JANKÓ**

Behandelt wird die analytische Ermittlung des Membranspannungszustandes und der Membranformänderungen der durch ein gleichmäßig verteiltes horizontales Randkraftsystem belasteten flachen elliptischen Paraboloidschale. Die durch symmetrisch bzw. antimetrisch angeordnete, auf den einander gegenüberliegenden Rändern wirkenden Kraftsysteme hervorgerufene Effekte beschreibenden Funktionen wurden auch zur Erleichterung der Handrechnung in graphischer Form ausgearbeitet. Es wurde hingewiesen, daß durch Anwendung dieses statischen Grundproblems, im Rahmen der Membrantheorie auch die Schnittkräfte und Formänderungen solcher elliptischen Paraboloidschalen annäherungsweise untersucht werden können, die durch Randträger gestützt sind, welche in der horizontalen Richtung nicht vernachlässigbare Biege —, bzw. Drillsteifigkeit besitzen.

1. Bezeichnungen

f_x, f_y	Pfeilhöhen der in den x bzw. y Richtungen liegenden Bogen;
h	Schalenwandstärke;
$l_x = 2a, l_y = 2b$	Spannweiten der Bogen in den x, bzw. y Richtungen;
p	Belastung in der Richtung der Achse z, bezogen auf der Flächeneinheit der Grundrißprojektion;
$n_x = \ddot{F},\ n_{xy} = -\dot{F}',\ n_y = F''$	spezifische Werte der auf die Seitenlängenprojektionen bezogenen (reduzierten) Schnittkräfte;
u, v	Verschiebungen in den Richtungen der x- bzw. y-Achse gerichteten Tangenten;
u^*, v^*	Verschiebungen in den Richtungen x und y;
w	Verschiebung der Flächenpunkte in der Richtung der Flächennormale;
w^*	Verschiebung in der Richtung der z-Achse;
x, y	Orthogonalkoordinaten;
$z(x, y)$	Ordinaten der Schalenmittelfläche;
E	Elastizitätsmodul;
F	Spannungsfunktion der Membrankräfte;
$G = E/2(1 + \nu)$	Gleitmodul;
H	spezifischer Wert der in der Grundrißprojektion gleichmäßig verteilten horizontalen Randbelastung;
H^s, H^a	Intensitäten der symmetrischen, bzw. antimetrischen Randbelastung;
I	horizontales Biegeträgheitsmoment des Randbogenquerschnitts;
I_t	Drillträgheitsmoment des Randbogenquerschnitts;
$L_p(\ ) = \ddot{z}(\ )'' - 2\dot{z}'(\ )'{}^{\cdot} + z''(\ )^{\cdot\cdot}$	der Puchersche Differentialoperator;
ϑ	Absolutverdrehung des Mittelquerschnitts des Randbogen;
ν	Querdehnungszahl (in den Berechnungen: $\nu = 0,2$);
$\partial(\ )/\partial x = (\ )'$	Symbol der Ableitung nach x;
$\partial(\ )/\partial y = (\ )^{\cdot}$	Symbol der Ableitung nach y;
$\Delta\Delta(\ ) = (\ )^{\mathrm{IV}} + 2(\ )^{\mathrm{II}\cdot\cdot} + (\ )^{\cdot\cdot\cdot\cdot}$	biharmonischer Differentialoperator.

* Dr. E. DULÁCSKA Ráth Gy. u. 64. H-1122. Budapest Ungarn.
** Dr. L. JANKÓ Lajos u. 142. H-1036. Budapest Ungarn.

2. Einleitung

Zur Ermittlung der Membrankräfte und Membranformänderungen der flachen elliptischen Paraboloidschale, die durch gleichmäßig verteilte Flächenbelastung, bzw. durch das Eigengewicht hervorgerufen werden, stehen wohlbekannte Berechnungsverfahren zur Verfügung [1], [2], [3], [4]. Diese Methoden setzen voraus, daß die Randträger der Schale in ihrer eigenen Ebene gegen Biegung unendlich steif, während senkrecht auf diese Ebene vollkommen weich (sog. "halbsteife" Träger) sind.
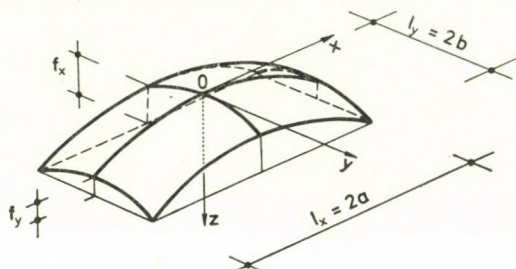

Bild 1. Geometrische Angaben der elliptischen Paraboloidschale

Es fragt sich, ob es möglich wäre, eine flache elliptische Paraboloidschale, die an einem ihrer Ränder durch gleichmäßig verteilte horizontale Kräfte belastet ist, bloß durch Membrankräfte in Gleichgewicht zu halten.

Im folgenden wird es biewiesen, daß dies möglich ist; es werden die auf den Membranspannungszustand und auf die Membranformänderungen bezügliche analytische Lösung und deren in Diagrammen verarbeitete Werte angegeben. Nur die auf die Ebene xz symmetrische Lösung *(Bild 1)* wird gesucht.

Die vorgeführte Methode hat mehrere praktische Anwendungsmöglichkeiten. Zur Untersuchung der räumlichen Stabilität der Randbogen — auch noch im Falle, wo der Gewölbedruck aus dem Gesichtspunkt der Schale betrachtet vernachlässigt werden kann — ist die Kenntnis der horizontalen Verbindungskräfte zwischen Schale und Randträgern unbedingt erforderlich.

Im allgemeinen entsprechen die in der Praxis angewandten Randbogen nicht der Definition des sog. "halbsteifen Randträgers", da sie endlich große Drill — und horizontale Biegesteifigkeit haben. Infolge dieser Steifigkeiten können die Randträger den nach der Membrantheorie entstehenden Randverschiebungen nicht ohne Widerstand folgen. Demzufolge entwickelt sich zwischen der Schale und dem Randträger ein Verbindungskraftsystem, d.h., die Schale wird von dem Seitendruck nicht vollkommen frei.

Die obenerwähnte Stabilitätsuntersuchung, bzw. die Berücksichtigung der Auswirkung der endlichen horizontalen Steifigkeit der Randträger kann mit Hilfe der hier vorgelegten Methode näherungsweise durchgeführt werden.

3. Gleichgewichts- und Formänderungsdifferentialgleichungen der flachen Membranschalen

Im folgenden werden die Untersuchungen aufgrund der Theorie der flachen Membranschalen durchgeführt [1], [2], [3]. Um der Behandlung eine klare Übersichtlichkeit zu geben, werden unten die das Gleichgewicht und die Verträglichkeit der Formänderungen der flachen Membranschalen beschreibenden partiellen Differentialgleichungen zusammengefaßt.

Die Puchersche Differentialgleichung

$$L_p(F) = -p \tag{3.1}$$

des Gleichgewichts der Membranschalen [1], [3] ist auch für beliebig steile Schalen gültig, jedoch kann die wie folgt geschriebene Form der Verträglichkeitsgleichung

$$L_p(w) = -\frac{1}{Eh} \Delta\Delta F \tag{3.2}$$

[1], [2], [3], [4] nur im Fall von flachen Membranschalen gebraucht werden.

Wie bekannt, bedeutet die Annahme der Flachheit in Zusammenhang mit den Membranschalen, daß die geodetischen Krümmungen der Fläche infolge ihrer Kleinheit vernachlässigt und die Metrik der Fläche mit der euklidischen (ebenen) Metrik identisch angenommen werden können.

Die Flachheit kann auch mit Hilfe der Richtungstangenten der Fläche wie folgt

$$1 + \acute{z}\grave{z} \approx 1,$$
$$1 + \acute{z}^2 \approx 1, \tag{3.3a—c}$$
$$1 + \grave{z}^2 \approx 1$$

definiert werden.

Infolge der Flachheit der Schale können die mit den Richtungen der im Bild 2 eingezeichneten Orthogonalkoordinaten parallelen Verschiebungen u, v, w mit den in den Richtungen der x, y und z Achsen des Cartesischen Koordinatensystems fallenden Verschiebungen u^*, v^* und w^* identisch angenommen werden [1]:

$$u \approx u^*, \ v \approx v^*, \ w \approx w^*. \tag{3.4}$$

Die Verschiebungen u und v können nach der (die entsprechenden Randbedingungen befriedigenden) Lösung der partiellen Differentialgleichungen (3.1), (3.2) durch Auswertung der Ausdrücke

$$u = \int \acute{z}w\,dx + \frac{1}{Eh} \int (\ddot{F} - v\overset{\shortparallel}{F})dx + u_1(y), \tag{3.5}$$

9*

$$v = \int \ddot{z} w \, dy + \frac{1}{Eh} \int (\overset{\shortmid\shortmid}{F} - \nu \ddot{F}) dy + v_1(x) \qquad (3.6)$$

erhalten werden [1]. Die Integrationsfunktionen $u_1(y)$ und $v_1(x)$ sind aus den Randbedingungen zu ermitteln.

Die Mittelfläche der elliptischen Paraboloidschale ist durch die Gleichung

$$z = \frac{4f_x}{l_x^2} x^2 + \frac{4f_y}{l_y^2} y^2 \qquad (3.7)$$

beschrieben *(Bild 1)*.
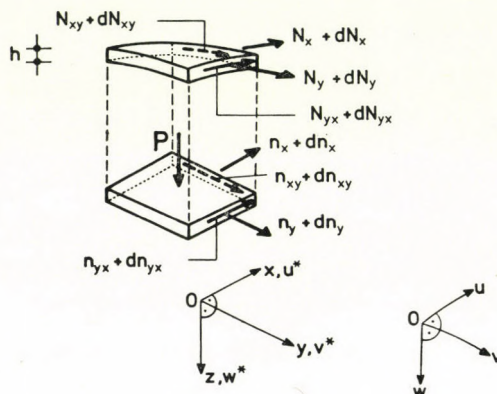
Bild 2. Vorzeichenregel der Innenkräfte und der Verschiebungen

4. Herstellung einer beliebigen Randbelastung

Im Bild 3 ist es demonstriert, daß bei Kenntnis der Effekte, die durch die symmetrische Randbelastung H^s und durch die antimetrische Randbelastung H^a entstehen, auch die durch eine beliebige Randbelastung H verursachten Membrankräfte und Membranformänderungen ermittelt werden können.

Im folgenden werden die Lösungen für H^s und H^a gezeigt.
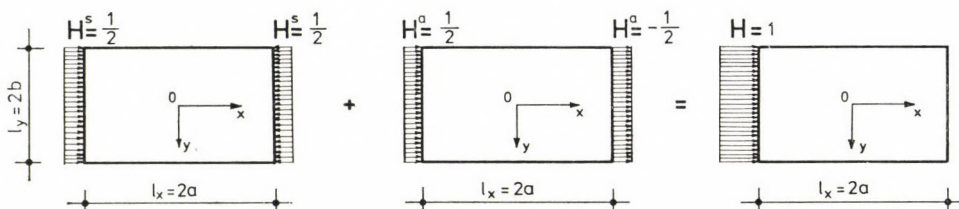
Bild 3. Zerlegung der Randbelastung $H = 1$ an der Stelle $x = -a$ in symmetrische ($H^s = 1/2$) und in antimetrische ($H^a = \pm 1/2$) Komponente

5. Untersuchung der symmetrischen Randbelastung H^s

Die Ränder $x = \pm a$ sind durch das gleichmäßig verteilte horizontale Kraftsystem H^s angegriffen. In diesem Fall sind die Randbedingungen der Schale, deren Randbogen dem Seitendruck nicht widerstehen kann, — wenn man den Druck mit Minusvorzeichen bezeichnet — wie folgt:

$$\ddot{F}\Big|_{x=\pm\frac{l_x}{2}} = n_x\Big|_{x=\pm\frac{l_x}{2}} = -H^s_{(y)}, \tag{5.1a—b}$$

$$\overset{\shortparallel}{F}\Big|_{y=\pm\frac{l_y}{2}} = n_y\Big|_{y=\pm\frac{l_y}{2}} = 0. \tag{5.1c—d}$$

Man setzt voraus, daß die Randbogen in ihrer eigenen Ebene unendlich steif sind. Infolgedessen gilt:

$$w\Big|_{x=\pm\frac{l_x}{2}} = 0, \tag{5.2a—b}$$

$$w\Big|_{y=\pm\frac{l_y}{2}} = 0. \tag{5.2c—d}$$

Da unser Lösungsverfahren aufgrund der Membrantheorie fußt, d.h., die Biegesteifigkeit der Schale außer acht gelassen ist, wird der Wert der Verdrehung der Rändern entlang nicht festgelegt, denn die vollkommen elastische Membran kann jeder am Rand gültigen Verdrehung ohne Widerstand folgen.

Im Verlauf der Ableitung soll man erstens die gleichmäßig verteilte Last H^s in eine Fourierische Reihe entwickeln

$$H^s_{(y)} = \frac{4}{\pi} H^s \sum_{m=1,3,5,\ldots} \frac{1}{m} \sin\frac{m\pi}{2} \cdot \cos\frac{m\pi}{l_y} y, \tag{5.3}$$

sodann die Gleichgewichtsgleichung (3.1) auf die Form

$$\ddot{F} + \frac{l_x^2}{l_q^2}\frac{f_y}{f_x}\overset{\shortparallel}{F} = 0 \tag{5.4}$$

bringen. Danach stellt man die die Gleichung (5.4) und die Randbedingungen (5.1) befriedigende Spannungsfunktion F her. Man soll die Lösung mit Hilfe der Fourierischen Methode suchen [5].

Setzt man den Produktenansatz

$$F(x, y) = X(x) \cdot Y(y) \tag{5.5}$$

in die Gleichung (5.4), so erhält man den Ausdruck

$$\frac{\ddot{Y}}{Y} + \frac{l_x^2}{l_y^2}\frac{f_y}{f_x}\frac{\overset{\shortparallel}{X}}{X} = 0 \, , \tag{5.5a}$$

der in die zwei gewöhnlichen Differentialgleichungen

$$\overset{\shortparallel}{X} - k^2\frac{l_y^2}{l_x^2}\frac{f_x}{f_y}X = 0 \tag{5.6a}$$

und

$$\ddot{Y} + k^2Y = 0 \tag{5.6b}$$

zerfällt (die Ziffer k läßt sich aus den Randbedingungen ermitteln).

Die allgemeine Lösung der Gleichung (5.6a) stellt die Funktion

$$X = C_{1m}\cosh k\,\frac{l_y}{l_x}\sqrt{\frac{f_x}{f_y}}\,x + C_{2m}\sinh k\,\frac{l_y}{l_x}\sqrt{\frac{f_x}{f_y}}\,x \tag{5.7a}$$

und die der Gleichung (5.6b) den Ausdruck

$$Y = C_{3m}\cos ky + C_{4m}\sin ky \tag{5.7b}$$

dar.

Die Randbedingungen (5.1a – b) sollten durch die Funktion X befriedigt werden. Das ergibt:

$$C_{2m} = 0 \, . \tag{5.8}$$

Nimmt man in Betracht, daß unsere Lösung auf den zur Ebene xz symmetrischen Fall bezogen ist, so erhält man aus den Randbedingungen (5.1c – d):

$$C_{4m} = 0 \, . \tag{5.9}$$

Die Funktion F wird demzufolge die Form annehmen:

$$F(x, y) = \sum_{m=1,3,5\ldots} C_m\cosh k\,\frac{l_y}{l_x}\sqrt{\frac{f_x}{f_y}}\,x\cos ky \, . \tag{5.10}$$

Setzt man die Ausdrücke (5.3) und (5.10) in die Randbedingungen (5.1a – b) ein, so ergibt sich die Beziehung:

$$C_m k^2\cosh k\,\frac{l_y}{2}\sqrt{\frac{f_x}{f_y}}\cos ky = \frac{4}{\pi}\,H^s\frac{1}{m}\sin\frac{m\pi}{2}\cos\frac{m\pi}{l_y}\,y \, , \tag{5.10a}$$

woraus

$$k = \frac{m\pi}{l_y} \tag{5.11}$$

und

$$C_m = H^s \frac{4l_y^2}{\pi^3} \frac{1}{m^3} \frac{\sin\dfrac{m\pi}{2}}{\cosh\dfrac{m\pi}{2}\sqrt{\dfrac{f_x}{f_y}}} \tag{5.12}$$

folgt. Letzten Endes erhält man für die Spannungsfunktion F den folgenden Ausdruck:

$$F = \frac{4H^s}{\pi^3} l_y^2 \sum_{m=1,3,5\ldots} \frac{1}{m^3} \frac{\sin\dfrac{m\pi}{2}}{\cosh\dfrac{m\pi}{2}\sqrt{\dfrac{f_x}{f_y}}} \cosh\frac{m\pi}{l_x}\sqrt{\frac{f_x}{f_y}}\, x \cos\frac{m\pi}{l_y}\, y. \tag{5.13}$$

Die Membranschnittkräfte ergeben sich als die Ableitungen der Funktion F wie folgt:

$$n_x = -\frac{4H^s}{\pi} \sum_{m=1,3,5\ldots} \frac{1}{m} \frac{\sin\dfrac{m\pi}{2}}{\cosh\dfrac{m\pi}{2}\sqrt{\dfrac{f_x}{f_y}}} \cdot \cosh\frac{m\pi}{l_x}\sqrt{\frac{f_x}{f_y}}\, x \cdot \cos\frac{m\pi}{l_y}\, y, \tag{5.14}$$

$$n_y = -\frac{f_x}{f_y} \frac{l_y^2}{l_x^2} n_x, \tag{5.15}$$

$$n_{xy} = \frac{4H^s}{\pi}\sqrt{\frac{f_x}{f_y}}\frac{l_y}{l_x} \sum_{m=1,3,5\ldots} \frac{1}{m} \frac{\sin\dfrac{m\pi}{2}}{\cosh\dfrac{m\pi}{2}\sqrt{\dfrac{f_x}{f_y}}} \sinh\frac{m\pi}{l_x}\sqrt{\frac{f_x}{f_y}}\, x \cdot \sin\frac{m\pi}{l_y}\, y. \tag{5.16}$$

Diese Ausdrücke wurden in den 25 charakteristischen Punkten ersten Viertels des Koordinatensystems mit Hilfe einer elektronischen Rechenanlage ausgewertet; die Ergebnisse sind in den Bildern 4 und 5 in Abhängigkeit von f_x/f_y dargestellt.

Zur Ermittlung der Membranverschiebungen benötigt man auch den Wert des Operators $\Delta\Delta F$:

$$\Delta\Delta F = \frac{4H^s\pi}{l_y^2}\left(\frac{f_x}{f_y}\frac{l_y^2}{l_x^2}-1\right)^2 \sum_{m=1,3,5\ldots} m\, \frac{\sin\dfrac{m\pi}{2}}{\cosh\dfrac{m\pi}{2}\sqrt{\dfrac{f_x}{f_y}}} \cosh\frac{m\pi}{l_x}\sqrt{\frac{f_x}{f_y}}\, x \cdot \cos\frac{m\pi}{l_y}\, y. \tag{5.17}$$
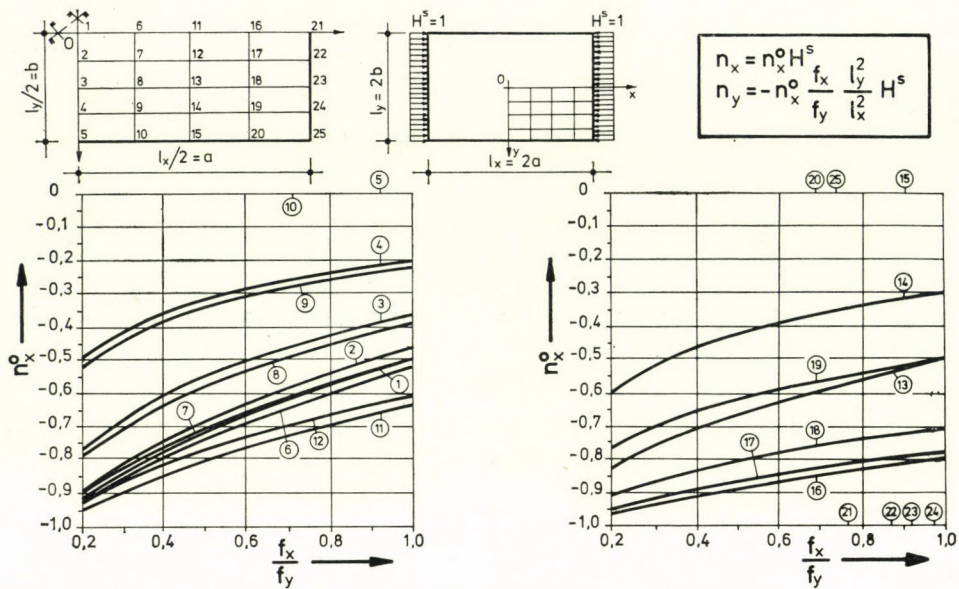
Bild 4a. Die Membrankräfte n_x und n_y aus der symmetrischen Randbelastung $H^s = 1$
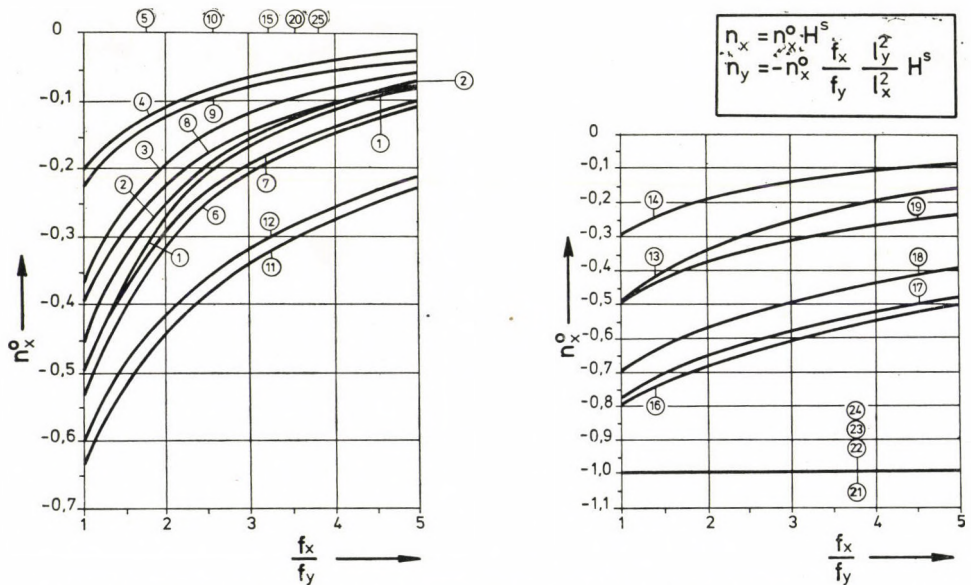

Bild 4b. Membrankräfte n_x und n_y aus der symmetrischen Randbelastung $H^s = 1$
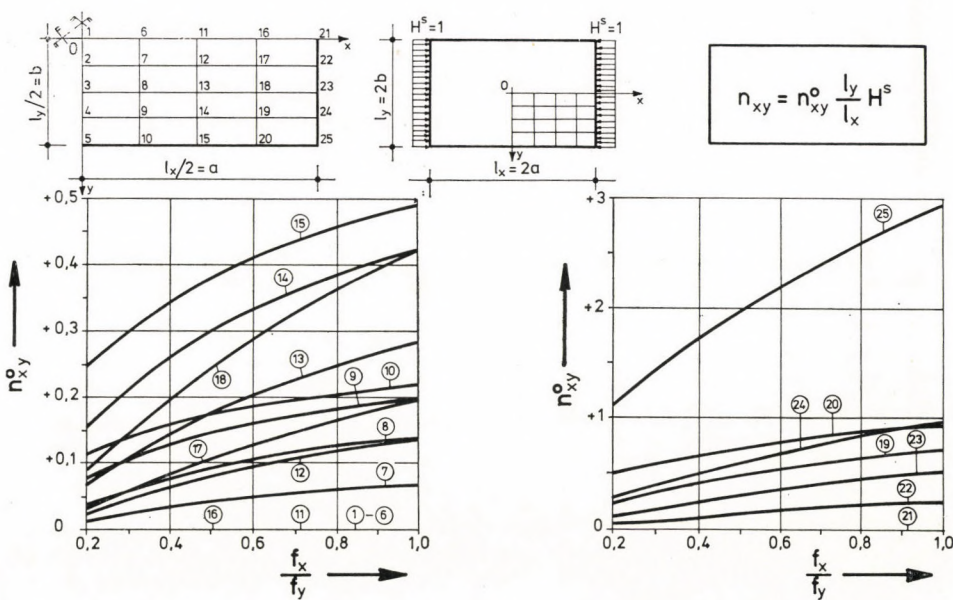
Bild 5a. Membranschubkraft n_{xy} aus der symmetrischen Randbelastung $H^s = 1$
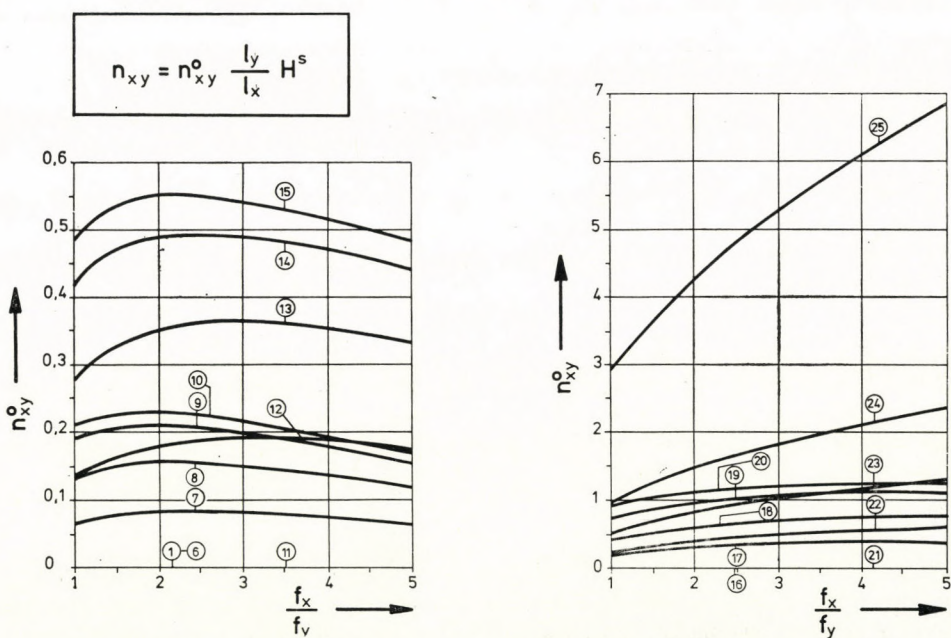
Bild 5b. Membranschubkraft n_{xy} aus der symmetrischen Randbelastung $H^s = 1$

Die Verträglichkeitsgleichung (3.2) nimmt die folgende ausführlichere Form an:

$$\ddot{w} + \frac{l_x^2}{l_y^2}\frac{f_y}{f_x}\overset{\shortparallel}{w} = -\frac{l_x^2}{8f_x Eh}\,\varDelta\varDelta F. \tag{5.18}$$

Zur auch die Randbedingungen (5.2) befriedigenden Lösung der Differentialgleichung (5.18) (Dirichletsche Aufgabe) wurde die Funktion

$$w = \sum_{m=1,3,5\ldots} w_m \cos\frac{m\pi}{l_y}y\left(x\sinh\frac{m\pi}{l_x}\sqrt{\frac{f_x}{f_y}}\,x - \right.$$
$$\left. -\frac{l_x}{2}\tanh\frac{m\pi}{2}\sqrt{\frac{f_x}{f_y}}\cosh\frac{m\pi}{l_x}\sqrt{\frac{f_x}{f_y}}\,x\right) \tag{5.19}$$

hergestellt, worin

$$w_m = -\frac{H^s}{4Eh}\left(\frac{f_x}{f_y}\frac{l_y^2}{l_x^2}-1\right)^2\sqrt{\frac{f_x}{f_y}}\frac{l_x^2}{f_x}\frac{\sin\dfrac{m\pi}{2}}{\cosh\dfrac{m\pi}{2}\sqrt{\dfrac{f_x}{f_y}}}. \tag{5.20}$$

Die Werte der Verschiebungen können durch Einsetzung der Ausdrücke (5.13) bzw. (5.19) von F bzw. w in (3.5) bzw. (3.6) erhalten werden:

$$u = \frac{H^s}{\pi Eh}l_x\sum_{m=1,3,5\ldots}\frac{\sin\dfrac{m\pi}{2}}{\cosh\dfrac{m\pi}{2}\sqrt{\dfrac{f_x}{f_y}}}\cos\frac{m\pi}{l_y}y\left\{\frac{1}{m}\sinh\frac{m\pi}{l_x}\sqrt{\frac{f_x}{f_y}}\,x\cdot\left[\left(\frac{f_x}{f_y}\frac{l_y^2}{l_x^2}-1\right)^2\cdot\right.\right.$$

$$\cdot\tanh\frac{m\pi}{2}\sqrt{\frac{f_x}{f_y}}-\frac{4}{\pi m}\sqrt{\frac{f_y}{f_x}}\left(1+\nu\frac{f_x}{f_y}\frac{l_y^2}{l_x^2}\right)-\frac{2}{\pi m}\sqrt{\frac{f_y}{f_x}}\left(\frac{f_x}{f_y}\frac{l_y^2}{l_x^2}-1\right)^2\right]-$$
$$\left.-\frac{2}{ml_x}\left(\frac{f_x}{f_y}\frac{l_y^2}{l_x^2}-1\right)^2 x\cosh\frac{m\pi}{l_x}\sqrt{\frac{f_x}{f_y}}\,x\right\}, \tag{5.21}$$

$$v = \frac{H^s}{\pi Eh}l_y\sum_{m=1,3,5\ldots}\frac{1}{m}\frac{\sin\dfrac{m\pi}{2}}{\cosh\dfrac{m\pi}{2}\sqrt{\dfrac{f_x}{f_y}}}\sin\frac{m\pi}{l_y}y\left\{\cosh\frac{m\pi}{l_x}\sqrt{\frac{f_x}{f_y}}\,x\cdot\right.$$

$$\cdot\left[\sqrt{\frac{f_y}{f_x}}\frac{l_x^2}{l_y^2}\left(\frac{f_x}{f_y}\frac{l_y^2}{l_x^2}-1\right)^2\tanh\frac{m\pi}{2}\sqrt{\frac{f_x}{f_y}}+\frac{4}{\pi m}\left(\frac{f_x}{f_y}\frac{l_y^2}{l_x^2}+\nu\right)\right]-$$
$$\left.-2\sqrt{\frac{f_y}{f_x^2}}\frac{l_x}{l_y}\left(\frac{f_y}{f_x}\frac{l_y^2}{l_x^2}-1\right)^2 x\cdot\sinh\frac{m\pi}{l_x}\sqrt{\frac{f_x}{f_y}}\,x\right\}. \tag{5.22}$$

Infolge der Symmetrie werden die Funktionen $u_1(y)$ und $v_1(x)$ gleich Null.

Die aus praktischen Gesichtspunkten wichtigen Verschiebungswerte $w = (0,0)$, $u = (a, 0)$, $v = (0, b)$ können aus den Bildern 6 und 7 in Abhängigkeit von f_x/f_y und l_x/l_y abgelesen ($v = 0,2$) bzw. können ihre charakteristischen Werte aus der Tafel 1 herausgenommen werden.

Untersuchen wir nun die Fälle $f_x = f_y = f$ und $l_x = l_y = 1$, d.h., die Membrankräfte und Membranverschiebungen des Rotationsparaboloids:

$$n_x = - \frac{4H^s}{\pi} \sum_{m=1,3,5\ldots} \frac{1}{m} \frac{\sin \dfrac{m\pi}{2}}{\cosh \dfrac{m\pi}{2}} \cosh \frac{m\pi}{l} x \cos \frac{m\pi}{l} y , \qquad (5.23)$$

$$n_y = -n_x , \qquad (5.24)$$

$$n_{xy} = \frac{4H^s}{\pi} \sum_{m=1,3,5\ldots} \frac{1}{m} \frac{\sin \dfrac{m\pi}{2}}{\cosh \dfrac{m\pi}{2}} \sinh \frac{m\pi}{l} x \sin \frac{m\pi}{l} y , \qquad (5.25)$$

$$w \equiv 0 , \qquad (5.26)$$

$$u = - \frac{4H^s l}{\pi^2 E h} (1 + v) \sum_{m=1,3,5\ldots} \frac{1}{m} \frac{\sin \dfrac{m\pi}{2}}{\cosh \dfrac{m\pi}{2}} \sinh \frac{m\pi}{l} x \cos \frac{m\pi}{l} y , \quad (5.27)$$
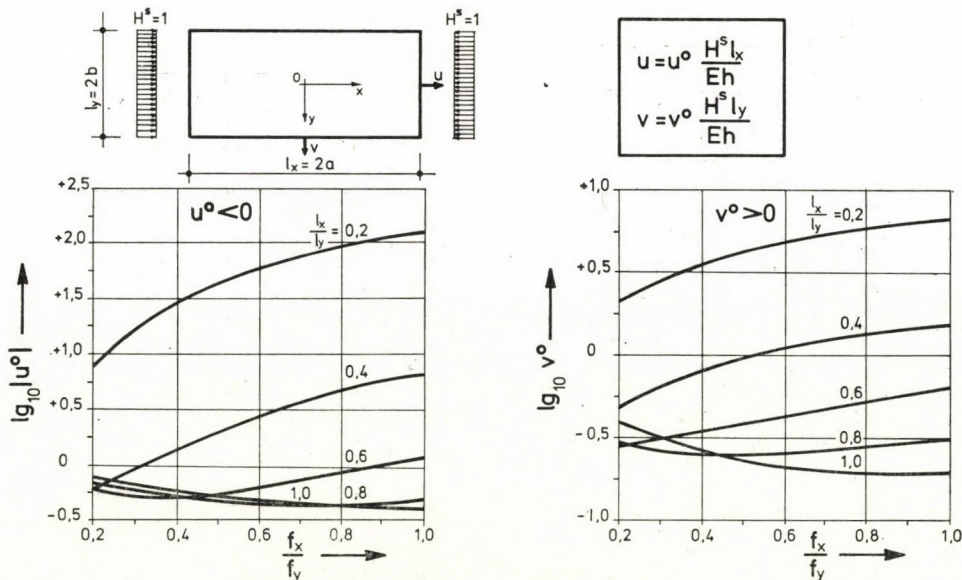

Bild 6a. Verschiebungen $u = u(a,0)$ und $v = v(0, b)$ infolge der symmetrischen Randbelastung $H^s = 1$; ($w_{\text{Rand}} = 0$)

$$u = u^o \frac{H^s l_x}{Eh}$$

$$v = v^o \frac{H^s l_y}{Eh}$$
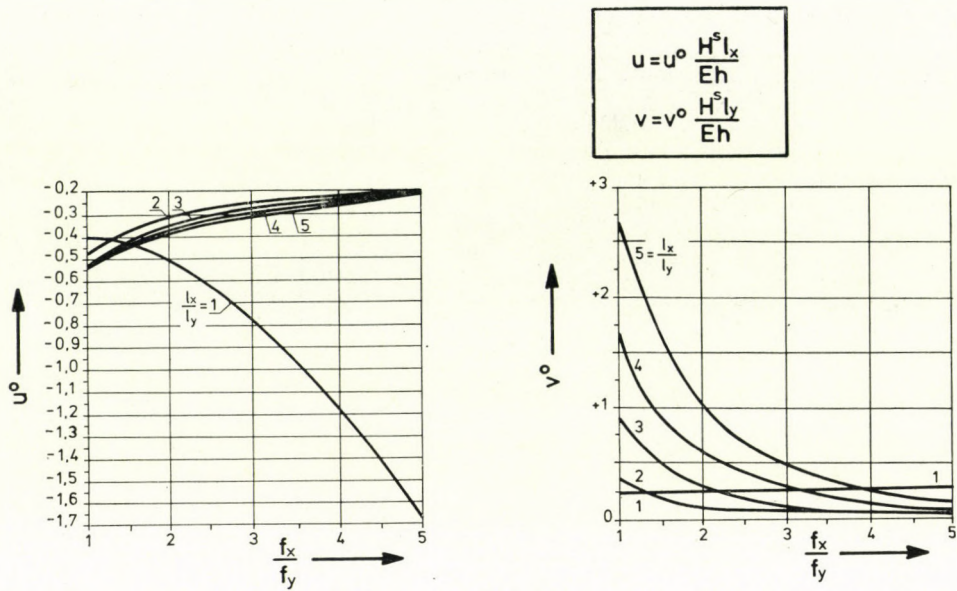
Bild 6b. Verschiebungen $u = u(a, 0)$ und $v = v(0, b)$ infolge der symmetrischen Randbelastung
$H = 1$; $(w_{\text{Rand}} = 0)$

$$w = w^o \frac{H^s l_x^2}{Eh f_x}$$

$$w = w^o \frac{H^s l_x^2}{Eh f_x}$$
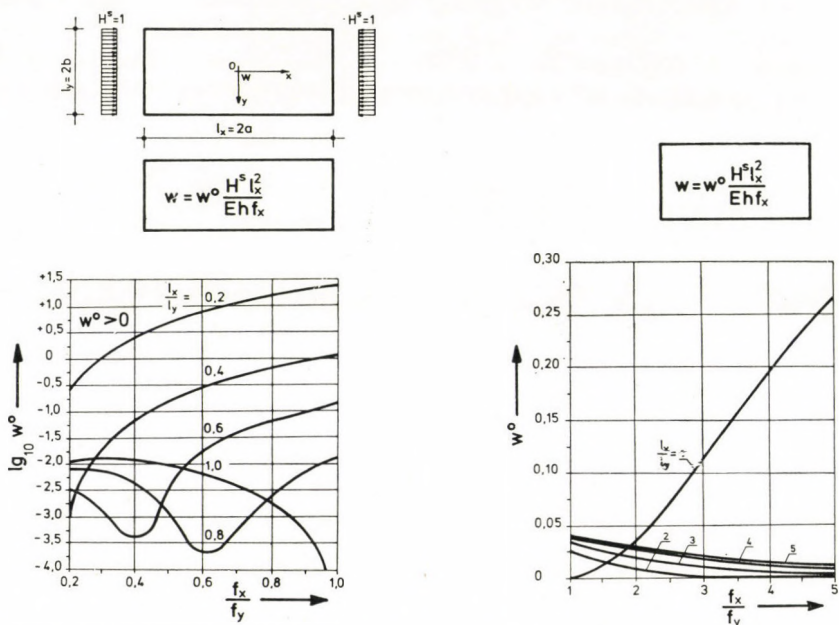
Bild 7a. Durchbiegung $w = w(0, 0)$ infolge
der symmetrischen Randbelastung
$H^s = 1$; $(w_{\text{Rand}} = 0)$

Bild 7b. Durchbiegung $w = w(0, 0)$ infolge
der symmetrischen Randbelastung
$H^s = 1$; $(w_{\text{Rand}} = 0)$

Tafel 1a

		H^s symmetrisch		
$\dfrac{f_x}{f_y}$	$\dfrac{l_x}{l_y}$	$u^0 = u \dfrac{E}{H^s} \dfrac{h}{l_x}$	$v^0 = v \dfrac{E}{H^s} \dfrac{h}{l_y}$	$w^0 = w \dfrac{E}{H^s} \dfrac{h f_x}{l_x^2}$
0,2	0,2	$-7,8913$	1,9999	0,2658
	0,4	$-0,6224$	0,4888	0,0010
	0,6	$-0,6148$	0,2816	0,0033
	0,8	$-0,7110$	0,2949	0,0079
	1,0	$-0,7728$	0,3952	0,0106
0,4	0,2	$-29,6873$	3,6071	2,5979
	0,4	$-1,4381$	0,8218	0,0722
	0,6	$-0,5336$	0,3536	0,0004
	0,8	$-0,5365$	0,2458	0,0045
	1,0	$-0,5939$	0,2574	0,0115
0,6	0,2	$-58,7543$	4,9221	7,7634
	0,4	$-2,6975$	1,1176	0,2995
	0,6	$-0,6565$	0,4478	0,0176
	0,8	$-0,4704$	0,2543	0,0002
	1,0	$-0,4392$	0,2097	0,0063
0,8	0,2	$-92,0706$	5,9780	15,4363
	0,4	$-4,7277$	1,3657	0,6842
	0,6	$-0,8990$	0,5382	0,0639
	0,8	$-0,4704$	0,2800	0,0027
	1,0	$-0,4320$	0,1949	0,0017
1,0	0,2	$-128,4235$	6,8168	25,0777
	0,4	$-6,8084$	1,5688	1,2000
	0,6	$-1,2191$	0,6180	0,1376
	0,8	$-0,5128$	0,3101	0,0138
	1,0	$-0,4054$	0,1948	0,0000

$$v = \frac{4 H^s l}{\pi^2 E h} (1 + v) \sum_{m=1,3,5\ldots} \frac{1}{m} \frac{\sin \dfrac{m\pi}{2}}{\cosh \dfrac{m\pi}{2}} \cosh \frac{m\pi}{l} x \sin \frac{m\pi}{l} y \; . \quad (5.28)$$

Nach der Gleichung (5.26) ist der Wert von w überall gleich Null. Dies erklärt sich aus der Tatsache, daß in jedem Punkt der in beiden Richtungen x und y identisch gekrümmten Schale rufen die mit umgekehrten Vorzeichen jedoch mit gleichem Absolutwert ($|n_x| = |n_y| = n$) auftretenden Schnittkräfte entgegengesetzte Durchbiegungen hervor, die einander gegenseitig aufheben.

Tafel 1b

H^s symmetrisch				
$\frac{f_x}{f_y}$	$\frac{l_x}{l_y}$	$u^0 = u\,\frac{E}{H^s}\,\frac{h}{l_x}$	$v^0 = v\,\frac{E}{H^s}\,\frac{h}{l_y}$	$w^0 = w\,\frac{E}{H^s}\,\frac{hf_x}{l_x^2}$
5,0000	5,0000	—0,2262	0,1452	0,0106
	4,0000	—0,2158	0,0764	0,0079
	3,0000	—0,2008	0,0333	0,0033
	2,0000	—0,2125	0,0371	0,0010
	1,0000	—1,6758	0,2612	0,2658
4,0000	5,0000	—0,2578	0,2540	0,0151
	4,0000	—0,2475	0,1389	0,0121
	3,0000	—0,2307	0,0606	0,0066
	2,0000	—0,2219	0,0420	0,0000
	1,0000	—1,1865	0,2701	0,1930
3,0000	5,0000	—0,3040	0,4801	0,0217
	4,0000	—0,2941	0,2732	0,0185
	3,0000	—0,2762	0,1240	0,0125
	2,0000	—0,2512	0,0565	0,0018
	1,0000	—0,7866	0,2658	0,1121
2,0000	5,0000	—0,3808	1,0257	0,0310
	4,0000	—0,3715	0,6080	0,0280
	3,0000	—0,3536	0,2944	0,0221
	2,0000	—0,3172	0,1082	0,0091
	1,0000	—0,5009	0,2387	0,0366
1,0000	5,0000	—0,5428	2,7647	0,0401
	4,0000	—0,5349	1,7063	0,0383
	3,0000	—0,5187	0,8918	0,0344
	2,0000	—0,4782	0,3392	0,0245
	1,0000	—0,4054	0,1948	0,0000

6. Untersuchung der antimetrischen Belastung H^a

Wenn am Rande $x = +a$ eine Zuglast H^a und am Rande $x = -a$ eine Drucklast derselben Grösse wie die erste wirkt, so können wir die statischen und Randbedingungen der durch in ihrer eigenen Ebene unendlich steif angenommenen, jedoch in der Seitenrichtung weichen Randträger unterstützten Schale folgenderweise beschreiben:

$$\ddot{F}\Big|_{x=+\frac{l_x}{2}} = n_x\Big|_{x=+\frac{l_x}{2}} = +H^a, \tag{6.1a}$$

$$\overset{\shortparallel}{F}\Big|_{x=-\frac{l_x}{2}} = n_x\Big|_{x=-\frac{l_x}{2}} = -H^a\,, \tag{6.1b}$$

$$\overset{\shortparallel}{F}\Big|_{y=\pm\frac{l_y}{2}} = n_y\Big|_{y=\pm\frac{l_y}{2}} = 0\,, \tag{6.1c—d}$$

$$w\Big|_{x=\pm\frac{l_x}{2}} = 0\,, \tag{6.2a—b}$$

$$w\Big|_{y=\pm\frac{l_y}{2}} = 0\,. \tag{6.2c—d}$$

Die Belastung H^a kann natürlich in die Fouriersche Reihe

$$H^a_{(y)} = \frac{4}{\pi}\,H^a \sum_{m=1,3,5\dots} \frac{1}{m}\,\sin\frac{m\pi}{2}\cdot\cos\frac{m\pi}{l_y}\,y \tag{6.3}$$

entwickelt werden, die die gleiche Form, wie (5.4) hat.

In diesem Fall erhalten wir die im Bezug auf die Ebene xz symmetrische, auch mit Hilfe des Fourierschen Verfahren hergeleitete und die Randbedingungen (6.1) befriedigende Lösung der Gleichgewichtsdifferentialgleichung (5.4):

$$F = -\frac{4H^a}{\pi^3}\,l_y^2 \sum_{m=1,3,5\dots} \frac{1}{m^3}\,\frac{\sin\dfrac{m\pi}{2}}{\sinh\dfrac{m\pi}{2}\sqrt{\dfrac{f_x}{f_y}}}\,\sinh\frac{m\pi}{l_x}\sqrt{\frac{f_x}{f_y}}\,x\cdot\cos\frac{m\pi}{l_y}\,y\,, \tag{6.4}$$

deren im Punkte 2 erwähnte partielle Differentialableitungen die gesuchten Membrankräfte ergeben:

$$n_x = \frac{4H^a}{\pi} \sum_{m=1,3,5\dots} \frac{1}{m}\cdot\frac{\sin\dfrac{m\pi}{2}}{\sinh\dfrac{m\pi}{2}\sqrt{\dfrac{f_x}{f_y}}}\cdot\sinh\frac{m\pi}{l_x}\sqrt{\frac{f_x}{f_y}}\,x\cdot\cos\frac{m\pi}{l_y}\,y\,, \tag{6.5}$$

$$n_y = -\frac{f_x}{f_y}\,\frac{l_y^2}{l_x^2}\,n_x\,, \tag{6.6}$$

$$n_{xy} = -\frac{4H^a}{\pi}\sqrt{\frac{f_x}{f_y}}\,\frac{l_y}{l_x} \sum_{m=1,3,5\dots} \frac{1}{m}\,\frac{\sin\dfrac{m\pi}{2}}{\sinh\dfrac{m\pi}{2}\sqrt{\dfrac{f_x}{f_y}}}\,\cosh\frac{m\pi}{l_x}\sqrt{\frac{f_x}{f_y}}\,x\cdot\sin\frac{m\pi}{l_y}\,y\,. \tag{6.7}$$

Die für die 25 charakteristischen Punkte der ersten Viertels des Koordinaten-
systems ausgerechneten Werte dieser Funktionen sind in den Bildern 8 und 9
graphisch dargestellt.
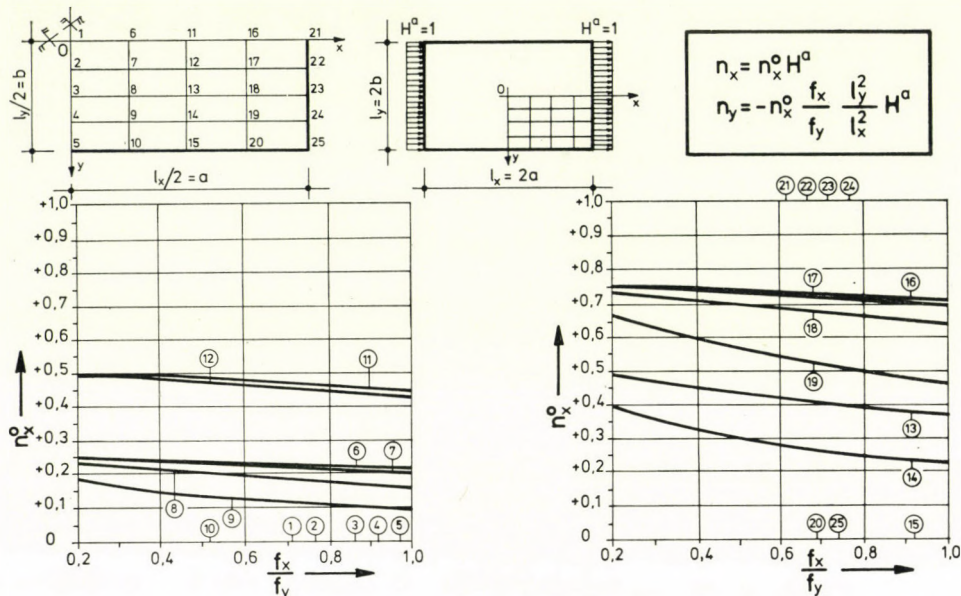
Bild 8a. Membrankräfte n_x und n_y aus der antimetrischen Randbelastung $H^a = 1$
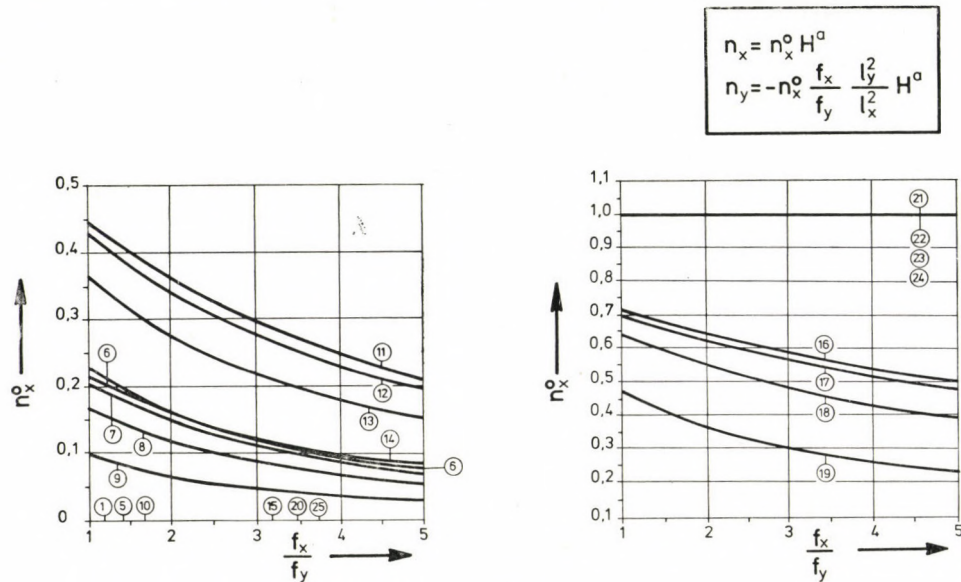

*Bild 8b.* Die Membrankräfte n_x und n_y aus der antimetrischen Randbelastung $H^a = 1$
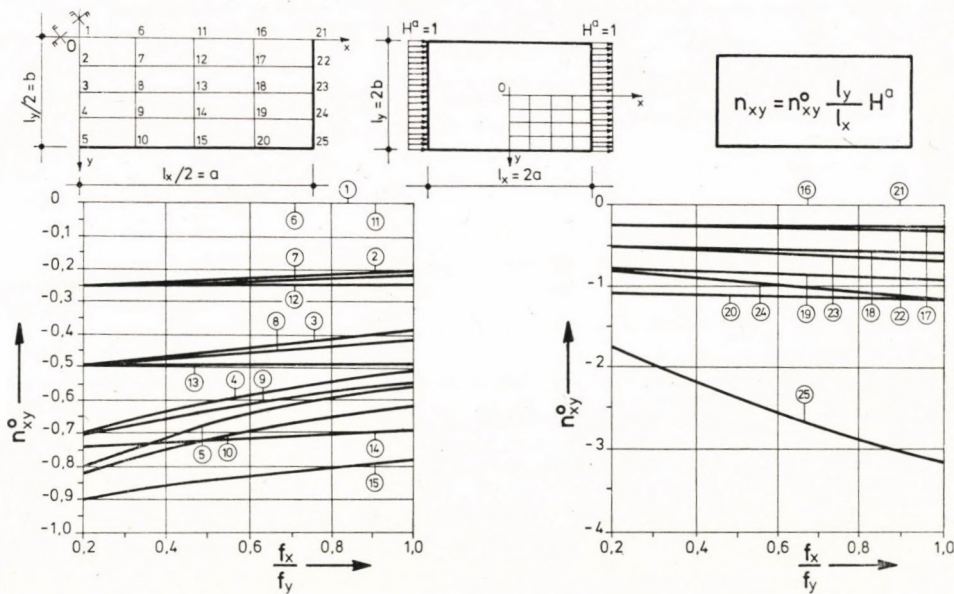
*Bild 9a.* Die Membranschubkraft n_{xy} aus der antimetrischen Randbelastung $H^a = 1$
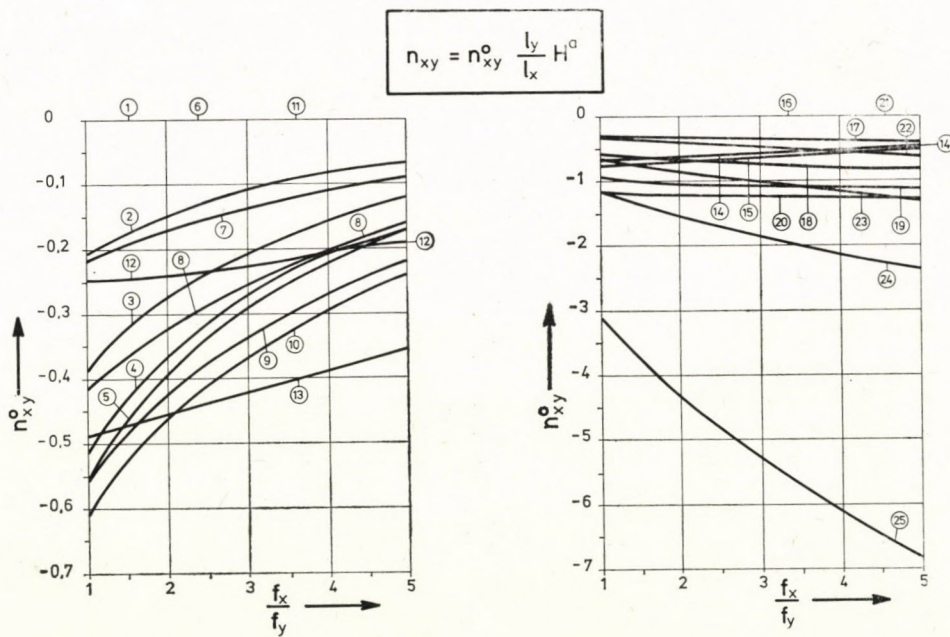
Bild 9b. Die Membranschubkraft n_{xy} aus der antimetrischen Randbelastung $H^a = 1$

10

Wendet man nun den biharmonischen Operator für F an, erhält man die Form

$$\Delta\Delta F = -\frac{4H^a\pi}{l_y^2}\left(\frac{f_x}{f_y}\,\frac{l_y^2}{l_x^2}-1\right)^2 \sum_{m=1,3,5\ldots} m\,\frac{\sin\dfrac{m\pi}{2}}{\sinh\dfrac{m\pi}{2}\sqrt{\dfrac{f_x}{f_y}}}\,\sinh\frac{m\pi}{l_x}\sqrt{\frac{f_x}{f_y}}\,x\cdot\cos\frac{m\pi}{l_y}y\,.$$

$$(6.8)$$

Zur Lösung der Verträglichkeits-Differentialgleichung (5.18), die auch die Randbedingungen (6.2) befriedigt, erhält man den Ausdruck

$$w = \sum_{m=1,3,5\ldots} w_m\cos\frac{m\pi}{l_y}y\left(x\cosh\frac{m\pi}{l_x}\sqrt{\frac{f_x}{f_y}}\,x - \frac{l_x}{2}\coth\frac{m\pi}{2}\sqrt{\frac{f_x}{f_y}}\sinh\frac{m\pi}{l_x}\sqrt{\frac{f_x}{f_y}}\,x\right).$$

$$(6.9)$$

Hier bedeutet:

$$w_m = \frac{H^a}{4Eh}\left(\frac{f_x}{f_y}\,\frac{l_y^2}{l_x^2}-1\right)^2\sqrt{\frac{f_x}{f_y}}\,\frac{l_x^2}{f_x}\,\frac{\sin\dfrac{m\pi}{2}}{\sinh\dfrac{m\pi}{2}\sqrt{\dfrac{f_x}{f_y}}}\,.$$

$$(6.10)$$

Setzt man (6.4) und (6.9) in (3.5) bzw. in (3.6) ein, so erhält man für u bzw. für v die folgenden Zusammenhänge:

$$u = \frac{H^a}{\pi Eh}\,l_x \sum_{m=1,3,5\ldots} \frac{\sin\dfrac{m\pi}{2}}{\sinh\dfrac{m\pi}{2}\sqrt{\dfrac{f_x}{f_y}}}\cos\frac{m\pi}{l_y}y\left\{\frac{1}{m}\cosh\frac{m\pi}{l_x}\sqrt{\frac{f_x}{f_y}}\,x\cdot\left[-\left(\frac{f_x}{f_y}\,\frac{l_y^2}{l_x^2}-1\right)^2\cdot\right.\right.$$

$$\cdot\coth\frac{m\pi}{2}\sqrt{\frac{f_x}{f_y}} + \frac{4}{\pi m}\sqrt{\frac{f_y}{f_x}}\left(1+\nu\frac{f_x}{f_y}\,\frac{l_y^2}{l_x^2}\right) - \frac{2}{\pi m}\sqrt{\frac{f_y}{f_x}}\left(\frac{f_x}{f_y}\,\frac{l_y^2}{l_x^2}-1\right)^2\right] +$$

$$+ \frac{2}{ml_x}\left(\frac{f_x}{f_y}\,\frac{l_y^2}{l_x^2}-1\right)^2 x\cdot\sinh\frac{m\pi}{l_x}\sqrt{\frac{f_x}{f_y}}\,x\right\},$$

$$(6.11)$$

$$v = \frac{H^a}{\pi Eh}\,l_y \sum_{m=1,3,5\ldots} \frac{1}{m}\,\frac{\sin\dfrac{m\pi}{2}}{\sinh\dfrac{m\pi}{2}\sqrt{\dfrac{f_x}{f_y}}}\sin\frac{m\pi}{l_y}y\left\{\sinh\frac{m\pi}{l_x}\sqrt{\frac{f_x}{f_y}}\,x\cdot\right.$$

$$\cdot\left[-\sqrt{\frac{f_y}{f_x}}\,\frac{l_x^2}{l_y^2}\left(\frac{f_x}{f_y}\,\frac{l_y^2}{l_x^2}-1\right)^2\coth\frac{m\pi}{2}\sqrt{\frac{f_x}{f_y}} - \frac{4}{\pi m}\left(\frac{f_x}{f_y}\,\frac{l_y^2}{l_x^2}+\nu\right)\right] +$$

$$+ 2\sqrt{\frac{f_y}{f_x}}\,\frac{l_x^2}{l_y^2}\left(\frac{f_x}{f_y}\,\frac{l_y^2}{l_x^2}-1\right)^2 x\cdot\cosh\frac{m\pi}{l_x}\sqrt{\frac{f_x}{f_y}}\,x\right\}.$$

$$(6.12)$$

Die Funktionen $u_1(y)$ und $v_1(x)$ sind infolge der Symmetrie bzw. Antimetrie gleich Null.

Für die Praxis benötigen wir vor allem die Verschiebungswerte $w = w(s/2,0)$, $u(a, o)$, $v(a, b)$.

Diese Werte sind in den Bildern 10 und 11 in der Abhängigkeit von f_x/f_y und l_x/l_y dargestellt ($\nu = 0{,}2$).

Die charakteristischen Werte derselben sind auch in der Tafel 2 wiedergegeben.

Im Fall eines Rotationsparaboloids ($f_x = f_y = f$, $l_x = l_y = l$) werden die hergeleiteten Abhängigkeiten folgenderweise vereinfacht:

$$n_x = \frac{4H^a}{\pi} \sum_{m=1,3,5\ldots} \frac{1}{m} \frac{\sin\dfrac{m\pi}{2}}{\sinh\dfrac{m\pi}{2}} \sinh\frac{m\pi}{l}x \cos\frac{m\pi}{l}y \,, \qquad (6.13)$$

$$n_y = -n_x \,, \qquad (6.14)$$

$$n_{xy} = -\frac{4H^a}{\pi} \sum_{m=1,3,5\ldots} \frac{1}{m} \frac{\sin\dfrac{m\pi}{2}}{\sinh\dfrac{m\pi}{2}} \cosh\frac{m\pi}{l}x \sin\frac{m\pi}{l}y \,, \qquad (6.15)$$
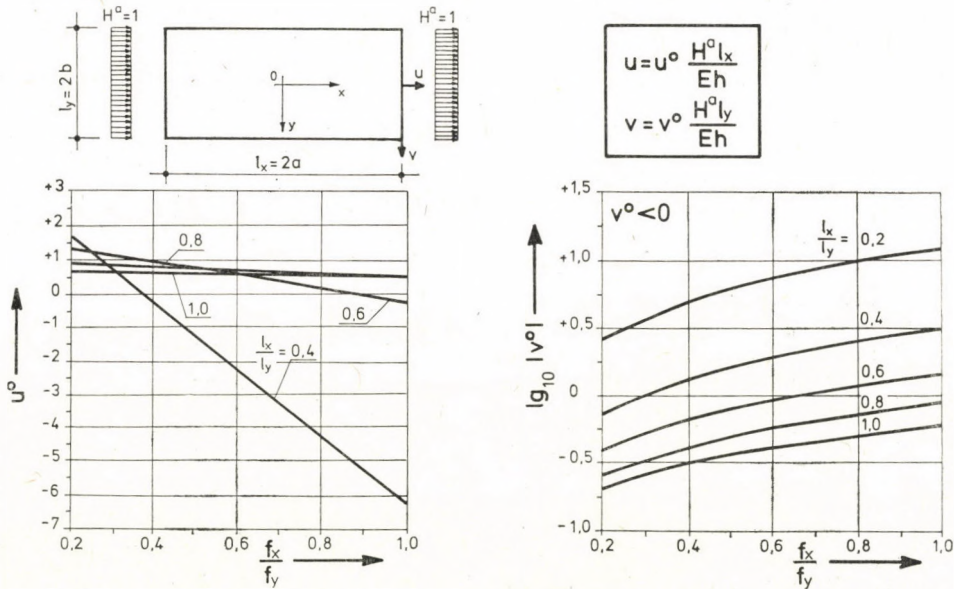

Bild 10a. Verschiebungen $u = u(a, o)$, und $v = v(a, b)$ infolge der antimetrischen Randbelastung $H^a = 1$; ($w_{\text{Rand}} = 0$)

$$u = u^0 \frac{H^a l_x}{Eh}$$
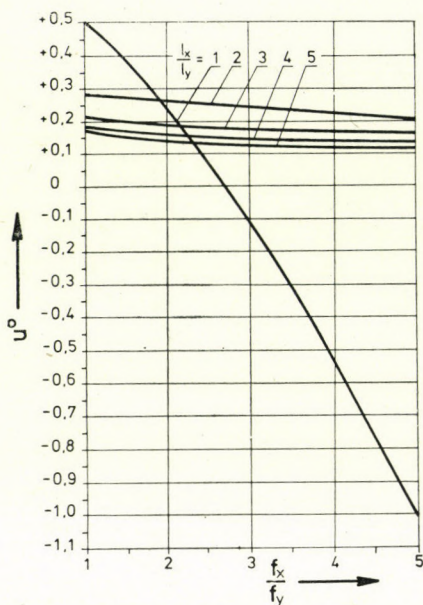
$$v = v^0 \frac{H^a l_y}{Eh}$$
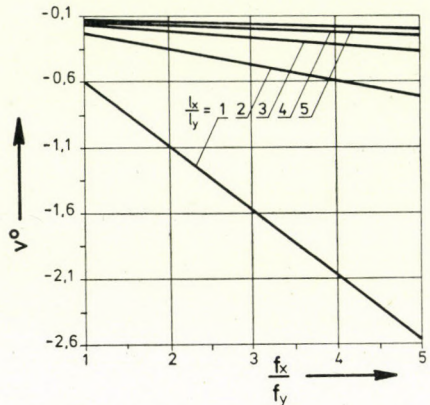
Bild 10b. Verschiebungen $u = u(a, o)$ und $v = v(a, b)$ infolge der antimetrischen Randbelastung $H^a = 1$; $(w_{Rand} = 1)$

$$w = w^0 \frac{H^a l_x^2}{Ehf_x}$$

$$w = w^0 \frac{H^a l_x}{Eh}$$
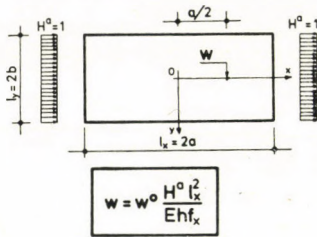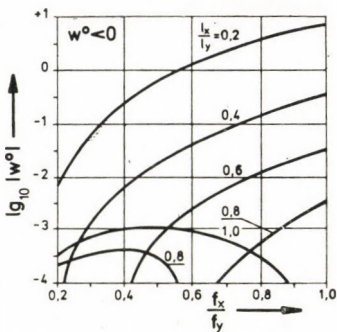
Bild 11a. Durchbiegung $w = w(a/2,\ 0)$ aus der antimetrischen Randbelastung $H^a = 1$; $(w_{Rand} = 0)$
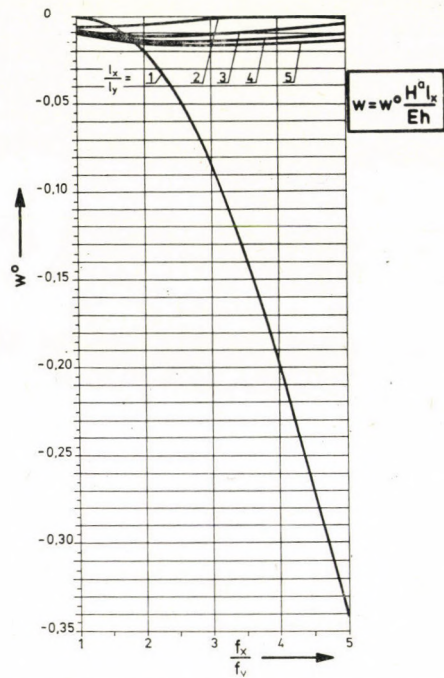
Bild 11b. Durchbiegung $w = w(a/2,\ 0)$ aus der antimetrischen Randbelastung $H^a = 1$; $(w_{Rand} = 0)$

Tafel 2a

		H^a antimetrisch		
$\dfrac{f_x}{f_y}$	$\dfrac{l_x}{l_y}$	$u^0 = u\,\dfrac{E}{H^a}\,\dfrac{h}{l_x}$	$v^0 = v\,\dfrac{E}{H^a}\,\dfrac{h}{l_y}$	$w^0 = w\,\dfrac{E}{H^a}\,\dfrac{hf_x}{l_x^2}$
0,2	0,2	−17,1794	−2,5690	−0,0080
	0,4	1,6929	−0,7164	−0,0000
	0,6	1,3272	−0,3733	−0,0001
	0,8	0,9142	−0,2532	−0,0002
	1,0	0,6730	−0,1976	−0,0003
0,4	0,2	−48,5493	−5,0392	−0,2229
	0,4	−0,2287	−1,3339	−0,0062
	0,6	0,9584	−0,6477	−0,0000
	0,8	0,8009	−0,4076	−0,0004
	1,0	0,6275	−0,2964	−0,0010
0,6	0,2	−80,7745	−7,5094	−1,0944
	0,4	−2,1911	−1,9515	−0,0422
	0,6	0,5850	−0,9222	−0,0025
	0,8	0,6871	−0,5620	−0,0000
	1,0	0,5818	−0,3952	−0,0009
0,8	0,2	−114,3603	−9,9796	−2,9987
	0,4	−4,2270	−2,5690	−0,1329
	0,6	0,2006	−1,1967	−0,0124
	0,8	0,5714	−0,7164	−0,0005
	1,0	0,5361	−0,4940	−0,0003
1,0	0,2	−149,6567	−12,4498	−6,1764
	0,4	−6,3604	−3,1866	−0,2956
	0,6	−0,1999	−1,4711	−0,0339
	0,8	0,4519	−0,8707	−0,0034
	1,0	0,4896	−0,5928	−0,0000

$$w = 0, \qquad (6.16)$$

$$u = \frac{4H^a l}{\pi^2 Eh}\,(1 + v)\sum_{m=1,3,5\ldots}\frac{1}{m}\,\frac{\sin\dfrac{m\pi}{2}}{\sinh\dfrac{m\pi}{2}}\cosh\frac{m\pi}{l}\,x\cos\frac{m\pi}{l}\,y\,, \quad (6.17)$$

$$v = -\frac{4H^a l}{\pi^2 Eh}\,(1 + v)\sum_{m=1,3,5\ldots}\frac{1}{m}\,\frac{\sin\dfrac{m\pi}{2}}{\sinh\dfrac{m\pi}{2}}\sinh\frac{m\pi}{l}\,x\sin\frac{m\pi}{l}\,y\,. \quad (6.18)$$

Tafel 2b

$\dfrac{f_x}{f_y}$	$\dfrac{l_x}{l_y}$	$u^0 = u\,\dfrac{E}{H^a}\,\dfrac{h}{l_x}$	$v^0 = v\,\dfrac{E}{H^a}\,\dfrac{h}{l_y}$	$w^0 = w\,\dfrac{E}{H^a}\,\dfrac{hf_x}{l_x^2}$
		H^a antimetrisch		
5,0000	5,0000	0,1191	−0,1976	−0,0137
	4,0000	0,1370	−0,2532	−0,0101
	3,0000	0,1682	−0,3733	−0,0042
	2,0000	0,2028	−0,7164	−0,0013
	1,0000	−1,0167	−2,5690	−0,3421
4,0000	5,0000	0,1250	−0,1779	−0,0154
	4,0000	0,1420	−0,2223	−0,0122
	3,0000	0,1735	−0,3184	−0,0067
	2,0000	0,2238	−0,5928	0,0000
	1,0000	−0,5249	−2,0750	−0,1959
3,0000	5,0000	0,1335	−0,1581	−0,0264
	4,0000	0,1495	−0,1914	−0,0139
	3,0000	0,1803	−0,2635	−0,0094
	2,0000	0,2418	−0,4693	−0,0013
	1,0000	−0,1089	−1,5809	−0,0845
2,0000	5,0000	0,1467	−0,1383	−0,0155
	4,0000	0,1613	−0,1606	−0,0140
	3,0000	0,1906	−0,2086	−0,0111
	2,0000	0,2589	−0,3458	−0,0046
	1,0000	0,2272	−1,0869	−0,0183
1,0000	5,0000	0,1679	−0,1186	−0,0099
	4,0000	0,1810	−0,1297	−0,0094
	3,0000	0,2084	−0,1537	−0,0085
	2,0000	0,2799	−0,2223	−0,0060
	1,0000	0,4896	−0,5928	0,0000

7. Anwendung zur näherungsweise Berücksichtigung der Auswirkung der Verdrehungs- und seitlichen Biegesteifigkeit der Randträger

7.1. Theoretische Grundlagen

Wären die Drillsteifigkeiten (GI_{tx}, GI_{ly}) und die seitlichen Biegesteifigkeiten (EI_x, EI_y) gleich Null, so könnten die Randträger ohne Widerstand den durch die Flächenbelastung p hervorgerufenen horizontalen Verschiebungen folgen, und damit würde der Spannungszustand der elliptischen Paraboloidschale im Rahmen der Membrantheorie (d.h., mit Vernachlässigung der

Biegesteifigkeit der Schale) gelöst. Die in der einschlägigen Sachliteratur behandelten Verfahren [1] setzen außer der Annahme der unendlichen Steifigkeit der Randträger in ihren eigenen Ebenen ($w_{Rand} = 0$) auch die Vernachlässigung der obenerwähnten Randträgersteifigkeiten voraus.

In der Wirklichkeit können jedoch die Randträger — infolge ihrer endlich großen Drillsteifigkeit GI_t und Biegesteifigkeit in der horizontalen Ebene EI — den horizontalen Schalenverschiebungen nicht ohne Behinderung folgen.
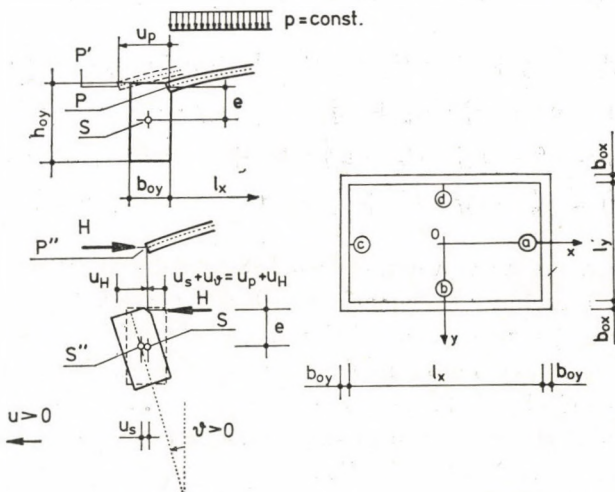

Bild 12. Gleiche horizontale Verschiebung der Schale und des Randträgers ($w_{Rand} = 0$)

Setzt man voraus, daß die Randträger gegen die in ihren Ebenen auftretende Biegung steif sind (was im allgemeinen zutrifft), so kann die Verträglichkeit zwischen der Membranschale und den Randträgern durch ein horizontales Anschlußkraftsystem gewährleistet werden.

Da die Randverformungen der mit gleichmäßig verteilten Flächenbelastung belegten Schale und auch dieselben der durch ein gleichmäßig verteiltes horizontales Randkraftsystem belasteten Schale durch Fouriersche Reihen von identischer Struktur beschrieben werden können, kann man mit guter Näherung annehmen, daß das Verbindungskraftsystem durch den gleichmäßig verteilten Durchschnittswert entsprechend charakterisiert werden kann. Demzufolge kann man durch Anwendung der im vorhergehenden abgeleiteten Resultate ein Näherungsverfahren zur Ermittlung der an den Schalenrändern auftretenden Seitendrücke ausarbeiten.

Das Zustandekommen der erwähnten Verträglichkeit ist im Bild 12 dargestellt.

Die Verträglichkeitsgleichungen werden auf die Mittelpunkte (a, b, c, d) der Schalenrandträger bezogen aufgeschrieben, infolge dessen wird die Verträglichkeit mit vollkommener Genauigkeit nur an diesen Punkten erfüllt.

Bezeichnet man mit u_s (v_s) die horizontale Verschiebung des Querschnittsschwerpunktes des durch das Kraftsystem $H = 1$ belasteten parabolischen Bogenträgers; mit u_ϑ (v_ϑ) die infolge der Verdrehung des Randträgers auftretende Verschiebung des Anschlußpunktes P; und mit u_H (v_H) die durch die Horizontalkräfte $H = 1$ hervorgerufenen Schalenverschiebungen, so kann man das inhomogene lineare Gleichungssystem wie folgt aufschreiben:

$$
\begin{aligned}
H_a(u_s^{aa} + u_\vartheta^{aa}) &= u_p^a + u_H^{aa} \cdot H_a + u_H^{ab} \cdot H_b + u_H^{ac} \cdot H_c + u_H^{ad} \cdot H_d, \\
H_b(v_s^{bb} + v_\vartheta^{bb}) &= v_p^b + v_H^{bb} \cdot H_b + v_H^{bc} \cdot H_c + v_H^{bd} \cdot H_d + v_H^{ba} \cdot H_a, \\
H_c(u_s^{cc} + u_\vartheta^{cc}) &= u_p^c + u_H^{cc} \cdot H_c + u_H^{cd} \cdot H_d + u_H^{ca} \cdot H_a + u_H^{cb} \cdot H_b, \\
H_d(v_s^{dd} + v_\vartheta^{dd}) &= v_p^d + v_H^{dd} \cdot H_d + v_H^{da} \cdot H_a + v_H^{db} H_b + v_H^{dc} H_c,
\end{aligned}
\qquad (7.1a-d)
$$

wo der erste bzw. zweite von den oberen Indexen die Stelle der Verschiebung bzw. der die Verschiebung hervorrufenden Kraft bezeichnet.

Das Gleichungssystem bezieht sich der Einfachheit halber auf den Fall, wo die stützenden Randbogen in der horizontalen Ebene entweder gelenkig gestützt oder steif eingespannt sind $(u_s^{ab} = u^{ab} = \ldots = 0$ usw.$)$.

Die Kräfte H sind positiv im Falle, wo sie auf die Schale Druck ausüben, während die Einheits- und Lastkoeffizienten im Sinne vom Rande der Schale nach außen wirkend als positiv betrachtet werden. Die Einheitsbeiwerte können mit Hilfe der bekannten Methoden der Statik ohne weiteres ermittelt werden (siehe Punkt 7.2).

Zur Berechnung der durch die Flächenlast P hervorgerufenen Belastungsbeiwerte wurden die an den Seiten 264 bis 266 des im Literaturverzeichnis unter [1] befindlichen Werks vorgeführten Fourierschen Reihen mit Hilfe von einer elektronischen Rechenanlage ausgewertet und das Ergebnis in den Bildern 13a bis c graphisch dargestellt. Diese Ergebnisse sind auch in der Tafel 3 wiedergegeben.

Diese Berechnung kann im wesentlichen dem folgenden Zwecke dienen. Für gewisse Flächentragwerke konstruiert man verhältnismäßig starke Randträger, bei den die Größe des Gewölbedrucks schon einen wesentlichen Wert erreichen kann. Das behandelte Berechnungsverfahren kann — wenn man nämlich die an den vier Rändern seitendruckfrei unterstützte Schale als Grundsystem annimmt [1] — auch zur Näherungsuntersuchung von elliptischen Paraboloidschalen angewendet werden, die an beliebigen Rändern mit auf Verdrehung und auf horizontale Biegung steifen Randträgern verbunden sind. Die Methode kann auch für den Fall herangezogen werden, wo infolge des Zusammenbaus mit anderen Schalen (Tonnenschale, elliptische Paraboloid-
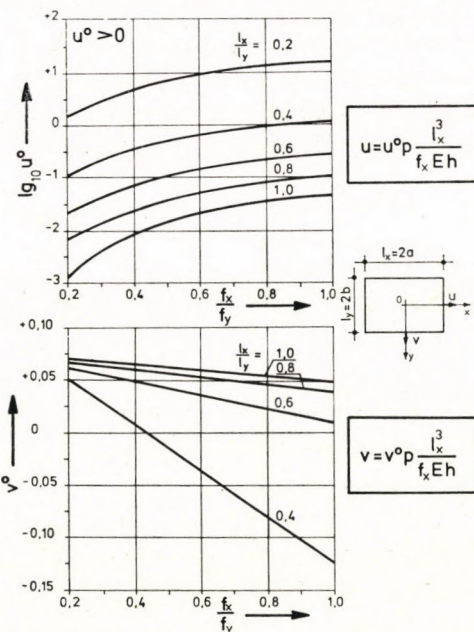
Bild 13a. Die Membranverschiebungen $u = u(a, 0)$ und $v = v(0, b)$ entlang des Randes der elliptischen Paraboloidschale ohne Seitendruck, hervorgerufen durch die konstante Last p; $(w_{\text{Rand}} = 0)$
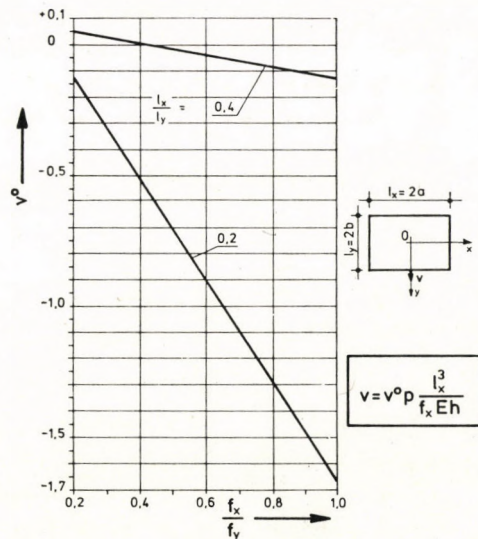
Bild 13b. Die Membranverschiebungen $v = v(0, b)$ entlang des Randes der elliptischen Paraboloidschale ohne Seitendruck, hervorgerufen durch die konstante Belastung $p = \text{const.}$ $(w_{\text{Rand}} = 0)$
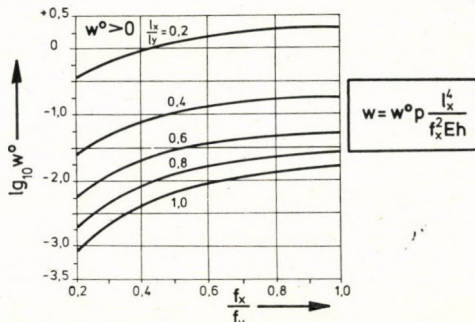

Bild 13c. Membrandurchbiegung $w = w(0, 0)$ der seitendruckfreien elliptischen Paraboloidschale, hervorgerufen durch die konstante Belastung p $(w_{\text{Rand}} = 0)$

schale) die elliptische Paraboloidschale auch praktisch verschiebungslose Randträger hat.

Es soll noch erwähnt werden, daß man an den Seiten 272 bis 282 des Werks [1] für derartige Rotationsparaboloidschalen gültige Lösungen finden kann, deren beliebige Randträger gegen Biegung und Verdrehung unendlich steif sind.

Tafel 3

		aus konstanter Belastung P		
$\dfrac{f_x}{f_y}$	$\dfrac{l_x}{l_y}$	$u^0 = u \, \dfrac{E}{P} \, \dfrac{f_x h}{l_x^3}$	$v^0 = v \, \dfrac{E}{P} \, \dfrac{f_x h}{l_x^3}$	$w^0 = w \, \dfrac{E}{P} \, \dfrac{f_x^2 h}{l_x^4}$
0,2	0,2	1,442842	$-0,123526$	0,336646
	0,4	0,106183	0,048646	0,024374
	0,6	0,023619	0,060511	0,005616
	0,8	0,006898	0,065550	0,001936
	1,0	0,001298	0,071142	0,000738
0,4	0,2	4,608036	$-0,498996$	0,941938
	0,4	0,337049	0,012177	0,073502
	0,6	0,077621	0,051388	0,019128
	0,8	0,026069	0,059612	0,007953
	1,0	0,009094	0,064014	0,004160
0,6	0,2	8,554988	$-0,911730$	1,465292
	0,4	0,622653	$-0,034327$	0,119870
	0,6	0,145563	0,038650	0,033219
	0,8	0,051816	0,053550	0,014887
	1,0	0,021277	0,059318	0,008508
0,8	0,2	12,931970	$-1,303521$	1,802736
	0,4	0,935116	$-0,081634$	0,154225
	0,6	0,219455	0,024547	0,044913
	0,8	0,080155	0,046744	0,021120
	1,0	0,035205	0,054560	0,012647
1,0	0,2	17,602950	$-1,654735$	1,939704
	0,4	1,263915	$-0,125803$	0,174762
	0,6	0,296279	0,010648	0,053461
	0,8	0,109523	0,039801	0,026178
	1,0	0,049767	0,049767	0,016215

Es existiert jedoch im Bezug auf elliptische Paraboloidschalen von allgemeiner Geometrie ($l_x \neq l_y$, $f_x \neq f_y$) keine exakte Lösung weder im Falle der Randträger von endlicher Steifigkeit, noch im Falle von unendlich steifen Randträgern. Demnach scheint uns das wichtigste Anwendungsgebiet der behandelten statischen Grundaufgabe die Näherungsanalyse dieser letzteren Probleme zu sein.

Schließlich muss darauf hingewiesen werden, daß zur Analyse der räumlichen Stabilität der Randträger — selbst im Falle, wo aus dem Gesichtspunkt der Schale der Gewölbedruck vernachlässigt werden kann — die Kenntnis der horizontalen Anschlußkräfte zwischen der Schale und Randträgern unerläßlich ist.

7.2 Numerische Beispiele

Untersuchen wir die durch die geometrischen Parameter

$$l_x = l_y = l = 20 \text{ m},$$

$$f_x = f_y = f = 2,5 \text{ m},$$

$$h = 0,08 \text{ m}$$

definierte und mit $p = 0,3$ Mp/m² belastete elliptische Paraboloidschale für zwei unterschiedliche Unterstützungsfälle.

7.21 Erster Fall. Alle vier Randträger der im *Bild 12* dargestellten Schale seien gegen Biegung und Verdrehung unendlich steif (infolge der Verbindung durch Zusammenbau mit den benachbarten Schalen). Von der Flächenbelastung p (siehe Bild 13, bzw. Tafel 3) tritt die nach Außen gerichtete Verschiebung

$$u_P = u_P^a = v_P^b = u_P^c = v_P = 0,0498 \; \frac{20^3}{25 \cdot 0,08} \; \frac{P}{E} = 1992 \; \frac{P}{E} = 598 \; \frac{1}{E} \; [m]$$

an den Punkten *a, b, c* und *d* auf. Die an einem Rand durch die Randbelastung $H = H^s + H^a = (1/2) + (1/2) = 1$, am anderen Rand durch die Randbelastung $\overline{H} = H^s + H^a = (1/2) - (1/2) = 0$ hervorgerufenen Schalenverschiebungen (s. Bilder 6a und 10 bzw. Tafeln 1 und 2) sind wie folgt:

$$u_H^{aa} = v_H^{bb} = \frac{1}{2} \; \frac{20}{E \, 0,08} \; (-0,4054 - 0,4896) = -112 \; \frac{1}{E} \; [m],$$

$$u_H^{ab} = u_H^{ad} = v_H^{bc} = v_H^{qb} = \frac{1}{2} \cdot 0,1948 \; \frac{20}{E \, 0,08} = +24,35 \; \frac{1}{E} \; [m],$$

$$u_H^{ac} = v_H^{bd} = \frac{1}{2} \; \frac{20}{E \, 0,08} \; (-0,4054 + 0,4896) = +10,53 \; \frac{1}{E} \; [m].$$

Die Verträglichkeitsgleichung ist:

$$H(-112 + 2 \cdot 24,35 + 10,53) + 598 = 0$$

$$H = \frac{598}{193,11} = 3,1 [M/pm].$$

Nach der exakten Lösung ([1] S. 287) ergibt sich ein Gewölbedruck

$$H = \frac{0,3}{2} \; \frac{20^2}{8 \cdot 2,5} = 3 [Mp/m],$$

d. h., der Fehler unseres Näherungsverfahrens beträgt 3 Prozent.

7.22 Zweiter Fall. Die Schale sei an den Rändern *a* und *c* durch unendlich steife Randträger und an den Rändern *b* und *d* durch seitlich weiche Randträger unterstützt. Die Biegesteifigkeit der Bogen mit der Geometrie $b_0 = 0,25$ m, $h_0 = 0,50$ m beträgt

$$EI = 0,5 \; \frac{0,25^3}{12} \; E = 6,51 \cdot 10^{-4} \; E [Mpm^2],$$

und die Verdrehungssteifigkeit

$$GI_t = 0,23 \cdot 0,5 \cdot 0,25^3 \; \frac{E}{2(1 + 0,2)} = 7,49 \cdot 10^{-4} E [Mpm^2].$$

Der Anschlußpunkt der Mittelquerschnitte der Randbogen an der Schale wird infolge der Biegung und Verdrehung aus der gleichmäßig verteilten Belastung $H = 1$ um das Maß

$$u_s + u_\vartheta = (640000 + 4170)\frac{1}{E}\,m = 644170\,\frac{1}{E}\,m$$

verschoben.

$$v_s + v_\vartheta = 0\,.$$

Infolge der doppelten Symmetrie sind

$$H_a = H_c\,,$$

und

$$H_b = H_d\,.$$

Das Verträglichkeits-Gleichungssystem lautet:

$$H_a\,644170 = 598 + H_d(-112 + 10{,}53) + H_b\,24{,}35 \cdot 2\,,$$

$$0 = 598 + H_b(-112 + 10{,}53) + H_a \cdot 24{,}35 \cdot 2\,,$$

$$H_a\,644271 - H_b\,48{,}70 = 598\,,$$

$$-H_a\,48{,}70 + H_b\,101{,}47 = 598\,.$$

Die Lösung ist:

$$H_a = 0{,}0014\ [Mp/m]\,.$$

$$H_b = 5{,}893\ \ [Mp/m]\,.$$

Demnach wird beinahe die ganze Last in der Richtung der steifen Ränder durch Gewölbewir kung getragen.

SCHRIFTTUM

1. BELEŞ, A. A.—SOARE, M. V.: Das elliptische und hyperbolische Paraboloid im Bauwesen. Akademie-Verlag, Bukarest, 1970
2. BÖLCSKEI, E.: Déformation des voiles minces. *Acta Techn. Hung.*, 5 (1952)
3. FLÜGGE, W.: Stresses in Shells. Second Edition. Springer Verlag Berlin (Heidelberg) New York
4. GEYLING, F. T.: A General Theory of Deformations of Membrane Shells. Dissertation. Stanford University, Stanford, Cal. 1953.
5. SOMMERFELD, A.: Vorlesungen über theoretische Physik. Bd. VI. Partielle Differentialglei-chungen der Physik. Akademische Verlagsgesellschaft Geest und Portig, Leipzig 1954

Membrane Forces and Membrane Deflections of Flat Elliptic Paraboloid Shells Subjected to Uniformly Distributed Horizontal Load at the Edges. An analytic method of solution of the membrane stress pattern and membrane deflections of flat elliptic paraboloid shells subjected to uniformly distributed horizontal edge load is presented. The functions describing the effects of the symmetrical and antisymmetrical system of forces acting on the edges have been worked out also in graphic form in order to make easier the calculation by hand. It has been pointed out that by making use of this basic static problem, in the framework of the membrane theory also the internal forces and deflections of the elliptic paraboloid shells supported by edge beams, having non negligible flexural and torsional stiffnesses in the horizontal plane can be analyzed in an approximate way.

Мембранные усилия и мембранные деформации плоских эллиптических параболоид-ных оболочек с равномерно распределяющейся горизонтальной краевой нагрузкой. В работе дается аналитическое решение работы мембранных усилий и мембранных деформаций плоских эллиптических параболоижных оболочек, нагруженных равномерно распределяющейся горизонтальной системой краевых усилий. Функции, — описывающие воздействия, вызванные системой симметрических и, соответственно, антиметрических усилий, работающих на противоположных краях, — обработаны также в графической форме, облегчающей вычисления ручным способом. В работе показано, что путем использования данной основной статической задачи в рамках мембранной теории в приближен-ной форме можно исследовать также внутренние усилия и деформации эллиптических параболоидных оболочек, обладающих краевыми балками, имеющими в горизонтальном направлении непренебрежимые жесткости на изгиб и, соответственно, кручение.

SOME PROBLEMS OF MAINS VOLTAGE REGULATION IN L. T. NETWORKS

L. GÁDOR*

CAND. OF TECHN. SCI.

In relatively sparsely populated settlements large voltage drops may arise in the long radial lines of the secondary network. This fact justifies voltage regulation. If an extended system is regulated in one point, a multi-step or a continuous regulator has no advantages, a two-step regulator is completely satisfactory. If the feeding point voltage varies too, a two-parameter regulation must be applied with simultaneous sensing of the current and the voltage. A relatively large feeding point voltage variation can be eliminated only with a regulator placed in the feeding point and here multi-step or continuous regulation is justified.

1. Introduction

In electric energy distribution systems covering a large area the emplacements of production and consumption are distant from each other, therefore, the varying production and consumption arise in a complicated current distribution. As a consequence of the voltage drops in the system, the voltage changes from place to place.

In order to keep the voltage at the place of consumption within prescribed limits, voltage regulation must be applied. According to the structure of the network the voltage regulation has several levels: the generator voltage itself must be regulated, in like manner the voltage must be regulated in the more important junctions of the high and the medium voltage network, and regulation must be used mostly in the L.T. secondary network.

In Hungary we have dealt for several years with the regulation of the L.T. consumers' network. This regulation is especially justified in those consumer districts where the specific consumption per unit area is small. So this is not valid for the densely populated town centres, but for the thinly built-up town borders and villages, where from one feeding point long lines branch out and on these considerable voltage drops can arise. Let us remark that in the improvement of voltage conditions of secondary networks in Hungary pioneer work of international standing has been done.

The regulator is connected to the network at a single point, there it senses and there it controls the system. Even theoretically it is impossible in an extended system to attain perfect constancy of values with one regulator, where the regulated parameter is also a function of the point.

* L. GÁDOR, Attila u. 111. 1012 Budapest Hungary.

If the aim is to keep the voltage as constant as possible in one single place, for one single consumer, then the continuous or finely stepped regulator is the perfect solution. The same can be said for such a consumer system where *within* the system there arise no considerable voltage differences, while the system changes its voltage as a whole in consequence of the feeding point voltage fluctuation.

But the task of regulating a secondary network differs from this, its aim is to improve the voltage conditions of lines with a high voltage drop, to moderate the voltage drops arising on unregulated lines, i.e. to keep them within the tolerance limits.

For the solution of this special problem the two-step regulator has been proposed as being the most suitable and also the most economic. Subsequently the author will examine which are the reasonable limits for the use of this extraordinarily simple and efficient means, as opposed to the continuous and multi-step regulators.

In order to simplify the examination several simplifying assumptions are introduced, so that the conditions are easier to review without reducing the value of the comparative statements.

The first simplification is to take the voltage drop as if were proportional to the length co-ordinate of the examined line. Furthermore, secondary effects due to the regulation will be neglected, e.g. that of the load varying in consequence of the regulation. It will be left out of consideration that the regulator is a transformer with a definite turns ratio, therefore, the absolute value of the voltage is not independent of the value of the input voltage. Neither will it be considered as a necessary dead zone needed for regulation. As a first step the feeding point voltage will also be taken as being constant.

2. Continuous regulation

The continuous regulator is placed at the k-th of the line length, taken as unit. Neglecting secondary effects as has been mentioned, the operation of the regulator does not change conditions on the line section between the feed point and the regulator.

Due to the working of the voltage regulation, peaks arise at three points: at the regulator input, at the regulator output and at the line end (Fig. 1). The voltage deviation will be minimum when the whole voltage drop of the unregulated line is divided into three parts. This determines the location of the regulator: $k = 1/3$.

If b is the voltage drop at the end of the unregulated line at full load, the maximum voltage deviation of the regulated line will be

$$f = \frac{b}{3}.\tag{1}$$

The type rating of the regulator is given by the maximum voltage rise occurring:

$$c = 2f = \frac{2b}{3} \, . \tag{2}$$
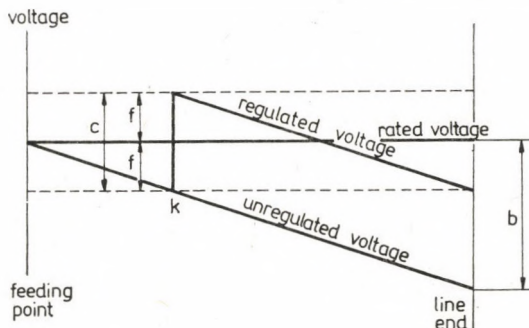
Fig. 1. Line voltages with continuous regulation

3. Two-step regulator

Conditions of the two-step regulator are shown on Fig. 2. Again b will be the maximum voltage deviation at the end of the unregulated line, which is reduced to f by the operation of the regulator. The regulator placed at k will either not affect, or it will rise the voltage by c.

The regulator will not come into action to that load at which the unregulated voltage at the end of the line reaches f. Then the regulator operates and rises the voltage from the level existing at the location k by c in such a way that its value deviates by f from the rated voltage.

With the load further increasing the voltage at each point drops and at full load the voltage drop f is reached simultaneously at the input and at the line end.
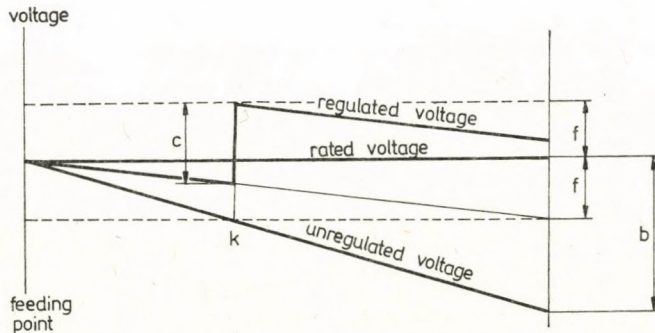

Fig. 2. Line voltages with two-step regulation

Fig. 2 provides the following relations:

$$f = kb \, , \tag{3}$$

$$c = (1 + k)f \, , \tag{4}$$

$$f + c = b \, . \tag{5}$$

These three equations give the following equation for k, which is independent of the voltage drop:

$$k^2 + 2k - 1 = 0 \, , \tag{6}$$

wherefrom

$$k = 0{,}41 \, . \tag{7}$$
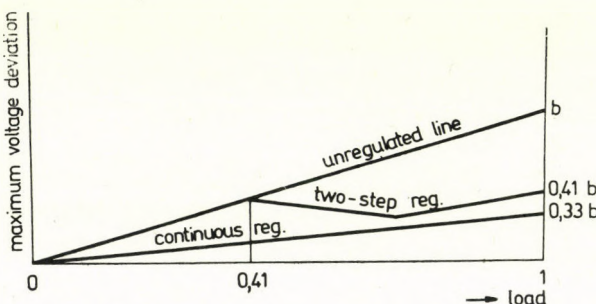
Fig. 3. Maximum voltage deviation in the line as a function of load

For the location of the two-step regulator, thus an unequivocal optimum is obtained, independently of the value of the voltage drop. The maximum voltage deviation will be

$$f = 0{,}41 \, b \, , \tag{8}$$

the type rating of the regulator will be determined by

$$c = 0{,}59 \, b \, . \tag{9}$$

Hence on a given line, with a two-step regulator it is impossible to obtain a voltage deviation smaller than 41% of the maximum drop and for this a 0,59 b voltage step is required. If a voltage step is chosen to be larger, the situation only deteriorates.

Fig. 3 shows the maximum voltage deviation as a function of the load. The regulator operates at 0,41 load, until that moment the characteristic of the voltage deviation is equal to that of the unregulated line. At the moment of switching over the operation of the regulator does not reduce the actual voltage deviation, however, it does not appear at the line end but at the regu-

lator output. Then with increasing load the voltage deviation is somewhat reduced, until the increasing voltage deviation at the regulator input is beginning to dominate, finally at full load, the deviation becomes $0,41\,b$ again.

For the sake of comparison Fig. 3 also shows the maximum voltage deviation arising under the action of the continuous regulator. Proportionally to the load this increases to the maximum value of $f = b/3$. As the diagram shows a considerable difference appears at small loads, before the two-step regulator operates at all. In the range of larger voltage deviations which in fact provides the real reason for the voltage regulation, the differences are not considerable.

Let us complete the comparison by remarking that $0,33\,b$ voltage range with the continuous regulator instead of $0,41\,b$ is obtained at the price of its type rating being $0,67\,b$ as opposed to $0,59\,b$ for the two-step regulator. Not to speak of the much more complicated and more expensive construction by which the continuous regulator differs from the extraordinarily simple and reliable two-step regulator.

4. Feed point voltage varying in proportion to the load

To get a better approach to the real operating conditions, in the subsequent treatment one of the simplifying conditions, the constance of the voltage of the feeding point is disregarded.

The feeding point voltage can change for two reasons and in two ways. Because of the voltage drop in the transformer the feeding point voltage can change proportionally to the load even if the primary transformer voltage is constant. But presumably, this will not be constant either, the voltage of the higher order network also varies within certain limits and this voltage variation is practically independent of the load in the secondary consumer line.

The voltage conditions of the line for a feeding point voltage changing only proportionally to the load are shown by Fig. 4. The feeding point voltage drop for a full load is a, that of the line is b, the whole drop is $a + b$.
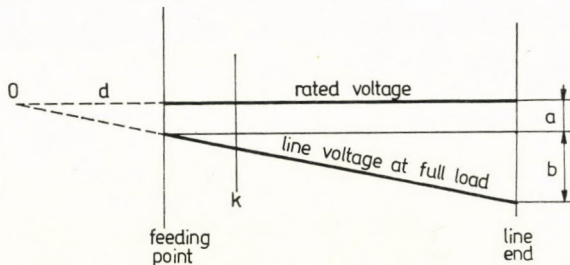

Fig. 4. Line voltage distribution with feeding point voltage varying proportional to the load

The situation is the same as if the line were fed at a fictitious feeding point 0 behind the feed point by d of a fixed voltage. For a line of unit length,

$$d = \frac{a}{b} \tag{10}$$

therefore, the problem is reduced to the problem already solved, the earlier formulae should be applied only.

For a feeding point voltage dependent on the load the continuous regulator must be placed in such a way that the distance between the fictitious feed point 0 and the line end should be divided by three and that the maximum voltage deviation arising as a consequence of regulation should be one third of the total voltage drop $a + b$. With a two-step regulator the situation is similar, the division into 0,41 obtained for the location of the regulator must be calculated for the line length increased by d, i.e. from the fictitious feeding point. In the formulae for the maximum voltage deviation and for the voltage rise $a + b$ takes the place of b.

If e.g. $a = 3\%$, $b = 9\%$, so for a

	continuous regulator	two-step regulator
k	0,11	0,21
f %	4	4,9
c %	8	7,1

As opposed to the case of a fixed feeding point voltage a qualitative difference is that k is not constant, the optimum location of the regulator depends on the ratio of feeding point voltage drop to line voltage drop. The greater the feeding point voltage variation compared to that of the line is, the farther is the fictitious feeding point and the better the regulator approaches the real feed point. Finally, if for a continuous regulation $a = 0,5\ b$ or for a two-step regulation $a = 0,7\ b$, the regulator gets into the feeding point. Assuming therefore, a feeding point voltage variation as compared to that of the line as large as stated above or even more, the feeding point voltage itself must be regulated. What is the continuous regulator able to do at the feeding point and what can the two-step one do?

In the most favourable case the continuous regulator can bring about a situation according to Fig. 5. And that is also the maximum of what can be done with a single regulator. In this situation the maximum voltage deviation is $f = b/2$. The regulator is able to compensate the feeding point voltage completely, while it reduces the line voltage deviation to one half. The voltage rise characterizing the type rating of the regulator is $c = a + b/2$.

For the operation of the two-step regulator mounted in the feeding point the voltage conditions are somewhat more complicated, they can be described on the base of Fig. 6. If f is the maximum voltage deviation occurring on the line, the regulator must switch over at that load condition, for which the voltage drop at the line end attains f. After switching-over, the voltage at the regulator
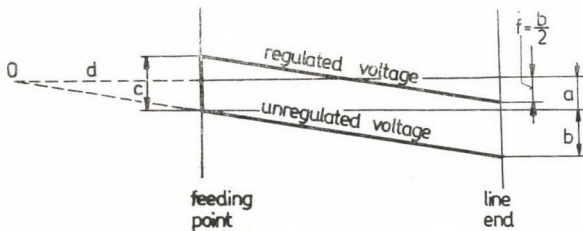

Fig. 5. Influence of continuous feeding point regulation in case of feeding point voltage varying proportional to the load
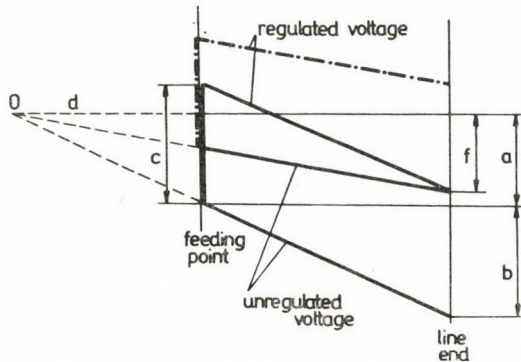
Fig. 6. Influence of two-step feeding point regulation in case of feeding point voltage varying proportional to the load

output i.e. at the beginning of the line must not deviate from the rated value by more than f. From this

$$f\frac{d}{1+d}+f=c,$$

i.e.

$$c=f\frac{1+2d}{1+d} \tag{11}$$

where $d=a/b$. The other critical condition is a full load, when at the line end appears the maximum voltage deviation f, which is the value of the full voltage drop reduced by c:

$$a+b-c=f. \tag{12}$$

Introducing c from (11),

$$f = \frac{(1 + d)^2}{2 + 3d} \, b = \frac{(a + b)^2}{3a + 2b} \, b \qquad (13)$$

and re-introducing this into (11),

$$c = \frac{(1 + d)(1 + 2d)}{2 + 3d} \, b = \frac{(a + b)(2a + b)}{3a + 2b} \, b \; . \qquad (14)$$
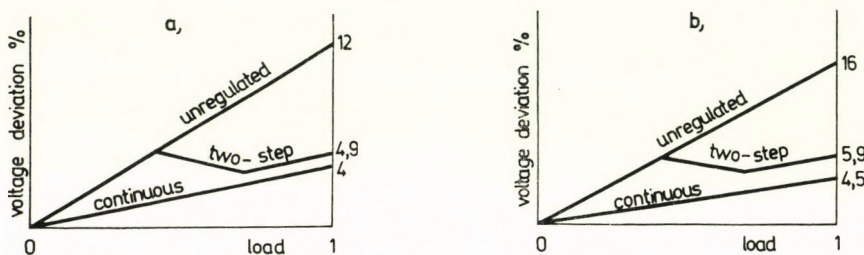
Fig. 7. Maximum voltage deviation in the line, as a function of the load, for feeding point voltage varying proportional to the load, *a)* regulator in the line, *b)* with feeding point regulation

Let there be   e.g. $a = 7\%$, $b = 9\%$. Then $k = 0$, furthermore for a

	continuous regulator	two-step regulator
$f\ \%$	4,5	5,9
$c\ \%$	11,5	8,5

The voltage deviation as a function of the load is shown in Fig. 7; *a)* shows the first example for a line regulator, *b)* the second one for a feeding point regulator, comparing continuous and two-step regulation. The continuous regulation is favourable for small loads, but then the voltage deviation is within tolerance limits anyhow. In the proximity of the rated load there is nearly no difference; in no case is it so large that it could counterbalance the smaller type rating of the two-step regulator and its incomparably simpler design.

5. Variation of the feeding point voltage independent of the load

Let us denote the maximum value of the independent symmetrical feeding point voltage deviation by a — the variation is therefore $\pm a$ —, the maximum line voltage drop by b. Fig. 8 shows that the voltage, considering

the whole length of the line and every value of the independent variables, can assume any place within the area surrounded by thick lines.

Under extreme operating conditions, the most favourable, i.e. smallest voltage deviation obtainable by continuous regulation is one third of the maxi-
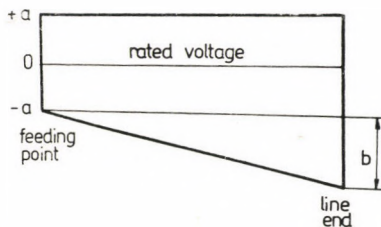

Fig. 8. Possible voltage range with feeding point voltage varying independently of the load
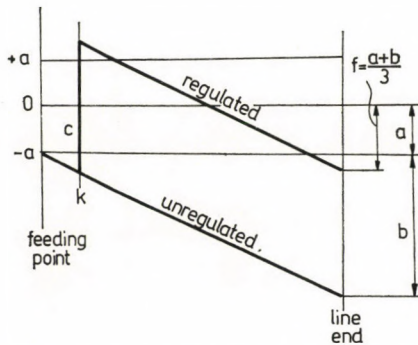

Fig. 9. Influence of continuous line regulation with feeding point voltage varying independently of the load

mum deviation $a + b$ of the unregulated line. Its value is $f = a + kb$, as it is obvious from Fig. 9. From this the location of the regulator along the line is

$$k = \frac{1}{3}\left(1 - 2\,\frac{a}{b}\right),\tag{15}$$

the maximum voltage deviation is

$$f = \frac{a + b}{3}\tag{16}$$

and the voltage rise is

$$c = 2\,\frac{a + b}{3}\,.\tag{17}$$

If $a = 0$, then in accordance with the foregoing $k = 1/3$. As a increases in relation to b, the regulator approaches the feeding point more and more,

for $b = 2a$ there is $k = 0$, the regulator gets into that point and then the maximum voltage deviation is $f = b/2$.

The results agree with those of the preceding para., from the point of view of the continuous regulator it is irrelevant whether the feeding point voltage variation is proportional to the load or independent of it.

Let us return to the case when the regulator is placed in the line at some distance k from the feeding point (Fig. 10). The feeding point voltage assumes some value a_x independent of the load. Let the ratio of the load be related to the full load i, while the voltage drop at the line will be ib. The regulator
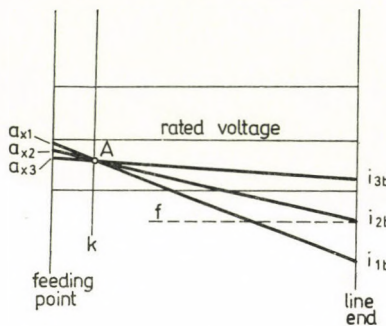

Fig. 10. For different voltage — load pairs the voltage drop line passes through the same point A

fulfils its task, i.e. the voltage variations are the most favourable if the regulator rises the voltage above the zero line by half of the voltage drop $(1 - k)ib$ arising behind it. But as the figure also shows, the straight line characterizing the voltage drop passes through the same point A for different simultaneous feeding point voltage — load pairs. Therefore, the regulator is not able to operate satisfactorily by sensing the voltage u in point A only. The regulating order for the voltage rise c must also contain information about the load:

$$c = u + \frac{1}{2}(1 - k)ib, \tag{18}$$

the condition for its execution is the simultaneous sensing of both parameters, u and i.

The regulator located at the feeding point works in the same way, but logically a_x replaces u and instead of $1/2(1 - k)ib$ we have $1/2\,ib$, k being zero. Hence, the required voltage variation is

$$c_x = a_x + \frac{1}{2}ib. \tag{19}$$

a_x may deviate from the zero line in any sense, so the operation may also be regulating downwards.

Let us point out one more thing. In the preceding para. that situation was dealt with where the feeding point changes its voltage according to the load. Although changing feeding point voltage was dealt with here too, the problem could be solved on the base of sensing one single parameter, the voltage. The voltage varying in dependence on the load already contains the information related to the load, but if the two change independently of each other, sensing both variables cannot be avoided.
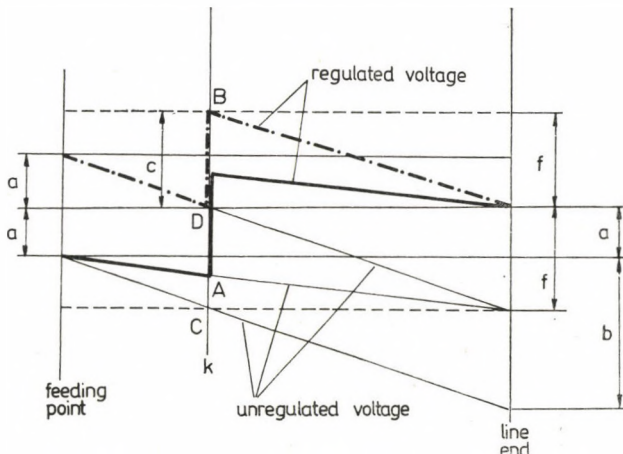

Fig. 11. Influence of the two-step regulator placed in the line in case of relatively small feeding point voltage variation

The next task is the examination of the influence of the two-step regulator in case of a feeding point voltage varying independently of the load.

If the independent variation a of the feeding point voltage is small, conditions develop according to Fig. 11. In the most unfavourable case at the regulator input a voltage corresponding to point C appears which will be at the same time the maximum voltage deviation:

$$f = a + kb. \qquad (20)$$

But the voltage deviation at the line end must not be larger than this. If the same voltage deviation is permitted, then

$$a + b = f + c. \qquad (21)$$

The regulator must start to operate already at point A, but even at D it must not rise the voltage above B. This latter condition provides

$$(1 - k)(a + f) + c = 2f. \qquad (22)$$

The foregoing three Eqs result in the ratio k defining the location of the regulator, the maximum voltage deviation f and the voltage rise c:

$$k = \sqrt{\left(1 + \frac{a}{b}\right)^2 + 1} - \left(1 + \frac{a}{b}\right), \tag{23}$$

$$f = \left(\frac{a}{b} + k\right)b, \tag{24}$$

$$c = (1 - k)b. \tag{25}$$
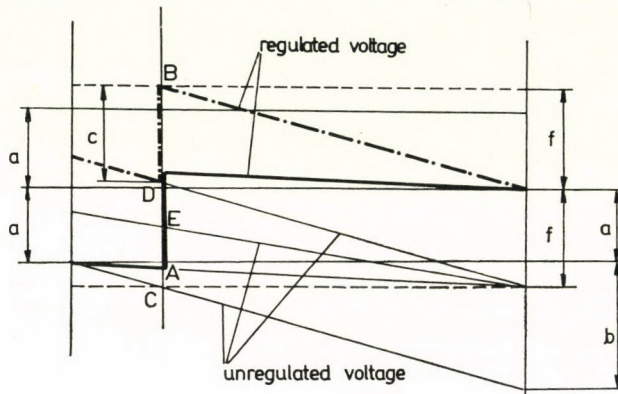
Fig. 12. Influence of the two-step regulator placed in the line in case of relatively large independent feeding point variation

If $a = 0$, these relations naturally will give the earlier values for the fixed feeding point voltage: $k = 0$, $f = 0{,}41\,b$, $c = 0{,}59\,b$.

A somewhat larger independent variation will result in the situation of Fig. 12. It differs from the preceding that the straight line passing through D remains in the feeding point below the maximum feeding point voltage. Eqs (20) and (21) remain valid without change, but (22) is replaced by

$$(1 - k)b + c = 2f, \tag{26}$$

wherefrom

$$k = \frac{1 - \dfrac{a}{b}}{2}, \tag{27}$$

and

$$\frac{c}{b} = \frac{f}{b} = \frac{1 + \dfrac{a}{b}}{2}. \tag{28}$$

The boundary of the two ranges is $a/b = 1/3$, the regulation parameters belonging to that ratio are from (23)...(25) and from (27), (28) identically $k = 1/3$ and $f = c = 2/3\ b$. Finally if $a/b \geq 1$, there is $k = 0$, the regulator gets into the feeding point.

Returning to Fig. 12, the regulator must also operate at the intermediate point E if the voltage and the load are simultaneously such that the line end voltage deviation reaches f. If u is the coordinate of point E and i the relative load, the above condition can be formulated as follows:

$$u + (1 - k)ib = f. \tag{29}$$
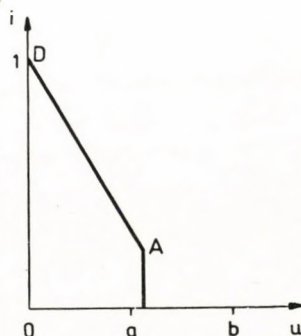
Fig. 13. Working characteristic of regulator with two parameters

Therefore, the regulator must sense the voltage as well as the current. As an example, Fig. 13 shows such a working characteristic.

If the regulator gets into the feeding point, the situation is qualitatively changed. The input voltage of the regulator does not appear on the line, therefore, from the point of view of voltage deviation there remain two critical places, the feeding point and the line end. The voltage drop appearing along the line cannot be influenced from the feeding point, but the feeding point end of the voltage-drop straight line can be shifted to and fro in order to place it symmetrically onto the zero line. The voltage fluctuation $2a$ of the feeding point is halved by the two-step regulator. This only regulates in one direction, practically always upwards, therefore, the desirable symmetrical placement of the voltage deviations is attained by an appropriate shifting of the zero line. Generally this is possible by switching over the tap of the feeding transformer.

In case of symmetry the voltage deviation obtainable with the aid of the two-step regulator is half of the whole variation, $f = (a + b)/2$. Here a finer regulation is justified, with three steps $f = a/3 + b/2$, in general with n steps $f = a/n + b/2$, with continuous regulation, as has been shown earlier, $f = b/2$. Fig. 14 gives a general diagram of k and f as a function of a/b for dependent

and independent variation of the feeding point voltage, and for two-step and continuous regulation, respectively. As has been stated the continuous regulation has the same line of the curve for dependent and independent feeding point voltage variation.

Finally let us deal with the case when the two kinds of the feeding point voltage variations combine. If a_1 is the voltage variation proportional to the load and a_2 the independent one, so let there be $a_1 + a_2 = a$. The total voltage variation a can be composed in the most different ways.
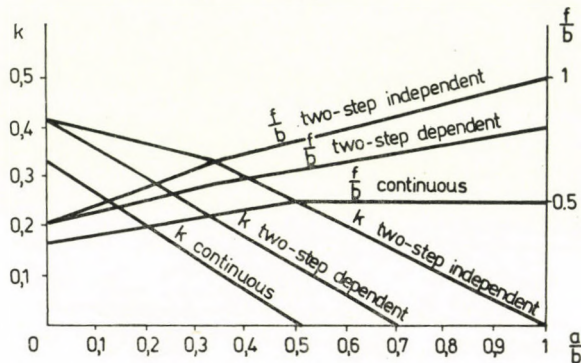
Fig. 14. General view of the emplacement k of the regulator and the maximum voltage deviation f according to the kind of regulation and as a function of the load

It is pointed out again that from the point of view of continuous regulation the origin of the feeding point variation is indifferent, determinant is the total variation. With two-step regulation the situation is more intricate, therefore, for information only the results are published here.

1. If

$$0 \leq \frac{a_2}{b} - \frac{a_1}{3b} \leq \frac{1}{3},$$

k is the root of the Eq.:

$$k^2 + 2k \left(1 + \frac{2a_1 + a_2}{b} \right) - \left(1 - \frac{2a_1^2}{b^2} - \frac{2a_1 a_2}{b^2} \right) = 0,$$

$$\frac{f}{b} = k + \frac{a_1 + a_2}{b},$$

$$\frac{c}{b} = 1 - k.$$

2. If

$$\frac{a_1 + a_2}{b} > 1\,,$$

$$k = 0\,,$$

$$\frac{f}{b} = \frac{c}{b} = a_1 + a_2\,.$$

3. If

$$\frac{a_1 + a_2}{b} > 1\,,$$

$$k = 0\,,$$

$$\frac{f}{b} = \frac{c}{b} = a_1 + a_2\,.$$

Summing-up, for the regulation of the secondary network the following principles can be laid down. If the voltage variation of the secondary network exceeds tolerance limits and the feeding point voltage is constant, or does not deviate from the rated value more than by half the line voltage variation, a two-step regulator must be inserted into the line. If the feeding point voltage variation is larger than that, a feeding point regulator must be used. Finally, if the feeding point voltage variation approximates the line voltage drop or even surpasses it, it is justified to apply a multi-step feeding point voltage regulator. If the feeding point voltage variation independent of the load is even only $1-2\%$, for the correct operation of the regulator the current must be sensed, too.

When really dimensioning the regulator, of course, one must leave the domain of the simplifying assumptions and account for the real voltage distribution of the line, the branches, the dead zone etc. But the simplified discussion greatly clarifies the essential relations. The laws of free fall could not be taught either in school if the air friction, the aerodynamical effects, the Coriolis force and the gravitational anomalies were to be considered.

REFERENCES

1. GÁDOR, L.: Control of Secondary Networks. *VKI Communications* **3** (1969)
2. CZIGÁNY, B., GÁDOR, L.: Automatic Voltage Control in Distribution Networks. *Villamosság* **21** (1973), 8—9
3. NÉMETH, I.: Apparatus Developed for Regulating and Controlling the Voltage of Electric Distribution Networks. *VKI Communications* **5** (1974)

Wirtschaftliche Spannungsregelung von Niederspannungsnetzen. In verhältnismäßig locker besiedelten Gebieten können an den langen Radialleitungen der Niederspannungsnetze große Spannungsabfälle auftreten; dies begründet die Verwendung von Spannungsreglern. Wenn das räumlich ausgedehnte System in einem Punkt geregelt wird, bringt die vielstufige oder die kontinuierliche Regelung keine Vorteile, ein Zweipunktregler genügt vollkommen. Wenn auch die Speisepunktspannung schwankt, muß eine zweiparametrige Regelung angewendet werden: gleichzeitige Erfassung der Spannung und des Stromes. Verhältnismäßig große Schwankungen der Speisepunktspannung können nur mit einem im Speisepunkt aufgestellten Regler eliminiert werden; hier ist die Verwendung eines mehrstufigen oder eines kontinuierlichen Spannungsreglers begründet.

Экономичное регулирование напряжения низковольтных сетей. В районах с относительно неплотной населенностью могут возникать значительные падения напряжения на длинных радиальных линия вторичной сети. Это обстоятельство обосновывает применение регуляторов напряжения. Если производить регулирование в одной точке системы, распространяющейся в пространстве, тогда не выгодным производить регулирование в несколько ступеней или же плавное регулирование; данную цель будет полностью удовлетворять регулятор с двумя позициями. Если напряжение в точке отбора энергии также колеблется, тогда необходимо применять двухпараметровое регулирование при одновременном восприятии напряжения и тока. Относительно большое колебание напряжения в точке отбора мощности можно устранить только с помощью регулятора, установленного в точке отбора мощности. Здесь обосновано применение многоступенчатого или плавного регулятора напряжения.

A REMARK ON THE UPPER LIMIT OF THE TORSIONAL STIFFNESS OF PRISMATIC BARS

I. ECSEDI*

The present paper deals with the torsional stiffness of the simply consistent region of rectifiable border curve and with the generalization of an inequality concerning the basic frequency of an oscillating membrane extended to the same bordering curve.

Symbols

The following symbols are used in this paper:

D simply consistent range in the plane x, y with rectifiable border curve,
∂D border of D,
x, y coordinates,
S torsional stiffness,
Φ Prandtl's stress function,
A area of region D,
$dA = dx\ dy$,
$f(u + jv), g(x + jy)$ functions of complex variables ($\sqrt{-1} = j$),
u, v coordinates,
B image of region D in plane u, v,
∂B border of region B,
C area of region B,
$dC = du\ dv$,
λ_i frequency,
φ_i eigenfunction,
C_i coefficient,
Λ basic frequency of region B,

Other quantities are interpreted in the text.

The free torsion of prismatic bars of homogeneous material with a solid, constant cross section, as is known, leads to the following boundary value problem: The function of two variables $\Phi = \Phi(x, y)$, continuous in the region D and on its border ∂D, is to be determined which satisfies in the region D the partial differential equation.

$$\frac{\partial^2 \Phi}{\partial x^2} + \frac{\partial^2 \Phi}{\partial y^2} = -2 \tag{1}$$

and meets at the border ∂D of the region D the homogeneous boundary condition (Fig. 1)

$$\Phi = 0 \,. \tag{2}$$

* Dr. I. Ecsedi, Vászonfehérítő u. 24, 3531-Miskolc, Hungary

By knowing the function $\Phi = \Phi(x, y)$, from the equation

$$S = 2 \int_D \Phi dA \tag{3}$$

the torsional stiffness S of the cross section may be calculated. Let the mutual unequivocal conform projection of the Region D of the plane x, y upon the region B of the plane u, v be considered (Fig. 2).

The conform projection is defined by the functions

$$\left. \begin{matrix} x = x(u, v) \\ y = y(u, v) \end{matrix} \right\} , \quad \left. \begin{pmatrix} u = u(x, y) \\ v = v(x, y) \end{pmatrix} \right\} . \tag{4}$$
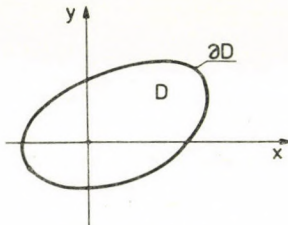
Fig. 1. Region D

The conform projection determined by (4) might also be given by the analytic, single-valued complex function

$$x + jy = f(u + jv), \ |u + jv = g(x + jy)| . \tag{5}$$

Let us transform the boundary value problem defined by (1) and (2) from the system of coordinates x, y into the system of coordinates u, v. The transformation results in the partial differential equation

$$\frac{\partial^2 \psi}{\partial x^2} + \frac{\partial^2 \psi}{\partial y^2} = -2H^2(u, v) \tag{6}$$

and at the border B of the region B in the homogeneous boundary condition

$$\psi = 0 \tag{7}$$

where

$$\psi = \psi(u, v) = \Phi[x(u, v), y(u, v)] , \tag{8}$$

further $B + \partial B$ is the image in the plane x, y of $D + \partial D$ in the plane u, v, and

$$H^2 = H^2(u, v) = \left(\frac{\partial x}{\partial u}\right)^2 + \left(\frac{\partial y}{\partial u}\right)^2 = \left(\frac{\partial x}{\partial v}\right)^2 + \left(\frac{\partial y}{\partial v}\right)^2 = |f'(u + jv)|^2. \qquad (9)$$

The torsional stiffness S of the region D of the plane x, y may be deter-mined with the aid of the function $\psi = \psi(u, v)$ from the equation

$$S = 2 \int_B \psi H^2 dC \qquad (10)$$

wherein

$$dC = du dv. \qquad (11)$$

The solution of the natural oscillation problem of the elastic membrane of homogeneous material and in uniform thickness, extended to the region B
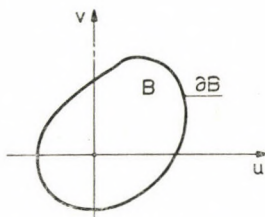
Fig. 2. Region B

of the plane u, v and fixed at the border ∂B, may be realized by the determi-nation of the whole system of the eigenfunctions.

$$\varphi_1, \varphi_2, \varphi_3, \dots$$

and the corresponding frequencies

$$\lambda_1, \lambda_2, \lambda_3, \dots .$$

It is known that the functions φ_i and the values λ_i might be obtained by the non-trivial solution of the following eigenvalue problem

$$\frac{\partial^2 \varphi_i}{\partial u^2} + \frac{\partial^2 \varphi_i}{\partial v^2} + \lambda_i^2 \varphi_i = 0, \qquad (12)$$

at the border ∂B

$$\varphi_i = 0. \qquad (13)$$

We know further that the eigenfunctions are orthogonal, [3], and in the present paper it can be assumed that they are also normated, i.e.,

$$\int_B \varphi_i \varphi_j dC = \delta_{ij} = \begin{cases} 1 & i = j, \\ 0 & i \neq j. \end{cases} \qquad (14)$$

The frequencies constitute a non-decreasing sequence with positive terms, i.e.,

$$0 < \lambda_1 \leq \lambda_2 \leq \lambda_3 \leq \ldots . \tag{15}$$

The frequency λ_1 is called the basic frequency of the region B and is designated by Λ, i.e.,

$$\lambda_1 = \Lambda . \tag{16}$$

One tries to produce the solution for the boundary value problem defined by (6), (7) in the form

$$\psi = \sum_{i=1}^{\infty} \frac{C_i}{\lambda_i^2} \varphi_i . \tag{17}$$

This function satisfies the boundary condition (7) at any values of the coefficients c_i $(i = 1, 2, \ldots)$. However, it satisfies the partial differential equation then and only then (as it may be proved by direct substitution), if

$$\sum_{i=1}^{\infty} c_i \varphi_i = 2 H_i^2 . \tag{18}$$

Multiplication of (18) with φ_j, and integration as well as the application of the assumption (14) yields

$$C_i = 2 \int_B \varphi_i H^2 dC . \tag{19}$$

Replacing (17) into (10), and reversing the order of the integration and addition, taking (19) into account, the equation

$$S = \sum_{i=1}^{\infty} \frac{C_i}{\lambda_i^2} \tag{20}$$

may be deduced. By making use of the inequality (15) as well as Bessel's inequality

$$\sum_{i=1}^{\infty} C_i^2 \leq 4 \int_B H^4 dC \tag{21}$$

[3], from (20) we obtain for the torsional stiffness

$$S \leq \frac{4 \int_B H^4 dC}{\Lambda^2} . \tag{22}$$

Introducing the variable

$$k = \frac{\int_B H^4 dC}{C} \tag{23}$$

AIR CIRCULATION IN BUILDINGS BY THE FLOW IN NETWORKS METHOD

By

A. ZÖLD

Department of Heating and Ventilating II, Institute of Building Constructions and Equipment
Technical University, Budapest

Introduction

Changes in both the numerical values and proportions of building parameters made with up-to-date construction methods and structures controlling the energy transfer fundamentally altered the respective role of doors and windows, responsible for most of the energy transfer of the buildings.

Energy exchange may have different forms both in winter and in summer such as heat transfer by transmission, thermal exchange by radiation, and air infiltration. Transmission and radiation heat transfer depend on the properties of the structure of doors and windows, but infiltration depends on features of the entire building as a coherent, homogeneous aerodynamic structure, hence it is more difficult to compute. The following will be a short description of the method of computing the infiltration rate of air, and the conclusions drawn therefrom.

Infiltration air circulation is due to the combined effect of three factors such as:
— pressure difference due to wind (between windward and leeward sides),
— stack effect,
— auxiliary mechanical ventilation.

The wind effect, stochastic in character, is of different rate for rooms with similar topological relation, because of orientation.

Also the stack effect varies stochastically. Probable durations of various outdoor temperature intervals are known.

Stack effect and wind are in a weak correlation. Auxiliary mechanical ventilation has a theoretically regular effect.

Accordingly,
— infiltration air circulation depends on several parameters;
— in the heating season, infiltration air circulation undergoes complex variation due to practically independent factors;
— infiltration air circulation changes differently in different rooms, and on different storeys.

4

A smaller part of transmission heat loss of rooms with poor insulation or with great cooling surfaces results from infiltration heat transfer, thus — in spite of an important heat flow by absolute value — infiltration heat transfer variation involves minor design and control problems. In case of well insulated buildings, however, infiltration heat transfer is high compared to the transmission heat loss, stressing design, control problems related to its variation. Under no-wind conditions, the infiltration heat transfer of several rooms in the test buildings was as high as 80 to 100% of the transmission heat loss ! In general, heat transfer in living rooms is about 50% of the transmission heat
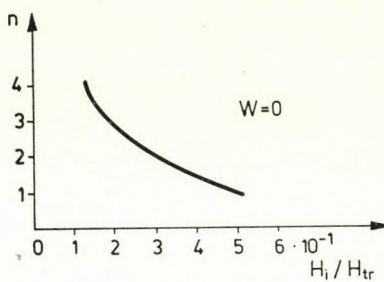
Fig. 1

Legend to figures

H_i	infiltration heat loss
H_{tr}	transmission heat loss
n	storey number
t_0	outdoor temperature
$\bar{t}_0$	outdoor mean temperature
w	wind velocity
w_d	design wind velocity

loss. About this value, there is of course an important scatter according to both building types and storey numbers. In low-rise houses, flats on each storey receive outer air, a phenomenon also connected with the exhaust ventilation in kitchens, toilets and bathrooms. For greater storey numbers, stack effect overrules exhaust ventilation to a degree that flats on upper storeys receive air from the staircase, as seen from diagrams made at an outdoor temperature $t_0 = -15°\,\mathrm{C}$ and calm (Figs 1, 2). In four-storey houses there is only flow in; flats in ten-storey buildings are likely to receive staircase air from the eighth or ninth storey upwards, while in sixteen-storey buildings, "regular" development of the neutral plane is seen.

Beside exhaust ventilation, development of a neutral plane is also much affected by the quality of doors and windows. Better doors and windows raise or cancel at all the neutral zone: gravity-induced air circulation is less, at a fixed exhaust air volume.

The flow pattern much depends also on the number of flats on each storey. Namely, every flat contains kitchen, bath, toilet, hence, with many single-room or one-and-a-half-room flats on a storey, there is a big exhaust air volume, offsetting the stack effect.

The less the building depth and the more articulated the ground plan outlines, the more the wind influences the infiltration heat transfer. Comparing the model buildings it can be stated that the wind effect was reacted on the most sensitively by the building with a little depth and vice versa. Other
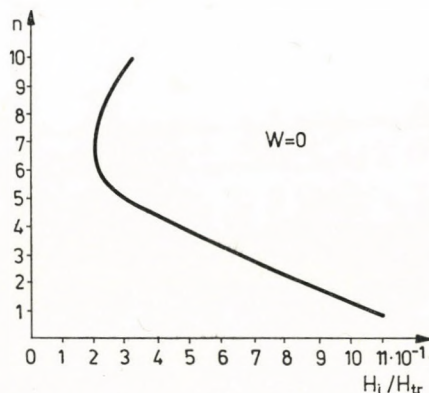
Fig. 2

conditions being equal, the infiltration heat transfer of the former changed three times as much upon wind effect as that of the latter. Ground plans where staircases join long corridors each storey with windows in different façades are unfavourable. Also articulated ground plans worsen sensitivity to wind of infiltration heat transfer of some unfavourably oriented rooms as shown by several examples. Of course, sensitivity to wind depends on the storey number, on the wind velocity and on the shielding of lower storeys.

Better doors and windows much reduce sensitivity to wind. This is of importance not only by reducing heat demand in windy wheater but also because of the poor correlation between wind and outdoor temperature, contributing to ease regulation difficulties and to reduce overheating due to regulation deficiencies.

Serious regulation difficulties are due to the variation of infiltration heat transfer as a function of outdoor temperature. Both stack effect and variation of temperature difference can be considered as linear but the law of resistance is of a character to cause the air mass flow to vary exponentially. Computations show the infiltration heat transfer to decrease as an average with increasing outdoor temperature, and the diagram to be of steeper ascent, the neutral

Thus, a frequency-based design reduces the magnitude and duration of indoor temperature differences between storeys. Economically operating heating systems can only be designed by starting from the frequency of outside conditions: replacing "performance-centric" by "operation-centric" approach. Heating and ventilating system of a dwelling house is no bridge to be designed against collapse at high safety for extreme cases but a machinery expected to operate at its optimum under usual conditions, permitted to behave poorer under extreme conditions of infrequent occurrence.
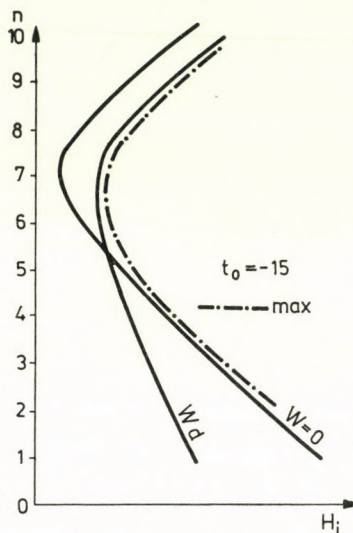
Fig. 4. Leeward side

Infiltration heat transfer of ground floor and lower-storey rooms has its maximum at the lowest outdoor temperature. The expected minimum of outdoor temperature ("design temperature") occurs for a very short time concluding cooling periods, caused by weathering processes accompanied normally by wind. Wind velocities are high at the beginning of cooling periods to gradually decrease. By the end of cooling periods — at outdoor temperature minima — wind velocities are as low as 2 m/s or even below. Thus, infiltration air circulation is due primarily to stack effect and accessory ventilation. Even for single-storey buildings, however, windward and leeward sides have to be distinguished. Namely on the windward side, maximum infiltration heat transfer pertains of course to the design wind velocity for the expected temperature minimum, but on the leeward side mostly to the calm.

In occurrence of the expected temperature minimum and calm, the so-called neutral plane may develop as a function of storey number, number of flats on a storey, and of ground plane features of the building. In this con-

dition, the storeys in and near the neutral plane have a low infiltration heat transfer. Even, if no neutral plane develops, infiltration heat transfer may be distributed among storeys so as to be low in the top. Variability of the infiltration heat transfer according to storeys is seen by the slope of lines in the diagram.

With varying outdoor temperature also the curve slope varies to a degree depending on the effect of accessory ventilation, shifting the neutral plane upwards. (Even, if no neutral plane develops within the building height,
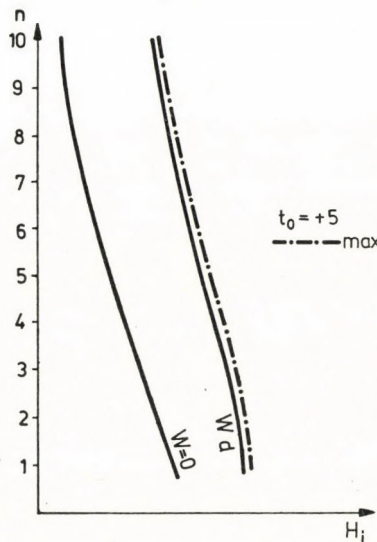
Fig. 5. Windward side

the phenomenon can be imagined by starting from a point in the curve of zero air mass flow.) Identity between outdoor and indoor temperature results in a vertical straight-line diagram.

According to the precedings, infiltration air mass flows vary so that rooms in or near the neutral plane for, e.g. $t_0 = -15°$ C get below it for higher outdoor temperatures. Thereby changed pressure conditions intensify and maybe deflect infiltration air circulations. (For example, at a lower outdoor temperature, air gets from the staircase into the room, windows exhibit exfiltration, higher outdoor temperatures generate infiltration through windows and cause air to leave through the ventilation system.) In a given case, air circulation may grow faster than thermal difference $(t_i - t_\sigma)$ decreases, hence infiltration heat transfer will grow for increasing outdoor temperatures. Of course, this is not true for the entire range of $t_i - t_\sigma$ during the heating season but only for a given interval.
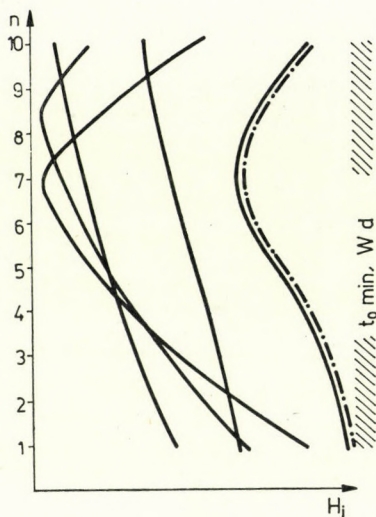
Fig. 10. Windward side
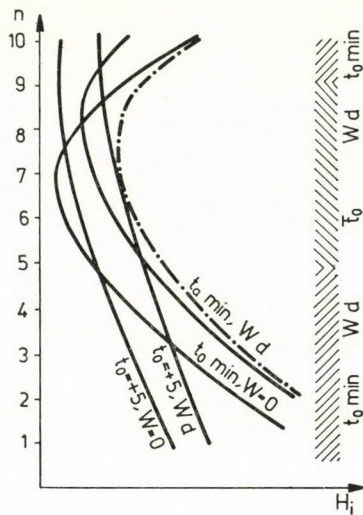
Fig. 11. Windward side

— the less flats there are on a storey,
— the poorer the doors and windows.

For a room much below the neutral plane (i.e. in the lower storeys, if a neutral plane develops within the building height at $t_{\sigma,\min}$; else in any storey)

— infiltration heat transfer has its maximum at $t_{\sigma,\min}$ and this at wind on the windward side, and mostly at calm on the leeward side.
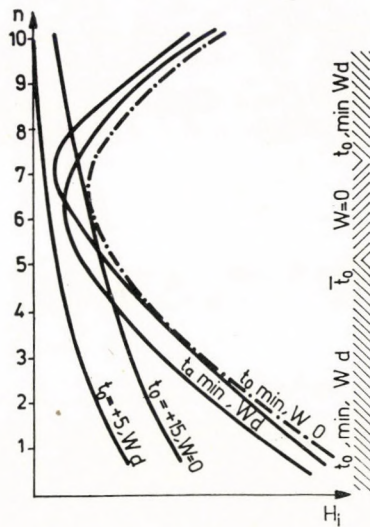
Fig. 12. Leeward side
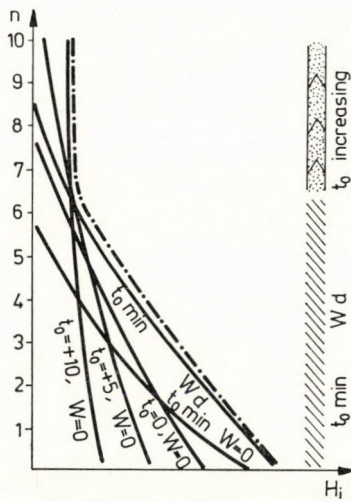
Fig. 13. Room not connected to entrance hall. Windward side

For a room in or over the neutral plane at $t_{\sigma,\min}$
— infiltration heat transfer has its maximum
   a) on the windward side at $t_{\sigma,\min}$ or at an outdoor temperature near the average;
   b) on the leeward side near the average outdoor temperature.

B)

$$\left.\begin{array}{l} f_s + d_p > h_p \\ f_s \leq h_p \\ h_j > h_p \\ f_s + d_p > h_j \end{array}\right\} \qquad \text{(VIII')}$$

or

$$\left.\begin{array}{l} f_s + d_p > h_p \\ f_s > h_p \\ f_s \leq h_j \\ f_s + d_p > h_j \end{array}\right\} \qquad \text{(VIII'')}$$

B.1) $\qquad f_{s-1} + d_p < h_p$

If $\qquad \dfrac{k_j}{k_p} \geq \dfrac{f_s + d_p - h_p}{f_s + d_p - h_j}, \quad \text{then} \quad j \prec p.$ $\qquad$ (VIII/1)

B.2) $\qquad f_{s-1} + d_p \geq h_p$

If $\qquad \dfrac{k_j}{k_p} \geq \dfrac{d_j}{f_s + d_p - h_j}, \quad \text{then} \quad j \prec p.$ $\qquad$ (VIII/2)

C)

$$\left.\begin{array}{l} f_s + d_p > h_p \\ f_s > h_p \\ f_s > h_j \end{array}\right\} \qquad \text{(IX)}$$

C.1) $\qquad f_{s-1} + d_p < h_p$

If $\qquad \dfrac{k_j}{k_p} \geq \dfrac{f_s + d_p - h_p}{d_p}, \quad \text{then} \quad j \prec p.$ $\qquad$ (IX/1)

C.2) $\qquad f_{s-1} + d_p \geq h_p$

If $\qquad \dfrac{k_j}{k_p} \geq \dfrac{d_j}{d_p}, \quad \text{then} \quad j \prec p.$ $\qquad$ (IX/2)

If in cases (VII), (VIII) or (IX) the criteria $j \prec p$ of points A), B) and C) are satisfied, that is to say: if their joint penalty is lower in case of a j, p order, then job p is scheduled as the job immediately following job j, i.e. with the next sequence number, in the table. (It is advisable to keep this order of the jobs even if the condition on k_j/k_p is satisfied with equality, i.e. when the total penalty of the two jobs is independent of their order in the sequence.)

After this Rule 5 is applied again.

If — on the other hand — the criterion for the order j, p is not satisfied, then job p is scheduled preceding job j, and gets the sequence number s in the table, while job j gets sequence number $s + 1$.

13 $\qquad\qquad\qquad\qquad\qquad\qquad$

For the job with index $s - 1$ and job p, Rule 7 is applied again and we return to Rule 5 only in the case when job p does not precede any other job.

D)

$$\left.\begin{array}{l} f_s + d_p > h_p \\ f_s \leq h_p \\ h_j > h_p \\ f_s + d_p \leq h_j \end{array}\right\} \tag{X'}$$

or

$$\left.\begin{array}{l} f_s + d_p > h_p \\ f_s > h_p \\ f_s \leq h_j \\ f_s + d_p \leq h_j \end{array}\right\} \tag{X''}$$

In this case the correct order is p, j, since now

$$g_j = h_j - f_s \geq d_p,$$

where

$$f_s = f_{s-1} + d_j,$$

and this corresponds to case (IV), only the float, g_j has not been registered. Job p comes into the place of job j

$$f_s = f_{s-1} + d_p$$

and job j gets sequence number $s + 1$

$$f_{s+1} = f_s + d_j.$$

Then Rule 7 is applied again for job p.

It can be seen that in order to sequence a work optimally, the application of Rule 7 must be repeated every time, when a job gets new sequence number, and even then can only be performed with penalty.

If at the beginning of the sequencing ($f_0 = 0$) case (II) held for job p, then job p gets into the first place of the sequence,

$$s_1 = p \quad \text{and} \quad f_1 = d_p.$$

Rule 8: if all deadlines after the sequence number s can be satisfied, that is

$$h_i \geq f_s + \sum_{e=s+1}^{i} d_e$$

(for every further i, where $e = s + 1, s + 2, \ldots, i$ denotes the order according to the deadlines), then the further order of the jobs is given by the deadlines.
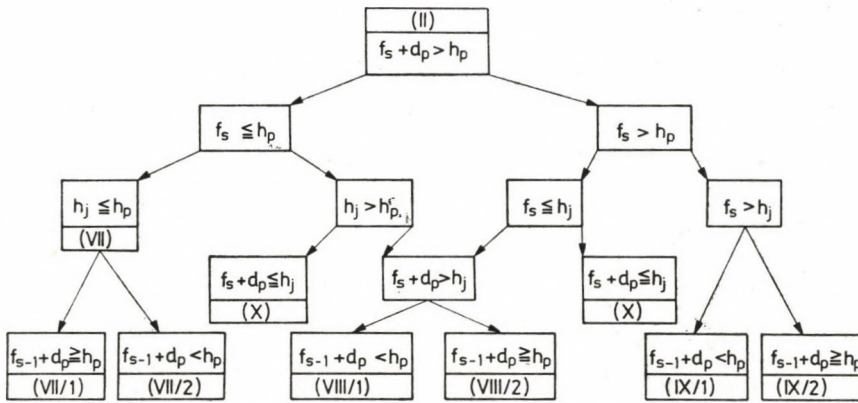
The tree of situations showing how to decide the criterion of sequence in case (II)

Fig. 1

The following, heuristic principles of optimization are easy to explain and can be realized if we follow the above described rules:

1. a job with lower penalty per time unit can only precede a job with higher penalty per time unit *without further investigation*, if it does not endanger the possibility of fulfilment of the latter by its deadline,

2. if neither of two neighbouring jobs can be fulfilled by its deadline, then the decreasing order of their penalty per time unit is the correct order.

2.3. *Heuristic solution of the numerical example*

Let us return to our numerical example given in Table 4, which requires the sequencing of 6 jobs. The order according to the deadlines: 1, 2, 3, 4, 5, 6. The order according to the penalties: 5, 1, 2, 3, 4, 6.

Let us approximate the optimal solution with our sequencing rules.

Step 1: the condition of Rule 2 is not satisfied, because here each deadline is shorter than the total time-span.

Step 2: the condition of Rule 3 is not satisfied for every i either (it is not satisfied already for the job with the shortest deadline, job 1), therefore the schedule — for the whole problem — is not given by the deadlines. Let us prepare the table of sequence and apply Rule 5.

Step 3: $f_0 = 0$; $p = 5$; $h_5 = 13$, $d_5 = 2$

$\qquad d_5 < h_5 \rightarrow$ (I)

$\qquad g_5 = 13 - 2 = 11$

Apply Rule 6.

Step 4: $f_0 = 0$; $r = 1$; $h_1 = 2$, $d_1 = 5$

$\qquad h_1 < h_5$ and $g_5 > d_1 \rightarrow$ (IV) $\qquad\qquad\qquad 1 \prec 5$

We introduce job 1 into the table with sequence number $s = 1$ and $f_1 = 5$, $g_5' = 11 - 5 = 6$.

$\qquad$ Rule 6 is applied further.

Step 5: $f_1 = 5$, $j = 1$; $p = 5$; $r = 2$; $h_2 = 4$, $d_2 = 4$

$\qquad h_2 < h_5$ and $g_5' > d_2 \rightarrow$ (IV) $\qquad\qquad\qquad 2 \prec 5$

Job 2 is scheduled with sequence number $s = 2$ ($f_2 = 9$) and $g_5'' = 6 - 4 = 2$. Then Rule 7 is applied for job 2.

Step 6: $f_1 = 5$, $j = 1$, $p = 2$, $h_2 = 4$, $d_2 = 4$

$\qquad f_1 + d_2 > h_2$, $f_1 > h_2$, $f_1 > h_1$, $f_0 + d_2 = h_2 \rightarrow$ (IX/2)

$\qquad k_1 = 5$, $k_2 = 4$, $k_1/k_2 = d_1/d_2$

therefore the order of jobs 1 and 2 does not matter, but — according to our agreement — we schedule them in the order j, p that is 1, 2.

$\qquad$ Since there is still float ($g_5'' = 2$), Rule 6 is applied further.

Step 7: $f_2 = 9$, $j = 2$, $p = 5$, $r = 3$, $h_3 = 8$, $d_3 = 3$

$\qquad h_3 < h_5$ and $g_5'' < d_3 \rightarrow$ (V) $\qquad\qquad\qquad 5 \prec 3$

So job 3 is scheduled with sequence number $s = 3$ ($f_3 = 11$), and then Rule 7. is applied for job 3.

Step 8: $f_3 = 11$, $j = 5$, $p = 3$, $h_3 = 8$, $d_3 = 3$

$\qquad f_3 + d_3 > h_3$, $f_3 > h_3$, $f_3 < h_5$

$\qquad f_3 + d_3 > h_5$, $f_2 + d_3 > h_3 \rightarrow$ (VIII/2)

$\qquad k_5 = 7$, $k_3 = 2$, $k_5/k_3 > d_5/f_3 + d_3 - h_5 \rightarrow \qquad 5 \prec 3$.

Hence job 3 is scheduled with sequence number $s = 4$ ($f_4 = 14$), and then Rule 5 is applied.

Step 9: $f_4 = 14$, $j = 3$, $p = 4$, $h_4 = 12$, $d_4 = 5$.

$\qquad f_4 + d_4 > h_4 \rightarrow$ (II)

Apply Rule 7.

Step 10: $f_4 + d_4 > h_4$, $f_4 > h_4$, $f_4 > h_3$.

$f_3 + d_4 > h_4 \rightarrow$ (IX/2)

$k_3 = 2$, $k_4 = 1$

$k_3/k_4 > d_3/d_4$ hence $\qquad\qquad\qquad\qquad$ $3 \prec 4$.

Job is scheduled with sequence number $s = 5$ ($f_5 = 19$) and Rule 5 is applied again.

Step 11: $f_5 = 19$, $j = 4$, $p = 6$, $h_6 = 17$, $d_6 = 7$.

$f_5 + d_6 > h_6 \rightarrow$ (II)

Apply Rule 7.

Step 12: $f_5 + d_6 > h_6$, $f_5 > h_6$, $f_5 > h_4$

$f_4 + h_6 > h_6 \rightarrow$ (IX/2)

$k_4 = 1$, $k_6 = 1$, $k_4/k_6 > d_4/d_6$ hence $\qquad\qquad$ $4 \prec 6$.

Job 6 is scheduled with sequence number $s = 6$ ($f_6 = 26$) and Rule 5 is applied again.

Step 13: no more jobs.

The optimal sequence according to our heuristic rules:

1, 2, 5, 3, 4, 6

and the penalty belonging to this schedule: $Q = 63$.

Figure 2 shows the schedule determined with the help of our heuristic rules. The delay of the jobs can also be seen.

This example has served our purpose to show that it is not always and not unconditionally most practical to solve a problem of operations research with the exact methods of mathematical programming. At the same time it

Table 5

Table of sequence

Sequence number (s)	Number of job (i)	f_s	h_i	Penalty
1	1	5	2	15
2	2	9	4	20
3	5	11	13	—
4	3	14	8	12
5	4	19	12	7
6	6	26	17	9
				63

must not be forgotten that we have not proved the sufficiency of our heuristic rules and therefore we cannot exclude the possibility that they can be improved. (As it happens, the rules presented here developed out of an earlier version [4].)

In the present case counter-examples can be given of either Rule 4 or Rule 4* is applied to determine the priority. In certain examples the two priorities of consideration result in different sequences. Therefore, it is practical to perform the planning of the sequence with both priorities separately and to accept the better solution. In the examples studied so far one of these two
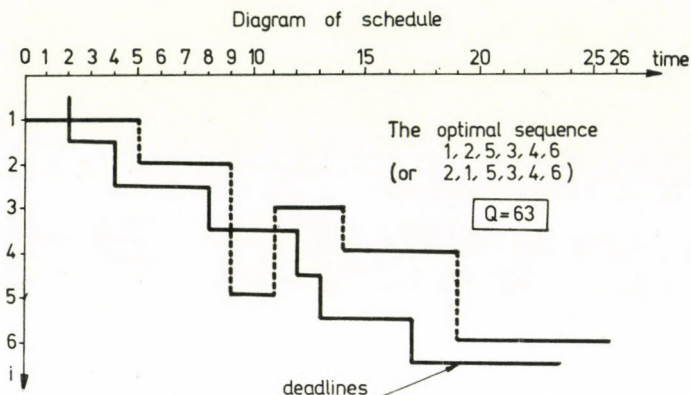
Fig. 2

solutions was always the optimal one, but we cannot claim yet that no counter-example exists. It is not impossible however, that — analyzing the inner connections of the problem further and improving the procedure — the necessity and sufficiency of heuristic rules developed after thorough analysis and investigations can be proved logically. But then the heuristic algorithm becomes exact algorithm.

Until then no more can be said about the solution achieved that it is a good approximation of the optimum. How good the approximation is, depends on our rules.

In any case it is advisable to evaluate the results we get — after performing a greater number of problems — with a method capable to determine the neighbourhood of the exact optimum, i.e. its lowest upper and highest lower bounds which can possibly be estimated, e.g. with a branch and bound method which can be terminated reaching the specified interval-length, or, in case of smaller problems, can determine the exact optimum.

REFERENCES

1. JÁNDY, G.: Approximate Algorithm for the Fixed Charge Capacitated Site Location Problem. Technical Report No 67—3, Stanford University, California
2. JÁNDY, G.: The Location Problem of Given and Indivisible Different Units. *Environment and Planning* **2** (1970)
3. JÁNDY, G.: Operations Research in the Planning and Controlling of Capacities. Technical Publishing House, Budapest (1971), (in Hungarian)
4. JÁNDY, G.: Introduction to Operations Research II. Tankönyvkiadó, Budapest 1974 (in Hungarian)
5. McMILLAN, C. JR.: Mathematical Programming. An Introduction to the Design and Application of Optimal Decision Machines, Wiley, New York, 1970.
6. PRITSKER—WATTERS—WOLFE: Mathematical Formulation. A Problem in Design, The Rand Corporation, Report P-3790, February 1968.
7. McMILLAN, C. JR.: Mathematical Programming, Wiley, New York, 1975.

Erkennung und Verwendung von heuristischen Regeln in der Problemlösung der Operationsforschung. In der vorliegenden Arbeit weist der Verfasser — auch unter Berufung auf seine früheren heuristischen Algorithmen — darauf, daß die Schulbeispiele der Operationsforschung bei gewissen Aufgabentypen oft viel mehr innere Schranken enthalten, als welche das allgemeiner gültige Modell der Aufgabentype ausdrückt. Dabei ist mit den Modellen die Bestimmung der optimalen Lösung im Verhältnis zur Bedeutung der Aufgabe gegebenenfalls zu kostspielig, ja mit wachsender Zahl der Varianten und der Bedingungen wird sie verhältnismäßig schnell praktisch unausführbar. Hingegen können bei eingehenderer Problemanalyse regelmäßig heuristische Regel erkannt werden, mit deren Hilfe die optimalen Lösungen solcher Aufgaben gut angenähert werden können. Diese Annahme beweist der Verfasser mit für zwei verschiedene Aufgabentypen *(Produktionsprogrammierung für mehrere Perioden und Planung der Reihenfolge für den Durchgang durch einen Engpaß)* ausgearbeiteten heuristischen Algorithmen. Inzwischen ermöglicht er einen Einblick in das heuristische Gedankenlaboratorium.

Опознание и применение хеуристических правил при решении проблем в области операционных исследований. Автор в данной статье (ссылаясь также на прежние свои хеуристические алгоритмы) желает указать на то, что примеры методики операционных исследований часто в случае определенных типов задач содержат значительно большее число внутренних ограничений, чем это выражено моделью более общего характера данного типа задачи. В то же время в случае этих моделей определение оптимального решения по сравнению со значением задачи может быть возможно слишком дорогим, более того с ростом числа переменных и условий относительно быстро становится также практически невозможным. А если лучше ознакомиться с некоторым данным типом задачи, то с помощью более глубокого анализа проблемы такие виды задач при применении оптимального решения дают удовлетворительное приближенное решение. Данное предположение подтверждается автором разработанными им для различных типов задач *(программирование производства на ряд периодов и проектирование порядка следования через узкое сечение)* хеуристическими алгоритмами.

АВТОМАТИЗАЦИЯ ПРОЕКТИРОВАНИЯ С ПОМОЩЬЮ ДИСКРЕТНОГО ПРОГРАММИРОВАНИЯ

М. ГРОС*

В статье в общей форме описана одна из возможных моделей автоматизации статического проектирования. Задача проектирования сформулирована следующим образом: требуется найти такой проект конструкции с заданной геометрией и заданным набором элементов, для элементов которого удовлетворяются условия равновесия, совместимости и ограничения, а также то, что с какой-либо точки зрения (вес, стоимость или их сотношение) конструкция будет оптимальной. Для сформулированной задачи записывается математическая модель в случае линейных ограничений, а позже она распространяется и на случай нелинейных ограничений. В обоих случаях задача сводится к решению дискретной задачи «0—1» программирования, для решения которой эффективно могут быть применены методы перебора. Для применения метода перебора необходимо было бы на каждом шагу обращать матрицу большого размера. Чтобы избежать это требование доказывается теорема и приводится метод решения задачи. На основе данного метода проведены успешные испытания программы на ЭВМ «СИМЕНС 4004/151» института САМГЕП.

1. Введение

В статье обсуждается вопрос автоматизации статического проектирования из сборных элементов. Приводимый метод после введения соответствующих изменений может быть применен для автоматизации других процессов технического проектирования.

Под автоматизацией статического проектирования подразумеваем проектирование статически неопределимых конструкций с заданной геометрией, которые строятся индустриализированными методами производства и элементы которых удовлетворяют статическим и экономическим требованиям и вся конструкция с какой-либо точки зрения является оптимальной.

При построении модели кроме условий равновесия и совместимости не рассматриваем конкретную запись других ограничений (ограничения на перемещение, на прочность), их считаем заданными. Однако, рассматриваем отдельно случай, когда эти ограничения линейны и когда они могут быть заданы в виде нелинейной векторной функции.

* 1025. Budapest, II. Csalit u. 9. II. em. 3.

2. Инженерная формилировка задачи

Согласно теории первого порядка запишем в матричной форме уравнения равновесия и совместимости. Как известно из теории, матрица G зависит только от геометрии конструкции и в случае статически определимых и неопределимых систем ранг этой матрицы равен числу ее столбцов.

Матрица F содержит матрицы упругости отдельных элементов системы. x_1 и, соответственно, x_2 — неизвестные перемещения и внутренние силы, p^1 — нагрузки в узловых точках системы, а p^2 — кинематические нагрузки. В системе уравнений (1) каждому элементу конструкции соответствует некоторый гипервектор b_i. Если для простоты предположим, что может быть

$$\tag{1}$$

Рис. 1

заменен только i-й элемент, то это равносильно замене гипервектора b_i на b_i' в матрице системы уравнений (1). Гипервекторы b_i и b_i' отличаются друг от друга только матрицами упругости F_i. Таким образом, проектирование конструкции заданной геометрии равносильно вводу в базис системы уравнений (1) тех гипервекторов, для которых удовлетворяются ограничения задачи и которые оптимальны с какой-либо точки зрения [3].

Теперь рассмотрим те дополнительные ограничения, которые возможны при проектировании конструкций из сборных типовых элементов. Здесь используем такие ограничения, которые не описывают переход из одного состояния в другое, поэтому могут быть рассмотрены как произвольные и независимые от изменения состояния ограничения, не имеющие физического смысла. Содержание ограничений определяется конструкционными и техническими требованиями.

В правой части ограничений содержатся величины, на основании которых решается вопрос, какие гипервекторы необходимо заменить в базисе.

Возможны два случая ограничений:

1. Ограничения можно записать в виде системы линейных неравенств;
2. Ограничения можно записать в виде системы нелинейных неравенств.

В дальнейшем оба случая рассматриваются отдельно. Среди ограничений могут быть такие условия, которые предписывают совпадение типов применяемых элементов в определенных местах конструкции.

3. Математическая модель задачи для случая линейных ограничений

Пусть дана система линейных равенства и неравенств:

$$A(\mathbf{b}) \cdot \mathbf{x} + \mathbf{p} = 0 , \tag{2}$$

$$B \cdot \mathbf{x} < S(\mathbf{b}) , \tag{3}$$

где $A(\mathbf{b})$ — несингулярная матрица, зависящая от актуального базиса $\mathbf{b}$ и имеющая форму, описанную в (1),

$S(\mathbf{b})$ — заданная векторная функция, зависящая также от актуального базиса системы,

B — матрица заданных ограничений,

$\mathbf{b} = (\mathbf{b}_1^{j_1}, \ldots, \mathbf{b}_n^{j_n})$ — актуальный базис матирцы A.

Гипервекторы элементов, вводимых в базис матрицы A на место i-ого гипервектора образуют множество E_i:

$$E_i = \{\mathbf{b}_i^j\} \quad i \in J, j = 1, 2, \ldots, j^*(i), |J| = n$$

где J — множество мест для элементов в конструкции,

$j^*(i)$ — число типов элементов, применяемых на i-ом месте конструкции.

Если в матрице A произошла замена базиса $\mathbf{b}_i^j \to \mathbf{b}_i^{j'}$, то соответствующим образом изменяются компоненты вектора $\mathbf{s}$, т. е. $\mathbf{s}$ является функцией базиса $\mathbf{b}$.

Система (2)—(3) одновременно должна быть удовлетворена для случая нескольких векторов p в правой части уравнения (2), поэтому, записав их в столбцы матрицы P, систему (2)—(3) можно переписать в следующем виде:

$$A(\mathbf{b})X + P = 0 \tag{4}$$

$$BX < S(\mathbf{b}) , \tag{5}$$

где матрицы X, P и S имеют одинаковое число столбцов.

В случае замены базиса в матрице S соответствующим образом изменяются целые строки, так как неравенство должно быть одновременно удовлетворено для одной и той же правой части, и матрица S состоит из одинаковых столбцов.

Теперь покажем, как система ограничений (4)—(5) может быть заменена такой системой неравенств, из которой исключена матрица X, так как в дальнейшем нас будет интересовать не конкретная величина сил и перемещений, а то, что удовлетворены ли ограничения задачи или нет. Введем матрицу Y, для которой

$$BX + Y = S . \tag{6}$$

Так как $\mathbf{A}$ — несингулярная матрица, то система уравнений (4) всегда имеет единственно решение

$$\mathbf{X} = -\mathbf{A}^{-1}\mathbf{P}\,.$$

Подставляя это равенство в (6),выразим матрицу $\underline{\mathbf{Y}}$:

$$-\mathbf{B}\mathbf{A}^{-1}\mathbf{P} + \mathbf{Y} = \mathbf{S}$$
$$\mathbf{Y} = \mathbf{B}\mathbf{A}^{-1}\mathbf{P} + \mathbf{S}\,.$$

Теорема 1. Если $\mathbf{A}$ несингулярная матрица, то система (4)—(5) имеет тогда и только тогда решение, если $\mathbf{Y} > 0$.

Необходимость. Допустим, что система (4)—(5) имеет решение, т. е.

$$\mathbf{X} = -\mathbf{A}^{-1}\mathbf{P} \text{ и } \mathbf{B}\mathbf{X} < \mathbf{S}\,.$$

Подставим выражение для $\mathbf{X}$ в неравенство, получим:

$$\mathbf{S} + \mathbf{B}\mathbf{A}^{-1}\mathbf{P} > 0\,, \quad \text{т. е.} \quad \mathbf{Y} > 0\,.$$

Достаточность. Допустим, что $\mathbf{Y} > 0$, т. е.

$$-\mathbf{B}\mathbf{A}^{-1}\mathbf{P} < \mathbf{S}\,.$$

Так как $\mathbf{A}$ несингулярная матрица, то

$$\mathbf{X} = -\mathbf{A}^{-1}\mathbf{P}\,, \quad \text{поэтому} \quad \mathbf{B}\mathbf{X} < \mathbf{S}\,.$$

Этим самым мы доказали *Теорему 1.*

На основе теоремы система (4)—(5) может быть заменена следующим условием:

$$\mathbf{B}\mathbf{A}^{-1}(\mathbf{b})\mathbf{P} + \mathbf{S}(\mathbf{b}) > 0\,.$$

Рассмотрим следующий вектор:

$$\boldsymbol{\delta} = (\delta_1^1,\, \delta_1^2,\, \ldots,\, \delta_1^{j*(1)},\; \delta_2^1,\, \ldots\, \delta_2^{j*(2)},\, \ldots,\, \delta_n^{j*(n)})\,,$$

где

$$\delta_i^j = \begin{cases} 1,\ \text{если гипервектор } \mathbf{b}_i^j \text{ относится к базису } \mathbf{b}, \\ 0\ \text{ в противном случае.} \end{cases}$$

После этого нашу задачу можно записать в виде следующей модели:

$$\sum_{i=1}^{n}\sum_{j=1}^{j*(i)} c_i^j \cdot \delta_i^j \to \min \qquad\qquad (7)$$

$$\sum_{j=1}^{j^*(i)} \delta_i^j = 1 \quad i = 1, 2, \ldots, n \tag{8}$$

$$\sum_{i \in H_s} (\delta_{i_1}^j - \delta_{i_2}^j) = 0 \quad s = 1, 2, \ldots, s^*; \quad i_1, i_2 \in H_s \tag{9}$$

$$\mathsf{B}[\mathsf{A}(\boldsymbol{\delta})]^{-1}\mathsf{P} + \mathsf{S}(\boldsymbol{\delta}) > 0 \tag{10}$$

где c_i^j — вес, стоимость (или их соотношение) i-ого элемента j-ого типа,

n — число гиперстолбцов матрицы F,

$j^*(i)$— число элементов множества E_i, т. е. число типов i-ого элемента,

H_s — множество индексов тех мест конструкции, в которых должны быть выбраны элементы одинакового типа,

s^* — число множеств H_s.

Условие (8) означает, что на i-овом месте конструкции всегда может быть выбран только один элемент множества E_i. Условие (9) означает, что на те места конструкции, индексы которых принадлежат можеству H_s, должны быть выбраны элементы одинакового типа.

Каждое множество E_i пополним двумя фиктивными элементами: очень «сильным» и очень «слабым» типом элемента. Первый тип необходим для того, чтобы всегда существовало хотя бы одно возможное решение. Если же второй тип попадает в решение, то это означает, что на i-ом месте конструкции элемент не нужен. Если очень «сильный» тип элемента попадает в оптимальное решение, то это означает, что множество E_i необходимо пополнить другими типами элементов. Величины c_i^j, соответствующие фиктивным элементам, выбирают очень «большими» и соответственно, очень «малыми» (например, в сто раз больше самого дорогого элемента).

Таким образом, задачу, описанную в пункте 2, удалось свести к решению задачи дискретного «0—1» программирования, для решения которой существуют известные по литературе [4, 5] методы. В данном случае наиболее эффективными методами решения задачи считаем методы перебора, так как по построению они не зависят от того, что ограничения являются линейными или нелинейными, и за конечное число шагов дают оптимальное решение. В результате применения метода перебора на каждом шагу необходимо проверять удовлетворение ограничений для каждой комбинации вектора $\boldsymbol{\delta}$. Для этого постоянно нужно было бы обращать матрицу большого размера. В следующем пункте рассмотрим такой метод вычисления элементов матрицы Y, в случае которого нет необходимости выполнять эту операцию и для расчета достаточно знать матрицы жесткости и упругости различных типов элементов.

4. Метод решения задачи

4.1 Вычисление матрицы Y *при замене базиса в случае линейных ограничений*

С помощью разбивки на четыре блока запишем матрицу, обратную матрице A [1]:

$$A^{-1} = \begin{bmatrix} -(G*F^{-1}G)^{-1} & (G*F^{-1}G)^{-1}G*F^{-1} \\ F^{-1}G(G*F^{-1}G)^{-1} & F^{-1} - F^{-1}G(G*F^{-1}G)^{-1}G*F^{-1} \end{bmatrix}.$$

Рассмотрим матрицу

$$M = (G*F^{-1}G)^{-1},$$

принимающую участие во всех четырех блоках. В случае произвольной замены базиса матрица F изменяется, поэтому для вычисления матрицы M необходимо обращать матрицу больших размеров. Для устранения этого затруднения рассмотрим следующую теорему:

Теорема 2. Если ранг матрицы G равен числу столбцов и F — несингулярная матрица, то

$$(G*F^{-1}G)^{-1} = G^+F(G^+)*,$$

где

$$G^+ = (G*G)^{-1}G*.$$

Доказательство. Так как F — несингулярная матрица, то

$$\varrho(G*F^{-1}) = \varrho(G*) = \varrho(G) = m.**$$

На основе этого можно применить следующую [2] теорему: если матрица A имеет размеры $n \times m$, а матрица B $m \times k$ и $\varrho(A) = \varrho(B) = m$, то

$$(A \cdot B)^+ = B^+ \cdot A^+.$$

Поэтому, если примем $A = G*F^{-1}$ и $B = G$, то

$$(G*F^{-1}G)^{-1} = G^+(G*F^{-1})^+.$$

Теперь применим следующую теорему [2]: $(A \cdot B)^+ = B^+ \cdot A^+$ тогда и только тогда, если

$$A^+ABB*A* = BB*A* \tag{12}$$

$$BB^+A*AB = A*AB. \tag{13}$$

---

* Знаком $+$ обозначаем обобщенную обратную матрицу.
** Знаком ϱ обозначаем ранг матрицы.

В нашем случае $A = G^*$ и $B = F^{-1}$.
Проверим удовлетворение условия (12):

$$(G^*)^+ G^* F^{-1}(F^{-1})^* G = F^{-1}(F^{-1})^* G . \qquad (14)$$

Так как ранг матрицы G равен числу ее столбцов, то согласно [2]:

$$G^+ = (G^*G)^{-1}G^* \text{ и } (G^+)^* = [(G^*G)^{-1}G^*]^* = \\ = G[(G^*G)^{-1}]^* = G[(G^*G)^*]^{-1} = G(G^*G)^{-1} \qquad (15)$$

Подставим (15) в (14), получим:

$$G(G^*G)^{-1} \cdot G^* F^{-1}(F^{-1})^* G = F^{-1}(F^{-1})^* G .$$

Умножим уравнение слева на матрицу G^*:

$$G^*G(G^*G)^{-1} \cdot G^* F^{-1}(F^{-1})^* G = G^* F^{-1}(F^{-1})^* G ,$$

получим тождество:

$$G^* F^{-1}(F^{-1})^* G = G^* F^{-1}(F^{-1})^* G .$$

Этим самым доказано удовлетворение условия (12). Условие (13) удовлетворяется тривиально, так как

$$(F^{-1})(F^{-1})^+ = E .$$

Таким образом, уравнение (11) можно переписать так:

$$M = G^+ F(G^*)^+ .$$

Учитывая тот факт, что $(G^*)^+ = (G^+)^*$, теорема доказана.
На основе теоремы 2 вычисление обратной матрицы A возможно с помощью единственного обращения симметрической матрицы G^*G, так как G^+ — постоянная матрица на протяжении всех вычислений, а матрица F^{-1} вычисляется по формулам.

$$A^{-1} = \begin{bmatrix} -G^+F(G^+)^* & G^+FGG^+F^{-1} \\ F^{-1}GG^+F(G^+)^* & F^{-1} - F^{-1}GG^+FGG^+F^{-1} \end{bmatrix} ,$$

так как

$$(G^+)^* \cdot G^* = [(G^* \cdot G)^{-1} \cdot G^*]^* \cdot G^* = G(G^* \cdot G)^{-1} \cdot G^* = GG^+ .$$

Дальнейшей нашей целью является получение такого алгоритма, с помощью которого элементы матрицы Y можно вычислять без лишнего умножения матриц больших размеров, как можно более экономно.

Разобьем матрицы P и B на блоки соответственно блокам матрицы A:

$$B = [B^1 B^2], \quad P = \begin{bmatrix} P^1 \\ P^2 \end{bmatrix},$$

где матрица B^1 размера $\tau \times m$, $B^2 - \tau \times n$, $P^1 - m \times \kappa$, $P^2 - n \times \kappa$. Матрица P^2 представляет собой кинематические нагрузки. В дальнейшем для простоты изложения предположим, что $P^2 = 0$. Матрица Y в блочном виде может быть записана так:

$$Y = - B^1 G^+ F(G^+)^* P^1 + B^2 F^{-1} G G^+ F(G^+)^* P^1 + S.$$

Введем следующие обозначения:

$$B^1 G^+ = C^1, \quad (G^+)^* P^1 = C^2 \quad \text{и} \quad G G^+ = C^3.$$

F — гипердиагональная матрица, поэтому обратная ей также будет гипердиагональной. Разобьем матрицы C^1, C^2, C^3, B^2 и S на блоки соответственно блокам матрицы F. В таком случае произвольный элемент матрицы Y может быть записан так:

$$y_{et} = \sum_{i \in J} \sum_{j \in J} \left(- C^1_{ei} F_{ij} C^2_{jt} + \sum_{k \in J} \sum_{m \in J} B^2_{li} F^{-1}_{ij} C^3_{jk} \cdot F_{km} \cdot C^2_{mt} \right) + S_{et}.$$

Так как $F_{ij} = F^{-1}_{ij} = 0$, если $i \neq j$, то

$$y_{et} = - \sum_{i \in J} C^1_{ei} F_{ii} C^2_{it} + \sum_{i \in J} \sum_{j \in J} B^2_{ei} F^{-1}_{ii} C^3_{ij} F_{jj} C^{2t}_{jt} + S_{et}. \tag{16}$$

Для решения поставленной задачи каждый раз необходимо было бы вичислять правую часть уравнения (16). С целью уменьшения вычислений рассмотрим, как изменяется произвольный элемент матрицы Y при замене базиса.

Допустим, что хотим произвести замену базиса в нескольких местах, их индексы образуют множество J^*. Пусть

$$J' = J \backslash J^*,$$

то есть J' множество индексов тех гипервекторов, в которых не происходит замены базиса. Подставим (16) в тривиальное уравнение

$$\hat{y}_{et} = (\hat{y}_{ei} - y_{et}) + y_{et},$$

получим

$$\hat{y}_{et} = - \sum_{i \in J} C^1_{li} (\hat{F}_{ii} - F_{ii}) C^2_{it} + \sum_{i \in J} \sum_{j \in J} (B^2_{ei} \hat{F}^{-1}_{ii} C^3_{ij} \hat{F}_{jj} C^2_{jt} - \\ - B^2_{ei} F^{-1}_{ii} C^3_{ij} F_{jj} C^2_{jt}) + \hat{S}_{et} - S_{et} + y_{et}. \tag{17}$$

Преобразуем первую сумму:

$$\sum_{i \in J} C^1_{ei}(\hat{F}_{ii} - F_{ii})C^2_{it} = \sum_{i \in J^*} C^1_{ei}(\hat{F}_{ii} - F_{ii})C^2_{it} +$$

$$+ \sum_{i \in J'} C^1_{ei}(F_{ii} - F_{ii})C^2_{it} = \sum_{i \in J^*} C^1_{ei}(\hat{F}_{ii} - F_{ii})C^2_{it} \,. \tag{18}$$

Теперь преобразуем вторую сумму уравнения (17):

$$\sum_{i \in J} \sum_{j \in J} = \sum_{i \in J^*} \sum_{j \in J} + \sum_{i \in J'} \sum_{j \in J} = \sum_{i \in J^*} \sum_{j \in J} + \sum_{i \in J'} \sum_{j \in J'} + \sum_{i \in J'} \sum_{j \in J^*} \,.$$

После этих преобразований (17) можно записать в виде:

$$y_{et} = - \sum_{i \in J^*} C^1_{ei}(\hat{F}_{ii} - F_{ii})C^2_{it} + \sum_{i \in J^*} \sum_{j \in J} B^2_{ei}(\hat{F}^{-1}_{ii} - C^3_{ij}\hat{F}_{jj} -$$

$$- F^{-1}_{ii}C^3_{ij}F_{jj})C^2_{jt} + \sum_{i \in J'} \sum_{j \in J^*} B^2_{ei}F^{-1}_{ii}C^3_{ij}(\hat{F}_{jj} - F_{jj})C^2_{jt} + \hat{S}_{et} - S_{et} + y_{et} \,, \tag{19}$$

так как по определению множества J'

$$\sum_{i \in J'} \sum_{j \in J'} B^2_{ei}(F^{-1}_{ii}C^3_{ij}F_{jj} - F^{-1}_{ii}C^3_{ij}F_{jj})C^2_{jt} = 0 \,.$$

Таким образом, по уравнению (19) видно, что произвольный элемент матрицы Y можно вычислить без обращения матриц больших размеров.

4.2 Случай нелинейных ограничений

Теперь рассмотрим тот случай, когда ограничения задачи задаются в виде нелинейной векторной функции и системы линейных уравнений:

$$\left.\begin{array}{l} A(\delta)X + P = 0 \\ D(X) < S(\delta) \end{array}\right\} \,.$$

Не повторяя рассуждения предыдущего пункта, здесь приведем только основные результаты алгоритма.

С учетом теоремы 2 и условия $P^2 = 0$ можно записать:

$$X = - A^{-1}(\delta)P \,, \quad \begin{bmatrix} X^1 \\ X^2 \end{bmatrix} = \begin{bmatrix} G + F(G+)*P^1 \\ - F^{-1}GG + F(G+)*P^1 \end{bmatrix} \,.$$

Если матрицы $G^+, GG^+, (G^+)*P^1$ разобьем на блоки соответственно блокам матрицы $\bar{F}$, то произвольный блок матрицы X можно записать следующим образом:

$$X_{et}^1 = \sum_{i \in J} G_{ei}^+ F_{ii} C_{it}^1 \quad (l = 1, 2, \ldots, m; \; t = 1, 2, \ldots, k)$$

$$X_{St}^2 = - \sum_{l=1}^{m} F_{SS}^{-1} G_S X_{et}^1 = - \sum_{i \in J} F_{SS}^{-1} C_{Si}^2 F_{ii} C_{it}^1 \quad (s = 1, 2, \ldots, n) \,,$$

где

$$C^1 = (G^+)^* \cdot P^1, \; C^2 = GG^+.$$

Исходя из этих формул, можно получить формулы для расчета произвольного блока матрицы X после замены базиса:

$$\hat{X}_{et}^1 = \sum_{i \in J^*} G_{ei}^+ (\hat{F}_{ii} - F_{ii}) C_{it}^1 + X_{et}^1$$

$$\hat{X}_{St}^2 = - \sum_{i \in J^*} F_{SS}^{-1} C_{Si}^2 (\hat{F}_{ii} - F_{ii}) C_{it}^1 + X_{St}^2 \quad s \notin J^*$$

$$\hat{X}_{St}^2 = - \sum_{i \in J^*} (\hat{F}_{SS}^{-1} C_{Si}^2 \hat{F}_{ii} - F_{SS}^{-1} C_{Si}^2 F_{ii}) C_{it}^1 + X_{St}^2 \quad s \in J^*$$

Эти формулы перерасчета проще формул, известных автору по литературе [6—8], а также легко программируемы.

Таким образом, в случае нелинейных ограничений в модель задачи [7]—[10] вместо условий [10] нужно ввести следующее условие:

$$S(\delta) - D(X) > 0 \,.$$

ЛИТЕРАТУРА

1. Szabó, J.—Roller, B.: Rúdszerkezetek elmélete és számítása, Műszaki Könyvkiadó, Budapest, 1971
2. Albert, A.: Regression and the Moore-Penrose Pseudoinverse, Academic Press, New York, 1972
3. Holnapy, D.: Adatbank alkalmazása a műszaki tervezés automatizálásához SZÁMOLÓGÉP, NIM IGÜSZI 1975/2
4. Garfinkel, R. S.—Nemhauser, G. L.: Integer Programming, John Wiley, New York, 1972
5. Gallagher, R. H.—Zienkiewicz, O. C.: Optimum Structural Design, London, John Wiley, 1973
6 Sobieszczanski, J.: Matrix Algorithm for Structural Modification Based upon Parallel Element Concept, *AIAA Journal* (1969) 11.
7. СЕРГЕЕВ, Н. Д.: Расчет статически неопределимых систем при их многоэтапной последовательной модификации, Строительная механика и расчет сооружений, 1976/4.
8. ПЕРЕЛЬМУТЕР, А. В.: О влиянии изменения жесткостей на перераспределение усилий в статически неопределимой системе, Строительная механика расчет сооружений, 1974/5.

Automatisiertes Projektieren mittels integer Programmierung. — In der vorhegenden Arbeit wird ein mögliches Modell für die Automatisierung des statischen Projektierens in allgemeiner Form definiert. Die Projektierungsaufgabe wird so interpretiert, daß ein, aus dem gegebenen Vorrat an Elementen herstellbares Projekt mit gegebener Geometrie gesucht wird, bei welchem für die Elemente die Gleichgewichts-, Kompabilitäts- und einschränkeneden Bedingungen erfüllt sind und wo ferner unter irgendeinem Gesichtspunkt (Gewicht, Kosten oder deren Verhältnis) die Konstruktion optimal ist. Für das so definierte Problem wird das mathematische Modell für lineare einschränkende Bedingungen aufgeschrieben und dann auch auf nichtlineare Fälle ausgedehnt. In beiden Fällen werden die Probleme auf eine "0—1" ganzzahlige Programmierungsaufgabe zurückgeführt, für deren Lösung die Abzählmethode wirksam angewendet werden kann. Bei der Verwendung der Abzählmethode wäre bei jedem Schritt die Inversion einer großen Matrix notwendig. Es sind auch Lösungsverfahren vorgeführt, wo dies vermieden wird.

Automated Designing with Integer Programming. — In this paper the author presents a possible model for the general solution of automated designing. The design problem is defined as follows: a design of a structure with given geometry and composed from a given stock of elements is looked for, where for the elements the equilibrium, compatibility and limiting conditions are fulfilled and where the structure is optimum from some point of view (weight, cost, or their ratio). For the problem thus defined the mathematical model for linear limiting conditions is established and then it is extended to the case of non-linearity. In both cases the problems are reduced to that of a "0—1" integer programming task to which the enumerative method can be applied. For this method the inversion of a large matrix would be necessary. A solution method is shown for avoiding this.

ELECTROMAGNETIC WAVE PROPAGATION IN INHOMOGENEOUS MEDIA: STRONG AND WEAK INHOMOGENEITIES

CS. FERENCZ*

The paper deals with a classification of the inhomogeneities in a way which seems to be more objective than the earlier methods. It gives a simple form for Maxwell's equations which means general usability in examination of propagation, and also gives variations for the dispersion equations, investigating several questions of the commonly used method of 6-dimensional designation.

Investigating of propagation of electromagnetic waves in inhomogeneous media does not only meet the needs, but — apart from the favourable results — it has led to many problems, which are still open, so it is necessary to go on analyzing those questions which might possibly have general consequences. In a similar manner to earlier papers [1, 2, 3, 4] the monochromatic signal will be considered only, that is the solution will take the form of $\exp{(j\omega t - \varphi)}$.

The existence of that solution will not be dealt with, as it can only be decided by examining the medium parameters and the boundary conditions [3] in a concrete case. But, according to the Floquet-theorem [5] it is clear, that the existence of the solution in the form

$$\bar{F}(\bar{x} + \bar{p}_i) = \bar{F}(\bar{x})e^{j\Phi i} \,, \quad i = 1, 2, 3$$

is fulfilled on the condition that the

$$\omega = f(\Phi_1, \Phi_2, \Phi_3)$$

dispersion equation exists, the investigations based on the dispersion equation will be emphasized. According to the heading of that paper — and paying attention to the dispersion equations — the classification of strong and weak inhomogeneities will be examined here, from the point of view of solving the equations. Before that, it is necessary to analyze the dispersion equations.

The relation between media and electromagnetic wave will be taken as linear, that is, permeability, permittivity, etc. do not depend on the intensity, phase, etc. of the electromagnetic field, except for the frequency of the signal.

* Dr. Cs. FERENCZ Puskin u. 24. H-1088 Budapest, Hungary.

1. The investigation of the former classification

Previously [1, 3, 4, 6] a generally accepted method was followed in classifying the inhomogeneities as strong and weak, which was based on the formal examination of those derivatives which can be found in the Maxwell-equations. This means the following:

Let the solution be sought in the form

$$\bar{F} = \bar{F}_0 e^{j(\omega_0 t - \varphi)} \tag{1}$$

where $\bar{F}$ is the unknown electrical or magnetic field, respectively, or may be something else, $\bar{F}_0$ is the amplitude vector (defined generally), ω_0 the frequency of the monochromatic signal, t is time, and φ the phase function. Let the components of tensors of medium parameters (permeability, permittivity, etc.) be designated for a_{ik}. The Maxwell's equations are:

$$
\begin{aligned}
\bar{\nabla} \times \bar{H} &= \bar{J} + \varepsilon_0 \frac{\partial \bar{D}}{\partial t}, \\
\bar{\nabla} \times \bar{E} &= -\mu_0 \frac{\partial \bar{B}}{\partial t}, \\
\bar{\nabla} \bar{B} &= 0, \\
\bar{\nabla} \bar{D} &= \varrho / \varepsilon_0
\end{aligned}
\tag{2}
$$

where $\bar{E}$ is the electrical intensity field, $\bar{H}$ is the magnetic intensity field, $\bar{D}$ is the electric displacement field, $\bar{B}$ is the magnetic induction field, ε_0 and μ_0 are the permittivity and permeability of vacuum, respectively, $\bar{J}$ is the density of electrical current, ϱ is the density of electric charge. By differentiating these equations the following terms will be obtained [3]

$$\left(\frac{1}{a_{ik}} \frac{\partial a_{ik}}{\partial x_i} + \frac{1}{F_{0k}} \frac{\partial F_{0k}}{\partial x_i} - j \frac{\partial \varphi}{\partial x_i} \right) a_{ik} F_k \tag{3}$$

where x_i means the independent variables.

It is known that in the case of homogeneous media

$$\frac{\partial \varphi}{\partial x_i} = k_i = \text{const}$$

and therefore (3) leads to the well-known form of

$$(-jk_i a_{ik} F_k), \quad j^2 = -1.$$

In the following, let the variation of the medium parameters be small if the distance is commensurable with wavelength λ, that is

$$\Delta a_{ik} = \frac{\partial a_{ik}}{\partial x_i} \lambda \simeq \eta$$

where η is elementary small. In multiplying (3) by λ and estimating the values of each term:

$$\lambda \cdot \text{Term (3)} \simeq \left[\frac{\eta}{a_{ik}} + \frac{\eta}{F_{0k}} - j \left(\frac{\partial \varphi}{\partial x_i} \lambda \right) \right] a_{ik} F_k \simeq$$

$$\simeq -j \left(\frac{\partial \varphi}{\partial x_i} a_{ik} F_k \right) \lambda \sim -j(k_i a_{ik} F_k) \lambda . \tag{4}$$

In this way those media are considered as weakly inhomogeneous ones, where all the terms are negligible as compared to $j \cdot \partial \varphi / \partial x_i$, and those, where this comparison cannot be executed, are considered as strongly inhomogeneous ones.

It seems to be arbitrary when examining (4) in more details, that however small the neglected terms are, they are not multiplied by j, and it is not necessary when in estimating their importance and magnitude they should be compared to a term multiplied by j. (Their meaning differs even physically, as they describe the variation of amplitude and phase, respectively).

Statement

As the terms, not being multiplied by j in (4) disappear only in a homogeneous case and they obviously appear in any inhomogeneous case and are commensurable with $(\partial \varphi / \partial x_i - k_i)$. The mentioned — generally accepted — way only serves for defining quasi-homogeneous media.

Thus to classify inhomogeneities is a problem still to be solved.

2. Form of Maxwell's equations

In order to solve the mentioned problem the Maxwell's equations are to be solved for propagating electromagnetic signal. Let the process be begun by analyzing the forms of Eqs (2). Let us take the role of terms $\bar{J}$ and ϱ/ε_0 into consideration. The generally used method in the wave theory [1, 3, 6, 7, 8] can be seen e.g. in the case of describing propagation in plasma.

a) First of all it is to be noted, that for the above two terms the continuity equation is valid

$$\text{rot } \bar{H} = \dot{J} + \varepsilon_0 \frac{\partial \bar{D}}{\partial t}$$

$$\text{div rot } \bar{H} = 0 = \text{div } \bar{J} + \varepsilon_0 \text{ div} \left(\frac{\partial \bar{D}}{\partial t} \right).$$

Furthermore

$$\text{div } \bar{D} = \frac{\varrho}{\varepsilon_0}.$$

Therefore, if

$$\text{div} \left(\frac{\partial \bar{D}}{\partial t} \right) = \partial/\partial t (\text{div } \bar{D}), \tag{5}$$

the equation of continuity is valid in the usual form. (Therefore, it seems to be important to investigate the validity of the different forms of the equation of continuity for inhomogeneous media, or for "quickly" or "specially" varying media in time.)

In this case, assuming that (5) is valid:

$$\bar{\nabla} \bar{J} + \frac{\partial \varrho}{\partial t} = 0. \tag{6}$$

b) It is known that in plasma in the presence of a static magnetic field [7, 8, etc.]

$$\bar{J} = \sigma \bar{E}$$

where σ is the tensor of conductivity.

Therefore — as no other effects exist if it is linear — in the plasma

$$\text{rot } \bar{H} = \sigma \bar{E} + \varepsilon_0 \frac{\partial \bar{E}}{\partial t}$$

and from that

$$\text{rot } \bar{H} = \varepsilon_0 \frac{\partial}{\partial t} \left(\frac{1}{\varepsilon_0} \int^t \sigma \bar{E} \mathrm{d}t + \bar{E} \right) = \varepsilon_0 \frac{\partial \bar{D}}{\partial t}.$$

If the variation is assumed for the form $\exp(j\omega_0 t)$, then

$$\text{rot } \bar{H} = j\varepsilon_0 \omega_0 \left(\frac{\sigma}{j\varepsilon_0 \omega_0} + 1 \right) \bar{E} = j\varepsilon_0 \omega_0 \varepsilon \bar{E}.$$

It is simultaneously a definition for permittivity as well.

c) It is known that the deduction of the medium parameters follows a similar method in other cases, too. Thus, in investigations of wave propagation

a generalized definition may be accepted for the displacement vector — if it is sensible mathematically —

$$\overline{\mathfrak{D}} = \frac{1}{\varepsilon_0} \int^t \bar{J} dt + \overline{D} \,, \tag{7}$$

or in another form:

$$\varepsilon_0 \frac{\partial \overline{\mathfrak{D}}}{\partial t} = \bar{J} + \varepsilon_0 \frac{\partial \overline{D}}{\partial t} \,. \tag{8}$$

From this it follows, that

$$\operatorname{div} \overline{\mathfrak{D}} = \frac{1}{\varepsilon_0} \operatorname{div} \left(\int^t \bar{J} dt \right) + \operatorname{div} \overline{D} = \frac{1}{\varepsilon_0} \int^t (\operatorname{div} \bar{J}) dt + \operatorname{div} \overline{D} \,.$$

If (6) is valid, — taking into consideration the last equation of Eqs (2) —

$$\operatorname{div} \overline{\mathfrak{D}} = \frac{1}{\varepsilon_0} \int^t \left(-\frac{\partial \varrho}{\partial t} \right) dt + \frac{\varrho}{\varepsilon_0} \equiv 0 \,. \tag{9}$$

Now, if $\overline{\mathfrak{D}}$ is always defined by (7) or (8) (as it is commonly used), then:

Statement

In investigations of wave propagation it is sufficient to use the form

$$\overline{\nabla} \times \overline{H} = \varepsilon_0 \frac{\partial \overline{D}}{\partial t} \,,$$

$$\overline{\nabla} \times \overline{E} = -\mu_0 \frac{\partial \overline{B}}{\partial t} \,,$$

$$\overline{\nabla} \overline{B} = 0 \,,$$

$$\overline{\nabla} \overline{D} = 0 \tag{10}$$

of Maxwell's equations without any restrictions of general validity, where $\overline{D}$ is defined in the same way as $\overline{\mathfrak{D}}$ in (8). In this way all effects of the media will be assembled in $\overline{D}$ and $\overline{H}$ (included the active generative effects as well). This statement in this form is valid, till Eq. (6) is valid. NB: The validity of Eq. (6) depends not only on the investigated phenomenon but on the functions (that is, distributions) which describe the medium parameters of the applied model, as well.

— Form (10) may be inexpedient for examining certain problems of excitation or radiation.

In the following the form (10) of Maxwell's equations will be used.

d) Before analyzing the dispersion equation based on Eq (10), several comments must be made to restrict the validity of the following statements. The way of generalizing the results has already been shown [3, 4, 9] but the execution of this generalization is a further step. This will not be dealt with in this paper.

d) 1. Let the signal be assumed now as strictly monochromatic. Therefore, and because of 2.*a*, the propagation in media varying in time will not be investigated, for then an examination of signals of general $S(\omega)$ spectra would not be negligible.

d) 2. In the followings general — bianisotropic — media will be examined, but then moving media will not be investigated, because of the following reasons:

Formally applying Maxwell's equations to a moving media, they appear in a bianisotropic form. [5, 10, 11, 12, 13, 14]. Therefore, a general bianisotropic refraction index will usually be used. But in this form the Doppler-effects completely disappear. If it seems advisable for some reason, the Doppler-effect will be taken into account by supplementary relations [15, 16]. These treatments are arbitrary and contradict the contemplation of the theory of relativity [3, 4].

Further, the usual ways of investigation also carry other difficulties. One of them originates in formal reasons. The bianisotropic relation among $\bar{E}, \bar{D}, \bar{B}$ and $\bar{H}$ have a rather complicated form when written in 3-dimensions, and do not even formally exist in 4-dimensions.

So in general the bianisotropic relation is given for 6-dimensional vectors [5, 10, 11, 12, 13, 14] fabricated from a 3-dimensional electric and a 3-dimensional magnetic component, and it then takes a simple form of a 6-dimensional tensor. This formal treatment, however, substantially contradicts the 4-dimensional electromagnetic tensor [17], and therefore, it seems inexpedient to use it.

Another difficulty is, that the more precise investigation of electromagnetic wave propagation in a moving media produced fundamental contradictions e.g. transformation of phase-velocity of electromagnetic plane waves, etc. [17, 18, 19, 20], and these contradictions have not been definitively solved yet. Neither is a better way given for solving the problem on investigating the medium parameters (permeability, permittivity, etc.) under relativistic circumstances [17, 21].

The reason of these difficulties can well be seen on the introduction of $\bar{D}$ and $\bar{H}$. To apply the method of separating the forms of propagating energy, which is ligitimate in case of "stationary" observers, for "moving" observers by even defining the mode of separation, is not justified [3, 22]. Only that treatment can be accepted, which is based on the transformation of total

energy. The question of the energy propagation will be dealt with in a later paper.

Keeping in mind the physical conception, a work was successfully done earlier for giving a ray-tracing method suitable for practical investigation concerning moving media (relativistic ray-tracing) [3, 24], which produced in a number of cases the consistent and uniform explanation [23, 24, 25, 26] of "extraordinary" frequency changes [27, 28, 29, 30, 31, 32] and the conclusions were later justified [40], e.g. by Pioneer-6 experiment [33, 34]. So in the recent paper moving media may be excluded from the investigation and the results can be generalized later, keeping in mind, what was mentioned above.

3. Forms of dispersion-equation

a) Previously [3, 4, 35] the dispersion equation for stationary, invarying in time and — according to the new definition — quasi-homogeneous media was deduced in the following form:

$$\bar{F} = \bar{F}(\bar{r})e^{j[\omega_0 t - \varphi(\bar{r})]} .$$

Let be

$$\bar{K} = \text{grad } \varphi ,$$

and

$$\bar{D} = \varepsilon\bar{E} , \quad \bar{B} = \mu\bar{H} .$$

Then, taking the quasi-homogeneity into consideration, Eq (10) can be rewritten

$$\bar{K}\times\bar{H} = -\omega_0\varepsilon_0\varepsilon\bar{E} ,$$
$$\bar{K}\times\bar{E} = \omega_0\mu_0\mu\bar{H} ,$$
$$\mu_0\bar{K}\mu\bar{H} = 0 ,$$
$$\varepsilon_0\bar{K}\varepsilon\bar{E} = 0 .$$

From here solving the equations in a similar manner for $\bar{E}$ or $\bar{H}$, [4], i

$$\begin{aligned} \Lambda &= \bar{K}\times(\bar{K}\times\ldots) , & \varepsilon &= 1 + \mathbf{e} , \\ \mathbf{P} &= \bar{K}\times\mathbf{e}\ldots , & \mu &= 1 + \mathbf{m} , \\ \mathbf{M} &= \bar{K}\times\mathbf{m}\ldots , & k_0 &= \omega_0\sqrt{\varepsilon_0\mu_0} , \end{aligned}$$

then the solutions non-trivially exist if one of the two equivalent dispersion equations will be fulfilled. These are:

$$\left| \left(\frac{\Lambda}{k_0} + k_0\varepsilon\right) + \mathbf{M}\left(\frac{\Lambda}{k_0} + k_0\mu\right)^{-1}\mathbf{P} \right| = 0 ,$$

or

$$\left| \left(\frac{\Lambda}{k_0} + k_0\mu\right) + \mathbf{P}\left(\frac{\Lambda}{k_0} + k_0\varepsilon\right)^{-1}\mathbf{M} \right| = 0 .$$

(11)

Here however two questions remain unanswered in connection with Eqs (11) and their deductions. The one is, that though the equivalence of the two equations follows from the deduction, it is not directly conceivable. The other is, that for the sake of the existence of Eqs (11) in the given form restrictions have to be accepted, which cannot be fulfilled, generally.

It is namely a determinant of hypermatrices, and if $\mathbf{A}^{-1}$ exists and (by the second step) the matrices are interchangeable [36], then

$$\begin{vmatrix} \mathbf{A} & \mathbf{B} \\ \mathbf{C} & \mathbf{D} \end{vmatrix} = \begin{vmatrix} \mathbf{1} & \mathbf{0} \\ \mathbf{CA}^{-1} & \mathbf{1} \end{vmatrix} \begin{vmatrix} \mathbf{A} & \mathbf{B} \\ \mathbf{0} & (\mathbf{D} - \mathbf{CA}^{-1}\mathbf{B}) \end{vmatrix} = 0 \,, \tag{12}$$

that is

$$\begin{vmatrix} \mathbf{A} & \mathbf{B} \\ \mathbf{C} & \mathbf{D} \end{vmatrix} = |\, \mathbf{AD} - \mathbf{CB}\,| = 0 \,. \tag{13}$$

That Eqs (12) and (13) should equal zero, this is necessary only in the dispersion equation. From Eqs (12) and (13) it can be seen, that both forms of Eq. (11) and other forms can be deduced as well, if restrictions are made for the matrices. However, these restrictions cannot generally be made.

b) It is important and can be seen from *a)*, that though a 6-dimensional formalism will be applied, still when it comes to further calculation, one has to return to the 3-dimensional form and must even then be cautious.

c) In the following the problem of the dispersion equation of, in time invarying and not moving, quasi-homogeneous media will be dealt with, generally, without any restrictions concerning the tensors. At the same time the equivalency of the different forms will be verified.

For the sake of generality bianisotropic media will be investigated, where

$$\begin{aligned} \bar{D} &= \varepsilon\bar{E} + \varkappa\bar{H} \,, \\ \bar{B} &= \nu\bar{E} + \mu\bar{H} \,, \end{aligned} \tag{14}$$

or choosing those $(\bar{E}, \bar{B})$ pairs, which belong together

$$\begin{bmatrix} \bar{D} \\ \bar{H} \end{bmatrix} = \begin{bmatrix} \mathbf{P} & \mathbf{L} \\ \mathbf{M} & \mathbf{Q} \end{bmatrix} \begin{bmatrix} \bar{E} \\ \bar{B} \end{bmatrix} \tag{15}$$

where

$$\begin{aligned} \varepsilon &= \mathbf{P} - \mathbf{LQ}^{-1}\mathbf{M} \,, & \varkappa &= \mathbf{LQ}^{-1} \,, \\ \nu &= -\mathbf{Q}^{-1}\mathbf{M} \,, & \mu &= \mathbf{Q}^{-1} \,. \end{aligned} \tag{16}$$

Maxwell's equations then become

$$\begin{aligned} \bar{K} \times \bar{H} &= -\omega_0\varepsilon_0(\varepsilon\bar{E} + \varkappa\bar{H}) \,, \\ \bar{K} \times \bar{E} &= \omega_0\mu_0(\nu\bar{E} + \mu\bar{H}) \,, \\ \bar{K}(\varepsilon\bar{E} + \varkappa\bar{H}) &= 0 \,, \\ \bar{K}(\nu\bar{E} + \mu\bar{H}) &= 0 \end{aligned} \tag{17}$$

where the third and forth equations hold automatically, so they may be neglected.

Let the

$$\mathbf{K} = \begin{bmatrix} 0 & -K_3 & K_2 \\ K_3 & 0 & -K_1 \\ -K_2 & K_1 & 0 \end{bmatrix} \Lambda = \mathbf{KK} \tag{18}$$

nominations now be introduced, then

$$
\begin{aligned}
(\mathbf{K} + \omega_0\varepsilon_0\varkappa)\bar{H} + \omega_0\varepsilon_0\varepsilon\bar{E} &= 0 \,, \\
(\mathbf{K} - \omega_0\mu_0\nu)\bar{E} - \omega_0\mu_0\mu\bar{H} &= 0 \,.
\end{aligned}
\tag{19}
$$

In solving it for $\bar{E}$ or $\bar{H}$, the solutions will be non-trivial, if

or

$$
\begin{aligned}
|\, (\bar{\mathbf{K}} + \omega_0\varepsilon_0\varkappa)\mu^{-1}(\mathbf{K} - \omega_0\mu_0\nu) + k_0^2\varepsilon \,| &= 0 \,, \\
|\, (\bar{\mathbf{K}} - \omega_0\mu_0\nu)\varepsilon^{-1}(\mathbf{K} + \omega_0\varepsilon_0\varkappa) + k_0^2\mu \,| &= 0 \,.
\end{aligned}
\tag{20}
$$

Meanwhile the tensors can be completely general.

ε^{-1}, μ^{-1} and the inverse of the other tensors exist without any restrictions, as for

$$\varepsilon = 1 + e \,, \quad \mu = 1 + m$$

which follows from the deduction of the medium parameters as well. (In some cases there are exceptions as well: e.g. ideal resonance-cases assumed to be lossless. When in such cases one insists on neglecting the not negligible losses, it must be controlled, which equations-form exists from the possible forms of Eqs (20).)

1. *Statement*

From the existence of the inverse-tensors trivially follows the equivalence of Eqs (20).

2. *Statement*

As for $|\mathbf{K}| = 0$, $\mathbf{K}^{-1}$ does not exist. Now neglecting the bianisotropic terms, the individual rearrangements in the equations cannot be executed between the equivalent forms of Eqs (20). If a case is more simple than bi-anisotropic, the equivalence cannot be seen directly.

Note: It can be simply seen, that the tensors of the (19) hypermatrix, in general, are not interchangeable. Therefore, the 6-dimensional formalism proposed, directly for these cases, [5, etc.] not only contradict the 4-dimensional picture, but it involves difficulties in the calculation as well! (This however does not mean, that the results are automatically wrong in the 6-dimensional treatment, so it is worth further investigation.)

4. Strong inhomogeneities

a) In that case, when the inhomogeneities cannot be treated as quasi-homogeneous ones, all the terms in Eq (3) must be taken into account. Now the method of inhomogeneous basic modes can be applied for deciding the propagating electromagnetic wave pattern. [3, 4, 38, 39]. The relations will not be repeated here because of their great length, they are known, anyway. It is characteristic though, that no higher derivatives occur in them: this fact makes a difference among this and the further methods of investigation, and at the same time produces a restriction for its applicability.

b) In that case, when the inhomogeneities are rather strong, accepting several restrictions, a different way from 4.*a* can also be found for obtaining the result [3, 9]. If the higher derivatives will not be neglected, for simple anisotropic cases (when either ε or μ characterizes alone the medium) the form of dispersion equation is the following:

$$| \Lambda + k_0^2 \varepsilon - j(\mathbf{Grad}\ \bar{K} + \bar{\nabla}\bar{K} \cdot \mathbf{1}) | = 0 , \tag{21.a}$$

or

$$| \Lambda + k_0^2 \mu - j(\mathbf{Grad}\ \bar{K} + \bar{\nabla}\bar{K} \cdot \mathbf{1}) | = 0 . \tag{21.b}$$

It is important, however, that now not only $\bar{K} = \mathbf{grad}\ \varphi$, but the derivatives of it should also occur.

c) Further, in case of step-functions (ray-tracing method) a general method for giving the propagating signal was found [3, 4, 38, 39]. In this case — the multiple refraction-reflection law — at the step (a very strong inhomogeneity) the higher derivatives also appear.

The first investigations concerning the analysis of Maxwell's equations in the presence of distributions, though not striving for the description of wave propagation, showed a similar feature [37].

d) If interpreting the medium parameters ($\varepsilon, \varkappa, \nu$ and μ) and the "rot" operation ($\bar{\nabla} \times \ldots = \mathbf{K}_{\bar{\nabla}} \ldots$) as operators, then developing Maxwell's equations e.g. for $\bar{E}$, it results in the following form:

$$\varepsilon^{-1}(\mathbf{K}_{\bar{\nabla}} - j\omega_0\varepsilon_0\varkappa)\mu^{-1}(\mathbf{K}_{\bar{\nabla}} + j\omega_0\mu_0\nu)\bar{E} = k_0^2\bar{E} . \tag{22}$$

(The equations for $\bar{H}$ has a similar form).

At present Eq. (22) will not be further analyzed, only settled, after applying $\bar{\mathbf{K}}_{\bar{\nabla}}$ repeatedly, that in case of strong inhomogeneities not only the first, but the higher derivatives also generally appear.

In case of not so strong inhomogeneities, already the derivatives of the second order disappear or are negligible.

5. Consequences

a) Both the phase (the derivative of which is the propagation vector) and the amplitude vector of propagating signal will be influenced by the medium if the latter is really inhomogeneous.

If the variation of the amplitude may be neglected, the phenomenon may be called expediently quasi-homogeneous.

In the course of the discussions, the inhomogeneous (weakly inhomogeneous) and strongly inhomogeneous media differ in producing derivatives of second order (of the phase, e.g.) negligibly or not, when solving the equations of Maxwell.

b) The equivalence of dispersion equations originating from Maxwell's equations for $\bar{E}$ or $\bar{H}$ was directly verified in this paper.

c) According to the present investigations, the 6-dimensional formalism, often used in preference to the bianisotropic media, not only does not make a real simplification in calculations, but also does not fit into the accepted theories in physics. Therefore, either it seems expedient not to use it or one must be rather cautious when using it. (If showing the physical conception — though it is not probable — of the 6-dimensional formalism would have rather heavy consequences).

REFERENCES

1. BRANDSTÄTTER, J. J.: An Introduction to Waves, Rays and Radiation in Plasma Media; McGraw-Hill Book Co., Inc.; New York 1963
2. CHOUDHARY, S.—FELSEN, L. B.: Asymptotic Theory for Inhomogeneous Waves; *IEEE Trans. on Ant. and Prop.* **AP-21** (1973), 827.
3. FERENCZ, Cs.: Electromagnetic Wave Propagation in Inhomogeneous Linear Media; Thesis submitted for the degree of Candidate of Sciences, Budapest 1970, Library of the Hungarian Academy of Sciences (in Hungarian)
4. FERENCZ, Cs.: Wave Propagation in Inhomogeneous Linear Media; Acta Techn. Hung. **68** (1970), 215
5. ARNAUD, J. A.—SALEH, A. A. M.: Theorems for Bianisotropic Media; *Proc. IEEE* **60** (1972), 639
6. BUDDEN, K. G.: Radio Waves in the Ionosphere; Cambridge at the Univ. Press, 1966
7. ALLIS, W. P.—BUCHSBAUM, S. J.—BERS, A.: Waves in Anisotropic Plasmas, M. I. T. Press; Cambridge, Mass. 1963
8. ÁRKOS I. F.: Refraction Coefficient of Ionosphere; Híradástechnika, **21** (1970), 219 (in Hungarian)
9. FERENCZ, Cs.: Wave Propagation in Arbitrary Linear Media; *Acta Techn. Hung.* **71,** (1971) 109
10. KONG, J. A.—CHENG, D. K.: Modified Reciprocity Theorem for Bianisotropic Media, *Proc. IEEE,* **117,** (1970), 349
11. LINDELL, I. V.: On the Definiteness of the Constitutive Parameters of a Moving Anisotropic Medium, *Proc. IEEE,* **60** (1972), 638
12. CHENG, D. K.—KONG, J. A.: Time-Harmonic Fields in Source-Free Bianisotropic Media, *J. of Appl. Phys.,* **39** (1968), 5792
13. KONG, J. A.—CHENG, D. K.: Wave Behavior at an Interface of a Semi-Infinite Moving Anisotropic Medium, *J. of Appl. Phys.* **39** (1968), 2282.
14. CENSOR, D.: First-Order Propagation in Moving Media, *IEEE Trans. on Microwave Theory and Techn.,* MTT-16, (1968), 565
15. MIDDLETON, D.: A Statistical Theory of Reverberation and Similar First-Order Scattered Fields-Part. III. *IEEE Trans. on Inf. Theory,* IT-18 (1972), 35

16. Censor, D.: Propagation and Scattering in Radially Flowing Media, *IEEE Trans. on Microwave Theory and Techn.*, *MTT* **17**, (1969), 374
17. Novobátzky, K.: Theory of Relativity; Tankönyvkiadó, Budapest 1951 (In Hungarian)
18. Tamm, I. E.: Basic Theory of Electrodynamics, Izd. Nauka; Moscow 1966 (in Russian)
19. Synge, J. L.: Relativity, the Special Theory, North-Holland Publ. Co., Amsterdam 1965
20. Laue, M. v.: Die Relativitätstheorie, I., Fr. Vieweg und Sohn, Braunschweig 1955
21. Marx, G.: Das elektromagnetische Feld in bewegten anisotropen Medien; *Acta Phys. Hung.*, **3** (1953), 75
22. Károlyházy, F.: Personel information.
23. Ferencz, Cs.—Tarcsai, Gy.: A New Experimental Possibility of Investigating the Solar Corona: Frequency Measurements on Radio Sources when Occultated by the Sun, *Planet. Space Sci.*, **13** (1970), 1213
24. Ferencz, Cs.—Tarcsai, Gy.: Theoretical Explanation of the Solar Limb Effect, *Planet Space Sci.*, **19** (1971), 659
25. Ferencz, Cs.—Tarcsai, Gy.: Interaction of Gravitational and Electromagnetic Field or Another Effect?, *Nature*, **233** (1971) 404
26. Ferencz, Cs.—Tarcsai, Gy.: Refraction Effects due to Moving Media in Doppler Measurements, *Space Research* **12**, 595, Akademie-Verlag, Berlin 1972
27. Sadeh, D.—Knowles, S. H.—Yaplee, B. S.: Search for a Frequency Shift of the 21 centimeter Line from Taurus A Near Occultation by the Sun, *Science*, **159** (1968), 307
28. Adam, M. G.: Interferometric Measurements of Solar Wavelength and an Investigation of the Einstein Gravitational Displacement, *Mon. Not. Roy. Astron. Soc.*, **108** (1948), 446
29. Higgs, L. A.: The Solar Red-Shift, *Mon. Not. Roy. Astron. Soc.*, **121** (1960), 421
30. StJohn, C. E.: Evidence for the Gravitational Displacement of Lines in the Solar Spectrum predicted by Einstein's Theory; *Astrophys. J.*, **57** (1928), 195
31. Birkemeier, W. P.—Merril, H. S.—Sargeant, D. H.—Thomson, D. W.—Beamer, C. W.—Bergemann, G. T.: Observation of Wind-Produced Doppler-Shifts in Tropospheric Propagation, *Radio Science*, **3** (1968), 309
32. Jacobs, J. A.—Watanabe, T.: Doppler Frequency Changes in Radio Waves Propagating Through a Moving Ionosphere, *Radio Science*, **1** (1966), 257
33. Merat, P.—Pecker, J. C.—Vigier, J. P.: Possible Interpretation at an Anomalous Redshift Observed at the 2292 MHz Line Emitted by Pioneer-6 in the Close Vicinity of the Solar Limb, *Astr. Astrophys*, **30** (1974), 167
34. Chastel, A. A.—Heyvaerts, J. F.: Perturbations of Pioneer 6 Telemetry Signal During Solar Occultation, *Nature*, **249**, (1974) 21
35. Ferencz, Cs.: Wave Propagation in Inhomogeneous, Anisotropic, Time-Varying Medium, *Per. Pol. E. E.* **12** (1968), 347
36. Lovass-Nagy, V.: Matrix Calculations, Tankönyvkiadó, Budapest 1956 (in Hungarian)
37. M. Idemen: The Maxwell's Equations in the Sense of Distributions; *IEEE Trans. on Ant. and Prop.*, *AP-21* (1973), 736
38. Drahos, D.—Ferencz, Cs.—Ferencz, I.—Horváth, F.—Tarcsai, Gy.: Some Theoretical Contributions Concerning Doppler Geodetical Measurements, *Space Research* **10**, 43, North-Holland, Publ. Co., Amsterdam 1970
39. Ferencz, Cs.—Ferencz, I.—Tarcsai, Gy.: Refraction Problems and Wave Propagation in Doppler Geodetical Measurements, *Nabl. I. Sz. Z.* **9** (1970), 361
40. Ferencz, Cs.—Tarcsai, Gy.: Redshift During Pioneer-6 Solar Occultation — Unexplained or Predicted?, *Nature* **252** (1974), 615

Die Ausbreitung elektromagnetischer Wellen in inhomogenen Medien. I. Starke und schwache Inhomogenität. Die Arbeit beschäftigt sich mit einer Klassifizierung der Inhomogenitäten, welche objektiver erscheint als die bisherige. Eine allgemein anwendbare, einfache Form der Maxwellschen Gleichungen wird angegeben, welche bei der Untersuchung von Ausbreitungsfragen allgemein verwendet werden kann. Außerdem werden Varianten der Dispersionsgleichungen abgeleitet. Einige Fragen der üblichen sechsdimensionalen Untersuchungsmethode werden untersucht.

Распространение электромагнитных волн в негомогенной среде, I. Сильная и слабая негомогенность. Статья занимается вопросом отнесения негомогенностей к одному классу, которая кажется более объективной, чем применявшиеся ранее принципы. Даются простая по виду форма уравнений Максвелла, которую можно применять при исследовании вопросов распространения в общем виде, а также измененения уравнений дисперсий. Исследуются некоторые вопросы шестимерного способа обозначения.

DETERMINATION OF THE YARN FORCE ARISING IN THE BALLOON IN RING SPINNING

B. GREGA*

CAND. OF TECHN. SCI.

The author gives a formula for the determination of the yarn force valid for any point of the ring spinning balloon. In deriving the formula of the yarn force, from the forces acting on the yarn element, the centrifugal force, the air resistance and the two pulling forces at opposite directions acting on the yarn element moving in the balloon, have been taken into account. The importance of the formula lies in the fact that no means for measuring yarn force at balloon points were available so far.

The number of spindle revolutions and the frequency of yarn breakages — the latter being closely related to the former — are among the most decisive factors in ring spinning, as their influence is considerable on mill productivity. The increasing quality requirements of weaving demand yarns less uneven, i.e. reduced yarn breaking frequency, which is closely connected with higher efficiency and economy, respectively. However, the index of yarn breakages per 1000 spindle hours does not correctly express the relations of technological conditions, yarn properties and yarns breakages. In ring spinning, technological operation is mostly measured by the number of yarn breakages, and their frequency in respect to time, machine and production unit, naturally also taking into consideration the raw material generally processed. In view of rentability, but above all the quantity and quality of the yarn produced, yarn breakage frequency has to be kept as low as possible.

The frequency of yarn breakages are mostly influenced by the following factors: *a)* the unevenness of the yarn, *b)* the weakness of the fibre strand between top and bottom delivery rollers, *c)* too low or too high twist, *d)* variations in yarn force during twisting and winding-on of the yarn, respectively.

We shall determine the yarn force at an arbitrary point of the balloon taking into account the centrifugal force, from the forces acting on the yarn element the air resistance, and the pulling forces of opposite directions acting on the balloon and on the yarn element passing towards the bobbin. The weight of the yarn element and the Coriolis force being too small (of about $1,3 \cdot 10^{-3} — 1,7 \cdot 10^{-3}$) will be neglected.

* B. GREGA Németvölgyi út 22, H-1126 Budapest, Hungary

Let us choose the axis y of our coordinate system to be the axis of the spindle, and the axes x and z be in the plane of the ring. Taking into consideration the air resistance but because of it being too small, neglecting the weight of the yarn element, the centrifugal force originating from the fairly slow motion towards the yarn, and hence also the Coriolis force, we obtain for the system of differential equations of the balloon curve (Fig. 1.)
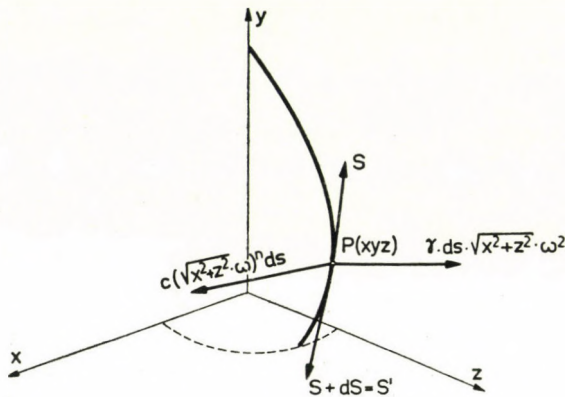
Fig. 1

$$\sigma \cdot ds \sqrt{x^2 + z^2} \cdot \omega^2 \cdot \frac{x}{\sqrt{x^2 + z^2}} + S' \cos \alpha' - S \cos \alpha + c(\sqrt{x^2 + z^2} \cdot \omega)^n ds \frac{x}{\sqrt{x^2 + z^2}} = 0 ,$$

$$S' \cos \beta' - S \cos \beta = 0 ,$$

$$\sigma \cdot ds \sqrt{x^2 + z^2} \cdot \omega^2 \frac{z}{\sqrt{x^2 + z^2}} + S' \cos \gamma' - S \cos \gamma - c(\sqrt{x^2 + z^2} \cdot \omega)^n ds \frac{x}{\sqrt{x^2 + z^2}} = 0$$

where

(x, y, z) = the coordinates of the place considered,
γ = the linear density of the yarn,
ds = the length of the yarn element,
ω = the angular velocity of the rotation round the spindle axis,
S and S' = tangential tensioning forces of different values acting on the two end points of the yarn element
α, β, γ = angles formed by the force S (and at the same time by the tangent) and the coordinate axes x, y, z
α', β', γ' = angles formed by force $S' = S + dS$ and the coordinate axes x, y, z
c = factor of proportionality of the air resistance.

Since

$$S' \cos \alpha' = (S + dS) \cos (\alpha + d\alpha) = (S + dS)(\cos \alpha \cos d\alpha - \sin \alpha \sin d\alpha) \approx$$

$$\approx (S + dS)(\cos \alpha - d\alpha \cdot \sin \alpha) =$$

$$= S \cos \alpha - S d\alpha \sin \alpha + dS \cos \alpha - dS d\alpha \sin \alpha \approx$$

$$\approx S \cos \alpha - S d\alpha \sin \alpha + dS \cos \alpha .$$

Similarly,

$$S' \cos \beta' = S \cos \beta - S d\beta \sin \beta + dS \cos \beta \,,$$

$$S' \cos \gamma' = S \cos \gamma - S d\gamma \sin \gamma + dS \cos \gamma \,.$$

Considering the above and after simplification, the system of differential equation takes the form

$$\sigma \cdot \omega^2 \cdot x \cdot ds + dS \cos \alpha - S \cdot d\alpha \cdot \sin \alpha = - c(\sqrt{x^2 + z^2} \cdot \omega)^n ds \frac{z}{\sqrt{x^2 + z^2}} \,,$$

$$dS \cos \beta - S \cdot d\beta \cdot \sin \beta = 0 \,,$$

$$\sigma \cdot \omega^2 \cdot z \cdot ds + dS \cos \gamma - S \cdot d\gamma \sin \gamma = c(\sqrt{x^2 + z^2} \cdot \omega)^n ds \frac{x}{\sqrt{x^2 + z^2}} \,.$$

From the integration of the second differential equation:

$$\int_{S=S_0}^{S} \frac{dS}{S} = - \int_{\beta=\beta_0}^{\beta} \frac{- \sin \beta}{\cos \beta} d\beta \,,$$

$$\frac{S}{S_0} = \frac{\cos \beta_0}{\cos \beta} \,,$$

$$S \cos \beta = S_0 \cos \beta_0 = S_0 \frac{V_0}{S_0} = V_0 = \text{const.,}$$

hence, the component of the yarn tension pointing to the spindle axis is constant.

Furthermore since

$$dS \cdot \cos \alpha - S \cdot d\alpha \cdot \sin \alpha = \frac{d}{dx} (S \cdot \cos \alpha) dx \,,$$

$$dS \cdot \cos \gamma - S \cdot d\gamma \cdot \sin \gamma = \frac{d}{dx} (S \cdot \cos \gamma) dx \,,$$

the first and third differential equations:

$$\sigma \cdot ds \cdot \omega^2 \cdot x + \frac{d}{dx} (S \cos \alpha) dx = - c(\sqrt{x^2 + z^2}\omega)^n \, ds \frac{z}{\sqrt{x^2 + z^2}}$$

$$\sigma \cdot ds \cdot \omega^2 z + \frac{d}{dx} (S \cos \gamma) dx = c(\sqrt{x^2 + z^2}\omega)^n \, ds \frac{x}{\sqrt{x^2 + z^2}} \,.$$

From these

$$\sigma \cdot \omega^2 x^2 \frac{ds}{dx} + x \frac{d}{dx} (S \cos \alpha) = - \sigma \cdot \omega^2 z^2 \frac{ds}{dx} - z \cdot \frac{d}{dx} (S \cos \gamma) \,,$$

$$- \sigma \cdot \omega^2 \frac{ds}{dx} (x^2 + z^2) = x \frac{d}{dx} (S \cos \alpha) + z \frac{d}{dx} (S \cos \gamma) \,.$$

Since

$$\cos \alpha = \frac{1}{\sqrt{1 + y'^2 + z'^2}},$$

$$\cos \gamma = \frac{z'}{\sqrt{1 + y'^2 + z'^2}},$$

$$\frac{d}{dx}(\cos \alpha) = -\frac{y'y'' + z'z''}{(\sqrt{1 + y'^2 + z'^2})^3},$$

$$\frac{d}{dx}(\cos \gamma) = \frac{z''(1 + y'^2 + z'^2) - z'(y'y'' + z'z'')}{(\sqrt{1 + y'^2 + z'^2})^3},$$

$$\frac{ds}{dx} = \sqrt{1 + y'^2 + z'^2}.$$

The differential equation to be solved for the yarn tension:

$$\frac{dS}{dx}(x \cos \alpha + z \cos \gamma) + S \cdot x \cdot \frac{d}{dx}(\cos \alpha) + S \cdot z \cdot \frac{d}{dx}(\cos \gamma) = - \sigma \omega^2(x^2 + z^2)\frac{ds}{dx},$$

or in detail:

$$\frac{dS}{dx}\frac{x + zz'}{\sqrt{1 + y'^2 + z'^2}} +$$

$$+ S \cdot \frac{- x(y'y'' + z'z'') + zz''(1 + y'^2 + z'^2) - zz'(y'y'' + z'z'')}{(\sqrt{1 + y'^2 + z'^2})^3} =$$

$$= - \sigma \cdot \omega^2(x^2 + z^2)\sqrt{1 + y'^2 + z'^2}.$$

Divided by

$$(x \cos \alpha + z \cos \gamma) = \frac{x + zz'}{\sqrt{1 + y'^2 + z'^2}},$$

$$\frac{dS}{dx} - S \cdot \frac{(x + zz')(y'y'' + z'z'') - zz''(1 + y'^2 + z'^2)}{(x + zz')(1 + y'^2 + z'^2)} =$$

$$= - \sigma \cdot \omega^2 \cdot (x^2 + z^2)\frac{1 + y'^2 + z'^2}{x + zz'}.$$

If

$$\frac{(x + zz')(y'y'' + z'z'') - zz''(1 + y'^2 + z'^2)}{(x + zz')(1 + y'^2 + z'^2)} = A(x),$$

$$- \sigma \cdot \omega^2(x^2 + z^2)\frac{1 + y'^2 + z'^2}{x + zz'} = F(x),$$

where except for the apex of the balloon the nominator always differs from zero, thus

$$\frac{dS}{dx} = A(x) \cdot S = F(x) .$$

The general solution of the reduced equation of

$$\frac{dS}{dx} - A(x) \cdot S = 0$$

is

$$S = C \cdot e^{\int_{x_0}^{x} A(x)dx} .$$

Solving the complete equation and integrating for the section from the yarn guide up to the point $P(xyz)$ of the balloon curve

$$S = \left(\int_{x_0}^{x} (F(x) \cdot e^{-\int_{x_0}^{x} A(x)dx} \, dx + k \right) e^{\int_{x_0}^{x} A(x)dx} .$$

In the apex of the balloon the measured peak tension is $S = S_0$, since at the point $P(xyz)$ of the space curve of the balloon the yarn tension amounts to

$$S = \left(S_0 + \int_{x_0}^{x} F(x) e^{-\int_{x_0}^{x} A(x)dx} \, dx \right) e^{\int_{x_0}^{x} A(x)dx} .$$

The convergent integrals contained in the formula are calculated from $x_0 = = 0 + \varepsilon$ up to the abscissa of the point of the balloon space curve concerned.

In the case of a plane balloon there are neither coordinate axis (z) nor coordinate planes (x, z) and (y, z) and since $z = z' = z'' = 0$,

$$A(x) = \frac{y'y''}{1 + y'^2} = \frac{1}{2} \frac{\dfrac{d}{dx}(1 + y'^2)}{1 + y'^2} ,$$

$$F(x) = - \sigma\omega^2 x(1 + y'^2) .$$

With these

$$\int_{x_0}^{x} A(x)dx =$$

$$= \frac{1}{2} \int_{x_0}^{x} \frac{\dfrac{d}{dx}(1 + y'^2)}{1 + y'^2} \, dx = \frac{1}{2} \ln (1 + y'^2) - \frac{1}{2} \ln (1 + y_0'^2) = \ln \sqrt{\frac{1 + y'^2}{1 + y_0'^2}} ,$$

$$e^{\int_{x_0}^{x} A(x)dx} = \sqrt{\frac{1 + y'^2}{1 + y_0'^2}} , \qquad e^{-\int_{x_0}^{x} A(x)dx} = \sqrt{\frac{1 + y_0'^2}{1 + y'^2}} ,$$

furthermore

$$\int_{x_0}^{x} F(x) \cdot e^{-\int_{x_0}^{x} A(x)dx} \, dx = - \sigma \cdot \omega^2 \int_{x_0}^{x} x(1 + y'^2) \sqrt{\frac{1 + y_0'^2}{1 + y'^2}} \, dx =$$

$$= - \sigma \cdot \omega^2 \int_{x_0}^{x} \sqrt{1 + y_0'^2} \cdot x \sqrt{1 + y'^2} \, dx \, .$$
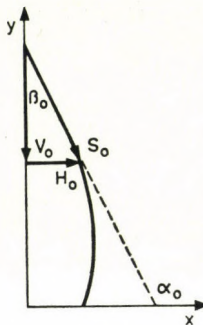
Fig. 2

With these, the yarn tension in the plane (Fig. 2.)

$$S = \left(S_0 - \sigma \cdot \omega^2 \sqrt{1 + y_0'^2} \int_{x_0}^{x} x \sqrt{1 + y'^2} \, dx \right) \sqrt{\frac{1 + y'^2}{1 + y_0'^2}} \, ,$$

or

$$\frac{S}{\sqrt{1 + y'^2}} = \frac{S_0}{\sqrt{1 + y_0'^2}} - \sigma \cdot \omega^2 \int_{x_0}^{x} x \sqrt{1 + y'^2} \, dx \, ,$$

i.e.

$$S \cos \alpha = S_0 \cos \alpha_0 - \sigma \cdot \omega^2 \int_{x_0}^{x} x \sqrt{1 + y'^2} \, dx \, .$$

Since at the yarn guide

$$\cos \alpha_0 = \frac{1}{\sqrt{1 + y_0'^2}} = \cos \left(\frac{\pi}{2} + \beta_0 \right) = - \sin \beta_0 = - \frac{H_0}{S_0}$$

hence

$$S \cos \alpha = - H_0 - \sigma \cdot \omega^2 \int_{x_0}^{x} x \sqrt{1 + y'^2} \, dx \, . \tag{1}$$

This latter formula can directly be put into the formula of the plane balloon, also taking the equation

$$\frac{d}{dx} (S \cdot \sin \alpha) = 0$$

into consideration obtained from the integration of the equilibrium equation of the plane balloon

$$S \cdot \sin \alpha = V_0 . \tag{2}$$

Namely, the quotient of the equations (1) and (2)

$$\frac{\cos \alpha}{\sin \alpha} = \frac{1}{y'} = - \frac{\sigma \cdot \omega^2}{V_0} \int_{x_0}^{x} x \sqrt{1 + y'^2} \, dx - \frac{H_0}{V_0} ,$$

whence by differentiating with respect to x the differential equation

$$\frac{y''}{y'^2} = - \frac{\sigma \cdot \omega^2}{V_0} \cdot x \cdot \sqrt{1 + y'^2}$$

is obtained, which is the differential equation of the plane balloon.

With the first integration and the initial conditions

$$- \frac{\sqrt{1 + y'^2}}{y'} = \frac{\sigma \cdot \omega^2}{2V_0} x^2 - \frac{S_0}{V_0}$$

and multiplying this by the equation

$$S \cdot \sin \alpha = S \frac{y'}{\sqrt{1 + y'^2}} = V_0$$

$$S = S_0 - \frac{\sigma \omega^2}{2} \cdot x^2 ,$$

the formula of the yarn tension of the plane balloon is obtained.

By taking the air resistance into account let us now calculate the tensioning force of the yarn at the point P_2 (4,2; 7,6; -2) of the balloon with a maximum radius. The equations of the projections can be defined on the basis of photos with the aid of the points lying on the projection curves.

In the a case of a cotton weft yarn $Nm = 60$, and at a spindle revolution of $n = 10{,}500$ rev/min, the photos for the three points of the projection curve gave:
$P_1(2{,}25; 0; 0{,}4)$, $P_2(4{,}2; 7{,}6; -2)$ and $P_3(0; 20; 0)$.
With the aid of these the equations of the projections falling onto the coordinate planes (xy) and (yz):

$$x = 2{,}25 + 0{,}4835 \, y - 0{,}0298 \, y^2,$$

$$z = 0{,}4 - 0{,}5 \, y + 0{,}024 \, y^2.$$

Thus, we have to determine the forms of the functions $A(x)$ and $F(x)$. To this, we shall determine the derived functions of the equations of the projection curves. In the first place we shall establish the equations of the bottom and top branches of the projections, respectively.

From the first equation:

$$0,0298\, y^2 - 0,4835\, y + x - 2,25 = 0$$

and

$$y_{1,2} = 8,12 \pm 5,78\, \sqrt{4,22 - x}\,.$$

In the projection plane (xy) the equation of the top branch

$$y_1 = 8,12 + 5,78\, \sqrt{4,22 - x}\,,$$

while that of the bottom branch

$$y_2 = 8,12 - 5,78\, \sqrt{4,22 - x}\,.$$

Substituting the value of $y_{1,2}$ into the second equation

$$z_{1,2} = 0,4 - 0,5\, (8,12 \pm 5,78\, \sqrt{4,22 - x}) + 0,024(8,12 \pm 5,78\, \sqrt{4,22 - x})^2$$

Accordingly, z as a function of x on the top branch:

$$z_1 = 1,325 - 0,805\, x - 0,63\sqrt{4,22 - x}\,,$$

while on the botton branch:

$$z_2 = 1,325 - 0,805\, x + 0,63\,\sqrt{4,22 - x}\,.$$

Thus, the derivatives of the top branch:

$$y_1 = 8,12 + 5,78\,\sqrt{4,22 - x}\,,$$

$$y_1' = -\frac{2,89}{\sqrt{4,22 - x}}\,,$$

$$y_1'' = -\frac{1,445}{\sqrt{(4,22 - x)^3}}\,,$$

i.e.

$$z_1 = 1,325 - 0,805\, x - 0,63\,\sqrt{4,22 - x}\,,$$

$$z_1' = -0,805 + \frac{0,315}{\sqrt{4,22 - x}}\,,$$

$$z_1'' = -\frac{0,157}{\sqrt{(4,22 - x)^3}}\,.$$

With the aid of $y(x)$ and $z(x)$, i.e. together with their derivatives the functions $A(x)$ and $F(x)$ can be calculated.

$$A(x) = \frac{(x + zz')(y'y'' + z'z'') - zz''(1 + y'^2 + z'^2)}{(x + zz')(1 + y'^2 + z'^2)} =$$

$$= \frac{4,2295 - 0,1265\,\sqrt{4,22 - x}}{(4,22 - x)15,42 - 1,65\, x - 0,413\,\sqrt{4,22 - x}} -$$

$$- \frac{0,24 - 0,1265\, x - 0,099\,\sqrt{4,22 - x}}{(4,22 - x)(1,65\, x - 1,263)\,\sqrt{4,22 - x} + 2,547 - 0,76\, x}\,.$$

Thus

$$\int_{x_0}^{x} A(x)dx = -4,7678\,.$$

Now we shall set up the function $F(x)$ for the top branch of the balloon:

$$F(x) = -\sigma \cdot \omega^2 (x^2 + z^2) \frac{1 + y'^2 + z'^2}{x + zz'} =$$

$$= -0{,}19104208(1{,}645x^2 - 2{,}525x + 3{,}4 -$$

$$-0{,}65\sqrt{4{,}22 - x}) \frac{1{,}65(4{,}22 - x) + 8{,}45 - 0{,}413\sqrt{4{,}22 - x}}{(1{,}65x - 1{,}263)(4{,}22 - x) + 0{,}507\sqrt{(4{,}22 - x)3} + (0{,}417 - 0{,}253x)\sqrt{4{,}22 - x}}$$

hence

$$\int_{x_0}^{x} F(x)dx = 13{,}38268 .$$

Under processing, the tension in the cotton weft yarn $Nm = 60$ at $n = 10500$ rev/min spindle revolutions and at $So = 13{,}3$ g peak tension is, at the point $P_2(4{,}2; 7{,}6; -2)$, of the balloon with the highest radius

$$S = (13{,}3 + 13{,}38268 \cdot e^{4{,}7679}) \cdot e^{-4{,}7679} = \frac{13{,}3}{e^{4{,}7679}} + 13{,}38268 = 0{,}114 + 13{,}38268 =$$

$$= 13{,}49668 \approx 13{,}5 \text{ grs} .$$

The yarn tension is affected by the yarn count. Under equal spinning conditions the tension arising in finer yarn counts is lower than that in courses counted ones.

The highest influence exerted on yarn tension is that of the number of spindle revolutions. The tensioning force increases rapidly with the square of the number of spindle revolutions. Hence, increased number of spindle revolutions leads to a higher tension and thus to more yarn breakages, unless higher quality and/or of improved composition materials can be processed.

REFERENCES

1. BANKE, K. H.: *Deutsche Textiltechnik,* **11**, 10 (1960)
2. WEGENER, W.—PEUCKER, R.: Textil Praxis, Stuttgart, 1955
3. DE BARR, A. E.: *Textile Manufacturer* **87** (1961), No. 1034.
4. GRISHIN, P. F.: *Platts Bulletin* **9**, 219—236
5. GREGA, B.: Thesis for candidature, Budapest 1973

Bestimmung der Fadenkraft im Ballon beim Ringspinnen. Der Verfasser gibt eine Formel für die Bestimmung der Fadenkraft in jedem Punkt des Ringspinnballons bekannt. Bei der Ableitung der Fadenkraft wurden von den auf das Fadenelement wirkenden Kräften die Zentrifugalkraft, der Luftwiderstand und die zwei entgegengesetzt gerichteten Zugkräfte am im Ballon sich bewegenden Fadenelement in Betracht gezogen. Die Bedeutung der vom Verfasser angegebenen Formel liegt darin, daß nach unseren Kenntnissen die Fadenkraft nicht gemessen werden kann.

Определение усилия пряжи, возникающего в баллоне при кольцепрядении. Автор дает формулу, пригодную для вычисления усилия пряжи в произвольной точке баллона кольцепрядения. При выводе формулы усилия пряжи из числа усилий, воздействующих на элемент пряжи, автор учитывает центробежную силу, сопротивление воздуха и два растягивающих усилия противоположного направления, действующих на движущийся элемент пряжи. Приведенная автором формула является значительной вследствие того, что в точках баллона на основе существовавших до сих пор сведениям нельзя измерить усилие пряжи.

THE FUNCTIONS OF FLOTATION PLANT DESIGN AND PROCESS CONTROL

SZ. PETHŐ*

DOCTOR OF TECHN. SCI.

By using the experimental results of one single cell of operational dimensions the separation functions of flotation systems, thus their mass yield, their component yields and their composition can be determined. The functions are suitable for the designing, the optimization and the process control of flotation systems. The practical application is demonstrated on the calculation of the separation parameters of sulfide copper ore flotation systems.

1. Introduction

With a cell of volume v, discontinuous feed, and based on a test of duration T, the separation functions of a flotation plant with continuous feeding consisting of cells of volume v a T flotation time can be deduced, if during the experiment several products are produced and if their mineral composition is determined at the time of feeding.

2. Evaluation of experimental results

The results of the experiments carried out with one single cell are summed up in Fig. 1. In the experiments a number of p products has been made. The gangue remaining in the cell is the product p. The mass yield of the product l is M_l ($l = 1, 2, \ldots, p$), the flotation time is t_l. The further parts of the table show the mineral composition. The product contains a n mineral: the mass proportion of the mineral i in the product l is $m_i^{(l)}$ ($i = 1, 2, \ldots, n$). The mass proportion of the mineral i in the feed is m_i. The relations between the direct measurements recorded in the Table are

$$\sum_{l=1}^{p} M_l = 1 \, , \tag{1}$$

$$T = \sum_{l=1}^{p-1} t_l \, , \tag{2}$$

* Dr. Sz. PETHŐ, Ásványelőkészítési Tanszék H-3515 Miskolc-Egyetemváros, Hungary

$$\sum_{i=1}^{n} m_i^{(l)} = 1 \; ; \quad l = 1, 2, \ldots, p \; , \tag{3}$$

$$\sum_{i=1}^{n} m_i = 1 \; , \tag{4}$$

$$\sum_{l=1}^{p} m_i^{(l)} M_l = m_i \; ; \quad i = 1, 2, \ldots, n \; . \tag{5}$$
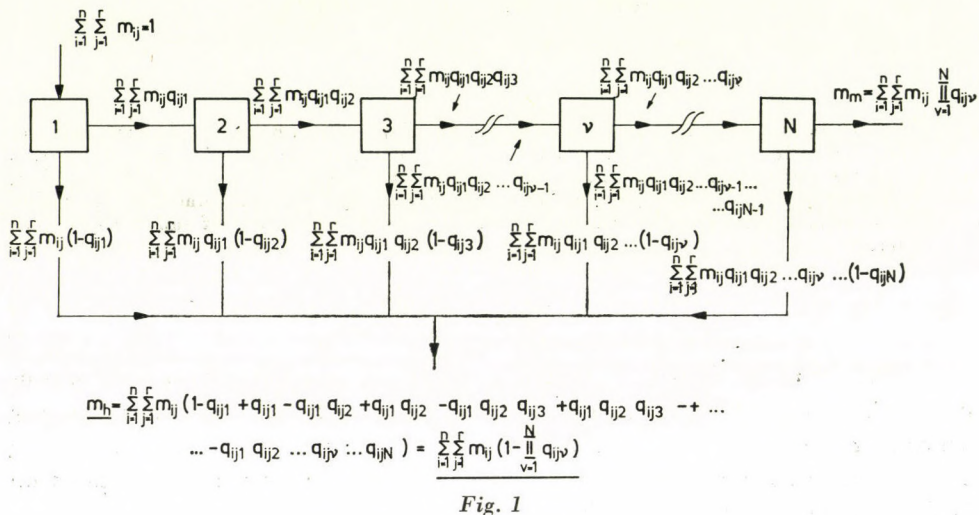
Fig. 1

The component yield of mineral i in the product l is

$$k_i^{(l)} = M_l \, \frac{m_i^{(l)}}{m_i} \; ; \quad i = 1, 2, \ldots, n; \quad l = 1, 2, \ldots, p \; . \tag{6}$$

The relation between the component yields is

$$\sum_{l=1}^{p} k_i^{(l)} = 1 \; ; \quad i = 1, 2, \ldots, n \; . \tag{7}$$

With aid of the values $k_i^{(l)}$ the constituent yield function of each mineral can be plotted. The functions follow some kinetic equation. — The results of the flotation can always be described by the kinetic equation of the first order [2], [3], [8], [9], [10]. It is useful in such cases to represent the yields on logarithmic ordinates. With such a representation the yield function of any one mineral is not always a straight, as the mineral content of the raw material m_i consists of parts with different flotation tendencies. By a construction due to KELSALL [2], [3] the parts with equal flotation tendency

can be separated. The mineral of mass fraction m_i can be separated into r parts, for the yield of the jth part of the ith mineral the well-known relation stands

$$k_{ij} = 1 - e^{-\lambda_{ij}t} ; \quad i = 1, 2, \ldots, n ; \quad j = 1, 2, \ldots, r , \tag{8}$$

λ_{ij} is the flotation tendency. Its reciprocal $(1/\lambda_{ij})$ is the mean flotation time of the mineral grains with equal flotation tendency, if the experiment is continued until the separation of the last mineral grain [1]. The composition of the raw material charged to the flotation cell can be given by minerals, within that according to the flotation characteristics [6].

$$\sum_{i=1}^{n} \sum_{j=1}^{r} m_{ij} = 1 . \tag{9}$$

3. Separation functions of flotation plants

The separation functions of flotation plants can be separated with the aid of Fig. 1 [6]. In the figure N cells of volume v m³ each are connected in series [7]. The feed is V m³/h of pulp.

The flotation time T_1 of the first cell is

$$T_1 [\text{min}] = 60 \frac{v}{V} . \tag{10}$$

In the froth product of this cell the yield p_{ij1} of jth fraction of the ith mineral is

$$p_{ij1} = 1 - \exp(-\lambda_{ij}T_1) . \tag{11}$$

In the inert product the yield q_{ij1} of the same product is

$$q_{ij1} = 1 - p_{ij1} = \exp(-\lambda_{ij}T_1) . \tag{12}$$

The mass yields m_{h1} and m_{m1} of the froth and gange products for the first cell, are

$$m_{h1} = \sum_{i=1}^{n} \sum_{j=1}^{r} m_{ij}(1 - q_{ij1}) , \tag{13}$$

$$m_{m1} = \sum_{i=1}^{n} \sum_{j=1}^{r} m_{ij}q_{ij1} . \tag{14}$$

The second cell is fed with less pulp, therefore, the flotation time will be longer. If the density of the pulp remains unchanged (from now on this will be assumed) the flotation time in the second cell is

$$T_2 = 60 \frac{v}{V \sum_{i=1}^{n} \sum_{j=1}^{r} m_{ij}q_{ij1}} . \tag{15}$$

If the pulp density changes, the flotation time T_2 will differ from the foregoing value, but will be proportional to it.

The mass yield of the two products of the second cell is

$$m_{h2} = \sum_{i=1}^{n} \sum_{j=1}^{r} m_{ij} q_{ij1} (1 - q_{ij2}) , \qquad (16)$$

and

$$m_{m2} = \sum_{i=1}^{n} \sum_{j=1}^{r} m_{ij} q_{ij1} q_{ij2} . \qquad (17)$$

The flotation time T_ν of the νth cell and the two yields $(m_{h\nu}, m_{m\nu})$ are

$$T_\nu = 60 \, \frac{\nu}{V \sum_{i=1}^{n} \sum_{j=1}^{r} m_{ij} q_{ij1} q_{ij2} \cdots q_{ij\nu-1}} \qquad (18)$$

and

$$m_{h\nu} = \sum_{i=1}^{n} \sum_{j=1}^{r} m_{ij} q_{ij1} q_{ij2} \cdots q_{ij\nu-1} (1 - q_{ij\nu}) , \qquad (19)$$

$$m_{m\nu} = \sum_{i=1}^{n} \sum_{j=1}^{r} m_{ij} q_{ij1} q_{ij2} \cdots q_{ij\nu} . \qquad (20)$$

The values $q_{ij\nu}$ are the cell yields. From them the Tromp curve of any flotation cell can be constructed [4], [5].

The mass yield of the froth product of the flotation plant is, in the sense of the summation, shown on Fig. 1:

$$m_h = \sum_{i=1}^{n} \sum_{j=1}^{r} m_{ij} \left(1 - \prod_{\nu=1}^{N} q_{ij\nu} \right) . \qquad (21)$$

The mass yield of the gangue is

$$m_m = \sum_{i=1}^{n} \sum_{j=1}^{r} m_{ij} \prod_{\nu=1}^{N} q_{ij\nu} . \qquad (22)$$

The mineral contents b_i and c_i of the concentrate and the gangue are

$$b_i = \frac{1}{m_h} \sum_{r=1}^{r} m_{ij} \left(1 - \prod_{\nu=1}^{N} q_{ij\nu} \right) \qquad (23)$$

and

$$c_i = \frac{1}{m_m} \sum_{j=1}^{r} m_{ij} \prod_{\nu=1}^{N} q_{ij\nu} . \qquad (24)$$

The mineral yields k_i and K_i are the following:

$$k_i = \frac{1}{m_i} \sum_{j=1}^{r} m_{ij} \left(1 - \prod_{\nu=1}^{N} q_{ij\nu} \right) \tag{25}$$

and

$$K_i = \frac{1}{m_i} \sum_{j=1}^{r} m_{ij} \prod_{\nu=1}^{N} q_{ij\nu} \,. \tag{26}$$

For the deduced separation functions there is

$$m_h + m_m = 1 \,, \tag{27}$$

$$\sum_{i=1}^{n} b_i = 1 \,, \quad \sum_{i=1}^{n} c_i = 1 \,, \tag{28}$$

and

$$k_i + K_i = 1 \,; \quad i = 1, 2, \ldots, n \,. \tag{29}$$

The flotation time of the row of cells and the mean flotation time $\overline{T}$ of a simple cell are

$$T = \sum_{\nu=1}^{N} T_v \quad \text{and} \quad \overline{T} = T/N \,. \tag{30}$$

If the useful mineral content of the flotated raw material and with this the mass yield of the concentrate are small, the flotation times T_ν and the cell yields $q_{ij\nu}$ $(\nu = 1, 2, \ldots, N)$ are practically equal. In this case the mass yield m_h of the concentrate will be, considering the equal cell yields $q_{ij1} = q_{ij2} = \ldots = q_{ijN} = q_{ij}$

$$m_h = \sum_{i=1}^{n} \sum_{j=1}^{r} m_{ij} \left(1 - q_{ij}^{N} \right) \,. \tag{31}$$

Correspondingly the other separation function can also be calculated.

4. Practical application

Table 2 shows the results of a flotation experiment with chalcopyritic-pyritic ore [11], [12].

The product was analyzed for Cu and Fe (columns 4 and 5), and from the results the chalcopyrite, the pyrite and the gangue contents were determined. $m_1 = 0{,}0166$, $m_2 = 0{,}0897$ and $m_3 = 0{,}8937$. From the mineral contents (columns 6, 7, 8) the yields (columns 9, 10, 11) can be calculated. In Fig. 2 the yield function of the chalcopyrite has been plotted. With the graphical method shown in the figure the chalcopyrite can be separated into three parts accord-

Table 1

Evaluation of Experimental Results

Product	Mass part	Flotation time	Mineral composition	
			1. Mineral	
1.	2.	3.	4.	5.
1. Product	M_1	t_1	$m_1^{(1)}$	$k_1^{(1)}$
2. Product	M_2	t_2	$m_1^{(2)}$	$k_1^{(2)}$
$\vdots$	$\vdots$	$\vdots$	$\vdots$	$\vdots$
l. Product	M_l	t_l	$m_1^{(l)}$	$k_1^{(l)}$
$\vdots$	$\bullet$	$\vdots$	$\vdots$	$\vdots$
p. Product	M_p	—	$m_1^{(p)}$	$k_1^{(p)}$
Feed	1	T	m_1	1

Table 2

Evaluation of flotation

Product	Mass yield	Flotation Time min.	Metal Content	
			Cu	Fe
1.	2.	3.	4.	5.
$K_1 + K_2$	0,1038	10	0,0420	0,1212
$K_3 + K_4$	0,1518	20	0,0130	0,1846
$K_5 + K_6$	0,1870	20	0,0058	0,1029
Gangue	1,0000	—	0,00070	0,0268
Material		50	0,00574	0,0468

Table 3

Mass Yields m_{ij}, Flotation Tendencies

Chalcopyrite			Pyrite
Mass Proportion	Flotation Tendency	Cell Yield	Mass Proportion
1.	2.	3.	4.
$m_{11} = 0,00966$	$\lambda_{11} = 0,5640$	$q_{111} = 0,5222$	$m_{21} = 0,0296$
$m_{12} = 0,00385$	$\lambda_{12} = 0,1077$	$q_{121} = 0,8833$	$m_{22} = 0,0601$
$m_{13} = 0,00309$	$\lambda_{13} = 0,0128$	$q_{131} = 0,9854$	
$m_1 = 0,01660$			$m_2 = 0,0897$

Obtained with One Flotation Cell

$(m_i^{(l)})$ and yield $(k_i^{(l)})$

2. Mineral		i. Mineral		n. Mineral	
6.	7.	8.	9.	10.	11.
$m_2^{(1)}$	$k_2^{(1)}$	$m_i^{(1)}$	$k_i^{(1)}$	$m_n^{(1)}$	$k_n^{(1)}$
$m_2^{(2)}$	$k_2^{(2)}$	$m_i^{(2)}$	$k_i^{(2)}$	$m_n^{(2)}$	$k_n^{(2)}$
$\vdots$	$\vdots$	$\vdots$	$\vdots$	$\vdots$	$\vdots$
$m_2^{(l)}$	$k_2^{(l)}$	$m_i^{(l)}$	$k_i^{(l)}$	$m_n^{(l)}$	$k_n^{(l)}$
$\vdots$	$\vdots$	$\vdots$	$\vdots$	$\vdots$	$\vdots$
$m_2^{(p)}$	$k_2^{(p)}$	$m_i^{(p)}$	$k_i^{(p)}$	$m_n^{(p)}$	$k_n^{(p)}$
m_2	1	m_i	1	m_n	1

experiments

Mineral Content			Mineral Yields		
Chalcopyrite	Pyrite	Gangue	Chalcopyrite	Pyrite	Gangue
6.	7.	8.	9.	10.	11.
0,1212	0,1810	0,6978	0,758	0,210	0,081
0,0376	0,3714	0,5910	0,867	0,408	0,113
0,0167	0,2096	0,7737	0,902	0,491	0,143
0,00202	0,0562	0,9418	1,000	1,000	1,000
0,0166	0,0897	0,8937			

q_{ij1} and Cell Yields q_{ij1}

		Gangue		
Flotation Tendency	Cell Yield	Mass Proportion	Flotation Tendency	Cell Yield
5.	6.	7.	8.	9.
$\lambda_{21} = 0{,}08140$	$q_{211} = 0{,}9105$	$m_{31} = 0{,}0554$	$\lambda_{31} = 0{,}30400$	$q_{311} = 0{,}7045$
$\lambda_{22} = 0{,}00585$	$q_{222} = 0{,}9933$	$m_{32} = 0{,}8383$	$\lambda_{32} = 0{,}00188$	$q_{321} = 0{,}9978$
		$m_3 = 0{,}8937$		

16

ing to its flotability $(0{,}5819 \cdot 0{,}0166 = 0{,}00\,966, \ldots,)$. The figures for the two other yields are not published here. The resulting mass proportions m_{ij} and flotation tendencies λ_{ij} are listed in Table 3.

The cell volume v is 16 m³, the pulp volume feed is $V = (5/6)10^3\ m^3/h$; $T_1 = 1{,}152$ min. With the flotation tendency λ_{ij} and the flotation time T the cell yields q_{ij1} which can be calculated; they are also shown in Table 3. Let us choose a $N = 48$ cells.

Table 4 shows the mass yield of the concentrate, the mineralic composition of the three products (feed, concentrate and gangue) and their mass yields.

The calculation based on the corresponding relations have been carried out on a computer. The separation functions of the flotation systems can be calculated for any cell circuit.

$$CuFeS_2 : \quad \begin{aligned} m'_{11} &= 0{,}5819 \\ m'_{12} &= 0{,}2319 \\ m'_{13} &= \underline{0{,}1861} \\ &\ 0{,}9999 \end{aligned}$$
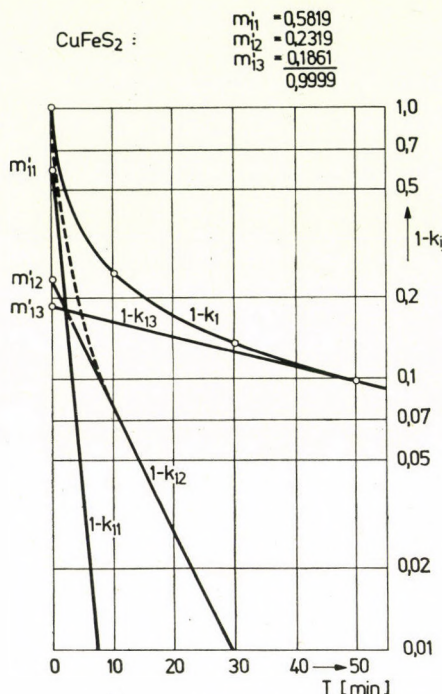
Fig. 2

Table 4

Separation Parameters of Flotation Plant ($N = 48$, $T = 64{,}846$ min)

Separation parameters		Feed	Concentration	Gangue
1.		2.	3.	4.
Mass yield		1,—	0,2153	0,7847
Mineral Composition	Chalcopyrite	0,0166	0,0708	0,0017
	Pyrite	0,0897	0,2249	0,0526
	Gangue	0,8937	0,7043	0,9457
	Total	1,0000	1,0000	1,0000
Mineral Yields	Chalcopyrite	1,—	0,9186	0,0814
	Pyrite	1,—	0,5398	0,4602
	Gangue	1,—	0,1696	0,8304

5. Some conclusions

With the separation functions flotation systems can be designed, using the experiments made with one single cell of operational size. Designing is aimed at determining the connection of the cells, the masses of final and intermediate products, their qualities and their yields. With the functions optimization is also possible if the purpose is the production of products with fixed quality and yields, or if the purpose is the fulfillment of a contract between the mine and the siderurgical plant with maximum economical profit and minimum investment costs (e.g. minimum number of cells).

In case of such aims the functions are also suitable for realizing process control with computers.

REFERENCES

1. Pethő, Sz.: Investigation of the Velocity Equations Describing Flotation Processes (in Hungarian). *Oszt. Közl.* **35** (1965), 99—106
2. Kelsall, F. D.: Application of Probability in the Assessment of Flotation Systems. *Bull. of the Inst. of Mining and Metallurgy*, (1961), No. 650, 191—204
3. Tarján, G.: Mineral Preparation (in Hungarian). Manuscript. Tankönyvkiadó, Budapest 1974
4. Steiner, H. J.: Zur Frage einer Projektierung von Flotationsanlagen auf flotationskinetischer Grundlage. 2. Arbeitstagung des Fachausschusses für Erzaufbereitung der Ges. Deutscher Metallhütten- und Bergleute, 1971 Oct. 14—16, Hameln/Weser.
5. Steiner, H. J.: Das Flotationsverhalten verwachsener Körner aus kinetischer Sicht, *Berg- u. Hüttenmännische Monatshefte*, **118** (1963), 245—251
6. Pethő, Sz.—Tompos, E.—Böhm, J.: Functions of the Optimum Designing and Process Control of Flotation Systems (in Hungarian). Manuscript.
7. Schuber, H.: Aufbereitung fester mineralischer Rohstoffe. Band II, VEB Deutscher Verlag f. Grundstoffindustrie, Leipzig 1967
8. Panu, H.: Beitrag betreffend Gleichungen und Methoden zur Berechnung der Flotationsergebnisse, *IX. Internat. Kongress für Aufbereitung der mineralischen Rohstoffe*, Praha 1960, 123—132 *(Rudy)*.
9. Ek, G.: Cinétique de flotation (études en laboratoires — essais industriels), *IXème Congrès international de la préparation des minerais*, Praha 1970, 115—121 *(Rudy)*.
10. Inoue, T.—Imaizumi, T.: Some Aspects of the Flotation Kinetics, *VIII. Internat. Mineral Processing Congress*, Leningrad 1968, 15
11. Budai, L.: Diplome Project. Manuscript, 1976.
12. Szigeti, L.: Diplome Project. Manuscript, 1976.

Die Funktionen der Planung und Prozeßsteuerung von Flotationsanlagen. Unter Verwendung der Versuchsergebnisse einer einzigen Zelle von Betriebsausmaßen können die Separationsfunktionen von Flotationsanlagen, d. h. die Massenausbringung der Endprodukte, ihre Bestandteilausbringungen und ihre Zusammensetzungen, abgeleitet werden. Die Funktionen eignen sich für den Entwurf, die Optimierung und die Prozeßsteuerung von Flotationsanlagen. Die praktische Anwendung wird für die Berechnung der Separationsparameter eine Flotationsanlage für sulfidisches Kupfererz gezeigt.

Функции проектирования и управления процессами работы флотационных агрегатов. Путем использования экспериментальных результатов одной единственной секции производственных масштабов можно вывести функции разделения флотационных агрегатов, т. е. определить массовые выходы конечных продуктов, выходы компонентов и состав конечных продуктов. Выведенные функции пригодны для проектирования, оптимизации и управления процессами работы флотационных агрегатов. Практическое применение демонстрируется в статье вычислением параметров разделения флотационного агрегата, пригодного для флотации сульфидной медной руды.

AN ESTIMATION OF THE TORSIONAL STIFFNESS OF A PRISMATIC BAR OF HETEROGENEOUS MATERIAL AND SOLID CROSS SECTION

I. ECSEDI*

The present paper treats the generalization of one of the results of J. BARTA, who deduced the lower and upper bounds for the estimation of the torsional stiffness of prismatic bars made of homogeneous material and having solid cross section. In the paper the extensions of these bounds to prismatic bars of heterogeneous material is dealt with.

The following symbols are used in this paper:

x, y orthogonal coordinates,

i, j unit vectors of system of coordinates xy,

T simply connected domain in plane xy, cross section of torsioned prismatic bar,

g boundary of T, smooth (at least by sections smooth) rectifiable closed curve,

R torsional stiffness of cross section,

$\nabla = \dfrac{\partial}{\partial x} i + \dfrac{\partial}{\partial y} j$ Hamilton's differential operator,

$\Delta = \nabla \cdot \nabla$ Laplace operator,

$\cdot$ designs scalar product of two vectors,

γ smooth closed curve,

D region surrounded by curve γ,

$\dfrac{\partial}{\partial s}$ derivative calculated along the tangent of boundary curve,

$\dfrac{\partial}{\partial n}$ derivative calculated along the normal unit vector n of the boundary curve,

s arc coordinate interpreted on the boundary curve,

$u = u(x, y)$ two-variable function,

u_0 value of u on the boundary curve g,

$H = -\nabla \cdot \left(\dfrac{\nabla u}{G}\right)$ auxiliary function,

T_i $(i = 1, 2, \ldots \ldots n)$ domain in plane xy,

$g_i = g_{i0} + \Sigma g_{ij}$ boundary of T_i,

g_{i0} part of boundary T_i falling on boundary g of region $T = T_1 + T_2 + \ldots$,

g_{ij} curve separating regions T_i and T_j,

G_i shear modulus of elasticity of material within region T_i.

It is well known that the torsional problem of a prismatic bar of heterogeneous material having a solid cross section $G = G(x,y)$ shown in Fig. 1, represents the following boundary value problem [1]:

To be determined in the closed domain $T + g$ continuous function which satisfies in region T the partial differential equation

$$\nabla \cdot \left(\frac{1}{G} \nabla F\right) = -2, \quad P \in T, \tag{1}$$

* Dr. I. ECSEDI, Vászonfehérítő u. 24, IV/1., H-3531, Miskolc, Hungary

and on the boundary of region T, on the curve g the homogeneous boundary condition

$$F = 0, \qquad P \in g .$$ (2)

By knowing the solution of the boundary value problem established by Eqs (1) and (2), the torsional stiffness R of the cross section may be calculated with the aid of the formula

$$R = 2 \int_T F dT .$$ (3)
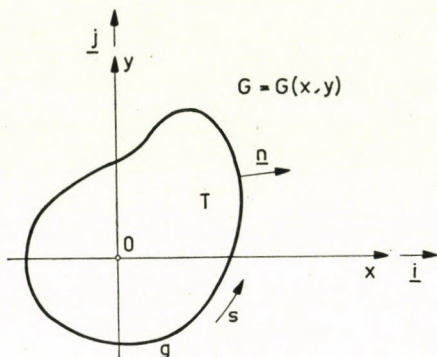
Fig. 1. Solid cross section
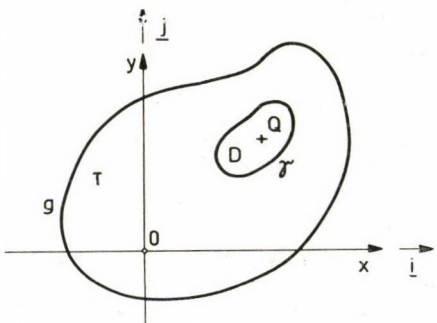
Fig. 2. Drawing to verification of $F \geq 0$, $P \varepsilon T$

First it will be pointed out that the consequence of Eqs (1) and (2) is the validity of the inequality

$$\frac{1}{G} \frac{\partial F}{\partial n} \leq 0 , \qquad P \in g$$ (4)

at the points of the boundary curve g. The verification will be carried out in two steps. First, it will be proved that F is not negative in T, i.e.

$$F \geqslant 0 , \qquad P \in T .$$ (5)

Let us assume that in T there is a point S where F is negative. In this case, due to the continuity of F the point Q has, in all events, a neighbourhood defined by a closed curve γ (Fig. 2) where F is negative, i.e.,

$$F < 0, \qquad P \in D + \gamma .\tag{6}$$

Herein, D denotes the region in plane xy bordered by the curve γ. After the *Gaussian* integral transformation and simultaneous application of the rules of product derivation the following identity might be deduced:

$$\int_D \frac{(\nabla F)^2}{G}\, dT = 2\int_D F dT + \int_\gamma \frac{1}{G}\frac{\partial F}{\partial n}\, F ds .\tag{7}$$

The left-hand side of Eq. (7) always being positive, equality may only exist (due to the assumption $F < 0$, $P \in D + \gamma$ being true), if the condition

$$\frac{1}{G}\frac{\partial F}{\partial n} \leqslant 0, \quad P \in \gamma\tag{8}$$

is fulfilled at the points of curve γ. In turn, from (8) it follows that $F = F(x,y)$ does not increase in the direction n (see Fig. 2), thus, the region D where $F < 0$, may be extended to the region T, but $F = 0$ $P \in g$ and thus on the basis of (8) may be written

$$\int_T \frac{(\nabla F)^2}{G}\, dT = 2\int_T F dT .\tag{9}$$

By this equation, being the left-hand side positive and the right-hand side negative, we arrived to a contradiction. Therefore, our basic condition was faulty, thus

$$F \geqslant 0, \qquad P \in T .\tag{10}$$

The second part of the verification presents itself immediately from Eqs (2) and (10). Since F is not negative in T and at the boundary T is equal to zero, in the direction of n (n being the normal of the curve g), proceeding toward the curve g, $F = F(x, y)$ surely does not increase, accordingly ($G > 0$) at the points of the curve g it is true that

$$\frac{1}{G}\frac{\partial F}{\partial n} \leqslant 0, \quad P \in g .\tag{11}$$

Be the function $u = u(x,y)$ continuous in the region $T + g$ and twice continuously derivable in T. Let us express the value of $u = u(x,y)$ on the

boundary curve g by the function $u_0 = u_0(x, y)$. The maximum of u_0 is designated by $u_{0\max}$ and its minimum by $u_{0\min}$. Let the following identity be considered

$$- 2F\nabla \cdot \left(\frac{1}{G} \nabla u \right) = 2 \left[- \nabla \cdot \left(\frac{1}{G} \nabla F \right) \right] (u - u_{0\max}) +$$
$$+ 2 \left\{ (u - u_{0\max}) \left[\nabla \cdot \left(\frac{1}{G} \nabla F \right) \right] - F\nabla \cdot \left[\frac{1}{G} \nabla (u - u_{0\max}) \right] \right\}. \tag{12}$$

For transforming Eq. (12), the Eq. (15) derivable from Eqs (13) and (14) may be used:

$$\int_T F\nabla \cdot \left(\frac{1}{G} \nabla v \right) dT = - \int_T \frac{\nabla v \cdot \nabla F}{G} dT + \int_g F \frac{\partial v}{\partial n} \frac{1}{G} ds, \tag{13}$$

$$\int_T v\nabla \cdot \left(\frac{1}{G} \Delta F \right) dT = - \int_T \frac{\nabla v \cdot \nabla F}{G} dT + \int_g v \frac{\partial F}{\partial n} \frac{1}{G} ds, \tag{14}$$

$$\int_T v\nabla \cdot \left(\frac{1}{G} \nabla F \right) dT - \int_T F\nabla \cdot \left(\frac{1}{G} \nabla v \right) dT =$$
$$= \int_g v \frac{1}{G} \frac{\partial F}{\partial n} ds - \int_g F \frac{1}{G} \frac{\partial v}{\partial n} ds. \tag{15}$$

From Eq. (12) by integration extended to T, and by application of the identity (15) to the function

$$v = u - u_{0\max} \tag{16}$$

may arrived to Eq. (17)

$$- 2 \int_T \left[\nabla \cdot \left(\frac{1}{G} \nabla u \right) \right] F dT = 4 \left(\int_T u dT - u_{0\max} T \right) +$$
$$+ 2 \int_g (u_0 - u_{0\max}) \frac{1}{G} \frac{\partial F}{\partial n} ds. \tag{17}$$

For writing down Eq. (17) the fact has been utilized that $F = F(x, y)$ is the solution of the boundary value problem designated by Eqs (1) and (2). Be

$$H = H(x, y) = - \nabla \cdot \left(\frac{1}{G} \nabla u \right) \tag{18}$$

and let us denote by $H_{\max}$ the highest value of H in region T. By application of the inequalities

$$- 2 \int_T \left[\nabla \cdot \left(\frac{1}{G} \nabla u \right) \right] F dT \leqslant H_{\max} \int_T 2 F dT \,, \tag{19}$$

and

$$(u_0 - u_{0\max}) \frac{1}{G} \frac{\partial F}{\partial n} \geqslant 0 \,, \qquad P \in g \tag{20}$$

and by taking into account Eq. (17), the inequality describing the torsional stiffness may readily be written down as:

$$H_{\max} R \geq 4 \left(\int_T (u dT - u_{0\max} T) \right) . \tag{21}$$

By a similar consideration, with the aid of the function

$$v = u - u_{0\min} \tag{22}$$

the inequality

$$H_{\min} R \leqslant 4 \left(\int_T u dT - u_{0\min} T \right) \tag{23}$$

may be established as characterizing the torsional stiffness, wherein $H_{\min}$ is the lowest value of the function $H = H(x,y)$ in the region T. The inequalities (21) and (23) are the generalization of the result deduced by J. BARTA to the prismatic bar made of homogeneous material and having a solid cross section. By way of verification the method described in [3] by J. BARTA has essentially been followed.

Now, it will be pointed out that the pair of inequalities (21), (23) might also be used for the estimation of the torsional stiffness of a prismatic bar composed of combined materials.

In the case of a prismatic bar made of combined materials, in the sub-region T_i of the cross section the material has a shear modulus of elasticity G_i. From G_i one assumes that in T_i it is constant. In case of this constraint, the solution of the torsion problem involves the following boundary value problem [2]:

The following function $F_i = F_i(x,y)$ is to be determined which is continuous in the region $T_i + g_i$ and which satisfies in T_i the partial differential equation

$$\Delta F_i = - 2G \,, \qquad P \in T \,, \tag{24}$$

in region T_i, g_{i0} border falling on the boundary curve g the homogeneous boundary condition

$$F_i = 0 \,, \qquad P \in g_{i0} \,, \tag{25}$$

and at the points of the smooth (at least by sections smooth) curve g_{ij} separating the regions T_i and T_j, the fitting condition

and

$$F_i = F_j, \quad P \in g_{ij} \tag{26}$$

$$\frac{1}{G_i} \frac{\partial F_i}{\partial n} = \frac{1}{G_j} \frac{\partial F_j}{\partial n}, \quad P \in g_{ij} \tag{27}$$
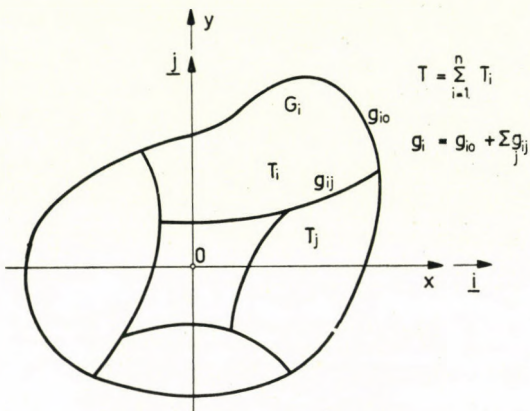
Fig. 3. Prismatic bar of composite material

(see Fig. 3). Recognizing the solution of the boundary value problem $F_i (i = 1, 2, \ldots \ldots n)$ defined by (24), (25), (26), (27), the torsional stiffness of the cross section may be determined from the formula

$$R = 2 \sum_{i=1}^{n} \int_{T_i} F_i dT . \tag{28}$$

From the structure of the boundary value problem defined by (24), (25), (26), (27) it follows that the estimation which may be given by (21) and (23) remains valid if one interpretes the function in the region T_i as

1. $u_i = u_i(x, y), \quad P \in T_i + g_i$

are continuous in $T_i + g_i$ and

2. $u_i = u_i(x, y)$

is, at least, twice continuously derivable in T_i

3. $u_i = u_j, \quad P \in g_{ij}, \tag{29}$

4. $\frac{1}{G_i} \frac{\partial u_i}{\partial n} = \frac{1}{G_j} \frac{\partial u_j}{\partial n}, \quad P \in g_{ij}. \tag{30}$

In the case, H_{max} denotes the highest value of the expression $H_i =$ $= -\Delta u_i / u_i \, (i = 1, 2, \ldots \ldots n)$ in the region $T = T_1 + T_2 + \ldots \ldots + T_n$, and H_{min} designates the minimum value of the expression $H_i = -\Delta u_i / u_i$, in the region $T = T_1 + T_2 + \ldots \ldots T_n$. Further u_{0min} designates the lowest value of $u_i (i = 1, 2, \ldots, n)$ and u_{0max} designates the highest value of u_i $(i = 1, 2, \ldots n)$ along the boundary curve

$$g = g_{10} + g_{20} + \ldots \ldots + g_{n0} \, .$$
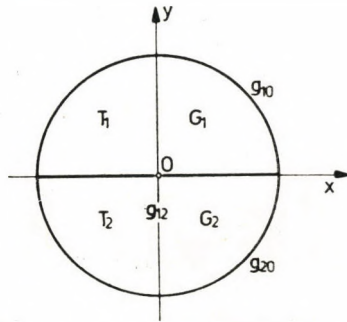
Fig. 4. Solid circular cross section of composite material

In the following the estimation of the torsional stiffness of a prismatic bar of heterogeneous material and a solid cross section will be demonstrated.

The estimation of the torsional stiffness of the solid cross section depicted in Fig. 4 will be discussed. In the region T_1 of the cross section a material of a shear modulus of elasticity G_1 and in the region T_2 that of G_2 is to be found. Be

$$G_1 = 1 \, , \quad G_2 = 2 \, .$$

The function

$$u = x^2 + y^2 = \begin{cases} u_1 = u_1(x, y) \, , & P \in T_1 \\ u_2 = u_2(x, y) \, , & P \in T_2 \end{cases} \tag{31}$$

satisfies the fitting conditions (26) and (27) prescribed along the curve g_{12}, thus, with its aid bounds might be formed for the torsional stiffness of the cross section. To the above function, according to (18), the following $H =$ $= H(x, y)$ is associated:

$$H = H(x, y) = \begin{cases} -4 \, , & P \in T_1 \, , \\ -2 \, , & P \in T_2 \, , \end{cases} \tag{32}$$

further

$$u_{0min} = u_{0max} = 1 \, . \tag{33}$$

With these values, and by making use of (21) and (23) the lower and upper bounds (limits) are obtained

$$R < \pi = 3{,}14159 \,, \tag{34}$$

$$R > 0{,}5\pi = 1{,}57079 \tag{35}$$

respectively, for the torsional stiffness R. Let us consider the function

$$u = 1 - (x^2 + y^2) = \begin{cases} u_1 = u_1(x, y) \,, & P \in T_1 \,, \\ u_2 = u_2(x, y) \,, & P \in T_2 \,, \end{cases} \tag{36}$$

as satisfying the fitting conditions (26) and (27). The $H = H(x,y)$ associated to the above function will be

$$H = H(x, y) = \begin{cases} 3 \quad, & P \in T_1 \,, \\ 1{,}5 \,, & P \in T_2 \,, \end{cases} \tag{37}$$

and, in the case discussed

$$u_{0\min} = u_{0\max} = 0 \,. \tag{38}$$

On the basis of the above results in (36), (37), (38), from the inequalities (21), (23) the estimations

$$R < 1{,}3333\pi = 4{,}18889 \,, \tag{39}$$

$$R > 0{,}6666\pi = 2{,}09439 \tag{40}$$

may be deduced for the torsional stiffness.

Lastly, taking the functions

$$u_1 = u_1(x, y) = 1 - (x^2 + y^2) - \frac{1}{8}(y - x^2 y - y^3) \,, \quad P \in T_1 \,, \tag{41}$$

$$u_2 = u_2(x, y) = 1 - (x^2 + y^2) - \frac{1}{4}(y - x^2 y - y_3) \,, \quad P \in T_2 \tag{42}$$

as starting points the lower and upper bound for R can be established.

The $u_i (i = 1,2)$ functions under (41) and (42) satisfy the fitting conditions prescribed to the curve g_{12}. These functions are associated with the following $H = H(x,y)$ function

$$H = H(x, y) = \begin{cases} 3 - y \,, & P \in T_1 \\ 2 - y \,, & P \in T_2 \,. \end{cases} \tag{43}$$

Thus, we have

$$H_{\max} = 3, \quad H_{\min} = 2 \tag{44}$$

and

$$u_{0\min} = u_{0\max} = 0 \,. \tag{45}$$

By evolving in detail the inequalities (21) and (23) to the upper and lower bounds are arrived at

$$R < 3{,}698 \,, \tag{46}$$

$$R > 2{,}4666 \tag{47}$$

respectively, to the torsional stiffness. Taking (47) and (34) into account, yields

$$2{,}4666 < R < 3{,}1416 \,. \tag{48}$$

The arithmetical mean of the lower and upper limit entering in the inequalities (48) will be

$$R^* = 2{,}804 \tag{49}$$

which may differ from the exact value of the torsional stiffness of the cross section no more than $0{,}5(3{,}1416 - 2{,}466) = 0{,}338$.

REFERENCES

1. С. Г. ЛЕХНИЦКИЙ: Кручение анизотропных и неоднородных стержней. Физ-мат. Лит. Москва 1971.
2. Н. Х. АРУТЮНЯН, Б. Л. АБРАМЯН: Кручение упруих мел. Физ.-Мат. Лит. Москва 1963.
3. Barta, J.: On the Estimation of Torsional Rigidity. Nederl. Akademie Van Wetenschappen. Amsterdam Series B. 58. No. 1 1955 Pp. 80—99.

Eine Schätzungsmethode zur Ermittelung der Verdrehungssteifigkeit eines prismatischen Stabes mit Vollquerschnitt aus heterogenem Material. Die Verallgemeinerung eines Ergebnisses von J. Barta wird behandelt. J. Barta hat nämlich zur Abschätzung der Verdrehungssteifheit eines aus homogenem Material hergestellten prismatischen Stabes untere und obere Grenzen abgeleitet. In dieser Abhandlung werden diese Grenzen auf prismatische Stäbe aus heterogenem Material erstreckt.

Об одном способе оценки жесткости на кручение призматического стержня из гетерогенного материала, имеющего сплошное сечение. Данная статья посвящена обобщению результатов, достигнутых Й. Барта. Статья занимается распространением нижних и верхних ограничений, выведенных Й. Барта для оценки жесткости на кручение призматического стержня из гомогенного материала со сплошным сечением, на случай призматического стержня из гетерогенного материала.

INDEX

Printed in Hungary

SZENDY, K.: *Planning of Optimal Investment Capacities for Interconnected Power Systems Using Probabilistic Constrained Programming*

By means of probabilistic constrained programming the paper gives a useful tool for determining the optimal enlargement of generating and transfer capacities in an interconnected system. In the described method the instantaneous transfer powers are eliminated. The admissibility and reliability of the power supply are investigated by generation and interconnection constraints. The available generating and transfer capacities, as well as the peak load deviations are considered as random variables. In addition to technical constraints the optimization process contains the prescribed reliability level as a lower limit Furthermore, the cost of load shedding can also be taken into consideration. The method is illustrated by a simple example.

LUKÁCS, J.—GADÁNYI, P.: *Preliminary Study of the Interactions of Low Energy Oxigen Ions with Solid Carbon and Platinum Targets*

The aim of this study was to show the possibility of measuring the energy distribution of charged particles produced by the interaction of low energy oxygen ions with carbon. The oxygen ions were produced by a Kistemaker-ionsource working with a hot cathode Penning-discharge. In a first step the beam was not mass-analyzed and the measurements were made only in the pressure range of 10^{-5}—10^{-6} torr. Authors succeeded in producing an oxygen ion beam having, first about 45 eV and now about 15 eV kineti energy, with 20—30 nA intensity. They made preliminary measurements with an 45 eV oxygen ion beam. The targets were outgassed on the temperature of about 1000 °C for several hours in high vacuum. Short discussion of the results of the calculated energy distributions of the backscattered charged particles from carbon and platinum targets, and of the possible reaction mechanisms will be given.

KINZE, M.: *Investigation of Soil Mechanics on an Economical Design of Technology for the Construction and Compaction of Dams.*

Earth dams should, in all phases of construction and in all of its working conditions have a satisfactory stability safety. Besides, the deformations resulting from the effects of the dead weight and water pressure should not challange the correct function of the dams, in particular, their watertightness, watertight joints and protective layers. The paper deals with these problems on the basis of laboratory and field tests.
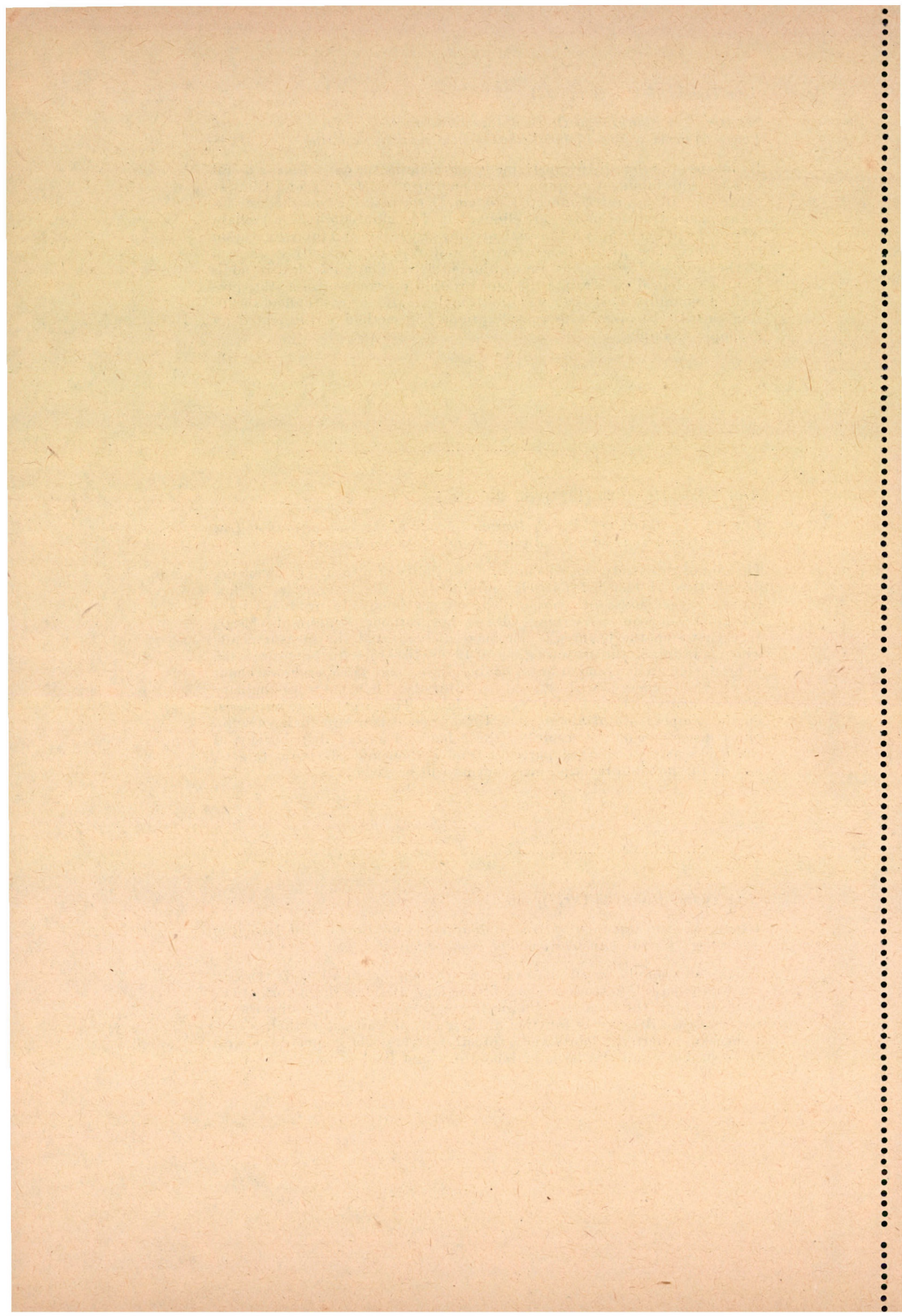
Acta Techn. Hung. **85** (1977), pp. 281—305

BERCELI, T.: *Large Signal Properties of Injection Locked Diode Oscillators*

A large signal model is used to investigate the properties of injection locked diode oscillators. Relations between the input and output signals are derived and used, to determined the locking band. It is shown that the locking band is shifted to lower frequencies as the diode susceptance non-linearity is increased. Transmission characteristics such as output power and phase, further group delay time, AM-to-PM conversion and AM compression are determined. Frequency dependence of the parameters is investigated of different values of input power, load and diode susceptance non-linearity. This latter parameter has the effect of causing unsymmetry, resulting in the lowest distortion at a frequency which is higher than the band centre.

Acta Techn. Hung. **85** (1977), pp. 307—320

ABDEL—MONEIM—HAMOUDA: *A Comparative Experimental Study of the Accuracy and Precision of Measurements of External Screw Threads by Different Methods*

The main objective of this paper is to compare experimentally among three methods applied for measuring the effective diameter of external screw threads namely, the optical, optical with knife edge and the three wire method regarding — a) the degree of accuracy and b) the degree of the result computed from the measurements taken by each method on a screw threads plug gauge. The three methods are different and each has its own caused system of erros, both the controllable and uncontrollable errors inherent in the measuring system of each method.

Acta Techn. Hung. **85** (1977), pp. 321—334

ANTAL, K. G.—GÁTI, E.: *The Excitation Mechanism of the $6^I D_2$ Level of Hg Atoms in the Positive Column of a Low-Pressure Mercury-Argon-Discharge*

In the paper the radial structure of the positive column of a discharge in $6 \cdot 10^-$, Torr Hg vapour and 2,5 Torr Ar working gas in investigated experimentally and theoretically. The assumed plasma model is checked by probe measurements, and by a spectroscopic method, the radial distribution of the intensity of the 579,1 nm wavelength line is determined. As an evaluation of the obtained profile the ratio of the direct and the indirect processes is determined using a simple population model. The dependence of this ratio from the microparameters of the discharge and the integrated transition probabilities has been calculated.

Acta Techn. Hung. **85** (1977), pp. 335—338

GREGA, B.: *Determination of the Equation of the Balloon Plane Curve in Ring Spinning Taking the Weight of the Yarn Into Consideration*

The author set up the system of differential equations of the plane balloon by taking into cinsideration the tensioning forces of opposite directions acting at the two end points of the yarn element. As there is no possibility for a solution in a closed form, expansion in series is suggested for defining the equation of the plane balloon.

*Acta Techn. Hung.* **85** (1977), pp. 339—347

PETHŐ SZ.: *The Error Functions and the Most Favourable Measuring Conditions for Mass Yield and Component Yield.*

The main parameters for evaluating the separation operations are the mass yield, the component yield and the efficiency. Their functions can be calculated by using the law of error propagation. By fixing the errors of the parameters the accuracy of product analysis can also be deduced.

Acta Techn. Hung. **85** (1977), pp. 349—376

DULÁCSKA, E.—JANKÓ, L.: *Membrane Forces and Membrane Deflections of Flat Elliptic Paraboloid Shells Subjected to Uniformly Distributed Horizontal Load at the Edges.*

An analytic method of solution of the membrane stress pattern and membrane deflections of flat elliptic paraboloid shells subjected to uniformly distributed horizontal edge load is presented. The functions describing the worked out also in graphic form in order to make easier the calculation by hand. It has been theory also the internal forces and deflections of the elliptic paraboloid shells supported by edge beams having non negligible flexural and torsional stiffnesses in the horizontal plane can be analyzed in an approximate way.
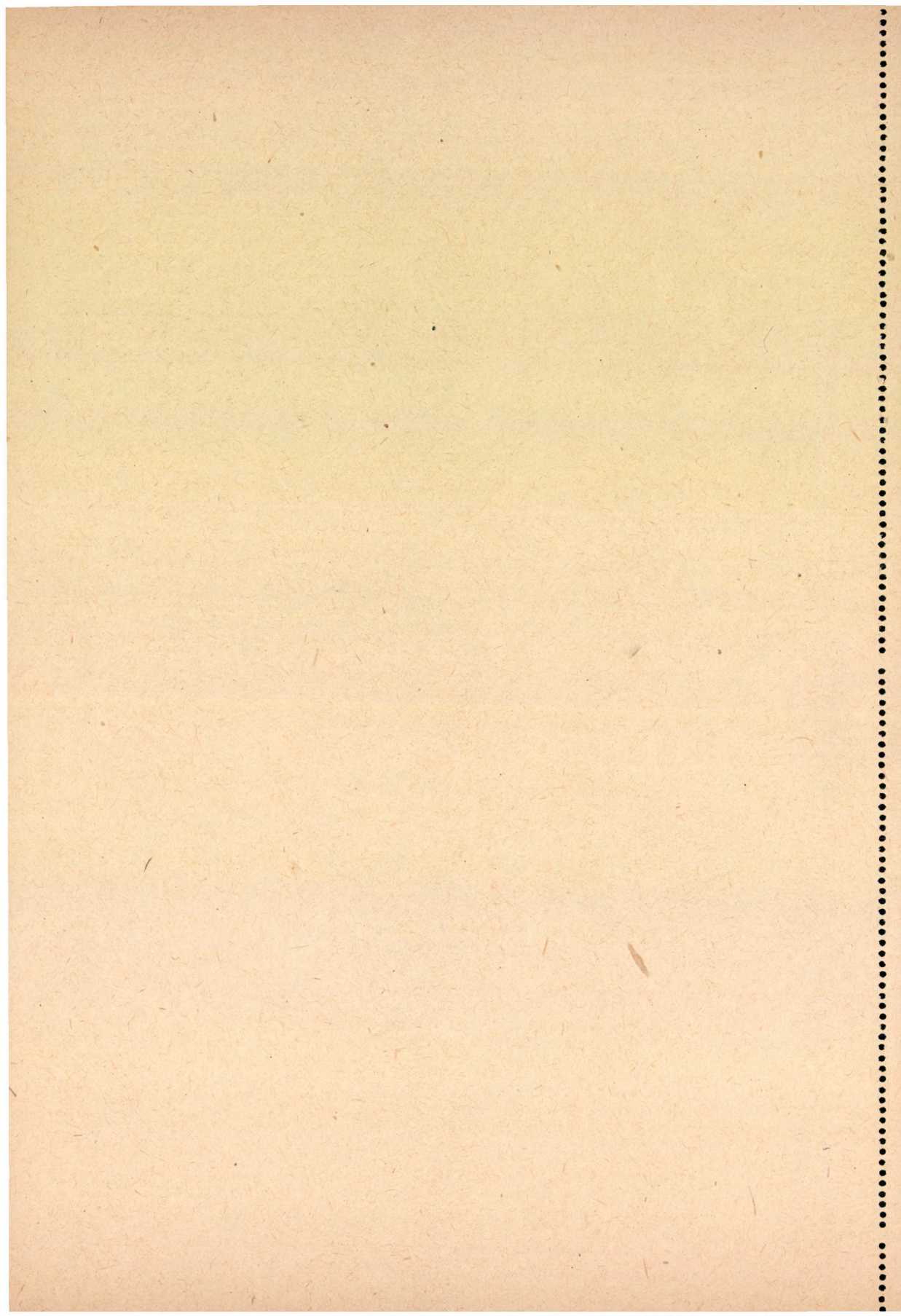
GÁDOR, L.: *Some Problems of Mains Voltage Regulation in L. T.*

In relatively sparsely populated settlements large voltage drops may arise in the long radial lines of the secondary network. This fact justifies voltage regulation. If an extended system is regulated in one point, a multi-step or a continuous regulator has no advantages, a two-step regulator is completely satisfactory. If the feeding point voltage varies too, a two-parameter regulation must be applied with simultaneous sensing of the current and the voltage. A relatively large feeding point voltage variation can be eliminated only with a regulator placed in the feeding point and here multi-step or continuous regulation is justified.

ECSEDI, I.: *A Remark on the Upper Limit of the Torsional Stiffness of Prismatic Bars*

The present paper deals with the torsional stiffness of the simply consistent region of rectifiable border curve and with the generalization of an inequality concerning the basic frequency of an oscillating membrane extended to the same bordering curve.

JÁNDY, G.: *Recognizing and Utilizing Heuristic Rules in the Problemsolving of Operations Research*

In the present paper the author wants to show — referring also to his earlier heuristic algorithms — that the school-examples of operational research teaching often imply much more inner bounds than is expressed by the more general model of the type of problem. Also the finding of the optimum solution in these models may be too expensive considering the importance of the task and even with increasing number of variables and conditions relatively soon the models get practically unolvables. But with recognizing better the type of problem, a deeper analysis usually shows such heuristic rules by which the optimum solutions of such problems can be approximated very well. The author proves this assumption by *heuristic algorithmus* elaborated for two different types of problems *(production programming of several periods and planning of the sequence of passing through a bottleneck)*. In-between it is possible to gain insight into the mental laboratory of heuristics.
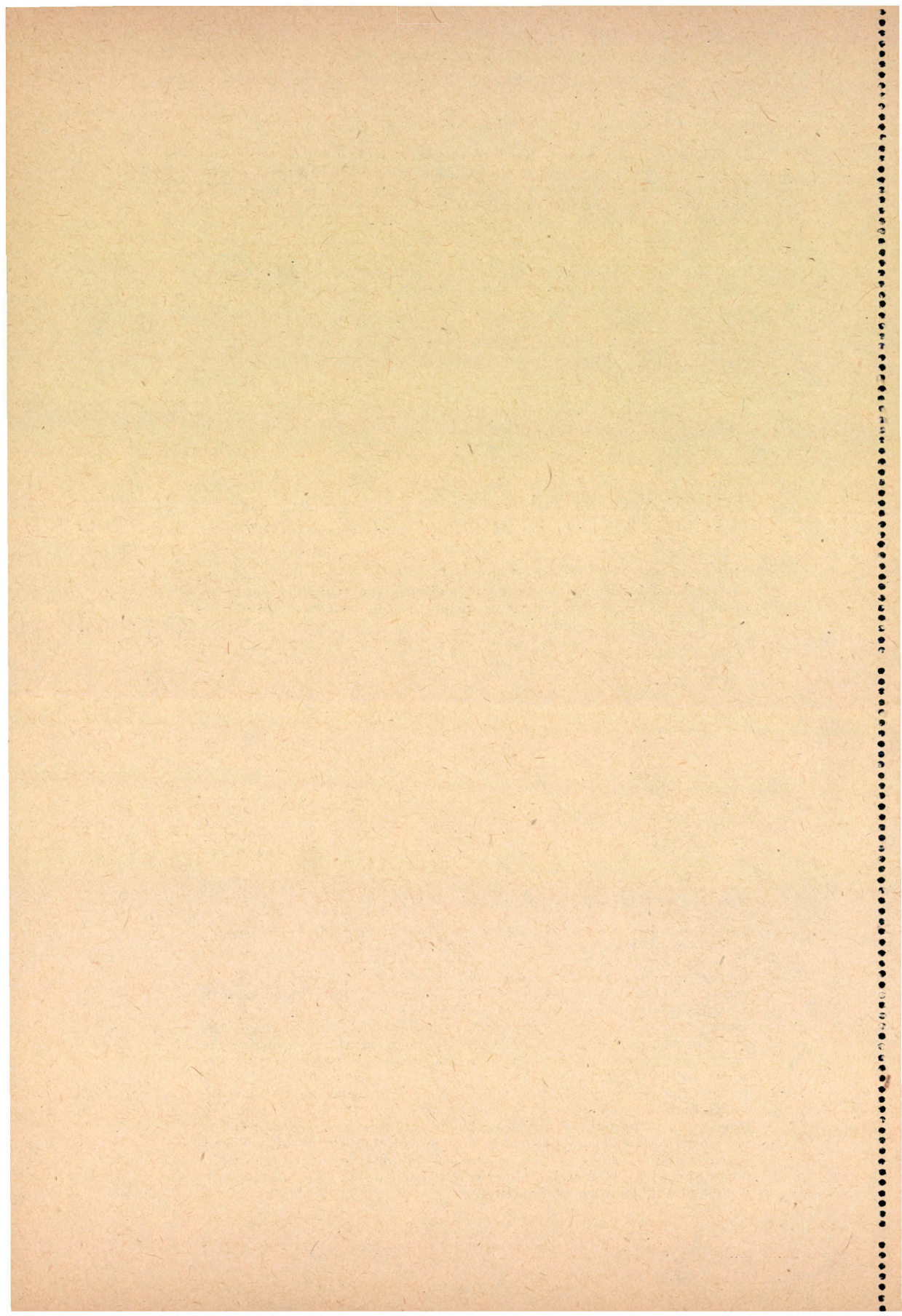
GRÓSZ, M.: *Automated Designing with Integer Programming*

In this paper the authors presents a possible model for the general solution of automated designing. The design problem is defined as follows: a design of a structure with given geometry and composed from a given stock of elements is locked for, where for the elements the equilibrium, compatibility and limiting conditions are fulfilled and where the structure is optimum from some point of view (weight, cost, or their ratio). For the problem thus defined the mathematical model for linear limiting conditions is established and then it is extended to the case of non-linearity. In both cases the problems are reduced to that of a "0—1" integer programming task to which the enumerative method can be applied. For this method the inversion of a large matrix would be necessary. A solution method is shown for avoiding this.

FERENCZ, Cs.: *Electromagnetic Wave Propagation in Inhomogeneous Media: Strong and Weak Inhomogeneities*

The paper deals with a classification of the inhomogeneities in a way which seems to be more objective than the earlier methods. It gives a simple form for Maxwell's equations which means general usability in examination of propagation, and also gives variations for the dispersion equations, investigating several questions of the commonly used method of 6-dimensional designation.

GREGA, B.: *Determination of the Yarn Force Arising in the Balloon in Ring Spinning*

The author gives a formula for the determination of the yarn force valid for any point of the ring spinning balloon. In deriving the formula of the yarn force, from the forces acting on the yarn element, the centrifugal force, the air resistance and the two pulling forces at opposite directions acting on the yarn elements moving in the balloon, have been taken into account. The importance of the formula lies in the fact that no means for measuring yarn force at balloon points were available so far.
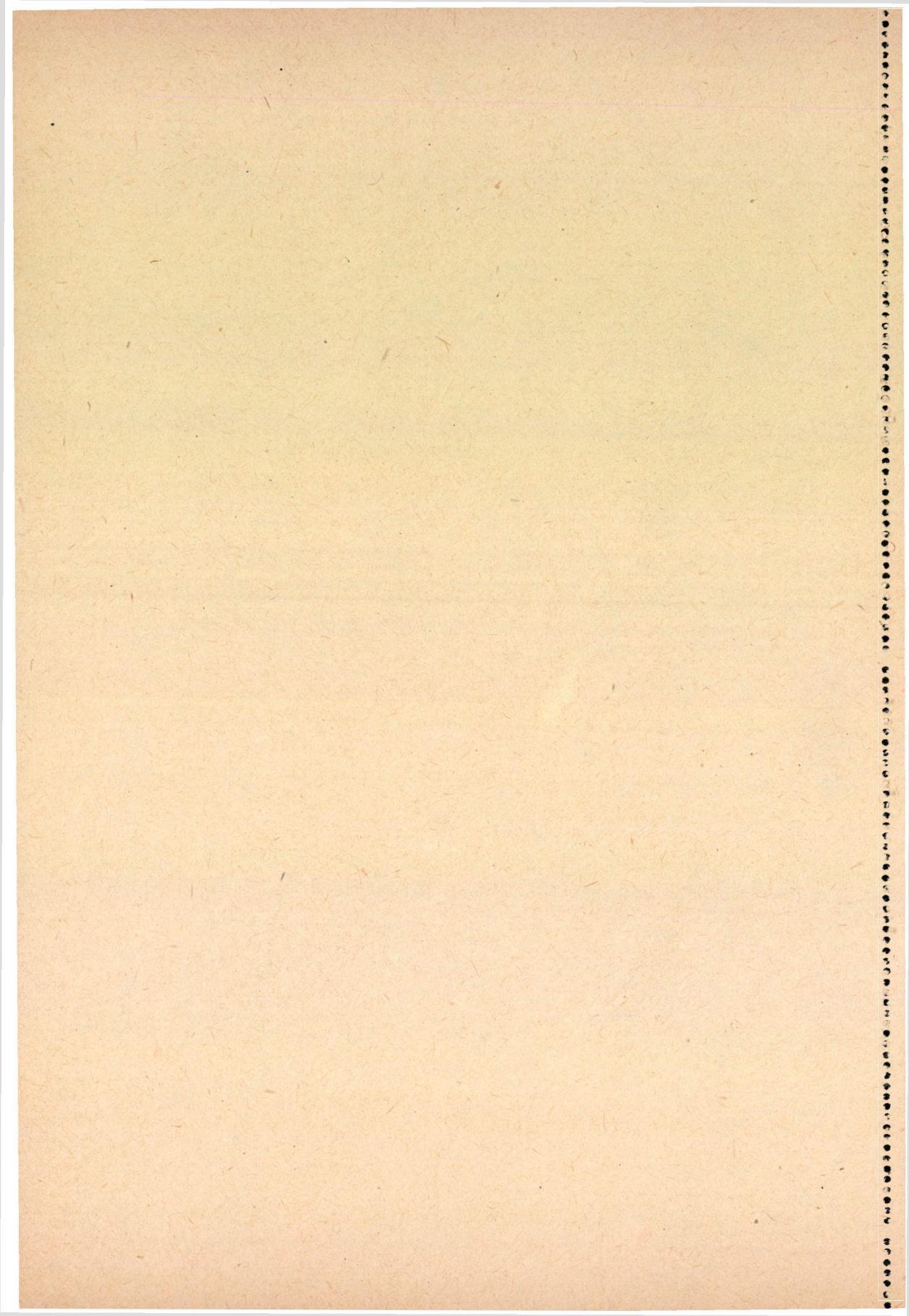
PETHŐ, Sz.: *The Functions of Flotation Plant Design and Process Control*

By using the experimental results of one single cell of operational dimensions the separation functions of flotation systems, thus their mass yield, their component yields and their composition can be determined. The functions are suitable for the designing, the optimization and the process control of flotation systems. The practical application is demonstrated on the calculation of the separation parameters of sulfide copper ore flotation systems.

ECSEDI, I.: *An Estimation of the Torsional Stiffness of a Prismatic Bar of Heterogeneous Material and Solid Cross Section*

The present paper treats the generalization of one of the results of J. BARTA, who deduced the lower and upper bounds for the estimation of the torsional stiffness of prismatic bars made of homogeneous material and having solid cross section. In the paper the extensions of these bounds to prismatic bars of heterogeneous material is dealt with.

The *Acta Technica* publish papers on technical subjects in English, French, German and Russian.

The *Acta Technica* appear in parts of varying size, making up one volume.

Manuscripts should be addressed to

Acta Technica
1051 Budapest
Münnich Ferenc u. 7.
Hungary

Correspondence with the editors and publichers should be sent to the same address, Subscription rate: $ 36.00 a volume.

Orders may be placed with "Kultura" Foreign Trading Company (1389 Budapest 62, P. O. B. 149. Account No. 218 10990) or its representatives abroad.

Les *Acta Technica* paraisent en français, allemand, anglais et russe et publient des travaux du domaine des sciences techniques.

Les *Acta Technica* sont publiés sous forme de fascicules qui seront réunis en volumes.

On est prié d'envoyer les manuscrits destinés à la rédaction à l'adresse suivante:

Acta Technica
1051 Budapest
Münnich Ferenc u. 7.
Hongrie

Toute correspondance dait être envoyée à cette même adresse.

Le prix de l'abonnement: $ 36.00 par volume.

On peut s'abonner à l'Entreprise du Commerce Extérieur «Kultura» (1389) Budapest 62, P. O. B. 149. Compte courant No. 218-10990) on chez représentants à l'étranger.

«*Acta Technica*» публикуют трактаты из области технических наук на русском, немещном, английском и французском языках.

«*Acta Technica*» выходят отдельными выпусками разного объема. Несколько выпусков составляют один том.

Предназначенные для публикации рускописи следует направлять по адресу:

Acta Technica
1051 Budapest
Münnich Ferenc u. 7.
Венгрия

По этому же адресу направлять всякую корреспонденцию для редакции и администрации.

Подписная цена — $ 36.00 за том. Заказы принимает предприятие по внешней торговле «Kultura» (1389 Budapest 62, P. O. B. 149 Текущий счет № 218 10990) или его заграничные представительства и уполномоченные.

Reviews of the Hungarian Academy of Sciences are obtainable at the following addresses:

AUSTRALIA
C.B.D. LIBRARY AND SUBSCRIPTION SERVICE, Box 4886, G.P.O., *Sydney N.S.W. 2001*
COSMOS BOOKSHOP, 135 Ackland Street, *St. Kilda (Melbourne), Victoria 3182*

AUSTRIA
GLOBUS, Höchstädtplatz 4, *1200 Wien XX*

BELGIUM
OFFICE INTERNATIONAL DE LIBRAIRIE, 30 Avenue Marnix, *1050 Bruxelles*
LIBRAIRIE DU MONDE ENTIER, 162 Rue du Midi, *1000 Bruxelles*

BULGARIA
HEMUS, Bulvar Ruszki 6, *Sofia*

CANADA
PANNONIA BOOKS, P.O. Box 1017, Postal Station "B", *Toronto, Ontario M5T 2T8*

CHINA
CNPICOR, Periodical Department, P.O. Box 50, *Peking*

CZECHOSLOVAKIA
MAD'ARSKÁ KULTURA, Národní třida 22, *115 66 Praha*
PNS DOVOZ TISKU, Vinohradská 46, *Praha 2*
PNS DOVOZ TLAČE, *Bratislava 2*

DENMARK
EJNAR MUNKSGAARD, Norregade 6, *1165 Copenhagen*

FINLAND
AKATEEMINEN KIRJAKAUPPA, P.O. Box 128, *SF-00101 Helsinki 10*

FRANCE
EUROPERIODIQUES S. A., 31 Avenue de Versailles, *78170 La Celle St. Cloud*
LIBRAIRIE LAVOISIER, 11 rue Lavoisier, *75008 Paris*
OFFICE INTERNATIONAL DE DOCUMENTATION ET LIBRAIRIE, 38 rue Gay-Lussac, *75240 Paris Cedex 05*

GERMAN DEMOCRATIC REPUBLIC
HAUS DER UNGARISCHEN KULTUR, Karl-Liebknecht-Strasse 9, *DDR-102 Berlin*
DEUTSCHE POST ZEITUNGSVERTRIEBSAMT, Strasse der Pariser Kommüne 3—4, *DDR-104 Berlin*

GERMAN FEDERAL REPUBLIC
KUNST UND WISSEN ERICH BIEBER, Postfach 46, *7000 Stuttgart 1*

GREAT BRITAIN
BLACKWELL'S PERIODICALS DIVISION, Hythe Bridge Street, *Oxford OX1 2ET*
BUMPUS, HALDANE AND MAXWELL LTD., Cower Works, *Olney, Bucks MK46 4BN*
COLLET'S HOLDINGS LTD., Denington Estate, *Wellingborough, Northants NN8 2QT*
W.M. DAWSON AND SONS LTD., Cannon House, *Folkestone, Kent CT19 5EE*
H. K. LEWIS AND CO., 136 Gower Street,
London WC1E 6BS

GREECE
KOSTARAKIS BROTHERS, International Booksellers, 2 Hippokratous Street, *Athens-143*

HOLLAND
MEULENHOFF-BRUNA B.V., Beulingstraat 2, *Amsterdam*
MARTINUS NIJHOFF B.V., Lange Voorhout 9—11, *Den Haag*

SWETS SUBSCRIPTION SERVICE, 347b Heereweg, *Lisse*

INDIA
ALLIED PUBLISHING PRIVATE LTD., 13/14 Asaf Ali Road, *New Delhi 110001*
150 B-6 Mount Road, *Madras 600002*
INTERNATIONAL BOOK HOUSE PVT. LTD., Madame Cama Road, *Bombay 400039*
THE STATE TRADING CORPORATION OF INDIA LTD., Books Import Division, **Chandralok** 36 Janpath, *New Delhi 110001*

ITALY
EUGENIO CARLUCCI, P.O. Box 252, *70100 Bari*
INTERSCIENTIA, Via Mazzé 28, *10149 Torino*
LIBERIA COMMISSIONARIA SANSONI, Via Lamarmora 45, *50121 Firenze*
SANTO VANASIA, Via M. Macchi 58, *20124 Milano*
D. E. A., Via Lima 28, *00198 Roma*

JAPAN
KINOKUNIYA BOOK-STORE CO. LTD., 17-7 Shinjuku-ku 3 chome, Shinjuku-ku, *Tokyo 160-91*
MARUZEN COMPANY LTD., Book Department, P.O. Box 5056 Tokyo International, *Tokyo 100-31*
NAUKA LTD. IMPORT DEPARTMENT, 2-30-19 Minami Ikebukuro, Toshima-ku, *Tokyo 171*

KOREA
CHULPANMUL, *Phenjan*

NORWAY
TANUM-CAMMERMEYER, Karl Johansgatan 41—43, *1000 Oslo*

POLAND
WĘGIERSKI INSTYTUT KULTURY, Marszalkowska 80, *Warszawa*
CKP I W ul. Towarowa 28 *00-958 Warsaw*

ROMANIA
D. E. P., *Bucureşti*
ROMLIBRI, Str. Biserica Amzei 7, *Bucureşti*

SOVIET UNION
SOJUZPETCHATJ — IMPORT, *Moscow*
and the post offices in each town
MEZHDUNARODNAYA KNIGA, *Moscow G-200*

SPAIN
DIAZ DE SANTOS, Lagasca 95, *Madrid 6*

SWEDEN
ALMQVIST AND WIKSELL, Gamla Brogatan 26, *101 20 Stockholm*
GUMPERTS UNIVERSITETSBOKHANDEL AB Box 346, *401 25 Göteborg 1*

SWITZERLAND
KARGER LIBRI AG, Petersgraben 31, *4011 Basel*

USA
EBSCO SUBSCRIPTION SERVICES, P.O. Box 1943, *Birmingham, Alabama 65201*
F. W. FAXON COMPANY, INC., 15 Southwest Park, *Westwood, Mass, 02090*
THE MOORE-COTTRELL SUBSCRIPTION AGENCIES, *North Cohocton, N. Y. 14838*
READ-MORE PUBLICATIONS, INC., 140 Cedar Street, *New York, N. Y. 10003*
STECHERT-MACMILLAN, INC., 7250 Westfield Avenue, *Pennsauken N. J. 08110*

VIETNAM
XUNHASABA, 32, Hai Ba Trung, *Hanoi*

YUGOSLAVIA
JUGOSLAVENSKA KNJIGA, Terazije 27, *Beograd*
FORUM, Vojvode Mišića 11, *21000 Novi Sad*